

**Optimisation of IMPAXX EPS Foam Energy Absorber with Applications for
Amphibian Aircraft Landing on Water**

By

Kamarul Bin Amir Mohamed

A thesis submitted to the University of Hertfordshire in partial fulfilment of the
requirements of the degree of Doctor of Philosophy

School of Engineering and Technology

November 2018

Abstract

The research aims to optimise the design of IMPAXX EPS foam energy absorber for enhanced landing performance of an amphibian aircraft. Extensive transient dynamic simulations have been carried out to investigate the effect of IMPAXX EPS foam layer arrangements to landing performance with LS-DYNA. The design parameters of the IMPAXX EPS foam were systematically assessed for impact performance using LS-DYNA simulation. The research started with material characterisation of IMPAXX EPS foam related to impact application. Three IMPAXX EPS foams of different densities were tested at 2 m/s, 3 m/s, and 4 m/s impact velocity for blocks with various combinations of foam types. There were 12 flat layered design of foams that were evaluated through experiment and simulation to observe the characteristic of IMPAXX EPS foams. Later, optimised design of flat layer configuration were selected. The selected design then were used with shape configurations such as Arc (ARC), Sinusoidal (SIN), square (SQ) and Trapezium (TR). These shapes were then incorporated with space (S) and no-space (NS) design respectively. The final

optimised foam design was then installed at the front (FRONT) and back (BACK) position of the amphibian aircraft. This is to determine the best installation location based on acceleration (g) and displacement (mm) with specified impact load. A statistical analysis has been carried out to determine the optimum value of acceleration (g) and displacement (mm) effects through experiment and simulation. Average approach and time (t) average approach has been used to determine the best design. Results showed the design configuration of square space (SQ-S) with CBA design is the best material configuration and has been used for the landing performance analysis of the full aircraft. Hence, position of the energy absorber gives significant effect in reducing the acceleration (g) impact towards the structure and occupant for 3 m/s and 4 m/s impact velocity. For these impact velocities, it is found that foams installed at BOTH position provides a significant reduction of acceleration (g) to the occupant which is 8.82 g for 3 m/s and 14.5 g for 4 m/s. Meanwhile, for 2 m/s, it does not provide any improvement to the structure and occupant.

Dedication

*My Father, Amir Mohamed,
I've taken many parts of him.*

*My Mother, Maimon,
My love for you will always remain.*

Without you all, I'm nothing.

Beloved wife, Zaiton...

I always love you till heaven

My clever & beautiful kids, Hanna & Hafiy

Thank you for being good kids & always patient facing me

Mother in-law, Kamariah

thank you for believing me in everything

Thank you for everything.

Table of Contents

Abstract	ii
Dedication	iv
Table of Contents	v
List of Figures	xiii
List of Tables	xxv
Acknowledgements	xxxii
Declaration	xxxiii
Publications Associated with This Research Work	xxxiii
Chapter 1: Introduction	1
1.1 Project Background	1
1.2 Problem Statement	5
1.3 Aims and Objectives	6
1.4 Scope of Research	7
	v

1.5	Novelty and Contribution to New Knowledge	8
1.6	Thesis Arrangement	9
Chapter 2:	Literature Review	11
2.1	Brief History of Amphibian Aircraft	11
2.2	Comparison of Landing Parameters	13
2.2.1	Normal Landing	17
2.2.2	Crosswind Landing	18
2.2.3	Downwind Landing	20
2.2.4	Glassy Water Landing	20
2.2.5	Rough Water Landing	21
2.2.6	Confined Area Landing	22
2.2.7	Emergency Landing	22
2.3	Impact on Pilot/Occupant During Landing	22
2.3.1	Aircraft and Seated Human Coordinate System.	23
2.3.2	Acceleration (g) and Impact	24
2.3.3	Human Tolerance Curves (Eiband Curves)	26
2.3.4	Nature of Human Tolerance Towards Acceleration Rate	28

2.3.5	Aircraft Seat Crashworthy Evaluation	30
2.4	Polymeric Foams	33
2.4.1	Deformation Mechanisms in Foams	35
2.4.2	Manufacturing Process of Expanded Polystyrene (EPS)	38
2.4.3	Energy Absorption Characteristics of EPS	40
2.4.4	Advantages and Applications of EPS	41
2.5	High Energy Absorption – IMPAXX EPS Foam	45
2.5.1	Stress-Strain Curve of IMPAXX EPS Foam	48
2.6	Finite Element (FE) Modelling	50
2.6.1	IMPAXX Foam Modelling in LS-DYNA	50
2.6.2	Aircraft Structure–Carbon Fibre with Airex Foam Core	52
2.6.3	Water Modelling in LS-DYNA	54
2.6.4	Seat: DAX55 and Confor Green Modelling in LS-DYNA	56
2.7	Summary of Literature Survey	58
Chapter 3:	Research Strategy	60
3.1	Introduction	60
3.2	Phase One: Data Collection and Analysis	63

3.3	Phase Two: Determine Best Flat Design	64
3.4	Phase Three: Determine Best Shape Design	67
3.5	Phase Four: Determine Best Position	69
3.6	Phase Five: Conclusions	71
3.7	Summary of Research Strategy	71
Chapter 4:	Setup for Experimental and Numerical Study	72
4.1	Introduction	72
4.2	Experimental Setup	72
4.2.1	Drop Tower Test- Machine	72
4.2.2	Composite Sandwich Structure	75
4.2.3	IMPAXX 300, 500 and 700	76
4.3	Numerical Setup	76
4.3.1	IMPAXX EPS Foam	76
4.3.2	Layer Configuration	81
4.3.3	Shape Configuration	83
4.3.4	Water	85
4.3.5	Seating Foam	89

4.3.6	Finite Element Dummy Model and Seatbelt	92
4.3.7	Aircraft Composite Sandwich Finite Element Model	93
Chapter 5:	Result and Analysis of Simulation and Experiment	97
5.1	Experiment and Simulation Results	99
5.1.1	Acceleration Results for Layer Design Configuration	102
5.1.2	Displacement Results for Layer Design Configuration	105
5.1.3	Summary of Acceleration and Displacement Measurement Result	108
5.2	Analysis of Foam Design Based on Layer	109
5.2.1	Single Layer Foam Configuration	109
5.2.2	Multiple Layer Foam Configuration	117
5.2.3	Combination (Hybrid) Layer Foam Configuration	125
5.2.4	Summary of Flat Foam Design Based on Layer Configuration	129
5.3	Analysis of Foam Design Based on Impact Velocity	130
5.3.1	Impact Velocity Analysis at 2 m/s	131
5.3.2	Impact Velocity Analysis at 3 m/s	136
5.3.3	Impact Velocity Analysis at 4 m/s	141
5.3.3	Summary of Foam Design Based on Impact Velocity	146

Chapter 6:	Best Design Configuration for Impact Absorption	147
6.1	Analysis to Determine Best Design Configuration for Material Design Based on Average Value	148
6.1.1	Analysis by Using Average Values at 2 m/s	148
6.1.2	Analysis by Using Average Values at 3 m/s	150
6.1.3	Analysis by Using Average Values at 4 m/s	152
6.1.4	Summary of the Best Materials Analysis Based on Average Values Approach for Experiment and Simulation	155
6.2	Analysis to Determine Best Design Configuration for Material Foam Design Based on Time (t) Parameter	155
6.2.1	Analysis Using Time (t) Average Approach at 2 m/s	155
6.2.2	Analysis Using Time (t) Average Approach at 3 m/s	159
6.2.3	Analysis Using Time (t) Average Approach at 4 m/s	163
6.2.4	Summary of Best Materials Selection Based on Time (t) Average Approach for Experiment and Simulation	167
6.3	The Analysis on Space (S) vs. No-Space (NS) to Determine Best Design Configuration	167
6.3.1	Space (S) vs. No-Space (NS) Design Based on Average Values of Acceleration and Displacement	173

6.3.2	Space (S) vs. No-Space (NS) Design Based on Time (t) Approach	185
6.4	Summary	198
Chapter 7: Optimised Position in Equator P2 Aircraft Landing on Water		200
7.1	Aircraft with No-Foam Installed	203
7.2	Foam Installed in Aircraft - FRONT Position	205
7.3	Foam Installed in Aircraft – BACK Position	208
7.4	Foam Installed in Aircraft - BOTH Position	210
7.5	Summary of Optimised Foam Location for Equator P2 Aircraft	213
Chapter 8: Conclusions and Recommendations		215
8.1	Conclusions	215
8.2	Future Research and Suggestions	217
References		218
Appendix A		229
Appendix B		231
Appendix C		238
Appendix D		242

Appendix E	246
Appendix F	276
Appendix G	298
Appendix H	309

List of Figures

Figure 1-1 : Modifications of Twin Engine Land-Based Aircraft	2
Figure 1-2: Modifications of Single Engine Land-Based Aircraft	2
Figure 1-3: P2 Xcursion Aircraft by Equator SA, Norway	3
Figure 1-4: IMPAXX EPS Foam Compared to Other Energy Absorbing Material	4
Figure 2-1 : Grumman Goose G-21 (1937)	11
Figure 2-2: Evolution of Sea Base Capable Seaplanes	12
Figure 2-3: State-of-the-art Electric Propelled Amphibian Aircraft	13
Figure 2-4: Basic landing Conditions for land aircraft	14
Figure 2-5: The Touchdown Attitude and Hull Components for Most Seaplanes	16
Figure 2-6: Equator Aircraft P2 Landing Trigonometry	17
Figure 2-7 : Excessive Crosswind Effect	18
Figure 2-8: Dropping the Upwind Wing Uses a Horizontal Component of Lift to Counter the Crosswind Drift	19
Figure 2-9: Downwind Arc to Compensate the Crosswind	19

Figure 2-10: Consequences of Misjudging the Altitude)	20
Figure 2-11: Landing Attitude, Airspeed and Rate of Descent for Landing on Glassy Water	21
Figure 2-12: Aircraft Coordinates	23
Figure 2-13: Human Coordinates	23
Figure 2-14: Triangular Crash Pulse	25
Figure 2-15: Eiband Curve of $+G_z$	26
Figure 2-16: Eiband Curve of $-G_x$	27
Figure 2-17: Effect of rate of onset	29
Figure 2-18: Test Condition 1 Simulation Setup	31
Figure 2-19: Test Condition 2 Simulation Setup	32
Figure 2-20: Sled Test Results on the Cushioned Seat	33
Figure 2-21: Typical Compressive Response Stress-Strain Curve for Elastomeric Foam	35
Figure 2-22: Un-Deformed Mechanical Model of a Closed Cell Foam	37
Figure 2-23: Deformed Mechanical Model of a Closed Cell Foam	37
Figure 2-24: Model from Skochdopole and Ruben Which Shows the Force Acting Parallel for Air and Polymer Cell Walls	38

Figure 2-25: Raw Bead	39
Figure 2-26: Polymerisation Reaction of the Monomer ‘Styrene’	39
Figure 2-27: Pre-puff Bead	39
Figure 2-28: Process of Manufacturing EPS	40
Figure 2-29: ATMOS™- Bicycle Helmet by GIRO	42
Figure 2-30: Equestrian Helmets with EPS Foam by Troxel	43
Figure 2-31: Helmets Main Component Made by Dainese	44
Figure 2-32: EPS Foam for Product Packaging	45
Figure 2-33: IMPAXX Foam by DOW Automotive	46
Figure 2-34: IMPAXX Fixed Inside NASCAR Race Car Door	46
Figure 2-35: (a) Side View of Closed-cell Structure of IMPAXX (with SEM, TU/e), (b) Top view of Closed-cell Structure of IMPAXX(with SEM, TU/e)	47
Figure 2-36: Compressive Response of IMPAXX Energy Absorbing Foam	48
Figure 2-37: Quasi-static Compression Comparison of 48 kg/m ³ Foams	49
Figure 2-38: Quasi-static vs. Dynamic Response Compression Curve	49
Figure 2-39: Carbon Fibre Sandwich with Airex C70 core	53
Figure 2-40: Experimental and Simulation Stress-Strain Curve; (a) DAX 55, (b) CONFOR Green	57

Figure 3-1: Flowchart of the Research Activities	61
Figure 3-2: Phase One: Data Collection and Analysis	64
Figure 3-3: Phase Two: Best Flat Design Determination	64
Figure 3-4: Phase Three : Best Shape Determination	68
Figure 3-5: The Best Design Configuration Position for Foam Location	70
Figure 3-6: Phase Four: Foam Position in Equator P2 Aircraft	70
Figure 3-7: Phase Five: Conclusion	71
Figure 4-1: IMATEK IM-10R Drop Weight Impact Tester in UNIMAP	73
Figure 4-2: Compression impactor	74
Figure 4-3: Specimen Clamp Positioned in the Machine for Indentation Testing	74
Figure 4-4: Semi Sphere 20mm Diameter Indenter	74
Figure 4-5: (a) Sandwich Composite Panel, (b) Detail Sandwich Structure	75
Figure 4-6: IMPAXX Foam Used for the Testing	76
Figure 4-7: Compressive Response of IMPAXX Energy Absorbing Foam	77
Figure 4-8: LS-DYNA Material Model Input Deck Listing for IMPAXX™ 300	78
Figure 4-9: LS-DYNA Material Model Input Deck Listing for IMPAXX™ 500	78

Figure 4-10: LS-DYNA Material Model Input Deck Listing for IMPAXX™ 700	78
Figure 4-11: Foam and Impactor Setup in LS Dyna	79
Figure 4-12: Mesh Size Setup	79
Figure 4-13: Mesh Size Analysis for IMPAXX 300	80
Figure 4-14: Layered Foam Setup in LS-DYNA	82
Figure 4-15: IMPAXX Foam Shape Configurations	83
Figure 4-16: Simulation Image Showing Steel Ball Impacting Pure FE Model of Water at t=5 ms.	88
Figure 4-17: Comparison of the Acceleration for Water Impact Validation	89
Figure 4-18: Simulation of CONFOR Green and DAX55 in LS DYNA	90
Figure 4-19: Comparison of Stress-strain between Experimental Data and Numerical Simulations of CONFOR Green.	91
Figure 4-20: Comparison of Stress-Strain between Experimental Data and Numerical Simulations of DAX55	91
Figure 4-21: LS-DYNA HYBRID III Dummy and Seating Position Inside Equator P2 Aircraft	93
Figure 4-22: Dummy with 4-Point Harness System and Rigid Buckle	93

Figure 4-23: Stress-Strain Curve Extracted from Quasi-static Tests on AIREX C70.55 Cross-Linked PVC Foams	95
Figure 4-24: Indentation Result of Composite Sandwich at 2 m/s	96
Figure 5-1: Foam Condition After 3 m/s Impact	99
Figure 5-2: Effect of A (Lowest Density Foam) After 3 m/s Impact; (a) Design ABC, (b) Design BAC	100
Figure 5-3: The Comparison between Simulation vs. Experiment Data; (a) 2 m/s, (b) 3 m/s, (c) 4 m/s	101
Figure 5-4: Acceleration with Impact Velocity 2 m/s; (a) Design 2003, (b) Design 2006, (c) Design 2007	103
Figure 5-5: Displacement with Impact Velocity 2 m/s; (a) Design 2003, (b) Design 2006, (c) Design 2007	106
Figure 5-6: Simulation Result of Single Layer Acceleration Based on Material	112
Figure 5-7: Experiment Result of Single Layer Acceleration Based on Material	113
Figure 5-8: Simulation Values of Single Layer Displacement Based on Material	116
Figure 5-9: Experiment Values of Single Layer Displacement Based on Material	116

Figure 5-10: Simulation Values of Multiple Layer Acceleration Based on Material	120
Figure 5-11: Experiment Values of Multiple Layer Acceleration Based on Material	120
Figure 5-12: Simulation Values of Multiple Layer Displacement Based on Material	124
Figure 5-13: Experiment Values of Multiple Layer Displacement Based on Material	124
Figure 5-14: Simulation Values of Combination Layer (Hybrid) Acceleration Based on Material	126
Figure 5-15: Experiment Values of Combination Layer (Hybrid) Acceleration Based on Material	126
Figure 5-16: Simulation Values of Combination Layer (Hybrid) Displacement Based on Material.	128
Figure 5-17: Experiment Values of Combination Layer (Hybrid) Displacement Based on Material	129
Figure 5-18: Maximum and Average Point of Acceleration Based on Velocity 2 m/s. (a) Experiment; (b) Simulation; (c) Comparison of Maximum Point	132

Figure 5-19: Maximum and Average Point of Displacement Based on Velocity 2 m/s. (a) Experiment; (b) Simulation; (c) Comparison of Maximum Point.	134
Figure 5-20: Maximum and Average Point of Acceleration Based on Velocity 3 m/s. (a) Experiment; (b) Simulation; (c) Comparison of Maximum Point.	137
Figure 5-21: Maximum and Average Point of Displacement Based on Velocity 3 m/s. (a) Experiment; (b) Simulation; (c) Comparison of Maximum Point.	139
Figure 5-22: Maximum and Average Point of Acceleration Based on Velocity 4 m/s. (a) Experiment; (b) Simulation; (c) Comparison of Maximum Point.	142
Figure 5-23: Maximum and Average Point of Displacement Based on Velocity 4 m/s. (a) Experiment; (b) Simulation; (c) Comparison of Maximum Point.	144
Figure 6-1: Simulation Result of Acceleration vs. Displacement at 2 m/s	150
Figure 6-2: Experiment Result of Acceleration vs. Displacement at 2 m/s	150
Figure 6-3: Experiment Result of Acceleration vs. Displacement at 3 m/s	152
Figure 6-4: Experiment Result of Acceleration vs. Displacement at 3 m/s	152
Figure 6-5: Simulation Result of Acceleration vs. Displacement at 4 m/s	154
Figure 6-6: Experiment Result of Acceleration vs. Displacement at 4 m/s	154
Figure 6-7: Simulation: Acceleration at 2 m/s Based on Time (t)	157
Figure 6-8: Simulation: Displacement at 2 m/s Based on Time (t)	157
Figure 6-9: Experiment: Acceleration at 2 m/s Based on Time (t)	158

Figure 6-10: Experiment: Displacement at 2 m/s Based on Time (t)	158
Figure 6-11: Simulation: Acceleration at 3 m/s Based on Time (t)	161
Figure 6-12: Simulation: Displacement at 3 m/s Based on Time (t)	161
Figure 6-13: Experiment: Acceleration at 3 m/s Based on Time (t)	162
Figure 6-14: Experiment: Displacement at 3 m/s Based on Time (t)	162
Figure 6-15: Simulation: Acceleration at 4 m/s Based on Time (t)	165
Figure 6-16: Simulation: Displacement at 4 m/s Based on Time (t)	165
Figure 6-17: Experiment: Acceleration at 4 m/s Based on Time (t)	166
Figure 6-18: Experiment: Displacement at 4 m/s Based on Time (t)	166
Figure 6-19: The Acceleration Results of Material Design Configuration with Impact Velocity 2 m/s, 3 m/s, 4 m/s Between Space (S) and No-Space (NS)	170
Figure 6-20: The Displacement Results Material Design Configuration with Impact Velocity 2 m/s, 3 m/s, 4 m/s Between Space (S) and No-Space (NS)	172
Figure 6-21: The Best Design for Impact Velocity 2 m/s ; (a) Acceleration - Space Average and No-space Average, (b) Acceleration - Space and No-space Compared to Average Line	175

Figure 6-22: The Best Design for Impact Velocity 2 m/s; (a) Displacement - Space Average and No-Space Average, (b) Displacement - Space and No-Space Compared to Average Line	176
Figure 6-23: The Best Design for Impact Velocity 3 m/s ; (a) Acceleration - Space Average and No-Space Average, (b) Acceleration - Space and No-Space Compared to Average Line	179
Figure 6-24: The Best Design for Impact Velocity 3 m/s ; (a) Displacement - Space Average and No-Space Average, (b) Displacement - Space and No-Space Compared to Average Line	180
Figure 6-25: The Best Design for Impact Velocity 4 m/s ; (a) Acceleration - Space Average and No-Space Average, (b) Acceleration - Space and No-Space Compared to Average Line	183
Figure 6-26: The Best Design for Impact Velocity 4 m/s ; (a) Displacement - Space Average and No-Space Average, (b) Displacement - Space and No-Space Compared to Average Line	184
Figure 6-27: Acceleration: Space vs. No-Space for best shape design at 2 m/s	187
Figure 6-28: Displacement: Space vs. No-Space for Best Shape Design at 2 m/s	187
Figure 6-29: New Acceleration: Space vs. No-Space for best shape design at 2 m/s	188

Figure 6-30: New Displacement : Space vs. No-Space for Best Shape Design at 2 m/s	188
Figure 6-31: Acceleration: Space vs. No-Space for Best Shape Design at 3 m/s	190
Figure 6-32: Displacement: Space vs. No-Space for Best Shape Design at 3 m/s	190
Figure 6-33: New Acceleration: Space vs. No-Space for Best Shape Design at 3 m/s	192
Figure 6-34: New Displacement: Space vs. No-Space for Best Shape Design at 3 m/s	192
Figure 6-35: Acceleration: Space vs. No-Space for Best Shape Design at 4 m/s	194
Figure 6-36: Displacement: Space vs. No-Space for Best Shape Design at 4 m/s	194
Figure 6-37: New Acceleration: Space vs. No-Space for Best Shape Design at 4 m/s	195
Figure 6-38: New Displacement: Space vs. No-Space for Best Shape Design at 4 m/s	195
Figure 7-1: Full Aircraft setup in LS Dyna	201

Figure 7-2: Location Data Taken and Foam Installation Position; (a) Foam Installation Position, (b) Node Data Taken	203
Figure 7-3: : A1 Value When NO FOAM Installed at Various Velocity	204
Figure 7-4: A2 Value When NO FOAM Installed at Various Velocity	204
Figure 7-5: Full Simulation of Equator P2 Landing Contour Before-After for NO-FOAM Installed	205
Figure 7-6: A1 Value When FRONT Foam Installed at Various Velocity	206
Figure 7-7: A2 Value When FRONT Foam Installed at Various Velocity	207
Figure 7-8: Full Simulation of Equator P2 Landing Contour Before-After for FRONT	207
Figure 7-9: A1 Value When BACK Foam Installed at Various Velocity	208
Figure 7-10: A2 Value When BACK Foam Installed at Various Velocity	209
Figure 7-11: Full Simulation of Equator P2 Landing Contour Before-After for Back	210
Figure 7-12: A1 Value When BOTH Foam Installed at Various Velocity	211
Figure 7-13: A2 Value When BOTH Foam Installed at Various Velocity	212
Figure 7-14: Full Simulation of Equator P2 Landing Contour Before-After for Both	212

List of Tables

Table 2-1: Amphibian Aircraft Development Throughout the Years	12
Table 2-2: Consideration for Basic Landing Condition	14
Table 2-3: Equator Aircraft P2 Landing Parameters	16
Table 2-4: Aircraft and Human Body Movement Direction Coordinate	23
Table 2-5: Human Tolerance Limits According to Axes	27
Table 2-6: Seat/ Restraint System Dynamic Tests: Part 23.562 Normal, Utility or Acrobatic Category Airplanes	32
Table 2-7: Technical Data for Commercial Grade of IMPAXX	47
Table 2-8: LS-DYNA Material Model Input Deck Listing for IMPAXX™ 300, 500 and 700 Foam Aligned with Vertical Approach Angle	51
Table 2-9: Mesh Quality Criteria	52
Table 2-10: Properties of Carbon Fibre	53
Table 2-11: Properties of Airex C70 Foam Core	53
Table 2-12: Experimental Parameters for Ball Impacting Water	54

Table 2-13: Investigations Involving A Classical FE	55
Table 2-14: Mechanical Properties and LS-DYNA Materials Cards	56
Table 2-15: Additional Parameters for DAX55 for LS-DYNA MAT_57 Material's Card	57
Table 2-16: Summary of Literature Review	59
Table 3-1: Materials, Impact Velocity and Layer Design as the Parameter and Variable for the Study	62
Table 3-2: The Average Values of Displacement and Acceleration for 2 m/s	65
Table 3-3: Shape Design Configuration	67
Table 4-1: Data Recorded According to IMPAXX Foam Mesh Size of 2.5 mm, 5.0 mm and 10.0 mm	80
Table 4-2: Density, Volume and Mass Values for Commercial Grades of IMPAXX	81
Table 4-3: IMPAXX Foam Testing Sequence	82
Table 4-4: Water Simulation Parameters in LS Dyna	86
Table 4-5: Parameters of Rigid Steel Material	86
Table 4-6: Considered Test Cases for Simulation Validation Procedure	86
Table 4-7: Mechanical Properties of Cellular Materials and Additional Parameters in LS DYNA	90

Table 4-8: Plain Weave Carbon/Epoxy Laminate LS DYNA Material Card	95
Table 4-9: Material Properties of Cross-Linked PVC Foam C70.55	96
Table 5-1 : Categories and Naming Identification for Design Configuration	98
Table 5-2 : Naming List for Experiment and Simulation	98
Table 5-3: The Maximum Point of Acceleration (Simulation)	104
Table 5-4: The Maximum Point of Acceleration (Experiment)	104
Table 5-5: The Maximum Point of Displacement (Simulation)	107
Table 5-6: The Maximum Point of Displacement (Experiment)	108
Table 5-7: Acceleration Single Layer (Simulation and Experiment)	111
Table 5-8: Displacement Single Layer Percentage Difference (Simulation and Experiment)	114
Table 5-9: Acceleration Multiple Layer Percentage Difference (Simulation and Experiment)	118
Table 5-10: Displacement Multiple Layer Percentage Difference (Simulation and Experiment)	122
Table 5-11: Acceleration Combination Layer Percentage Difference (Simulation and Experiment)	125
Table 5-12: Displacement Combination Layer Percentage Difference (Simulation and Experiment)	128

Table 5-13: The Combination/Hybrid Layer Result of 2 m/s Impact Velocity	135
Table 5-14: The Combination/Hybrid Layer Result of 3 m/s Impact Velocity	140
Table 5-15: The Combination/hybrid Layer Result of 4 m/s Impact Velocity	145
Table 6-1: Simulation of Acceleration and Displacement at 2 m/s	149
Table 6-2: Experiment of Acceleration and Displacement at 2 m/s	149
Table 6-3: Simulation of Acceleration and Displacement at 3 m/s	151
Table 6-4: Experiment of Acceleration and Displacement at 3 m/s	151
Table 6-5: Simulation of Acceleration and Displacement at 4 m/s	153
Table 6-6: Experiment of Acceleration and Displacement at 4 m/s	153
Table 6-7: The Best Design Based on time (t) Average Approach of Acceleration Experiment vs. Displacement Experiment at 2 m/s	156
Table 6-8: The Best Design Based on time (t) Average Approach of Acceleration Simulation vs. Displacement Simulation at 2 m/s	156
Table 6-9: The Best Design Based on time (t) Average Approach of Acceleration Simulation vs. Displacement Simulation at 3 m/s	159
Table 6-10: The Best Design Based on time (t) Average Approach of Acceleration Experiment vs. Displacement Experiment at 3 m/s	159
Table 6-11: The Best Design Based on time (t) Average Approach of Acceleration Simulation vs. Displacement Simulation at 4 m/s	163

Table 6-12: The Best Design Based on time (t) Average Approach of Acceleration Experiment vs. Displacement Experiment at 4 m/s	163
Table 6-13: Design Configuration for Shape Simulation.	168
Table 6-14: The Acceleration Results of Shape Design Configuration for Space and No-Space	169
Table 6-15: The Displacement Results of Shape Design Configuration for Space and No-Space	171
Table 6-16: Data Computation Based on Average Approach at 2 m/s	174
Table 6-17: The Best Design Based on Average Approach of Acceleration vs. Displacement at 3 m/s	178
Table 6-18: The Best Design Based on Average Approach of Acceleration vs. Displacement at 4 m/s	181
Table 6-19: The Best Design Based on Time (t) Average Approach of Acceleration vs. Displacement at 2 m/s	186
Table 6-20: The Best Design Based on Time (t) Average Approach of Acceleration vs. Displacement at 3 m/s	189
Table 6-21: The Best Design Based on Time (t) Average Approach of Acceleration vs. Displacement at 4 m/s	193
Table 6-22: Best Shape Frequency at Impact Velocity 2 m/s	196
Table 6-23: Best Shape Frequency at Impact Velocity 3 m/s	197

Table 6-24: Best Shape Frequency at Impact Velocity 4 m/s	198
Table 7-1: Equator Aircraft P2 Xcursion Specification (Source: Equator, n.d.)	201
Table 7-2: Absorber Location Installed in the Aircraft and Node Location for Data Collection	202
Table 7-3: The Values of Simulation Results Based on Materials Installed in the Aircraft	213

Acknowledgements

First of all, I thank God, for giving me the knowledge and strength to complete this PhD thesis. The completion of the thesis would not have been possible without the support and encouragement of many individuals. I thank all the people who have supported me throughout my PhD study.

Thanks to my supervisor, Dr Andrew Lewis and Dr Yigeng Xu for their guidance and encouragement throughout this work. Dr William Tiu, without you, I would never have made it.

Special thanks to Mr. Tomas Brødreskift and Mr. Knut Brødreskift from Equator Aircraft AS, Norway for materials, valuable information and resources for me to complete this thesis.

I wish to express my gratitude to Universiti Malaysia Perlis, Universiti Teknikal Malaysia Melaka, Malaysia, Ministry of Higher Education Malaysia and to The University of Hertfordshire for their financial support and facilities to complete this project.

Declaration

This thesis is submitted in partial fulfilment for the degree of Doctor of Philosophy under the regulations set out by the Doctoral College at the University of Hertfordshire. All work reported in the thesis has been carried out by Kamarul Amir Mohamed, except where stated otherwise, between the dates of June 2012 and November 2018. No part of this thesis has been previously submitted to the University of Hertfordshire or any other academic institution for admission to a higher degree.

Kamarul Amir Mohamed

November 2018

Publications Associated with This Research Work

Kamarul A.M., Xu, Y., Lewis, A., Tiu, W. (2017). A Review on Hull Design for Amphibian Aircraft. *Engineering & Technology Research*, Vol. 1, No. 1 (pp. 10-15).

Chapter 1: Introduction

1.1 Project Background

The development of amphibian aircraft can be traced back through the vision of military development in countries that were directly involved in World War I and World War II. The first category of an amphibian aircraft is the floatplane that was fitted with pontoon-style floats. Since amphibian aircraft was an aircraft designed to take off and land on the surface of the water, these pontoons were attached in place of a conventional landing gear with wheels (Global, 2013).

The other category of amphibian aircraft is the one with modified lower part of the fuselage copying the shape of a boat hull, which could float on the surface of water during rest or low speed flight. This is how the term ‘flying boat’ arises (Loftin, 1985). Both categories of amphibian aircraft that flourished in the world war years were then transformed to large elegant flying boats for intercontinental air services. The capabilities of an amphibian aircraft that combines the speed and range are an advantage compared to conventional aircraft due to its ability to land and take-off on open water. They also have the

ability to operate without a hard surface runway and this feature is an additional advantage on safety for overwater operations. Figure 1-1 and Figure 1-2 show the differences between amphibian aircraft and normal land aircraft.

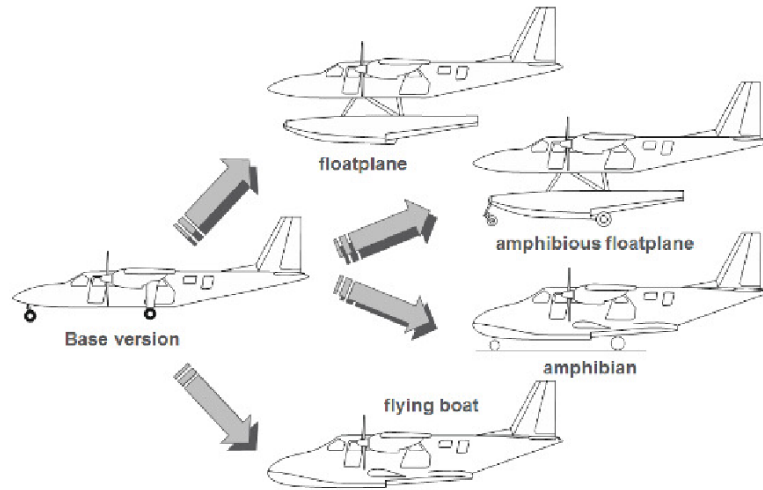


Figure 1-1 : Modifications of Twin Engine Land-Based Aircraft (Source: Gobbi et al., 2011; Majka, 2012)

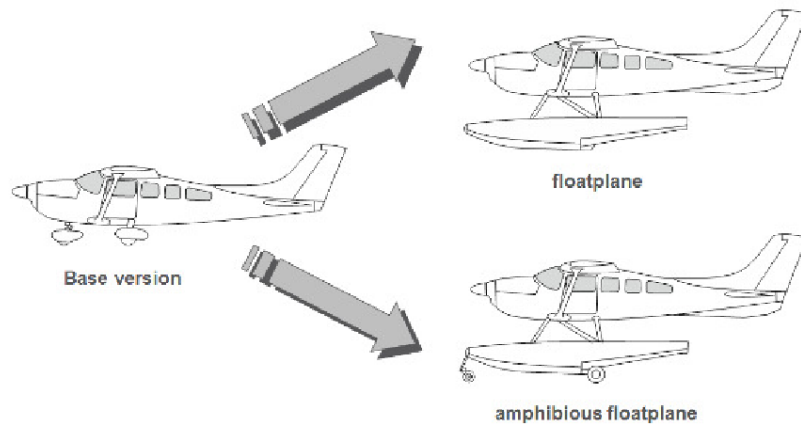


Figure 1-2: Modifications of Single Engine Land-Based Aircraft (Source: Gobbi et al., 2011; Majka, 2012)

In general, amphibian aircraft is more complex than a normal land plane due to its dual working environment (Liem, 2018). Equator P2 Xcursion aircraft (Figure 1-3) lands using its hull structure without any external absorber for water landing purposes. Considering

water landing is a service requirement for this type of aircraft, the hull structure should be able to withstand the impact during normal landing. The energy during contact with water should be absorbed accordingly by the aircraft's structure and at the same time providing protection for structural stability and occupant's safety (Xianfei et al., 2017). Therefore, it is important to design and install passive energy absorption device at Equator P2 to improve the landing performance of the aircraft.



Figure 1-3: P2 Xcursion Aircraft by Equator SA, Norway (Source: Equator, n.d.)

The LS-DYNA is a well-established commercial software for dynamic simulations. It provides the capability to study dynamic problems. It can be used for the stress analysis of structure excited by various types of impact loading and provides the capability to study non-linear dynamic problems. It can also be used for the stress analysis of structures excited by various types of impact loading. In addition, LS-DYNA simulation is able to provide highly accurate and reliable numerical results, and it has also been recognised by many global companies such as NASA , (Hunziker et al., 2018), aircraft manufacturer (Hu et al., 2016), military research agency (Jackson, 2018), oil and gas company (Li et al., 2018a) and so on. Due to these reasons, this research uses the LS-DYNA software to generate and assess

numerical results for optimum dynamic response of the structure.

Most polymeric foams are synthetic and made from petroleum products. However, there are many recent studies conducted using natural extract element based i.e. palm kernel (Septevani et al., 2015), soy based (Lubguban et al., 2017), castor oil (Hejna et al., 2017). Many experimental and numerical studies have been conducted using foam (synthetic and natural) to absorb impact energy in various applications such as the metal foam core for ballistic impact (Zhang et al., 2018), tube-reinforced foam in automotive (Zhou et al., 2018), foam-filled honeycomb structures under impact load (Mozafari et al., 2016). There is however no research reported on using IMPAXX EPS foam for impact energy absorbing structures for amphibian aircraft landing on water. IMPAXX foams is chosen since it is one of the best energy absorber foams which is widely used in automotive and aerospace applications. It is claimed that IMPAXX foam provides higher energy absorbing efficiency (Figure 1-4). It dissipates energy applied through 70% of strain. Furthermore, it comes with three different densities which are suitable for the interest of layer configuration in this study.

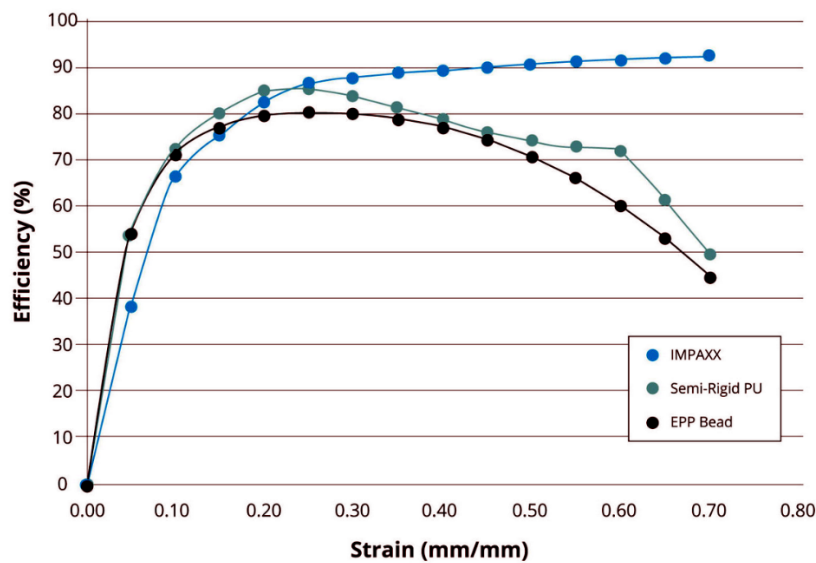


Figure 1-4: IMPAXX EPS Foam Compared to Other Energy Absorbing Material (Source: Coastal Automotive, n.d.)

1.2 Problem Statement

Many studies can be found in the literature with regard to the crashworthiness of common aircraft. There is however very little for amphibian aircraft on using foam for energy absorbing structures to improve the crashworthiness of amphibian aircraft landing on water. Most studies on amphibian aircraft were focussed on aspects such as the aircraft landing gear design and analysis method (Robinson, 2018), spin resistant aircraft configuration (Gionta et al., 2018), computational modelling of the cabin interior of the conceptual model of amphibian aircraft “Lapwing” (Abbasov and V’iacheslav, 2017), Seadrome - the safety of takeoff and landing operations in the seaplane basin (Voloshchenko, 2016), ultralight amphibious PrandtlPlane (Cipolla et al., 2016) optimisation of amphibious aircraft fuselage (Qiu and Song, 2015), VTOL twin fuselage amphibious aircraft (Morris, 2014).

Foam is commonly used for energy absorbing padding especially in sports and military gear (Lewis and Kim, 2018). Many researchers also concentrated on the design of the first contact face (normally hard surface – like composite, ceramic and metal surface) to prevent the impact energy from reaching the occupant (Wu et al., 2018). It is expected that foam installed behind the rigid surface may play an important factor to absorb more impact energy if the foam with proper density, layup configuration and geometry are used.

Researches related to the application of IMPAXX EPS foam were mostly used in sport products like bicycle helmet with IMPAXX foam liner (Teng et al., 2013) (Boshevski and Mircheski, 2017) , absorbing pads to reduce occupant injuries in vehicle side impact (Yıldızhan et al., 2016), polymeric foam composite for vehicle arresting system (Valentini et al., 2016), military helmets and roof padding on head injury protection from vertical

impacts (Franklyn and Laing, 2016). It is proven that IMPAXX EPS foam can absorb impact energy effectively when it has been used properly in the above products. There is however limited research publicly available on using IMPAXX EPS foam for aircraft application in the public domain especially for impact energy absorbers of amphibian aircraft. This project will fill the gap in exploiting the full potential of IMPAXX EPS foam for landing performance of amphibian aircraft through a systematic numerical study.

1.3 Aims and Objectives

The aim of this research is to develop an IMPAXX EPS foam structure for optimised crashworthiness performance of Equator P2 aircraft landing on water.

- i. To analyse the effect of different densities, sequence and shape of IMPAXX EPS foam through experiments and simulations.
- ii. To propose the optimum sequential and shape configuration of IMPAXX EPS foam as energy absorber for Equator P2 Xcursion aircraft.

To fulfil the above aims, following objectives are to be achieved:

- i. Characterise the dynamic response of IMPAXX EPS foam with different densities through experiment and simulation.
- ii. Determine the best design configuration of flat EPS foams based on displacement and acceleration (g) results via experiment and simulation.
- iii. Determine the effect of EPS foam shape based on displacement and acceleration (g) results via simulation.

- iv. Propose effective position of foam energy absorber for Equator P2 Xcursion amphibian aircraft application.

1.4 Scope of Research

The research scopes of the project are as follows:

- i. To study and critically review research on IMPAXX EPS foam application for energy absorbing materials. This is to identify important material parameters for energy absorption based on published experimental and numerical researches.
- ii. To study and critically review the research on crashworthiness of amphibian aircraft landing on water. This is to identify important parameters such as velocity, first impact contact area, aircraft main structure, angle of attack and other relevant information based on published experimental or numerical results.
- iii. To obtain actual mechanical and physical properties of IMPAXX EPS foam by conducting actual test on the proposed material. This is required due to the lack of material data of IMPAXX EPS foam in the literature.
- iv. To study IMPAXX EPS foams of different densities for the dynamic response at different impact velocity, stacking sequence, and interface shape. Experimental and numerical investigation will be carried out to determine the best material and design configuration towards impact energy absorption.
- v. To use statistical method to analyse data obtained from experiments and

simulations. This required careful assessment since a lot of data values are close to each other. This part is to determine the best design based on acceleration and displacement.

- vi. To determine the value of acceleration (g) and displacement as the main parameter for the identification of the best material and design. The acceleration (g) values are based upon different applied impact velocities.
- vii. To perform an analysis on P2 amphibian aircraft structure simulation using the optimised design parameters to reduce the acceleration (g) value.
- viii. To conduct a comprehensive analysis of the experimental and simulation results of the project. This is necessary to identify key results and their correlations in order to fill the research gap and contribute to the knowledge in this field.

1.5 Novelty and Contribution to New Knowledge

The novelty of this research are as follows:

- i. Use of IMPAXX foam as absorber material at different densities in amphibian aircraft landing by simulation and experimental. This also highlighted in research gap and comprehensive literature review subtopic.
- ii. Fully equator P2 amphibian aircraft model successfully developed by simulation to look at impact respond of IMPAXX foam when proposed at different position in the aircraft.

Meanwhile, the contribution to new knowledge are listed as below:

- i. Shifting of different density of IMPAXX foam in layer structure provides different performance and behaviour of impact response under different impact velocity.
- ii. Different sequence of optimised layer arrangement and shape design applied with different impact velocity reduce g values significantly.
- iii. Position of foam in the aircraft plays an important role to determine g value experienced by passenger and also amphibian aircraft structure.

1.6 Thesis Arrangement

This thesis is split into eight chapters. Firstly, Chapter 1 presents research background of the project, problem statements, project aims and objectives, scope of the research and thesis structure. The research gap has been identified and research work has been outlined to fill the gap. In addition, novelty and contribution to knowledge in the field are highlighted.

Chapter 2 presents a comprehensive review of relevant literature relevant to the project. In this literature review, brief history of amphibian aircraft has been presented first. Key aspects reviewed in this chapter include comparison of landing parameters, impact on pilot during landing, polymeric foams characteristics and parameters for energy absorption, capacity of IMPAXX EPS, and Finite Element (FE) Modelling.

Chapter 3 outlines the research strategy for the project. Five phases of research activities are defined with regards to the project aims and objectives to be achieved.

Chapter 4 presents details of the setup for experimental and numerical studies. For experimental setup, details of drop tower test machine, composite sandwich structure and IMPAXX foam with different densities are described. For numerical setup, replication of experimental procedure on IMPAXX foam, layer configuration, and the finite element model of the seating foam and composite sandwich structures are also presented in this chapter.

In Chapter 5, flat foam is first used to investigate the dynamic response of the blocks made of single, multiple and hybrid layers. This chapter mainly presents results from experiment and simulation of EPS Foams in order to examine the material characteristics. Analysis is carried out to characterise the dynamic response of the foam using acceleration and displacement as the evaluation parameters.

Chapter 6 focuses on the best design selection process which was later used to complement Chapter 7. Firstly, evaluation on best flat block of EPS foams were conducted using statistical method. This chapter includes evaluation of single block foams, multiple layered foams and also combination foams. Later, the best selected design of flat block foams was used for the shape effect procedures. The effect of foam shape is then investigated to identify the best one out of the four shapes considered. For this shape, configurations with space or no-space are investigated. The best material and design configuration for the impact energy absorber for the aircraft is proposed in the end.

Chapter 7 assesses the position effect and proposes the best position of the foam energy absorber in aircraft for optimum crashworthiness performance.

Finally, Chapter 8 summarises all the findings in relation to the project objectives defined in Chapter 1. Future research is suggested to enhance the work further

Chapter 2: Literature Review

2.1 Brief History of Amphibian Aircraft

Amphibian aircraft have been built in various nations since early 1900's but the sudden boost of its usage and demand started during World War II (Liem, 2018). During this period, the aircraft were mainly used for military purposes.

Pioneers such as Grumman Corporation introduced a light family utility amphibian aircraft (Figure 2-1). However, military potentials were seen on this type of aircraft which then were ordered by United States Army and its allies during World War II. It was used for air-sea rescue and anti-submarine patrol services. In addition, amphibian aircraft were also used as a supply carrier and bomber throughout the war.



Figure 2-1 : Grumman Goose G-21 (1937) (Source: Wikipedia, n.d.)

Figure 2-2 illustrates the brief history of sea planes evolution. A summary of the development from year 1900 till now is shown in Table 2-1.

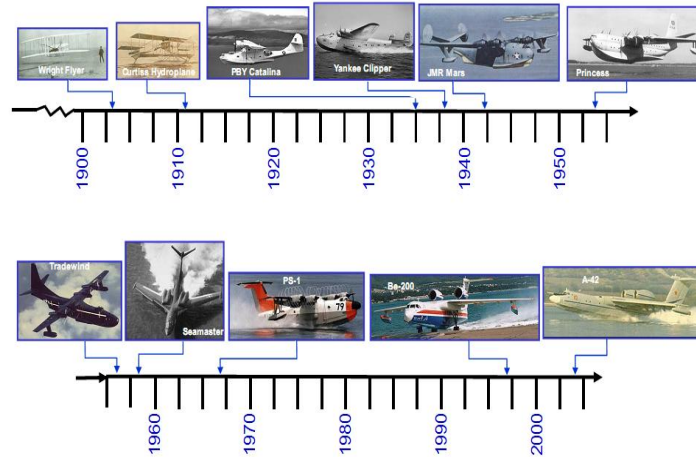


Figure 2-2: Evolution of Sea Base Capable Seaplanes (Source: Jessaji Odedra and Kennell, 2004)

Table 2-1: Amphibian Aircraft Development Throughout the Years (Source: Jessaji Odedra and Kennell, 2004; Bennett et al., 2005.; Vagianos and Thurston, 1970; Loftin, 1985)

Year	Development
1900's	Beginnings of amphibian aircraft development from the time of the Wright Bros Flyer aircraft, although alternative forms of amphibian aircrafts were being investigated before then, by Leonardo da Vinci, Alexander Graham Bell's AEA planes etc.
1910's	Initial developments included light weight aircraft, carrying only man & machine. Later developments saw ordinary land planes being converted to amphibian aircrafts and used as fighter aircraft and racing machines – Schneider Trophy.
1930-40's	The advent of the two World Wars provided suitable justification for developing amphibian aircrafts for various roles such as small fighters, large bomber/patrol aircraft and long distance (trans-Atlantic flights) passenger transportation
Post 1945	Development and interest in amphibian aircrafts reduced as land planes became superior both in aircraft performance and load carrying abilities, and were able to operate in any weather conditions
1950's	With new emerging threats, renewed interest in amphibian aircrafts was aimed at providing greater speed (jet engine), range (reduced weights & better fuselage designs) and mission role capabilities to match their land plane counterparts
1960-90's	The late 1960's provided more commercial and multipurpose use of amphibian aircrafts through firefighting, search and rescue and as well as low volume passenger transportation for short island transfers & leisure activities. However, the level of technology improvements and investment in these newly designed aircraft are not significant.
Present - Future	Recent developments include concept proposals from LM C130 floatplane conversion and the Boeing - Ultra Pelican for meeting military requirements of troop/equipment delivery. Some manufacturers tend to use latest technology such as composite hull and even electric propelled aircrafts (Figure 2-3).



Figure 2-3: State-of-the-art Electric Propelled Amphibian Aircraft (Source: Equator, n.d.)

2.2 Comparison of Landing Parameters

Typical landing types and parameters are briefly reviewed in this section to make sure that a proper arrangement for simulations can be achieved in the project. Amphibian aircraft landing is a bit different compared to its land counterpart. Consideration should be made on factors such as optimal impact point and landing speed to make a successful water landing. This is challenging since there were no cues such as lights and runway markings. Figure 2-4 and Table 2-2 show the basic landing conditions of a land-based aircraft and its configuration for landing.

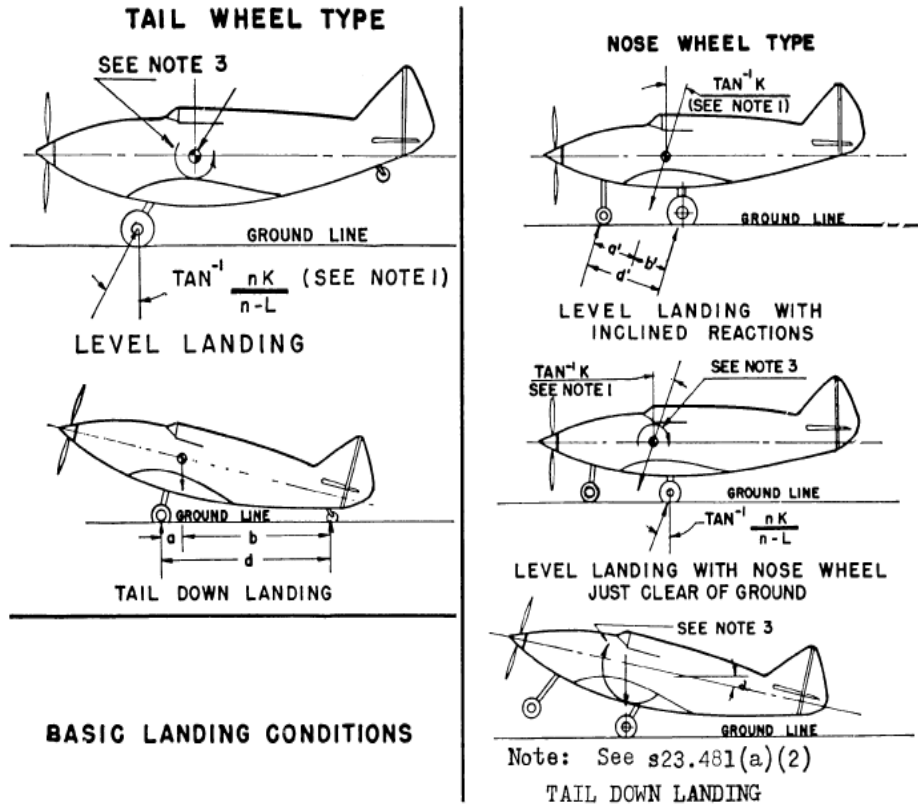


Figure 2-4: Basic landing Conditions for land aircraft (Source: EASA, 2012)

Table 2-2: Consideration for Basic Landing Condition (Source: EASA, 2012; Nguyen, 2010)

Parameters	TAIL WHEEL TYPE		NOSE WHEEL TYPE		
	Level landing	Tail-down landing	Level landing with inclined reactions	Level landing with nose wheel just clear of ground	Tail-down landing
Tail (nose) wheel loads (V_f)	0	$(n-L)W a/d$	$(n-L)W b'/d'$	0	0
Tail (nose) wheel loads (D_f)	0	0	$KnW b'/d'$	0	0
Notes	(1), (3), and (4)	(4)	(1)	(1), (3), and (4)	(3), and (4)
<p>NOTE (1). K may be determined as follows: $K=0.25$ for $W=3,000$ pounds or less; $K=0.33$ for $W=6,000$ pounds or greater, with linear variation of K between these weights.</p> <p>NOTE (2). For the purpose of design, the maximum load factor is assumed to occur throughout the shock absorber stroke from 25 percent deflection to 100 percent deflection unless otherwise shown and the load factor must be used with whatever shock absorber extension is most critical for each element of the landing gear.</p> <p>NOTE (3). Unbalanced moments must be balanced by a rational or conservative method.</p> <p>NOTE (4). L is defined in §23.735(b).</p> <p>NOTE (5). n is the limit inertia load factor, at the c.g. of the airplane, selected under §23.473 (d), (f), and (g).</p> <p>V_f= Reaction Force at the nose wheel, D_f= Drag Force</p>					

During landing, an aircraft need to be aligned with the centreline of the runway. Then, the flap and pitch attitude are adjusted accordingly to the required rate of descent. Basic adjustment to $1.3V_{so}$ + corrections should be used (FSF, 2000; FAA, 2004a; Moren, 1999). This is to make sure that the aircraft stabilises and then the pressure on controls will be relieved after the retrimmed adjustment. Pilots are trained to find a good place to land an aircraft and able to glide (if the engines fail) to a safe touchdown during emergency situations. An amphibian aircraft attached with water float will have a steeper power-off glide which would promote higher rate of descent. Therefore, this should also be considered by any amphibian aircraft pilot for spotting potential landing areas during flight. An advantage of amphibian aircraft is that, it permits more landing options during emergency landing since it is designed to land on both land and water. For land-based aircraft, water landing is the only option it has since smooth landing on grass, dirt runway usually cause damage to the fuselage. Therefore, amphibian aircraft with hull or floats would be a safer alternative in this situation (FAA, 2004b).

One of the objectives in water landing is to touch down at minimum possible speed and in a correct pitch attitude. In addition, minimal or no side drift and full control of the approach, landing, transition and finally taxiing should be achieved throughout the process.

There is a wide range of limits for pitch attitude angle or angle of attack during touchdown for land-based aircraft. Pitch attitude is the angle between the oncoming air or relative wind and a reference line on the airplane or wing. Aircraft with conventional landing gear, needed nearly zero or flat pitch attitude for angle of attack (FAA, 2004b). Correct pitch angle need to be obtained for various manoeuvres. The amphibian aircraft nose maybe a few degrees higher with means to touchdown on step. It should touch down on the steps with the

sterns of the floats or fuselage near to water. If the pitch is much higher or lower, the effects of excessive water drag on fuselage could cause the nose to pitch down in the water. Touching down on steps will keep the water drag minimum while allowing the energy to dissipate gradually. Figure 2-5 shows touchdown attitude and the hull components discussed earlier.

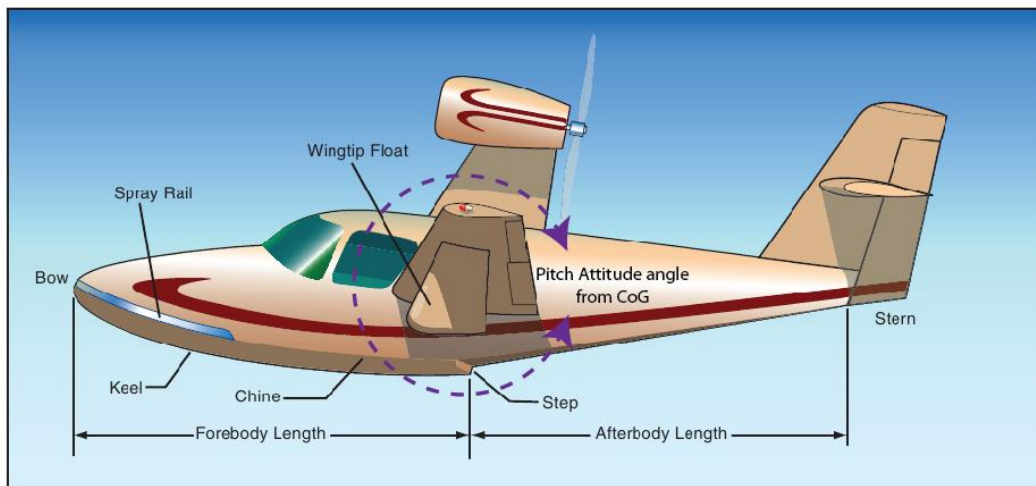


Figure 2-5: The Touchdown Attitude and Hull Components for Most Seaplanes (Source: FAA, 2004b)

The landing speed and sink rate are calculated from aircraft stall speed. Equator Aircraft P2 model has a stall speed of 52 Knots. Therefore, the sink or descent rate could be determined as shown in Table 2-3. These values were calculated using basic trigonometry shown in Figure 2-6.

Table 2-3: Equator Aircraft P2 Landing Parameters (Source: FSF, 2000; Equator, n.d.; Moren, 1999)

Parameters	Knots	m/s	Sink, m/s
Stall Speed, V_{so}	52	26.75	1.40
Stall Speed, $V_{so} \times 1.3 = V_{ref}$	67.6	34.77	1.82
V_{ref} + Corrections (maximum 20 knots)	87.6	45.07	2.35
* V_{so} – Without Flaps			

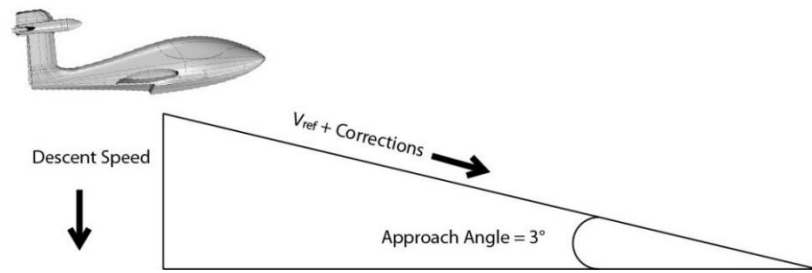


Figure 2-6: Equator Aircraft P2 Landing Trigonometry (Source: Moren, 1999)

There are several types of landing as listed in FAA Handbook for water landing such as normal landing, crosswind landing, downwind landing, glassy water landing, rough water landing, confined area landing and emergency landing.

2.2.1 Normal Landing

Preferably, direction of normal landings usually goes directly into the wind. One advantage for amphibian aircraft is that it could be landed with or without power. However, to gain positive control of the sinking rate, the power-on method is normally used by pilots. During normal landing, flaps are fully extended to get a minimal approach speed possible. Flaps, throttle and pitch would control the glide path of an amphibian aircraft which is similar to their land counterparts.

The greater difference in speed between the aircraft and water would increase the touchdown drag (FAA, 2004b) and this would promote a nose down condition. That's why the landing procedures emphasis on the slowest speeds possible. The whole process from touch down to taxiing would last for about 5-6 seconds which is quicker than landing on the runway.

2.2.2 Crosswind Landing

Crosswind landing is to indirectly land an amphibian aircraft into the wind. During this landing, pilots need to minimise the sideway drift component and maintain directional control which is similar to the land based aircraft (FAA, 2004b). For an aircraft equipped with float, this loss of control would be disastrous since it was mainly designed to take vertical and fore-and-aft loads rather than side loads. Excessive side force would capsize the aircraft as shown in Figure 2-7.

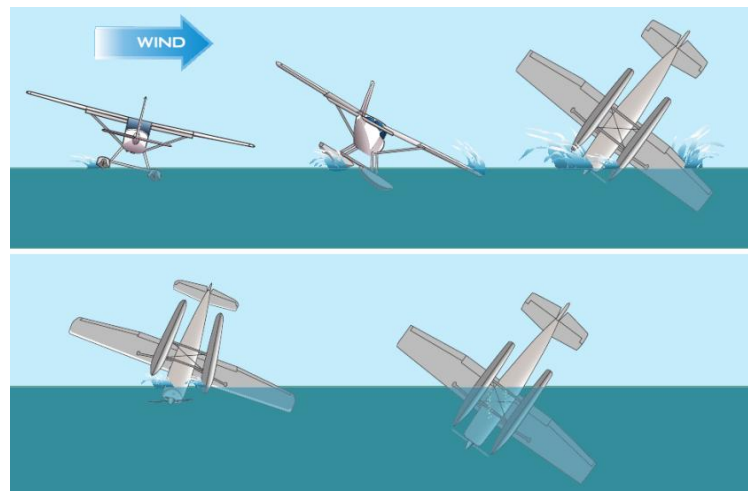


Figure 2-7 : Excessive Crosswind Effect (Source: FAA, 2004b)

After the landing, many pilots tend to turn to the downwind side to minimise weathervaning. This is the technique used to stabilise the aircraft during crosswind landing. It reduces centrifugal force on the aircraft by postponing weathervaning until anticipated speed acquired. This is shown clearly in Figure 2-8.

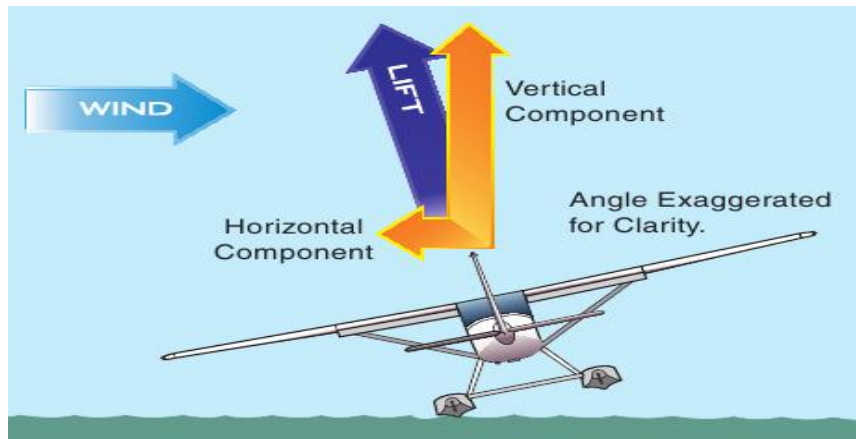


Figure 2-8: Dropping the Upwind Wing Uses a Horizontal Component of Lift to Counter the Crosswind Drift (Source: FAA, 2004b)

Another technique commonly used is the downwind arc method in which the sideward force (centrifugal force) is offset with the crosswind force as shown in Figure 2-9.

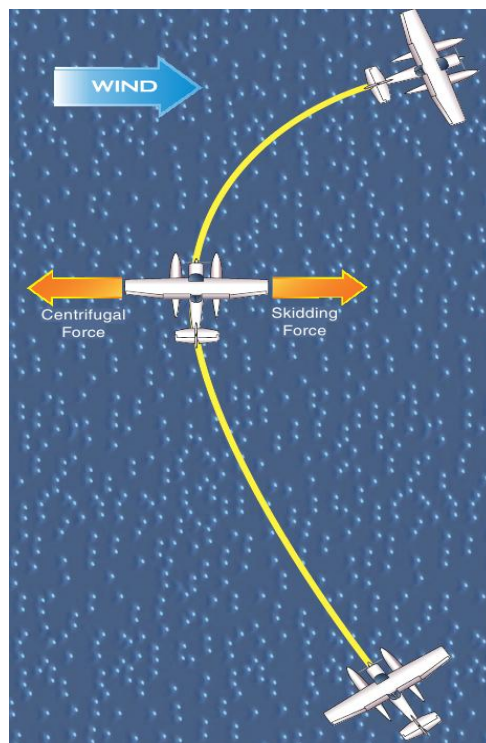


Figure 2-9: Downwind Arc to Compensate the Crosswind (Source: FAA, 2004b)

2.2.3 Downwind Landing

Downwind landing is considered as a more convenient and safer landing practise compared to the normal landing. However, this landing often required more watery area. Usually, upwind landing would be a long process therefore downwind landing is time saving. In order to complete a downwind landing, pilots need to have a thorough knowledge of water landing characteristics and environmental factors in the landing area.

2.2.4 Glassy Water Landing

This type of landing is considered as one of the trickiest and frequently more dangerous landing options. Glassy, calm and flat water could promote false sense of safety. It also gives an indicator of no wind present at that time. Therefore, factors such as direction to land, crosswind, weathervaning and rough water could be ignored. However, these physical and visual characteristics hold many potential hazards.

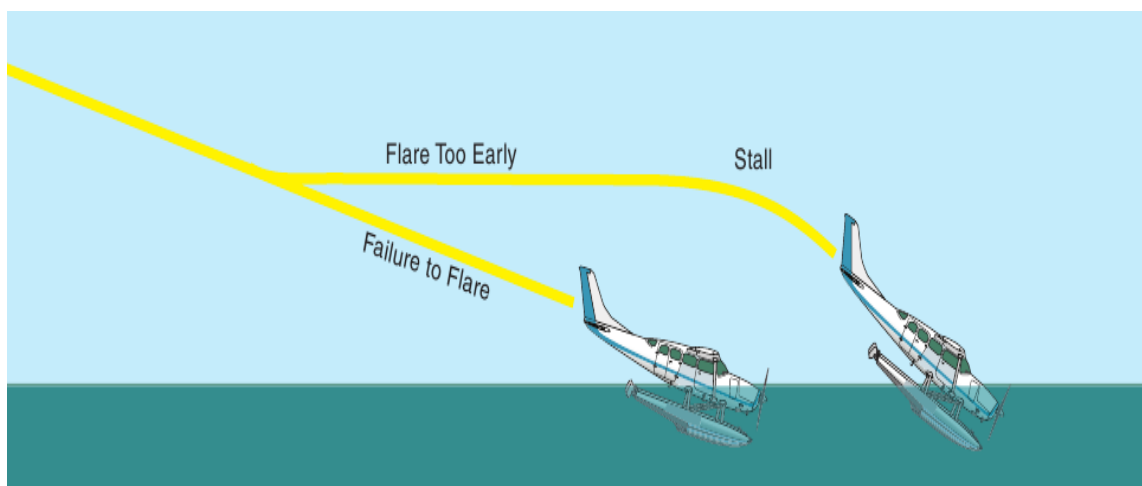


Figure 2-10: Consequences of Misjudging the Altitude (Source: FAA, 2004b)

The possibilities of misjudging the altitude are obvious due to the lack of surface

features. Even an experienced pilot would find it hard to judge the aircraft height from water. This could contribute to a catastrophic landing failure as shown in Figure 2-10. During this type of landing, pilots normally prepare their aircraft for a normal water contact. Approximately, 200 feet above the water surface, aircraft nose is raised to the normal touchdown attitude. The power is adjusted to the maximum of 150 feet/minute with airspeed of 10 knots above stall speed (V_{so}). This speed is maintained until the aircraft touches the water. Once the power settings and landing attitude is set, the airspeed should remain the same without any further adjustment (Figure 2-11).

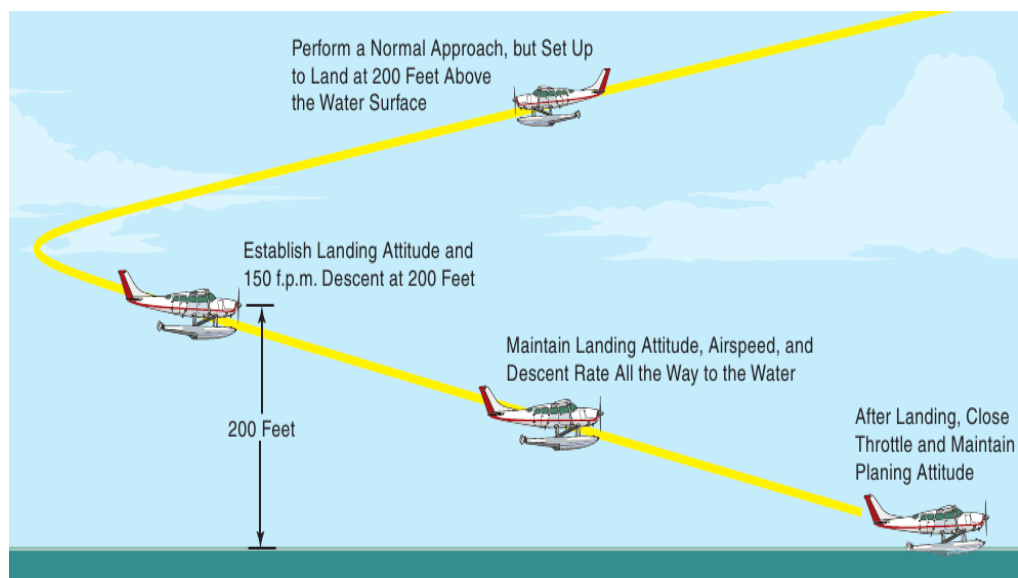


Figure 2-11: Landing Attitude, Airspeed and Rate of Descent for Landing on Glassy Water (Source: FAA, 2004b)

2.2.5 Rough Water Landing

This could be considered a relative and subjective terms for landing. Sometimes, what is good for small boats would be considered rough for an aircraft. Therefore, it is totally dependent on the pilot experience and the amphibian aircraft size to land on this type of water condition,

2.2.6 Confined Area Landing

One of the considerations that should be considered when landing an amphibian aircraft is whether the landing area is suitable for take-off or not. This is crucial since most amphibian aircraft needs a longer take-off run, compared to landing run. The pilot should also consider the air temperature because it would affect the take-off performance due to the air density.

2.2.7 Emergency Landing

Normally, an emergency landing within the gliding distance of water is not a major problem for an amphibian aircraft. However, there would be some leeway in landing attitude where suitable types of landing with regards to water condition should be applied.

2.3 Impact on Pilot/Occupant During Landing

Human tolerance towards acceleration should be studied in order to understand the impact environment during landing for any amphibian aircraft. This will provide maximum working limits for the IMPAXX foam and enabling the optimisation procedure to be conducted.

In this section, commonly used aircraft and seated human coordinate system will be discussed. Guidance were based on the literature related to crash situation, since this would be one of the worst impact condition that the aircraft would face throughout its service.

2.3.1 Aircraft and Seated Human Coordinate System.

Coordinate systems were used to simplify the description of landing or crash situations. The aircraft movements are defined by pitch, yaw and roll. Meanwhile, for the human, aircraft movements are presented in x, y and z coordinates. Both aircraft and human coordinate axes are arbitrarily assigned as shown in Table 2-4.

Table 2-4: Aircraft and Human Body Movement Direction Coordinate (Source: Shanahan, 2004)

Aircraft Movement	Human Movement During Impact
Roll	X
Pitch	Y
Yaw	Z

Figure 2-12 and Figure 2-13 present clearly the aircraft and human coordinate with description on the direction of accelerative force.

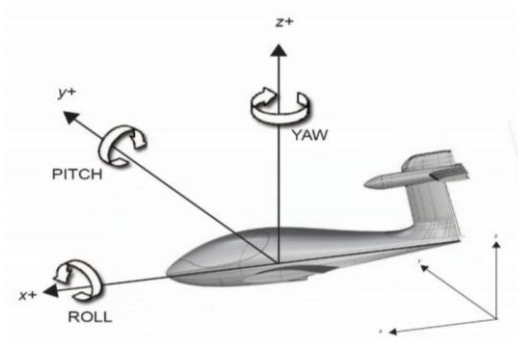


Figure 2-12: Aircraft Coordinates (Source: Shanahan, 2004)

	DIRECTION OF ACCELERATIVE FORCE	
	VERTICAL	
	HEADWARD	EYEBALLS- DOWN
	TAILWARD	EYEBALLS- UP
	TRANSVERSE	
	LATERAL RIGHT	EYEBALLS- LEFT
	LATERAL LEFT	EYEBALLS- RIGHT
	BACK TO CHEST	EYEBALLS- IN
CHEST TO BACK	EYEBALLS- OUT	
<i>NOTES: THE ACCELERATIVE FORCE ON THE BODY ACTS IN THE SAME DIRECTION AS THE ARROWS</i>		

Figure 2-13: Human Coordinates (Source: Shanahan, 2004)

Figure 2-12 represents the aircraft coordinate system and usually used as a guide in standards and publication worldwide. There are other coordinate system used but Shanahan (2004) uses 'left hand rule' coordinate system. Meanwhile, Figure 2-13 shows the most common coordinates system used and applied to a seated human. This system is used to define vectors of displacement, acceleration, velocity and force related to the occupant. Even though this model is not universal, it is used in many literatures related to human tolerances (FAA, 1989). The eyeball reference is also commonly used to describe the body inertial reaction to the applied accelerations during impact. This inertial reaction was the opposite to and equal to the applied acceleration (Shanahan, 2004)

Referring to the movement coordinates in Figure 2-13, any force or acceleration could be described easily to its components directed along the orthogonal axes.

2.3.2 Acceleration (g) and Impact

Acceleration could be defined as the velocity change rate for any given mass. Acceleration could also be described in g unit which represents the ratio between acceleration and gravity as shown in Equation 2-1. Normally, gravity is referred as 9.806 m/s² or;

$$\textit{Acceleration (g)} = a/g \quad (2-1)$$

Normally, acceleration values are calculated at the centre of mass. In addition, deceleration is a reverse action of acceleration which could also be called as negative acceleration.

The crash or impact event could be described using triangular crash pulse as shown in Figure 2-14. In this figure, the pulse describes the acceleration that occurs in the crash event over time or the acceleration-time history of the impact. Even though the crash or impact event is complicated and differs with different scenarios, this triangular pulse was agreed to be used generally for most aircraft crash situation. The assumptions of triangular pulse would simplify the calculation related to the crash while providing reasonable estimates of acceleration exposure (Shanahan, 2004). This could be achieved by assuming that the average acceleration of a pulse is one-half of a peak acceleration.

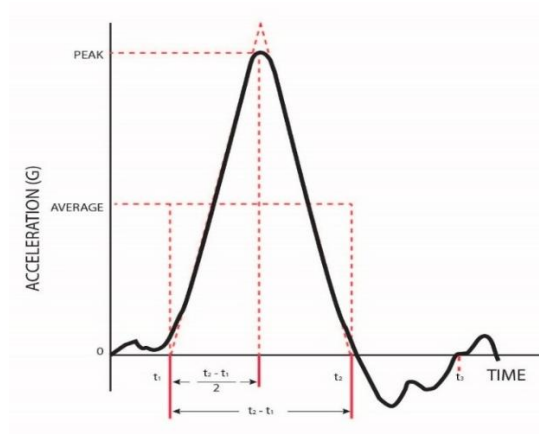


Figure 2-14: Triangular Crash Pulse (Source: Shanahan, 2004)

If the velocity value could be estimated and the stopping distance (displacement during impact) could be measured, the acceleration could also be estimated. This could be achieved by assuming the triangular pulse using Equation 2-2:

$$Peak\ G = \frac{v^2}{(g)s} \quad (2-2)$$

where, v is velocity change of the impact, s is stopping distance and, g is acceleration of gravity at sea level is 32.2 ft/s^2 or 9.806 m/s^2 . Therefore, average (g) is equal to one half of the peak acceleration (g) which applies similarly to get the average value of acceleration.

2.3.3 Human Tolerance Curves (Eiband Curves)

In 1959, Eiband compiled results of human tolerance towards abrupt acceleration under restrained condition. Figure 2-15 and Figure 2-16 were constructed to show typical human tolerance which later be called as Eiband Human Tolerance Curve (Eiband Curves).

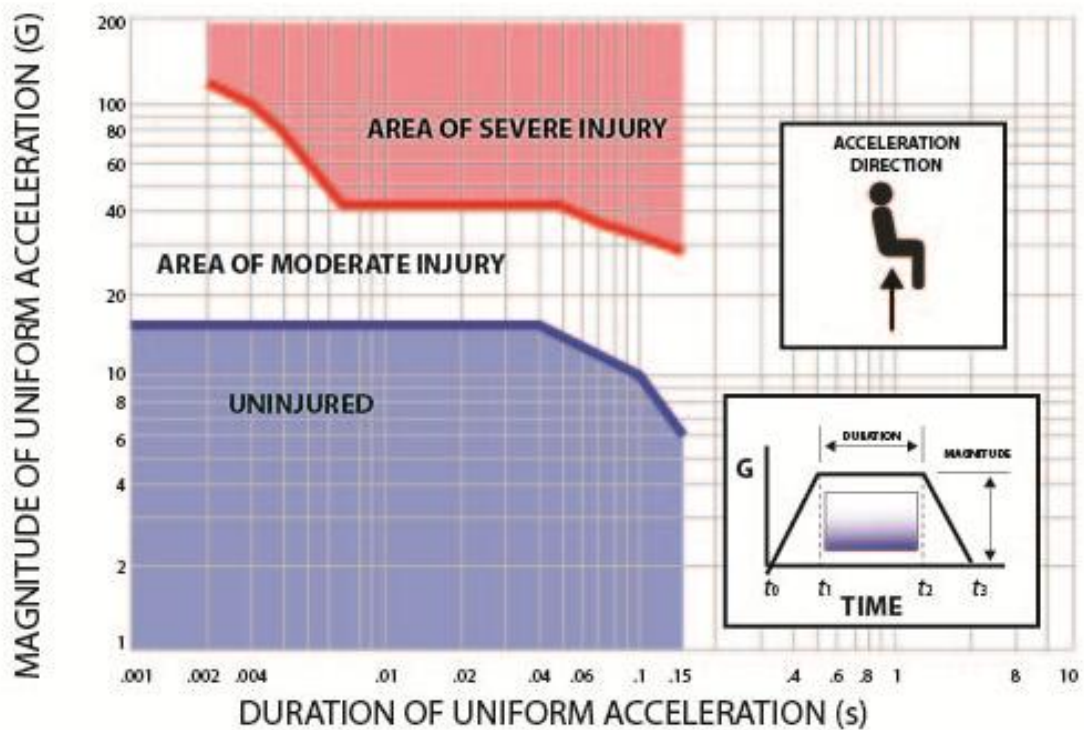


Figure 2-15: Eiband Curve of $+G_z$ (Source: Eiband, 1959; Shanahan, 2004)

Figure 2-15 represents forces experienced by the pilot on an ejection seat or during vertical crash condition. It was plotted with uniform acceleration of the vehicle vs. the duration of the acceleration pulse. From this graph, Eiband illustrated that any individuals would survive uninjured and could tolerate approximately 18 g of acceleration. He also mentioned that spinal injury does not occur for acceleration below 20-25 g.

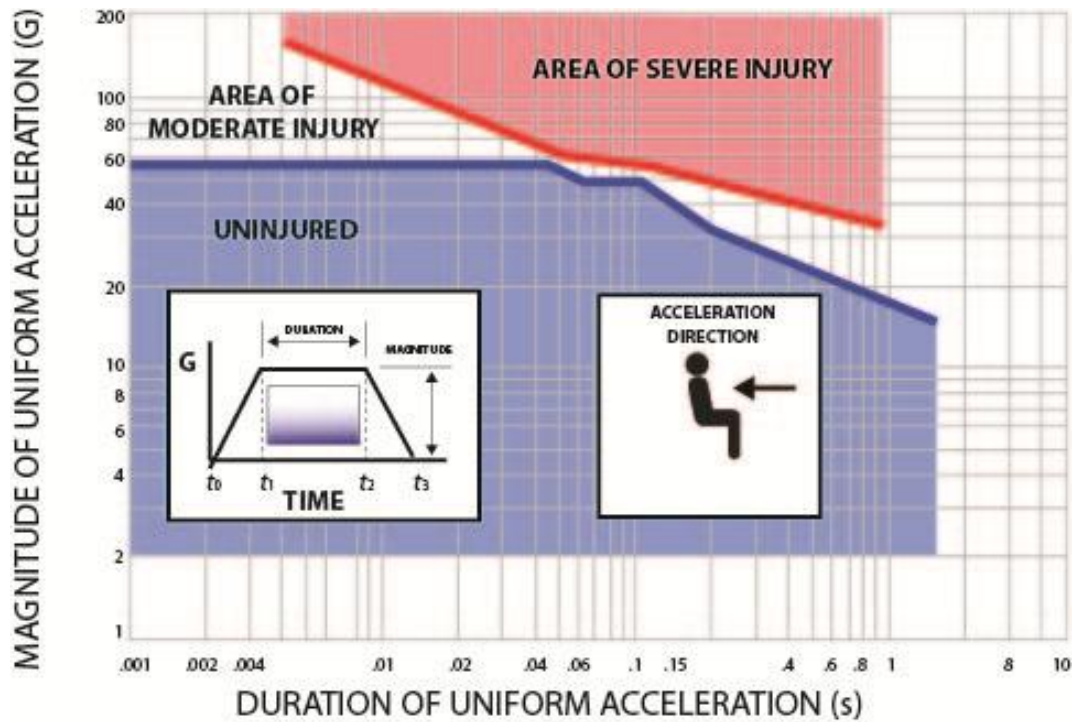


Figure 2-16: Eiband Curve of $-G_x$ (Source: Eiband, 1959; Shanahan, 2004)

In Figure 2-16, Eiband illustrated the curve for a head on collision scenario. In this instance, any individual could withstand up to 40 g of acceleration, if properly restrained. This proves that human could tolerate various acceleration rates depending on axes or direction of the applied acceleration. All of the results estimated by Eiband for human tolerance in all axes is summarised by Shanahan (2004) in Table 2-5.

Table 2-5: Human Tolerance Limits According to Axes (Source: Shanahan, 2004)

Direction of Accelerative Force	Occupant's Inertial Response	Tolerance Level
Headward (+ G_z)	Eyeballs Down	20-25 g
Tailward (- G_z)	Eyeballs Up	15 g
Lateral Right (+ G_y)	Eyeballs Left	20 g
Lateral Left (- G_y)	Eyeballs Right	20 g
Back to Chest (+ G_x)	Eyeballs Out	45 g
Chest to Back (- G_x)	Eyeballs In	45 g

2.3.4 Nature of Human Tolerance Towards Acceleration Rate

Generally, human could tolerate certain acceleration rates depending on factors such as:

i. Magnitude of acceleration

The magnitude of acceleration would be one of the major factors affecting human tolerance towards acceleration. In this instance, greater acceleration magnitude would be more likely to cause injury.

ii. Direction of the acceleration

Hence human tolerance towards accelerations is axes dependent (Shanahan, 2004). This could be seen clearly in Figure 2-12 and Figure 2-13. Eiband (1959) suggested that the most tolerable direction of acceleration by human body is +G_x and -G_x. The least tolerable direction is at the tailwards direction (-G_z).

iii. Duration of the acceleration

This factor is one of the main determinants of human tolerance towards acceleration. The shorter duration of acceleration would be tolerable.

iv. Rate of onset

This rate refers to the frequency and how rapidly the acceleration is applied. It is depicted in the graph area as shown in Figure 2-17. The magnitude and duration of acceleration determines the rate of onset. The higher rate of onset is less tolerable for human body.

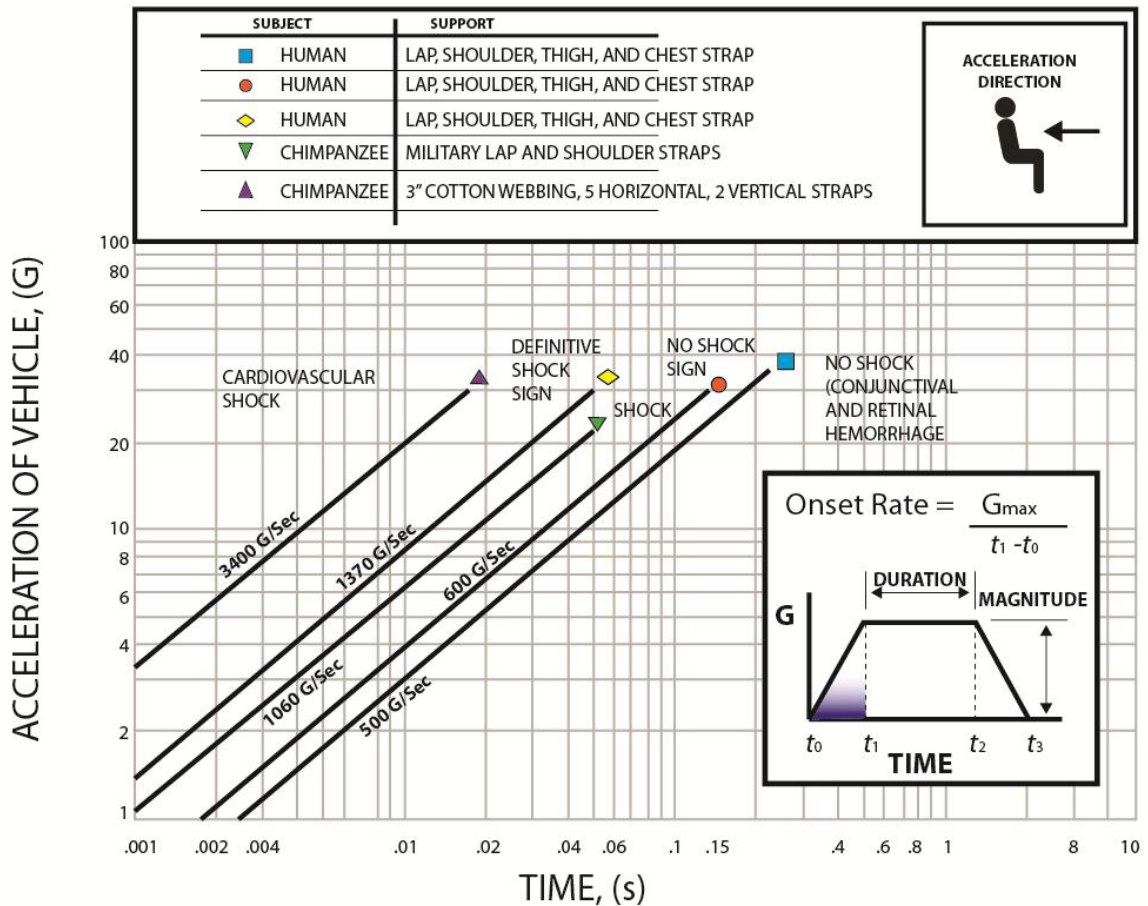


Figure 2-17: Effect of rate of onset (Source: Shanahan, 2004)

v. Position/Restraint/Support

How well the occupants were restrained and supported by the seat and restraint system would be the main criteria affecting human safety during the impact. In addition, the amount of loads distributed accordingly over the body surface would also affect the human safety. This is the determinant factor for survival in survivable impact condition.

2.3.5 Aircraft Seat Crashworthy Evaluation

Code of Federal Regulations (CFR), 14 CFR Parts § 23.562 and § 25.562 were used for aircraft seat crashworthy evaluation. This would be a proper guideline for this project since simulations will be conducted through various aspects of pilot seats during landing on water.

In this circular, Federal Aviation Administration (FAA) has outlined several definitions and methods which will be followed by this research. This dynamic test method as outlined in A 23.562-1 (FAA, 1989) to evaluate the performance of airplane seats, restraint system and related interior systems for demonstrating structural integrity and its ability to protect the occupant from serious injuries. It differs from static test which only concentrates on structural strength of the seat or restraint system only. This circular also helps to promote standardisation among all test method and criteria.

The dynamic performance of an aircraft seat type outlined by FAA emphasised on occupants impact protection criteria (Bhonge, 2008). There are two forms of dynamic test conditions for this test (Desjardins and Laananen, 1980; FAA, 2006; Olivares, 2010). In both test conditions, a 50th percentile male Anthropomorphic Test Devices (ATD) was used by Coltman et al. (1989); Bhonge (2008) and Olivares (2010) .

2.3.5.1 Dynamic Test Condition 1

This test condition combined vertical/longitudinal velocity to evaluate spinal injury and structural integrity for vertical load in emergency landing. It provides ideas on occupant protection if a predominant impact load component applied and directed along the spinal

column. The spinal protection is critical in this condition so there is a need to provide a material with an energy absorbing (load limiting) capabilities on the seat which would then comply to human injury criteria as specified in § 23.562(c) (7) (FAA, 1989). Figure 2-18 shows the test condition 1 setup in LS-DYNA.

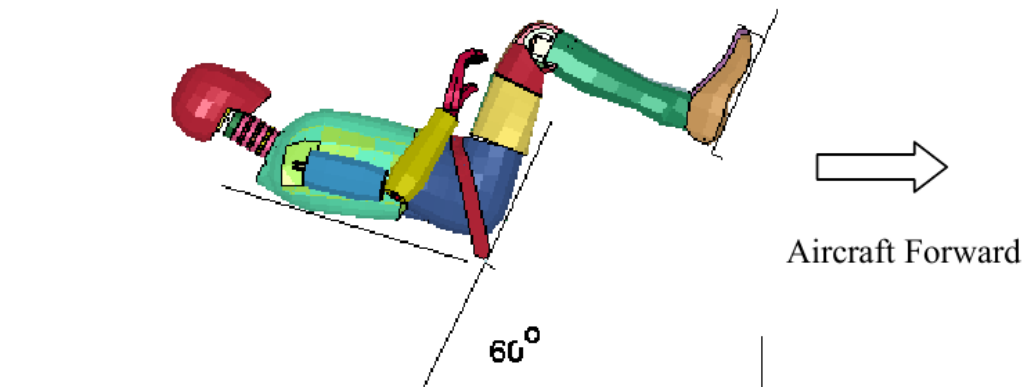


Figure 2-18: Test Condition 1 Simulation Setup (Source: Bhonge, 2008)

2.3.5.2 Dynamic Test Condition 2

The test evaluation was carried out on the protection provided in crashes where the predominant impact is in longitudinal direction with a combination of lateral components. In this test, occupants head need to avoid any impact allotted, using any interior compartment. This test is also used to examine the structural strength of the system. Both tests allow submarining assessment when the seat belt slips above the pelvis and roll out of the torso restraint system (of particular concern with some single diagonal torso restraint belts) (FAA, 1989). Simulated floor or sidewall deformations is used to replicate external crash forces. This would help to evaluate if the seat could accommodate such external forces (FAA, 2006; FAA, 1989). Figure 2-19 shows the test condition 2 setup in LS-DYNA.

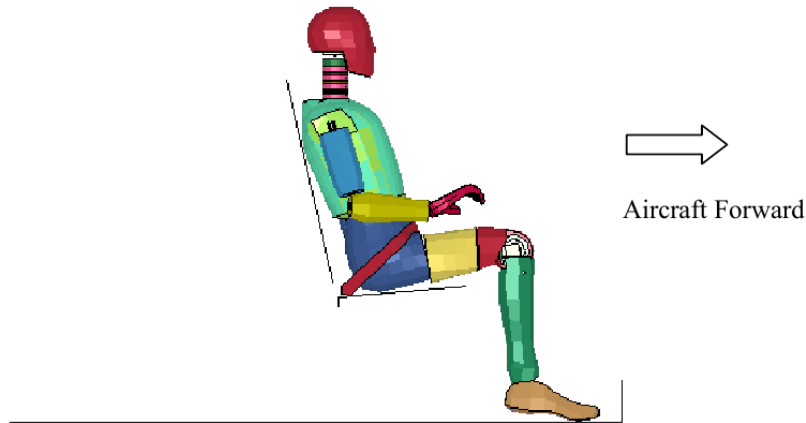


Figure 2-19: Test Condition 2 Simulation Setup (Source: Bhonge, 2008)

Table 2-6 shows the details of test conditions 1 and 2 in accordance to Federal Aviation Regulations (FAR) 23 and 25.

Table 2-6: Seat/ Restraint System Dynamic Tests: Part 23.562 Normal, Utility or Acrobatic Category Airplanes (Source: FAA, 1989; FAA, 2015; Bhonge, 2008)

Aircraft/ Certification Type	Part 23	Part 25	
	FAR 23562	FAR 25.562	
Test 1 Combined Vertical / Longitudinal			
Test Velocity (in ft/sec)	31	35	
Peak Deceleration (in g's)	19/15	14	
Time to Peak (in sec)	0	0	
Initial Conditions			
Seat Pitch Angle	0°	0°	
Seat Roll Angle	0°	0°	
Fixture Angle	60°	60°	
Test 2 Combined Vertical / Longitudinal			
Test Velocity (in ft/sec)	42	44	
Peak Deceleration (in g's)	26/21	16	
Time to Peak (in sec)	10°	10°	
Initial Conditions			
Seat Pitch Angle	10°	10°	
Seat Roll Angle	10°	10°	
Fixture Angle	0°	0°	
Compliance Criteria			
HIC	1000	1000	
Lumbar Load (lb)	1500	1500	
Strap Load (lb)	1750	1750	
Femur Load (lb)	NA	2250	

According to aircraft seat testing regulations (Table 2-6), the acceleration pulse for FAR Parts 23 is 15 g with rise times of 0.06 s and the maximum measured lumbar-column

pelvic compressive loads in the Anthropomorphic Test Device (ATD) must not exceed the 1500 pounds pass/fail criterion. Figure 2-20 shows example of results from previous studies on a cushion seat using DAX55 and Confor as the foam material (Beheshti and Lankarani, 2006).

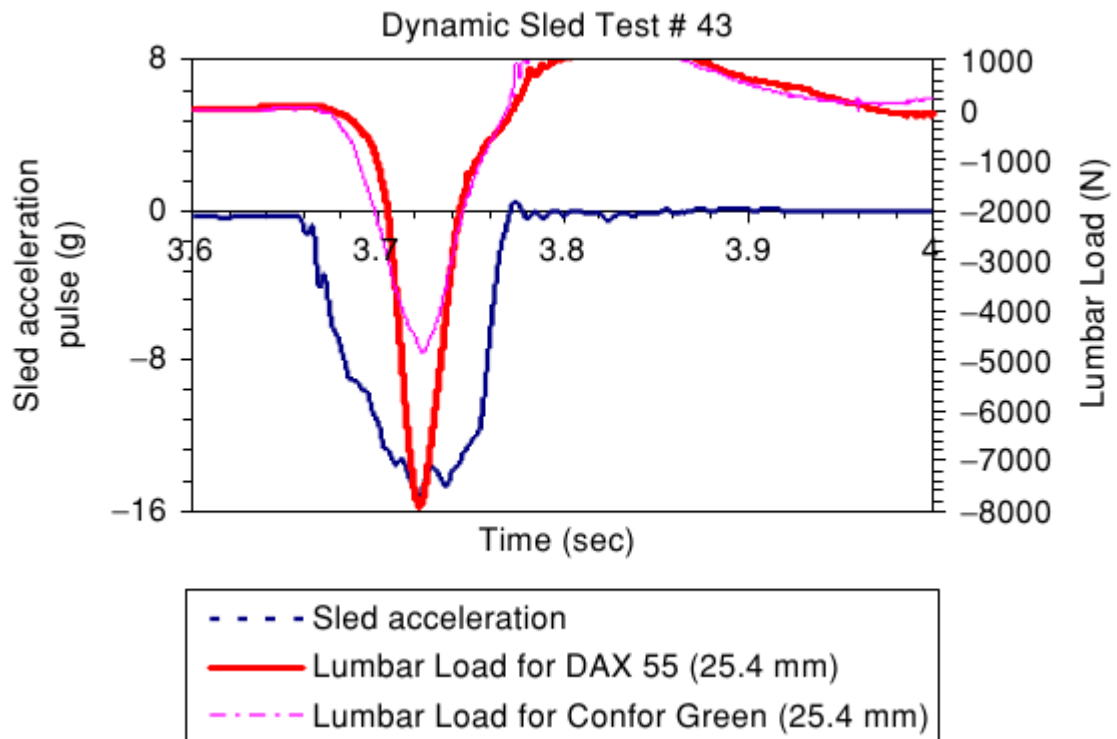


Figure 2-20: Sled Test Results on the Cushioned Seat (Source: Beheshti and Lankarani, 2006)

2.4 Polymeric Foams

Polymeric foam has been studied extensively in the area of impact energy absorption (Aktay et al., 2006; Mills et al., 2003; Slik et al., 2006; Atas and Sevim, 2010; Di Landro et al., 2002). All researchers agree that polymeric foam do have good energy absorption capabilities. Most polymeric foams show three distinctive loading phases that consists of initial elasticated phase, densification plateau and solidification phase when it fails. Factors affecting its absorption capacity include the density and the base polymer (Gover and

Gudimetla, 2011). Denser foams tend to have shorter densification plateau with higher reaction force (Di Landro et al., 2002).

Foam has been used in various applications such as thermal insulation, impact absorption and as a lightweight structure material. It is necessary to understand the foam behaviours to efficiently utilise its capabilities. Mechanical properties of the foam are closely related to the complex micro-structure and the properties of the material of which the cell walls are made. Gibson and Ashby (1997) specified that some salient structural features of foams such as:

- i. The relative density, $R = \frac{\rho^*}{\rho_s}$, in which the superscript * refers to the effective properties of the polymer foam and the subscript s refers to the properties of the solid;
- ii. The degree to which cells are open or closed;
- iii. The geometric anisotropy of the foams.

The important properties of the solid as mentioned by Gibson and Ashby (1997) are the polymer density ρ_s , Young's modulus E_s and yield strength σ_{ys} . These materials parameters are easily found in literatures and data sheet provided by the manufacturer. In this study, IMPAXX foam manufactured by Dow Chemicals will be used in the experiment and the parameters will be the input for simulation purposes.

2.4.1 Deformation Mechanisms in Foams

This section will be focussed on the use of closed-cell polystyrene foam in this research. A closed-cell foam deformation could be described by simplified mechanical models which refer to a network of beam (Gibson and Ashby, 1997; Hilyard, 1982). These models fit different phenomena that occur when the foam was subjected to mechanical loads. However, this approach is only applicable to few specific materials. For polystyrene models, the properties of cellular solid are dependent on (Di Landro et al., 2002):

- i. Parameters describing the foam structure – Density and cell size
- ii. Parameters describing the intrinsic properties of the material constituting the cell walls

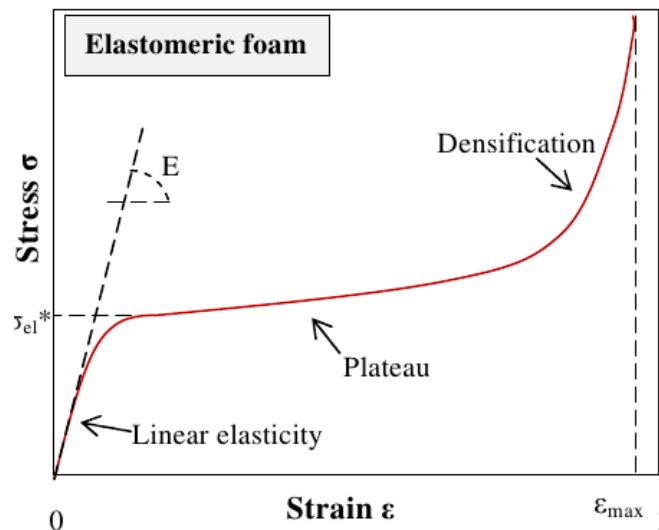


Figure 2-21: Typical Compressive Response Stress-Strain Curve for Elastomeric Foam
(Source: De Vries, 2009)

Figure 2-21 shows a typical stress-strain curve of elastomeric materials. It is shown clearly that the curve could be divided into three sections. There is a linear elasticity region during the initial load application. Then, it goes to the plateau region and finally leads to

densification of the foam where the stress rises steeply. Each section is controlled by some mechanism of deformation. Linear elastic section is mainly controlled by the wall bending cells which stretches the cells wall up to the strain limit. The elastomeric foam shows an elastic response even when a small strain applied to it. In this region, the compressive stress could be determined by $\sigma^* = E^*\epsilon$. The Young modulus E^* is the slope for stress strain response for the linear elasticity and can be described by Equation 2-3:

$$\frac{E^*}{E_b} = \frac{E_{c^*}}{E_b} + \frac{E_{g^*}}{E_b} + \frac{E_{f^*}}{E_b} \cong \phi^2 \cdot \left(\frac{\rho^*}{\rho_b}\right)^2 + \frac{P_0 \cdot (1 - 2\nu^*)}{1 - \left(\frac{\rho^*}{\rho_b}\right) \cdot E_b} + (1 - \phi) \cdot \frac{\rho^*}{\rho_b} \quad (2-3)$$

where,

$$\frac{\rho^*}{\rho_b} = 1,2 \cdot \left(\left(\frac{t_e}{l}\right)^2 + 0,7 \cdot \left(\frac{t_w}{l}\right)^2\right) \quad (2-4)$$

In Equation 2-3, ϕ is the fraction of bulk materials related to the cell edges of thickness t_e ; the remaining fraction $(1 - \phi)$, Equation 2-4, constitutes the walls of thickness t_w , l is the edge length (Di Landro et al., 2002). While in compression, the plateau is associated with partially collapsed cell. For elastomeric foam, there was no plastic deformation and the foam plateau was determined by elastic buckling. When the cells are completely collapsed, it would start to touch the opposing walls which leads to the final section bottoming out referred as densification. Due to the bending of cell edges (E_{c^*}), linear elastic deflection of a beam of unitary length is computed at its midpoint by load F (Figure 2-22). Uni-axial stress needs to be applied so that each cell would transfer the force F (Figure 2-23).

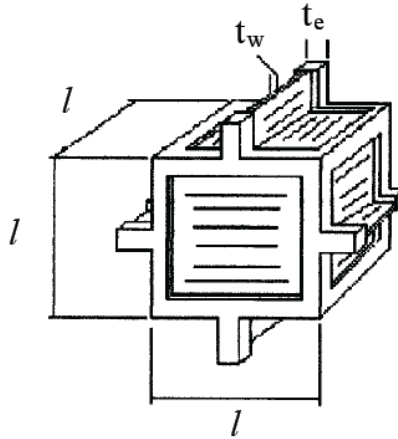


Figure 2-22: Un-Deformed Mechanical Model of a Closed Cell Foam (Source: Di Landro et al., 2002)

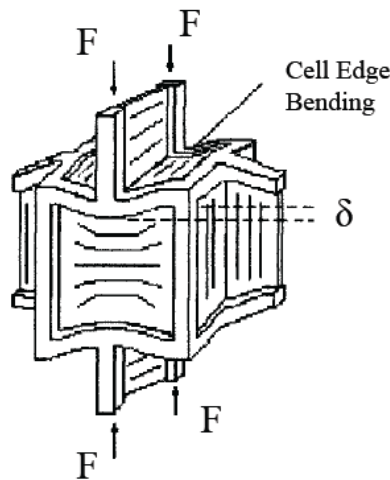


Figure 2-23: Deformed Mechanical Model of a Closed Cell Foam (Source: Di Landro et al., 2002)

When applied with force, the edge bends by itself and the linear elastic deflection δ of the structure as a whole is proportional to $(Fl^3)/(E_bI)$, where I is the second moment of inertia of the edge. ($I \propto t_e^4$). The force F and the strain ε are related to the compressive stress σ and the displacement δ by the relationships $F \propto \sigma l^2$ and $\varepsilon \propto \frac{\delta}{l}$ respectively. It follows that the elastic contribution to foam, Young's modulus is given by $E_g = \frac{\sigma}{\varepsilon} \propto \frac{E_b t^4}{l^4}$ (Di Landro et al., 2002). The deformation is also affected by the closed cell setup. This is because, when the closed cell is compressed, it would also compress the air inside the cells. This leads to an additional force, which can be calculated using Boyle's law (Mills, 2007). Qualitative

model was used by Skochdopole and Ruben's (1965) and Mills (2007) (Figure 2-24) which suggested that the cell which contains air and the polymer microstructure was acting in parallel during deformation (Figure 2-24).

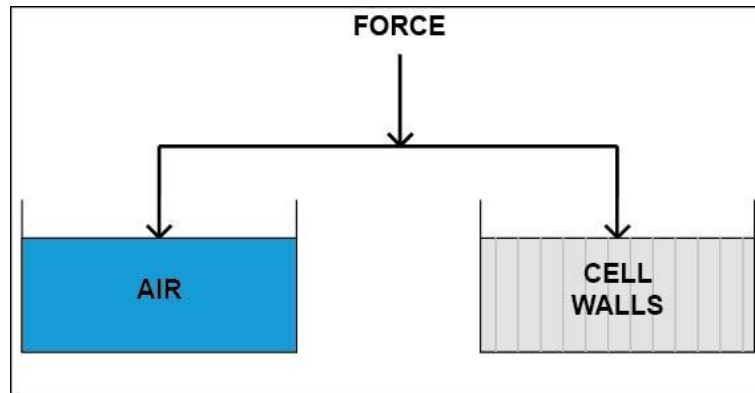


Figure 2-24: Model from Skochdopole and Ruben Which Shows the Force Acting Parallel for Air and Polymer Cell Walls (Source: Mills, 2007)

Furthermore, foams possessing a plastic yield point tend to have ductile failure if the load is beyond its linear elastic section. The plastic strain of the foam was not recoverable; it was often exploited in designing an energy absorption system (Di Landro et al., 2002).

2.4.2 Manufacturing Process of Expanded Polystyrene (EPS)

The common technique in producing EPS is as follows. First, liquid monostyrene were produced from crude oil. After several production steps, the raw bead of polystyrene was made. In raw form, the resin looks like glass-like globules (Figure 2-25). Then, it is added with foaming agent such as butane, ether and propane also called a pre-expansion phase. After the raw beads being treated with foaming agent, it is heated with steam which causes the bead to expand. This expansion process is called polymerisation (Figure 2-26) of monomer styrene and it changes the physical attributes of the raw beads to prepuff-bead.

Normally, resins would expand around 20-50 times of its original size depending on the required density (Figure 2-27) (Mark, 2009; HSV, 2013; Di Landro et al., 2002).



Figure 2-25: Raw Bead (Source: ICA, 2013)

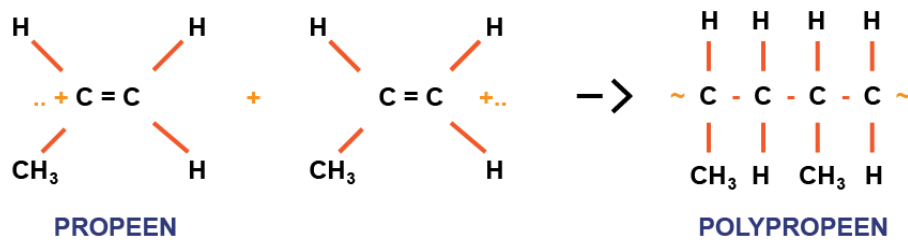


Figure 2-26: Polymerisation Reaction of the Monomer 'Styrene' (Source: HSV, 2013)



Figure 2-27: Pre-puff Bead (Source: ICA, 2013)

This expanded polystyrene would then be conveyed into a mould where it would be formed according to required specification. In manufacturing a polystyrene sheet, temperature range of 200-260° C is needed (Mark, 2009). There are two types of moulding process normally associated with EPS manufacturing: block moulded and shape moulded.

When the beads are heated again with steam, they melt to form a moulded part. All the beads are somewhat welded together and simultaneously trapping air inside its closed cell (HSV, 2013). This trapped air helps the energy absorption capabilities of EPS foam. The entire process is shown clearly in Figure 2-28.

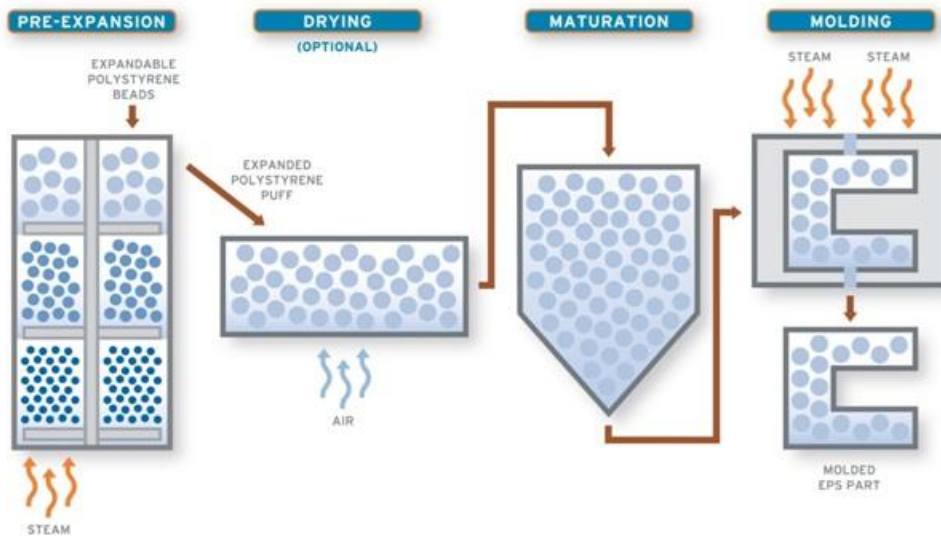


Figure 2-28: Process of Manufacturing EPS (Source: Styro, 2013)

2.4.3 Energy Absorption Characteristics of EPS

The most common type of foams used was EPS (Di Landro et al., 2002). EPS were known to be low cost, light and suitable for mass production. It could dissipate large amount of impact energy while showing low reaction force (Ozturk and Anlas, 2009). Since it has a high energy absorbing capability, EPS is often used in highly impact absorbing application such as motorcycle helmets. Impact-protection is achieved by the helmets outer shell, which distributes the impact energy over a large area of the shell. Meanwhile, closed-cell EPS foam used as helmets inner liner absorb most of the impact energy and reduce the load transmitted to the rider's head (Di Landro et al., 2002; Miyazaki et al., 2006). Ozturk and Anlas (2009)

mentioned that EPS could absorb impact energy while maintaining the reaction forces on the packaged object (stress) and the deformation of the package (strain).

2.4.4 Advantages and Applications of EPS

EPS is the most used material for consumer product packaging and liners. This was mainly due to its excellent characteristics such as energy absorption rate, lightweight and low cost which satisfies most of the required purposes (Cernicchi et al., 2008). This lightweight material creates a chain impact to the industry including fuel emission reduction during transportation of the product. EPS is considerably tough, and it is also used as a side impact barrier for race tracks. In addition, EPS is also waterproof, and is hence suitable for this research since the hull might be wet from the water taxiing situation. EPS is also easily available and by having localised production units, the cost would be tolerable (Plastipedia, 2013).

There are several common usages of EPS such as:

- i. **Bicycle Helmets**

Bicycle helmets were used to protect cyclists during accident especially when they hit the road surface (Mills, 2003). In this situation, the skull will be fractured if there is a high-pressure impact concentration over a small area. The bicycle helmet helps to distribute the load from the road to a large area of skull to reduce the stress concentration. It also helps to reduce the peak force during the impact via the controlled deformation of the foam. Example of the bicycle helmet is shown in Figure 2-29.



Figure 2-29: ATMOS™- Bicycle Helmet by GIRO (Source: ATMOS, 2014)

ii. Equestrian Helmets

It was shown from various studies that sports like horse racing is risky (Balendra et al., 2007; Turner et al., 2002; McIntosh and McCrory, 2005). Horse jockeys are prone to injury compared to other racing athletes (McIntosh and McCrory, 2005; Paix, 1999). It was suggested that the correct usage of helmet while riding would protect the head and reduced severity of head injury on impact (Rueda et al., 2009). The effectiveness of helmet usage in leisure riding was shown by the reduction in numbers of serious head injury among helmet users (Bond et al., 1995). Figure 2-30 shows an example of equestrian helmet for sports usage which has EPS foam in its structure.



Figure 2-30: Equestrian Helmets with EPS Foam by Troxel (Source: Troxel, 2014)

iii. Motorcycle Helmets

There were a number of works in the aspects of design and safety of motorcycle helmets with energy absorbing EPS foam liner (Aiello et al., 2007; Cernicchi et al., 2008; Kostopoulos et al., 2002; Halldin et al., 2001). The EPS which was used as the helmet's liner plays an important part especially to absorb the energy during impact and hence provide required protection for the motorcyclist (Kostopoulos et al., 2002). Figure 2-31 shows the main component of a motorcycle helmet. The main function for this liner is to provide some gap for the head to stop from contacting hard surface during impact. The crush deformation of EPS under loading would reduce the force allotted directly to the skull. In this instance, maximum acceleration and hence the peak force experienced by the rider would be reduced.



Figure 2-31: Helmets Main Component Made by Dainese (Source: Cernicchi et al., 2008)

iv. Product Packaging

Expanded polystyrene (EPS) was mostly used in packaging of consumer products (Ozturk and Anlas, 2009). Reasons for this include: known-lower-cost material, light-weight and good protection for products especially during transportation. Foam was certainly a diverse protective material in the packaging industry (Cui et al., 2009). Figure 2-32 shows some examples of EPS product packaging. As a summary, EPS is widely used in many applications due to its lower cost, light weight and good energy absorption.



Figure 2-32: EPS Foam for Product Packaging (Source: APP, 2014)

2.5 High Energy Absorption – IMPAXX EPS Foam

The mechanical properties of EPS are normally determined by the blowing agent, foaming ratio, injection or extrusion temperature and its rolling mechanism (Ahn et al., 2002). However, the research in this project will concentrate on closed-cell energy absorbing foam material by DOW Automotive. It is a highly engineered polystyrene-based thermoplastic foam. IMPAXX foam (Figure 2-33) was manufactured using extrusion method and contains a halogenated flame retardant system which were mixed with blowing agents and other additives (De Vries, 2009; Dow, 2009b).

Known for its lightweight and dynamic impact energy absorption, IMPAXX was mainly used for automotive applications and installed in bumpers and doors for protection to enhance passengers' safety in the event of a crash (Figure 2-34) (Dow, 2009b; Leslie-Pelecky, 2008; De Vries, 2009; Dow, 2009b). It is installed in vehicle cavities during assembly. IMPAXX foams can also be used for structural panel applications.

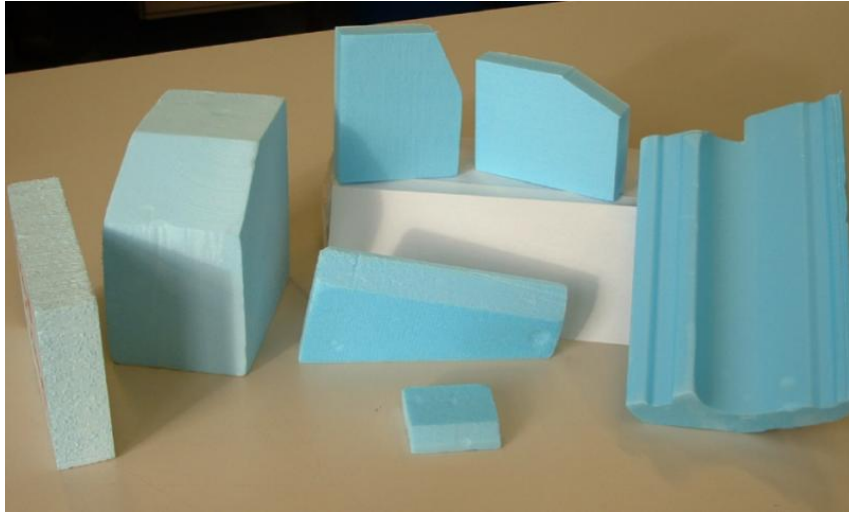


Figure 2-33: IMPAXX Foam by DOW Automotive (Source: Moritz, 2012)

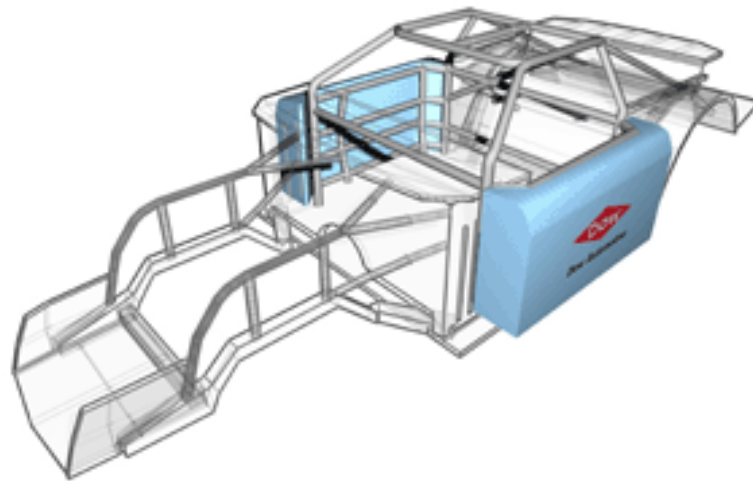


Figure 2-34: IMPAXX Fixed Inside NASCAR Race Car Door (Source: Leslie-Pelecky, 2008)

IMPAXX is strong, lightweight, and low in density, with a closed cell structure as shown in Figure 2-35 (Dow, 2009b). There are three commercial grades of IMPAXX foam, which are 300, 500 and 700. They were categorised based on its compressive strength and density (Dow, 2009a). This would maximise energy absorption because of anisotropy elongations which allows high elastic compression (Mills et al., 2003; Dow, 2009a).

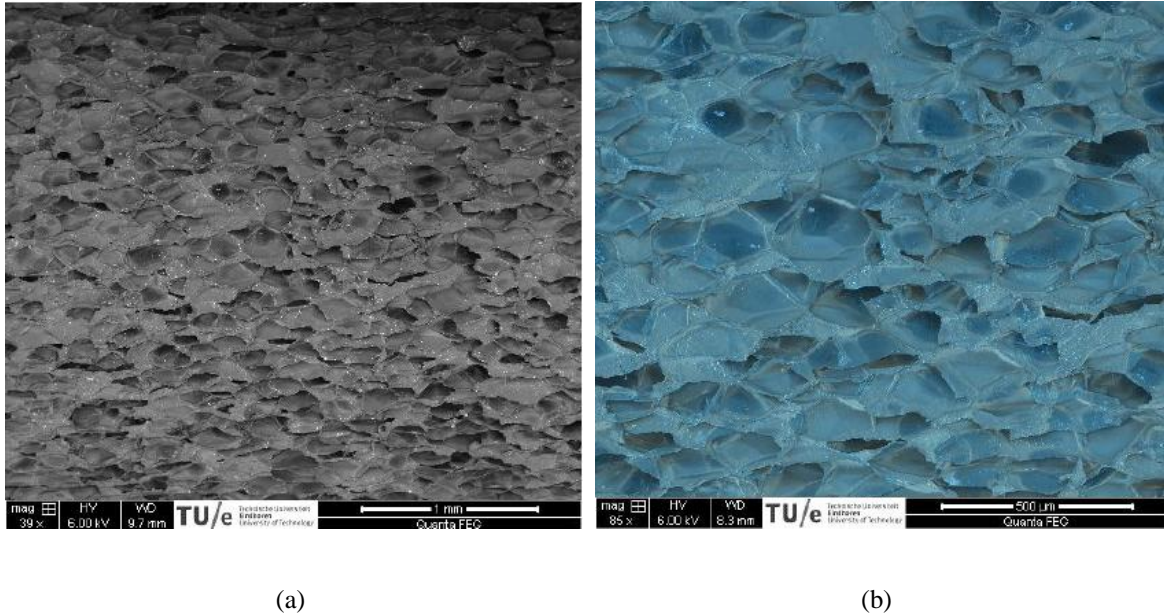


Figure 2-35: (a) Side View of Closed-cell Structure of IMPAXX (with SEM, TU/e), (b) Top view of Closed-cell Structure of IMPAXX (with SEM, TU/e) (Source: De Vries, 2009)

Table 2-7: Technical Data for Commercial Grade of IMPAXX (Source: Dow, 2006)

		TEST METHOD		
		ASTM D1621, 23°C		
IMPAXX	ρ^* (kg/m ³)	Compression Strength 10% (kPa)	Compression Strength 25% (kPa)	Compression Strength 50% (kPa)
300	35	345	375	434
500	43	512	544	612
700	45	700	718	835

Table 2-7 shows some technical data which were gathered from DOW Automotive literature. The technical data were obtained from the test conducted at room temperature, 23°C.

2.5.1 Stress-Strain Curve of IMPAXX EPS Foam

A comparison of the compressive responses for three specified commercial grades of IMPAXX foam is shown in Figure 2-36. The three lines represent the three foams with different densities. In addition, Figure 2-37 shows the comparison of IMPAXX and conventional material at the same density level of 48 kg/m³ foam under quasi-static compression.

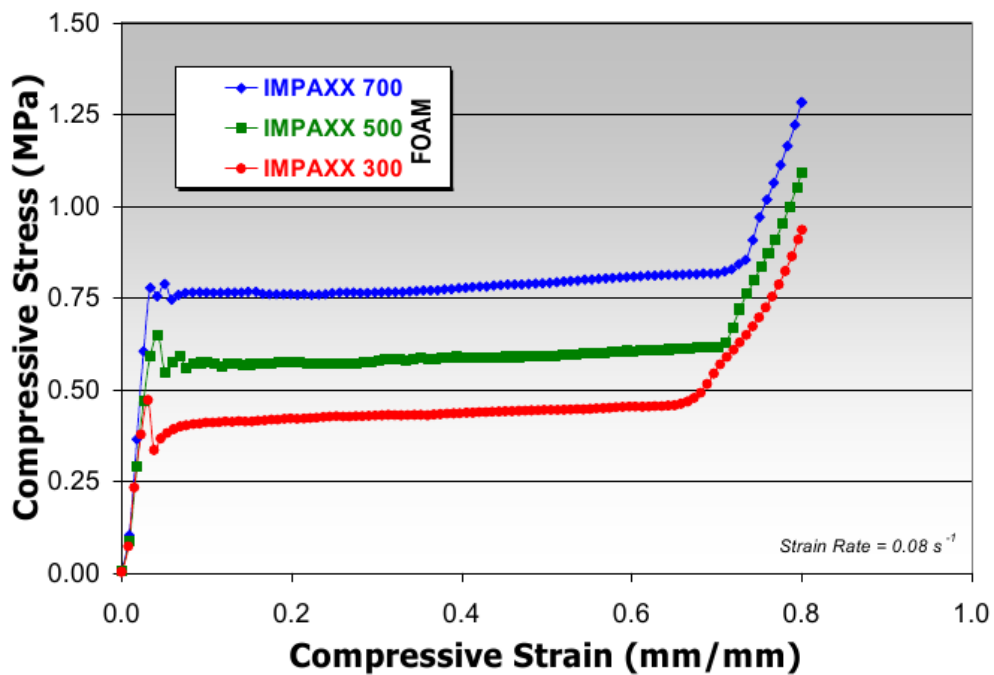


Figure 2-36: Compressive Response of IMPAXX Energy Absorbing Foam (Source: Dow, 2009a)

In this typical quasi-static stress-strain diagram, the characteristics of IMPAXX foam compared to high efficiency PU and EPP bead is depicted. The stress increases rapidly in the linear elastic region. Then it reaches the plateau and remains constant until 70% to 80% compression. After that, the densification phase begins. Based on above observation, IMPAXX could be considered as a good energy absorption material (Slik et al., 2006).

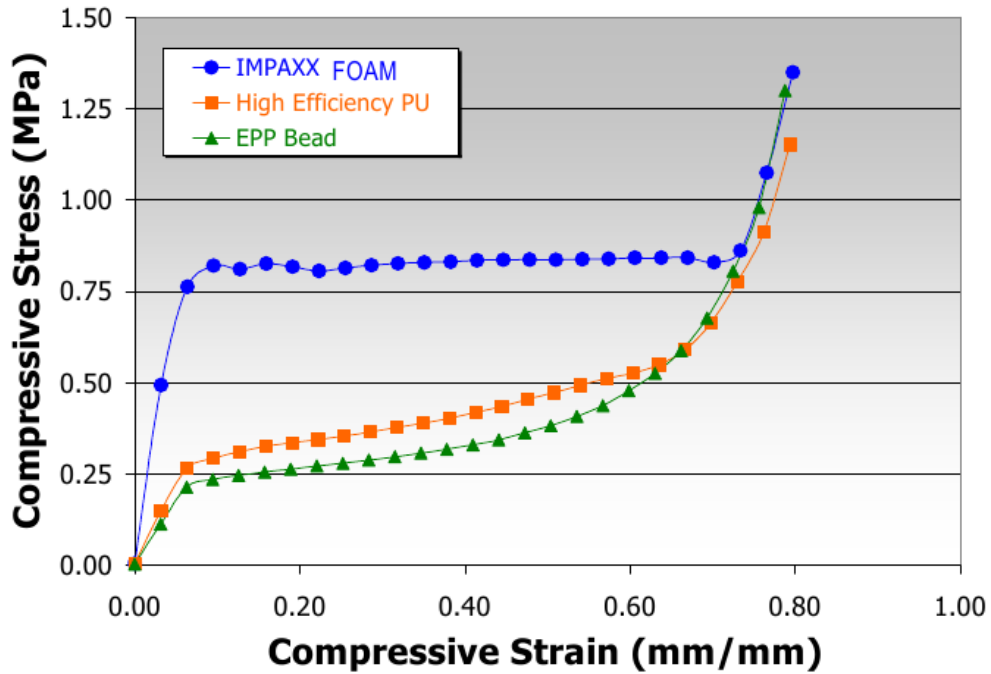


Figure 2-37: Quasi-static Compression Comparison of 48 kg/m³ Foams (Source: Dow, 2009a)

In addition, Slik et al. (2006) stated that IMPAXX foam is negligibly strain rate sensitive where low elastic recovery were observed from the compression curve (Figure 2-38) through a 65mm thickness sample. The foams were impacted at 4.5 m/s and 6.7 m/s with strain rates in the range of 70 ~ 100 1/s.

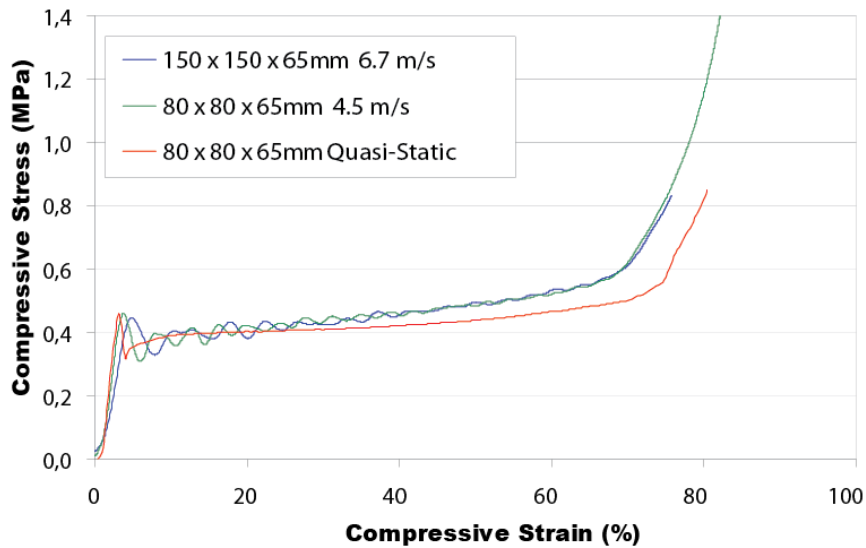


Figure 2-38: Quasi-static vs. Dynamic Response Compression Curve (Source: Slik et al., 2006)

2.6 Finite Element (FE) Modelling

In this study, there are four main models need to be constructed. Firstly, the energy absorbing polymeric foam (commercial IMPAXX foams) with different density will be modelled. Then, a simplified aircraft model will be constructed where the Equator P2 sandwich structure consisting of Carbon Fibre Reinforced Plastic (CFRP) as the skin material and Airex Foam for the core. Other than that, cushion seat will be constructed based on DAX55 which is widely used in commercial aircraft and recommended for aircraft seating certification as mentioned previously. Finally, the water model will be constructed to capture the water behaviour properly. Due to the complexity of the overall problem, this study concentrates on simplified model to balance the reliability of the results and the cost of the simulation.

2.6.1 IMPAXX Foam Modelling in LS-DYNA

2.6.1.1 Material Formulation

There are a few models for material formulation of polymeric foam in LS-DYNA. One of it is *MAT_57 which is for highly compressible, low density, elastic foams. This material model provides sufficient information for foam loading and unloading scenarios (Gover and Gudimetla, 2011; Slik et al., 2006; LSTC, 2007; Dow, 2009a). There are other options like Fu Chang Foam Damage Decay material model (MAT_83) and Modified Crushable Foam (MAT_163) (LSTC, 2007). However, both later material models will not be discussed here, since the research concentrates only on low density foam energy absorption capabilities. This low density foam is chosen because it provides good energy absorbing capabilities and low in weight. Furthermore, IMPAXX is manufactured at three

grades which differs in terms of density. This is viable for this study since this would create similarities in material composition but varies in density. As specified by the manufacturer, IMPAXX commercial grade foams could be formulated in LS-DYNA as shown in Table 2-8.

Table 2-8: LS-DYNA Material Model Input Deck Listing for IMPAXX™ 300, 500 and 700 Foam Aligned with Vertical Approach Angle (Source: Dow, 2009a; Bala, 2006)

MAT_57 * MAT_LOW_DENSITY_FOAM TITLE			
PARAMETERS	IMPAXX 300 (0-30°)	IMPAXX 500 (0-30°)	IMPAXX 700 (0-30°)
RO, kg/mm³	3.5e-8	4.3E-8	4.5E-8
E, N/mm²	0.0105	0.0105	0.0105
TC	1.0E+2	1.0E+2	1.0E+2
HU	0.101	0.101	0.101
DAMP	0.225	0.225	0.225
SHAPE	15	15	15
KCON	2.09	2.09	2.09
Units: kg,mm,ms			

2.6.1.2 Mesh/Element Quality Criteria for IMPAXX Foam.

The material models for rubber and metals were well established in Finite Element Analysis (FEA) (Mills, 2007). These isotropic formulations were also applied to polymeric foam models despite the foams showing a slight anisotropic characteristic due to its manufacturing process (Mills, 2007).

Despite having a complex microstructure on foam's cell, they are homogenous on a larger scale. Therefore, FEA treats the foam materials as a continuum. It calculates all the forces at mesh points. This mesh point is fully dependant on the mesh sizes which will normally be adjusted to get better accuracy and efficient computer processing cost (Mills, 2007).

Certain minimum and maximum limits were set as a guideline for mesh size. This could also be called working limits which would provide better accuracy and rapid solution. Normally, quality criteria elements for hexahedral brick (solid) or wedge elements should comply with this set of guidelines for better mesh quality and numerical stabilities. Table 2-9 shows the limits for elements sizing which will benefit the study in terms of simulation time and accuracy.

Table 2-9: Mesh Quality Criteria (Source: Bhonge, 2008; Mohan, 2009)

Parameters	Quadrilateral Shell Elements	Hexahedral Brick or Wedge Elements
Percentage of Elements in Model	95 %	5%
Aspect ratio	≤ 5	≤ 10
Skew Angle	$\leq 45^\circ$	≤ 60
Face warpage	$\leq 10^\circ$	$\leq 20^\circ$
Jacobian	≥ 0.7	≤ 0.6

2.6.2 Aircraft Structure–Carbon Fibre with Airex Foam Core

Airex C70-40 foam core is a unique closed cell, cross-linked polymer foam core and lightweight structural foam that has a good impact strength. It is suitable for high strength applications that require a low panel weight, a laminated carbon fibre foam core that can resist crushing forces and is able to supply an adequate mounting surface. For this study, the lay-up design used is quasi-isotropic, consists of carbon fibre on each side of an Airex foam core centre as shown in Figure 2-39. Table 2-10 and

Table 2-11 show the properties of carbon fibre and Airex foam core gathered from the manufacturer's datasheet.

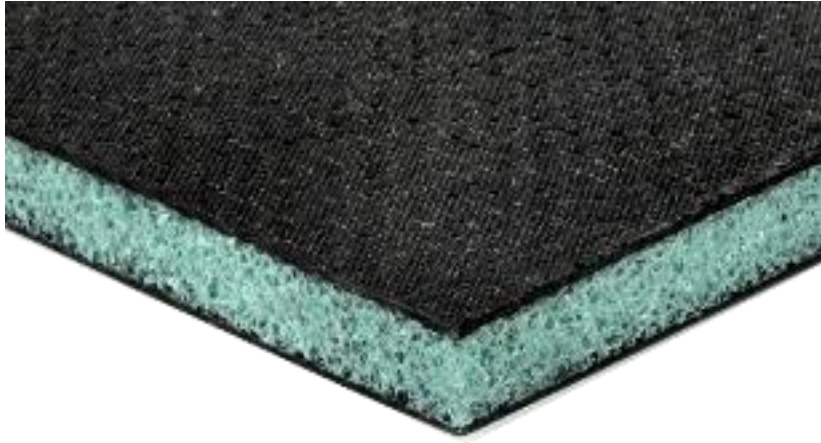


Figure 2-39: Carbon Fibre Sandwich with Airex C70 core

Table 2-10: Properties of Carbon Fibre (Source: Newcomb and Chae, 2018)

Parameters	Values
Tensile strength, GPa	3 – 7
Tensile modulus, GPa	200 – 935
Compressive strength, GPa	1 – 3
Compressive modulus, GPa	100 – 300
Density, g/cm ³	1.75 – 2.20

Table 2-11: Properties of Airex C70 Foam Core (Source: Airex, 2011)

Parameters	Values
Density, g/m ³	0.04
Compressive strength, MPa	0.45
Compressive modulus, MPa	37
Tensile strength, MPa	0.7
Tensile modulus, MPa	28
Shear strength, MPa	0.45
Shear modulus, MPa	13
Shear elongation at break, %	8

2.6.3 Water Modelling in LS-DYNA

The water medium's behaviours can be illustrated using two laws. They are isotropic elastic hydrodynamic law and Murnaghan equation of state. Based on the results from Toso (2009) it was suggested that the hydrodynamic isotropic elastic was more suitable to illustrate water behaviour due to the parameters that remain the same for all impact velocities in contrast to the Murnaghan material model that requires calibration. Therefore, this study will use isotropic elastic hydrodynamic law to model the water behaviour. The isotropic elastic hydrodynamic law was originally developed to be applied on ballistic impact in metals, where the materials behave like fluids above a certain impact energy level. It describes an isotropic elastic plastic material at low pressures with an equation of state (EOS) describing the 'hydrodynamic' pressure-volume behaviour at high pressures.

Modelling of water is sufficient with 8-node solids of pure FE mesh. This does not present any problem as the interest is in the first few milliseconds of the impact on water. This is true as long as the mesh elements is not too deformed. Reference test parameters based on experiment conducted by Troesch and Kang (1986) on a sphere impacting on water are shown in Table 2-12.

Table 2-12: Experimental Parameters for Ball Impacting Water (Source: Troesch and Kang, 1986)

Cases	Sphere diameter (m)	Weight (kg)	Velocity at impact (m/s)
Case 1	0.502	33.12	3.46
Case 2	0.502	33.12	4.89
Case 3	0.502	33.12	5.99

Firstly, the steel sphere was considered to remain undeformed during the drop. Therefore, it was modelled using shell element and define as *MAT_RIGID. Water surface has no waves (smooth) before the contact. Toso (2009) also suggested that, the water pool

was to be modelled using 8-node solid element. The boundary condition (symmetry, fixed and etc.) were applied to all side of the pool except on its top, to define normal displacement during a few milliseconds of the impact. Table 2-13 shows the summary of Toso (2009) work as the main literature for water modelling used in this study.

Table 2-13: Investigations Involving A Classical FE (Source: Toso, 2009)

Effects	Size Used	Description
Mesh size	(0.01 x 0.01 x 0.02) m (0.005 x 0.0005 x 0.01) m (0.003 x 0.0003 x 0.006) m	The coarser mesh shows high oscillations and leads to an over-estimation of the acceleration peak of 26%. The finer meshes are able to deliver acceleration time histories in better agreement with the measured data, whereas the middle-size mesh already delivers very acceptable results, where the acceleration peak is overestimated by only 9%. Finally, whatever the mesh size used, the acceleration plateau following the peak is overestimated. As a compromise with the computation time, it is decided to adopt the middle-size mesh (0.005 x 0.005 x 0.01) m for the following investigations.
Pool size	(0.34 x 0.34 x 0.25) m (0.44 x 0.44 x 0.25) m (0.56 x 0.56x 0.25) m	Independently of the pool size, the calculated peak remains unchanged. Nevertheless, the level of the acceleration plateau following the curve peak shows a dependency. For the smaller pool size (0.34 x 0.34 x 0.25) m, the plateau level amounts to approximately 30 g's compared to 20 g's for both higher pool sizes. This means that for the test case studied, a pool having a width and a length corresponding to two times the diameter of the sphere should be sufficient to minimise the boundary effects. It is proven, that the bigger the pool size is, the better it is to delay the reflection of compression waves able to parasitise the calculated curves. The oscillations in the calculated time histories remain nevertheless very acceptable compared to the general shape of the acceleration curve.
Symmetry conditions.	(0.44 x 0.44 x 0.25) m	The studies have been conducted using 0.44 m x 0.44 m x 0.25 m pool, shows that the calculation with a half and then a quarter model does not change the quality of the simulation results. Consequently, when the impactor presents a symmetry, this later will be used in order to reduce the computation time.

2.6.4 Seat: DAX55 and Confor Green Modelling in LS-DYNA

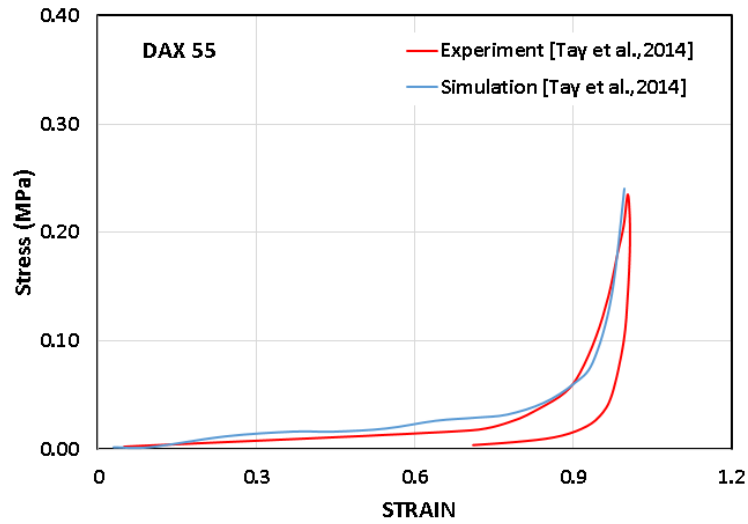
During landing, seat acts as a damper or spring to protect the occupant by reducing the acceleration (g) value. Therefore, proper selection of foam should be made for aircraft seating, to suits its major role in absorbing energy and reducing load transferred to the occupant.

As mentioned by Adams and Lankarani, 2003, improper selection of seat cushions could amplify the lumbar-column pelvic load of the seated occupant during a vertical impact conditions. Interest on recent studies used DAX foams as aircraft seat cushions to obtain high velocity and quasi-static loading rate (Adams and Lankarani, 2003; Beheshti and Lankarani, 2006; Bhonge et al., 2010).

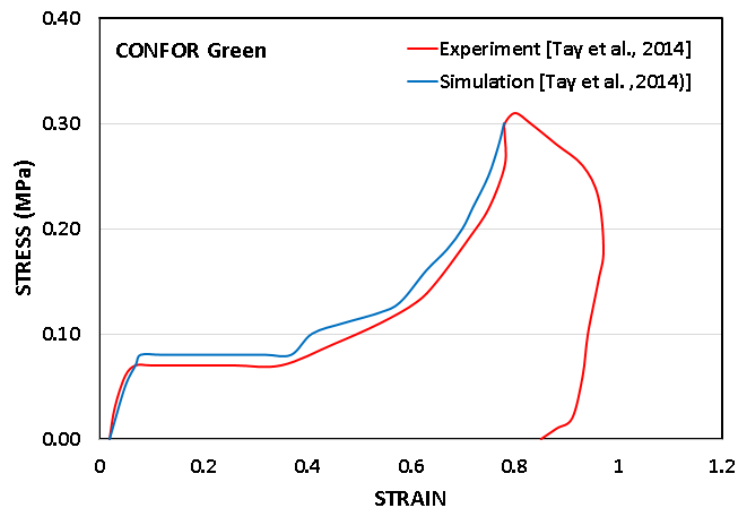
In their investigation, the seat cushions were modelled using 3D 8-node solid brick elements and in LS-DYNA, material model *MAT57_LOW DENSITY FOAM was used to model compressible foam for both materials. The model uses tabulated input data for the load curve – Nominal stress vs. strain. The stress-strain curve of these study as shown in Figure 2-40. These models can be utilised in the initial design of the aircraft seat, and thus reducing the cost and time of a full-scale sled test programme. In another study, Adams and Lankarani (2003) observed that DAX foam shows better stress behaviour compared to Confor foam. Beheshti and Lankarani (2006) also investigated on DAX foam and Confor foam for aircraft seat cushion. Table 2-14 illustrated mechanical properties and LS-DYNA materials cards of foam in aircraft seat cushion.

Table 2-14: Mechanical Properties and LS-DYNA Materials Cards (Source: Tay et al., 2014)

Cellular materials	ρ (kg/m ³)	E (MPa)	\dot{E} (MPa)	ν	LS-DYNA material card	Reference
DAX 55	35.0	0.05	25	0.31	MAT 57	Tay et al. (2014)
CONFOR Green	96.1	1.5	1200	0.33	MAT 57	Tay et al. (2014)



(a)



(b)

Figure 2-40: Experimental and Simulation Stress-Strain Curve; (a) DAX 55, (b) CONFOR Green (Source: Tay et al., 2014)

Table 2-15: Additional Parameters for DAX55 for LS-DYNA MAT_57 Material's Card (Source: Tay et al., 2014)

MAT 57 parameters	Value
Tension cut-off stress, τ_t	1.00E20 MPa
Hysteric unloading factor	0.101
Decay constant, β	0.0 s ⁻¹
Viscous damping coefficient	0.50
Shape factor	25.0
Young's relaxation modulus, E_d	0.0 MPa

In addition, aircraft seating cushion is part of the subsystem for the primary structure which act as an absorber from water impact to occupant on board. Other than ergonomically

comfortable, an aircraft seat should provide safety for passenger because of the interaction between occupant's body and the cushion. All seat cushion must pass FAA (2015) (Table 2-6) test condition prior to installation. These regulations require a dynamic sled test of the entire seat system in order to certify it. Perry et al. (2002) investigated the dynamic loads and the modified seat acceleration transmitted to a 50th percentile Anthropomorphic Test Device (ATD) from the seat cushion. It was reported that seat cushion is capable of transmitting and even amplify the load to the aircraft occupant if it was not designed properly. Hearon and Brinkley (1986) discovered that rate dependent foam cushion transfers less energy than operational cushion, consequently decreasing the possibility of spinal injury during impact.

2.7 Summary of Literature Survey

In summary, many interesting results regarding polymeric foam in impact energy absorption were found through the literature review. It is generally agreed that polymeric foam do have good energy absorption capabilities. Most of the polymeric foams show three distinct loading phases, that consist of initial elasticated phase, densification plateau and solidification phase when it fails. Factors affecting its energy absorption capacity are the density and the base polymer. However, there is no systematic experimental and numerical study about the effect of sequence and shape of IMPAXX EPS foam structures on impact energy absorption, which can be very valuable for the design of enhanced impact energy absorber for aircraft like Equator P2 aircraft. This is the research gap needed to be explored in details. Table 2-15, shows the summary of polymeric foam used in existing studies compared to the one used in this study.

Table 2-16: Summary of Literature Review

Authors	Foam Types	Density of foam	Skin/Shells	Sequent/Layer	Velocity	Simulation	Objective
Aktay et al. (2008)	Extruded closed cell polystyrene foam (EPS)	21.7 and 27.8 kg/m ³	Aluminium tube (Al)	Al/EPS/Al	2 mm/ms ⁻¹	ANSYS™	Crushing behaviour
Atas and Sevim (2010)	PVC foam core and Balsa wood core (BWC)	62 kg/m ³ and 157 kg/m ³	E-glass +45/-45	±45/core/±45	-	-	Impact response
Di Landro et al. (2002)	Expanded polystyrene (EPS) of different densities	28, 40, 55 and 70 g/l	Polycarbonate (PC)	PC/EPS	-	-	Energy absorption capability
Gover and Gudimetla (2011)	Foamular 250	35 kg/m ³	-	-	8.05 mm/min	LS-DYNA	Behaviour of EPS
Ozturk and Anlas (2009)	Expanded polystyrene (EPS) and Polyethylene	30 kg/m ³ and 58 kg/m ³	-	-	1000 mm/min	-	Phenomenological constitutive model
Halldin et al. (2001)	Expanded polystyrene (EPS)	40 kg/m ³	ABS thermoplastic	ABS/EPS	7.67 m/s	-	Oblique impact test on helmets
Tay et al. (2014)	IMPAXX, polyurethane foam, micro-agglomerated cork, DAX and CONFOR	33.6, 25.6, 293.0, 35.0, and 96.1 kg/m ³	-	-	14.98 m/s	LS-DYNA	Crashworthiness
Bhonge et al. (2010)	DAX 26 and 55	-	-	-	30 in/sec	LS-DYNA	Performance of the DAX foam
Caliskan and Apalak (2017; 2009)	Expanded polystyrene (EPS)	50, 100 and 180 kg/m ³	Aluminium plates (Al 6061-T6)	Al/EPS/Al	-	ABAQUS/Explicit (version 6.14)	Low velocity impact response of sandwich panels
Leijten et al. (2009)	Rohacell closed cell polymethacrylimide (PMI) foam (RF)	75 and 110 kg/m ³	Carbon non-crimp fabric (CF)	CF/RF/CF	-	-	Impact behaviour
Potes et al. (2016)	CORECORK® NL10 and NL20 cork agglomerates	120 and 200 kg/m ³	Aluminium plates	NL/Al	-	ABAQUS (version 6.14)	Impact response
Mahéo and Viot (2013)	Expanded polypropylene (EPP)	-	-	Multi-layered	-	LS-DYNA	Energy absorption capacities
Li et al. (2018b)	Closed-cell aluminium foam	0.45 g/cm ³	Aluminium alloy tubes (circular and square)	-	-	-	Crashworthy structures
This study	IMPAXX (IPX)	300, 500 and 700 kg/m ³	Carbon fibre (CF)	IPX/ IPX/ IPX	2, 3, 4 m/s	LS-DYNA	Impact response

Chapter 3: Research Strategy

3.1 Introduction

This chapter is about the strategy of the research adopted in this project to achieve the project aim and objectives. It explains in detail regarding methods used to perform tasks in this research work. In conducting any research, it is very important to decide the steps that will be taken in order to ensure the research is carried out smoothly and systematically. This includes the methodology flow, which explains in detail about the project and the troubleshooting steps to obtain the expected result.

In this section, an overview of all the research activities of the project is presented in accordance with the project aim and objectives defined in Chapter 1. The research work is divided into six phases with each phase dedicated to certain technical tasks associated with the project objective. This is important in defining the research tasks in order to complete this research. This flowchart shown in Figure 3-1 also provides aid if problems occur during this research carried out.

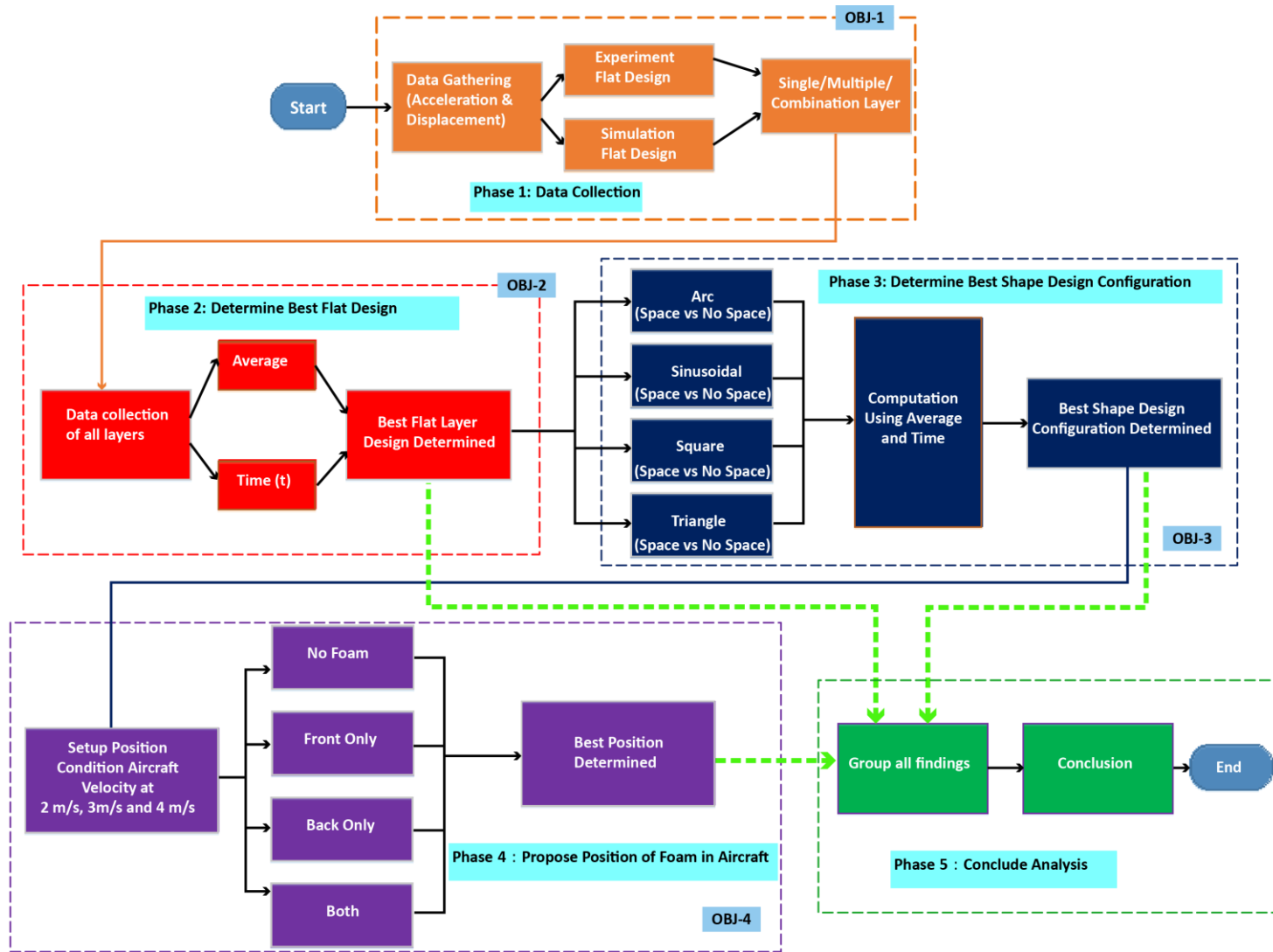


Figure 3-1: Flowchart of the Research Activities

The materials used in this study were carbon fibre reinforced plastics for the skin of the sandwich structure, foam for the core of the sandwich structure, foam for seating cushion and the water acting as the impact base. In this study, the experiment and simulation were conducted on the 3 types of foam material used (A, B, and C) where the impact velocity applied are 2 m/s, 3 m/s, and 4 m/s with shape/flat and no-space design of materials respectively (Table 3-1). Flat layer design consists of single, multiply and combination block of EPS foam. The difference between all flat designs is the arrangement of different density foams. Single block is main the individual block of the foam. While, multiple layer is the three-layered foam arranged with three same density material. Whereas combination layer foam is the arrangement of different density material to form a stack of three layer EPS foam. As for the combination or hybrid layer, specific shape was introduced in between the layers. Details of design configuration is described clearly in layer and shape configuration in section 4.2

Table 3-1: Materials, Impact Velocity and Layer Design as the Parameter and Variable for the Study

Composition	Velocity (m/s)	Layer Design
A	2	Flat / No-Space
B	3	Flat / No-Space
C	4	Flat / No-Space
Multiply		Flat / No-Space
Hybrid		Shape & No-Space

The experiment and simulation were carried out to assess IMPAXX foam material performance using parameters of acceleration and displacement. Configurations of flat or no-space, vs. shape materials design of each types materials are used to find the best type of material and the design (composition vs. shape/no-space).

In this study, IMPAXX 300, 500 and 700 were used as the energy absorbing

materials. IMATEK IM10R-15 Drop Weight Impact Tester was used in Universiti Malaysia Perlis (UNIMAP) mechanical testing lab. The foam was tested using dynamic compression test. Many efforts were made to study the impact characteristics of these foams since this will be one of the focus area for this study.

In addition to that, the Carbon Fibre Reinforced Polymer (CFRP) were also tested through dynamic indentation test using the same machine which is capable to test up to 10 m/s impact velocity. The material properties of CFRP were also gathered from Guida and Marulo (2014) . This is to make sure the behaviour of the experiment and simulation is accurate. DAXX 55 foam were used for the seating and its material properties were gathered from literature (Bhonge, 2008).

Toso (2009) did an extensive study of water modelling and simulation of aircraft structures impacting on water. This published work has been used as the reference for water parameters in LS Dyna simulation.

3.2 Phase One: Data Collection and Analysis

In order to find the best material and design, this phase needs to collect and analyse data based on experiments and simulations conducted for each type of materials and their combinations. The data collected were acceleration and displacement values for single, multiple and hybrid design under different impact velocities. Therefore, this research also needs to assess the effect of impact velocity on the acceleration and displacement, and to describe the dynamic characteristics of each material as a single layer as well as multiply layer and hybrid design (Figure 3-2).

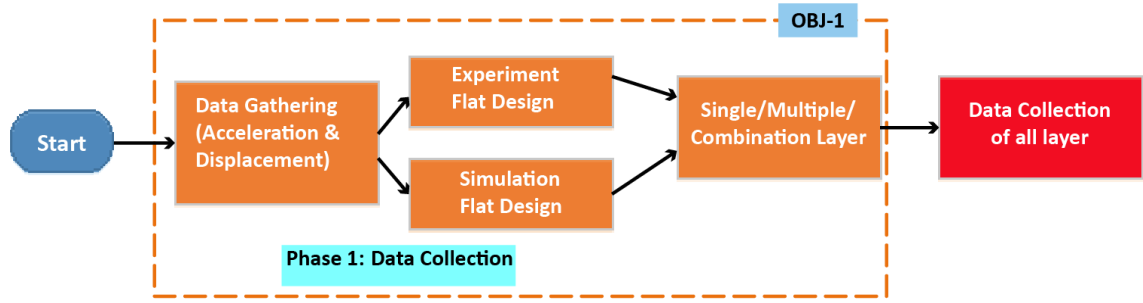


Figure 3-2: Phase One: Data Collection and Analysis

3.3 Phase Two: Determine Best Flat Design

Figure 3-3 shows methodology to determine the best flat design. Data collected from Phase one were carried forward to Phase two. The data were acceleration and displacement values for single, multiple and hybrid design under impact. In this phase, statistical approach was used by using average value and time (t). Best flat layer selection obtained will be one out of three material configurations. Material selected will be either Single Layer (A), Multiple Layer (AAA) or one out of six Combination Layer (ABC / CAB / BCA / CBA / BAC / ACB). This material will be tested under impact velocity of 2 m/s, 3 m/s and 4 m/s. The best flat layer selection will be recorded and carry forward to Phase five in conclusion section.

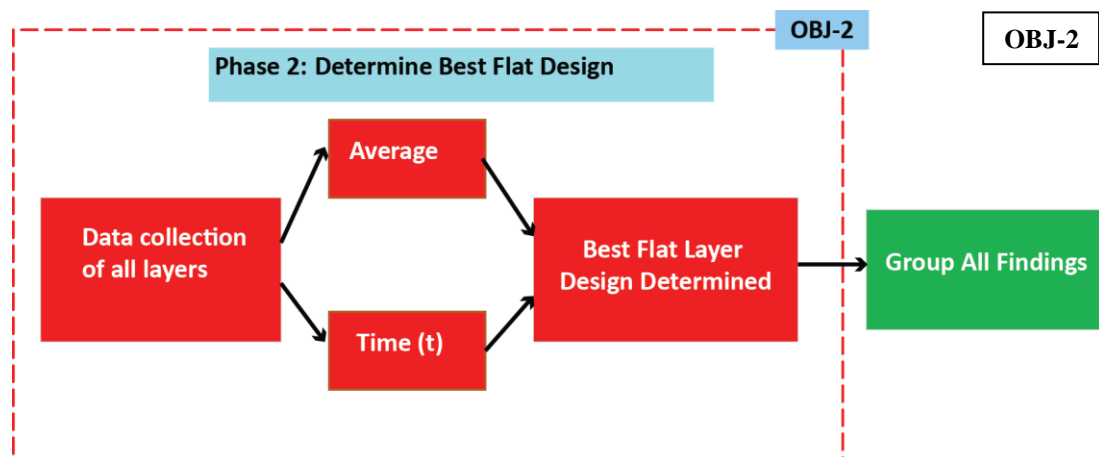


Figure 3-3: Phase Two: Best Flat Design Determination

In this study, to find the average value for acceleration and displacement were calculated based on Equation 3-1 below.

$$Average = \bar{A} = \frac{\sum_{i=1}^n x_i}{n} \quad (3-1)$$

where $i = n = 1, 2, 3, \dots, n$.

For example, Table 3-2 shows average values of displacement and acceleration for 2 m/s. Acceleration values for all material configuration were obtained, hence computation based on Equation 3-1 to obtain average value. Average acceleration value obtained from Table 3-2 was 44.60 g. Therefore, from the average value obtained, this value was plotted on every material configuration as boundary line.

This applied the same on method plotting the displacement line. Displacement values for all material configuration were obtained hence computation based on Equation 3-1 to obtain average value. Average displacement value obtained from Table 3-2 was 9.60 mm. Therefore, from the average value obtained, this value was plotted on every material configuration as boundary line.

Table 3-2: The Average Values of Displacement and Acceleration for 2 m/s

EXPERIMENT : ACCELERATION and DISPLACEMENT 2000													
MATERIAL	SINGLE LAYER			MULTIPLE LAYER			COMBINATION LAYER					AVE	
DESIGN	2001-E	2002-E	2003-E	2004-E	2005-E	2006-E	2007-E	2008-E	2009-E	2010-E	2011-E		2012-E
ACCELERATION -AVERAGE	33.37	58.03	77.49	31.49	61.81	71.81	32.96	33.29	33.06	32.53	34.52	34.87	44.60
Acceleration Average Line	44.60	44.60	44.60	44.60	44.60	44.60	44.60	44.60	44.60	44.60	44.60	44.60	
DISPLACEMENT -AVERAGE	9.27	7.69	7.16	11.07	9.73	7.94	11.66	10.78	10.71	9.13	9.79	10.35	9.60
Displacement Average Line	9.60	9.60	9.60	9.60	9.60	9.60	9.60	9.60	9.60	9.60	9.60	9.60	

Furthermore, the method to carry out the analysis using time (t) average is by using Equation 3-2. From this equation, displacement and acceleration obtained were

substituted. This calculation was used to obtain time for every single scenario. Set of time were added to obtain average time using Equation 3-2 as follows:

$$S = V_0 + \frac{1}{2} at^2 \quad (3-2)$$

where S = distance

V_0 = Initial velocity

a = acceleration

t = time

Equation 3-3 was derived from Equation 3-2 in order to obtain new value of displacement and acceleration. From this equation, two sets of calculation were carried out. First, the displacement and time play as fixed variable to obtain new acceleration. Secondly, the acceleration and time were used as fixed variable to obtain new displacement. These new set of acceleration and displacement were used to determine best material configuration.

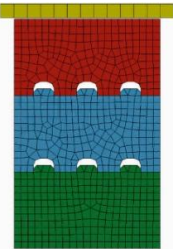
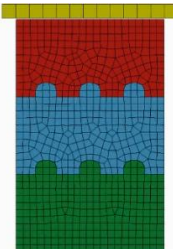
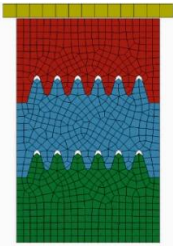
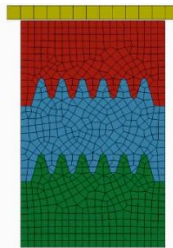
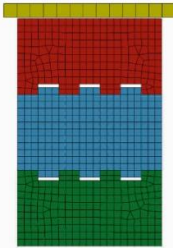
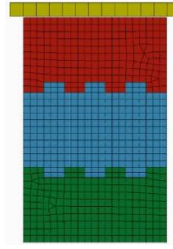
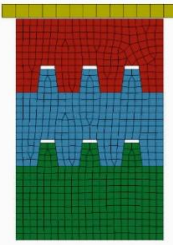
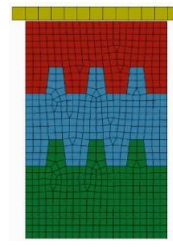
$$t = \sqrt{\frac{2S}{a}} \quad (3-3)$$

After obtaining new set of displacement and acceleration values, average was determined. This average line of displacement and acceleration were used as boundary limit to determine best material configuration. Any values fall below the both average line were selected as best foam design configuration.

3.4 Phase Three: Determine Best Shape Design

This phase is to determine best shape design configuration. There were four shapes under two different configurations. The four shapes are arc (ARC), sinusoidal (SIN), square (SQ) and trapezium (TR). The two configurations are space and no-space in between foam layers. Table 3-3 shows illustration of each shape and configuration, respectively.

Table 3-3: Shape Design Configuration

Shape	SPACE	NO-SPACE
Arc (ARC)		
Sinusoidal (SIN)		
Square (SQ)		
Trapezium (TR)		

Throughout this analysis, the data used were acceleration and displacement values with respect to each shape. The calculation here is same as phase three where average value and time (t) were carried out. Finding obtained from this phase was the best shape with either space or no-space configuration. Phase four answers will be recorded and carried forward to phase five to conclude overall findings. Figure 3-4 illustrates the activities for this phase.

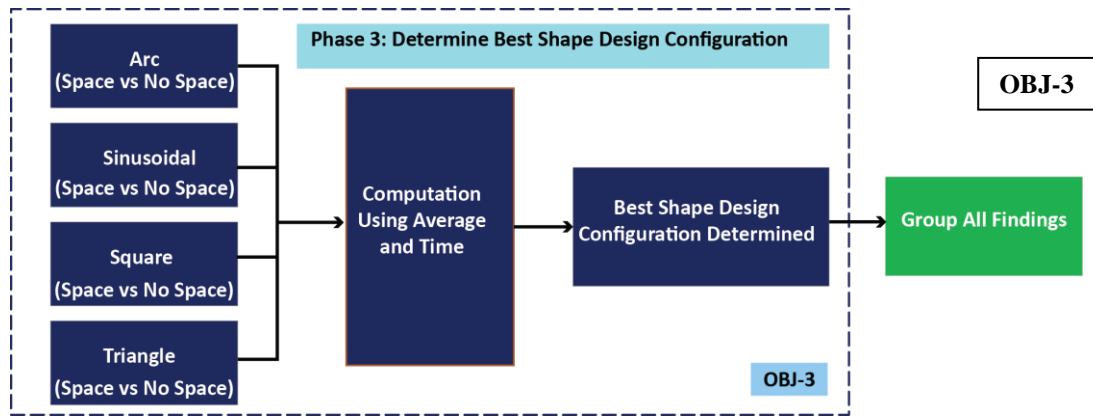


Figure 3-4: Phase Three : Best Shape Determination

The method to find the best shape configuration, for example, the acceleration towards material design with space using average is stated in Equation 3-4. The same approach for no-space used for acceleration, where the average for no-space is computed using Equation 3-5. Based on both equations, to obtain the average values based on average values of space and no-space is as Equation 3-6 as below:

$$Average_{space} = \bar{A}_S = \frac{\sum x_{iS}}{n_S} \quad (3-4)$$

$$Average_{No-Space} = \bar{A}_{NS} = \frac{\sum x_{iNS}}{n_{NS}} \quad (3-5)$$

$$Average = \bar{A} = \bar{A}_S \cup \bar{A}_{NS} \quad (3-6)$$

Since the x_{iS} signifies acceleration or displacement values, these values divided

by total number of data to obtain average of acceleration or average of displacement with space configuration ($\overline{A_S}$). While, data for acceleration and displacement with no-space configuration is x_{iNS} . The computation is similar with space configuration where all data from no-space configuration were added and divided by total number of data to obtain average acceleration or average displacement with no-space configuration ($\overline{A_{NS}}$). The first rule is to determine that the space result is smaller than average values of space. Same applies for data of no-space that should be smaller than average of no-space. Rule 1 (space) must intersect with Rule 2 (no-space) signifies as $x_{iS} < A_S \cap x_{iNS} < A_{NS}$. Thus, best design (BD) in Equation 3-7 configurations where data from space and no-space configuration should fall below average line. The data, $i = X007, X009, X010, \text{ and } X012$. The impact velocity remains the same, which were 2 m/s, 3 m/s, and 4 m/s.

$$BD_v = [x_{iSa} \cap x_{iNSa}] \cap [x_{iSD} \cap x_{iNSD}] \quad (3-7)$$

3.5 Phase Four: Determine Best Position

Figure 3-5 shows the positions where the foam could possibly be installed. The foams can be installed at the FRONT, BACK and BOTH positions. The positions were selected because of the first contact area and the only available space in the aircraft. Next, the data were taken from the dummy's pelvic acceleration (A1) and near the aircraft step (A2). Point A1 is mainly to evaluate the occupant's lower torso acceleration, which is critical for occupant safety during landing. Meanwhile, point A2 is to evaluate the acceleration (g) value of the structure during impact.

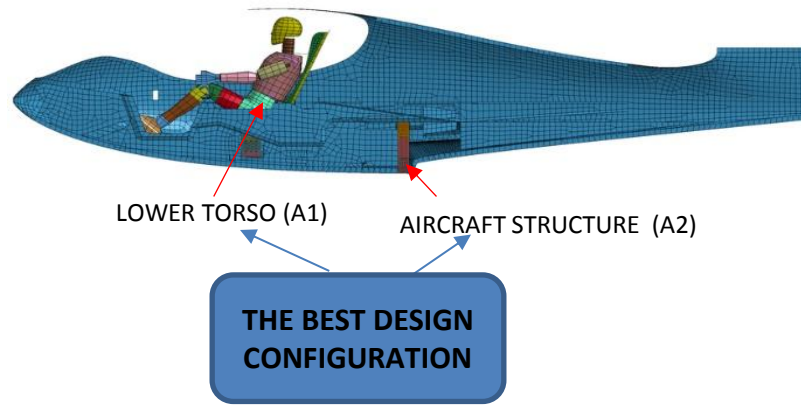


Figure 3-5: The Best Design Configuration Position for Foam Location

Phase four was to propose the best position of foam in aircraft. There were four options of position displayed in this analysis. The positions were, no foam in aircraft, only front position, only back position or both position installed with foam. This analysis was almost similar with phase two and three. The trend was identified by analysing the results at aircraft sink velocity of 2 m/s, 3 m/s and 4 m/s. Position with highest frequency was selected as the best position for the aircraft. The outcome of this phase was recorded and carried forward to phase five for conclusion of all findings. Figure 3-6 illustrates research activities in phase four.

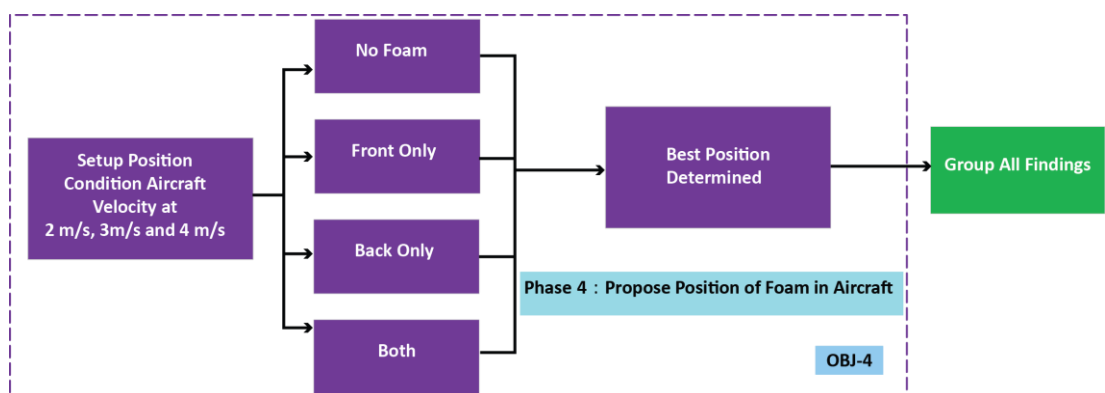


Figure 3-6: Phase Four: Foam Position in Equator P2 Aircraft

3.6 Phase Five: Conclusions

Final phase of this research project is to summarise key findings from the project. Figure 3-7 illustrates the process to draw a conclusion which reflect to respective objectives. The key findings include best flat design, applied to shape with space or no-space configuration and best position where the foam should be installed.

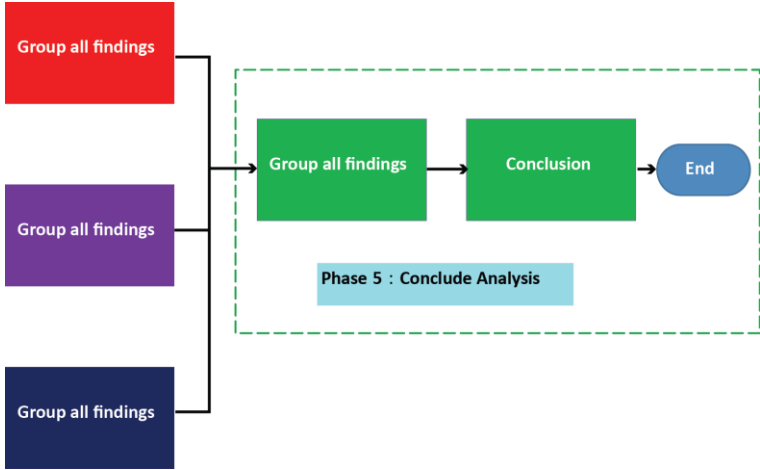


Figure 3-7: Phase Five: Conclusion

3.7 Summary of Research Strategy

To conclude, this chapter presents the overall research strategy of the project. The research has been divided into five phases. Technical focuses for each individual phase have been defined. The research work has been structured in corresponding to the project aim and objectives to ensure the successful completion of the project.

Chapter 4: Setup for Experimental and Numerical Study

4.1 Introduction

This chapter split into two parts: experimental setup and numerical setup. Topics under experimental setup are drop tower test machine, composite sandwich structure and IMPAXX 300, 500 and 700. Numerical setup includes details for IMPAXX foam, layer configuration, shape configuration, water, seating foam, finite element dummy model and seatbelt, and composite sandwich finite element model.

4.2 Experimental Setup

Experimental setup needs to be planned and defined properly in order to fulfil the aim and objectives of this study. Setup details for experimental study include the drop tower machine, composite sandwich coupon sample and IMPAXX foam.

4.2.1 Drop Tower Test- Machine

In this study, drop weight test will be conducted using IMATEK IM10R-20 (Figure 4-1). Drop weight test is usually conducted through a free-fall weighted striker, which is raised to a certain height. This weighted striker were then released, imparting load

to the test specimen (Brown, 2007). The desired impact velocity for this test is 2 m/s, 3 m/s and 4 m/s. The minimum velocity of 2m/s was determined based on FAA regulations specifying the maximum approach speed for the P2 aircraft. The other two velocities are to study the structural behaviour when higher impact velocity is encountered.

Two types of impactor were used. They are the compression impactor and indentation striker. The compression impactor is a 200 mm diameter with 14.253 kg mass (Figure 4-2). The specimen was clamped using coupon testing fixture as shown in Figure 4-3 for indentation testing. The indentation striker for CFRP indentation is a semi sphere striker with a diameter of 20 mm and mass of 13.661 kg (Figure 4-4). This machine incorporates a Kistler 30kN force transducer as the sensor, which is fitted at the weighted striker.



Figure 4-1: IMATEK IM-10R Drop Weight Impact Tester in UNIMAP



Figure 4-2: Compression impactor



Figure 4-3: Specimen Clamp Positioned in the Machine for Indentation Testing



Figure 4-4: Semi Sphere 20mm Diameter Indenter

4.2.2 Composite Sandwich Structure

The aircraft hull was constructed using a composite sandwich structure. It consists of composite fibre reinforced polymer (CFRP) face sheet on top surface, structural PVC Foam as the core and another CFRP face sheet at the bottom.

The face sheet (top and bottom) were constructed using 2 mm thick CFRP Prepreg single ply 180 g Bi Directional 45-degree woven fibre. The core is the Airex C70.40 PVC closed cell foam with 10 mm thickness. Equator AS, Norway supplied the materials for the purpose of this study. For the dynamic impact testing, the sandwich structure was cut into coupon sized 100 mm x 100 mm. Figure 4-5 shows the sandwich composite panel used in this test. Coupon testing was part of the certification process as stated by FAA (2009).

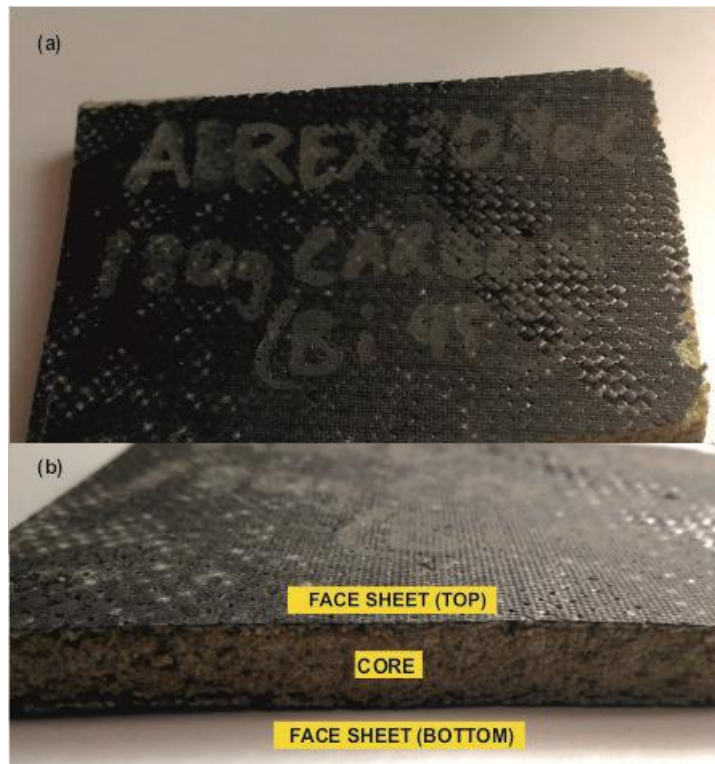


Figure 4-5: (a) Sandwich Composite Panel, (b) Detail Sandwich Structure

4.2.3 IMPAXX 300, 500 and 700

ASTM 1596-97 (ASTM, 2003) suggested 101.6 mm x 101.6 mm as a minimum value. The foams were cut into blocks, while the width and length were then rounded up to 105 mm x 105 mm x 55 mm size. Figure 4-6 shows IMPAXX foam used for testing purpose. Each layer were glued together using PVA glue to maintain the position during the first impact scenario.



Figure 4-6: IMPAXX Foam Used for the Testing

4.3 Numerical Setup

4.3.1 IMPAXX EPS Foam

Data collected through literature were used for material deck in LS Dyna. Work by Slik et al., (2006); Slik and Vogel, (2007); Dow, (2009a); Tay et al. (2014) and Segade et al., (2016) is referred to accordingly. Figure 4-7 to Figure 4-10 were the material input as suggested by the referred authors and the manufacturer in LS Dyna input format.

Material model MAT57 (*MAT_LOW_DENSITY_FOAM) were used to represent the IMPAXX foam performance. This material is suitable for modelling highly compressible low density and non-linear foams (Dow, 2009a; Croop and Lobo, 2009). As suggested by Dow (2009a), this material model is able to demonstrate the behaviour of IMPAXX foam.

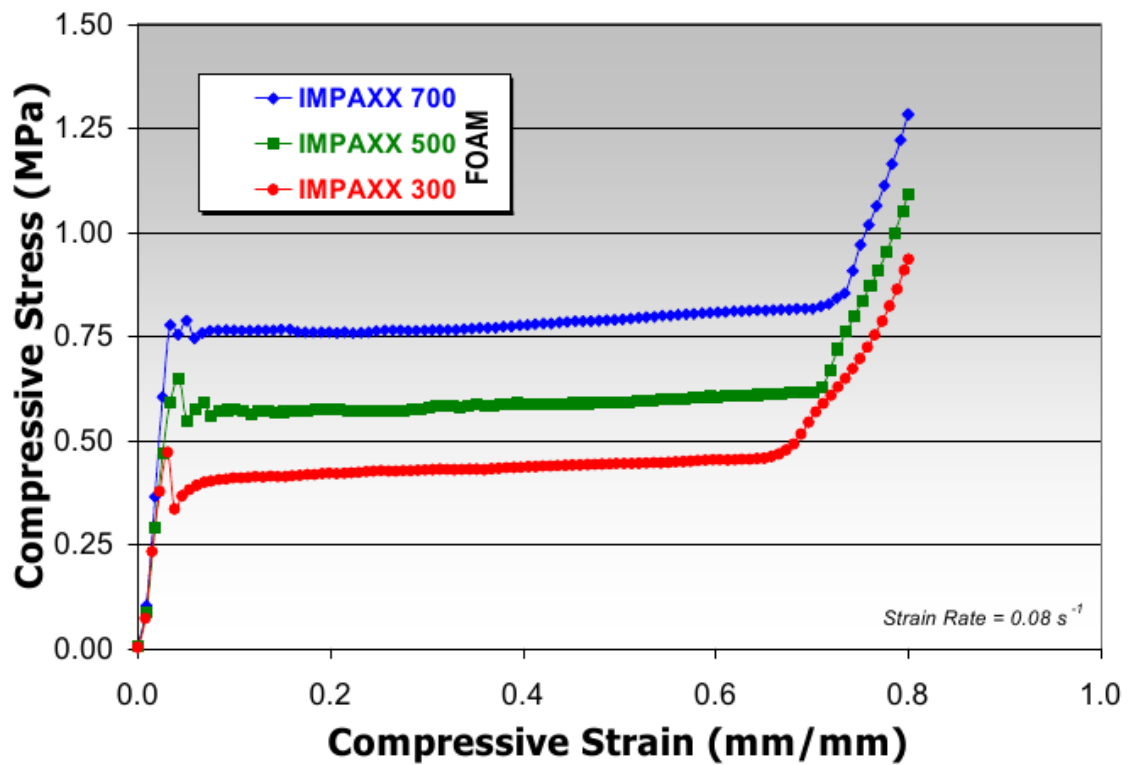


Figure 4-7: Compressive Response of IMPAXX Energy Absorbing Foam (Source: Dow, 2009a)

```

Units: Kg, mm,ms)
*MAT_LOW_DENSITY_FOAM_TITLE
IMPAXX 300 (0-30°)
  MID      RO      E      LCID    TC      HU      BETA    DAMP
  300     3.50E-08  0.0105  300    1.00E+02  0.101    0      0.225
  SHAPE    FAIL    BVFLAG  ED     BETA1   KCON    REF
           15      0      0      0      0      2.099    0

```

Figure 4-8: LS-DYNA Material Model Input Deck Listing for IMPAXX™ 300 (Source: Dow, 2009a)

```

Units: Kg, mm,ms)
*MAT_LOW_DENSITY_FOAM_TITLE
IMPAXX 500 (0-30°)
  MID      RO      E      LCID    TC      HU      BETA    DAMP
  500     4.30E-08  0.0105  500    1.00E+02  0.101    0      0.225
  SHAPE    FAIL    BVFLAG  ED     BETA1   KCON    REF
           15      0      0      0      0      2.099    0

```

Figure 4-9: LS-DYNA Material Model Input Deck Listing for IMPAXX™ 500 (Source: Dow, 2009a)

```

Units: Kg, mm,ms)
*MAT_LOW_DENSITY_FOAM_TITLE
IMPAXX 700 (0-30°)
  MID      RO      E      LCID    TC      HU      BETA    DAMP
  700     4.50E-08  0.0105  700    1.00E+02  0.101    0      0.225
  SHAPE    FAIL    BVFLAG  ED     BETA1   KCON    REF
           15      0      0      0      0      2.099    0

```

Figure 4-10: LS-DYNA Material Model Input Deck Listing for IMPAXX™ 700 (Source: Dow, 2009a)

Simulations were conducted for every individual foam of IMPAXX 300, 500 and 700. The simulation setup is shown in Figure 4-11 where the impactor is a rigid material with a mass of 14.25 kg and impacted at the velocity of 2 m/s, 3 m/s and 4 m/s. The foam size is exactly the same with the one used in experiment setup. Fixed boundary condition was introduced to the foam base, to fix it during impact simulation.

For this model, both impactor and foams were modelled using solid 8-node solid element. In addition to the foam setup, element formulation (ELFORM) Type-2 was selected. The *DEFINE_CURVE used was gathered from (Slik et al., 2006) to represent the compressive response of IMPAXX foam.

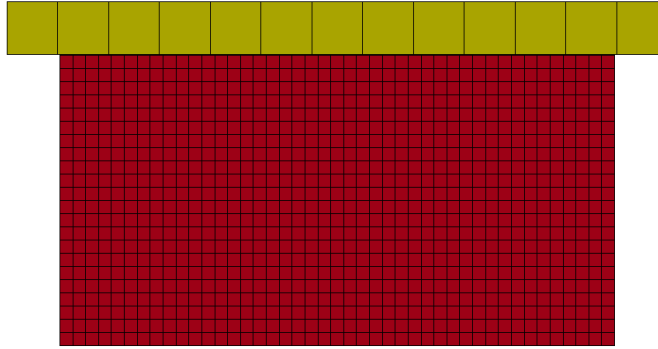


Figure 4-11: Foam and Impactor Setup in LS Dyna

For mesh size effect study, Cernicchi et al. (2008) suggested the use of cubic solid elements for the foam. The element size was constructed within the range of coarse to fine. This mesh size analysis was conducted to observe the effect of mesh density towards the simulation result. It is important task since this would reduce the computation cost without compromising the accuracy of the simulation results. The foam was constructed with element size of 2.5 mm, 5 mm and 10 mm (Figure 4-12). These three types of meshes were generated in order to investigate, if the simulation results would be affected by the mesh size.

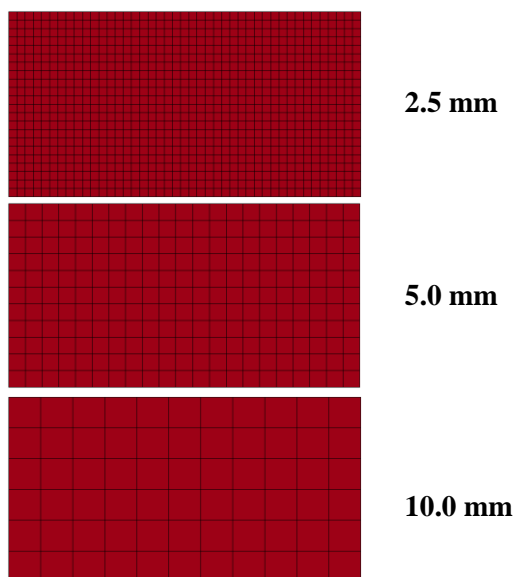


Figure 4-12: Mesh Size Setup

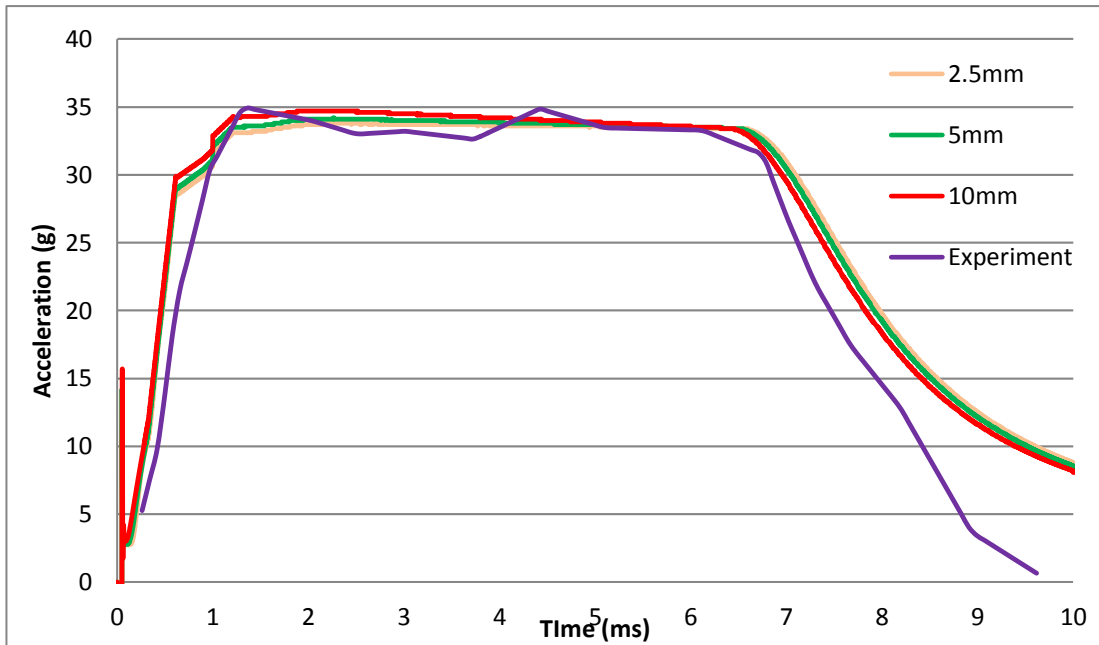


Figure 4-13: Mesh Size Analysis for IMPAXX 300

In Figure 4-13, the graph trend remains the same with the change of the mesh size. Small differences were shown on the maximum acceleration (g) recorded for all condition. Table 4-1 shows the recorded parameters including the Computer Processing Unit (CPU) and elapsed timing. The difference of 2.5 mm and 5.0 mm is recorded around 0.4 g but the CPU time difference is significantly increased by 92%. This would take longer in processing the whole model later. Therefore, 5 mm element size is selected for the IMPAXX foam simulation throughout this work.

Table 4-1: Data Recorded According to IMPAXX Foam Mesh Size of 2.5 mm, 5.0 mm and 10.0 mm

Mesh Size	2.5 mm	5.0 mm	10.0 mm
Maximum Acceleration (g)	33.8	34.2	34.7
Total CPU Time (s)	2134	152	19
Elapsed Time (s)	2135	154	20

4.3.2 Layer Configuration

The IMPAXX EPS foam block was constructed in Rhinoceros 3D modelling package. The block size was fixed at 105 x 105 x 55 mm, as specified in ASTM D 1596 Standards. It is critical to comply with the minimum requirements for this standard in order to simulate the pneumatic effect and buckling properties of cushioning materials. Solid 3D model was imported into LS-DYNA for meshing purposes. This solid mesh was constructed accordingly using 8-node 3D solid elements. The cushion for occupants seating has a strong influence on the lumbar load performance (FAA, 2006) (FAA, 1989). Therefore, it is critical to get accurate and reliable results from this simulation.

The foams then were simulated as an individual blocks or stacked layers with various density configurations. The density is gathered and calculated from the data sheet provided by the manufacturer (Table 4-2).

Table 4-2: Density, Volume and Mass Values for Commercial Grades of IMPAXX

IMPAXX Grades	Density (kg/m³)	Volume (cm³)	Mass (kg)	Layer Name
300	35	6.063 x10 ⁻³	0.0212	A
500	43	6.063 x10 ⁻³	0.0260	B
700	45	6.063 x10 ⁻³	0.0273	C

The blocks used in this study were stacked in layers of different densities placed at different positions. The stacking sequences are listed in Table 4-3 and the image in Figure 4-14 shows the foam setup in LS-DYNA. For the layered foams, there were two setups which is in interest for this study. Firstly, the multiple layer foam which consist of three layers of same density foam in this instance AAA, BBB and CCC. Finally, the combination layer or hybrid with individual foam was not repeated in

terms of grade such as ABC, CAB, BCA, CBA, BAC and ACB. This is to get better understanding of stacking sequence of same grade foams, different grade foams, compressive strength and density of the individual foam.

Table 4-3: IMPAXX Foam Testing Sequence

Sequence	Code	IMPAXX Type/ Grade	Composition
1	A	300	Single Layer
2	B	500	
3	C	700	
4	AAA	300, 300, 300	Multiple Layer
5	BBB	500, 500, 500	
6	CCC	700, 700, 700	
7	ABC	300, 500, 700	Combination Layer or Hybrid
8	CAB	700, 300, 500	
9	BCA	500, 700, 300	
10	CBA	700, 500, 300	
11	BAC	500, 300, 700	
12	ACB	300, 700, 500	

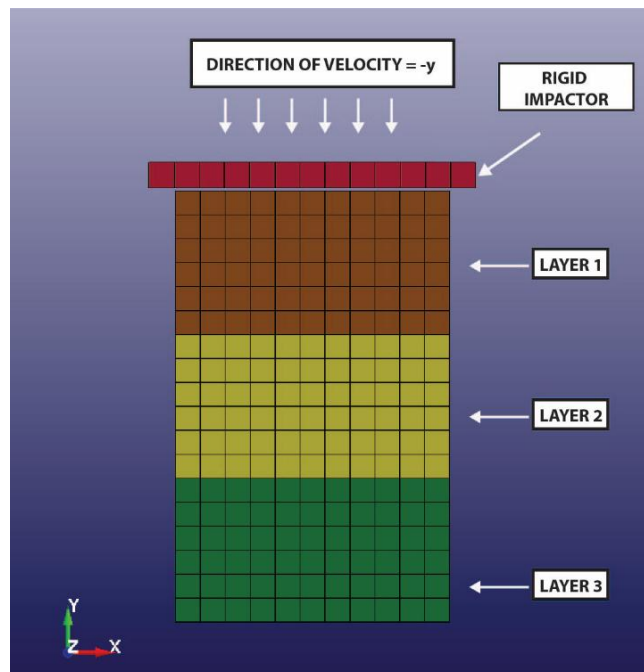


Figure 4-14: Layered Foam Setup in LS-DYNA

The simulation of blocks with different configurations will provide information on the best layer configuration which will be used for further simulation.

4.3.3 Shape Configuration

The next simulation incorporates the optimised EPS layers with several basic shapes such as square, arc and trapezium (Figure 4-15). The reason for using simulation for these stages was to lower the cost of procuring testing samples considering the cutting programme for such setup is quite costly. However, the final optimised result associated with the effect of the foam shape will be tested to validate simulation results.

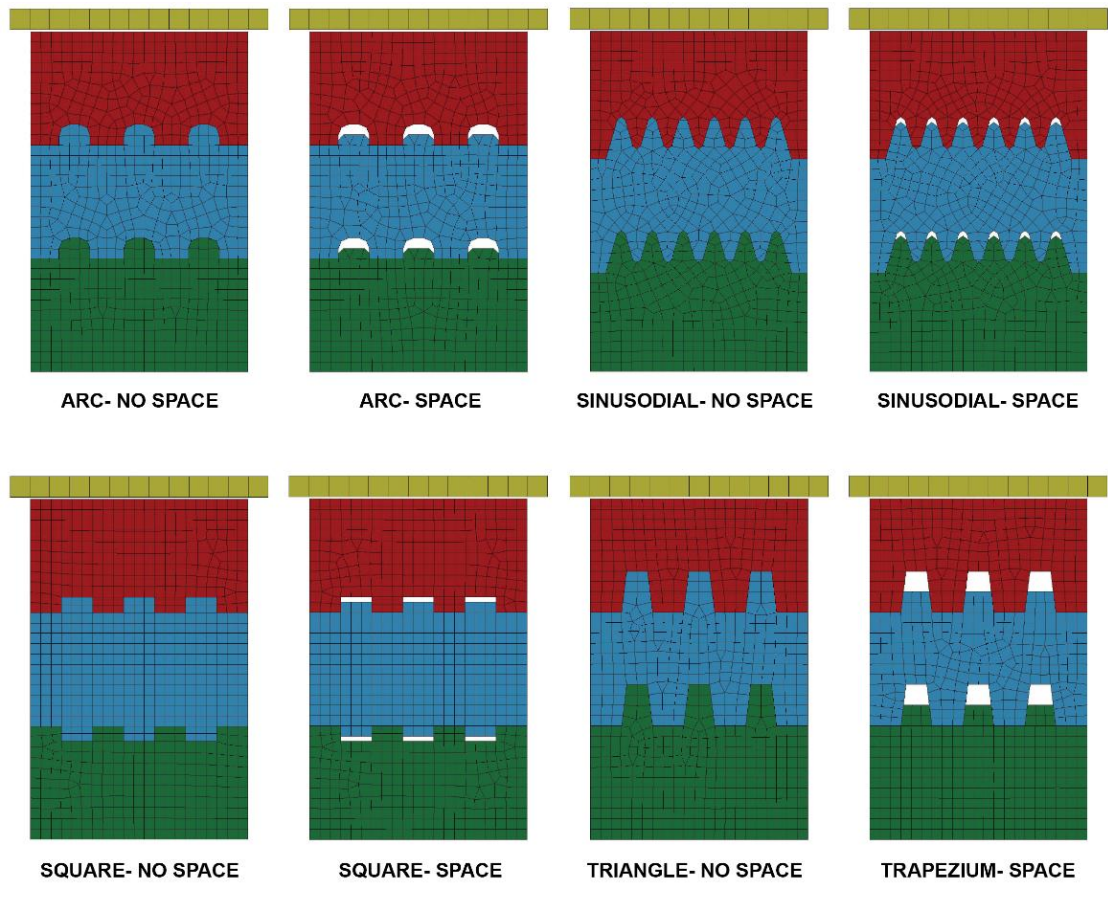


Figure 4-15: IMPAXX Foam Shape Configurations

The velocity that will be used for this simulation is chosen based on the actual landing regulations and the aircraft performance characteristics. The sink rate of Equator P2 Xcursion aircraft is set from minimum condition certified by FAA (2004b), which is 2 m/s. This was calculated according to the aircraft stall performance characteristics as specified in Table 2-3. Velocity used to test the material is in the range of 2 m/s - 4 m/s respectively.

A flat impactor with the mass of 14.253 kg was used for the experiment. Another aspect that needs to be considered is the accurate reference of stress strain curve (Cernicchi et al., 2008). The stress strain curve was acquired from the manufactures' software and should be reliable enough for this study.

Specific boundaries were applied to the nodes at the bottom part of layer 3 foam. This specific boundary was meant to hold the foam in places which have lateral and rotational constraint in all directions. Movement in x , y , and z direction was fixed. Similarly, rotational constraint was also applied in R_x , R_y and R_z direction respectively.

Furthermore, the components in the model was linked with contact algorithm which is available in LS-DYNA. *CONTACT_AUTOMATIC_SURFACE_TO_SURFACE was used for the impactor and the layer 1 foam element. Likewise, *CONTACT_AUTOMATIC_SURFACE_TO_SURFACE_TIEBREAK was used to link the foams at every layer. This layer integration algorithm would provide sufficient information to the software so that the motion induced by the impactor is restricted before onset of failure (Aiello et al., 2007). Surface contact connection's such as glued surface will transmit both tensile and compressive force until the failure of the glue,

hence the usage of this contact card is needed for this model. OPTION= 1 is selected so that all nodes are initially in contact will be tied together.

There is also a large difference in the elastic modulus of the impactor and the foam and it tends to promote penetration of the impactor on higher velocity test. Therefore, the stiffness coefficient needs to be adjusted accordingly to prevent such penetrations. As suggested by Bala (2006), LS-DYNA would compute the timestep and contact stiffness mainly on the maximum value of Young's modulus. However, LS-DYNA allows user to override this by using non-zero value of stiffness coefficient, KCON. In this instance, KCON of the foam material is set to 1% of the E value for the impactor, which is 2070.

4.3.4 Water

Toso (2009) contributed towards modelling and simulation of water. This study would follow results and suggestion from the author since it has been validated accordingly. Material type MAT010 (*MAT_ELASTIC_PLASTIC_HYDRO) was used with linear polynomial Equation of State (EOS) used for water. Parameters used were listed in Table 4-4. In addition, the water was constrained using *CONSTRAINED_LAGRANGE_IN_SOLID.

Table 4-4: Water Simulation Parameters in LS Dyna (Source: Toso, 2009; AWG, 2013)

Parameters	Value
Mass Density, RO	$1.0 \times 10^3 \text{ kg/m}^3$
Dynamic Viscosity	$1.0 \times 10^{-3} \text{ N-s/m}^2$
Pressure Cutoff, PC	-100 Pa
C ₀	0 GPa
C ₁	2.5 GPa
C ₂	7.5 GPa
C ₃	12.5 GPa

Material type for the ball is MAT020 (*MAT_RIGID) and considered as undeformable. Parameters for rigid steel material is shown in Table 4-5.

Table 4-5: Parameters of Rigid Steel Material (Source: LSTC, 2007)

Parameters	Value
Mass Density, RO	7850 kg/m^3
Young Modulus, E	$2.10 \times 10^2 \text{ GPa}$

Validity of material parameters were conducted through the experiment conducted by Troesch and Kang (1986) and simulation by Toso (2009). The specific parameters for the experiment and simulation are listed in Table 4-6.

Table 4-6: Considered Test Cases for Simulation Validation Procedure (Source: Toso, 2009; Troesch and Kang, 1986)

Test Cases	Sphere Diameter (m)	Weight (kg)	Velocity at impact (m/s)
Troesch_1	0.502	33.12	3.46
Troesch_2	0.502	33.12	4.89
Troesch_3	0.502	33.12	5.99

Toso (2009) also stated that, three factors should be considered in order to get reliable results for water modelling. The first would be the mesh sizes effect where three size conditions were examined such as:

- i. 10 mm x 10 mm x 20 mm
- ii. 5 mm x 5 mm x 10 mm
- iii. 3 mm x 3 mm x 6 mm

The coarser mesh shows high oscillations, which then lead to over estimation Toso (2009). Finer mesh would create a better time history. However, the middle-sized mesh also provides acceptable result and reduces the computational time. Therefore, this study will employ the 5mm x 5mm x 10mm mesh size for the water model.

Secondly, the water model would be affected by the pool size. The boundary size would create effects such as ripple or wave in real situation when the water flows back after reaching the boundary. Three pool sizes were considered which are 1.5, 2 and 2.5 times bigger than the sphere diameter. It was found that the pool having a length and width of 2 times the sphere diameter was sufficient to reduce the boundary effect (Toso, 2009).

Finally, Toso (2009) explained that there were no effect using quarter, half or full model sphere except for the computational time. Thus, the selection was based on computational time where full model was chosen for the validation test and a half model was used later for the actual aircraft simulation to reduce the computational time.

Toso (2009), showed a validation simulation of a sphere impacting water as suggested by Troesch and Kang (1986) and Toso (2009). It was plausible on the water

elevation around the sphere which shows the disturbance effect around the contact area. However, splash was not visible due to the topology of classical Lagrangian which shares common nodes on the neighbouring elements.

Figure 4-16 is the simulation image of a steel ball impacting water for model validation purposes.

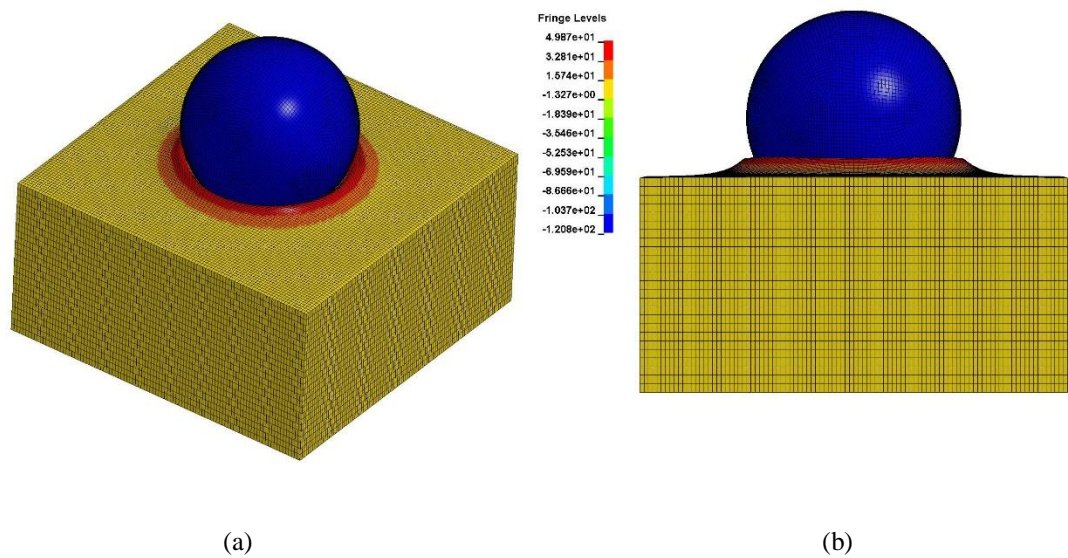


Figure 4-16: Simulation Image Showing Steel Ball Impacting Pure FE Model of Water at $t=5$ ms.

(a) Perspective View, (b) Side View

Toso (2009) work was followed closely since the author had proved the water impact simulation. Figure 4-17 presents a comparison of simulation and experimental acceleration (g) for three sets of cases. The results show a good agreement where the peak and plateau were well reproduced by the simulations for all the examined conditions. Even though, there were quite high oscillation towards the end, it was already sufficient since the impact situation only occurs in the first few milliseconds as suggested by Toso (2009).

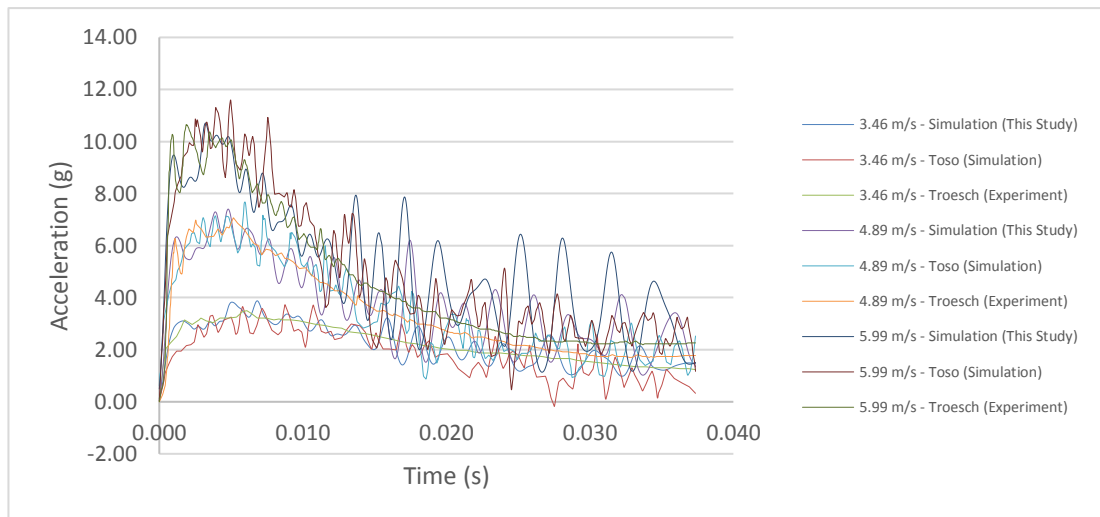


Figure 4-17: Comparison of the Acceleration for Water Impact Validation

4.3.5 Seating Foam

There are two common types of foam used in the aircraft industry which is DAX 55 and CONFOR Green (Bhonge, 2008), (Trelleborg, n.d.) . The density of both foams varies where the softer option which is the DAX55 would normally be used as the top layer. Meanwhile CONFOR Green is for the bottom layer nearest to the seat structure. This study will incorporate both foams and validated accordingly through literature results. Both of the foams are a viscoelastic material. This type of material showed instantaneous elasticity and will creep under stress (Veronika and Paul, 2012; Veronika et al., 2014).

The work of Tay et al. (2014) will be the guidance for this project since it provides extensive reference on the material validation for both DAX55 and CONFOR green. *MAT 057 – LOW DENSITY FOAM was used and the input details of parameters are shown in Table 4-7. This material was chosen since its capabilities of defining the unloading phase of cellular materials (Tay et al., 2014).

Table 4-7: Mechanical Properties of Cellular Materials and Additional Parameters in LS DYNA
(Source: Tay et al., 2014)

Foam	ρ Density	E Young's Modulus	Tension cut-off stress	Hysteric unloading factor	Decay constant	Viscous damping coefficient	Shape factor	Young's relaxation modulus
	(kg/m ³)	(MPa)	(MPa)			Ns/min		(MPa)
DAX 55	35	0.05	1.00E+20	0.101	0.0	0.50	25	0.0
CONFOR green	96.1	1.5						

All the information given were utilised for the modelling of DAX 55 and CONFOR green. *MAT 020- RIGID was applied to replicate the impactor and rigid base. Similar to the experimental and numerical setup conducted by Tay et al. (2014) the impactor velocity were set to 0.07 m/s. Model setup for the simulation is shown in Figure 4-18.

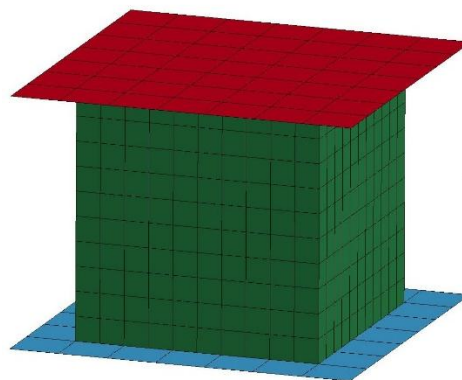


Figure 4-18: Simulation of CONFOR Green and DAX55 in LS DYNA

The stress strain-curve were taken from experiments conducted by Tay et al. (2014) as shown in Figure 4-19 and Figure 4-20. The tension cut-off stress was set to default value (Olivares et al., 2010). The shape and hysteric unloading factor were set to 25 and 0.101 respectively. The damping coefficient was set to 0.5 to increase stability because of the stiffness differences between the impactor and foams. Other than that, only default value was used for the parameters.

It is visible that by using parameters suggested by Tay et al. (2014), the result shows a good agreement for both CONFOR Green (Figure 4-19) and DAX55 (Figure 4-20). Therefore, this parameter will also be embedded in this work.

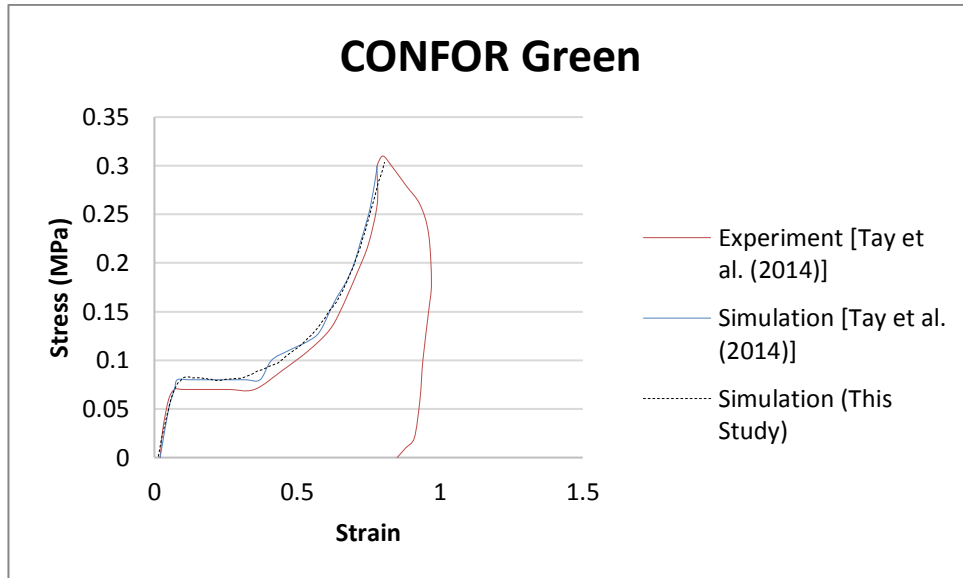


Figure 4-19: Comparison of Stress-strain between Experimental Data and Numerical Simulations of CONFOR Green.

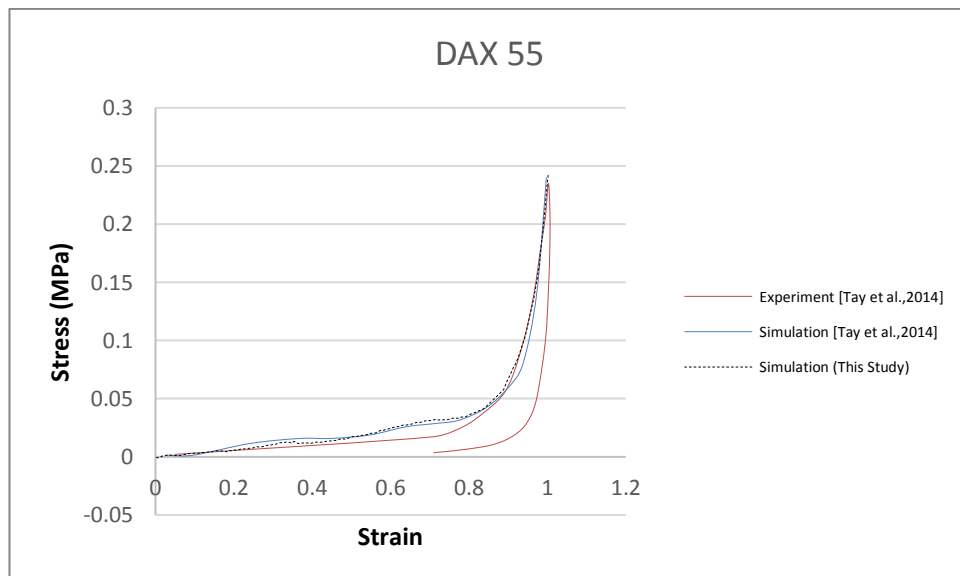


Figure 4-20: Comparison of Stress-Strain between Experimental Data and Numerical Simulations of DAX55

4.3.6 Finite Element Dummy Model and Seatbelt

The human occupant is simulated using a numerical 50th Percentile Hybrid III dummy developed and validated by Livermore Software Technology Corporation (LSTC). A full range of LSTC Hybrid III could be obtained in LS-DYNA format. The dummy used was modelled using rigid and deformable parts. It was validated by LSTC using standard impact testing method such as head impact, neck flexion and extension, chest impact and knee impact. These dummies are available for free and have been used for this study.

Various work (Tabiei et al., 2009; Kang and Xiao, 2008; Annett, 2010; Cheng et al., 2014) has been conducted using this type of dummy since it could provide vital information such as head, chest and dummy acceleration for injury assessment (Tabiei et al., 2009). Dummy model used with its seating position is shown in Figure 4-21.

The dummy was imported in LSPREPOST and adjusted accordingly to place it to the required position as in this case is on the Equator P2 aircraft seat. This is achieved by using 'H' point rotation and translation. Limb operation is also available to adjust the hands and legs position. After positioning the model on the aircraft' seat, only CONTACT_AUTOMATIC_SURFACE_TO_SURFACE was added to the dummy and seat.

The seatbelt was modelled as simple belt since it was meant just to put a restraint on the occupant during impact. Equator P2 aircraft uses a 4-point harness system therefore, a rigid steel buckle was also modelled using shell element to secure the

seatbelt constructed. Figure 4-22 shows the 4-point harness system and rigid buckle with its actual location on the FE model. The belts were then adjusted to fit the dummy model.

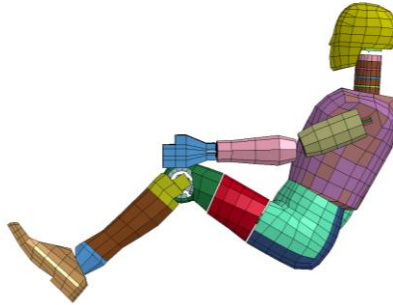


Figure 4-21: LS-DYNA HYBRID III Dummy and Seating Position Inside Equator P2 Aircraft

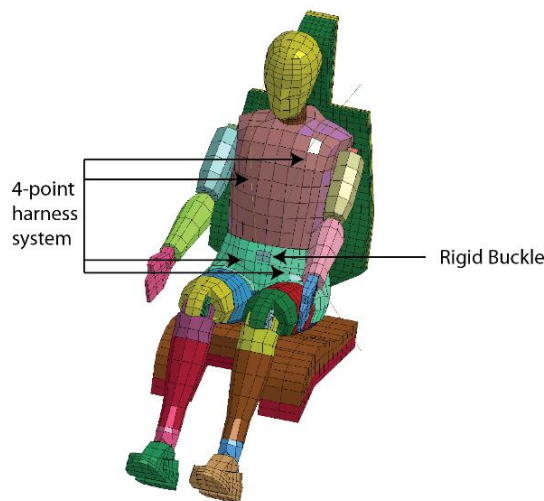


Figure 4-22: Dummy with 4-Point Harness System and Rigid Buckle

4.3.7 Aircraft Composite Sandwich Finite Element Model

The composite sandwich structure for the hull has both skins made from Carbon / Epoxy composite and the core made from AIREX C70.200 PVC foam. In order to incorporate the sandwich ply/layers *PART_COMPOSITE was applied to the shell element constructed. LS DYNA is known with its capabilities to simulate composite structure behaviours. However, the model generation for a complex layered might

become expensive. Therefore, LS DYNA introduced keyword *PART_COMPOSITE to simplify the modelling method of composite layups. There is no need to model several layers, integration points/shells. It only refers to the difference in material data and thickness applied with angle input relative to the material direction (Stelzmann and Hörmann, 2011). This is the best option for this study since the focus of this study is only on the dynamic behaviour of the structure not the damage related to cracks or delamination.

In a hull structure's case, the stress is transmitted from point of impact to the whole structure therefore the impact energy could be absorbed with higher total load preventing permanent damage. Crack and break would happen progressively, only when the load applied to the contact zone exceeds a threshold (Guida and Marulo, 2014). This is the case for this study as there is a concentration of impact at the point where the amphibian aircraft's hull touches the water surface during contact.

Lee et al. (2011) studied about Plain Weave (PW) Carbon/Epoxy composite which is similar to the one used in this study. Table 4-8 shows the material card used in LS DYNA. Guida and Marulo (2014) suggested that there was a problem on finding an appropriate formulation for the shell element to predict the damage characteristic of a composite material. In order to avoid unnecessary work done and to save computer cost, MAT_22 (MAT_COMPOSITE_DAMAGE) was used as suggested by Andersson and Larsson (2016). Since, MAT_22 is the simplest model that can provide shortest simulation time. This study is focussing on the absorber performance based on the overall dynamic response of the structure, not the composite damage, hence it is sufficient to use this type of material model. CONTACT_AUTOMATIC_

SURFACE_TO_SURFACE was used to define the contact between slave and master parts. The composite plate edges were constraint using Single Point Constraint (SPC) in LS DYNA.

Table 4-8: Plain Weave Carbon/Epoxy Laminate LS DYNA Material Card (Source: Lee et al., 2011)

RO (kg/mm ³) Mass	EA (GPa)	EB (GPa)	EC (GPa)	PRBA	PRCA	PRCB	GAB (GPa)	GBC (GPa)	GCA (GPa)
Mass density.	Young's modulus in a-direction	Young's modulus in b-direction	Young's modulus in c-direction	Poisson's ratio, ba	Poisson's ratio, ca	Poisson's ratio, cb	Shear modulus, ab	Shear modulus, bc	Shear modulus, ca
1.4975e-6	62.5	62.5	20.0	0.06	0.08	0.08	4.76	1.3	1.3

Core material properties were gathered from Hassan (2012) study on Polyvinyl Chloride (PVC) foams from Airex, C70.55. Typical stress strain curve for this material is shown in Figure 4-23 and its mechanical properties in Table 4-9.

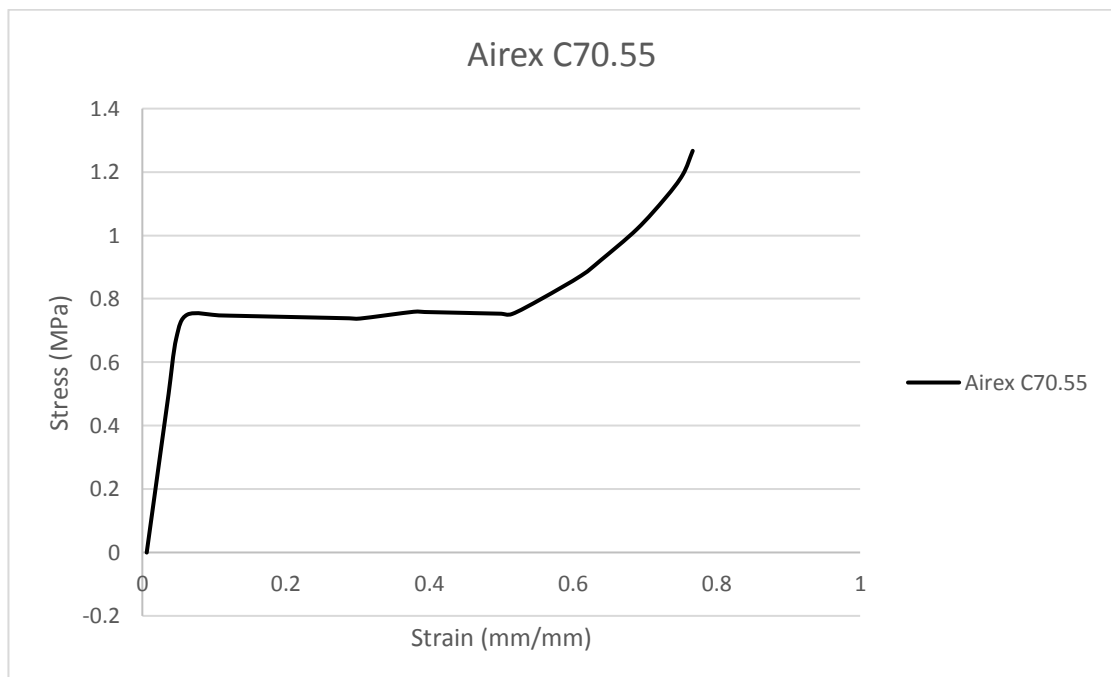


Figure 4-23: Stress-Strain Curve Extracted from Quasi-static Tests on AIREX C70.55 Cross-Linked PVC Foams (Source: Hassan, 2012)

Table 4-9: Material Properties of Cross-Linked PVC Foam C70.55 (Source: Hassan, 2012)

Density (kg/m ³)	60
Compression strength (MPa)	0.90
Compression modulus (MPa)	65
Shear strength (MPa)	0.9
Shear modulus (MPa)	22
Thermal conductivity (W/m.K)	0.031

The composite sandwich was validated using impact test result from experiment conducted in this study. The curve trend in Figure 4-24 shows agreement on both peaks. The peaks were the results of penetration between the upper skin, foam and the lower skin. Trials were made using different meshes which is 10 mm, 15 mm and 20 mm. Simulation with mesh of 20 mm shows an over predicted value on both peaks. The 10 mm mesh size simulation was under predicted compared to the experiment conducted. The 15 mm mesh size simulation showed a good agreement during the first peak. Since this study is interested on initial impact scenario, therefore 15 mm mesh size were chosen.

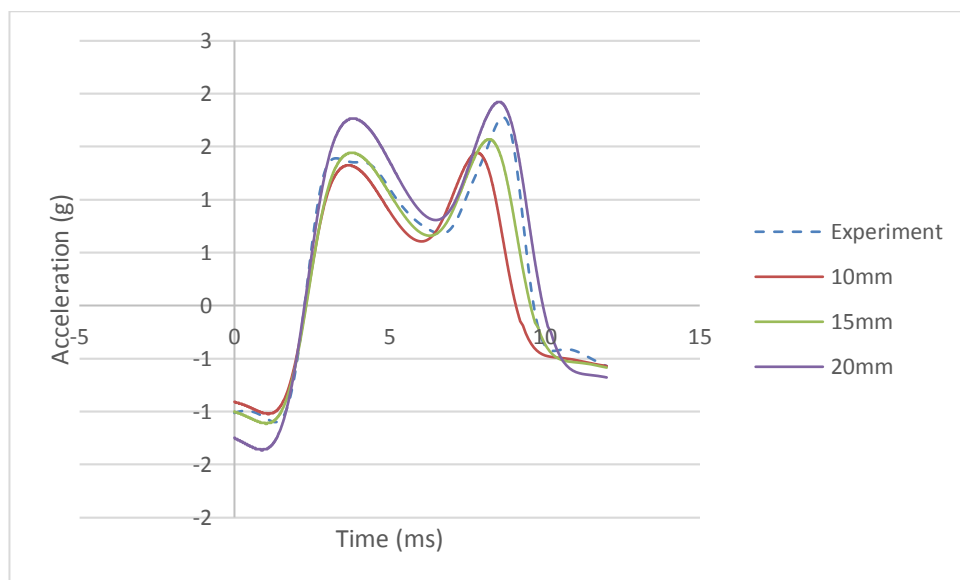


Figure 4-24: Indentation Result of Composite Sandwich at 2 m/s

Chapter 5: Result and Analysis of Simulation and Experiment

This chapter focuses on results and material characteristics of IMPAXX EPS Foam. By conducting simulation (S) and experiment (E), this study will come out with the different characteristic of all defined material design identified referring to the simulation and experiment.

Based on acceleration and displacement measurements, the characteristics of defined material design used in this study using impact velocity 2 m/s, 3 m/s, and 4 m/s (Table 5-1) is identified and constructed into table and graph. Specifically, this study uses three different density material where the layer of design no.1 is characterised as Material A, whilst design no.2 is for Material B, and design no.3 were meant for Material C (see Table 4-2). This study defined the single layer material design as representative of Material A, B and C. For multiple layers, this study defined material design AAA, BBB, and CCC are as triple of single layer Material of A, B, and C respectively. While, combination material design or hybrid material design are as combination of single layer material of Material A, B, and C. The combination material design or hybrid material design used in this study are ABC, CAB, BCA, CBA, BAC, and ACB. Table 5-2 showed the material design used in this study based on layer type configuration such as A, B, C, AAA, BBB, CCC, ABC, CAB, BCA,

CBA, BAC, and ACB (see Table 4-3 in 4.3.2).

Based on the acceleration or displacement measurement towards material design and impact velocity, as an example, the name of result towards the acceleration for sample no. 1 (Material A) which was impacted with 2 m/s impact velocity, it will be named as A2001-S. Similarly, for experiment conducted at 2 m/s and the result was on displacement value, it will be named as D2001-E. Such identification will be applied in following sub chapter as a guidance to understand the meaning of naming style used.

Table 5-1 : Categories and Naming Identification for Design Configuration

Type of Measurement	Velocity Impact	Design No.xx	Activities
Acceleration [A] or Displacement [D]	2 m/s [20xx] 3 m/s [30xx] 4 m/s [40xx]	xx=01 : xx=12	- Simulation [S] or Experiment [E]

Table 5-2 : Naming List for Experiment and Simulation

Name of Component Based Design	Design No. xx	Material Configuration
Single Layer	01	A
	02	B
	03	C
Multiple Layer	04	AAA
	05	BBB
	06	CCC
Combination Layer (Hybrid)	07	ABC
	08	CAB
	09	BCA
	10	CBA
	11	BAC
	12	ACB

5.1 Experiment and Simulation Results

Figure 5-1 shows the foam condition after impacted with 3 m/s. This figure proved that foam A is the most softer followed by B and C respectively (based on density of foam). The different densities foam of A (35 kg/m^3), B (43 kg/m^3), and C (55 kg/m^3) with same volume behave as expected as shown by the study (De Vries, 2009). The different in percentage a compared foam C is 4.4% (C to B), while C compared A is 22.2% and 18.6% for C compared to B. Thus, it clearly shows in Figure 5-1, C foam has small displacement as also shown for foam B and the most compressible is A foam.

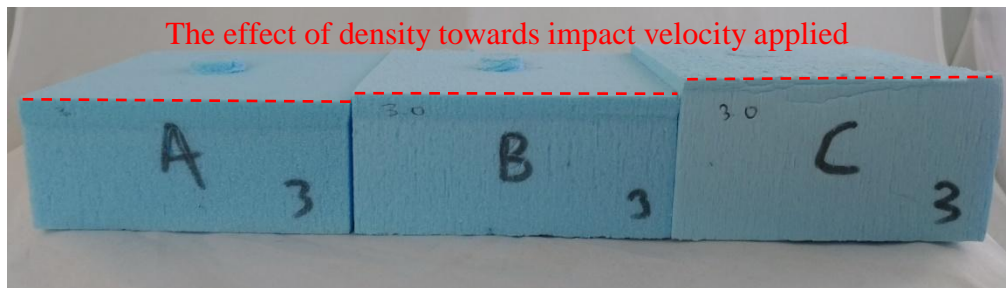


Figure 5-1: Foam Condition After 3 m/s Impact

Meanwhile, Figure 5-2 shows the effect of different density in terms of displacement when tested in multilayer and combination layer. Figure 5-2 is also selected to show that the softest (due to density) will influences overall structure with Material A becoming permanently compressed.

Figure 5-2 also proved that, the lowest density foam plays an important role in respond to the impact applied by becoming more compressible to absorb the impact energy. Even at different location as shown in Figure 5-2, where A located at centre of sequence will give same value of displacement, $AL_1=AL_2$ foam length (compressible length) at both location

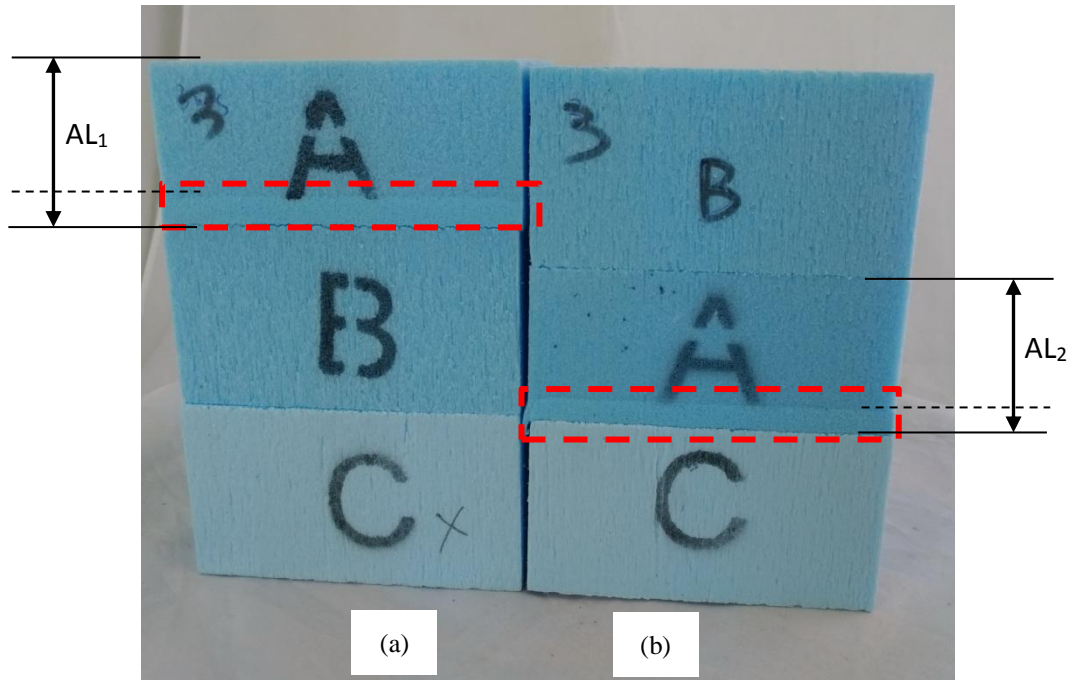


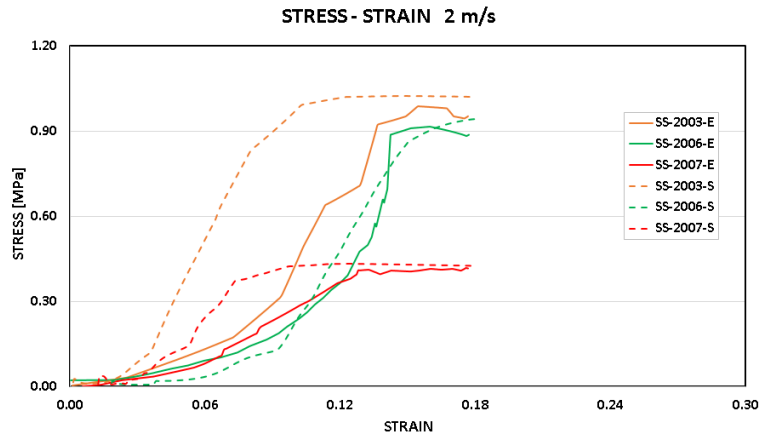
Figure 5-2: Effect of A (Lowest Density Foam) After 3 m/s Impact; (a) Design ABC, (b) Design BAC

Figure 5-1 and Figure 5-2 proved that a good combination arrangement/sequence are necessary to allocate the lowest density into the system when impacted with various impact velocity. This is the reasons why lower density foam need to be positioned accordingly to get maximum impact energy absorption with good value of acceleration (g) when human factors are considered. Arrangement of foam for experiment is shown in Appendix A.

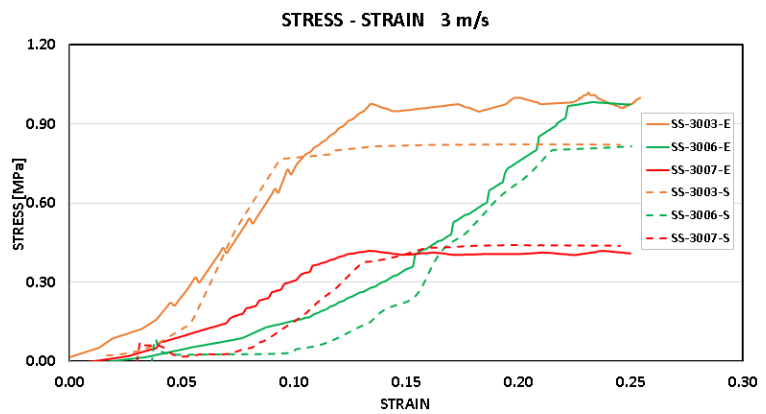
Figure 5.3 shows the comparison of stress-strain for simulation vs. experiment at 2 m/s, 3 m/s, 4 m/s. Figure 5-3(a) show the simulation result have high value for stress as compared to experiment. However, the trend of behaviours remains similar at all condition. Meanwhile for Figure 5-3(b) and Figure 5-3(c) show experiment result is slightly higher as compared to simulation. The complete data of on stress –strain

based on impact velocity 2 m/s, 3 m/s, and 4 m/s see in Appendix B.

(a)
Impact velocity 2 m/s



(b)
Impact velocity 3 m/s



(c)
Impact velocity 4 m/s

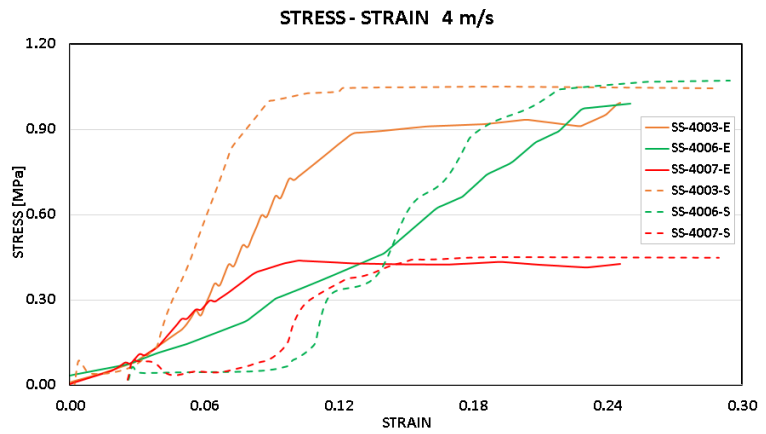


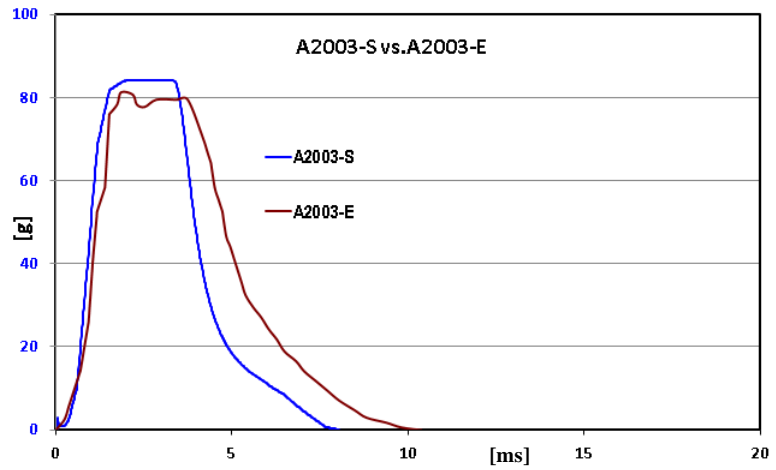
Figure 5-3: The Comparison between Simulation vs. Experiment Data;
(a) 2 m/s, (b) 3 m/s, (c) 4 m/s

5.1.1 Acceleration Results for Layer Design Configuration

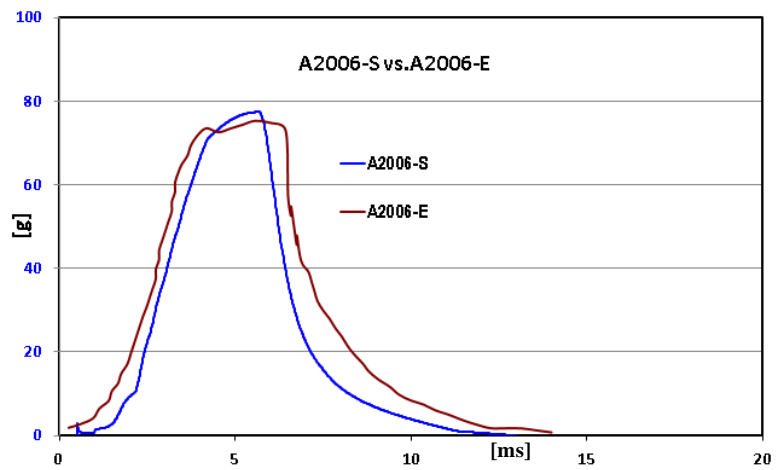
Figure 5-4 shows the example of acceleration results of simulation towards experiment for impact velocity 2 m/s. The figure shown the example based on each simulation and experiment towards single layer, multiple layer, and combination layer (hybrid). The complete of measurement for acceleration is in Appendix C.

Figure 5-4 shows selected example of single layer, multiple layer, and combination layer for acceleration resulted from experiment and simulation. A good argument obtained for the results and behaviours which clearly shown in Figure 5-4. Percentage difference between simulation and experiment for maximum acceleration recorded (at plateau region) were 3.6%, 3.09%, and 3.45% respectively. The gap between the ranges of all condition is 3.09 to 3.45% and considered acceptable value. This value and behaviour similar for impact velocity of 3 m/s and 4 m/s.

Single Layer
[Example: Design C]
(a)



Multiple Layer [Example:
Design CCC]
(b)



Combination Layer
[Example: Design ABC]
(c)

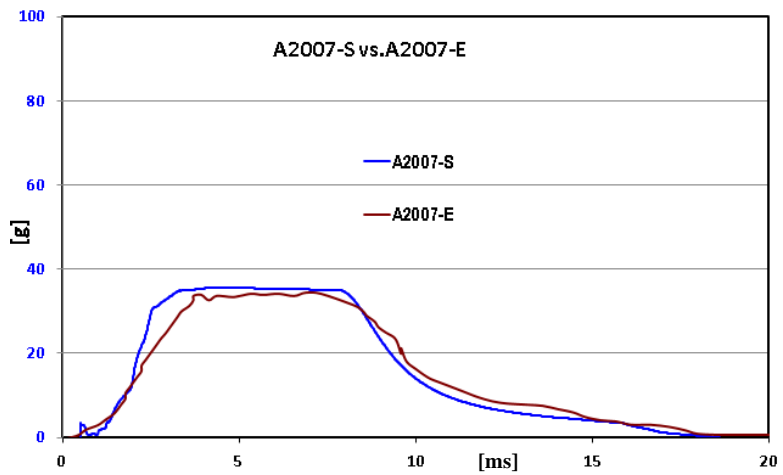


Figure 5-4: Acceleration with Impact Velocity 2 m/s;
(a) Design 2003, (b) Design 2006, (c) Design 2007

Table 5-3 showed that the highest acceleration results for simulation with impact velocity 2 m/s is material design C or A2003-S (84.31 g), for impact velocity 3 m/s is material design CCC or A3006-S (87.46 g) and for impact velocity 4 m/s is material design CCC or A4006-S (88.37 g). This is also shown in Table 5-4 for experiment where the highest of acceleration based on impact velocity 2 m/s is material design C or A2003-E (81.28 g), for impact velocity 3 m/s is material design C or A3003-E (84.94 g) and for impact velocity 4 m/s is material design CCC or A4006-E (86.06 g).

Table 5-3: The Maximum Point of Acceleration (Simulation)

ACCELERATION - 2 m/s – SIMULATION [in Acceleration (g)]												
Material Design	SINGLE LAYER			MULTIPLE LAYER			COMBINATION LAYER OR HYBRID					
	A	B	C	AAA	BBB	CCC	ABC	CAB	BCA	CBA	BAC	ACB
	A2001-S	A2002-S	A2003-S	A2004-S	A2005-S	A2006-S	A2007-S	A2008-S	A2009-S	A2010-S	A2011-S	A2012-S
Max	34.15	66.51	84.31	34.36	66.07	77.42	35.64	35.56	35.54	35.50	35.56	35.64
ACCELERATION - 3 m/s - SIMULATION [in Acceleration (g)]												
Material Design	SINGLE LAYER			MULTIPLE LAYER			COMBINATION LAYER OR HYBRID					
	A	B	C	AAA	BBB	CCC	ABC	CAB	BCA	CBA	BAC	ACB
	A3001-S	A3002-S	A3003-S	A3004-S	A3005-S	A3006-S	A3007-S	A3008-S	A3009-S	A3010-S	A3011-S	A3012-S
Max	34.80	67.54	85.47	35.29	68.93	87.46	36.36	36.31	36.53	36.31	36.31	36.36
ACCELERATION - 4 m/s- SIMULATION [in Acceleration (g)]												
Material Design	SINGLE LAYER			MULTIPLE LAYER			COMBINATION LAYER OR HYBRID					
	A	B	C	AAA	BBB	CCC	ABC	CAB	BCA	CBA	BAC	ACB
	A4001-S	A4002-S	A4003-S	A4004-S	A4005-S	A4006-S	A4007-S	A4008-S	A4009-S	A4010-S	A4011-S	A4012-S
Max	35.36	68.32	86.38	35.57	69.65	88.37	36.98	36.95	37.01	37.34	36.95	36.98

Table 5-4: The Maximum Point of Acceleration (Experiment)

ACCELERATION - 2 m/s - EXPERIMENT [in Acceleration (g)]												
Material Design	SINGLE LAYER			MULTIPLE LAYER			COMBINATION LAYER OR HYBRID					
	A	B	C	AAA	BBB	CCC	ABC	CAB	BCA	CBA	BAC	ACB
	A2001-E	A2002-E	A2003-E	A2004-E	A2005-E	A2006-E	A2007-E	A2008-E	A2009-E	A2010-E	A2011-E	A2012-E
Max	34.92	60.59	81.28	32.97	64.37	75.30	34.41	35.50	34.50	34.09	35.94	36.35
ACCELERATION - 3 m/s - EXPERIMENT [in Acceleration (g)]												
Material Design	SINGLE LAYER			MULTIPLE LAYER			COMBINATION LAYER OR HYBRID					
	A	B	C	AAA	BBB	CCC	ABC	CAB	BCA	CBA	BAC	ACB
	A3001-E	A3002-E	A3003-E	A3004-E	A3005-E	A3006-E	A3007-E	A3008-E	A3009-E	A3010-E	A3011-E	A3012-E
Max	34.69	67.31	84.94	34.56	65.03	82.12	34.61	35.68	36.22	36.47	36.71	35.47
ACCELERATION - 4 m/s- [in Acceleration (g)]												
Material Design	SINGLE LAYER			MULTIPLE LAYER			COMBINATION LAYER OR HYBRID					
	A	B	C	AAA	BBB	CCC	ABC	CAB	BCA	CBA	BAC	ACB
	A4001-E	A4002-E	A4003-E	A4004-E	A4005-E	A4006-E	A4007-E	A4008-E	A4009-E	A4010-E	A4011-E	A4012-E
Max	35.41	68.65	85.40	34.83	67.31	86.06	36.13	35.64	36.49	37.51	37.60	35.92

Since the acceleration values of combination layer (hybrid) close enough to the values of A (around 30 g) (Table 5-3 and Table 5-4) , so the conclusion is the Material A that control the acceleration g during impact.

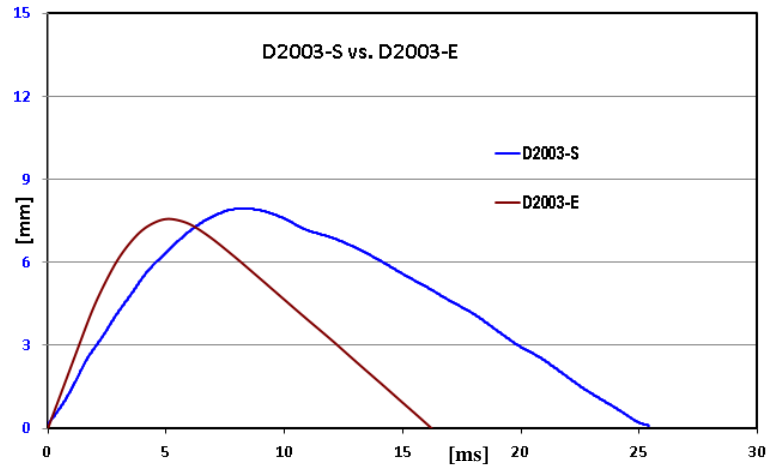
In addition, it can be concluded that the maximum values of acceleration with impact velocity 2 m/s for simulation and experiment occurred on material design C of single layer, whilst for impact velocity 4 m/s is on material design CCC of multiple layer. It is different for impact velocity 3 m/s, where the highest acceleration for the simulation occurred is on material design CCC (A3006-S) of multiple layer, while for the experiment occurred is on material design C (A3003-E) of multiple layer. Based on this finding, this study concluded that the highest values of acceleration were on single or multiple layer of the material design that having component of Material C.

5.1.2 Displacement Results for Layer Design Configuration

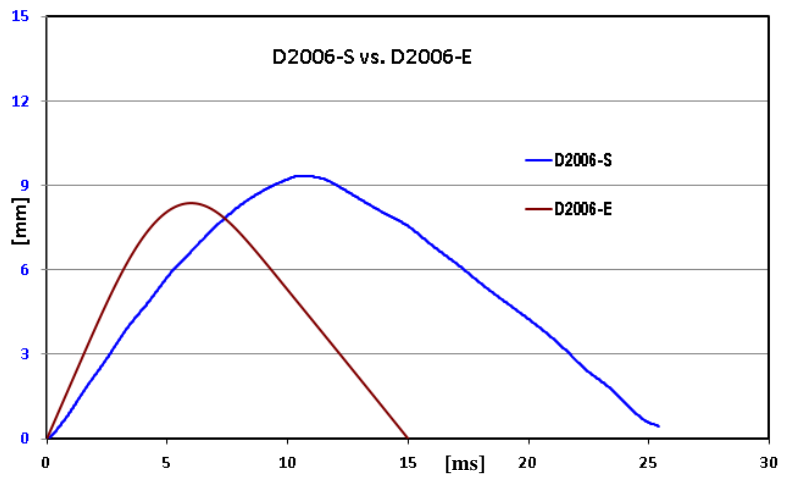
Figure 5-5 showed the example of displacements results of simulation towards experiment for impact velocity 2 m/s. The figure shows example based on each simulation and experiment towards single layer, multiple layer, and combination layer (hybrid). The complete of measurement for displacement is in Appendix D.

Figure 5-5 shows the result of displacement for impact velocity 2 m/s for single, multiple, and hybrid (combination) layer for selected design. The different displacement between simulation and experiment for (a) single, (b) multi, (c) hybrid were 4.53%, 10.4%, and 4.3% respectively. Thus, this also consider a good and acceptable agreement. This trend also similar for displacement at 3 m/s and 4 m/s.

Single Layer
[Example: Design C]
(a)



Multiple Layer
[Example: Design CCC]
(b)



Combination Layer [Example:
Design ABC]
(c)

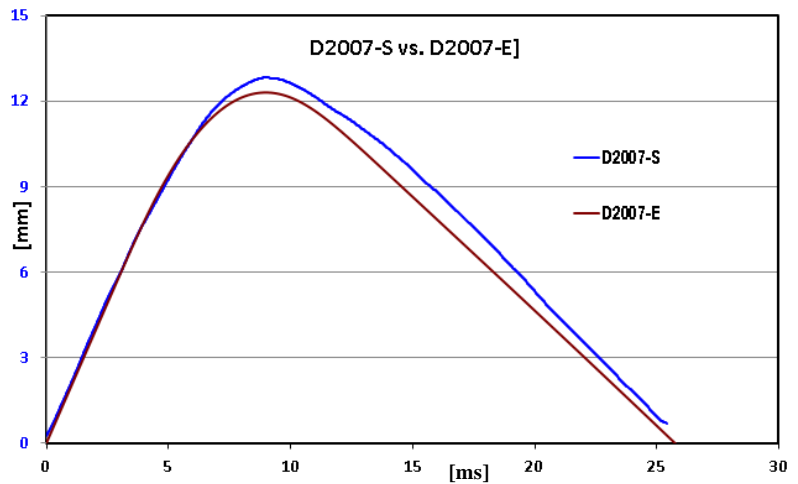


Figure 5-5: Displacement with Impact Velocity 2 m/s;
(a) Design 2003, (b) Design 2006, (c) Design 2007

Table 5-5 showed that the highest displacement results for simulation with impact velocity 2 m/s is material design AAA or A2004-S (12.04 mm), for impact velocity 3 m/s is material design AAA or A3004-S (19.77 mm) and for impact velocity 4 m/s is material design AAA or A4004-S (30.34 mm). This is also shown in Table 5-6, where the highest of displacement values based experiment using impact velocity 2 m/s is on material design AAA or A2004-E (11.68 mm). For impact velocity 3 m/s is on material design AAA or A3004-E (18.73 mm) and for impact velocity 4 m/s is on material design AAA or A4004-E (28.46 mm). This can be summarised that the higher values of displacement measurement (simulation and experiment) is on material design AAA of multiple layer.

Table 5-5: The Maximum Point of Displacement (Simulation)

DISPLACEMENT - 2 m/s - SIMULATION [in mm]												
Material Design	SINGLE LAYER			MULTIPLE LAYER			COMBINATION LAYER OR HYBRID					
	A	B	C	AAA	BBB	CCC	ABC	CAB	BCA	CBA	BAC	ACB
	D2001-S	D2002-S	D2003-S	D2004-S	D2005-S	D2006-S	D2007-S	D2008-S	D2009-S	D2010-S	D2011-S	D2012-S
Max	10.90	8.13	7.93	12.04	10.88	9.35	12.83	12.05	11.49	10.10	10.82	11.31
DISPLACEMENT - 3 m/s - SIMULATION [in mm]												
Material Design	SINGLE LAYER			MULTIPLE LAYER			COMBINATION LAYER OR HYBRID					
	A	B	C	AAA	BBB	CCC	ABC	CAB	BCA	CBA	BAC	ACB
	D3001-S	D3002-S	D3003-S	D3004-S	D3005-S	D3006-S	D3007-S	D3008-S	D3009-S	D3010-S	D3011-S	D3012-S
Max	16.49	12.55	8.31	19.77	17.54	14.29	17.29	20.21	16.61	21.10	18.09	19.51
DISPLACEMENT - 4 m/s - SIMULATION [in mm]												
Material Design	SINGLE LAYER			MULTIPLE LAYER			COMBINATION LAYER OR HYBRID					
	A	B	C	AAA	BBB	CCC	ABC	CAB	BCA	CBA	BAC	ACB
	D4001-S	D4002-S	D4003-S	D4004-S	D4005-S	D4006-S	D4007-S	D4008-S	D4009-S	D4010-S	D4011-S	D4012-S
Max	27.33	20.68	17.07	30.34	23.01	20.80	25.98	27.49	29.09	29.84	28.63	30.22

Table 5-6: The Maximum Point of Displacement (Experiment)

DISPLACEMENT - 2 m/s - SIMULATION [in mm]												
Material Design	SINGLE LAYER			MULTIPLE LAYER			COMBINATION LAYER OR HYBRID					
	A	B	C	AAA	BBB	CCC	ABC	CAB	BCA	CBA	BAC	ACB
	D2001-E	D2002-E	D2003-E	D2004-E	D2005-E	D2006-E	D2007-E	D2008-E	D2009-E	D2010-E	D2011-E	D2012-E
Max	9.80	8.13	7.57	11.68	10.27	8.37	12.31	11.37	11.31	9.64	10.33	10.92
DISPLACEMENT - 3 m/s - SIMULATION [in mm]												
Material Design	SINGLE LAYER			MULTIPLE LAYER			COMBINATION LAYER OR HYBRID					
	A	B	C	AAA	BBB	CCC	ABC	CAB	BCA	CBA	BAC	ACB
	D3001-E	D3002-E	D3003-E	D3004-E	D3005-E	D3006-E	D3007-E	D3008-E	D3009-E	D3010-E	D3011-E	D3012-E
Max	16.00	13.63	7.56	18.73	15.81	14.66	15.78	18.37	15.78	19.79	17.54	18.36
DISPLACEMENT - 4 m/s - SIMULATION [in mm]												
Material Design	SINGLE LAYER			MULTIPLE LAYER			COMBINATION LAYER OR HYBRID					
	A	B	C	AAA	BBB	CCC	ABC	CAB	BCA	CBA	BAC	ACB
	D4001-E	D4002-E	D4003-E	D4004-E	D4005-E	D4006-E	D4007-E	D4008-E	D4009-E	D4010-E	D4011-E	D4012-E
Max	25.92	20.31	16.99	28.46	21.31	18.99	25.45	25.43	26.96	27.94	26.74	28.88

5.1.3 Summary of Acceleration and Displacement Measurement Result

Based on acceleration and displacement measured through experiment and simulation, this study concluded that the highest values of acceleration were on single or multiple layer of the material design that having component Material C, whilst the higher values of displacement measurement are on material design AAA.

For acceleration, the highest values for 2 m/s and 4 m/s were consistent between the experiment and simulation. For 2 m/s, the highest value of acceleration for simulation and experiment is on the material design C, while for 4 m/s the highest value is on material design CCC. The phenomenon occurred when for 3 m/s, the highest value of simulation towards acceleration occurred on Material CCC, while for experiment is on C. This meant that the acceleration towards material design is very sensitive where there was error occurred in experiment and simulation that make the results between simulation and experiment for the highest is different. However, this

is not found in the displacement measured.

It needs to be noted that the displacement based on simulation and experiment is consistent for 2 m/s., 3 m/s, and 4 m/s where the material design AAA is having the highest values. Based on this finding, this study concluded that the use of displacement to determine the best design is critically important. In addition, there is need a method to justify that the experiment values were consequence to simulation results. In this context, Appendix F show how to find the tolerances towards acceleration and displacement based on simulation against experiment where this study justified with +/-15% (see section 3.3 about the formula and a method applied).

5.2 Analysis of Foam Design Based on Layer

In this section, the research focuses on the material characteristics based on the various velocity impact, such as 2 m/s, 3 m/s, and 4 m/s. Content such as maximum and average values of different material against velocity applied were shown clearly in tables. Other tables show maximum and average values of specified velocities against material configuration. The purpose of having this tables is to observe the increasing and decreasing trend of graph.

5.2.1 Single Layer Foam Configuration

5.2.1.1 The acceleration analysis of single layer configuration

Table 5-7 shows acceleration in single layer design configuration of both experiment and simulation. The difference of maximum point and average point were classified clearly using percentage difference. The percentage differences are

calculated based on maximum and average points of acceleration (g) for Material B vs. A, and C vs. B. For example, the percentage differences for maximum point of Material B (66.5 g) vs. A (34.15 g) is 32.36 g. This percentage differences are 94.8% (Material B compared to Material A). This method is also used to calculate the percentage difference of Material C vs. B.

Simulation values of maximum points for 2 m/s increased in acceleration (g). Increment of percentage of design 1 (A-2001-S) against design 2 (A-2002-S) was 94.8%. For percentage increment of design 2 (A-2002-S) against design 3 (A-2003-S) was 26.8%. Whilst, for the average values, it decreased by -56.7% then increased by 0.1% for velocity 2 m/s. To compare with experiment findings on velocity 2 m/s, maximum points increased in acceleration (g). Whilst for percentage increment of design 1 towards design 2 was 73.5%. For percentage, increment of design 2 towards design 3 was 34.1%. However, the increment of percentage average of design 1 towards design 2 was 11.5%. Whilst, the increment of percentage the average value of design 2 towards design 3 was 43.1%.

Simulation values of maximum points for 3 m/s increased in acceleration (g). Increment of percentage of design 1 (A-3001-S) against design 2 (A-2002-S) was 94.1%. For percentage increment of design 2 (A-3002-S) against design 3 (A-3003-S) was 26.5%. Whilst, for the average values, increased by 9.8% then increased by 0.1% for velocity 3 m/s. To compare with experiment findings on velocity 3 m/s, maximum points increased in acceleration (g). Whilst for percentage increment of design 1 towards design 2 was 94.0%. For percentage, increment of design 2 towards design 3 was 26.2%. However, percentage average of design 1 towards design 2 increased by

52.8%. Whilst, for the average value of design 2 against design 3 increased by 18.8%.

Table 5-7: Acceleration Single Layer (Simulation and Experiment)

SIMULATION - ACCELERATION [SINGLE LAYER] [in Acceleration (g)]									
IMPACT VELOCITY	2 m/s			3 m/s			4 m/s		
MATERIAL DESIGN	A	B	C	A	B	C	A	B	C
	A2001-S	A2002-S	A2003-S	A3001-S	A3002-S	A3003-S	A4001-S	A4002-S	A4003-S
MAXIMUM POINT	34.15	66.51	84.31	34.80	67.54	85.47	35.36	68.32	86.38
AVERAGE POINT	19.82	8.58	8.59	27.30	29.98	30.01	32.61	39.64	39.95
Percentage MAX	94.8%	26.8%		94.1%	26.5%		93.2%	26.4%	
Percentage AVE	-56.7%	0.1%		9.8%	0.1%		21.6%	0.8%	
EXPERIMENT - ACCELERATION [SINGLE LAYER] [in Acceleration (g)]									
IMPACT VELOCITY	2 m/s			3 m/s			4 m/s		
MATERIAL DESIGN	A	B	C	A	B	C	A	B	C
	A2001-E	A2002-E	A2003-E	A3001-E	A3002-E	A3003-E	A4001-E	A4002-E	A4003-E
MAXIMUM POINT	34.92	60.59	81.28	34.69	67.31	84.94	35.41	68.65	85.40
AVERAGE POINT	25.86	28.35	40.61	25.16	36.79	45.26	29.07	40.52	46.71
Percentage MAX	73.5%	34.1%		94.0%	26.2%		93.9%	24.4%	
Percentage AVE	11.5%	43.1%		52.8%	18.8%		40.8%	17.9%	

Simulation values of maximum points for 4 m/s increased in acceleration (g). Increment of percentage of design 1 (A-4001-S) against design 2 (A-4002-S) was 93.2%. For percentage increment of design 2 (A-4002-S) to design 3 (A-4003-S) was 26.4%. Whilst, for the average values, increased by 21.6% then increased by 0.8% for velocity 4 m/s. To compare with experiment findings on velocity 4 m/s, maximum points increased in acceleration (g). Whilst for percentage increment of design 1 towards design 2 was 93.9%. For percentage increment of design 2 towards design 3 was 24.4%. However, percentage average of design 1 towards design 2 increased by 40.8%. Whilst, for the average value of design 2 towards design 3 increased by 17.9%.

Figure 5-6 and Figure 5-7 shows that the maximum and average points based on Material A, B, and C for the acceleration based on simulation and experiment using impact velocity 2 m/s, 3 m/s and 4 m/s. However, it was visible, that there was an

increasing trend for the average points especially for Material B and C (see the blue dotted arrow in Figure 5-6 and Figure 5-7).

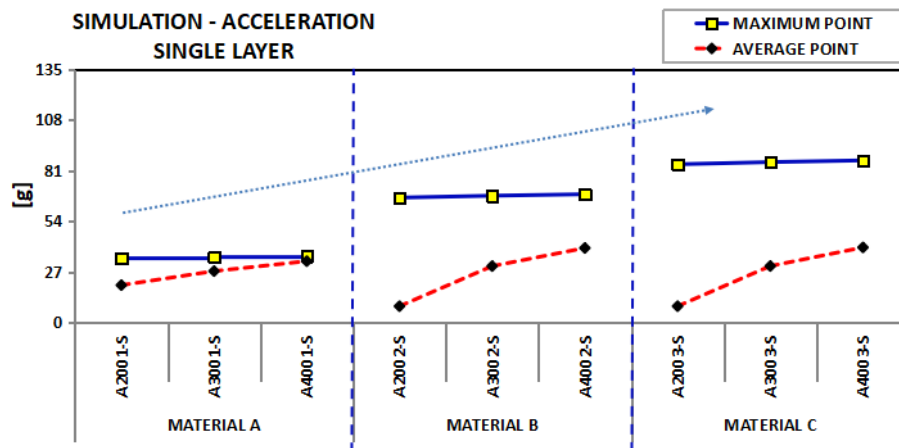


Figure 5-6: Simulation Result of Single Layer Acceleration Based on Material

Based from Figure 5-6, Material A, B and C were tested using specified velocities of 2 m/s, 3 m/s and 4 m/s. Observe from the simulation findings, average points increased as velocity increases. However, there is no significant changes for maximum points in all the materials. To summarise, Material C has the highest acceleration (g) values followed by Material B and Material C. Therefore, simulation shows, Material C is highest for single layer design configuration (blue dotted arrow).

Figure 5-7, Material A, B and C were tested using specified velocities of 2 m/s, 3 m/s and 4 m/s. Observe from the experiment findings, average points increased as velocity increases. However, there is no significant changes for maximum points in Material A. Whilst Material B showed a slight increase for 2 m/s to 3 m/s, but remain aligned for 3 m/s to 4 m/s. To summarise, Material C has the highest acceleration values followed by Material B and Material C (blue dotted arrow).

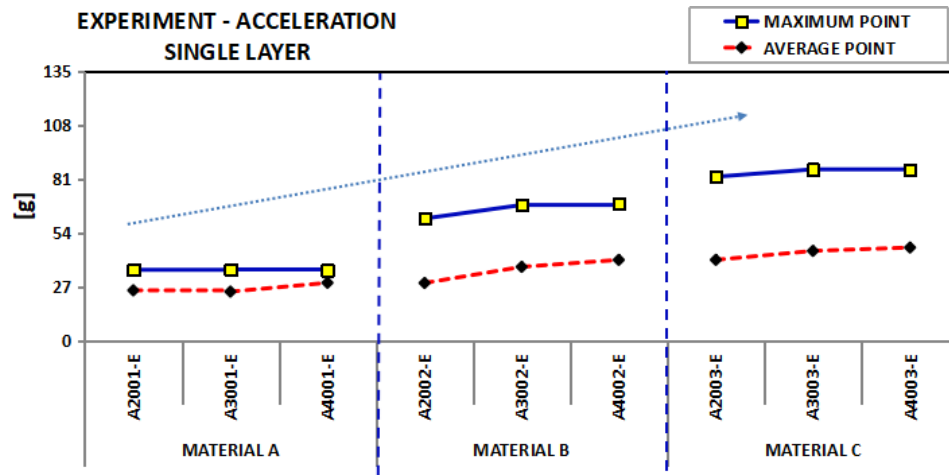


Figure 5-7: Experiment Result of Single Layer Acceleration Based on Material

To conclude, there were no significant difference between both simulation and experiment. However, the theory from simulation supported by experiment whereby Material C has the highest g value for single layer configuration.

5.2.1.2 The Displacement Analysis of Single Layer Configuration

Table 5-8 shows displacement in single layer design configuration of both experiment and simulation. The difference of maximum point and average point were classified clearly using percentage difference. The percentage differences are calculated based on maximum and average points of displacement (mm) for Material B vs. A, and C vs. B. For example, the percentage differences for maximum point of Material B (8.13 mm) vs. A (10.90 mm) is -2.77 mm. This percentage differences are -25.4 % (Material B compared to Material A). This method is also used to calculate the percentage difference of Material C vs. B.

Table 5-8: Displacement Single Layer Percentage Difference (Simulation and Experiment)

SIMULATION – DISPLACEMENT [SINGLE LAYER] [in mm]									
IMPACT VELOCITY	2 m/s			3 m/s			4 m/s		
MATERIAL DESIGN	A	B	C	A	B	C	A	B	C
	D2001-S	D2002-S	D2003-S	D3001-S	D3002-S	D3003-S	D4001-S	D4002-S	D4003-S
MAXIMUM POINT	10.90	8.13	7.93	16.49	12.55	8.31	27.33	20.68	17.07
AVERAGE POINT	6.45	4.07	3.96	11.13	6.88	4.03	18.80	13.77	10.71
Percentage MAX	-25.4%	-2.4%		-23.9%	-33.7%		-24.3%	-17.5%	
Percentage AVE	-26.2%	-3.2%		-33.6%	-34.6%		-29.8%	-22.0%	
EXPERIMENT – DISPLACEMENT [SINGLE LAYER] [in mm]									
IMPACT VELOCITY	2 m/s			3 m/s			4 m/s		
MATERIAL DESIGN	A	B	C	A	B	C	A	B	C
	D2001-E	D2002-E	D2003-E	D3001-E	D3002-E	D3003-E	D4001-E	D4002-E	D4003-E
MAXIMUM POINT	9.80	8.13	7.57	16.00	13.63	7.56	25.92	20.31	16.99
AVERAGE POINT	4.90	2.23	0.53	10.22	7.49	-0.02	18.25	13.03	9.58
Percentage MAX	-17.0%	-6.9%		-14.9%	-44.5%		-21.6%	-16.4%	
Percentage AVE	-17.6%	-6.0%		-26.4%	-45.4%		-28.4%	-26.2%	

Simulation values of maximum points for 2 m/s decreased in displacement (mm). Decrement of percentage of design 1 (D2001-S) against design 2 (D2002-S) was -25.4%. For percentage decrement of design 2 (D2002-S) against design 3 (D2003-S) was -2.4%. Whilst, for the average values, it decreased by -26.2% then decreased by -3.2% for velocity 2 m/s. To compare with experiment findings on velocity 2 m/s, maximum points also decreased in displacement (mm). Whilst for percentage decrement of design 1 (D2001-E) towards design 2 (D2002-E) was -17.0%. For percentage decrement based from design 2 (D2002-E) towards design 3 (D2003-E) was -6.9%. However, percentage average of design 1 based on design 2 slightly decreased by -17.6%. Whilst, for the average value of design 2 towards design 3 decreased by -6.0%.

Simulation values of maximum points for 3 m/s decreased in displacement (mm). Decrement of percentage of design 1 (D3001-S) against design 2 (D3002-S) was -23.9%. For percentage decrement of design 2 (D3002-S) against design 3 (D3003-S)

was -33.7%. Whilst, for the average values, decreased by -33.6% then decreased by -34.6% for velocity 3 m/s. To compare with experiment findings on velocity 3 m/s, maximum points decreased in displacement (mm). Whilst for percentage decrement of design 1 (D3001-E) towards design 2 (D3002-E) was -14.9%. For percentage decrement of design 2 (D3002-E) towards design 3 (D3003-E) was -44.5%. However, percentage average of design 1 towards design 2 decreased by -26.4%. Whilst, for the average value of design 2 towards design 3 decreased by -45.4%.

Simulation values of maximum points for 4 m/s decreased in displacement (mm). Decrement of percentage of design 1 (D4001-S) against design 2 (D4002-S) was -24.3%. For percentage decrement of design 2 (D4002-S) against design 3 (D4003-S) was -17.5%. Whilst, for the average values, decreased by -29.8% then decreased by -22.0% for velocity 4 m/s. To compare with experiment findings on velocity 4 m/s, maximum points decreased in displacement (mm). Whilst for percentage decrement of design 1 (D4001-E) towards design 2 (D4002-E) was -21.6%. For percentage decrement of design 2 (D4002-E) towards design 3 (D4003-E) was -16.4%. However, percentage average of design 1 towards design 2 decreased by -28.4%. Whilst, for the average value of design 2 based on design 3 decreased by -26.2%.

Figure 5-8 and Figure 5-9 shows that the maximum and average points based on Material A, B, and C for the displacement based on simulation and experiment using impact velocity 2 m/s, 3 m/s and 4 m/s. However, it was visible that a decreasing trend for the average points especially for Material B and C (see the blue dotted arrow in Figure 5-8 and Figure 5-9).

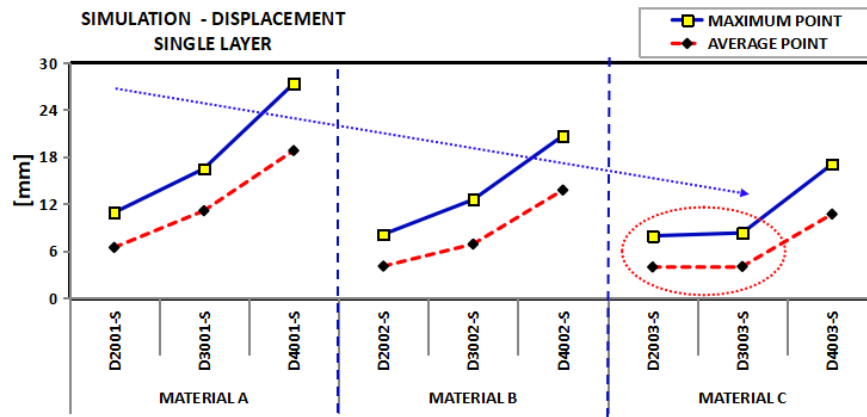


Figure 5-8: Simulation Values of Single Layer Displacement Based on Material

Based from Figure 5-8 Material A, B and C were tested using specified velocities of 2 m/s, 3 m/s and 4 m/s. Observe from the simulation findings, maximum and average points increased as velocity increases. However, there is no significant changes for maximum and average points for Material C when using 2 m/s and 3 m/s (red dotted circle). To summarise, Material C has the lowest displacement values followed by Material B and Material A (blue dotted arrow). Therefore, simulation showed that Material C has lowest displacement value for single layer design configuration.

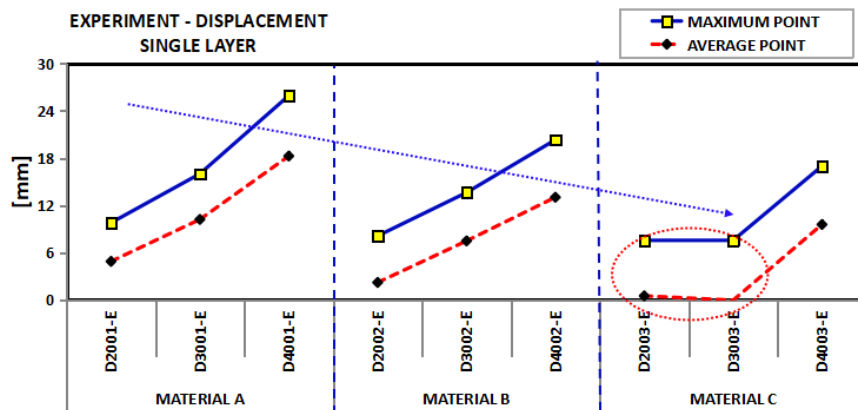


Figure 5-9: Experiment Values of Single Layer Displacement Based on Material

Based from Figure 5-9, Material A, B and C were tested using specified velocities of 2 m/s, 3 m/s and 4 m/s. Observe from the experiment findings, average points increased as velocity increases. However, there is no significant changes for maximum and average points for Material C when using 2 m/s and 3 m/s (red dotted circle). To summarise, Material C has the lowest displacement value followed by Material B and Material A (blue dotted arrow).

To conclude, there were no significant difference between both simulation and experiment. However, the theory from simulation supported by experiment whereby Material C has the lowest displacement value for single layer configuration.

5.2.2 Multiple Layer Foam Configuration

5.2.2.1 The Acceleration Analysis of Multiple Layer Foam Configuration

Table 5-9 shows acceleration in multiple layer design configuration of both experiment and simulation. The difference of maximum point and average point were classified clearly using percentage difference. The percentage differences are calculated based on maximum and average points of acceleration (g) for Material BBB vs. AAA, and CCC vs. BBB. For example, the percentage differences for maximum point of Material BBB (66.1 g) vs. AAA (34.36 g) is 31.72 g. This percentage differences are 92.3% (Material B compared to Material A). This method is also used

to calculate the percentage difference of Material CCC vs. BBB.

Simulation values of maximum points for 2 m/s increased in acceleration (g). Increment of percentage of design 4 (A2004-S) against design 5 (A2005-S) was 92.3%. For percentage increment of design 5 (A2005-S) against design 6 (A2006-S) was 17.2%. Whilst, for the average values, the trend aligned equally between all design about 0% for velocity 2 m/s. To compare with experiment findings on velocity 2 m/s, maximum points increased in acceleration (g). Whilst for percentage increment of design 4 (A2004-E) towards design 5 (A2005-E) was 95.2%. For percentage increment of design 5 (A2005-E) towards design 6 (A2006-E) was 17.0%. However, percentage average of design 4 towards design 5 increased by 103.6%. Whilst, for the average value of design 5 towards design 6 increased by 15.0%.

Table 5-9: Acceleration Multiple Layer Percentage Difference (Simulation and Experiment)

SIMULATION - ACCELERATION [SINGLE LAYER] [in Acceleration (g)]									
IMPACT VELOCITY	2 m/s			3 m/s			4 m/s		
MATERIAL DESIGN	AAA	BBB	CCC	AAA	BBB	CCC	AAA	BBB	CCC
	A2004-S	A2005-S	A2006-S	A3004-S	A3005-S	A3006-S	A4004-S	A4005-S	A4006-S
MAXIMUM POINT	34.36	66.07	77.42	35.29	68.93	87.46	35.57	69.65	88.37
AVERAGE POINT	8.60	8.60	8.60	12.88	12.89	12.90	17.15	17.18	17.18
Percentage MAX	92.3%	17.2%		95.3%	26.9%		95.8%	26.9%	
Percentage AVE	0.0%	0.0%		0.1%	0.0%		0.1%	0.0%	
EXPERIMENT - ACCELERATION [SINGLE LAYER] [in Acceleration (g)]									
IMPACT VELOCITY	2 m/s			3 m/s			4 m/s		
MATERIAL DESIGN	AAA	BBB	CCC	AAA	BBB	CCC	AAA	BBB	CCC
	A2004-E	A2005-E	A2006-E	A3004-E	A3005-E	A3006-E	A4004-E	A4005-E	A4006-E
MAXIMUM POINT	32.97	64.37	75.30	34.56	65.03	82.12	34.83	67.31	86.06
AVERAGE POINT	14.31	29.14	33.50	19.11	31.81	39.74	19.50	34.70	40.68
Percentage MAX	95.2%	17.0%		88.2%	26.3%		93.2%	27.9%	
Percentage AVE	103.6%	15.0%		73.9%	21.4%		77.9%	17.2%	

Simulation values of maximum points for 3 m/s increased in acceleration (g). Increment of percentage of design 4 (A3004-S) against design 5 (A3005-S) was 95.3%. For percentage increment of design 5 (A3005-S) against design 6 (A3006-S)

was 26.9%. Whilst, for the average values, increased by 0.1% then no increment for velocity 3 m/s. To compare with experiment findings on velocity 3 m/s, maximum points increased in acceleration (g). Whilst for percentage increment of design 4 (A3004-E) towards design 5 (A3005-E) was 88.2%. For percentage increment of design 5 (A3005-E) towards design 6 (A3006-E) was 26.3%. However, percentage average of design 4 towards design 5 increased by 73.9%. Whilst, for the average value of design 5 towards design 6 increased by 21.4%.

Simulation values of maximum points for 4 m/s increased in acceleration (g). Increment of percentage of design 4 (A4004-S) against design 5 (A4005-S) was 95.8%. For percentage increment of design 5 (A4005-S) against design 6 (A4006-S) was 26.9%. Whilst, for the average values, increased by 0.1%, then no increment at velocity 4 m/s. To compare with experiment findings on velocity 4 m/s, maximum points increased in acceleration (g). Whilst for percentage increment of design 4 (A4004-E) towards design 5 (A4005-E) was 93.2%. For percentage increment of design 5 (A4005-E) towards design 6 (A4006-E) was 27.9%. However, percentage average of design 4 towards design 5 increased by 77.9%. Whilst, for the average value of design 5 towards design 6 increased by 17.2%.

Figure 5-10 and Figure 5-11 shows that the maximum and average points based on Material AAA, BBB, and CCC for the acceleration based on simulation and experiment using impact velocity 2 m/s, 3 m/s and 4 m/s. However, it was visible that an increasing trend for the average points especially for Material BBB and CCC (see the blue dotted arrow Figure 5-10 and Figure 5-11).

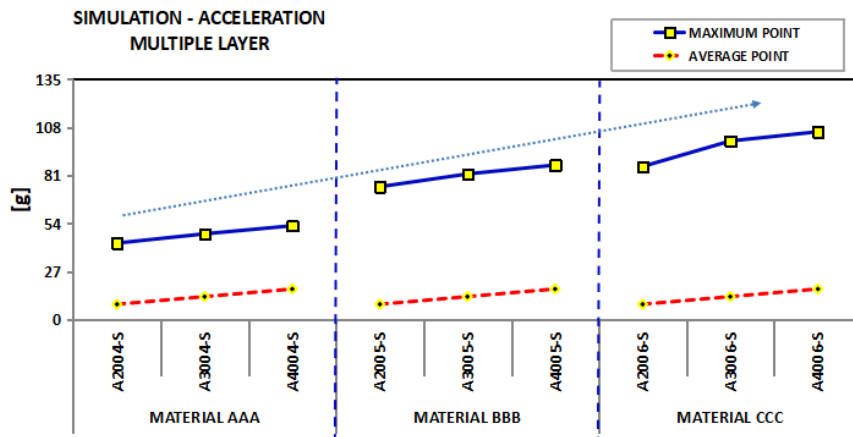


Figure 5-10: Simulation Values of Multiple Layer Acceleration Based on Material

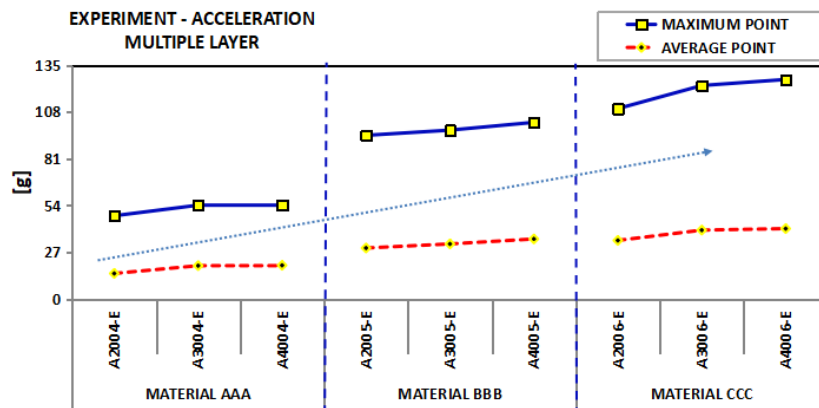


Figure 5-11: Experiment Values of Multiple Layer Acceleration Based on Material

Based from Figure 5-10, Materials AAA, BBB and CCC were tested using specified velocities of 2 m/s, 3 m/s and 4 m/s. Observe from the simulation findings, average points increased as velocity increases. However, there is no significant changes for maximum points in all the materials. To summarise, Material CCC has the highest acceleration (g) values followed by Material BBB and Material CCC. Therefore, simulation shows, Material CCC is highest for multiple layer design configuration.

Based from Figure 5-11, Materials AAA, BBB and CCC were tested using

specified velocities of 2 m/s, 3 m/s and 4 m/s. Observe from the experiment findings, average points increased as velocity increases. However, there is no significant changes for maximum points in all the materials. To summarise, Material CCC has the highest acceleration (g) values followed by Material BBB and Material CCC.

To conclude, there were no significant difference between both simulation and experiment. However, the theory from simulation supported by experiment whereby Material AAA has the lowest g value for multiple layer configuration.

5.2.2.2 The displacement analysis of multiple layer configuration

Table 5-10 shows displacement in multiple layer design configuration of both experiment and simulation. The difference of maximum point and average point were classified clearly using percentage difference. The percentage differences are calculated based on maximum and average points of displacement (mm) for Material BBB vs. AAA, and CCC vs. BBB. For example, the percentage differences for maximum point of Material BBB (10.88 mm) vs. AAA (12.04 mm) is -1.16 mm. This percentage differences are -9.6 % (Material B compared to Material A). This method is also used to calculate the percentage difference of Material CCC vs. BBB.

Simulation values of maximum points for 2 m/s decreased in displacement (mm). Decrement of percentage of design 4 (D2004-S) against design 5 (D2005-S) was -9.6%. For percentage decrement of design 5 (D2005-S) against design 6 (D2006-S) was -14.1%. Whilst, for the average values, it decreased by -11.0% then decreased by -13.0% for velocity 2 m/s. To compare with experiment findings on velocity 2 m/s,

maximum points also decreased in displacement (mm). Whilst for percentage decrement of design 4 (D2004-E) towards design 5 (D2005-E) was -12.1%. For percentage decrement of design 5 (D2005-E) towards design 6 (D2006-E) was -18.5%. However, percentage average of design 4 towards design 5 decreased by -12.2%. Whilst, for the average value of design 5 towards design 6 decreased by -17.7%.

Table 5-10: Displacement Multiple Layer Percentage Difference (Simulation and Experiment)

SIMULATION – DISPLACEMENT [MULTIPLE LAYER] [in mm]									
IMPACT VELOCITY	2 m/s			3 m/s			4 m/s		
MATERIAL DESIGN	AAA	BBB	CCC	AAA	BBB	CCC	AAA	BBB	CCC
	D2004-S	D2005-S	D2006-S	D3004-S	D3005-S	D3006-S	D4004-S	D4005-S	D4006-S
MAXIMUM POINT	12.04	10.88	9.35	19.77	17.54	14.29	30.34	23.01	20.80
AVERAGE POINT	6.03	5.32	4.64	11.35	8.69	6.91	22.89	14.82	12.53
Percentage MAX	-9.6%	-14.1%		-11.3%	-18.6%		-24.2%	-9.6%	
Percentage AVE	-11.0%	-13.0%		-24.7%	-15.8%		-27.6%	-34.3%	
EXPERIMENT – DISPLACEMENT [MULTIPLE LAYER] [in mm]									
IMPACT VELOCITY	2 m/s			3 m/s			4 m/s		
MATERIAL DESIGN	AAA	BBB	CCC	AAA	BBB	CCC	AAA	BBB	CCC
	D2004-E	D2005-E	D2006-E	D3004-E	D3005-E	D3006-E	D4004-E	D4005-E	D4006-E
MAXIMUM POINT	11.68	10.27	8.37	18.73	15.81	14.66	28.46	21.31	18.99
AVERAGE POINT	5.53	2.85	-0.65	11.92	8.09	5.00	19.98	12.58	9.68
Percentage MAX	-12.1%	-18.5%		-15.6%	-7.3%		-25.1%	-10.9%	
Percentage AVE	-12.2%	-17.7%		-27.4%	-9.6%		-36.8%	-20.3%	

Simulation values of maximum points for 3 m/s decreased in displacement (mm). Decrement of percentage of design 4 (D3004-S) against design 5 (D3005-S) was -11.3%. For percentage decrement of design 5 (D3005-S) against design 6 (D3006-S) was -18.6%. Whilst, for the average values, decreased by -24.7% then decreased by -15.8% for velocity 3 m/s. To compare with experiment findings on velocity 3 m/s, maximum points decreased in displacement (mm). Whilst for percentage decrement of design 4 towards design 5 was -15.6%. For percentage decrement of design 5 towards design 6 was -7.3%. However, percentage average of design 4 towards design 5 decreased by -27.4%. Whilst, for the average value of design 5 towards design 6 decreased by -9.6%.

Simulation values of maximum points for 4 m/s decreased in displacement (mm). Decrement of percentage of design 4 (D4004-S) against design 5 (D4005-S) was -24.2%. For percentage decrement of design 5 (D4005-S) against design 6 (D4006-S) was -9.6%. Whilst, for the average values, decreased by -27.6%, then decreased by -34.3% for velocity 4 m/s. To compare with experiment findings on velocity 4 m/s, maximum points decreased in displacement (mm). Whilst for percentage decrement of design 4 (D4004-E) towards design 5 (D4005-E) was -25.1%. For percentage decrement of design 5 (D4005-E) towards design 6 (D4006-E) was -10.9%. However, percentage average of design 4 towards design 5 decreased by -36.8%. Whilst, for the average value of design 5 towards design 6 decreased by -20.3%.

Figure 5-12 and Figure 5-13 shows that the maximum and average points based on Material AAA, BBB, and CCC for the displacement based on simulation and experiment using impact velocity 2 m/s, 3 m/s and 4 m/s. However, it was visible, that a decreasing trend for the average points especially for Material BBB and CCC (see the blue dotted arrow Figure 5-12 and Figure 5-13).

Based from Figure 5-12 and Figure 5-13, Materials AAA, BBB and CCC were tested using specified velocities of 2 m/s, 3 m/s and 4 m/s. Observe from the experiment findings, average point increases as velocity increase. Hence, the maximum points also increase. To summarise, Material CCC has lowest mm values followed by Material B and Material C.

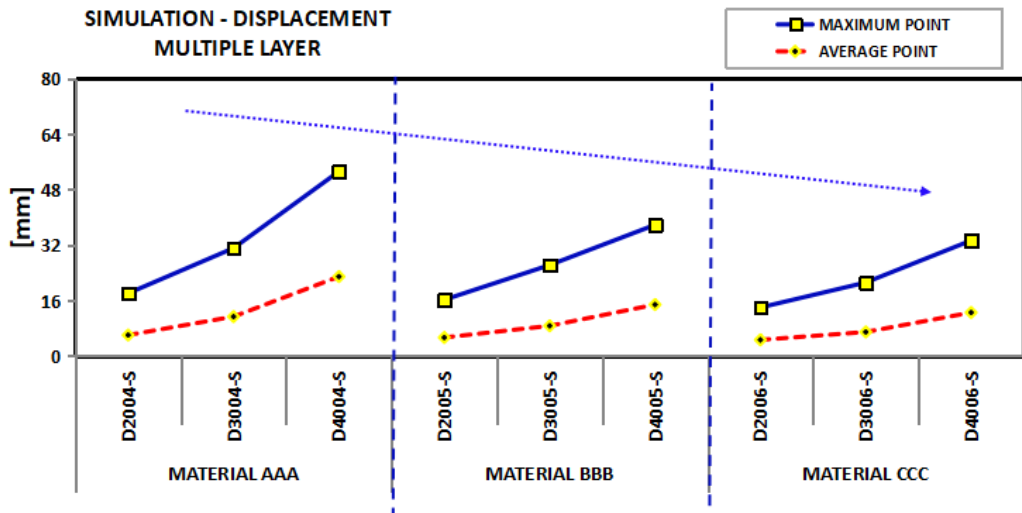


Figure 5-12: Simulation Values of Multiple Layer Displacement Based on Material

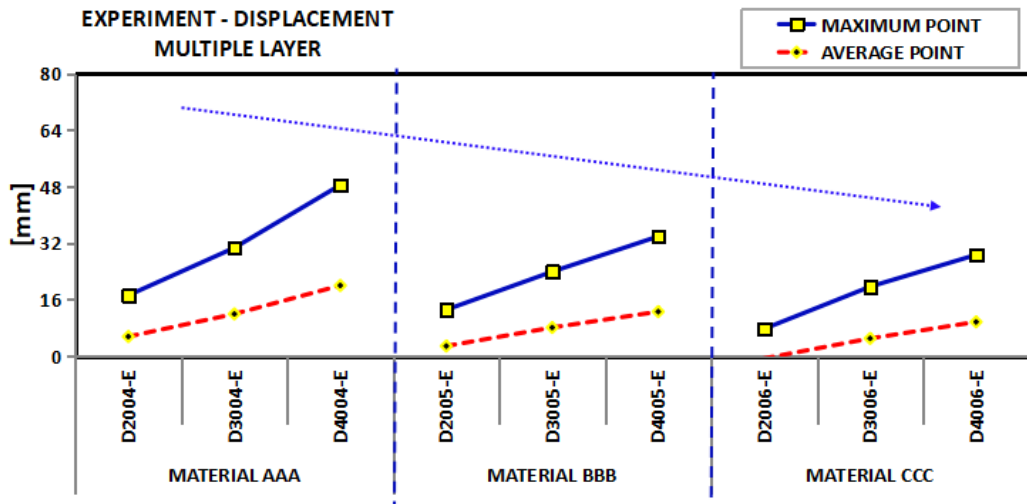


Figure 5-13: Experiment Values of Multiple Layer Displacement Based on Material

To conclude, there were no significant difference between both simulation and experiment. However, the theory from simulation supported by experiment whereby Material CCC has the lowest mm value for single layer configuration.

5.2.3 Combination (Hybrid) Layer Foam Configuration

5.2.3.1 The acceleration analysis of combination (hybrid) layer configuration

Table 5-11 show the data related to the simulation and experiment of combination layer (hybrid) material configuration. The percentage differences are calculated based on maximum and average points of acceleration (g) for Material CAB vs. ABC, BCA vs. CAB, CBA vs. BCA, BAC vs. CBA and ACB vs. BAC. For example, the percentage differences for maximum point of Material CAB (35.56 g) vs. ABC (35.64 g) is -0.08 g. This percentage differences are -0.2 % (Material CAB compared to Material ABC). This method is also used to calculate the percentage difference of Material BCA vs. CAB, CBA vs. BCA, BAC vs. CBA and ACB vs. BAC.

Table 5-11: Acceleration Combination Layer Percentage Difference (Simulation and Experiment)

SIMULATION - ACCELERATION [COMBINATION LAYER] [in Acceleration (g)]																		
IMPACT VELOCITY	2 m/s						3 m/s						4 m/s					
MATERIAL DESIGN	ABC	CAB	BCA	CBA	BAC	ACB	ABC	CAB	BCA	CBA	BAC	ACB	ABC	CAB	BCA	CBA	BAC	ACB
	A2007-S	A2008-S	A2009-S	A2010-S	A2011-S	A2012-S	A3007-S	A3008-S	A3009-S	A3010-S	A3011-S	A3012-S	A4007-S	A4008-S	A4009-S	A4010-S	A4011-S	A4012-S
MAXIMUM POINT	35.64	35.56	35.54	35.50	35.56	35.64	36.36	36.31	36.53	36.31	36.31	36.36	36.98	36.95	37.01	37.34	36.95	36.98
AVERAGE POINT	8.57	8.57	8.57	8.57	8.57	8.57	12.80	12.80	12.80	12.80	12.80	12.80	16.99	16.99	16.99	16.99	16.99	16.99
Percentage MAX	-0.2%	0.0%	-0.1%	0.2%	0.2%		-0.1%	0.6%	-0.6%	0.0%	0.1%		-0.1%	0.2%	0.9%	-1.0%	0.1%	
Percentage AVE	0.0%	0.0%	0.0%	0.0%	0.0%		0.0%	0.0%	0.0%	0.0%	0.0%		0.0%	0.0%	0.0%	0.0%	0.0%	
EXPERIMENT - ACCELERATION [COMBINATION LAYER] [in Acceleration (g)]																		
IMPACT VELOCITY	2 m/s						3 m/s						4 m/s					
MATERIAL DESIGN	ABC	CAB	BCA	CBA	BAC	ACB	ABC	CAB	BCA	CBA	BAC	ACB	ABC	CAB	BCA	CBA	BAC	ACB
	A2007-E	A2008-E	A2009-E	A2010-E	A2011-E	A2012-E	A3007-E	A3008-E	A3009-E	A3010-E	A3011-E	A3012-E	A4007-E	A4008-E	A4009-E	A4010-E	A4011-E	A4012-E
MAXIMUM POINT	34.41	35.50	34.50	34.09	35.94	36.35	34.61	35.68	36.22	36.47	36.71	35.47	36.13	35.64	36.49	37.51	37.60	35.92
AVERAGE POINT	14.39	17.04	17.36	17.65	17.12	17.34	17.80	19.13	20.39	16.50	15.55	16.64	19.16	21.91	19.92	19.91	22.17	20.62
Percentage MAX	3.1%	-2.8%	-1.2%	5.4%	1.1%		3.1%	1.5%	0.7%	0.7%	-3.4%		-1.4%	2.4%	2.8%	0.2%	-4.5%	
Percentage AVE	18.4%	1.7%	0.5%	-3.0%	2.3%		19.8%	5.4%	-19.1%	-6.7%	8.2%		-2.8%	-9.1%	3.4%	7.6%	-3.3%	

Based on Figure 5-14, the study showed that the maximum and average acceleration values for all combined materials were in same trend. This is consistent when the research applies 2 m/s, 3 m/s, and 4 m/s of impact velocity. Also, the research found in simulation that the maximum and average values between the 2 m/s, 3 m/s and 4 m/s impact in the same trend. In simulation, the maximum and average values at 2 m/s was lower than 3 m/s impact velocity.

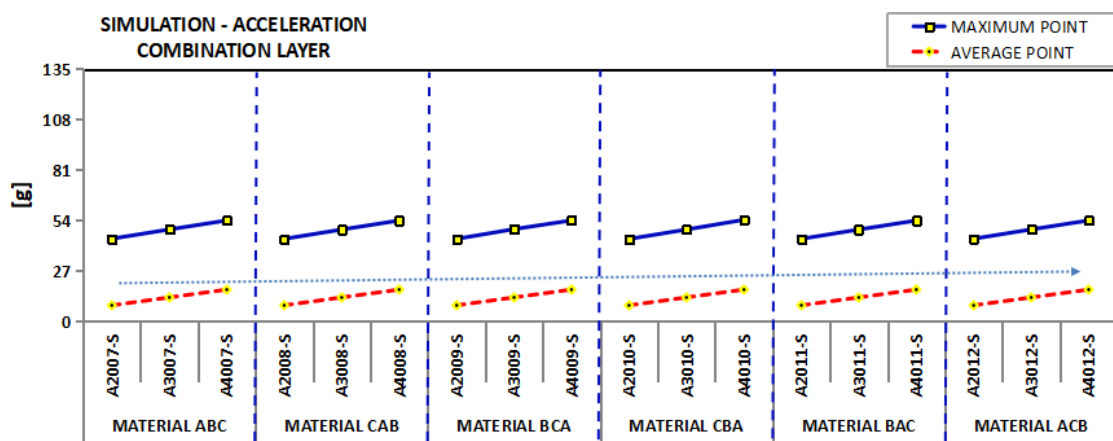


Figure 5-14: Simulation Values of Combination Layer (Hybrid) Acceleration Based on Material

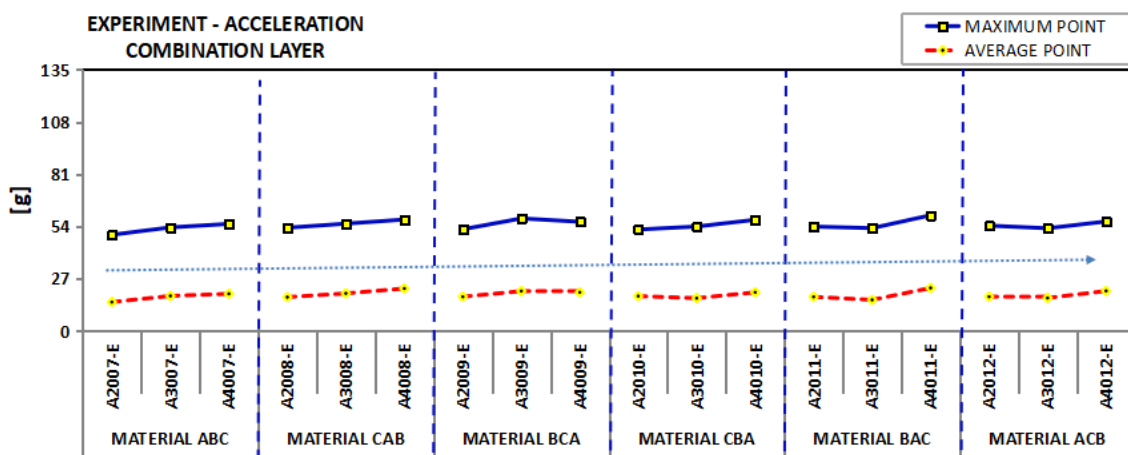


Figure 5-15: Experiment Values of Combination Layer (Hybrid) Acceleration Based on Material

Furthermore, Figure 5-14 and Figure 5-15 shows an increasing trend from 2 m/s to 4 m/s. This increasing trend applies to all configuration of combination or hybrid layer.

To conclude, there were no significant difference between both simulation and experiment. However, theory from simulation supported by experiment whereby the difference is not much of a different.

5.2.3.2 The displacement analysis of combination (hybrid) layer configuration

Table 5-12 shows displacement in combination layer design of both experiment and simulation. The difference of maximum point and average point were classified clearly using percentage difference. The percentage differences are calculated based on maximum and average points of displacement (mm) for Material CAB vs. ABC, BCA vs. CAB, CBA vs. BCA, BAC vs. CBA and ACB vs. BAC. For example, the percentage differences for maximum point of Material CAB (12.05 mm) vs. ABC (12.83 mm) is -0.78 mm. This percentage differences are -6.1 % (Material CAB compared to Material ABC). This method is also used to calculate the percentage difference of Material BCA vs. CAB, CBA vs. BCA, BAC vs. CBA and ACB vs. BAC.

Table 5-12: Displacement Combination Layer Percentage Difference (Simulation and Experiment)

SIMULATION - DISPLACEMENT [COMBINATION LAYER] [in mm]																		
IMPACT VELOCITY	2 m/s						3 m/s						4 m/s					
MATERIAL DESIGN	ABC	CAB	BCA	CBA	BAC	ACB	ABC	CAB	BCA	CBA	BAC	ACB	ABC	CAB	BCA	CBA	BAC	ACB
	A2007-S	A2008-S	A2009-S	A2010-S	A2011-S	A2012-S	A3007-S	A3008-S	A3009-S	A3010-S	A3011-S	A3012-S	A4007-S	A4008-S	A4009-S	A4010-S	A4011-S	A4012-S
MAXIMUM POINT	12.83	12.05	11.49	10.10	10.82	11.31	17.29	20.21	16.61	21.10	18.09	19.51	25.98	27.49	29.09	29.84	28.63	30.22
AVERAGE POINT	6.50	5.87	5.74	5.16	5.27	5.29	9.07	10.90	8.89	11.13	9.70	10.08	18.03	19.06	21.17	21.10	20.35	23.17
Percentage MAX	-6.1%	-4.6%	-12.1%	7.1%	4.5%		16.9%	-17.8%	27.0%	-14.2%	7.8%		5.8%	5.8%	2.6%	-4.0%	5.5%	
Percentage AVE	-9.8%	-2.2%	-10.1%	3.1%	0.2%		18.5%	-17.8%	24.7%	-7.3%	3.7%		5.7%	11.1%	-0.3%	-3.5%	13.8%	

EXPERIMENT - DISPLACEMENT [COMBINATION LAYER] [in mm]																		
IMPACT VELOCITY	2 m/s						3 m/s						4 m/s					
MATERIAL DESIGN	ABC	CAB	BCA	CBA	BAC	ACB	ABC	CAB	BCA	CBA	BAC	ACB	ABC	CAB	BCA	CBA	BAC	ACB
	A2007-E	A2008-E	A2009-E	A2010-E	A2011-E	A2012-E	A3007-E	A3008-E	A3009-E	A3010-E	A3011-E	A3012-E	A4007-E	A4008-E	A4009-E	A4010-E	A4011-E	A4012-E
MAXIMUM POINT	12.31	11.37	11.31	9.64	10.33	10.92	15.78	18.37	15.78	19.79	17.54	18.36	25.45	25.43	26.96	27.94	26.74	28.88
AVERAGE POINT	6.02	5.04	5.49	3.51	4.58	4.69	9.22	12.07	9.14	13.19	11.26	11.71	17.90	17.63	18.91	19.29	18.52	20.48
Percentage MAX	-7.6%	-0.6%	-14.8%	7.2%	5.7%		16.4%	-14.1%	25.4%	-11.4%	4.7%		-0.1%	6.0%	3.6%	-4.3%	8.0%	
Percentage AVE	-6.9%	-1.8%	-13.2%	5.6%	6.2%		30.4%	-24.0%	46.8%	-16.3%	3.9%		-1.5%	7.2%	2.0%	-4.0%	10.5%	

Figure 5-16 and Figure 5-17 shows increasing trend of the displacement maximum values for the simulation and experiment in tested velocity from 2 m/s to 3 m/s and 3 m/s to 4 m/s. The result was however, slightly aligned between the combination layer, especially for 2 m/s and 4 m/s (see the blue dotted arrow).

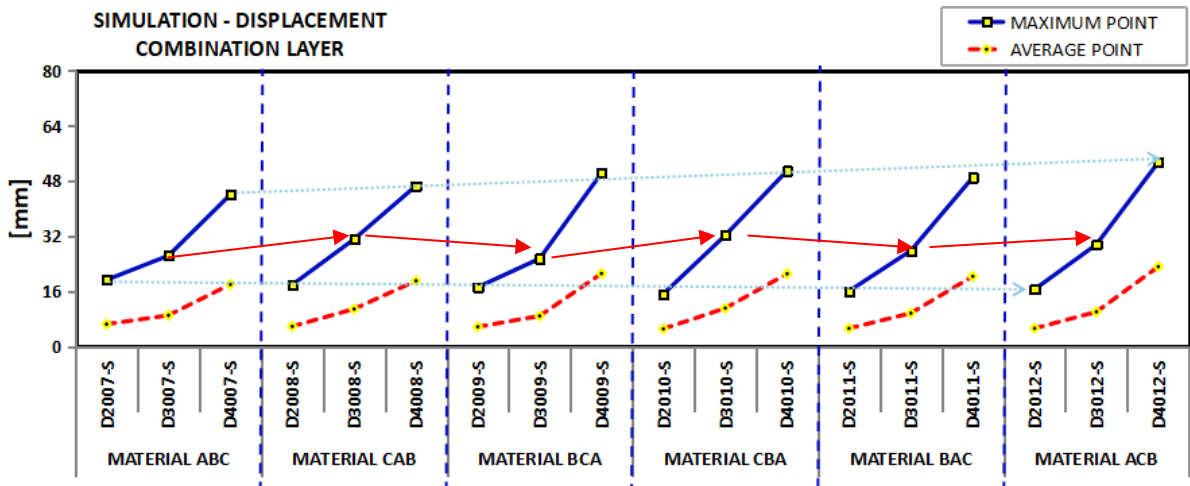


Figure 5-16: Simulation Values of Combination Layer (Hybrid) Displacement Based on Material.

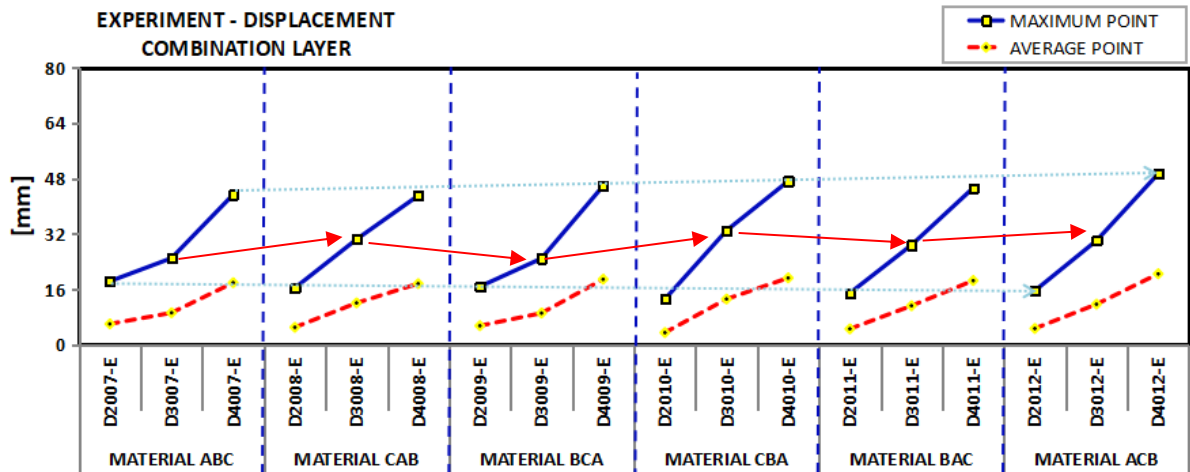


Figure 5-17: Experiment Values of Combination Layer (Hybrid) Displacement Based on Material

5.2.4 Summary of Flat Foam Design Based on Layer Configuration

Based on the experiment and simulation conducted, this research found that the maximum and average values of acceleration increased from A to C. It decreased for the maximum and average values of displacement. Differently, single layer and the multiple design result mirrors each other in terms of acceleration and displacement behaviour.

It showed that material configuration AAA (or design no.4) as a reflection of material configuration A (or design no 1) and material configuration BBB (or design no.5) as a reflection of material configuration B (or design no.2). In addition, material configuration CCC (or design no. 6) as a reflection of material configuration C (or design no 3).

Moreover, the material characteristic for the displacement (based on the experiments and simulations conducted) contradicted to acceleration. However, the characteristic of the combination layer (hybrid) material for the acceleration and

displacement showing slightly aligned trend, especially for 2 m/s and 4 m/s based on material configuration (Figure 5-16 and Figure 5-17) (blue dotted arrow). The interesting information to be noted are the maximum values of each combination layer (hybrid) were highly fluctuated compared to one another for velocity 3 m/s (in Figure 5-16 and Figure 5-17- red arrow lines).

As a remark, this study is necessary to enable the consideration of average values and standard deviations to evaluate material characteristic. Later, this would become useful on providing valuable information for statistical calculation in choosing the best design according to displacement and acceleration.

The average and maximum values of the combination layer materials based on displacement showed clear differences (fluctuated) when using 3 m/s impact velocity. This value however, will decrease for the impact velocity of 2 m/s and increases when impact velocity of 4 m/s introduced or applied. Hence, objective 2 were reflected in this portion of analysis.

5.3 Analysis of Foam Design Based on Impact Velocity

This section discusses foam configurations based on specified impact velocity at 2 m/s, 3 m/s and 4 m/s. The parameters that were looked into is the analysis of acceleration and displacement of all foam layer configuration.

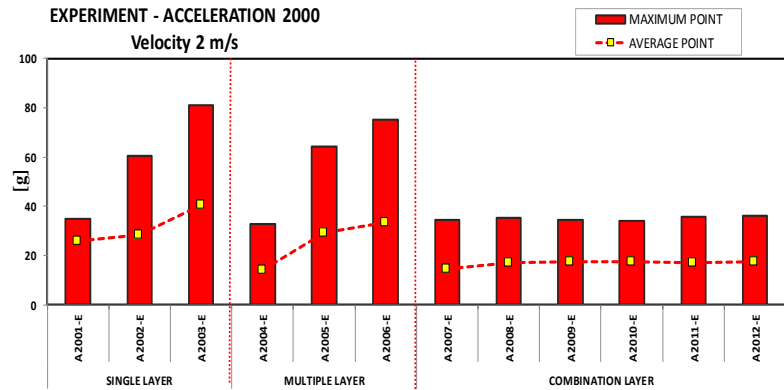
5.3.1 Impact Velocity Analysis at 2 m/s

In general, all material configurations were discussed based on acceleration and displacement value towards specified velocity 2 m/s as shown in Figure 5-18 (acceleration) and Figure 5-19 (displacement). Figure 5-18 consist of acceleration based on impact velocity at 2 m/s. Figure 5-18(a) shows experimental findings and Figure 5-18(b) shows simulation findings. Lastly, Figure 5-18(c) shows comparison between simulation and experimental values based on acceleration (g) parameter.

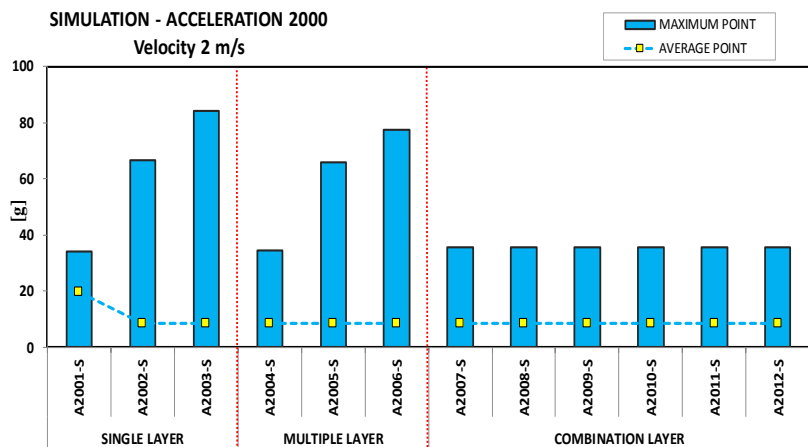
For Figure 5-18(a), three material configurations were compared experimentally. For single layer configurations, average and maximum points increased. Multiple layer configurations were similar to single layer whereby, average and maximum points also increased. Material configuration of combination (hybrid) layer shows that all maximum and average points were almost aligned.

For Figure 5-18(b), three material configurations were compared through simulation. For single layer configurations, average points decreased, but as for maximum points, the acceleration (g) values increased. The values differences between average points of experiment and simulation were influenced by the fluctuating point plotted in the experiment. Where, the range of data collected were determined by defined tolerance (Appendix E). For multiple layer configurations, maximum points increased significantly. In contrary, all the points for average values were aligned. Lastly, material configurations of combination (hybrid) layer shows that all maximum and average points were almost aligned.

(a)
Experiment – Acceleration
2 m/s



(b)
Simulation – Acceleration
2 m/s



(c)
Comparison of maximum
point – Acceleration
2 m/s

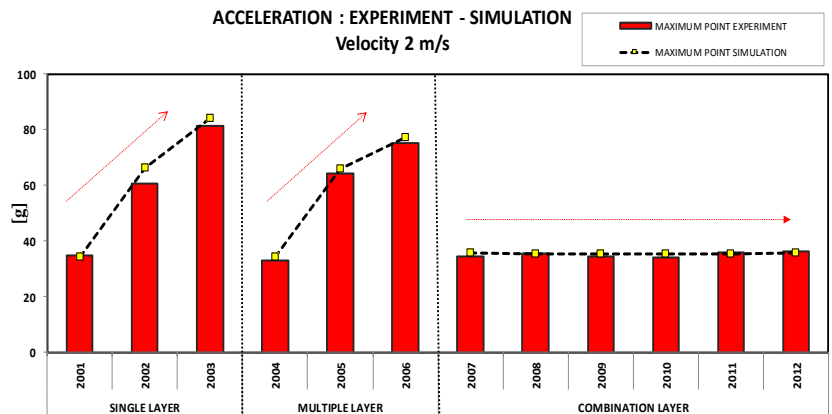


Figure 5-18: Maximum and Average Point of Acceleration Based on Velocity 2 m/s.
(a) Experiment; (b) Simulation; (c) Comparison of Maximum Point

For Figure 5-18(c), three material configurations were discussed through comparison between experiment and simulation. The comparison was observed using trend which refers to maximum points. For single layer configurations, both simulation

and experiment shows maximum points increased significantly. Multiple layer configurations were similar as single layer whereby, all maximum points increased significantly. Lastly, material configurations of combination (hybrid) layer shows that all maximum and average points were aligned.

Next discussion is based on displacement value towards specified velocity 2 m/s, shown in Figure 5-19 (displacement). Figure 5-19 consist of displacement values based on impact velocity at 2 m/s. For Figure 5-19(a) shows experimental findings and Figure 5-19(b) shows simulation findings. Lastly, Figure 5-19(c) shows the comparison between simulation and experiment based on displacement parameter.

For Figure 5-19(a), three material configurations were compared experimentally. For single layer configurations, average and maximum points decreased more than simulation findings. Multiple layer configurations were similar as single layer whereby, average and maximum points decreased compare to simulation. Lastly, material configurations of combination (hybrid) layer shows that all maximum and average points were not aligned.

For Figure 5-19(b), three material configurations were compared through simulation. For single layer configurations, average and maximum points decreased. The values differences between average points of experiment and simulation were influenced by the fluctuating point plotted in the experiment. Where, the range of data collected were determined by defined tolerance (Appendix E). Multiple layer configurations were similar as single layer whereby average and maximum points decreased significantly. Lastly, material configurations of combination (hybrid) layer

shows that all maximum and average points were not aligned.

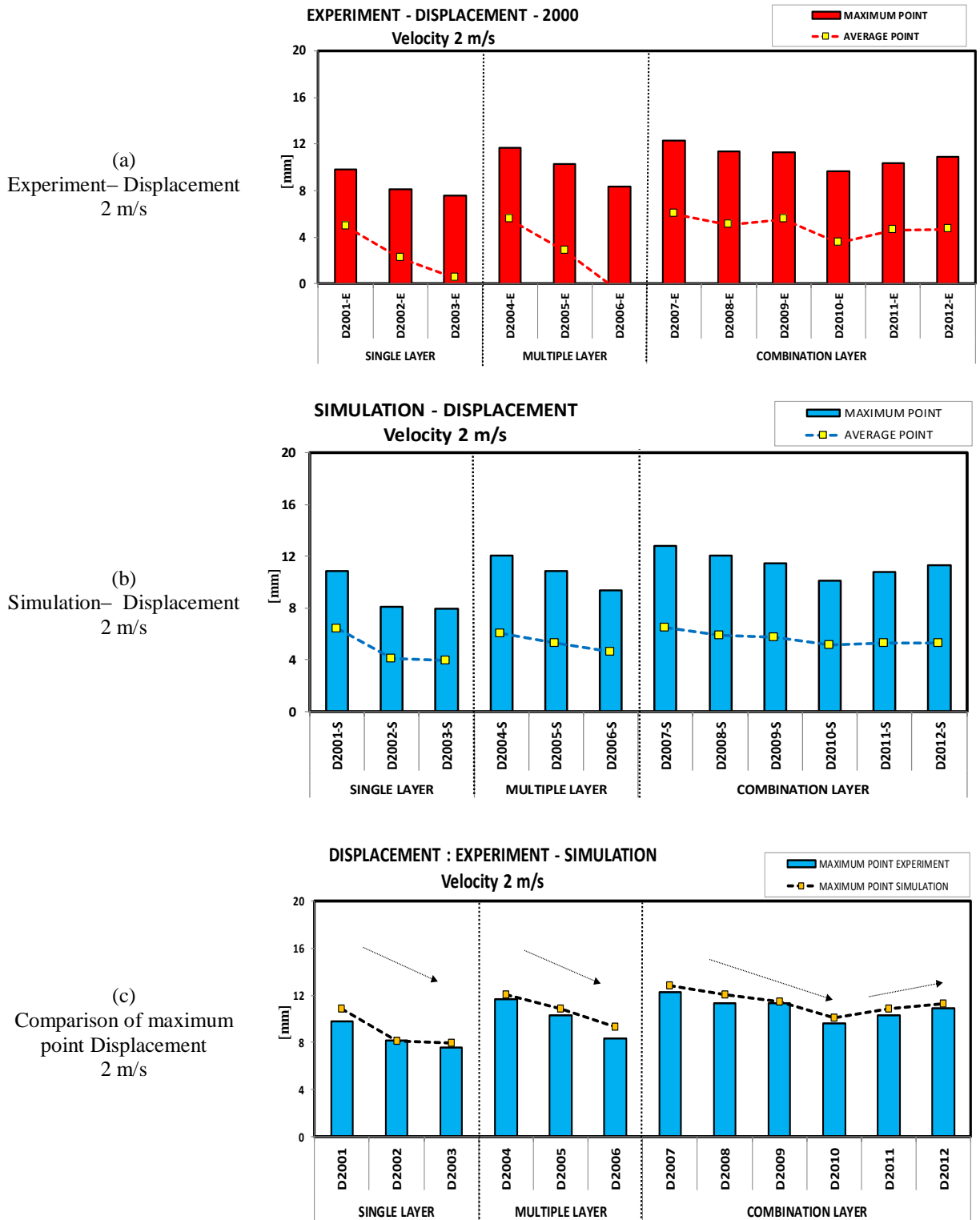


Figure 5-19: Maximum and Average Point of Displacement Based on Velocity 2 m/s. (a) Experiment; (b) Simulation; (c) Comparison of Maximum Point.

For Figure 5-19(c), three material configurations were discussed through comparison between experiment and simulation. The comparison were observed using trend which refers to maximum points. For single layer configurations, maximum points of simulation and experiment decreased significantly. Multiple layer configurations were similar as single layer whereby all maximum points decreased significantly. Lastly, all the maximum points of the experiment and simulation for combination (hybrid) were not aligned, especially design D2010. Maximum point for D2010 is lowest in displacement value.

Table 5-13: The Combination/Hybrid Layer Result of 2 m/s Impact Velocity

2007	2008	2009	2010	2011	2012
A	C	B	C	B	A
B	A	C	B	A	C
C	B	A	A	C	B

Based from previous comparison on acceleration and displacement, Table 5-13 shows summary of maximum point trends for hybrid layer. This is due to single and multiple layer have same maximum point trends that contradict between acceleration and displacement. Hence, single and multiple layer were excluded in this table. This table shows Material A gives huge impact towards material combination. To obtain highest optimisation, Material A should be placed lowest compared to Material B and C.

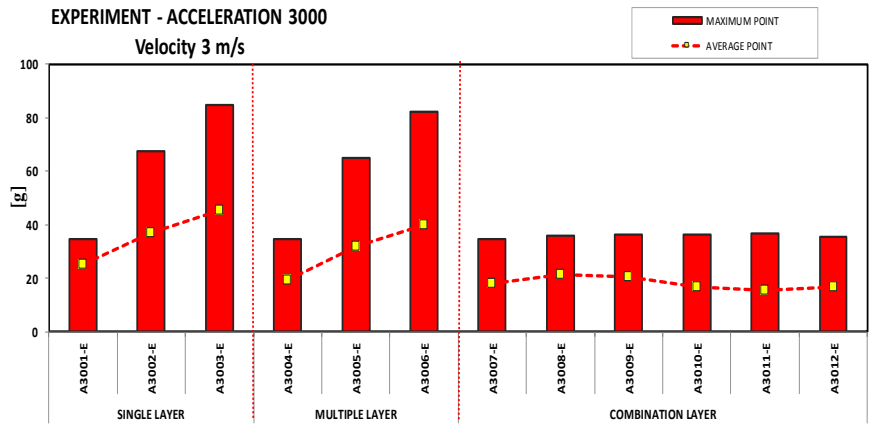
5.3.2 Impact Velocity Analysis at 3 m/s

In general, all material configurations were discussed based on acceleration and displacement values towards specified velocity 3 m/s as shown in Figure 5-20 (acceleration) and Figure 5-21 (displacement). Figure 5-20 consist of acceleration values based on impact velocity at 3 m/s. Figure 5-20(a) shows experimental findings and Figure 5-20(b) shows simulation findings. Lastly, Figure 5-20(c) shows the comparison between simulation and experiment based on acceleration parameter.

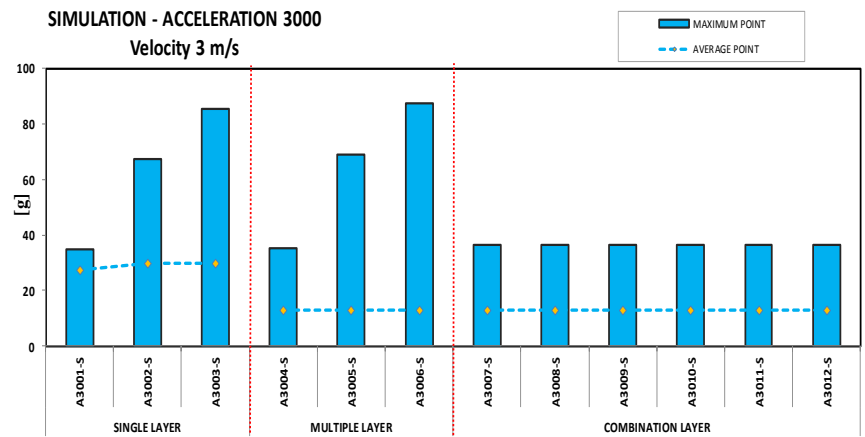
For Figure 5-20(a), three material configurations were compared using simulation. For single layer configuration, average and maximum points increased significantly. Multiple layer configurations were similar to single layer whereby average and maximum point also increased. Lastly, material configurations of combination (hybrid) layer shows that all maximum and average points were almost aligned.

For Figure 5-20 (b), three material configurations were compared experimentally. For single layer configurations, average points almost aligned, but as for maximum point, the acceleration (g) value increased. The values differences between average points of experiment and simulation were influenced by the fluctuating point plotted in the experiment. Where, the range of data collected were determined by defined tolerance (Appendix E). For multiple layer configurations, maximum points increased significantly. However, average points were aligned. Lastly, material configurations of combination (hybrid) layer shows that all maximum and average points were aligned.

(a)
Experiment – Acceleration
3 m/s



(b)
Simulation – Acceleration
3 m/s



(c)
Comparison of maximum
point – Acceleration
3 m/s

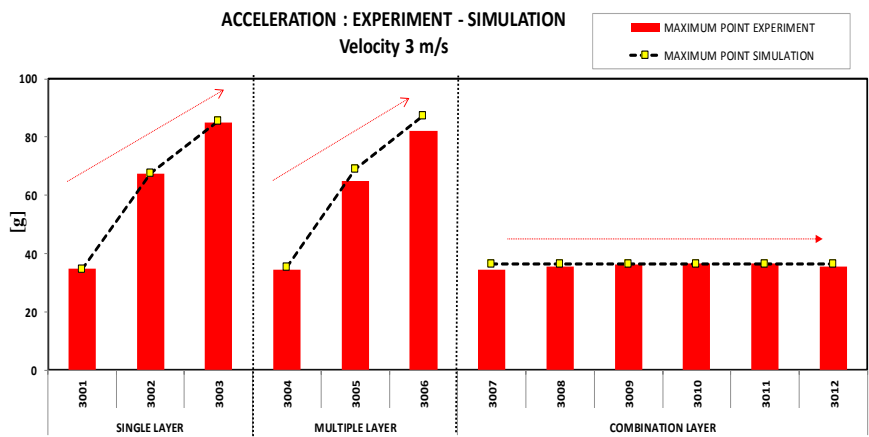


Figure 5-20: Maximum and Average Point of Acceleration Based on Velocity 3 m/s.
(a) Experiment; (b) Simulation; (c) Comparison of Maximum Point.

For Figure 5-20(c), three material configurations were discussed through comparison of experiment and simulation. The comparison was observed using trend referring to maximum points. For single layer configurations, both simulation and

experiment shows maximum points increased significantly. Multiple layer configurations were similar as single layer whereby, all maximum points increased significantly. Lastly, material configurations of combination (hybrid) layer shows all of maximum points were equally aligned.

Next discussion is on displacement value towards specified velocity 3 m/s, shown in Figure 5-21 (displacement). Figure 5-21 consist of displacement values based on impact velocity at 2 m/s. Figure 5-21(a) shows experimental findings and Figure 5-21(b) shows simulation findings. Lastly, Figure 5-21(c) shows the comparison between simulation and experiment based on displacement parameter.

For Figure 5-21(a), three material configurations were compared using simulation. For single layer configurations, average and maximum points decreased significantly. The configurations of multiple layer were similar to single layer configurations where the average and maximum points decreased significantly. Lastly, combination (hybrid) layer shows that all maximum and average points were fluctuating for all material configurations.

For Figure 5-21(b), three material configurations were compared experimentally. For single layer configurations, average and maximum points decreased significantly. The configurations of multiple layer were similar to single layer configurations where the average and maximum points decreased significantly. Lastly, combination (hybrid) layer shows that all maximum and average points were fluctuating for material configurations.

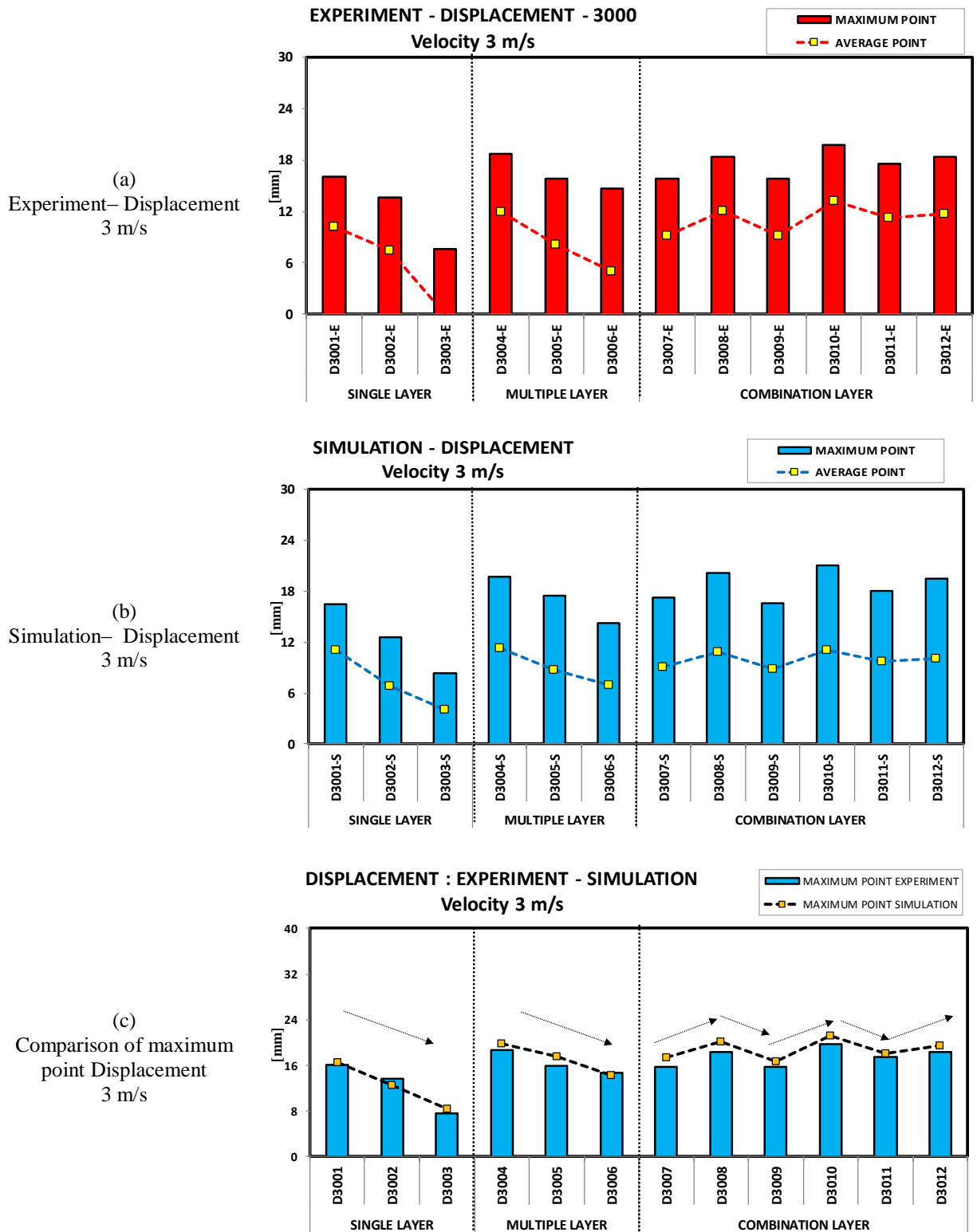


Figure 5-21: Maximum and Average Point of Displacement Based on Velocity 3 m/s.
(a) Experiment; (b) Simulation; (c) Comparison of Maximum Point.

For Figure 5-21(c), three material configurations were discussed through comparison of experiment and simulation. The comparison was observed using trend referring to maximum points. For single layer configuration, both simulation and experiment shows maximum points decreased significantly. Multiple layer configurations were similar as single layer whereby, all maximum points decreased significantly. Combination (hybrid) layer shows maximum points throughout all design configuration. Lowest displacement value is for design D3007 and highest maximum value is design D3010.

Based from previous comparison on acceleration and displacement, Table 5-14 shows summary of maximum point trends for hybrid layer. This is due to single and multiple layer have same maximum point trends that contradict between acceleration and displacement. Hence, single and multiple layer were excluded in this table. This table shows Material B gives huge impact towards material combination. To obtain highest optimisation, Material B should be placed middle or top position compared to Material A and C in term of both parameters acceleration and displacement.

Table 5-14: The Combination/Hybrid Layer Result of 3 m/s Impact Velocity

3007	3008	3009	3010	3011	3012
A	C	B	C	B	A
B	A	C	B	A	C
C	B	A	A	C	B

5.3.3 Impact Velocity Analysis at 4 m/s

In general, all material configurations were discussed based on acceleration and displacement value towards specified velocity 4 m/s as shown in Figure 5-22 (acceleration) and Figure 5-23 (displacement). Figure 5-22 consist of acceleration based on impact velocity at 4 m/s. Figure 5-22(a) shows experimental findings and Figure 5-22(b) shows simulation findings and Figure 5-22(c) shows the comparison between simulation and experiment based on acceleration parameter.

For Figure 5-22(a), three material configurations were compared using simulation. For single layer configurations, average and maximum points increased. The configurations of multiple layer were similar to single layer configurations where maximum and average points increased. Lastly, material configuration of combination (hybrid) layer shows that all maximum and average points were almost aligned.

For Figure 5-22(b), three material configurations were compared experimentally. For single layer configurations, average points increased slightly however maximum points increased significantly. For multiple layer configuration, maximum point increased significantly and for average values, all the points were aligned. Lastly, material configurations of combination (hybrid) layer shows that all maximum and average points were aligned.

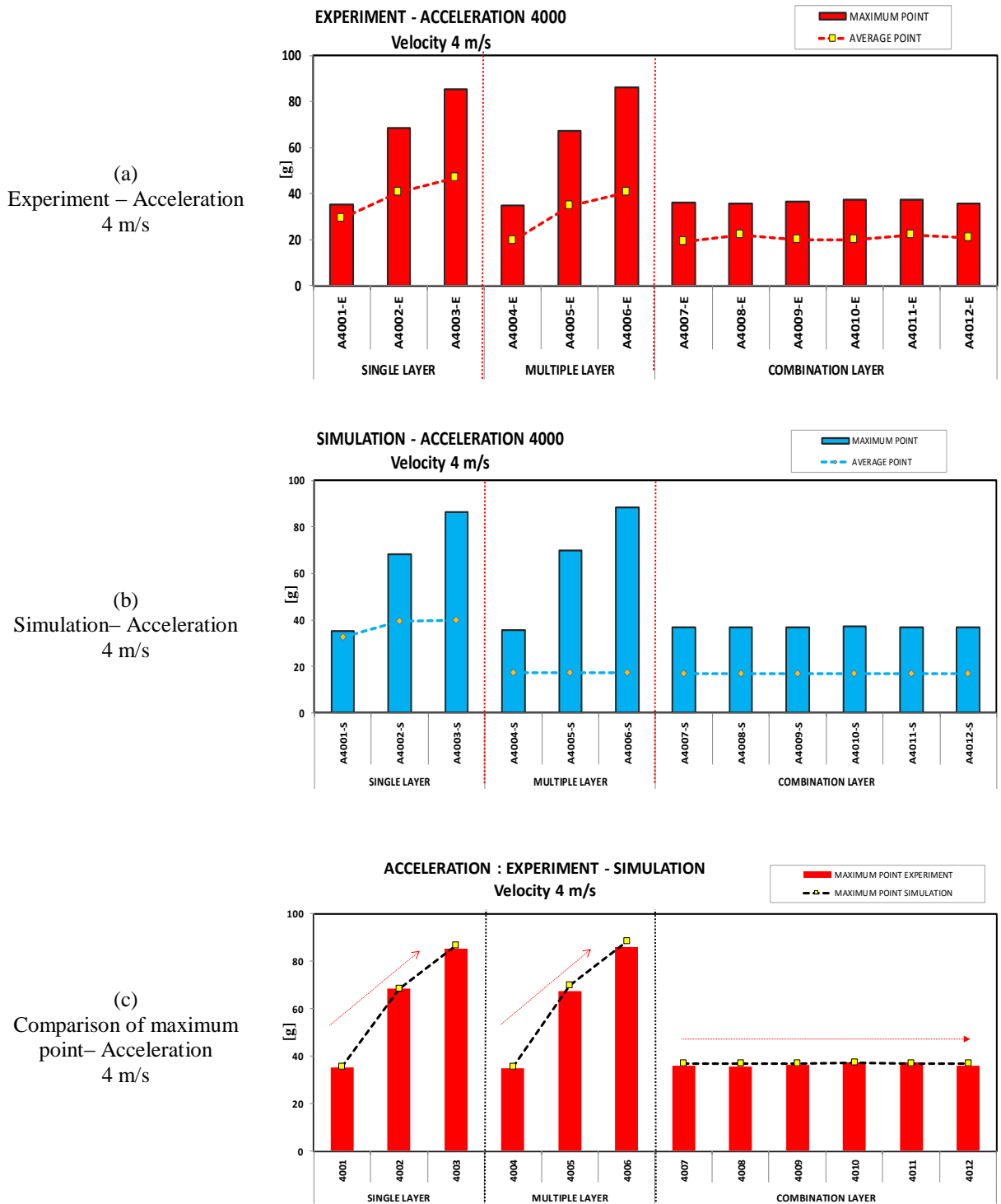


Figure 5-22: Maximum and Average Point of Acceleration Based on Velocity 4 m/s.
(a) Experiment; (b) Simulation; (c) Comparison of Maximum Point.

For Figure 5-22(c), three material configurations were discussed through comparison of experiment and simulation. The comparison was observed using trend

referring to maximum points. For single layer configurations, both simulation and experiment shows maximum points increased significantly. Multiple layer configurations were similar as single layer whereby all maximum points increased significantly. Lastly, material configurations of combination (hybrid) layer shows that all maximum and average points were equally aligned.

Next discussion is based on displacement value towards specified velocity 4 m/s, shown in Figure 5-23 (displacement). Figure 5-23 consist displacement based on impact velocity at 4 m/s. Figure 5-23(a) shows experimental findings, Figure 5-23(b) shows simulation findings and Figure 5-23(c) shows the comparison between simulation and experiment based on displacement parameter.

For Figure 5-23(a), three material configurations were compared using simulation. For single layer configurations, average and maximum points decreased more than simulation findings. The configurations of multiple layer were similar to single layer configurations where the average and maximum points decreased significantly compared to simulation. Lastly, material configurations of combination (hybrid) layer shows that all maximum and average points were slightly increased.

For Figure 5-23(b), three material configurations were compared experimentally. For single layer configurations, average and maximum points decreased significantly. Multiple layer configurations were similar as single layer whereby, the average and maximum points decreased significantly. Lastly, material configurations of combinations (hybrid) layer shows that all maximum and average points were slightly increased.

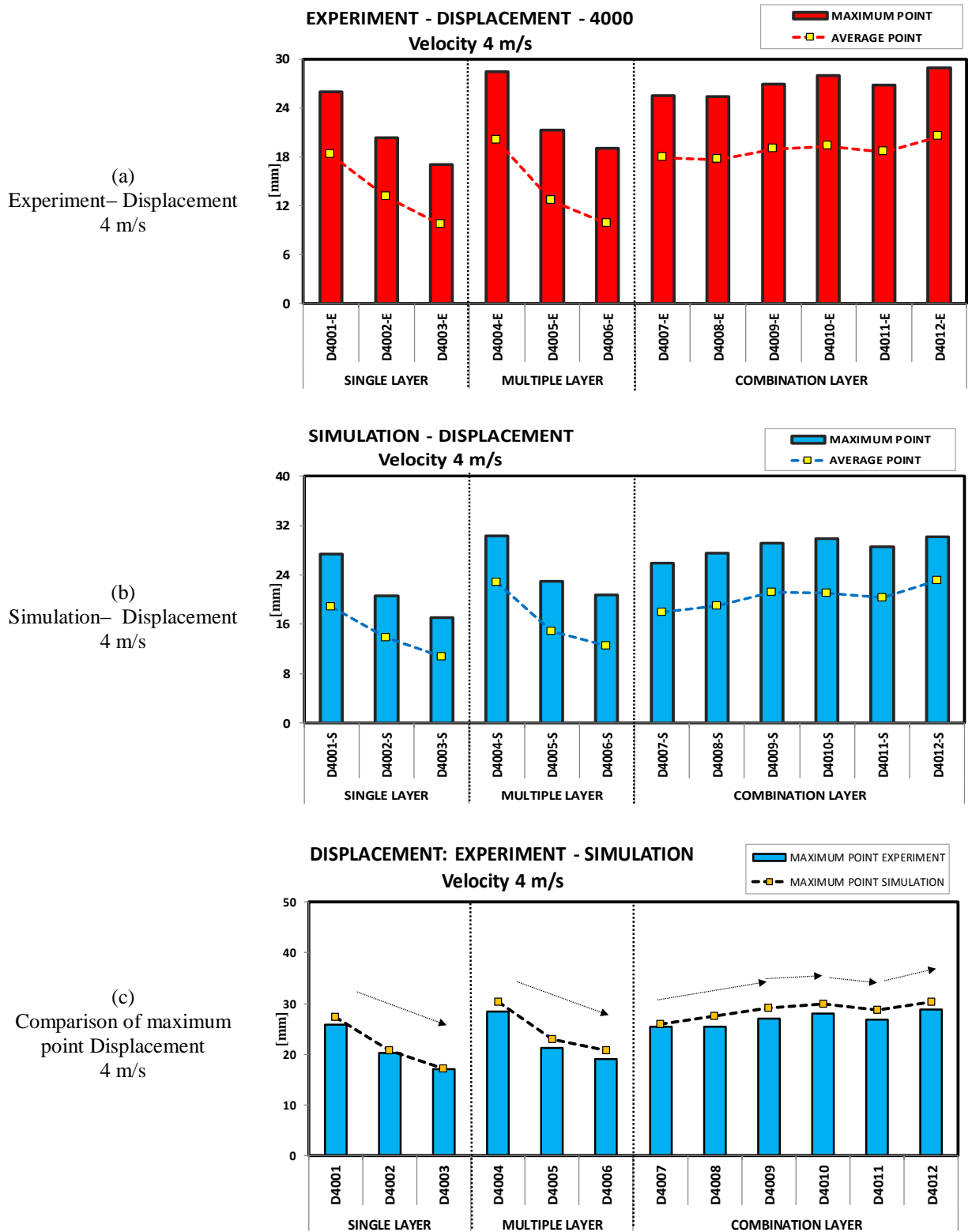


Figure 5-23: Maximum and Average Point of Displacement Based on Velocity 4 m/s.
(a) Experiment; (b) Simulation; (c) Comparison of Maximum Point.

For Figure 5-23(c), three material configurations were discussed through comparison of experiment and simulation. The comparison was observed using trend referring to maximum points. For single layer configurations, both simulation and experiment shows maximum points decreased significantly. Multiple layer configurations were similar as single layer whereby all maximum and average points decreased significantly. Lastly, material configurations of combination (hybrid) layer shows all maximum points increased. Lowest displacement value at design D4007 and highest displacement value at D4012.

Based from previous comparison on acceleration and displacement, Table 5-15 shows summary of maximum point trends for hybrid layer. This is due to single and multiple layer have same maximum point trends that contradict between acceleration and displacement. Hence, single and multiple layer were excluded in this table. This table shows Material C gives huge impact towards material combination. To obtain highest optimisation, Material C should be positioned either middle or top of design configuration.

Table 5-15: The Combination/hybrid Layer Result of 4 m/s Impact Velocity

4007	4008	4009	4010	4011	4012
A	C	B	C	B	A
B	A	C	B	A	C
C	B	A	A	C	B

5.3.3 Summary of Foam Design Based on Impact Velocity

To summarise, acceleration parameters based on impact velocity 2 m/s, 3 m/s, and 4 m/s were plotted out. However, hard to observe significant changes because the trends were almost aligned. Hence, acceleration parameter's graph trend was not discussed in this summary section. In addition, the characteristic of combination layer (hybrid) for the displacement showed dissimilarity to each impact velocity applied. For the impact velocity 2 m/s, the graph tends to be slightly aligned and went downward, whilst for the 3 m/s, the trend was fluctuating. The interesting part was, for the velocity 4 m/s, the graph shows an incremental trend.

Furthermore, based on the study conducted through the experiment and simulation, it was found that impact velocity gives significant dissimilarity on displacement for combination layer (hybrid) rather than acceleration. For 2 m/s, Table 5-13 shows Material A gives huge impact towards material combination. To obtain highest optimisation, Material A should be placed lowest compared to Material B and C. Impact velocity at 3 m/s, Table 5-14 shows Material B gives huge impact towards material combination. To obtain highest optimisation, Material B should be placed in middle or top position compared to Material A and C in term of both parameters acceleration and displacement. Finally, for impact velocity at 4 m/s, Table 5-15 shows Material C gives huge impact towards material combination. To obtain highest optimisation, Material C should be positioned either middle or top of design configuration. Hence, objective 1 was reflected in this portion of analysis.

Chapter 6: Best Design Configuration for Impact Absorption

This chapter focuses on IMPAXX EPS foam characteristics towards acceleration and displacement based on layer type configurations and shape designs. Simulation (S) and experiment (E) were conducted to determine the best material design based on layer configuration and shape. Simulation and experiment (with different impact velocity) were used to define material characteristics based on layer type configurations (or EPS foam arrangements) and shape designs.

Furthermore, four different types of shape designs (see in Figure 4-15) were tested, such as shape of arc (ARC), sinusoidal (SIN), square (SQ), and trapezium (TR). Each shapes consists of space and no-space configurations, which were applied in-between layers. This is mainly to determine the best material design configuration based on the shape and space effect, in regards to the overall performance of impact absorber for the aircraft.

In this research, the analysis conducted focuses on characteristics of material design configurations. Results showed that acceleration against the displacement is contradicting (opposite) between each other. Therefore, there is a need to use average and time (t) average method, to judge and decide the best materials that will be

employed in the aircraft.

6.1 Analysis to Determine Best Design Configuration for Material Design Based on Average Value

The analysis were carried out to determine best design configurations for flat foam design. The analysis were conducted to test different impact velocity of 2 m/s, 3 m/s and 4 m/s. To validate the findings, simulations were conducted simultaneously to support the results obtained from experimental procedures.

Based on the results, the values of displacement and acceleration were contradicting between each other. Therefore, it is difficult to observe the lowest values of acceleration and displacement. Hence, it is challenging to determine the best design from the results obtained. Basic statistical analysis were conducted for the ease of data collection. Comparisons between every single data and the average data were made throughout this chapter.

6.1.1 Analysis by Using Average Values at 2 m/s

Table 6-1 shows simulation of acceleration and displacement using impact velocity 2 m/s. The average values of acceleration and displacement were 46.80 g and 10.03 mm respectively. All the values were compared to the average value where values that were lower than average will be selected as best material design configuration. Table 6-1 shows that, only design 2010-S is below average values for acceleration and displacement.

Table 6-1: Simulation of Acceleration and Displacement at 2 m/s

SIMULATION : ACCELERATION (g) and DISPLACEMENT (mm) at 2 m/s													
MATERIAL DESIGN	SINGLE LAYER			MULTIPLE LAYER			COMBINATION LAYER						AVE
	A	B	C	AAA	BBB	CCC	ABC	CAB	BCA	CBA	BAC	ACB	
	2001-S	2002-S	2003-S	2004-S	2005-S	2006-S	2007-S	2008-S	2009-S	2010-S	2011-S	2012-S	
ACCELERATION -S-AVERAGE 2000	33.36	65.43	82.62	33.36	64.38	74.14	34.77	34.71	34.68	34.69	34.72	34.78	46.80
Acceleration Average Line	46.80	46.80	46.80	46.80	46.80	46.80	46.80	46.80	46.80	46.80	46.80	46.80	
DISPLACEMENT -S-AVERAGE 2000	10.30	7.65	7.46	11.33	10.23	8.78	12.09	11.30	10.81	9.47	10.23	10.67	10.03
Displacement Average Line	10.03	10.03	10.03	10.03	10.03	10.03	10.03	10.03	10.03	10.03	10.03	10.03	

Table 6-2: Experiment of Acceleration and Displacement at 2 m/s

EXPERIMENT : ACCELERATION (g) vs. DISPLACEMENT (mm) at 2 m/s													
MATERIAL DESIGN	SINGLE LAYER			MULTIPLE LAYER			COMBINATION LAYER						AVE
	A	B	C	AAA	BBB	CCC	ABC	CAB	BCA	CBA	BAC	ACB	
	2001-E	2002-E	2003-E	2004-E	2005-E	2006-E	2007-E	2008-E	2009-E	2010-E	2011-E	2012-E	
ACCELERATION -AVERAGE	33.37	58.03	77.49	31.49	61.81	71.81	32.96	33.29	33.06	32.53	34.52	34.87	44.60
Acceleration Average Line	44.60	44.60	44.60	44.60	44.60	44.60	44.60	44.60	44.60	44.60	44.60	44.60	
DISPLACEMENT -AVERAGE	9.27	7.69	7.16	11.07	9.73	7.94	11.66	10.78	10.71	9.13	9.79	10.35	9.60
Displacement Average Line	9.60	9.60	9.60	9.60	9.60	9.60	9.60	9.60	9.60	9.60	9.60	9.60	

Table 6-2 shows the experiment of acceleration and displacement with average values of 44.60 g and 9.60 mm respectively. All the values were compared to the average values. Values that are lower than average were selected as best material design configurations. Table 6-2 shows that, design 2001-E and 2010-E is below average values for acceleration and displacement.

To obtain a clear view on both tables, two bar charts were plotted separately from simulation and experiment. The highlighted boxes from Table 6-1 and Table 6-2 are shown by highlighting the bar charts 2010-S in simulation (Figure 6-1) and for experiment, 2 bars labelled 2001-E and 2010-E were highlighted (Figure 6-2). To conclude, for acceleration and displacement at 2 m/s, material 2010 from combination (hybrid) layer has the best material design configuration.

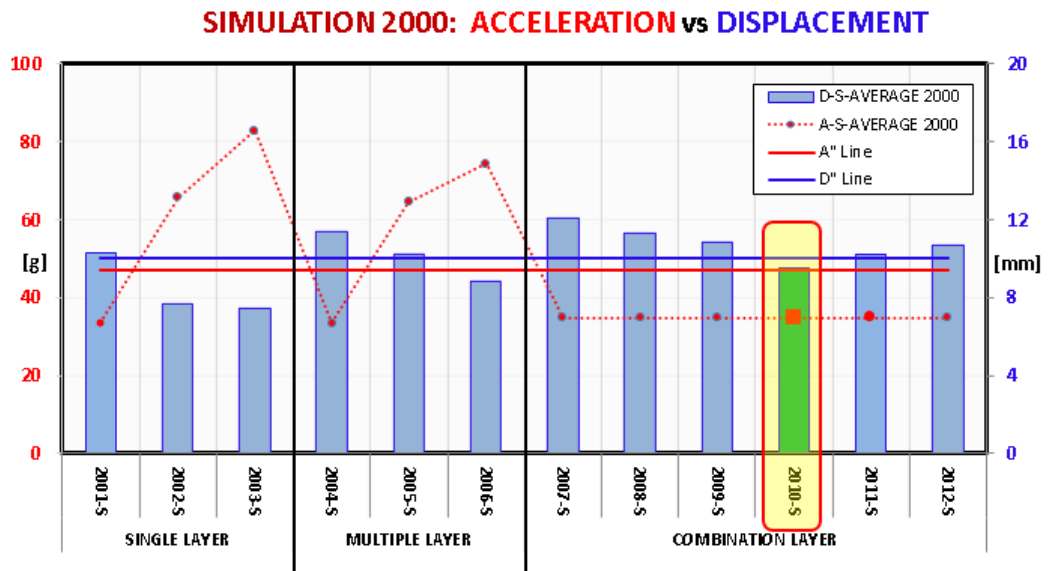


Figure 6-1: Simulation Result of Acceleration vs. Displacement at 2 m/s

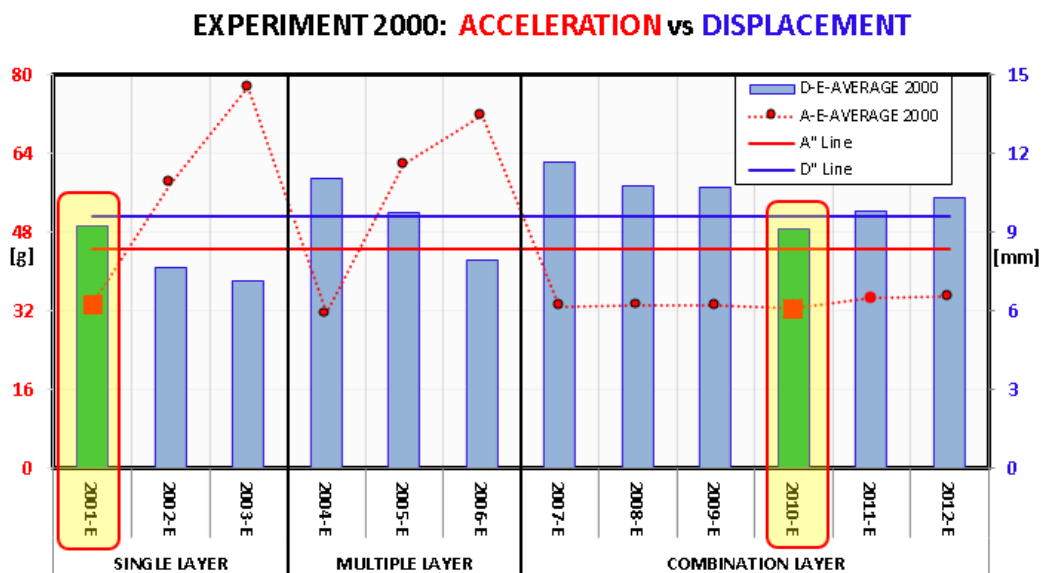


Figure 6-2: Experiment Result of Acceleration vs. Displacement at 2 m/s

6.1.2 Analysis by Using Average Values at 3 m/s

Table 6-3 shows simulation of acceleration and displacement using impact velocity 3 m/s. The average values of acceleration and displacement were 48.64 g and 15.80 mm respectively. All the values were compared to the average value where values that were lower than average will be selected as best material design

configuration. From Table 6-3, only two design 3001-S and 3009-S that having the values below average of acceleration and displacement.

Table 6-3: Simulation of Acceleration and Displacement at 3 m/s

SIMULATION : ACCELERATION (g) vs. DISPLACEMENT (mm) at 3 m/s													
MATERIAL DESIGN	SINGLE LAYER			MULTIPLE LAYER			COMBINATION LAYER						AVE
	A	B	C	AAA	BBB	CCC	ABC	CAB	BCA	CBA	BAC	ACB	
	3001-S	3002-S	3003-S	3004-S	3005-S	3006-S	3007-S	3008-S	3009-S	3010-S	3011-S	3012-S	
ACCELERATION -AVERAGE	33.83	66.46	84.26	34.51	67.60	84.96	35.39	35.32	35.33	35.31	35.33	35.39	48.64
Acceleration Average Line	48.64	48.64	48.64	48.64	48.64	48.64	48.64	48.64	48.64	48.64	48.64	48.64	
DISPLACEMENT -AVERAGE	15.55	11.83	7.74	18.65	16.40	13.46	16.19	18.99	15.72	19.76	16.95	18.38	15.80
Displacement Average Line	15.80	15.80	15.80	15.80	15.80	15.80	15.80	15.80	15.80	15.80	15.80	15.80	

Table 6-4: Experiment of Acceleration and Displacement at 3 m/s

EXPERIMENT : ACCELERATION (g) vs. DISPLACEMENT (mm) at 3 m/s													
MATERIAL DESIGN	SINGLE LAYER			MULTIPLE LAYER			COMBINATION LAYER						AVE
	A	B	C	AAA	BBB	CCC	ABC	CAB	BCA	CBA	BAC	ACB	
	3001-E	3002-E	3003-E	3004-E	3005-E	3006-E	3007-E	3008-E	3009-E	3010-E	3011-E	3012-E	
ACCELERATION -AVERAGE	32.59	64.53	80.79	32.52	61.85	79.74	33.18	34.12	34.36	35.42	34.80	34.02	46.49
Acceleration Average Line	46.49	46.49	46.49	46.49	46.49	46.49	46.49	46.49	46.49	46.49	46.49	46.49	
DISPLACEMENT -AVERAGE	15.12	12.87	7.15	17.73	14.97	13.88	14.93	17.36	14.93	18.69	16.58	17.36	15.13
Displacement Average Line	15.13	15.13	15.13	15.13	15.13	15.13	15.13	15.13	15.13	15.13	15.13	15.13	

Table 6-4 shows the experiment of acceleration and displacement with average values were 46.49 g and 15.13 mm respectively. All the values were compared to the average value where values that were lower than average will be selected as best material design configuration. From Table 6-4, only three designs which are 3001-E, 3007-E and 3009-E shows the values below average of acceleration and displacement.

To obtain a clear view on both tables, two bar charts were plotted out separated by simulation and experiment. The highlighted cells from Table 6-3 and Table 6-4 were shown clearly by highlighting the bar chart 3001-S and 3009-S in simulation (Figure 6-3). For experiment, 3 bars labelled 3001-E, 3007-E, and 3009-E were highlighted (Figure 6-4). To conclude, two materials which are 3001 (single layer) and 3009

(combination layer) have the best material design configuration for acceleration and displacement at 3 m/s.

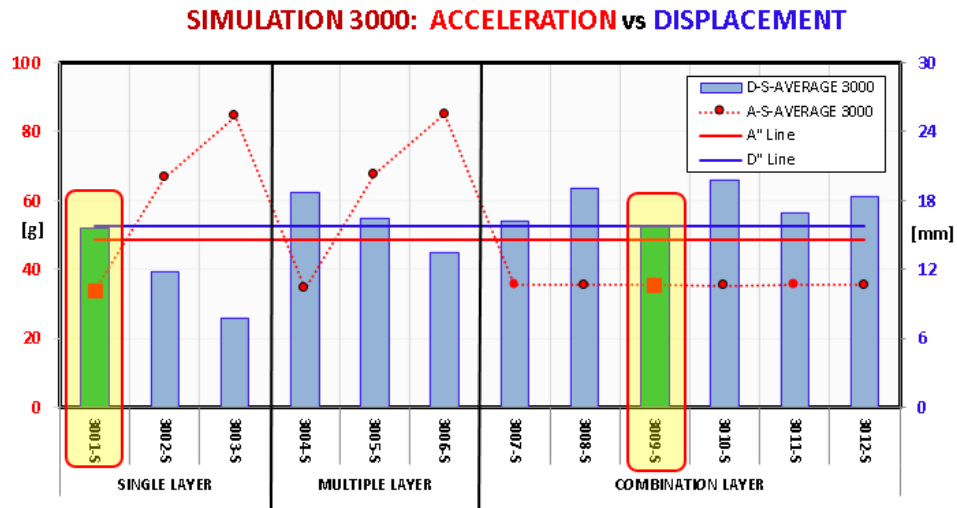


Figure 6-3: Experiment Result of Acceleration vs. Displacement at 3 m/s

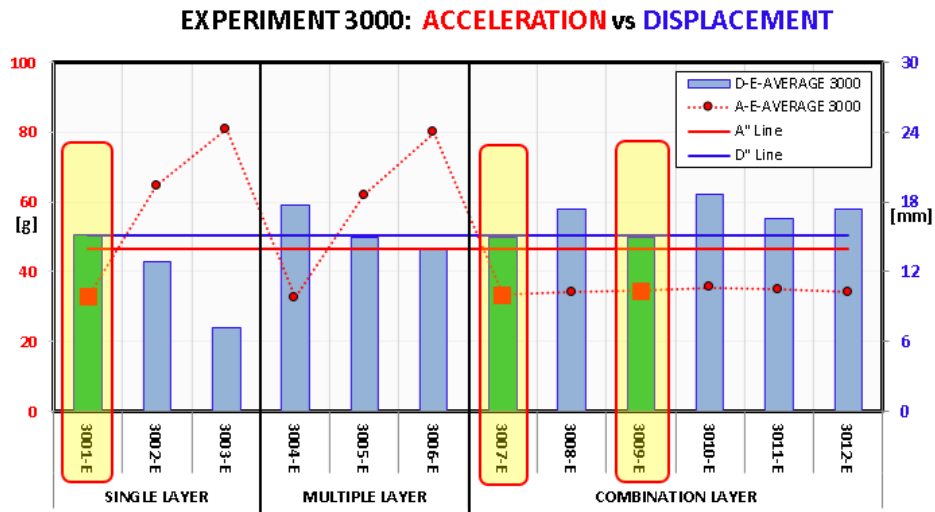


Figure 6-4: Experiment Result of Acceleration vs. Displacement at 3 m/s

6.1.3 Analysis by Using Average Values at 4 m/s

Table 6-5 shows simulation of acceleration and displacement using impact velocity 4 m/s. The average values of acceleration and displacement were 49.26 g and 24.38 mm respectively. All the values were compared to the average value where

values that were lower than average will be selected as best material design configuration. From Table 6-5, there were no values below average of acceleration and displacement.

Table 6-5: Simulation of Acceleration and Displacement at 4 m/s

SIMULATION : ACCELERATION (g) vs. DISPLACEMENT (mm) at 4 m/s													
MATERIAL DESIGN	SINGLE LAYER			MULTIPLE LAYER			COMBINATION LAYER						AVE
	A	B	C	AAA	BBB	CCC	ABC	CAB	BCA	CBA	BAC	ACB	
	4001-S	4002-S	4003-S	4004-S	4005-S	4006-S	4007-S	4008-S	4009-S	4010-S	4011-S	4012-S	
ACCELERATION -AVERAGE	34.22	66.96	84.87	34.88	68.68	86.74	35.85	35.79	35.75	35.77	35.80	35.85	49.26
Acceleration Average Line	49.26	49.26	49.26	49.26	49.26	49.26	49.26	49.26	49.26	49.26	49.26	49.26	
DISPLACEMENT -AVERAGE	25.75	19.48	16.18	28.71	21.56	19.55	24.55	25.80	27.41	28.04	27.02	28.52	24.38
Displacement Average Line	24.38	24.38	24.38	24.38	24.38	24.38	24.38	24.38	24.38	24.38	24.38	24.38	

Table 6-6: Experiment of Acceleration and Displacement at 4 m/s

EXPERIMENT : ACCELERATION (g) vs. DISPLACEMENT (mm) at 4 m/s													
MATERIAL DESIGN	SINGLE LAYER			MULTIPLE LAYER			COMBINATION LAYER						AVE
	A	B	C	AAA	BBB	CCC	ABC	CAB	BCA	CBA	BAC	ACB	
	4001-E	4002-E	4003-E	4004-E	4005-E	4006-E	4007-E	4008-E	4009-E	4010-E	4011-E	4012-E	
ACCELERATION -AVERAGE	33.02	64.41	80.27	32.52	64.28	82.50	34.21	34.27	34.83	34.12	35.76	33.79	47.00
Acceleration Average Line	47.00	47.00	47.00	47.00	47.00	47.00	47.00	47.00	47.00	47.00	47.00	47.00	
DISPLACEMENT -AVERAGE	24.46	19.18	16.02	26.90	20.16	17.96	24.03	24.02	25.46	26.40	25.26	27.25	23.09
Displacement Average Line	23.09	23.09	23.09	23.09	23.09	23.09	23.09	23.09	23.09	23.09	23.09	23.09	

Table 6-6 shows the experiment of acceleration and displacement with average values were 47.00 g and 23.09 mm respectively. All the values were compared to the average value where values that were lower than average will be selected as best material design configuration. From Table 6-6, there were no values below average of acceleration and displacement.

To obtain a clear view on both tables, two bar charts were plotted out separately from simulation and experiment (Figure 6-5 and Figure 6-6). There was no highlighted cells from Table 6-5 and Table 6-6. Therefore, Figure 6-5 and Figure 6-6 of simulation and experiment were not highlighted. To conclude, at 4 m/s, the foam material configuration regardless single, multiple or combination could not withstand the

impact velocity applied. Hence, there are no suitable selection could be made at 4 m/s.

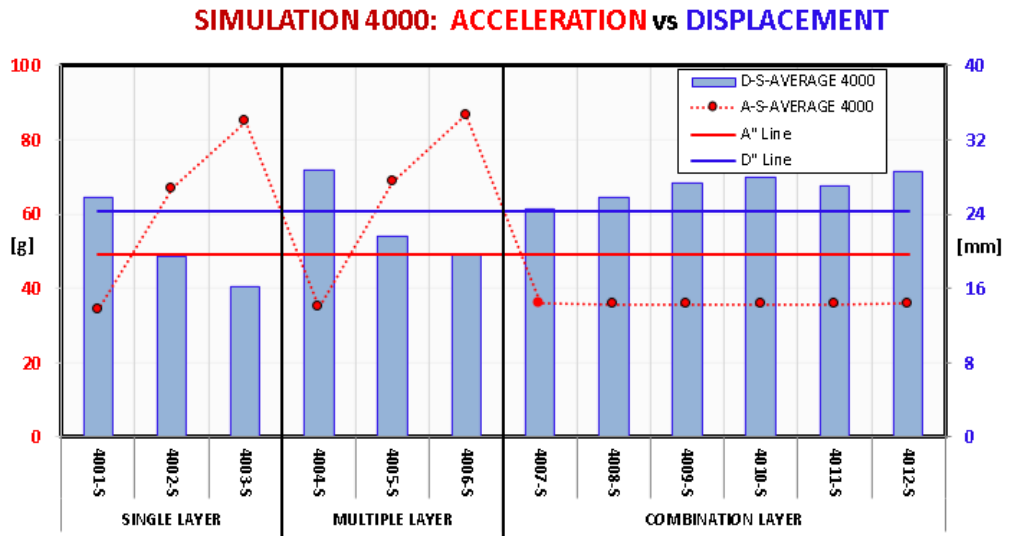


Figure 6-5: Simulation Result of Acceleration vs. Displacement at 4 m/s

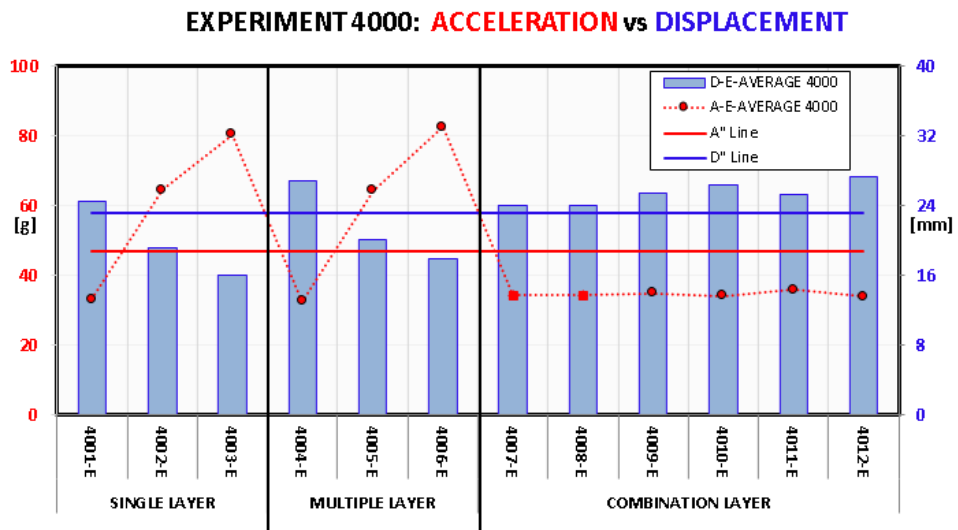


Figure 6-6: Experiment Result of Acceleration vs. Displacement at 4 m/s

6.1.4 Summary of the Best Materials Analysis Based on Average Values Approach for Experiment and Simulation

Several findings were obtained through analysis carried out at 2 m/s, 3 m/s and 4 m/s. Material 2010 (CBA) from combination (hybrid) layer has the best material design configuration at 2 m/s. The best material design configuration for impact velocity of 3 m/s are; single layer 3001 (A) and combination layer 3009 (BCA). Finally, no design could be selected for impact velocity 4 m/s, which can provide better information in terms of best material selection.

In conclusions, at 2 m/s and 3 m/s best material design configuration selected was combination layer. However, there are no suitable selection could be made at 4 m/s. Suitable impact velocity to test out foam material configurations were conducted at 2 m/s and 3 m/s. This theory will be used in the next subsection using time parameter. Hence, objective 2 is reflected in this portion of analysis.

6.2 Analysis to Determine Best Design Configuration for Material Foam Design Based on Time (t) Parameter

6.2.1 Analysis Using Time (t) Average Approach at 2 m/s

Table 6-7 shows simulation of acceleration and displacement using impact velocity 2 m/s. Based on time (t) average of 0.691 ms, the simulation average value of acceleration and displacement were calculated at 42.03 g and 11.17 mm respectively. All the values were compared to the average value where values that were lower than average will be selected as best material design configuration. From Table 6-7, only

design 2010-S (CBA) that fulfil both criteria of the values below average of acceleration (43.03 g) and displacement (11.17 mm).

Table 6-7: The Best Design Based on time (t) Average Approach of Acceleration Experiment vs. Displacement Experiment at 2 m/s

SIMULATION : ACCELERATION (g) vs. DISPLACEMENT (mm) at 2 m/s													
MATERIAL DESIGN	SINGLE LAYER			MULTIPLE LAYER			COMBINATION LAYER						AVE
	A	B	C	AAA	BBB	CCC	ABC	CAB	BCA	CBA	BAC	ACB	
	2001-S	2002-S	2003-S	2004-S	2005-S	2006-S	2007-S	2008-S	2009-S	2010-S	2011-S	2012-S	
A-S-AVERAGE 2000 (g)	33.36	65.43	82.62	33.36	64.38	74.14	34.77	34.71	34.68	34.69	34.72	34.78	
D-S-AVERAGE 2000 (mm)	10.30	7.65	7.46	11.33	10.23	8.78	12.09	11.30	10.81	9.47	10.23	10.67	
t =SQRT(2S/a)	0.786	0.483	0.425	0.824	0.564	0.487	0.834	0.807	0.790	0.739	0.768	0.783	0.691 ms
New A-S-AVERAGE 2000 (g)	43.15	32.06	31.26	47.50	42.88	36.82	50.67	47.37	45.33	39.70	42.89	44.71	42.03 g
New D-S-AVERAGE 2000 (mm)	7.96	15.61	19.71	7.96	15.36	17.69	8.29	8.28	8.27	8.28	8.28	8.30	11.17 mm

Table 6-8: The Best Design Based on time (t) Average Approach of Acceleration Simulation vs. Displacement Simulation at 2 m/s

EXPERIMENT : ACCELERATION (g) vs. DISPLACEMENT (mm) at 2 m/s													
MATERIAL DESIGN	SINGLE LAYER			MULTIPLE LAYER			COMBINATION LAYER						AVE
	A	B	C	AAA	BBB	CCC	ABC	CAB	BCA	CBA	BAC	ACB	
	2001-E	2002-E	2003-E	2004-E	2005-E	2006-E	2007-E	2008-E	2009-E	2010-E	2011-E	2012-E	
A-S-AVERAGE 2000 (g)	33.37	58.03	77.49	31.49	61.81	71.81	32.96	33.29	33.06	32.53	34.52	34.87	
D-S-AVERAGE 2000 (mm)	9.27	7.69	7.16	11.07	9.73	7.94	11.66	10.78	10.71	9.13	9.79	10.35	
t =SQRT(2S/a)	0.745	0.515	0.430	0.838	0.561	0.470	0.841	0.805	0.805	0.749	0.753	0.771	0.690 ms
New A-S-AVERAGE 2000 (g)	38.89	32.06	31.26	47.50	42.88	36.82	50.67	47.37	45.33	39.70	42.89	44.71	41.49 g
New D-S-AVERAGE 2000 (mm)	7.95	13.82	18.46	7.50	14.72	17.10	7.85	7.93	7.88	7.75	8.22	8.31	10.62 mm

Table 6-8 shows the average values of experiment for acceleration and displacement that were 41.49 g and 10.62 mm respectively. All the values were compared to the average value where values that were lower than average will be selected as best material design configuration. Based on time (t) average is 0.691 ms, from Table 6-8 there were only design 2001-E (A) and 2010-E (CBA) that fulfil both criteria of the values below average of acceleration (41.49 g) and displacement (10.62 mm).

To obtain a clear view on both tables, four bar charts were plotted out separated by simulation and experiment (Figure 6-7 to Figure 6-10). Green bar signifies the values

displacement average and acceleration average below displacement and acceleration line limits. However, blue bar signifies either the acceleration average falls above acceleration line limit or displacement average higher than displacement line limit. Green bar fulfils criteria for the selection of material configuration. The green bar should also be validated again by both acceleration and displacement via simulation and experiment. The green bars that present in both acceleration and displacement were highlighted in yellow.

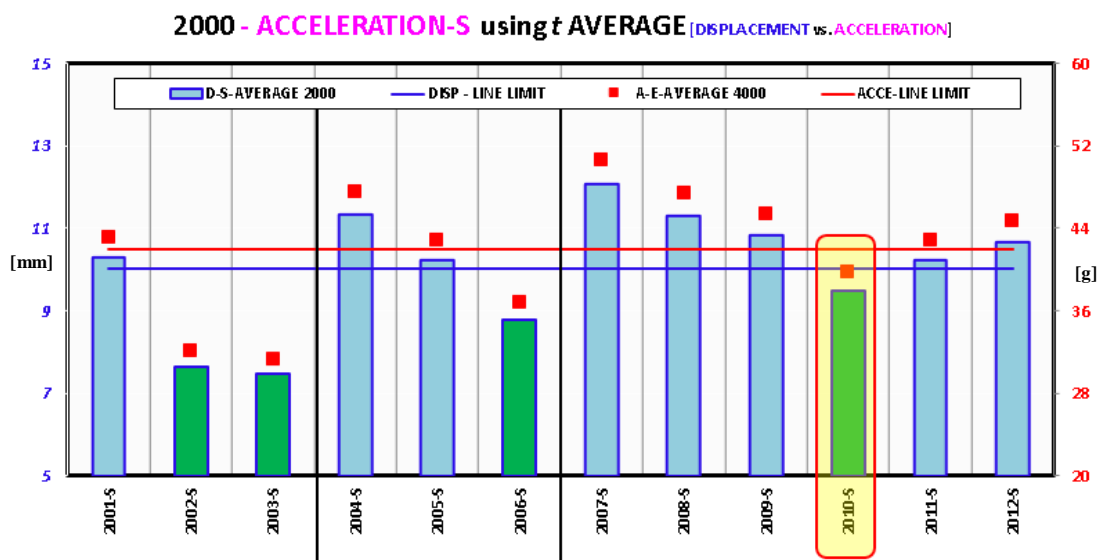


Figure 6-7: Simulation: Acceleration at 2 m/s Based on Time (t)

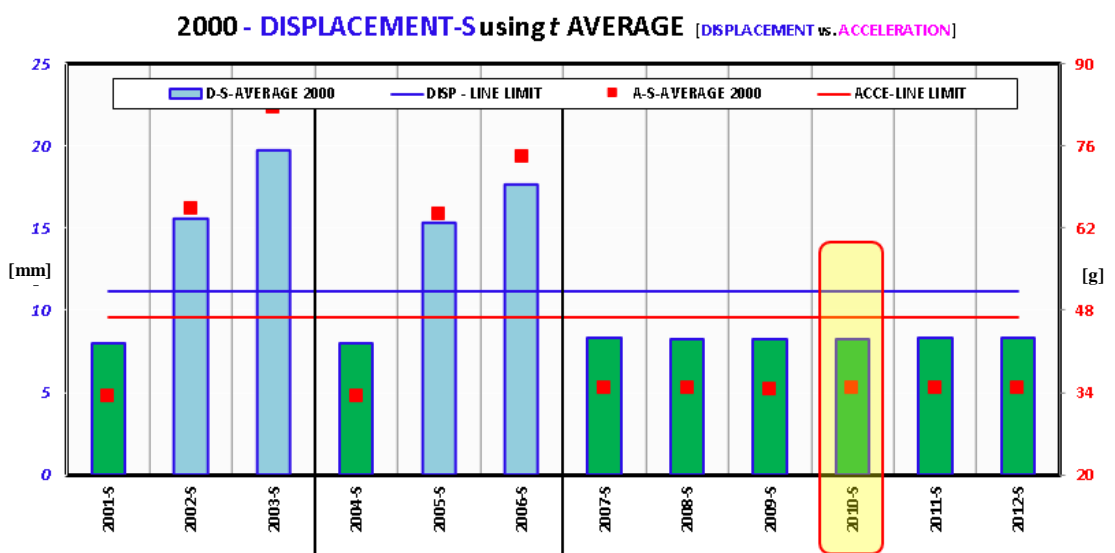


Figure 6-8: Simulation: Displacement at 2 m/s Based on Time (t)

The highlighted cells from Table 6-7 (simulation) were shown by highlighting the bar chart 2010-S (CBA) in simulation. Therefore, Figure 6-7 and Figure 6-8 shows design 2010-S of combination layer were selected as best material configuration.

Furthermore, there are two designs highlighted in Table 6-8 (experiment). Figure 6-9 and Figure 6-10 shows two highlighted bars that are; 2001-E (A) and 2010-E (CBA).

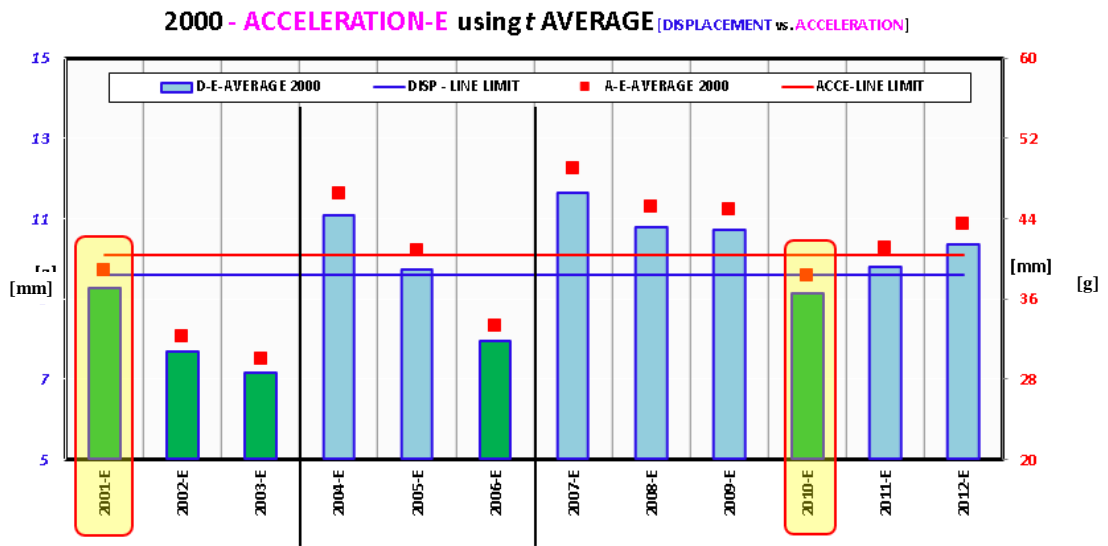


Figure 6-9: Experiment: Acceleration at 2 m/s Based on Time (t)

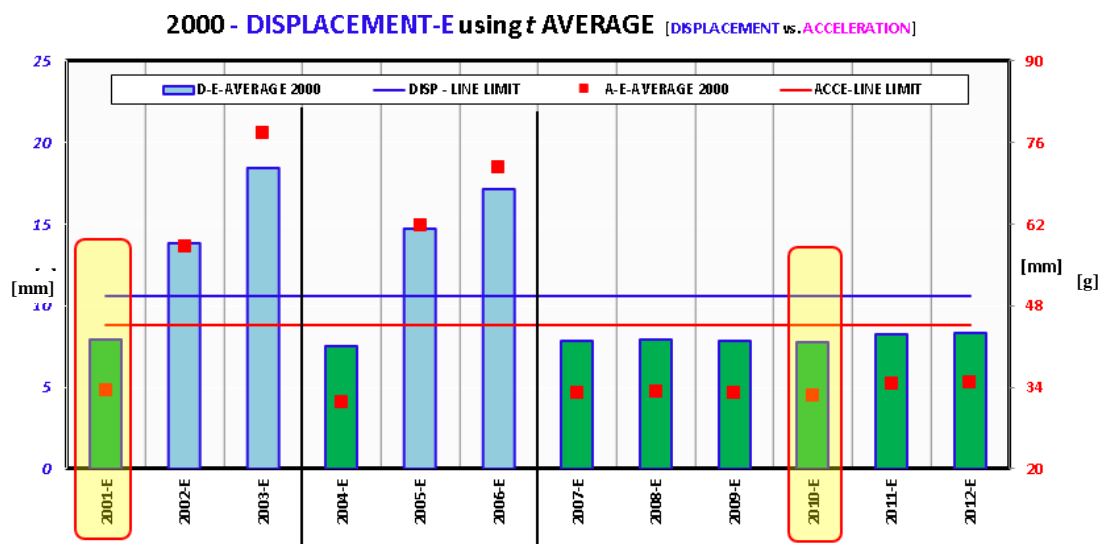


Figure 6-10: Experiment: Displacement at 2 m/s Based on Time (t)

Figure 6-7 to Figure 6-10 show the analysis based on time (t) average values for velocity at 2 m/s. The best material configuration was design 2010 (CBA) based on time (t) average values.

6.2.2 Analysis Using Time (t) Average Approach at 3 m/s

Table 6-9 shows simulation of acceleration and displacement using impact velocity 3 m/s. Based on time (t) average of 0.856 ms, the simulation average value of acceleration and displacement were 43.09 g and 17.84 mm respectively. All the values were compared to the average value where values that were lower than average will be selected as best material design configuration. From Table 6-9, only design 3001-S (A) and 3009-S (BCA) that fulfil both criteria of the values below average of acceleration (43.09 g) and displacement (17.84 mm).

Table 6-9: The Best Design Based on time (t) Average Approach of Acceleration Simulation vs. Displacement Simulation at 3 m/s

SIMULATION : ACCELERATION (g) vs. DISPLACEMENT (mm) at 3 m/s													
MATERIAL DESIGN	SINGLE LAYER			MULTIPLE LAYER			COMBINATION LAYER						AVE
	A	B	C	AAA	BBB	CCC	ABC	CAB	BCA	CBA	BAC	ACB	
	3001-S	3002-S	3003-S	3004-S	3005-S	3006-S	3007-S	3008-S	3009-S	3010-S	3011-S	3012-S	
A-S-AVERAGE 2000 (g)	33.83	66.46	84.26	34.51	67.60	84.96	35.39	35.32	35.33	35.31	35.33	35.39	
D-S-AVERAGE 2000 (mm)	15.55	11.83	7.74	18.65	16.40	13.46	16.19	18.99	15.72	19.76	16.95	18.38	
t =SQRT(2S/a)	0.959	0.597	0.428	1.040	0.697	0.563	0.956	1.037	0.943	1.058	0.980	1.019	0.856 ms
New A-S-AVERAGE 2000 (g)	42.41	32.26	21.09	50.87	44.72	36.70	44.15	51.79	42.87	53.88	46.23	50.13	43.09 g
New D-S-AVERAGE 2000 (mm)	12.40	24.37	30.90	12.66	24.79	31.16	12.98	12.95	12.95	12.95	12.96	12.98	17.84 mm

Table 6-10: The Best Design Based on time (t) Average Approach of Acceleration Experiment vs. Displacement Experiment at 3 m/s

EXPERIMENT : ACCELERATION (g) vs. DISPLACEMENT (mm) at 3 m/s													
MATERIAL DESIGN	SINGLE LAYER			MULTIPLE LAYER			COMBINATION LAYER						AVE
	A	B	C	AAA	BBB	CCC	ABC	CAB	BCA	CBA	BAC	ACB	
	3001-E	3002-E	3003-E	3004-E	3005-E	3006-E	3007-E	3008-E	3009-E	3010-E	3011-E	3012-E	
A-S-AVERAGE 2000 (g)	32.59	64.53	80.79	32.52	61.85	79.74	33.18	34.12	34.36	35.42	34.80	34.02	
D-S-AVERAGE 2000 (mm)	15.12	12.87	7.15	17.73	14.97	13.88	14.93	17.36	14.93	18.69	16.58	17.36	
t =SQRT(2S/a)	0.963	0.632	0.421	1.044	0.696	0.590	0.949	1.009	0.932	1.027	0.976	1.010	0.854 ms
New A-S-AVERAGE 2000 (g)	41.46	35.28	19.62	48.60	41.05	38.05	40.94	47.60	40.94	51.25	45.45	47.60	41.49 g
New D-S-AVERAGE 2000 (mm)	11.89	23.53	29.46	11.86	22.56	29.08	12.10	12.44	12.53	12.92	12.69	12.41	16.96 mm

Table 6-10 shows the average values of experiment for acceleration and displacement that were 41.49 g and 16.96 mm respectively. All the values were compared to the average value where values that were lower than average will be selected as best material design configuration. Based on time (t) average is 0.854 ms, from table below there were only design 3001-E (A), 3007-E (ABC) and 3009-E (BCA) that fulfil both criteria of the values below average of acceleration (41.49 g) and displacement (16.96 mm).

To obtain a clear view on both tables, four bar chart were plotted out separated by simulation and experiment. Green bar signifies the displacement average and acceleration average below displacement and acceleration line limits. However, blue bar signifies either the acceleration average falls above acceleration line limit or displacement average higher than displacement line limit. Green bar fulfils criteria for the selection of material configuration. The green bar should also be validated again by both acceleration and displacement via simulation and experiment. The green bars that present in both acceleration and displacement were highlighted in yellow. There are acceleration and displacement both simulation and experiment. The highlighted cells from Table 6-9 (simulation) were shown by highlighting the bar chart 3001-S (A) and 3009-S (BCA) in simulation. Therefore, Figure 6-11 and Figure 6-12 also shows design 3001-S and 3009-S from combination layer selected as best material configuration.

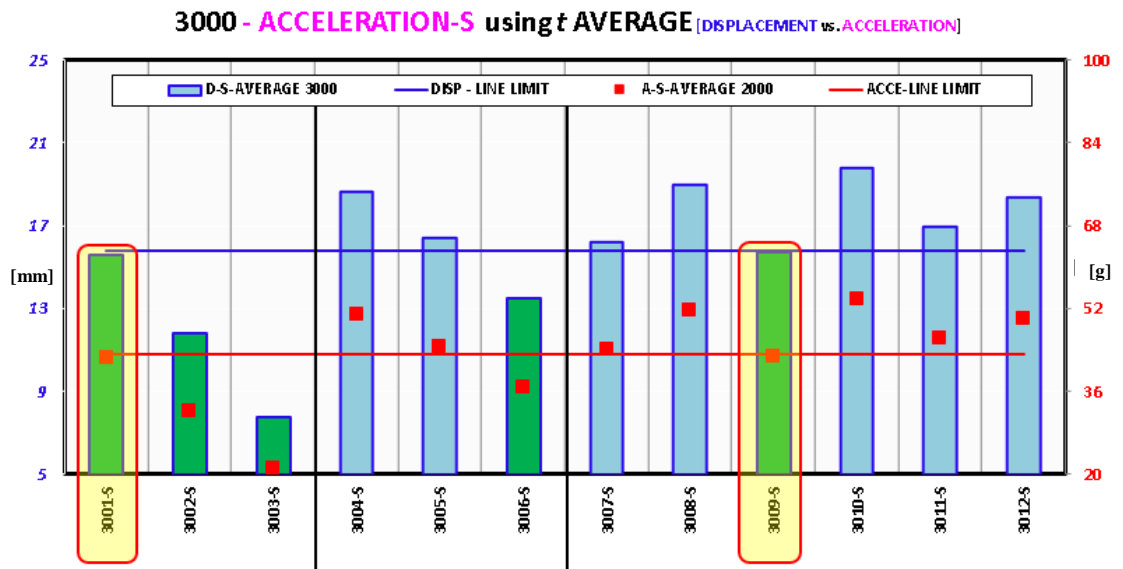


Figure 6-11: Simulation: Acceleration at 3 m/s Based on Time (t)

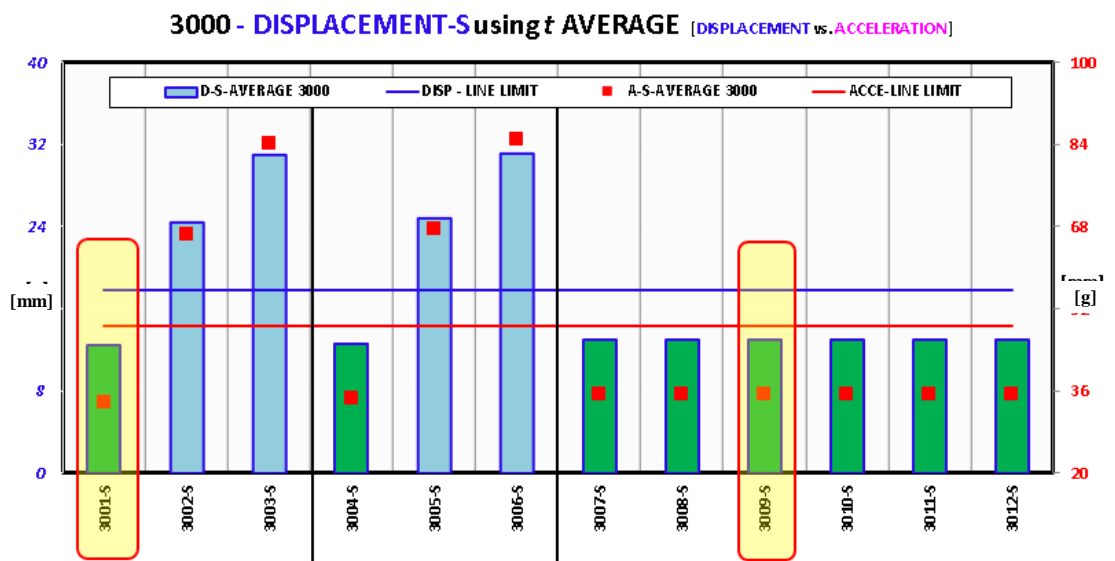


Figure 6-12: Simulation: Displacement at 3 m/s Based on Time (t)

Figure 6-13 shows that designs 3001-E (A), 3007-E (ABC), and 3009-E (BCA) have the best material configuration based on calculation from Table 6-10 (experiment). Figure 6-14 also shows that designs 3001-E (A), 3007-E (ABC), and 3009-E (BCA) have the best material configuration based on calculation from Table 6-9.

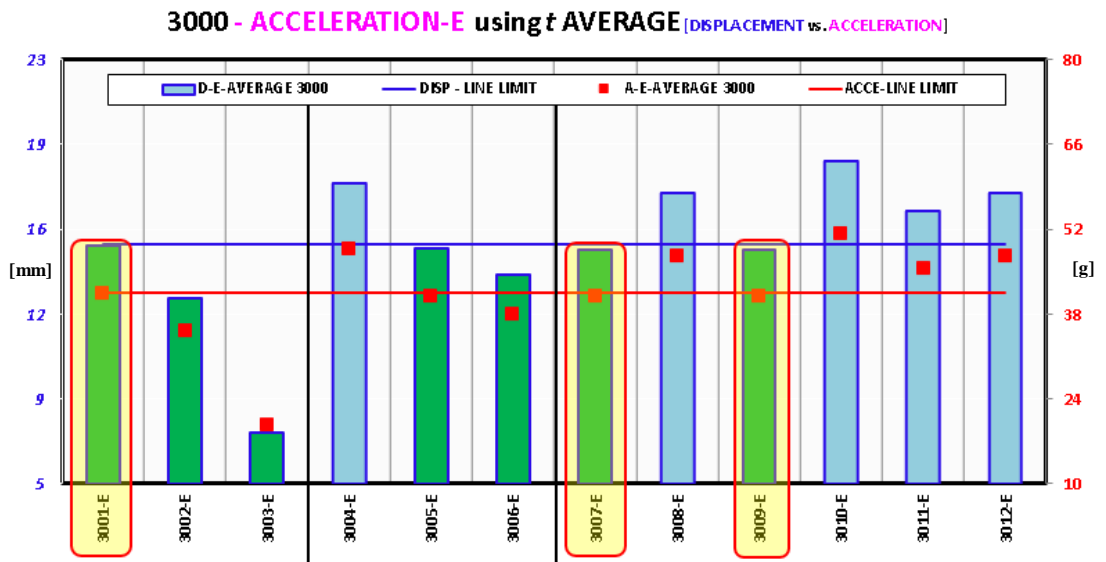


Figure 6-13: Experiment: Acceleration at 3 m/s Based on Time (t)

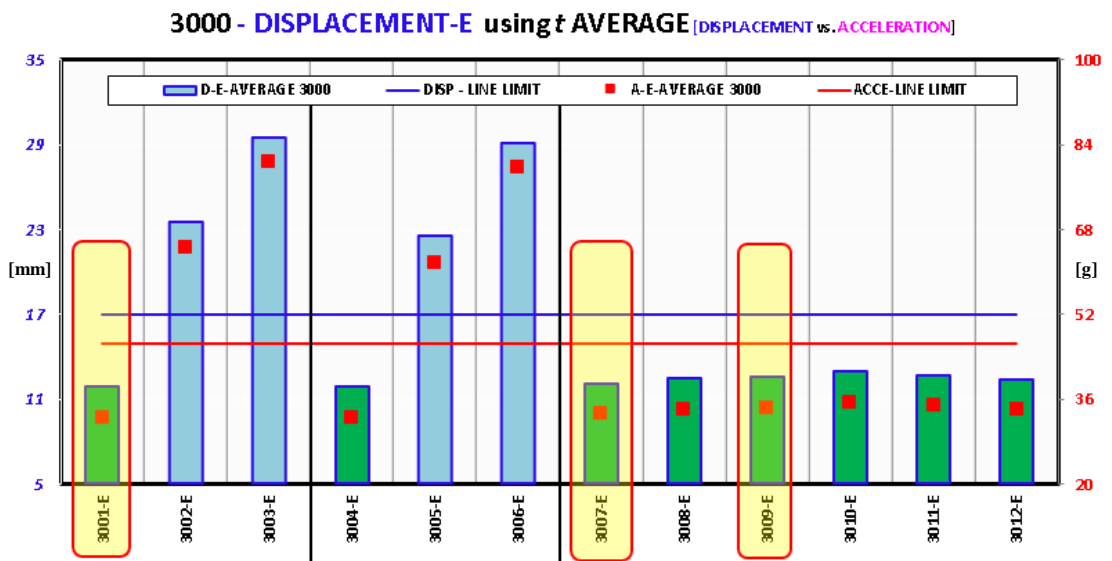


Figure 6-14: Experiment: Displacement at 3 m/s Based on Time (t)

Figure 6-11 to Figure 6-14 show the analysis based on time (t) average values for velocity at 3 m/s, there were proven by average value and parameter time as best material configuration. The best material configuration based on time (t) average values were design 3001(A) of single layer and 3009 (BCA) of combination layer.

6.2.3 Analysis Using Time (t) Average Approach at 4 m/s

Table 6-11 shows simulation of acceleration and displacement using impact velocity 4 m/s. Based on time (t) average of 1.0591 ms, the simulation average value of acceleration and displacement were 43.50 g and 27.61 mm respectively. All the values were compared to the average value where values that were lower than average will be selected as best material design configuration. Table 6-11 and Table 6-12 show no values that fulfil both criteria of the values below average of acceleration (43.50 g) and displacement (27.61 mm).

Table 6-11: The Best Design Based on time (t) Average Approach of Acceleration Simulation vs. Displacement Simulation at 4 m/s

SIMULATION : ACCELERATION (g) vs. DISPLACEMENT (mm) at 4 m/s													
MATERIAL DESIGN	SINGLE LAYER			MULTIPLE LAYER			COMBINATION LAYER						AVE
	A	B	C	AAA	BBB	CCC	ABC	CAB	BCA	CBA	BAC	ACB	
	4001-S	4002-S	4003-S	4004-S	4005-S	4006-S	4007-S	4008-S	4009-S	4010-S	4011-S	4012-S	
A-S-AVERAGE 2000 (g)	34.22	66.96	84.87	34.88	68.68	86.74	35.85	35.79	35.75	35.77	35.80	35.85	
D-S-AVERAGE 2000 (mm)	25.75	19.48	16.18	28.71	21.56	19.55	24.55	25.80	27.41	28.04	27.02	28.52	
$t = \sqrt{2S/a}$	1.227	0.763	0.617	1.283	0.792	0.671	1.170	1.201	1.238	1.252	1.229	1.261	1.059 ms
New A-S-AVERAGE 2000 (g)	45.94	34.76	28.87	51.23	38.47	34.88	43.80	46.02	48.90	50.04	48.20	50.89	43.50 g
New D-S-AVERAGE 2000 (mm)	19.18	37.53	47.57	19.55	38.50	48.62	20.10	20.06	20.04	20.05	20.06	20.10	27.61 mm

Table 6-12: The Best Design Based on time (t) Average Approach of Acceleration Experiment vs. Displacement Experiment at 4 m/s

EXPERIMENT : ACCELERATION (g) vs. DISPLACEMENT (mm) at 4 m/s													
MATERIAL DESIGN	SINGLE LAYER			MULTIPLE LAYER			COMBINATION LAYER						AVE
	A	B	C	AAA	BBB	CCC	ABC	CAB	BCA	CBA	BAC	ACB	
	4001-E	4002-E	4003-E	4004-E	4005-E	4006-E	4007-E	4008-E	4009-E	4010-E	4011-E	4012-E	
A-S-AVERAGE 2000 (g)	33.02	64.41	80.27	32.52	64.28	82.50	34.21	34.27	34.83	34.12	35.76	33.79	
D-S-AVERAGE 2000 (mm)	24.46	19.18	16.02	26.90	20.16	17.96	24.03	24.02	25.46	26.40	25.26	27.25	
$t = \sqrt{2S/a}$	1.217	0.772	0.632	1.286	0.792	0.660	1.185	1.184	1.209	1.244	1.189	1.270	1.053 ms
New A-S-AVERAGE 2000 (g)	44.10	34.58	28.88	48.49	36.34	32.37	43.31	43.30	45.90	47.59	45.53	49.12	41.63 g
New D-S-AVERAGE 2000 (mm)	18.32	35.73	44.53	18.04	35.66	45.77	18.98	19.01	19.32	18.93	19.84	18.74	26.07 mm

Table 6-12 shows the average values of experiment for acceleration and displacement that were 41.63 g and 26.07 mm respectively. All the values were

compared to the average value where values that were lower than average will be selected as best material design configuration. Table 6-11 and Table 6-12 show no values that fulfil both criteria for the values below average of acceleration (41.63 g) and displacement (26.07 mm).

To obtain a clear view on both tables, four bar chart were plotted out separated by simulation and experiment. Green bar signifies the displacement average and acceleration average below displacement and acceleration line limits. However, blue bar signifies either the acceleration average falls above acceleration line limit or displacement average higher than displacement line limit. Green bar fulfils criteria for the selection of material configuration. The green bar should also be validated again by both acceleration and displacement via simulation and experiment. The green bars that present in both acceleration and displacement were highlighted in yellow. There are acceleration and displacement both simulation and experiment. There were no highlighted cells from Table 6-11 and

Table 6-12, therefore no values were highlighted in Figure 6-15 to Figure 6-18: Hence, none of the design fulfil the criteria for best material configuration selected.

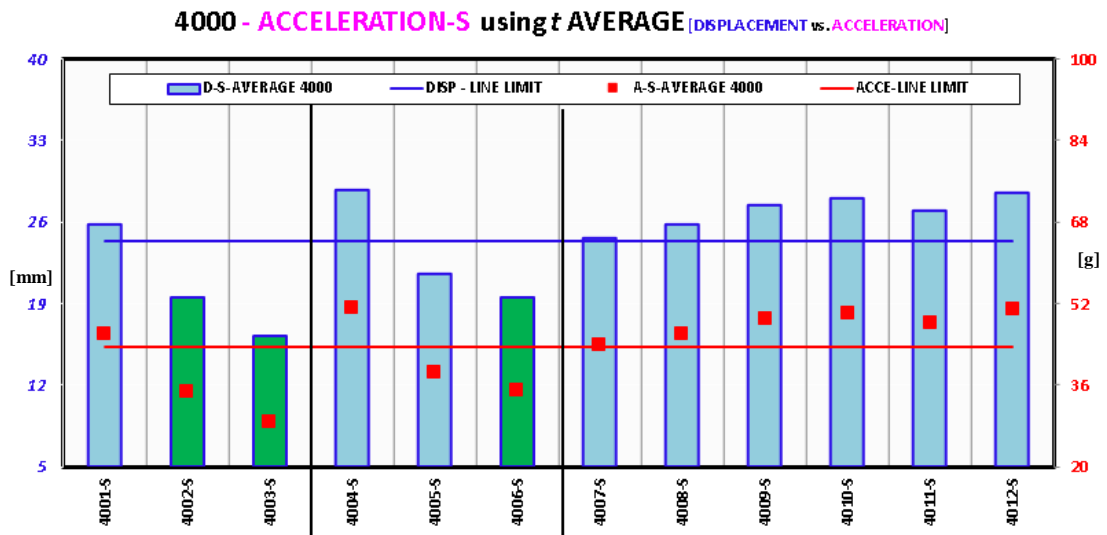


Figure 6-15: Simulation: Acceleration at 4 m/s Based on Time (t)

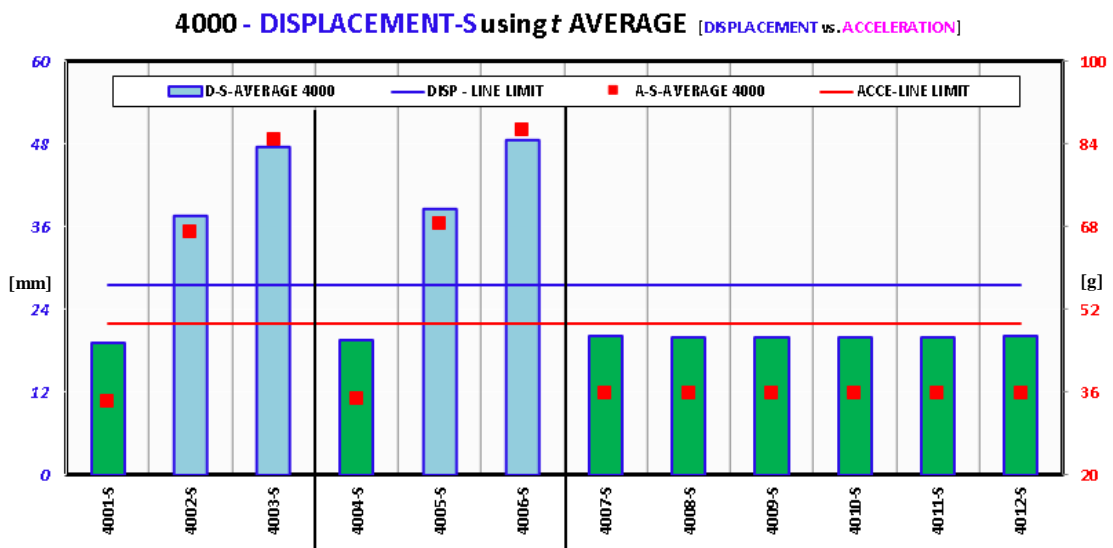


Figure 6-16: Simulation: Displacement at 4 m/s Based on Time (t)

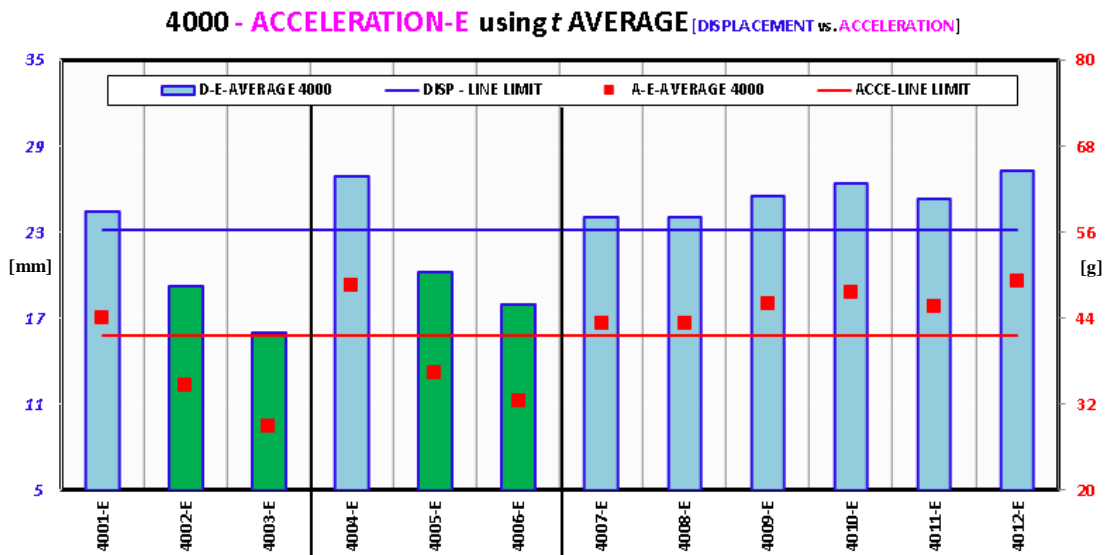


Figure 6-17: Experiment: Acceleration at 4 m/s Based on Time (t)

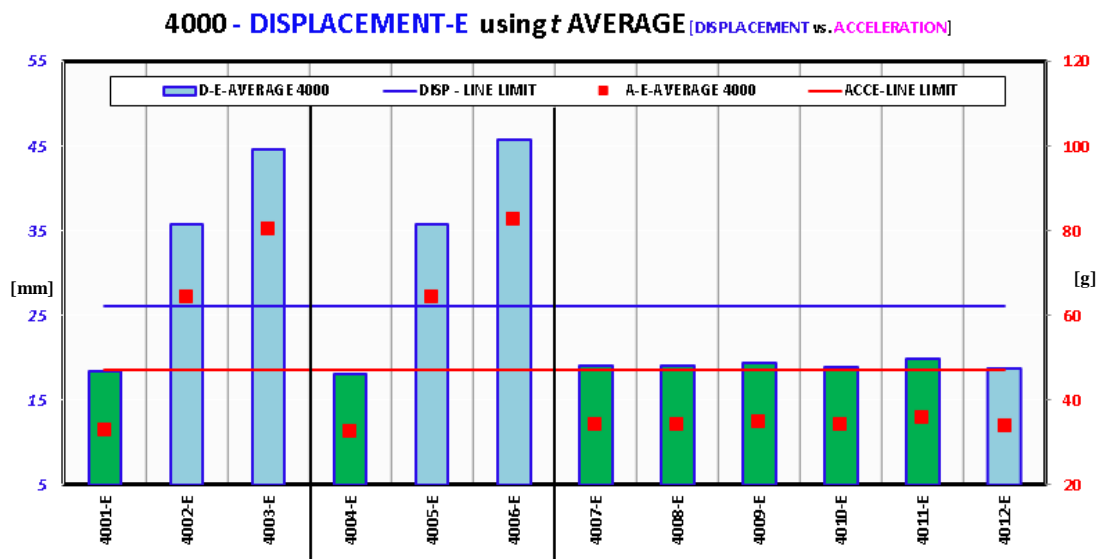


Figure 6-18: Experiment: Displacement at 4 m/s Based on Time (t)

Based on Figure 6-15 to Figure 6-18 , the analysis using average values with respect to time (t) does not provide best design configuration at impact velocity at 4 m/s.

6.2.4 Summary of Best Materials Selection Based on Time (t) Average Approach for Experiment and Simulation

Based on analysis carried out with respect to parameter time (t), at 2 m/s, design 2010 (CBA) was selected. For impact velocity 3 m/s, 3001 (A) of single layer and 3009 (BCA) of combination layer as best material configuration were selected. Finally, no best material could be selected for impact velocity 4 m/s.

To conclude the analysis of average values with respect to time (t), findings obtained were quite similar from section 6.1. This analysis however validate the previous experiment based on average value. Hence, objective 2 was reflected in this portion of analysis.

6.3 The Analysis on Space (S) vs. No-Space (NS) to Determine Best Design Configuration

Basically, this section discusses about comparison between space and no-space configuration. Refer to Figure 4-15, each space and no-space configurations were divided into 4 shapes design. Shapes proposed were Arc (ARC), Sinusoidal (SIN), square (SQ) and Trapezium (TR). Based from previous findings of acceleration and displacement from experiment, the best design found with impact velocity 2 m/s were the designs ABC (7), BCA (9) and CBA (10). Using impact velocity 3 m/s, only designs 7 (ABC) and 9 (BCA). Moreover, the best design based on simulation for acceleration and displacement with impact velocity 2 m/s is design no. 10 (CBA), while for velocity 3 m/s is design no. 9 (BCA).

Since design 9 (BCA) and 10 (CBA) shows Material A is arranged at lowest position (see Table 5-13), hence it is suitable for analysis conducted. Aside from design 9 (BCA) and 10 (CBA), design 7 (ABC) also being proposed for this analysis since the displacement value for this design is lower compared to displacement value of design 9 (BCA). Arrangement of Material A was at top position for impact velocity at 3 m/s and 4 m/s. In addition, the other design that suitable for analysis conducted is design 12 (ACB). The reason to include design 12 for analysis is because of displacement values for this design at all impact velocity incremental compared to design 7 (ABC). Also, design 12 have an arrangement of Material A that make this design obtained close displacement values than design 10 (CBA) at velocity 3 m/s. Furthermore, design 12 (ACB) have an arrangement of Material A at top position as suggested for impact velocity of 2 m/s and 4 m/s. Overall, design 7 (ABC), 9 (BCA), 10 (CBA) and 12 (ACB) were proposed for analysis.

Table 6-13 shows design configuration with naming style used from this section onwards. The terms for design with no-space and space, were “NS” and “S” respectively. The impact velocity remains at 2 m/s, 3 m/s and 4 m/s.

Table 6-13: Design Configuration for Shape Simulation.

SHAPE	NO-SPACE [NS] / SPACE[S]	DESIGN No. 7	DESIGN No. 9	DESIGN No. 10	DESIGN No. 12
ARC [ARC]	NS	1-2007-NS	9-2009-NS	17-2010-NS	25-2012-NS
	S	2-2007-S	10-2009-S	18-2010-S	26-2012-S
SINUSOIDAL [SIN]	NS	3-2007-NS	11-2009-NS	19-2010-NS	27-2012-NS
	S	4-2007-S	12-2009-S	20-2010-S	28-2012-S
SQUARE [SQ]	NS	5-2007-NS	13-2009-NS	21-2010-NS	29-2012-NS
	S	6-2007-S	14-2009-S	22-2010-S	30-2012-S
TRAPEZIUM [TR]	NS	7-2007-NS	15-2009-NS	23-2010-NS	31-2012-NS
	S	8-2007-S	16-2009-S	24-2010-S	32-2012-S

Table 6-14 shows the acceleration results of shape design configuration for ARC (arc), SIN (sinusoidal), SQ (square), and TR (trapezium) with impact velocity 2 m/s, 3 m/s, and 4 m/s for no-space (NS) and space (S). At impact velocity 2 m/s, design 2007 with TR (trapezium) shape shows highest maximum values of acceleration for no-space and space that are 34.88 g and 34.91 g respectively. At impact velocity 3 m/s, design 3007 with TR (trapezium) shape shows highest maximum values of acceleration, for no-space and space that are 35.87 g and 35.90 g. Whilst, design 3012 with TR (trapezium) shows the highest maximum values only for space configuration, that is 35.90 g. Moreover, for acceleration at impact velocity 4 m/s, design 4007 of TR (trapezium) shape shows highest maximum values for no-space and space that are, 36.56 g and 36.63 g respectively.

Table 6-14: The Acceleration Results of Shape Design Configuration for Space and No-Space

Acceleration (g) at IMPACT VELOCITY 2 m/s																
MATERIAL DESIGN	ARC (Arc)				SIN (Sinusoidal)				SQ (Square)				TR (Trapezium)			
	2007	2009	2010	2012	2007	2009	2010	2012	2007	2009	2010	2012	2007	2009	2010	2012
NO-SPACE [NS]	34.64	34.65	34.52	34.87	34.72	34.46	34.51	34.71	34.86	34.77	34.49	34.87	34.88	34.66	34.66	34.87
SPACE [S]	32.57	34.11	33.87	32.68	33.61	34.68	34.68	33.60	34.87	34.15	34.17	34.87	34.91	34.67	34.50	34.90
Acceleration (g) at IMPACT VELOCITY 3 m/s																
MATERIAL DESIGN	ARC (Arc)				SIN (Sinusoidal)				SQ (Square)				TR (Trapezium)			
	3007	3009	3010	3012	3007	3009	3010	3012	3007	3009	3010	3012	3007	3009	3010	3012
NO-SPACE [NS]	35.54	35.29	35.28	35.52	35.62	35.09	35.29	35.61	35.55	35.44	35.43	35.53	35.87	35.25	35.25	35.87
SPACE [S]	35.16	34.98	34.95	34.84	35.21	35.27	35.26	35.21	35.53	35.23	35.22	35.52	35.90	35.28	35.27	35.90
Acceleration (g) at IMPACT VELOCITY 4 m/s																
MATERIAL DESIGN	ARC (Arc)				SIN (Sinusoidal)				SQ (Square)				TR (Trapezium)			
	4007	4009	4010	4012	4007	4009	4010	4012	4007	4009	4010	4012	4007	4009	4010	4012
NO-SPACE [NS]	36.05	35.72	35.74	36.05	36.15	35.78	35.66	36.14	36.01	35.91	35.93	36.01	36.56	35.66	35.67	36.56
SPACE [S]	35.81	35.57	35.54	35.83	35.80	35.72	35.75	35.80	36.04	35.82	35.84	36.04	36.63	35.74	35.76	36.62

Figure 6-19 shows the examples of material design based on shape with space and no-space configuration for acceleration with impact velocity 2 m/s, 3 m/s, 4 m/s. All the graph of acceleration for no-space and space can be view in Appendix G.

Figure 6-19(a to f) shows the acceleration result of material design with space and no-space at different velocity. All figures show similar results with very small differences in percentage.

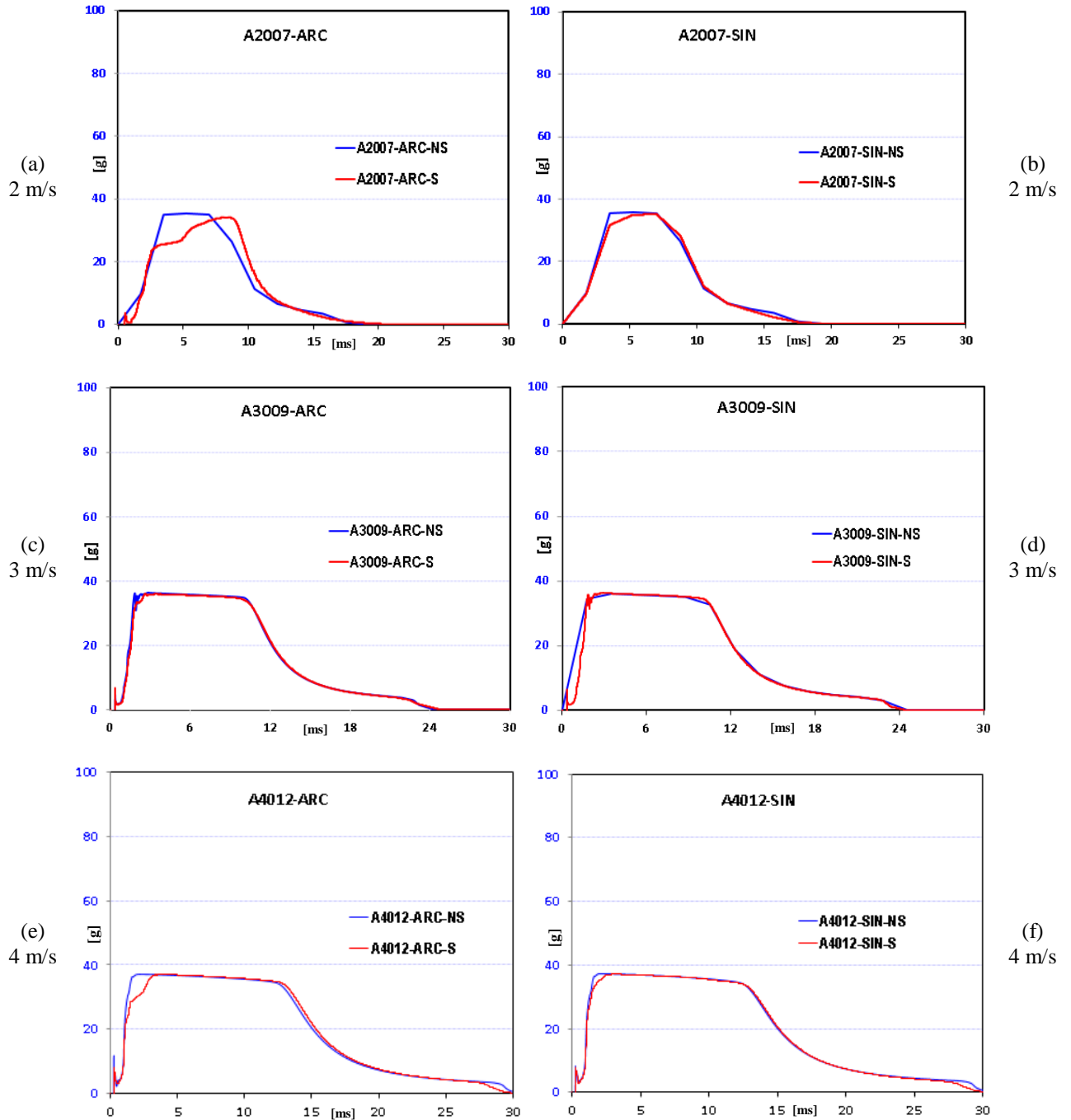


Figure 6-19: The Acceleration Results of Material Design Configuration with Impact Velocity 2 m/s, 3 m/s, 4 m/s Between Space (S) and No-Space (NS)

Table 6-15 shows the displacement results of shape design configuration such as ARC (arc), SIN (sinusoidal), SQ (square), and TR (trapezium) with impact velocity 2 m/s, 3 m/s, and 4 m/s for no-space (NS) and space (S). At impact velocity 2 m/s, design 2009 with SQ (square) shape shows highest maximum values of displacement for no-space that is 8.37 mm and for space is design 2007 with ARC (arc) shape that is 9.65 mm. At impact velocity 3 m/s, design 3009 with ARC (arc) shape shows highest maximum values of displacement for no-space that is 14.99 mm and for space is design 3007 with ARC (arc) shape that is 16.13 mm. Moreover, for displacement at impact velocity 4 m/s, design 4009 and 4010 of ARC (arc) shares the same highest maximum values for no-space that is 24.11 mm. Whilst, the highest values for space configuration is on design 4007 of ARC (arc) shape design, which is 25.07 mm.

Table 6-15: The Displacement Results of Shape Design Configuration for Space and No-Space

Displacement (mm) at IMPACT VELOCITY 2 m/s																
MATERIAL DESIGN	ARC (Arc)				SIN (Sinusoidal)				SQ (Square)				TR (Trapezium)			
	2007	2009	2010	2012	2007	2009	2010	2012	2007	2009	2010	2012	2007	2009	2010	2012
NO-SPACE [NS]	8.28	8.34	8.25	8.36	8.27	8.25	8.24	8.27	8.36	8.37	8.27	8.36	8.36	8.31	8.31	8.35
SPACE [S]	9.65	8.60	8.63	9.64	8.69	8.40	8.40	8.70	8.32	8.40	8.39	8.33	8.32	8.28	8.28	8.31
Displacement (mm) IMPACT VELOCITY 3 m/s																
MATERIAL DESIGN	ARC (Arc)				SIN (Sinusoidal)				SQ (Square)				TR (Trapezium)			
	3007	3009	3010	3012	3007	3009	3010	3012	3007	3009	3010	3012	3007	3009	3010	3012
NO-SPACE [NS]	14.97	14.99	14.98	14.90	14.88	14.91	14.90	14.87	14.95	14.96	14.96	14.96	14.87	14.96	14.95	14.87
SPACE [S]	16.13	15.27	15.30	16.06	15.26	15.04	15.04	15.26	14.92	15.02	15.01	14.93	14.82	14.92	14.92	14.82
Displacement (mm) IMPACT VELOCITY 4 m/s																
MATERIAL DESIGN	ARC (Arc)				SIN (Sinusoidal)				SQ (Square)				TR (Trapezium)			
	4007	4009	4010	4012	4007	4009	4010	4012	4007	4009	4010	4012	4007	4009	4010	4012
NO-SPACE [NS]	23.97	24.11	24.11	23.98	23.85	24.03	24.02	23.86	23.96	24.00	23.99	23.97	23.68	24.09	24.09	23.68
SPACE [S]	25.07	24.41	24.44	23.96	24.26	24.16	24.16	24.27	23.93	24.07	24.06	23.94	23.61	24.05	24.04	23.61

Figure 6-20 showed the examples of material design based on shape with space and no-space configuration for displacement with impact velocity 2 m/s, 3 m/s, 4 m/s. All the graph of displacement for no-space and space can be view in Appendix H.

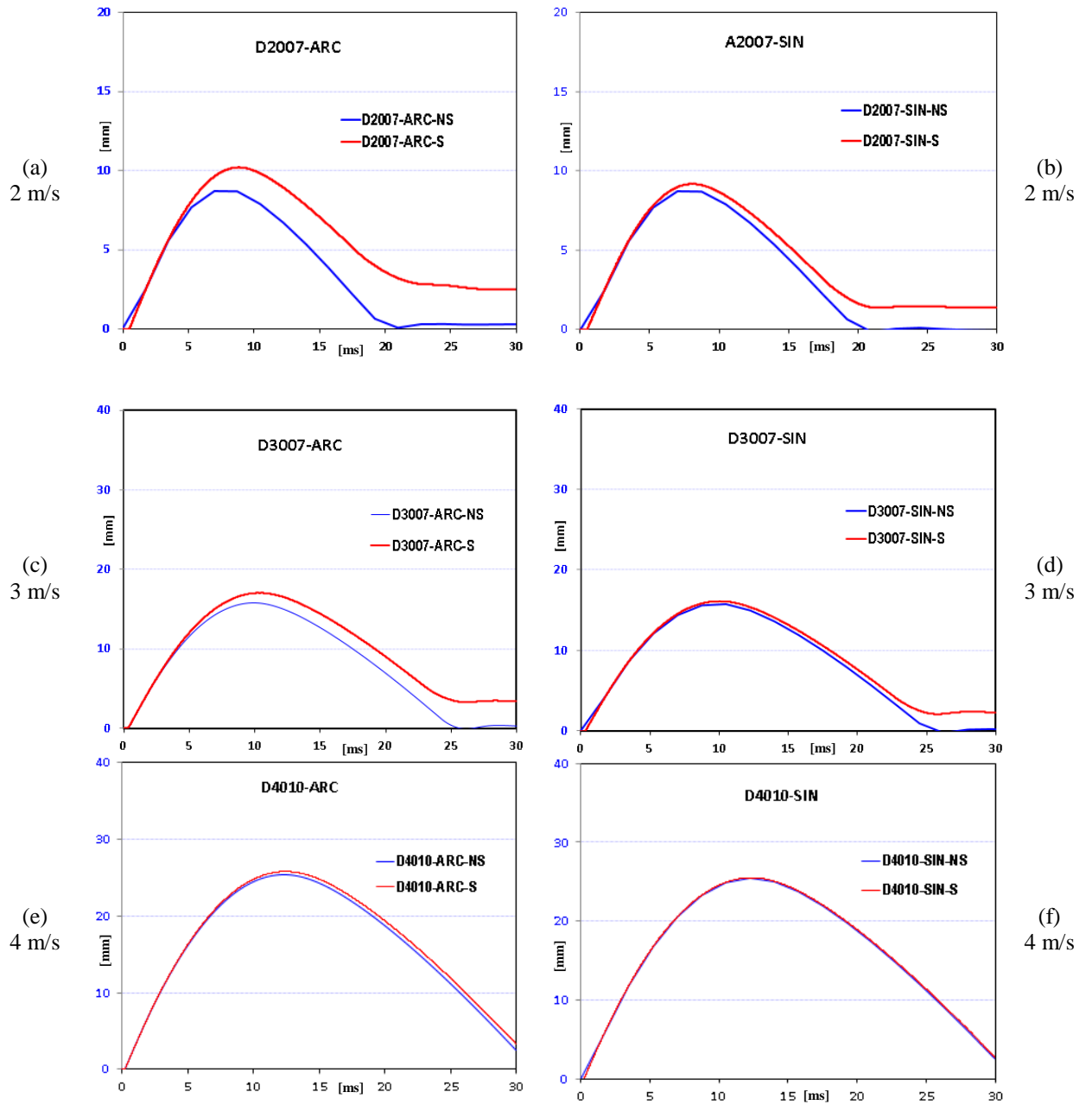


Figure 6-20: The Displacement Results Material Design Configuration with Impact Velocity 2 m/s, 3 m/s, 4 m/s Between Space (S) and No-Space (NS)

6.3.1 Space (S) vs. No-Space (NS) Design Based on Average Values of Acceleration and Displacement

The analysis were conducted using statistical approach while validation process were carried out using average values method. Data for acceleration and displacement of space and no-space acquired through simulations.

6.3.1.1 Average Values Approach at 2 m/s

Table 6-16 shows the acceleration and displacement data with average values approach applied. Blue shaded cells represent any single value of space and no-space data that are smaller than their respective average value. However, orange shaded cells show both values of space and no-space configuration that falls below average data values. Red-coloured-font values act as indicators to prove that both data from space and no-space plotted below than average line.

Table 6-16 shows displacement values of no-space in arc shape for design 7 and 10 that were below no-space average. Similarly, the selection using average value is also applied to no-space configuration to determine which design have lower values than average no-space in displacement.

Next, shape discussed was sinusoidal. For acceleration values, two cells highlighted in blue signify that design 9 and 10 are below no-space average. For displacement values, design 9 and 10 for space and no-space configuration were highlighted in orange colour with red-coloured-font. This signify that displacement values of space and no-space are lower than average space, average no-space and

overall average line.

Table 6-16: Data Computation Based on Average Approach at 2 m/s

2 m/s	ARC				SIN				SQ				TR			
	2007	2009	2010	2012	2007	2009	2010	2012	2007	2009	2010	2012	2007	2009	2010	2012
Acceleration NS (g)	34.64	34.65	34.52	34.87	34.72	34.46	34.51	34.71	34.86	34.77	34.49	34.87	34.88	34.66	34.66	34.87
Acceleration SPACE (g)	32.57	34.11	33.87	32.68	33.61	34.68	34.68	33.60	34.87	34.15	34.17	34.87	34.91	34.67	34.50	34.90
NO-SPACE Average (g)	34.70	34.70	34.70	34.70	34.70	34.70	34.70	34.70	34.70	34.70	34.70	34.70	34.70	34.70	34.70	34.70
SPACE Average (g)	34.18	34.18	34.18	34.18	34.18	34.18	34.18	34.18	34.18	34.18	34.18	34.18	34.18	34.18	34.18	34.18
Acceleration Ave -L(g)	34.44	34.44	34.44	34.44	34.44	34.44	34.44	34.44	34.44	34.44	34.44	34.44	34.44	34.44	34.44	34.44
Displacement NS (mm)	8.28	8.34	8.25	8.36	8.27	8.25	8.24	8.27	8.36	8.37	8.27	8.36	8.36	8.31	8.31	8.35
Displacement SPACE (mm)	9.65	8.60	8.63	9.64	8.69	8.40	8.40	8.70	8.32	8.40	8.39	8.33	8.32	8.28	8.28	8.31
NO-SPACE Average (mm)	8.31	8.31	8.31	8.31	8.31	8.31	8.31	8.31	8.31	8.31	8.31	8.31	8.31	8.31	8.31	8.31
SPACE Average (mm)	8.58	8.58	8.58	8.58	8.58	8.58	8.58	8.58	8.58	8.58	8.58	8.58	8.58	8.58	8.58	8.58
Displacement Ave -L (mm)	8.45	8.45	8.45	8.45	8.45	8.45	8.45	8.45	8.45	8.45	8.45	8.45	8.45	8.45	8.45	8.45

Next, square shape were analysed towards acceleration values where design 10 were highlighted with orange colour. Space value were highlighted in red-coloured font. This signify that only space value falls below average space and overall average line. For displacement values, only design 10 for space and no-space configurations were highlighted orange with red font. This signify that displacement values of space and no-space are lower than average space, average no-space and overall average line.

Last shape discussed was trapezium shape. Acceleration value with no-space for design 10 were highlighted in blue. The values of design 10 with no-space configuration shows below than average values of no-space. For displacement values, only design 10 for space and no-space configuration were highlighted in orange with red-coloured-font. This signify that displacement values of space and no-space are lower than average space, average no-space and overall average line.

ACCELERATION - 2000 SPACE vs. NO-SPACE

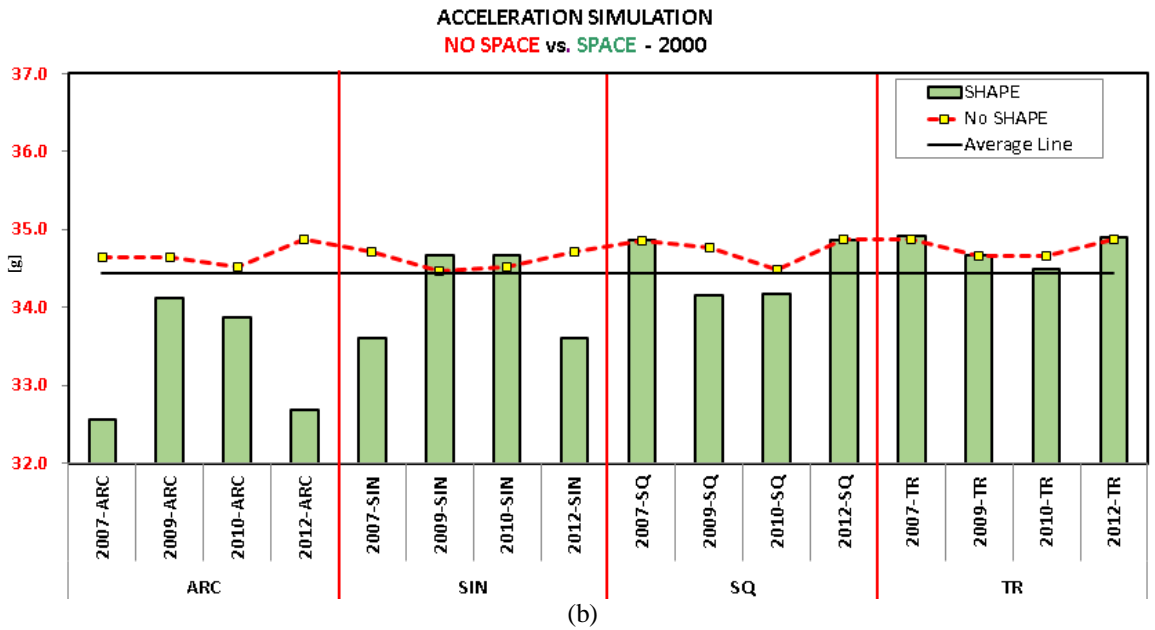
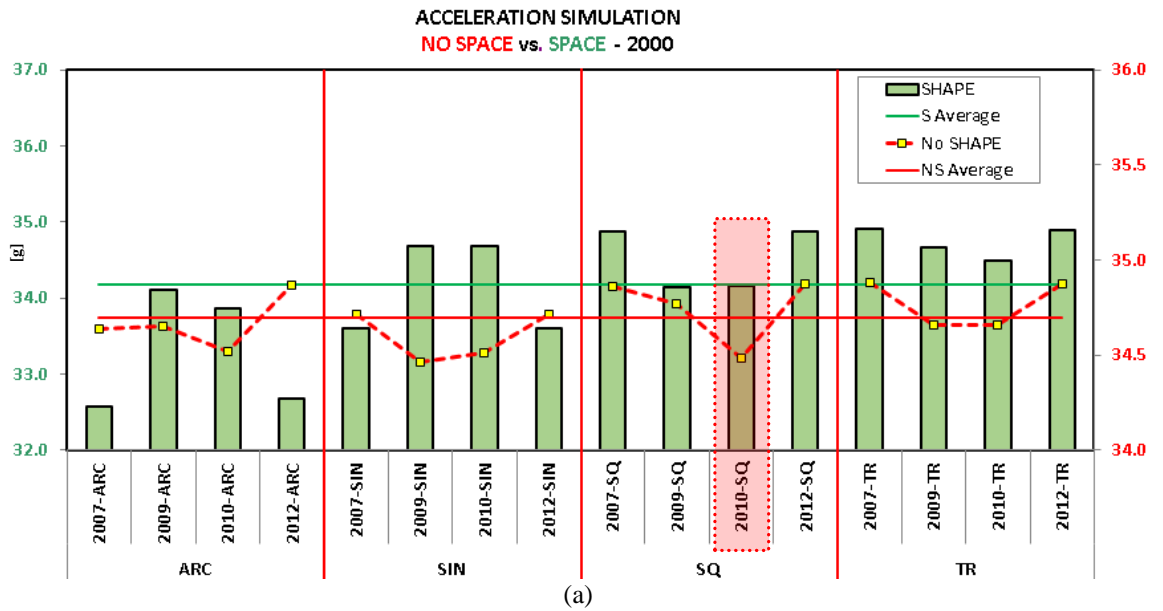


Figure 6-21: The Best Design for Impact Velocity 2 m/s ; (a) Acceleration - Space Average and No-space Average, (b) Acceleration - Space and No-space Compared to Average Line

Figure 6-21(a) was plotted based on Table 6-16, there is only design 2010 highlighted. This design was highlighted because the space and no-space value falls below space and no-space average line. However, in Figure 6-21(b), no design was highlighted because the space and no-space values does not fall completely below the

overall average line.

Figure 6-22(a) was plotted based on Table 6-16, where design 2009-SIN (sinusoidal), 2010-SIN (sinusoidal) and 2010-SQ (square) were highlighted. These designs were highlighted because space and no-space value falls below space and no-space average line.

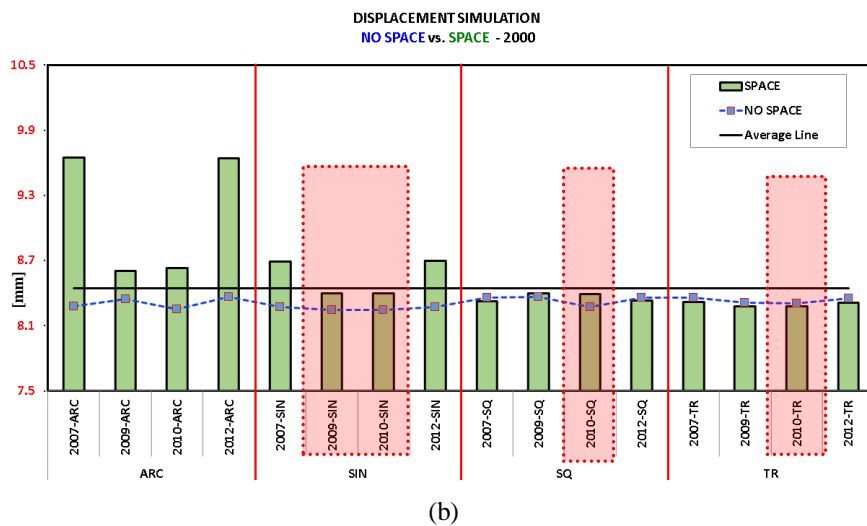
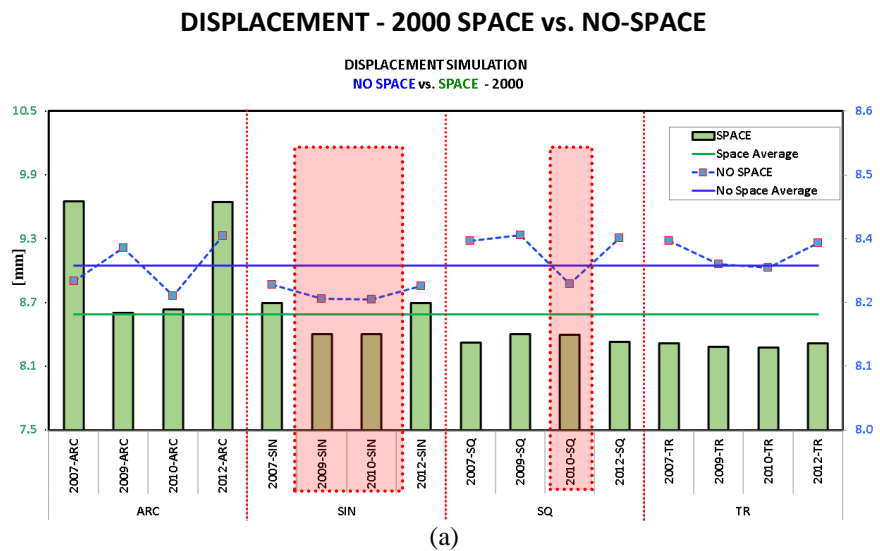


Figure 6-22: The Best Design for Impact Velocity 2 m/s; (a) Displacement - Space Average and No-Space Average, (b) Displacement - Space and No-Space Compared to Average Line

However, in Figure 6-22(b), four designs were selected due to both average space and no-space falls below overall average line. The designs selected were 2009-SIN

(sinusoidal), 2010-SIN (sinusoidal), 2009-SQ (square) and 2010-SQ (square).

6.3.1.2 Average Values Approach at 3 m/s

Table 6-17 shows the acceleration and displacement data with average values approach applied. Blue shaded cells represent any single value of space and no-space data that are smaller than their respective average value. However, orange shaded cells show both values of space and no-space configuration that falls below average data values. Red-coloured-font values act as indicators to prove that both data from space and no-space plotted below than average line.

Table 6-17 shows acceleration values in arc shape for design 9 and 10 plotted below average no-space, average space and overall average line. For displacement value, only design 12 from no-space configuration were plotted below than no-space average.

Next, shape discussed was sinusoidal. For acceleration values, two cells were highlighted in orange with red-coloured-font signify that design 9 and 10 values are below space average, no-space average and overall average line. For displacement values, design 9 and 10 for space and no-space configuration were highlighted in orange with red-coloured-font. This signify that displacement values of space and no-space are lower than average space, average no-space and overall average line. For design 7 and 12, only no-space value falls below no-space average.

Next shape analysed was square shape. For acceleration value, design 9 and 10 were highlighted in orange, which signifies space and no-space values that falls below

average space and no-space. For displacement values, all four designs of 7, 9, 10 and 12 for space configurations were highlighted in blue. This signify that displacement values of space configuration are lower than average space.

Table 6-17: The Best Design Based on Average Approach of Acceleration vs. Displacement at 3 m/s

3 m/s	ARC				SIN				SQ				TR			
	3007	3009	3010	3012	3007	3009	3010	3012	3007	3009	3010	3012	3007	3009	3010	3012
Acceleration NS (g)	35.54	35.29	35.28	35.52	35.62	35.09	35.29	35.61	35.55	35.44	35.43	35.53	35.87	35.25	35.25	35.87
Acceleration SPACE (g)	35.16	34.98	34.95	34.84	35.21	35.27	35.26	35.21	35.53	35.23	35.22	35.52	35.90	35.28	35.27	35.90
NO-SPACE Average (g)	35.46	35.46	35.46	35.46	35.46	35.46	35.46	35.46	35.46	35.46	35.46	35.46	35.46	35.46	35.46	35.46
SPACE Average (g)	35.30	35.30	35.30	35.30	35.30	35.30	35.30	35.30	35.30	35.30	35.30	35.30	35.30	35.30	35.30	35.30
Acceleration Ave -L(g)	35.38	35.38	35.38	35.38	35.38	35.38	35.38	35.38	35.38	35.38	35.38	35.38	35.38	35.38	35.38	35.38
Displacement NS (mm)	14.97	14.99	14.98	14.90	14.88	14.91	14.90	14.87	14.95	14.96	14.96	14.96	14.87	14.96	14.95	14.87
Displacement SPACE (mm)	16.13	15.27	15.30	16.06	15.26	15.04	15.04	15.26	14.92	15.02	15.01	14.93	14.82	14.92	14.92	14.82
NO-SPACE Average (mm)	14.93	14.93	14.93	14.93	14.93	14.93	14.93	14.93	14.93	14.93	14.93	14.93	14.93	14.93	14.93	14.93
SPACE Average (mm)	15.17	15.17	15.17	15.17	15.17	15.17	15.17	15.17	15.17	15.17	15.17	15.17	15.17	15.17	15.17	15.17
Displacement Ave -L (mm)	15.05	15.05	15.05	15.05	15.05	15.05	15.05	15.05	15.05	15.05	15.05	15.05	15.05	15.05	15.05	15.05

Lastly, characteristics of trapezium shape was discussed. Acceleration value of design 9 and 10 were highlighted in orange with red-coloured-font because the space and no-space values fall below average space, average no-space and overall average line. For displacement values, design 7 and 12 were highlighted in orange with red-coloured-font because the space and no-space values fall below average space, average no-space and overall average line. For design 9 and 10, only space value falls below average space.

Figure 6-23 and Figure 6-24 were plotted based on Table 6-17. Blue boxes indicate that there was no pairing between Figure 6-23(a) and (b), and Figure 6-24(a) and (b). However, orange boxes indicate that there was pairing between both figures. For acceleration, design 9 and 10 from sinusoidal shape were selected due to space and no-space value fall below the space average, no-space average and overall average. However, only sinusoidal shape was highlighted in orange because of the pairing and the values falls below average line that occurs between two figures.

ACCELERATION - 3000 SPACE vs. NO-SPACE

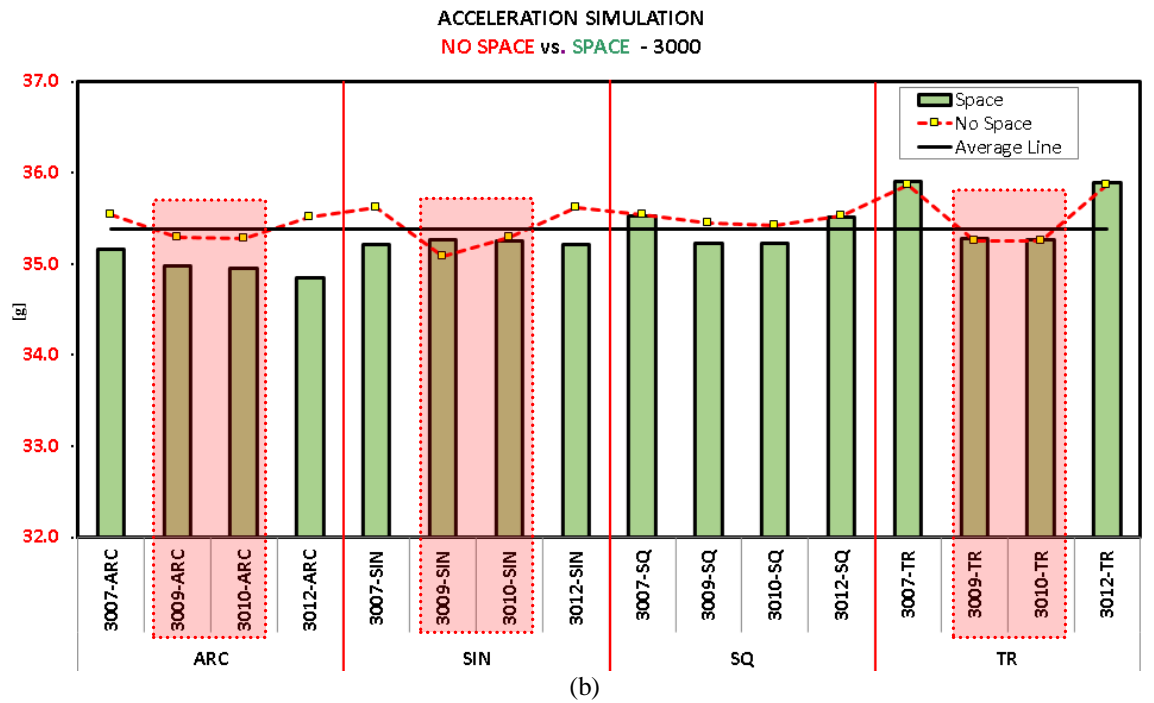
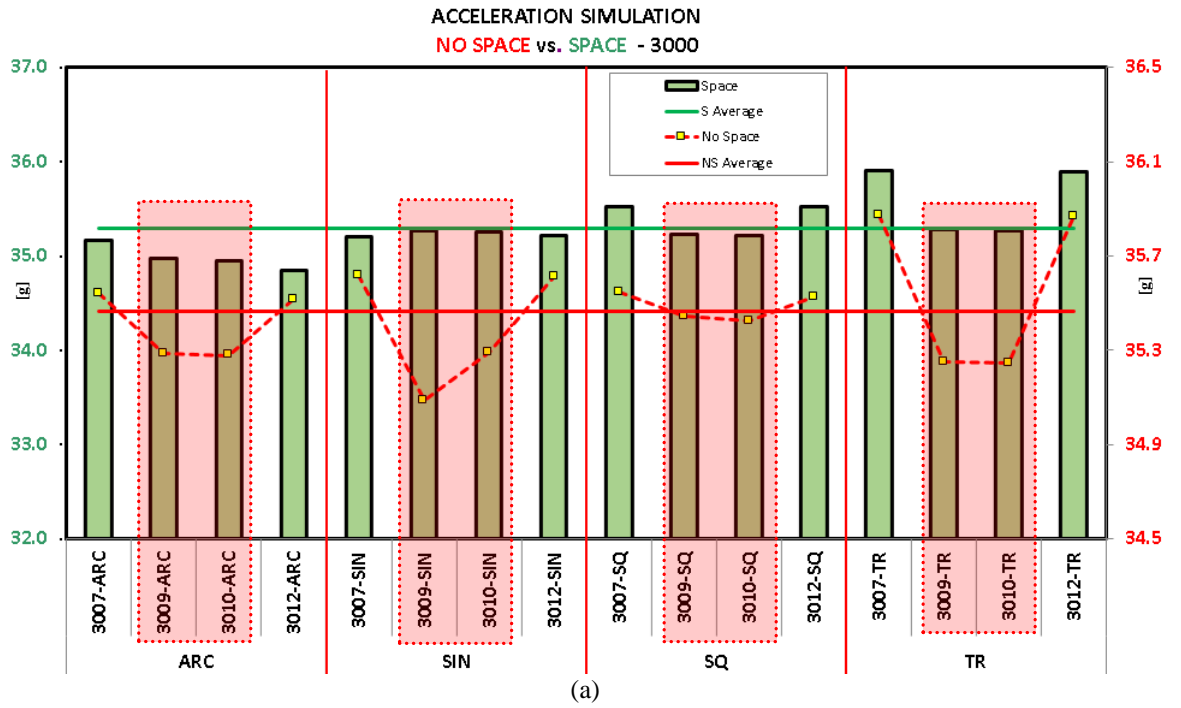


Figure 6-23: The Best Design for Impact Velocity 3 m/s ; (a) Acceleration - Space Average and No-Space Average, (b) Acceleration - Space and No-Space Compared to Average Line

DISPLACEMENT - 3000 SPACE vs. NO-SPACE

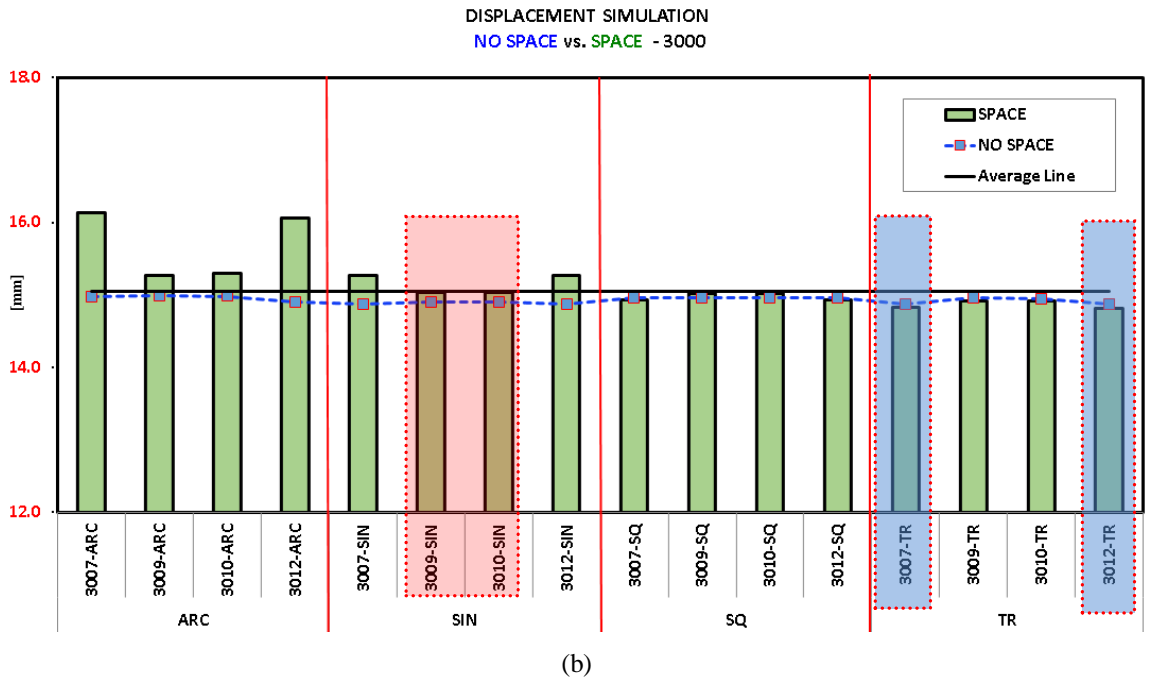
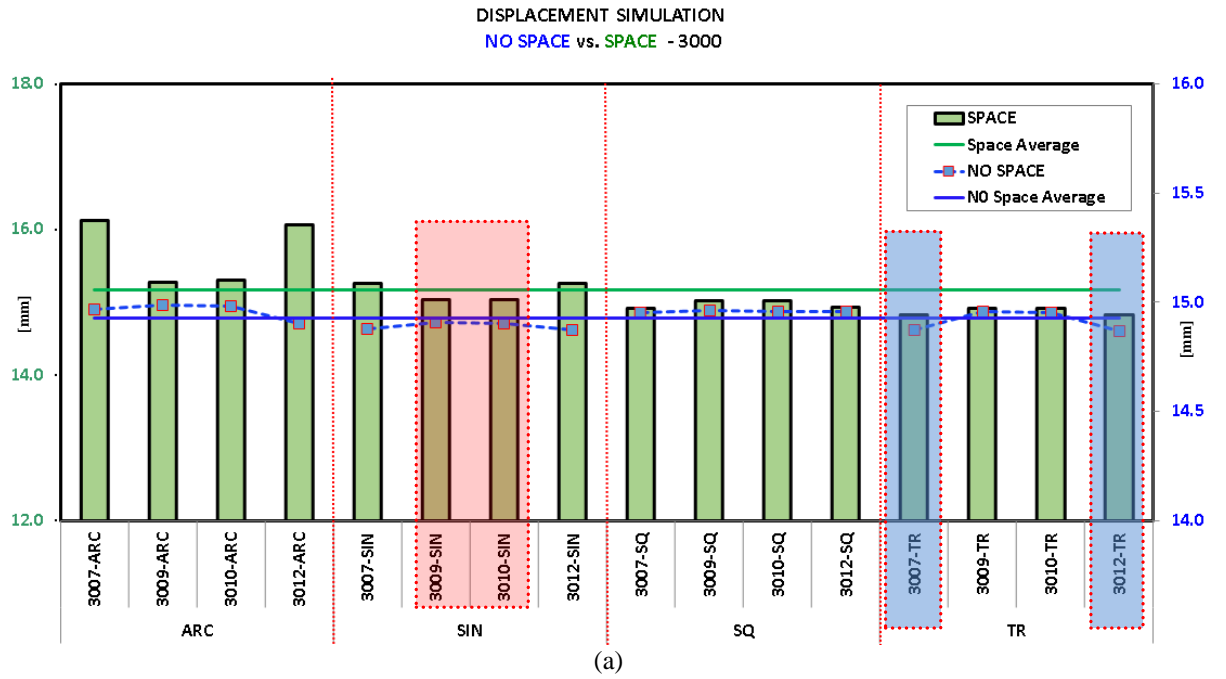


Figure 6-24: The Best Design for Impact Velocity 3 m/s ; (a) Displacement - Space Average and No-Space Average, (b) Displacement - Space and No-Space Compared to Average Line

6.3.1.3 Average Values Approach at 4 m/s

Table 6-18 shows the acceleration and displacement data with average values approach applied. Blue shaded cells represent any single value of space and no-space data that are smaller than their respective average value. However, orange shaded cells show both values of space and no-space configuration that falls below average data values. Red-coloured-font values act as indicators to prove that both data from space and no-space plotted below than average line.

Table 6-18 shows acceleration values for design 9 and 10 arc shape that are below average no-space, average space and overall average line. However, for design 7 and 12, only space configuration falls below space average values. For displacement, only design 12 was selected, because the displacement space configuration values fall below space average line.

Table 6-18: The Best Design Based on Average Approach of Acceleration vs. Displacement at 4 m/s

4 m/s	ARC				SIN				SQ				TR			
	4007	4009	4010	4012	4007	4009	4010	4012	4007	4009	4010	4012	4007	4009	4010	4012
Acceleration NS (g)	36.05	35.72	35.74	36.05	36.15	35.78	35.66	36.14	36.01	35.91	35.93	36.01	36.56	35.66	35.67	36.56
Acceleration SPACE (g)	35.81	35.57	35.54	35.83	35.80	35.72	35.75	35.80	36.04	35.82	35.84	36.04	36.63	35.74	35.76	36.62
NO-SPACE Average (g)	35.98	35.98	35.98	35.98	35.98	35.98	35.98	35.98	35.98	35.98	35.98	35.98	35.98	35.98	35.98	35.98
SPACE Average (g)	35.89	35.89	35.89	35.89	35.89	35.89	35.89	35.89	35.89	35.89	35.89	35.89	35.89	35.89	35.89	35.89
Acceleration Ave –L (g)	35.94	35.94	35.94	35.94	35.94	35.94	35.94	35.94	35.94	35.94	35.94	35.94	35.94	35.94	35.94	35.94
Displacement NS (mm)	23.97	24.11	24.11	23.98	23.85	24.03	24.02	23.86	23.96	24.00	23.99	23.97	23.68	24.09	24.09	23.68
Displacement SPACE (mm)	25.07	24.41	24.44	23.96	24.26	24.16	24.16	24.27	23.93	24.07	24.06	23.94	23.61	24.05	24.04	23.61
NO-SPACE Average (mm)	23.96	23.96	23.96	23.96	23.96	23.96	23.96	23.96	23.96	23.96	23.96	23.96	23.96	23.96	23.96	23.96
SPACE Average (mm)	24.13	24.13	24.13	24.13	24.13	24.13	24.13	24.13	24.13	24.13	24.13	24.13	24.13	24.13	24.13	24.13
Displacement Ave –L (mm)	24.04	24.04	24.04	24.04	24.04	24.04	24.04	24.04	24.04	24.04	24.04	24.04	24.04	24.04	24.04	24.04

Next shape discussed was sinusoidal. For acceleration values, two cells were highlighted in orange with red-coloured-font signifies that design 9 and 10 values are below space average, no-space average and overall average line. However, for design

7 and 12, only space configuration falls below space average. For displacement, only design 7 and 12 were selected, because the displacement value of no-space configuration falls below no-space average line.

Next shape analysed was square shape. For acceleration values, two cells highlighted orange with red-coloured-font signify that design 9 and 10 values are below space average, no-space average and overall average line. For displacement values, all four designs 7, 9, 10 and 12 for space configuration were highlighted in blue. This signify that displacement values of space configuration are lower than average space.

Last shape discussed was trapezium shape. Acceleration value of design 9 and 10 were highlighted in orange with red-coloured-font because the space and no-space values fall below average space, average no-space and overall average line. However, design 12 was highlighted in blue because space configuration value falls below space average line. For displacement values, design 7 and 12 were highlighted in orange with red-coloured-font because the space and no-space values fall below average space, average no-space and overall average line. For design 9 and 10, only space value falls below average space.

Figure 6-25(a) and (b) were plotted based on Table 6-18, all four shapes were selected and paired accordingly. For all shapes, design 9 and 10 were selected because all the space and no-space configuration values fall below space average, no-space average and overall average line.

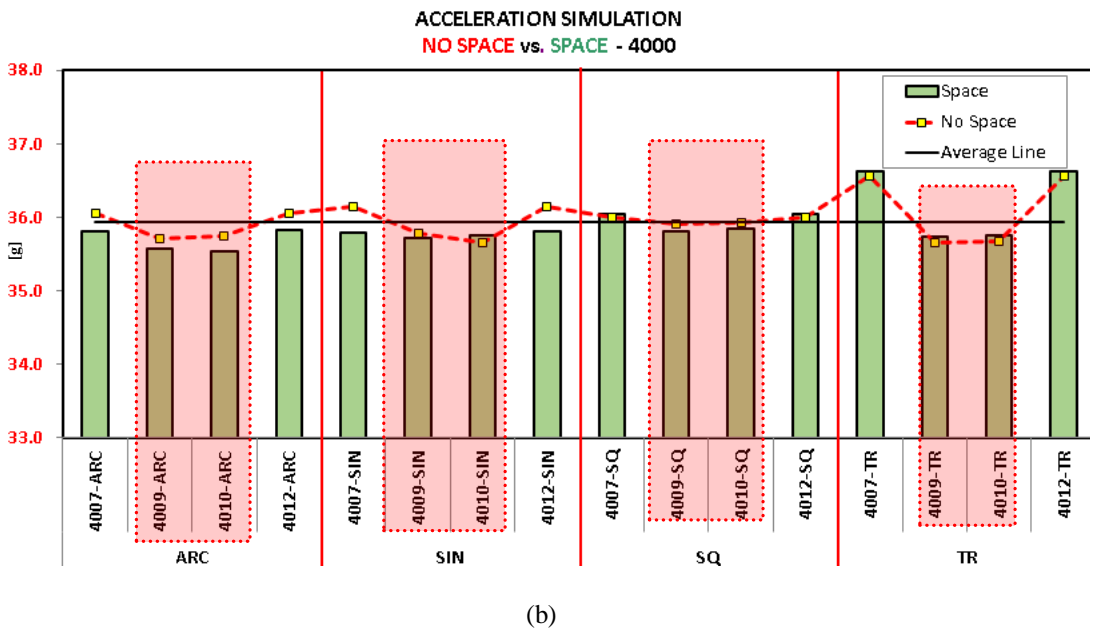
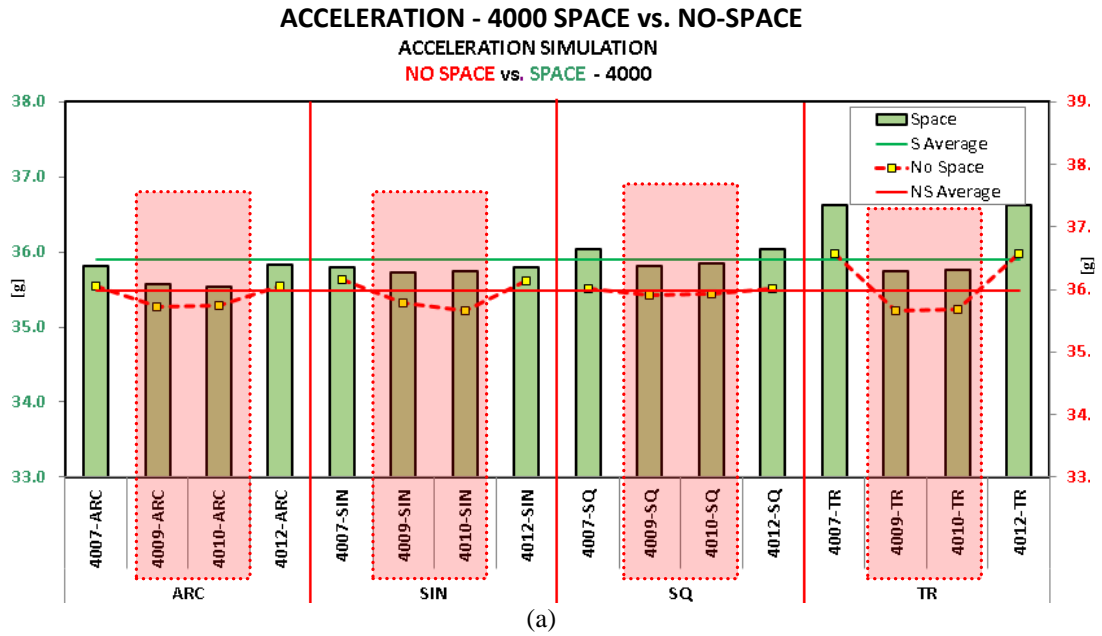
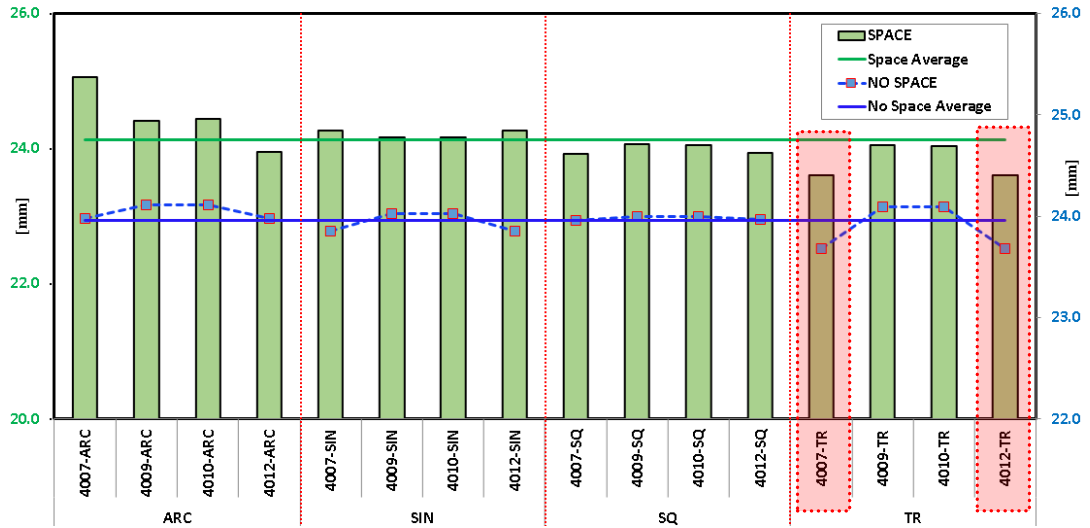


Figure 6-25: The Best Design for Impact Velocity 4 m/s ; (a) Acceleration - Space Average and No-Space Average, (b) Acceleration - Space and No-Space Compared to Average Line

Figure 6-26(a) and (b) were plotted based on Table 6-18. There was no pairing at all between space and no-space configuration except for trapezium shape. Design 7 and 12 from trapezium shape were selected due to displacement values, which are; below space average, no-space average and overall average.

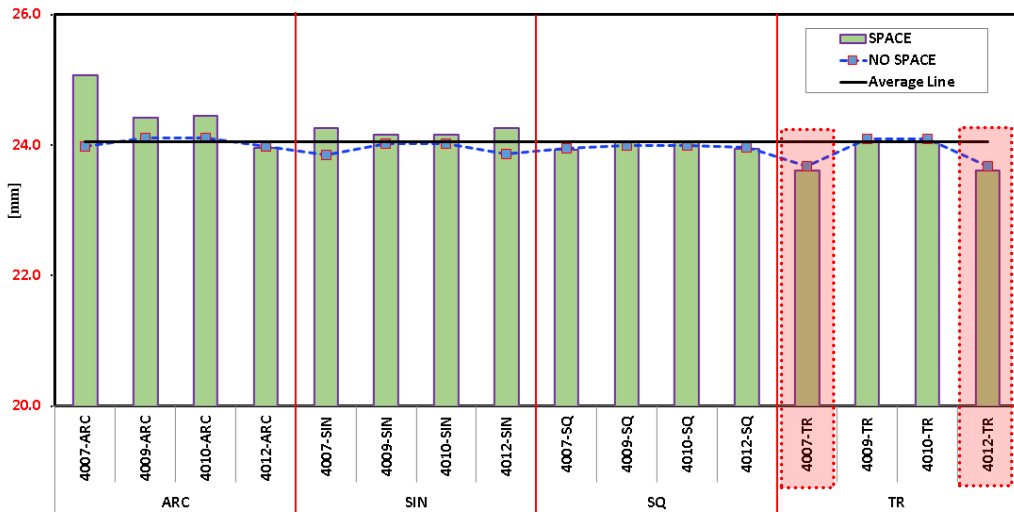
DISPLACEMENT - 4000 SPACE vs. NO-SPACE

DISPLACEMENT SIMULATION
NO SPACE vs. SPACE - 4000



(a)

DISPLACEMENT SIMULATION
NO SPACE vs. SPACE - 4000



(b)

Figure 6-26: The Best Design for Impact Velocity 4 m/s ; (a) Displacement - Space Average and No-Space Average, (b) Displacement - Space and No-Space Compared to Average Line

6.3.1.4 Summary of Space vs. No-Space Design Based on Average Values

To summarised, all analysis for space and no-space were conducted between four shapes at 2 m/s, 3 m/s and 4 m/s impact velocity. At 2 m/s, only square shape paired between acceleration and displacement value. Few sinusoidal shapes were highlighted, but highest recurring shape selected was square shape at 2 m/s.

However, at 3 m/s, all shapes for design 9 and 10. It could be observed that sinusoidal was repeatedly selected from both acceleration and displacement graph. Therefore, at 3 m/s, sinusoidal shape design was selected.

Lastly at 4 m/s, there were no pairing occurred in both acceleration and simulation graph. However, design 12 in trapezium shape was recalled several times due to the value mapped below space average, no-space average and overall average. Therefore, at 4 m/s, trapezium shape was selected.

To conclude overall findings, there are three materials selected except for arc shape. Therefore, to further determine the best shape. Another analysis was carried out using time parameter. Hence, objective 3 was reflected in this portion of analysis.

6.3.2 Space (S) vs. No-Space (NS) Design Based on Time (t) Approach

To carry out this analysis displacement and acceleration values were obtained from simulation. Time (t) approach was used to obtain time for every single scenario. Two sets of calculation were carried out throughout this process. Firstly, displacement and time play as a fixed variable to obtain new acceleration. Secondly, acceleration and time used as fixed variable to obtain new displacement. These new sets of acceleration

and displacement values were used to determine best material configuration.

After obtaining the displacement, acceleration, new displacement, and new acceleration, four different average values were calculated to plot a boundary line. The average lines are acceleration average, new acceleration average, displacement average and new displacement average. The best design configuration was selected based on acceleration and displacement values that fall below the average line for any space or no-space configuration. Hence, this analysis uses time (t) value approach to validate the finding from previous section.

6.3.2.1 Time (t) Value Approach at 2 m/s

Table 6-19 shows time at 2 m/s fixed at 0.70 ms. From this set of acceleration and displacement regardless space or no-space configuration, new set of acceleration and displacement were obtained. For average acceleration, the boundary line is at 34.44 g. Average displacement calculated was 8.45 mm. For new set of acceleration and displacement average were 34.43 g and 8.45 mm respectively.

Table 6-19: The Best Design Based on Time (t) Average Approach of Acceleration vs. Displacement at 2 m/s

2 m/s (t= 0.70)	ARC				SIN				SQ				TR				AVE NS - S	AVE
	2007	2009	2010	2012	2007	2009	2010	2012	2007	2009	2010	2012	2007	2009	2010	2012		
Acceleration NS (g)	34.64	34.65	34.52	34.87	34.72	34.46	34.51	34.71	34.86	34.77	34.44	34.87	34.88	34.66	34.66	34.87	34.70	34.44
Acceleration S (g)	32.57	34.11	33.87	32.68	33.61	34.68	34.68	33.60	34.87	34.15	34.17	34.87	34.91	34.67	34.50	34.90	34.18	
Displacement NS (mm)	8.28	8.34	8.25	8.36	8.27	8.25	8.24	8.27	8.36	8.37	8.27	8.36	8.36	8.31	8.31	8.35	8.31	8.45
Displacement S (mm)	9.65	8.60	8.63	9.64	8.69	8.40	8.40	8.70	8.32	8.40	8.39	8.33	8.32	8.28	8.28	8.31	8.58	
New Acceleration NS (g)	33.75	33.72	34.06	34.06	34.00	33.62	34.10	33.88	33.63	33.61	33.73	33.85	34.09	33.71	34.08	34.04	33.87	34.43
New Acceleration S (g)	39.33	35.44	33.93	33.91	35.07	34.24	34.23	33.75	35.19	34.24	34.22	33.73	39.30	35.45	33.95	33.89	34.99	
New Displacement NS (mm)	8.50	8.52	8.55	8.56	8.50	8.45	8.53	8.50	8.47	8.47	8.45	8.50	8.56	8.52	8.56	8.56	8.51	8.45
New Displacement S (mm)	7.99	8.25	8.56	8.56	8.37	8.51	8.38	8.51	8.31	8.51	8.38	8.46	8.02	8.24	8.56	8.56	8.39	

Figure 6-27 shows intersection of all shape regardless space or no-space configuration towards average acceleration line. Design 10 from square shape were

selected due to the value of acceleration from space or no-space configuration plotted below average acceleration line.

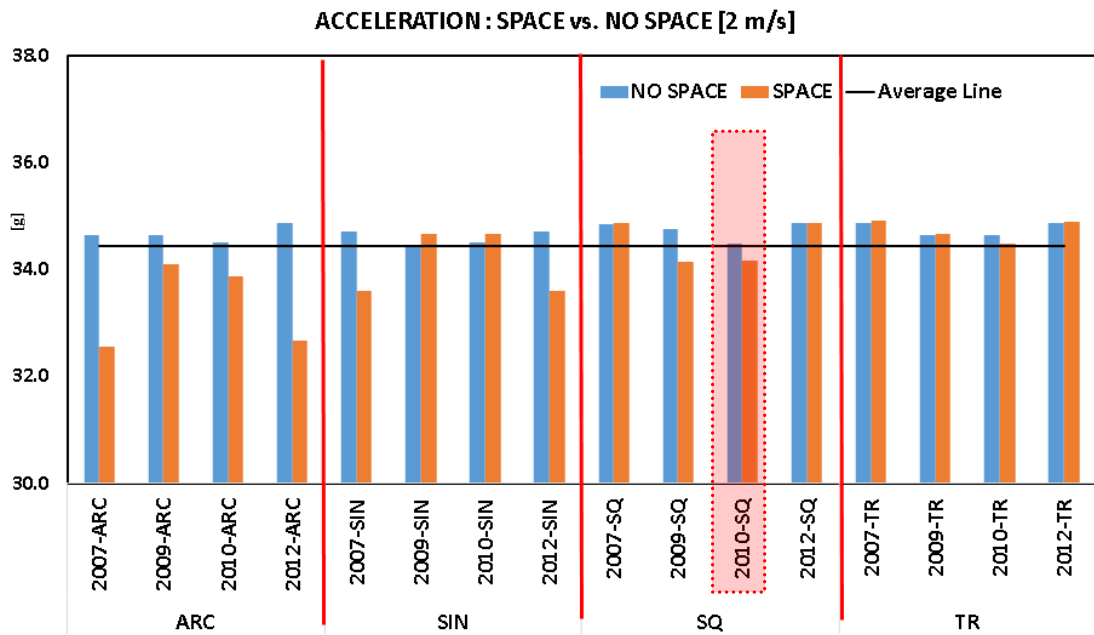


Figure 6-27: Acceleration: Space vs. No-Space for best shape design at 2 m/s

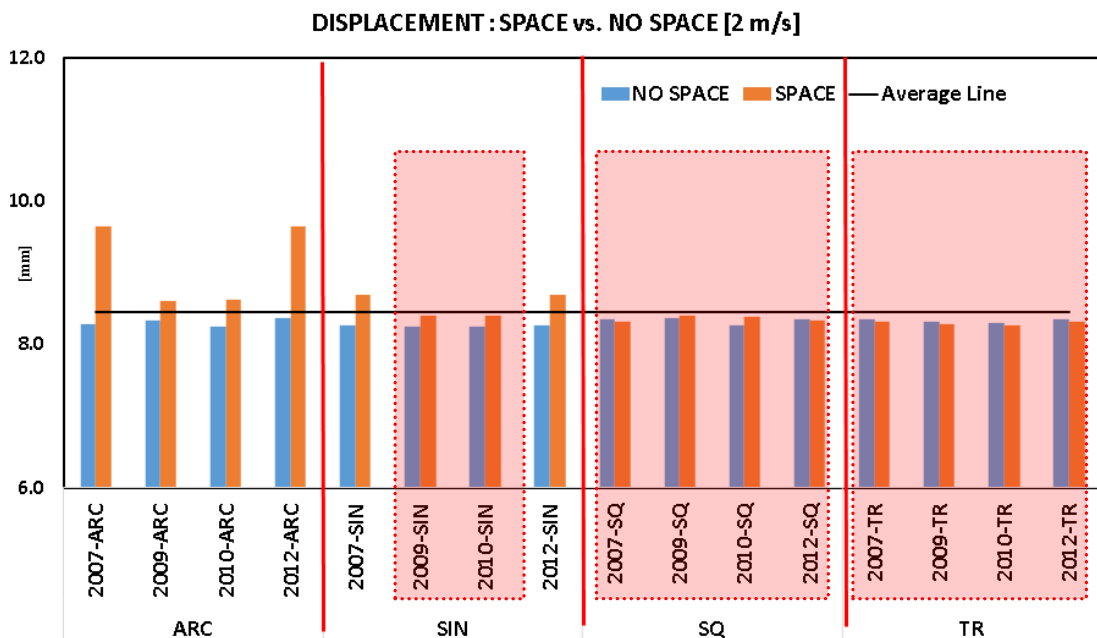


Figure 6-28: Displacement: Space vs. No-Space for Best Shape Design at 2 m/s

Figure 6-28 shows intersection of all shape regardless space or no-space

configuration towards average displacement line. Three shapes were selected because displacement values plotted below average displacement line. For sinusoidal shape, only design 9 and 10 were selected. However, all four designs were selected for square and trapezium shape.

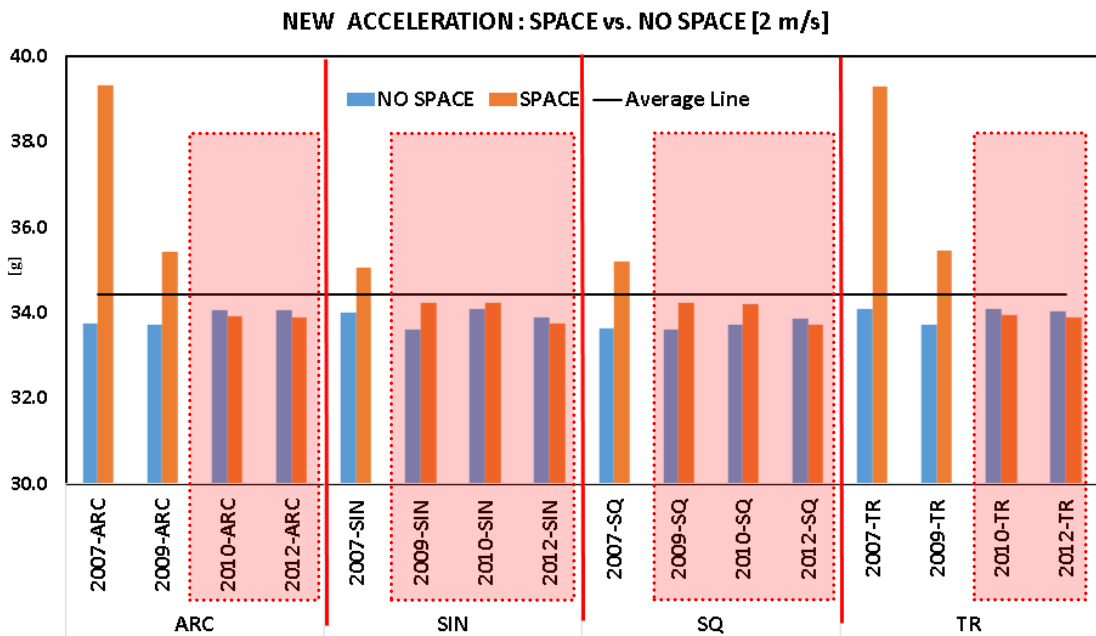


Figure 6-29: New Acceleration: Space vs. No-Space for best shape design at 2 m/s

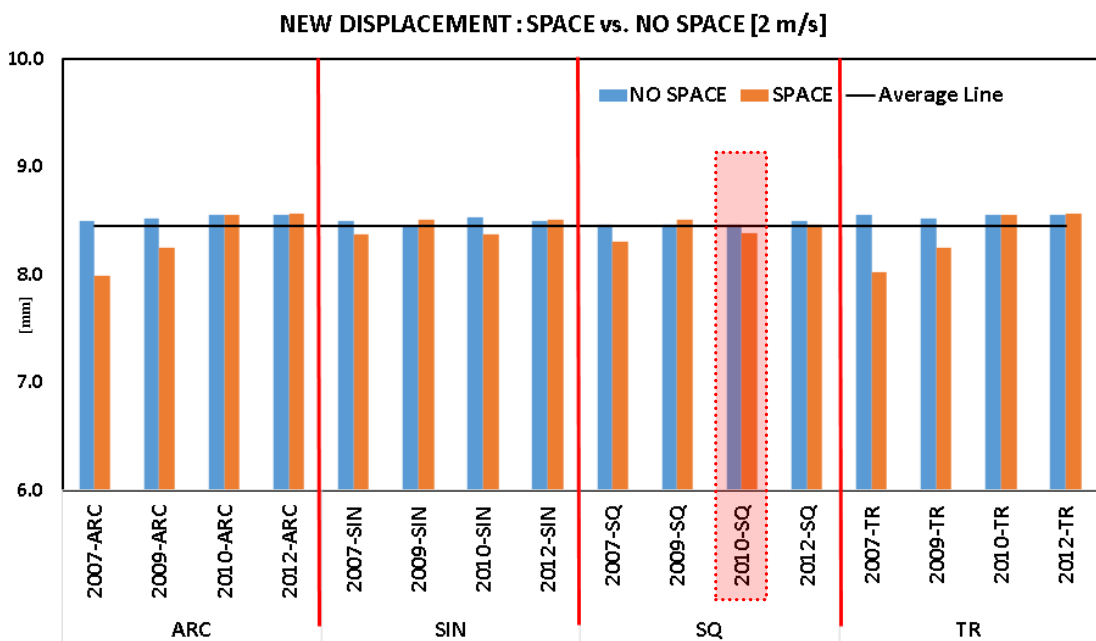


Figure 6-30: New Displacement : Space vs. No-Space for Best Shape Design at 2 m/s

Figure 6-29 shows intersection of all shape regardless space or no-space configuration towards new acceleration average line. Hence, four shapes were selected. For arc shape, design 10 and 12 meet the requirement. Design 9, 10 and 12 Sinusoidal and square shape were highlighted. Lastly, for trapezium shape, all design shows new acceleration value plotted below average line.

Figure 6-30 shows intersection of all shape regardless space or no-space configuration towards new displacement average line. It shows that only one shape was highlighted that is square at design 7. Design 7 meets the requirement whereby both space and no-space values fall below average line.

6.3.2.2 Time (t) Value Approach at 3 m/s

Table 6-20 shows set of computation. Time at 2 m/s fixed at 0.92 ms. From this set of acceleration and displacement regardless space or no-space configuration, new set of acceleration and displacement were obtained. For average acceleration, the boundary line is at 35.38 g. Average displacement calculated was 15.05 mm. For new set of acceleration and displacement average were 35.38 g and 15.05 mm respectively.

Table 6-20: The Best Design Based on Time (t) Average Approach of Acceleration vs. Displacement at 3 m/s

3 m/s (t= 0.92)	ARC				SIN				SQ				TR				AVE NS - S	AVE
	3007	3009	3010	3012	3007	3009	3010	3012	3007	3009	3010	3012	3007	3009	3010	3012		
Acceleration NS (g)	35.54	35.29	35.28	35.52	35.62	35.09	35.29	35.61	35.55	35.44	35.43	35.53	35.87	35.25	35.25	35.87	35.46	35.38
Acceleration S (g)	35.16	34.98	34.95	34.84	35.21	35.27	35.26	35.21	35.53	35.23	35.22	35.52	35.90	35.28	35.27	35.90	35.30	
Displacement NS (mm)	14.97	14.99	14.98	14.90	14.88	14.91	14.90	14.87	14.95	14.96	14.96	14.96	14.87	14.96	14.95	14.87	14.93	15.05
Displacement S (mm)	16.13	15.27	15.30	16.06	15.26	15.04	15.04	15.26	14.92	15.02	15.01	14.93	14.82	14.92	14.92	14.82	15.17	
New Acceleration NS (g)	35.19	34.97	35.15	34.96	35.23	35.04	35.18	35.16	35.22	35.04	35.16	35.15	35.03	34.96	35.16	34.95	35.10	35.38
New Acceleration S (g)	37.91	35.88	35.08	34.85	35.90	35.35	35.31	35.08	35.96	35.35	35.30	35.06	37.76	35.88	35.09	34.84	35.66	
New Displacement NS (mm)	15.12	15.15	15.12	15.26	15.01	14.93	15.08	14.99	15.01	15.01	15.05	14.99	15.11	15.15	15.11	15.26	15.09	15.05
New Displacement S (mm)	14.96	14.98	15.11	15.27	14.88	15.00	14.99	15.01	14.87	15.00	14.98	15.00	14.82	14.98	15.11	15.27	15.01	

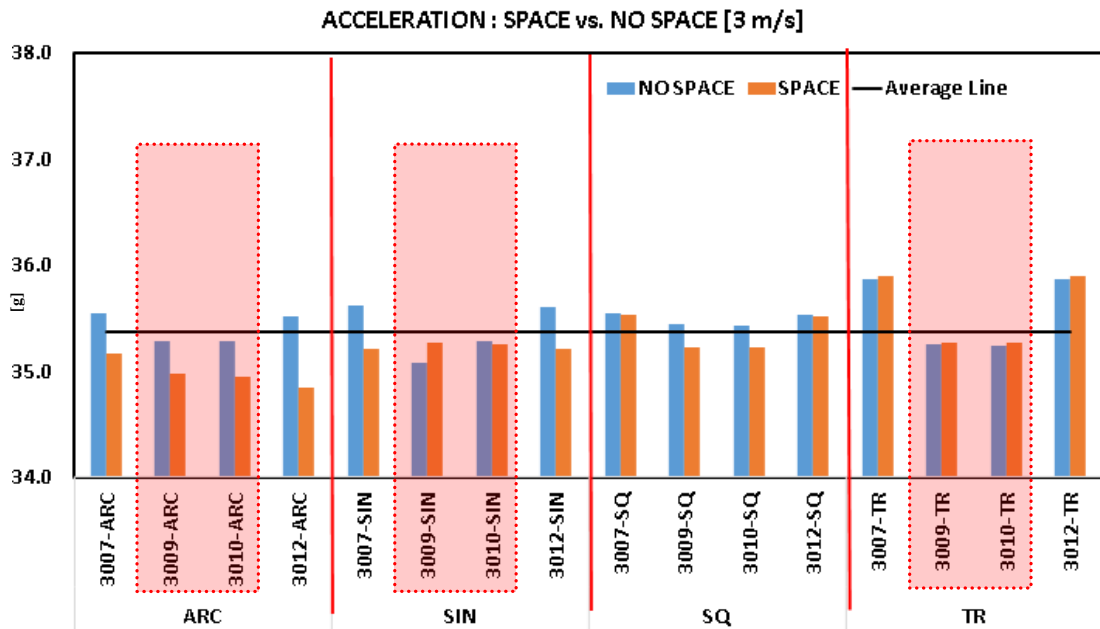


Figure 6-31: Acceleration: Space vs. No-Space for Best Shape Design at 3 m/s

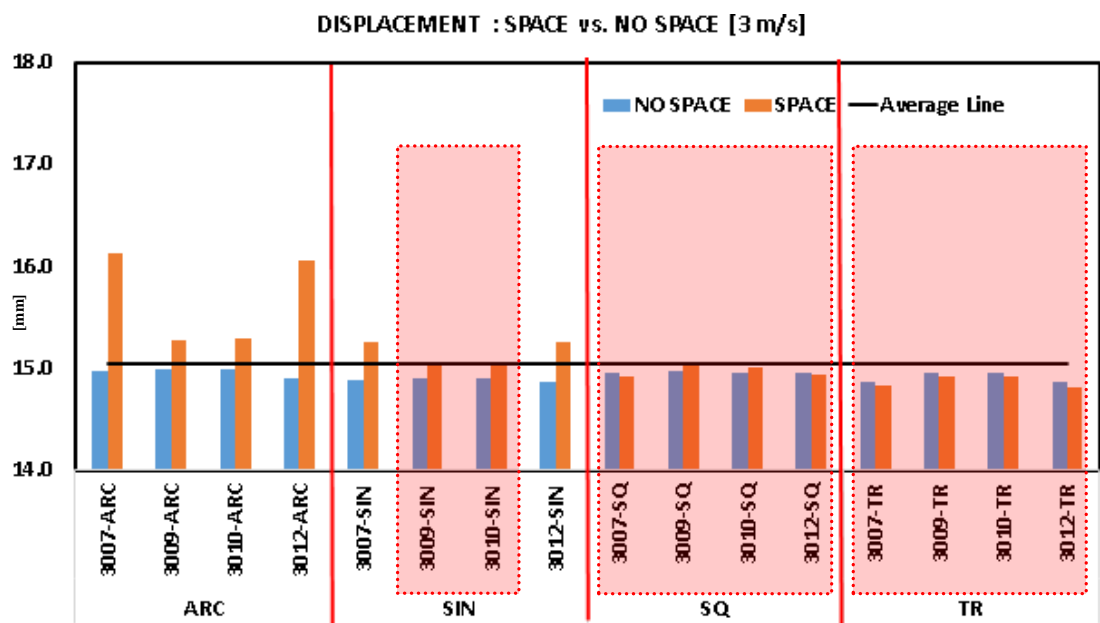


Figure 6-32: Displacement: Space vs. No-Space for Best Shape Design at 3 m/s

Figure 6-31 shows intersection of all shape regardless space or no-space configuration towards acceleration average line. Hence, three shapes were selected. For arc shape, design 9 and 10 meet the requirement. Sinusoidal and trapezium shapes

highlighted two same designs similar to arc which were design 9, and 10.

Figure 6-32 shows intersection of all shape regardless space or no-space configuration towards average displacement line. Hence, three shapes were selected because displacement values plotted below average displacement line. For sinusoidal shape, only design 9 and 10 were selected. However, all four designs were selected for square and trapezium shape.

Figure 6-33 shows intersection of all shape regardless space or no-space configuration towards new acceleration average line. Hence, two shapes were selected because new acceleration values plotted below new acceleration average line. For sinusoidal and square shape, all four designs meet the requirement.

Figure 6-34 shows intersection of all shape regardless space or no-space configuration towards new displacement average line. Hence, three shapes were selected. For ARC shape, design 9 and 10 meet the requirement. Sinusoidal and trapezium shape highlighted two same designs similar to arc which were design 9, and 10.

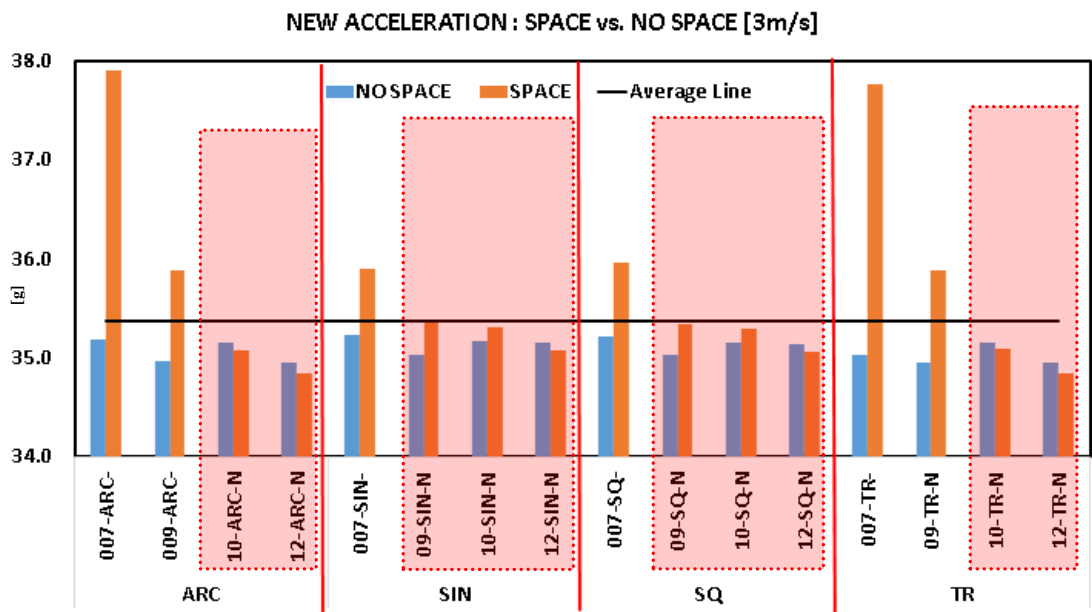


Figure 6-33: New Acceleration: Space vs. No-Space for Best Shape Design at 3 m/s

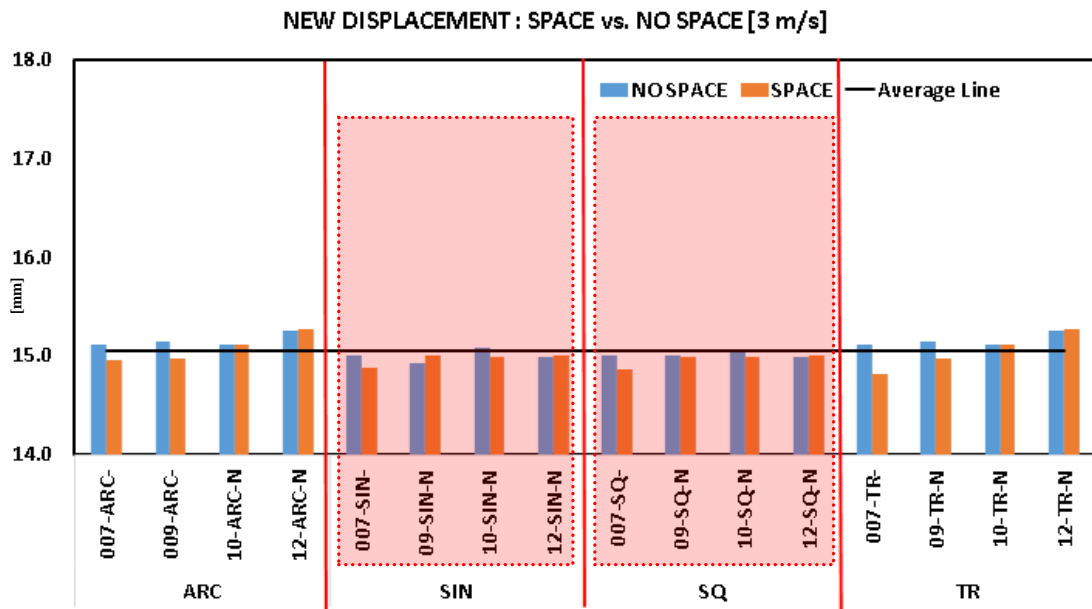


Figure 6-34: New Displacement: Space vs. No-Space for Best Shape Design at 3 m/s

6.3.2.3 Time (t) Value Approach at 4 m/s

Table 6-21 shows set of computation. Time at 2 m/s fixed at 1.16 ms. From this set of acceleration and displacement regardless space or no-space configuration, new set of acceleration and displacement were obtained. For average acceleration, the boundary line is at 35.94 g. Average displacement calculated was 24.04 mm. For new set of acceleration and displacement average were 35.93 g and 24.05 mm respectively.

Table 6-21: The Best Design Based on Time (t) Average Approach of Acceleration vs. Displacement at 4 m/s

4 m/s (t= 1.16)	ARC				SIN				SQ				TR				AVE	
	4007	4009	4010	4012	4007	4009	4010	4012	4007	4009	4010	4012	4007	4009	4010	4012	NS - S	AVE
Acceleration NS (g)	36.05	35.72	35.74	36.05	36.15	35.78	35.66	36.14	36.01	35.91	35.93	36.01	36.56	35.66	35.67	36.56	35.98	35.94
Acceleration S (g)	35.81	35.57	35.54	35.83	35.80	35.72	35.75	35.80	36.04	35.82	35.84	36.04	36.63	35.74	35.76	36.62	35.89	
Displacement NS (mm)	23.97	24.11	24.11	23.98	23.85	24.03	24.02	23.86	23.96	24.00	23.99	23.97	23.68	24.09	24.09	23.68	23.96	24.04
Displacement S (mm)	25.07	24.41	24.44	23.96	24.26	24.16	24.16	24.27	23.93	24.07	24.06	23.94	23.61	24.05	24.04	23.61	24.13	
New Acceleration NS (g)	35.83	35.65	35.80	35.39	36.04	35.91	35.86	36.01	36.03	35.90	35.86	36.00	35.83	35.65	35.82	35.39	35.81	35.93
New Acceleration S (g)	37.46	36.26	35.76	35.28	36.48	36.11	35.96	35.94	36.53	36.11	35.93	35.93	35.80	36.27	35.77	35.28	36.06	
New Displacement NS (mm)	24.13	24.19	24.09	24.47	23.90	23.94	24.03	23.86	23.91	23.86	24.04	23.87	24.12	24.19	24.09	24.47	24.07	24.05
New Displacement S (mm)	23.96	23.95	24.12	24.51	23.80	23.90	23.97	23.92	23.78	23.92	23.98	23.93	23.98	23.96	24.12	24.51	24.02	

Figure 6-35 shows intersection of all shape regardless space or no-space configuration towards acceleration average line. Hence, four shapes were selected. For all shapes, only design 9 and 10 were selected due to the acceleration value either space or no-space plotted below average line.

Figure 6-36 shows intersection of all shape regardless space or no-space configuration towards displacement average line. Hence, three shapes were selected. For arc shape, only design 12 was selected due to the displacement value was below displacement line. For square shape, design 7, 10 and 12 meets the requirement. Lastly, design 7 and 12 were selected for trapezium shape.

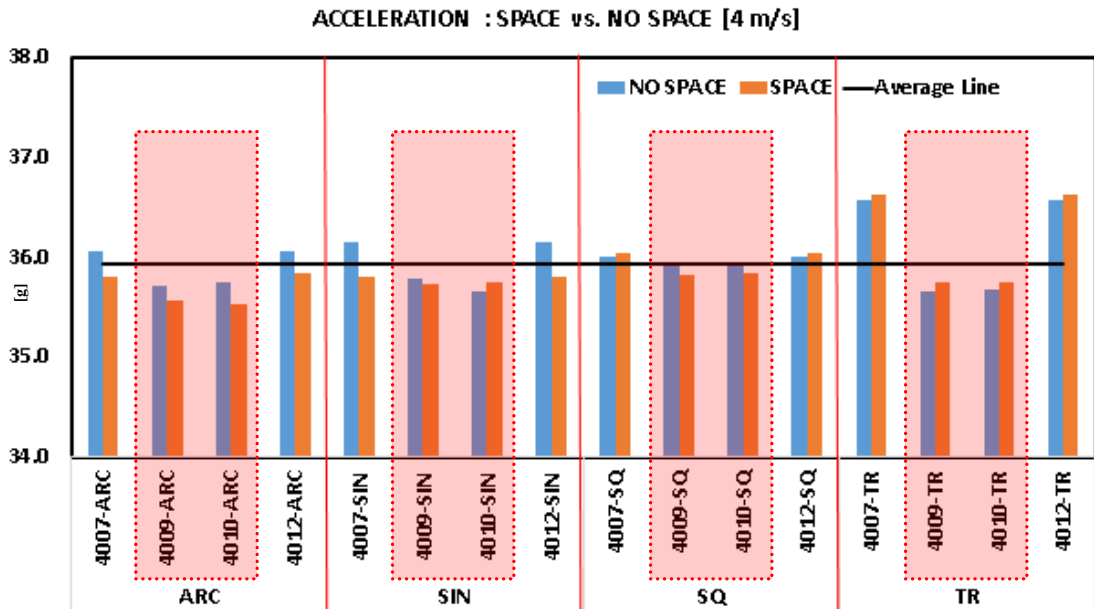


Figure 6-35: Acceleration: Space vs. No-Space for Best Shape Design at 4 m/s

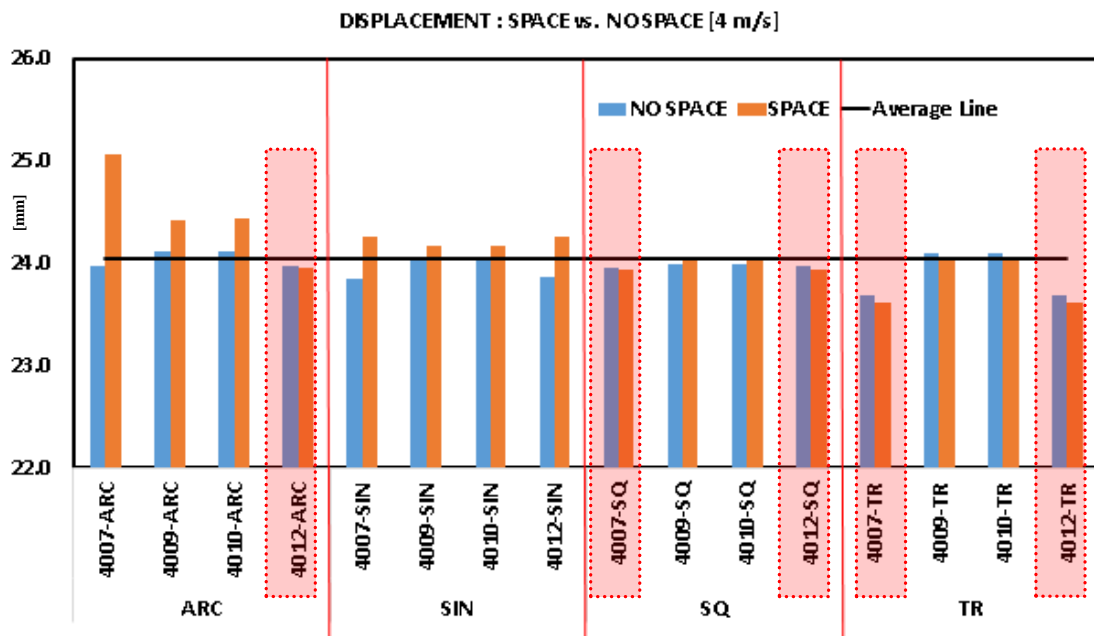


Figure 6-36: Displacement: Space vs. No-Space for Best Shape Design at 4 m/s

Figure 6-37 shows intersection of all shape regardless space or no-space configuration towards new acceleration average line. Hence, three shapes were selected. For arc shape, design 10 and 12 were selected due to the displacement value

was below displacement line. For square shape, only design 10 was selected. Lastly, design 7, 10 and 12 for trapezium shape were selected because new acceleration values point plotted below new acceleration average line.

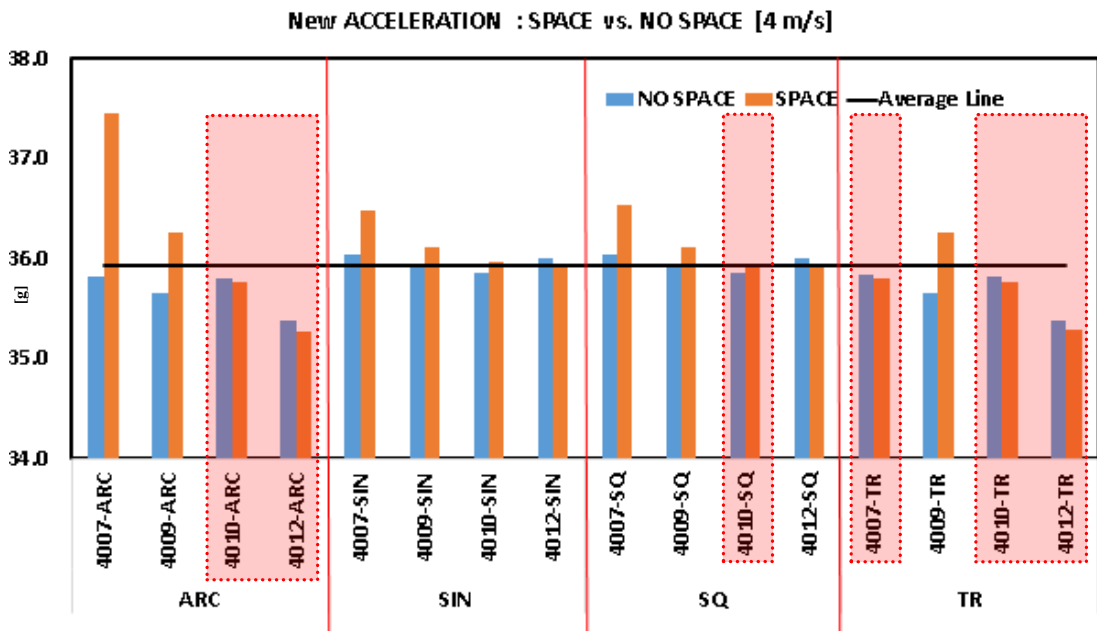


Figure 6-37: New Acceleration: Space vs. No-Space for Best Shape Design at 4 m/s

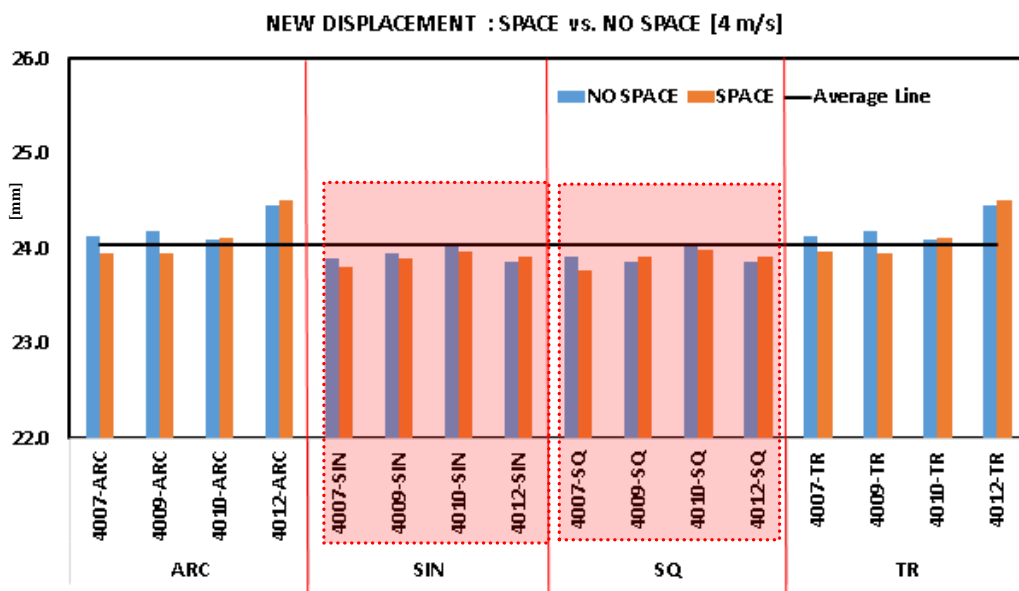


Figure 6-38: New Displacement: Space vs. No-Space for Best Shape Design at 4 m/s

Figure 6-38 shows intersection of all shape regardless space or no-space

configuration towards new acceleration average line. Hence, two shapes were selected because new acceleration values plotted below new acceleration average line. For SIN (sinusoidal) and SQ (square) shape, all four designs meet the requirement.

6.3.2.4 Summary of Space vs. No-Space Design Based on Time (t)

In summary, Figure 6-27 and Figure 6-28 show that acceleration, displacement, new acceleration and new displacement with respect to design configuration space and no-space. Frequency of same shape recalled in both figures based on the values below the average line were tabulated in Table 6-22.

Table 6-22: Best Shape Frequency at Impact Velocity 2 m/s

VELOCITY – 2 m/s						
		DESIGN 7	DESIGN 9	DESIGN 10	DESIGN 12	Frequency
ARC	ACCELERATION					2
	DISPLACEMENT					
	NEW ACCELERATION			X	X	
	NEW DISPLACEMENT					
SIN	ACCELERATION					5
	DISPLACEMENT		X	X		
	NEW ACCELERATION		X	X	X	
	NEW DISPLACEMENT					
SQ	ACCELERATION			X		9
	DISPLACEMENT	X	X	X	X	
	NEW ACCELERATION		X	X	X	
	NEW DISPLACEMENT			X		
TR	ACCELERATION					6
	DISPLACEMENT	X	X	X	X	
	NEW ACCELERATION			X	X	
	NEW DISPLACEMENT					

Table 6-22 shows the frequency of shapes based on the values lies below the average lines. The ARC shape were clearly observed twice in the condition where the points located below average line. For SIN (sinusoidal), SQ (square) and TR

(trapezium), there were 5, 9 and 6 occurrences of this shape.

Table 6-23 shows the frequency of shapes based on the values lies below the average lines. The ARC shape, were clearly observed four times where the points located below average line. For SIN (sinusoidal), SQ (square) and TR (trapezium), there were 10, 11 and 8 occurrences of this shape.

Table 6-23: Best Shape Frequency at Impact Velocity 3 m/s

VELOCITY – 3 m/s						
		DESIGN 7	DESIGN 9	DESIGN 10	DESIGN 12	Frequency
ARC	ACCELERATION		X	X		4
	DISPLACEMENT					
	NEW ACCELERATION			X	X	
	NEW DISPLACEMENT					
SIN	ACCELERATION		X	X		11
	DISPLACEMENT		X	X		
	NEW ACCELERATION		X	X	X	
	NEW DISPLACEMENT	X	X	X	X	
SQ	ACCELERATION					11
	DISPLACEMENT	X	X	X	X	
	NEW ACCELERATION		X	X	X	
	NEW DISPLACEMENT	X	X	X	X	
TR	ACCELERATION		X	X		8
	DISPLACEMENT	X	X	X	X	
	NEW ACCELERATION			X	X	
	NEW DISPLACEMENT					

Table 6-24 shows the frequency of shapes based on the values lies below the average lines. The ARC shape, were clearly observed five times where the points located below average line. For SIN (sinusoidal), SQ (square) and TR (trapezium), there were 6, 9 and 7 occurrences of this shape.

In summary, based on the findings regardless the impact velocity. The total of frequency regardless any impact velocity was totalled up. For ARC shape, total frequency was 11. For SIN (sinusoidal), SQ (square) and TR (trapezium) total were 21, 29 and 21 respectively. To conclude, square shape with space is suitable to be

selected based on high recurring number. Hence, objective 3 was reflected in this portion of analysis.

Table 6-24: Best Shape Frequency at Impact Velocity 4 m/s

VELOCITY – 4 m/s						
		DESIGN 7	DESIGN 9	DESIGN 10	DESIGN 12	Frequency
ARC	ACCELERATION		X	X		5
	DISPLACEMENT				X	
	NEW ACCELERATION			X	X	
	NEW DISPLACEMENT					
SIN	ACCELERATION		X	X		6
	DISPLACEMENT					
	NEW ACCELERATION					
	NEW DISPLACEMENT	X	X	X	X	
SQ	ACCELERATION		X	X		9
	DISPLACEMENT	X			X	
	NEW ACCELERATION			X		
	NEW DISPLACEMENT	X	X	X	X	
TR	ACCELERATION		X	X		7
	DISPLACEMENT	X			X	
	NEW ACCELERATION	X		X	X	
	NEW DISPLACEMENT					

6.4 Summary

To conclude overall findings in this chapter, the analysis was divided into several parts. The first analysis was to determine best foam configuration. Based on the findings, combination layer was proven suitable for this application. Next section of analysis was to observe the foam design based on impact velocity. Each impact velocity proposes different materials to be selected. However, Material A and C need to be arranged properly to achieve optimised design configuration.

Several calculations were carried out using simulation values and judgement based on statistical approach were introduced. Statistical approach used were average value and time (t) average approach. By using average value approach at 2 m/s and 3 m/s,

the best material design configuration selected was the combination layer. However, there are no suitable selection could be made at 4 m/s. Suitable impact velocity to test out foam material configuration were at 2 m/s and 3 m/s. This theory is used and validated in the next subsection using time (t) parameter.

Finally, Table 6-22 to Table 6-24 are using time (t) average. Total of frequency for ARC (arc), SIN (sinusoidal), SQ (square) and TR (trapezium) shapes were 11, 21, 29 and 21 respectively. Based on this highest frequency, square (SQ) shape with space was selected.

Chapter 7: Optimised Position in Equator P2 Aircraft Landing on Water

This section focuses on installing the best design selection from previous chapter into the aircraft structure. Figure 7-1 shows the full aircraft model in LS DYNA. Equator Aircraft SA, Norway, supplies the 3D model. It was simplified in Rhinoceros 3D software while the meshing was conducted in Hypermesh V13. Mixed element were chosen for the complex aircraft model. All aircraft structures were modelled using quadrilateral and triangular shell elements. In LS DYNA, both shell types are based on Belytchko-Tsay Shell theory.

Differently, the foams and water is maintained as solid. Geometry editing were done in Hypermesh in order to get a clean and connected mesh. Toggle edge function were applied with the tolerance of 0.5 to make sure any interconnecting surface is connected together while meshing. This is critical so that the model would work accordingly and minimise any instabilities issues in LS DYNA. Material card *PART_COMPOSITE were applied to the aircraft structure to minimise the calculation time. In addition, only symmetrical model was simulated to minimise computer-processing time. Table 7-1 listed the aircraft specification from

manufacturer's website. Mass and sink velocity were obtained from this specification.

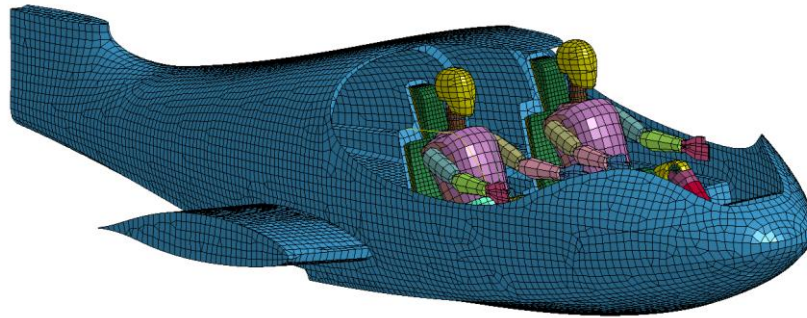


Figure 7-1: Full Aircraft setup in LS Dyna

Table 7-1: Equator Aircraft P2 Xcursion Specification (Source: Equator, n.d.)

EQUATOR AIRCRAFT P2 XCURSION SPECIFICATIONS	
TYPE:	EQUATOR P2 XCURSION (EQP2)
VERSION:	P.O.C PROTOTYPE
SERIAL NR	P2MK2V4 001 - EXPERIMENTAL
REG:	LN-EPX
SEATS:	2
MTOW	750kg
USEFUL LOAD (DRY):	240kg
MAX. CRUISE	130 KTS
ECONOMIC CRUISE	118 KTS (20l/h)
STALL	48KTS / 52KTS w/o FLAPS
RANGE	845NM / 1565km
GEAR	RETRACTABLE
MATERIAL	CARBON / KEVLAR COMPOSITE
AVIONICS	MGL iEFIS with remote transponder and radio
PROPELLER	DUC Flash, with custom DUC hub and spinner
ENGINE	ENGIRO M97 Electric (97 kW water cooled, 32 kgs)
GENERATOR	ENGIRO G60 (60kW, water cooled, 15kgs)
ICE:	WST KKM 352 Wankel (57kW) Multi Diesel (45kgs)
Controller:	Sevcon size 8 (2pcs, 8kgs per controller, water cooled)
Boost Battery:	Custom Lilon pack (6kWh) 32kgs
Test Battery:	LiPo pack (18kWh) (separate BMS), 100kgs
Ems:	Sevcon & Equator Aircraft custom screen solution
Cooling:	Common automotive heat exchangers 4pcs
<i>*Flight related data is theoretical, and are subject to change depending on the progress with test flights</i>	

Table 7-2 shows composition of absorber location installed in the aircraft and the location of data taken. Therefore, SQ-S design no. 10 based from section 6.4 is used for simulation in full aircraft to visualised the influence of the foam/absorber position in order to get optimised position. This location was determined based on the space available in the aircraft and the crucial spot. The lower torso point (A1) were chosen in order to examine the pelvic acceleration of the occupant. While, the other position is near the step area where this area is the first contact point of the aircraft during landing.

Table 7-2: Absorber Location Installed in the Aircraft and Node Location for Data Collection

FOAM POSITION IN AIRCRAFT	LOWER TORSO (A1)	STEP AREA (A2)	SUBCHAPTER
NO FOAM	0	0	7.1
FRONT	1	0	7.2
BACK	0	1	7.3
BOTH	1	1	7.4
Note: 0 = No 1 = YES			

Best design information was selected from previous part of this research. Impact velocity remains similar, which are 2 m/s, 3 m/s and 4 m/s. The foam design were installed in two areas of the aircraft, under the seat pan (FRONT) and aircraft step area (BACK) as shown clearly in Figure 7-2(a and b).

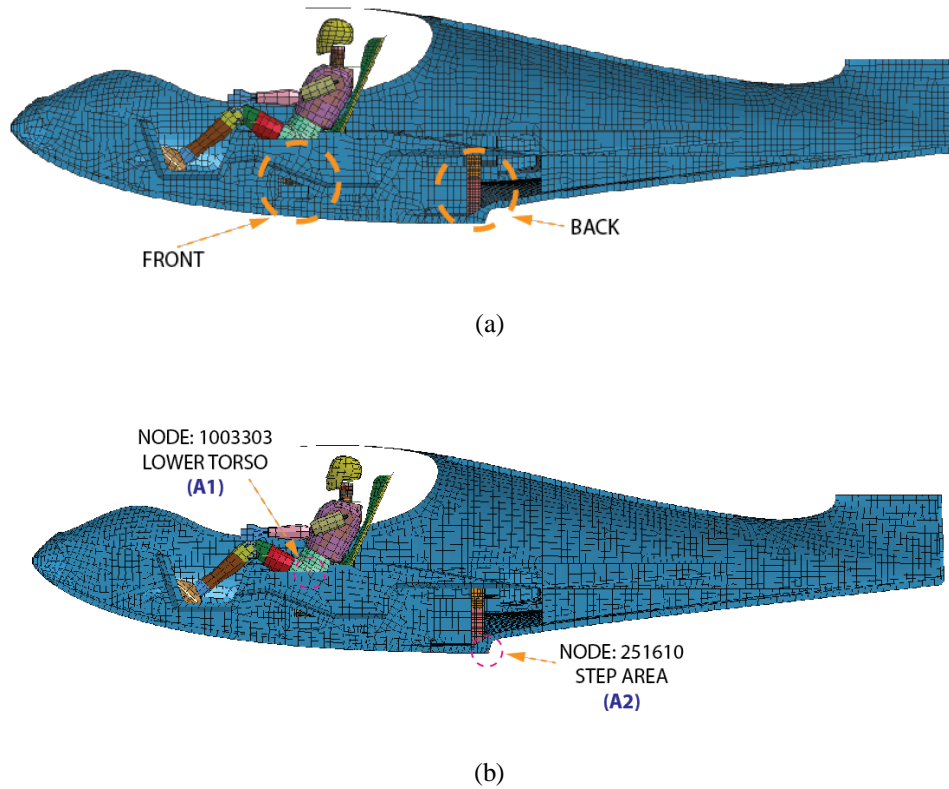


Figure 7-2: Location Data Taken and Foam Installation Position;
 (a) Foam Installation Position, (b) Node Data Taken

7.1 Aircraft with No-Foam Installed

Current aircraft design does not have foam installed as an absorber. Therefore, the hull structure of aircraft absorbs all the impact force while landing on water. The significance of this simulation is to identify the effects on using foam in two different locations. Based on Figure 7-2, two locations mentioned on the aircraft are the front below occupant and at the first contact point of impact during touchdown. Data collected were acceleration (g) against time (ms) at two points, which were Node 1003303 (A1) and Node 251610 (A2).

Figure 7-3 shows the results for impact velocity at 2 m/s, 3 m/s, and 4 m/s. This figure shows the effect of NO FOAM in the lower torso (A1) point. The peak values

for impact velocity at 2 m/s, 3 m/s, 4 m/s were 3.82 g, 10.49 g and 17.78 g respectively.

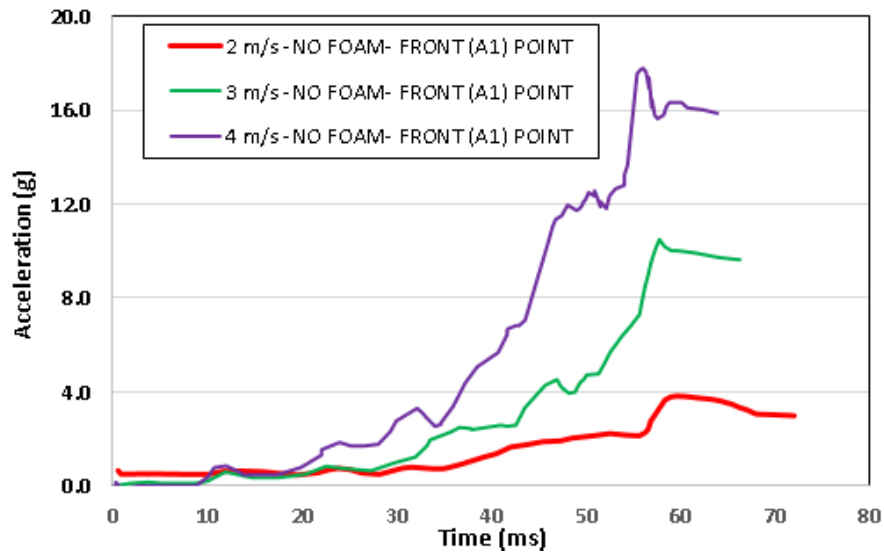


Figure 7-3: A1 Value When NO FOAM Installed at Various Velocity

Figure 7-4 shows three different line colours indicate three different velocities. This figure discusses the effect of NO FOAM in A2 point. The peak values recorded at impact velocity 2 m/s, 3 m/s and 4 m/s were 36.64 g, 60.41 g and 86.29 g respectively.

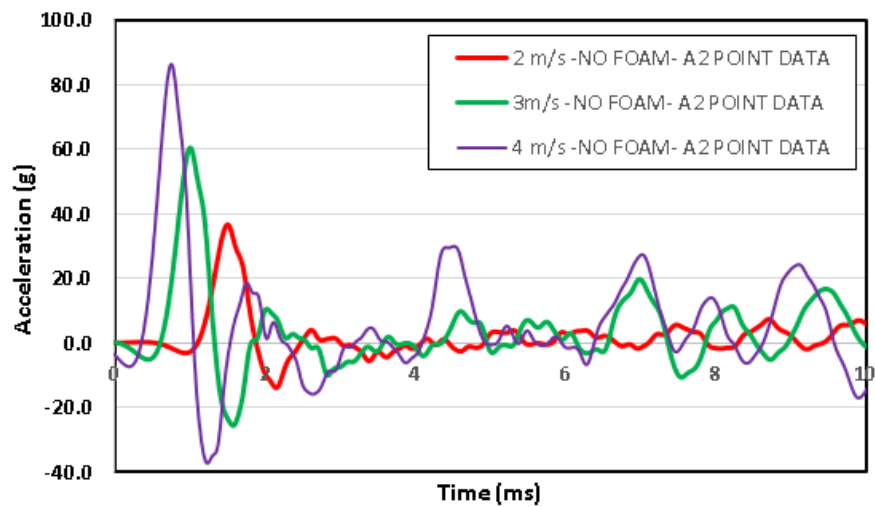


Figure 7-4: A2 Value When NO FOAM Installed at Various Velocity

Figure 7-5 shows full simulation of Equator P2 increased at impact velocity 2 m/s, 3 m/s, 4 m/s for before and after point of impact if NO-FOAM is installed. This figure shows that the material developed for simulation working without any instabilities or error. Thus, the reliability and result from this simulation are accurate and acceptable.

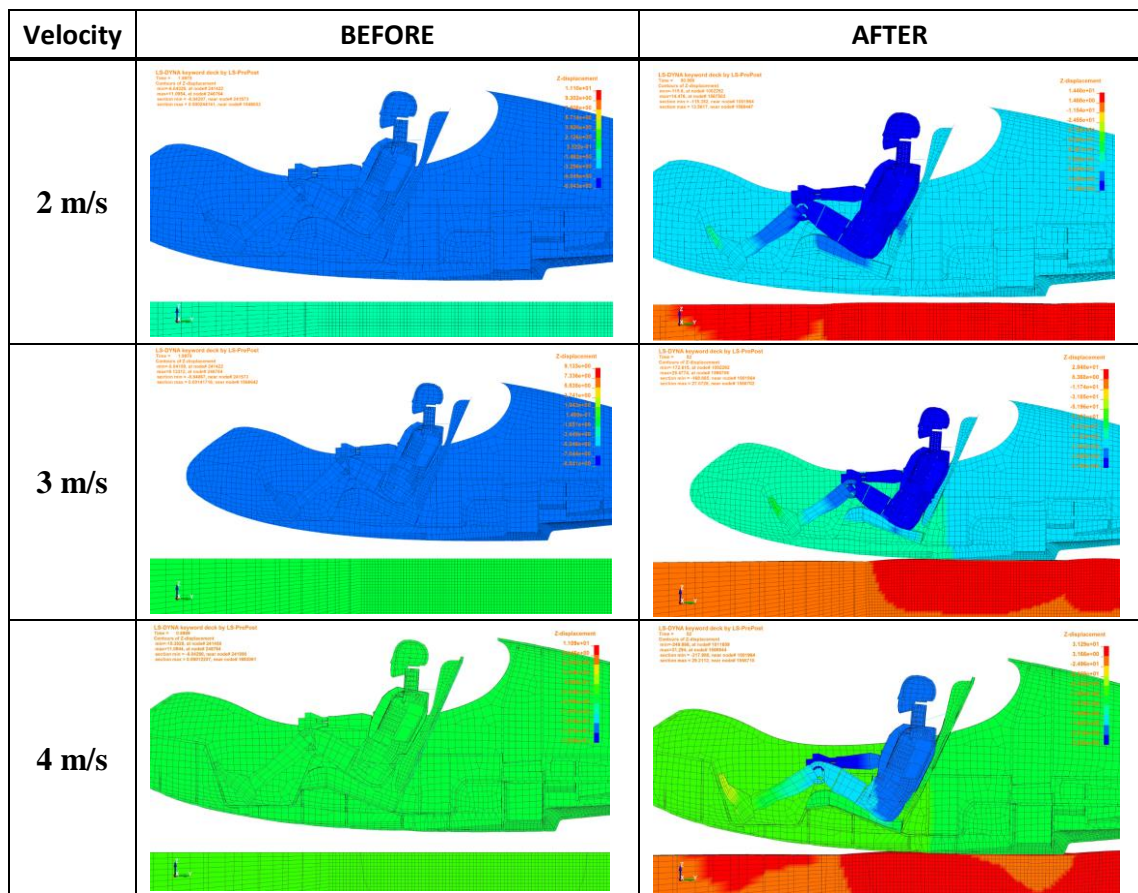


Figure 7-5: Full Simulation of Equator P2 Landing Contour Before-After for NO-FOAM Installed

7.2 Foam Installed in Aircraft - FRONT Position

This section discusses on the effect of placing foam in the FRONT position of aircraft. The significance of this simulation is to identify the effects on using foam in two different locations. Based on Figure 7-2, two locations mentioned on the aircraft are below the occupant and at the first contact point of impact during touchdown. Data collected were acceleration (g) against time (ms) at two positions which were Node

1003303 (A1) and Node 251610 (A2).

Figure 7-6 three different line colours indicate three different velocities. This figure discusses the effect of foam installed at FRONT position. The peak values recorded at impact velocity 2 m/s, 3 m/s and 4 m/s were 4.14 g, 10.34 g and 17.53 g respectively.

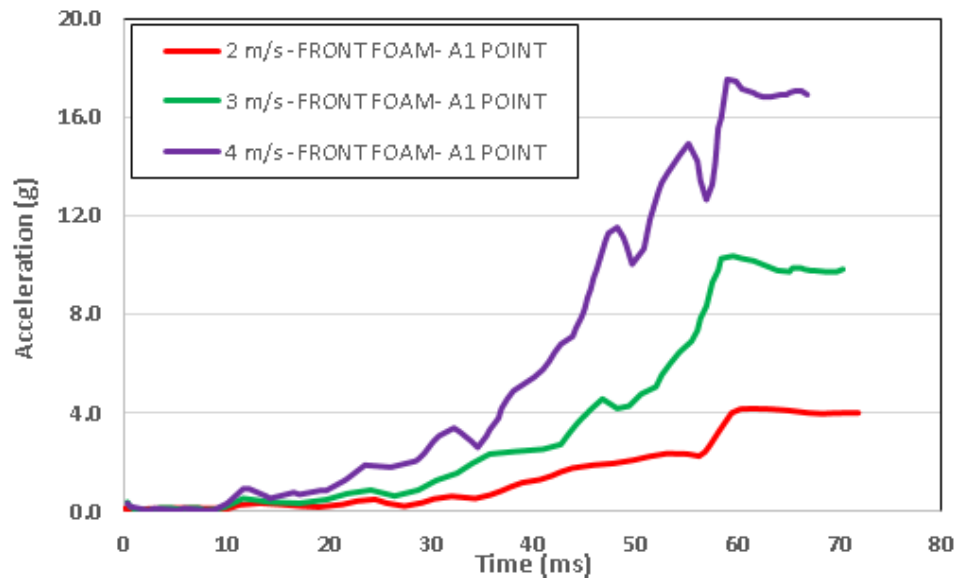


Figure 7-6: A1 Value When FRONT Foam Installed at Various Velocity

Figure 7-7 shows three different colour indicates three different velocities. This figure discusses the effect of foam installed at FRONT position. The peak values recorded at impact velocity 2 m/s, 3 m/s and 4 m/s were 35.67 g, 58.63 g and 86.30 g respectively.

Figure 7-8 shows full simulation of Equator P2 increased at impact velocity 2 m/s, 3 m/s, 4 m/s for before and after point of impact if only FRONT foam is installed. This figure shows that the material developed for simulation working without any instabilities or error. Thus, the reliability and result from this simulation are accurate and acceptable.

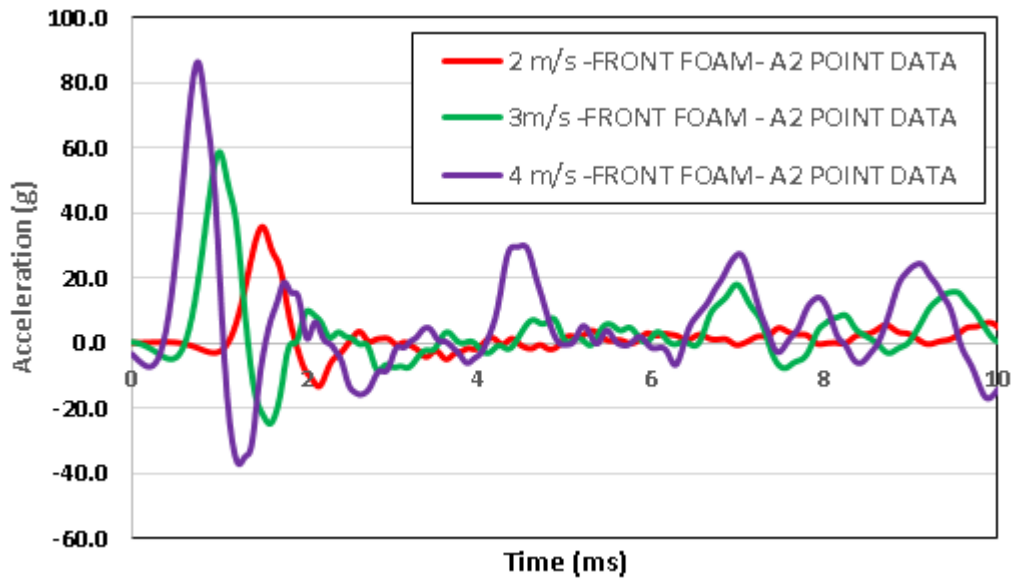


Figure 7-7: A2 Value When FRONT Foam Installed at Various Velocity

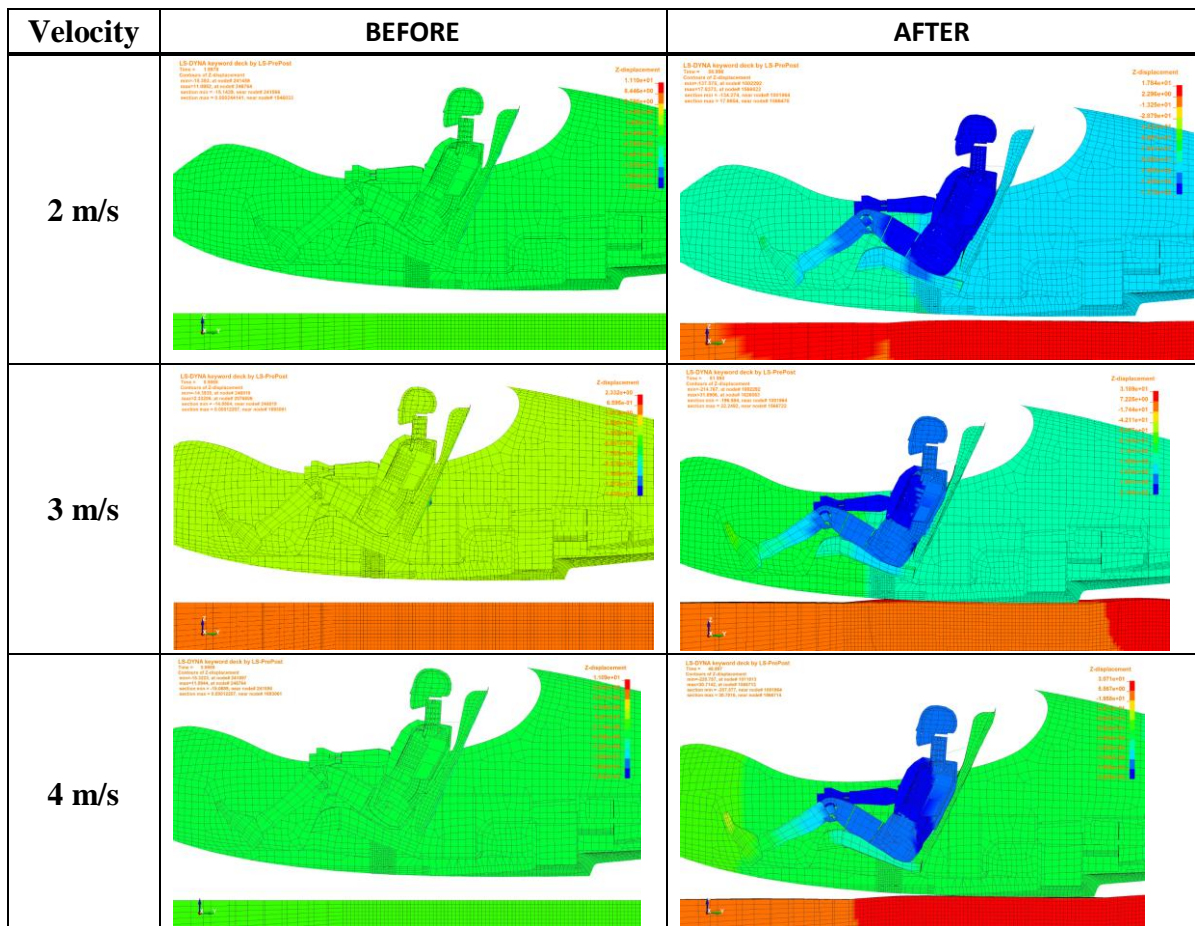


Figure 7-8: Full Simulation of Equator P2 Landing Contour Before-After for FRONT

7.3 Foam Installed in Aircraft – BACK Position

This section discusses on the effect of placing foam at the BACK position of aircraft. The significance of this simulation is to identify the effects on using foam in two different locations. Based on Figure 7-2, two locations mentioned on the aircraft are the front below occupant and at the first contact point of impact during touchdown. Data collected were acceleration against time at two position at lower torso (A1) and step area (A2).

Figure 7-9 shows three different colour indicates three different velocities. This figure discusses the effect of foam installed at BACK position. The peak values recorded at impact velocity 2 m/s, 3 m/s and 4 m/s were 4.18 g, 10.39 g and 16.55 g respectively

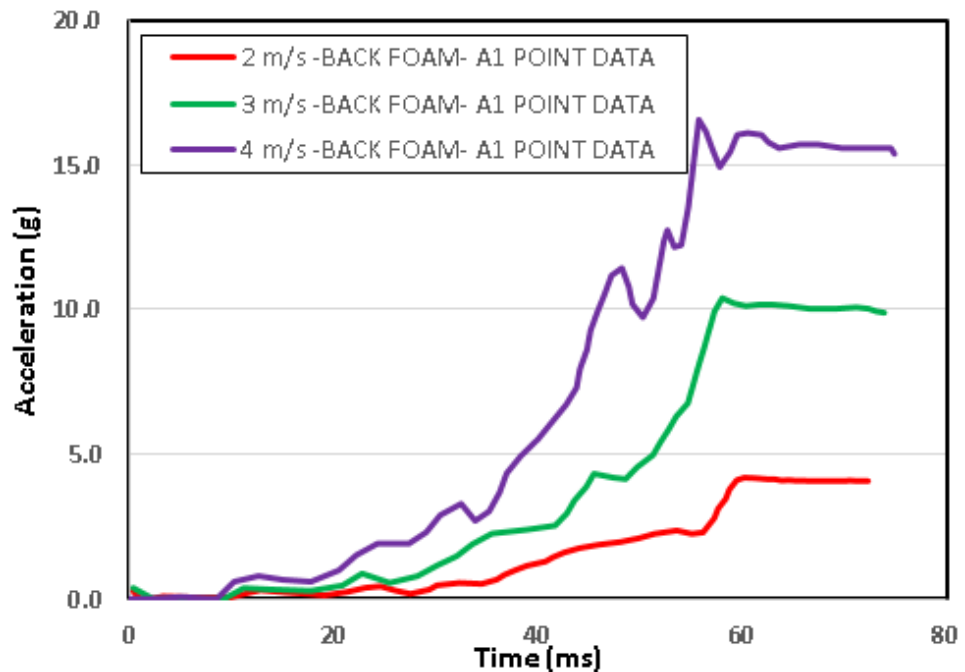


Figure 7-9: A1 Value When BACK Foam Installed at Various Velocity

Figure 7-10 shows three different colour indicates three different velocities. This figure discusses the effect of foam installed at BACK position. The peak values recorded at impact velocity 2 m/s, 3 m/s and 4 m/s were 35.67 g, 58.63 g and 83.67 g respectively.

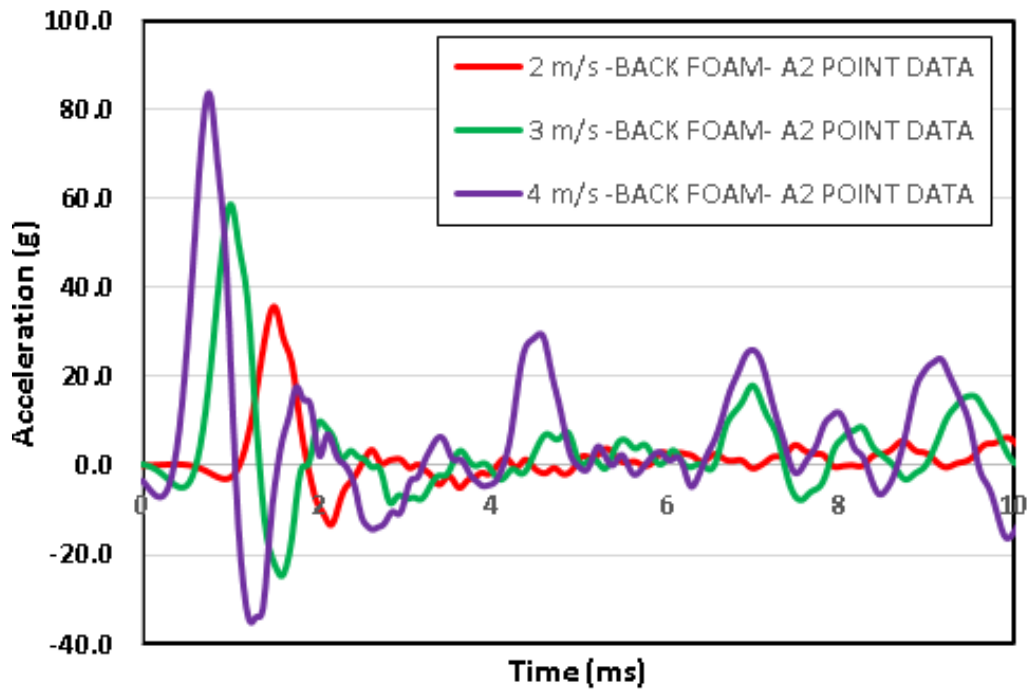


Figure 7-10: A2 Value When BACK Foam Installed at Various Velocity

Figure 7-11 shows full simulation of Equator P2 increased at impact velocity 2 m/s, 3 m/s, 4 m/s for before and after point of impact if BACK foam installed. This figure shows that the material developed for simulation working without any instabilities or error. Thus, the reliability and result from this simulation are accurate and acceptable.

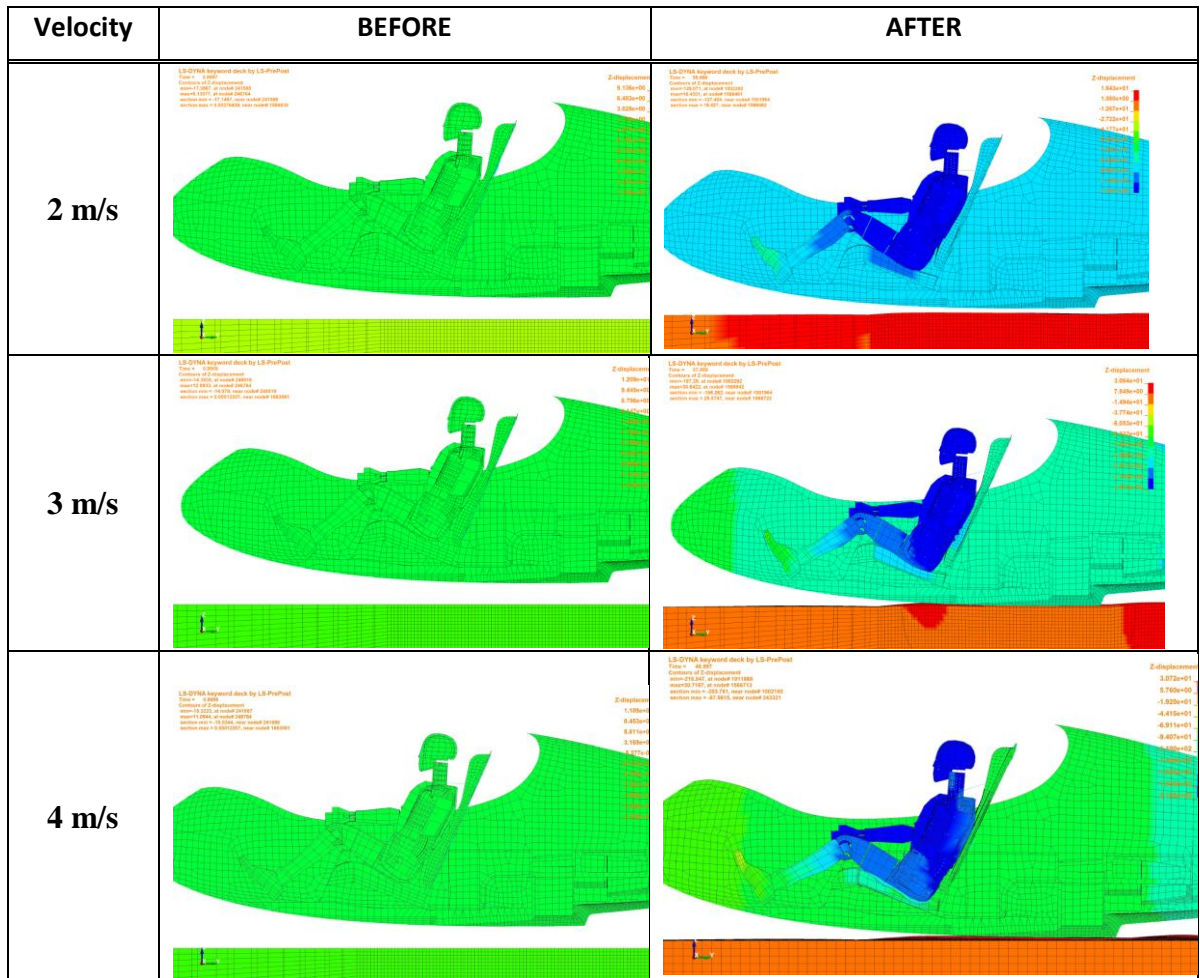


Figure 7-11: Full Simulation of Equator P2 Landing Contour Before-After for BACK

7.4 Foam Installed in Aircraft - BOTH Position

Last part of simulation is to observe on the effect when BOTH position were installed with foam. The significance of this simulation is to identify the effects on using foam in two different locations. Based on Figure 7-2 two locations mentioned on the aircraft are the front below occupant and at the first contact point of impact during touchdown. Data collected were acceleration against time at two position at lower torso (A1) and step area (A2).

Figure 7-12 shows three different colour indicates three different velocities. This figure discusses the effect of foam installed at BOTH position. The peak values recorded at impact velocity 2 m/s, 3 m/s and 4 m/s were 4.17 g, 8.82 g and 14.50 g respectively.

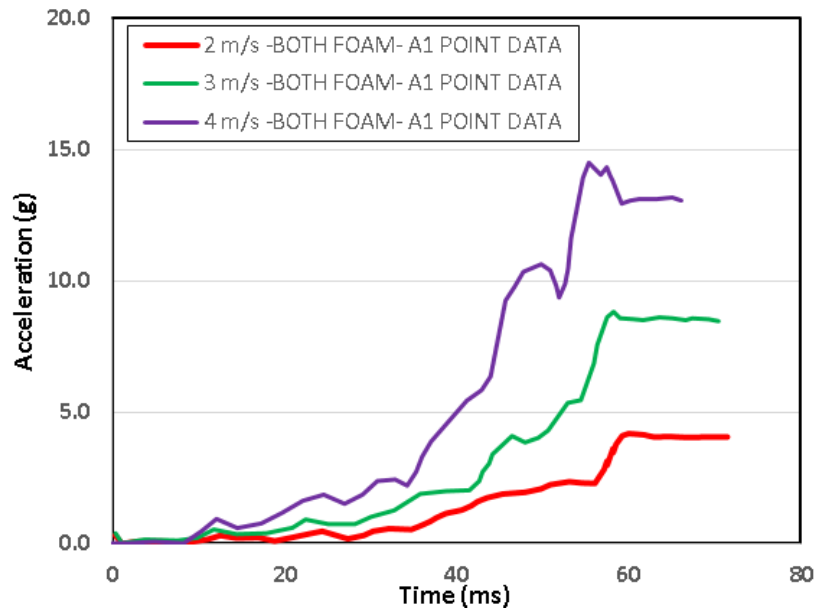


Figure 7-12: A1 Value When BOTH Foam Installed at Various Velocity

Figure 7-13 shows three different colour indicates three different velocities. This figure discusses the effect of foam installed at BOTH position. The peak values recorded at impact velocity 2 m/s, 3 m/s and 4 m/s were 35.67 g, 58.63 g and 83.67 g respectively.

Figure 7-14 shows full simulation of Equator P2 increased at impact velocity 2 m/s, 3 m/s, 4 m/s for before and after point of impact if BOTH location were installed with foams. This figure shows that the material developed for simulation working without any instabilities or error. Thus, the reliability and result from this simulation are accurate and acceptable.

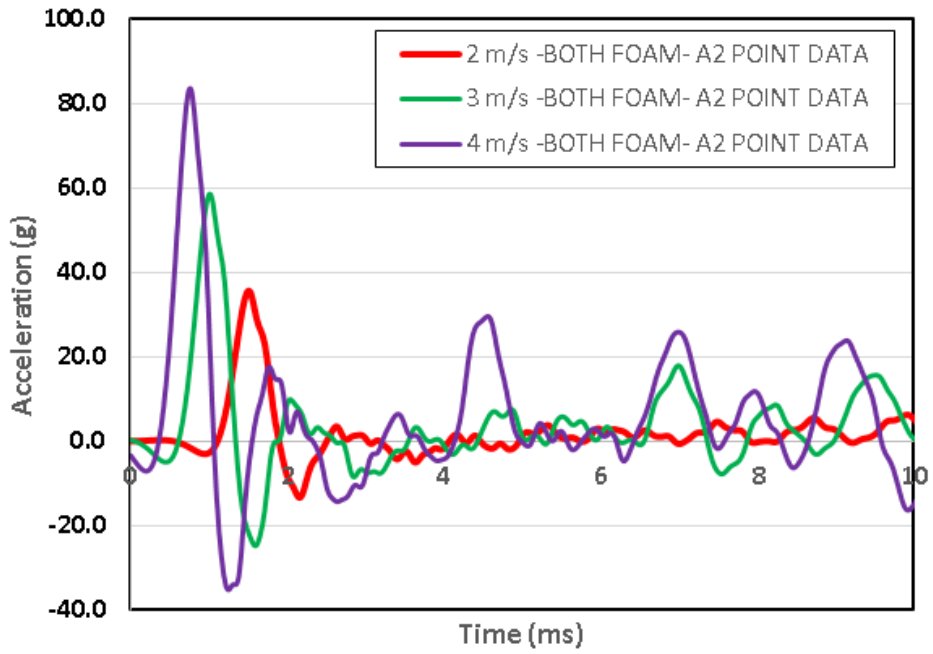


Figure 7-13: A2 Value When BOTH Foam Installed at Various Velocity

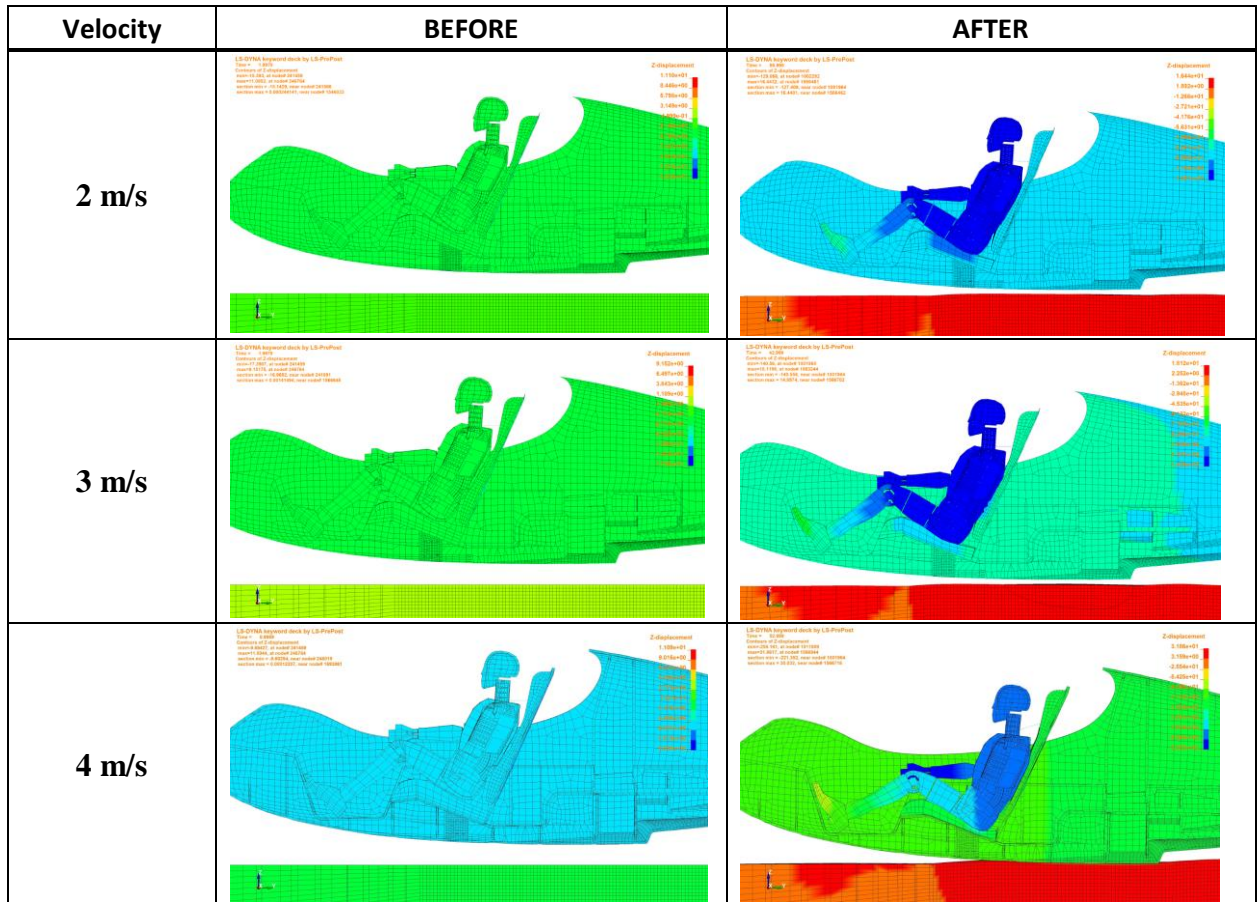


Figure 7-14: Full Simulation of Equator P2 Landing Contour Before-After for BOTH

7.5 Summary of Optimised Foam Location for Equator P2 Aircraft

Research focuses on the peak value of acceleration (g) recorded at the time (ms) of impact. Table 7-3 shows data and parameters related to the impact velocities and foam locations in detail.

Table 7-3: The Values of Simulation Results Based on Materials Installed in the Aircraft

IMPACT VELOCITY	2 m/s		3 m/s		4 m/s	
FOAM LOCATION	POINTS DATA COLLECTED					
	A1 (g)	A2 (g)	A1 (g)	A2 (g)	A1 (g)	A2 (g)
NO- FOAM	3.82	36.64	10.49	60.41	17.78	86.29
FRONT	4.14	35.67	10.34	58.63	17.53	86.30
BACK	4.18	35.67	10.39	58.63	16.55	83.67
BOTH	4.17	35.67	8.82	58.63	14.50	83.67
Note:	In g unit, $g = 9.81 \text{ m/s}^2$					

Table 7-3 shows the maximum value plotted for full aircraft simulation with foams installed at specified position to evaluate the effect of foam towards the acceleration (g) value. First discussion at 2 m/s, A1 point on aircraft shows lowest value of acceleration (g) is when NO FOAM installed. However, when foam is present in aircraft at any location, the values are similar. It was recorded at 3.82 g and this might be the spring action of the aircraft structure. Structure under the occupant section tend to be more solid when filled with foam absorber; there is limited space for deformation of the structure. However, when applied with 3 m/s and 4 m/s, the structure acceleration (g) value starts to increase. This shows that the foam absorber only useful for impact velocity higher than 2 m/s. This value is almost similar for any other location when the foam is present. To conclude the findings at impact velocity 2 m/s, NO FOAM resulting lowest acceleration (g) value for A1 point (3.82 g). In contrary, A2 point for NO FOAM shows the highest acceleration (g) (36.64 g).

Second discussion is the findings at 3 m/s. A1 point shows NO FOAM gives the highest value of acceleration (g) (10.49 g). The analysis shows when BOTH locations installed with foam give the lowest value of acceleration (g) (8.82 g). To conclude the findings at 3 m/s, NO FOAM result shows the highest acceleration (g) value in A2 point (60.41 g). Whilst, lowest acceleration (g) value in A1 point when BOTH locations installed with foam (8.82 g). Specifically, there are reduction of 15.985% compared to NO FOAM condition.

Next discussion is the findings on 4 m/s. Acceleration (g) values at installed position between NO FOAM and FRONT were almost similar. For foam position of BACK and BOTH at A2 point, same acceleration (g) values were recorder (86.3 g). At A1 position, lowest acceleration (g) values recorded when foam is installed in BOTH position (14.5 g). The different between BOTH foam installed and without foam recorded a reduction of 18.5%. Therefore, at 4 m/s, installation of foam at BOTH position is the best.

To summarise this chapter, aircraft with NO FOAM, BACK, FRONT and BOTH were simulated at impact velocity 2 m/s, 3 m/s and 4 m/s. The velocity increase shows that the acceleration (g) would also increase. However, in FRONT foam position, significant reduction only occurs at 3 m/s and 4 m/s. To conclude, installing foams under the seat pan (A1) and aircraft step area (A2) is better compared to NO-FOAM is installed in the aircraft. This proves, that the presence of foams are able to reduce more acceleration (g) while landing for position of under the seat pan (A1) and aircraft step area (A2). Hence, objective 4 was reflected in this portion of analysis,

Chapter 8: Conclusions and Recommendations

8.1 Conclusions

This research has been carried out by setting up the aims and objectives describes in Chapter 1, which all have been successfully achieved. There were four objectives of the research. First objective was to investigate the effects that occur during impact loading on IMPAXX EPS through experiment and simulation based on parameters such as velocities, densities and sequence configuration. It is found that to obtain highest optimisation; Material B should be placed in the middle or top position compared to Material A and C in terms of both parameters acceleration and displacement. Material C gives huge impact towards material combination. To obtain highest optimisation, Material C should be positioned either middle or top of design configuration.

The second objective was to determine best flat design configuration of EPS foam arrangements in terms of displacement and acceleration properties via experiment and simulation. Best flat design that was determined by this analysis is combination layer. To obtain highest optimisation, Material A should be placed in the lower or middle position. Material B should be placed in the middle or top arrangement. For Material

C, the position C must be placed at top or middle. From this rule, four designs were selected. Therefore, to complete objective two, material design 7 (ABC), 9 (BCA), 10 (CBA) and 12(ACB) were selected as best flat design configuration.

The third objective of this research was to analyse the shape effect on EPS foam in terms of displacement and acceleration (g) properties via simulation. There were four shapes introduced in this research. The shapes were arc (ARC) , sinusoidal (SIN), square (SQ) and trapezium (TR). Therefore, best shape selected was square (SQ) shape with space configuration. Based on average and time (t) average approach, the total frequency calculated for arc, sinusoidal, square and trapezium were 11, 21, 27 and 23 respectively. Therefore, by using these statistical approaches design 10 (CBA) square shape with Space was selected.

The last objective was to propose effective position of foam energy absorber for Equator P2 amphibian aircraft application. Based on analysis carried out in Chapter 7, the best position is when the foam were installed in BOTH position. To conclude, Design 10 using foam arrangement CBA with Space configuration must be installed in BOTH position of aircraft. This material design provides reduction of impact acceleration (g) for Equator P2 aircraft during landing on water. Hence, with this reduction, passenger experience minimum acceleration (g) value that indicates better passenger safety. Installed foam at BOTH position also improves structural integrity of the amphibian aircraft.

8.2 Future Research and Suggestions

The recommendations were made through the experience gained from this research and proposals for future considerations are as follows;

- i. Impact of aircraft landing on land/ solid surface is considered as a very interesting topic to be explored in the future, using similar parameters used in this research.
- ii. Besides small aircraft, future studies on passenger safety in commercial aircraft can also be considered.
- iii. A similar statistical approach can also be applied and used in automotive industries, especially to increase roles of passive impact device.
- iv. A more robust optimisation technique could be employed in order to verify the current technique with other types of material.
- v. The effect of the foam interface joining method to the dynamics of the system need to be considered for further study through experiment and simulation.
- vi. The effect due to the various load application in the numerical model (i.e. uniformly distributed load) and the experiment (i.e. concentrated load) need to be considered for further study through experiment and simulation.
- vii. The consideration towards energy dissipation by the material should be also studied in order to provide better understanding the dynamic characteristic of foam.

References

- Abbasov, I.B. and V'iacheslav, V.O. (2017) Computational modeling of the cabin interior of the conceptual model of amphibian aircraft "Lapwing." *Advances in Engineering Software*, 114: 227–234.
- Adams, A. and Lankarani, H. (2003) A modern aerospace modeling approach for evaluation of aircraft fuselage crashworthiness. *International Journal of Crashworthiness*, 8 (4): 401–413.
- Ahn, D.G., Lee, S.H. and Yang, D.Y. (2002). Mechanical properties and anisotropy of expanded polystyrene foam sheet for the VLM-S rapid prototyping process. *Journal of Materials Science Letters*, 21 (9): 747–749.
- Aiello, M., Galvanetto, U. and Iannucci, L. (2007) Numerical simulations of motorcycle helmet impact tests. *International Journal of Crashworthiness*, 12(1):1–7.
- Airex (2011) AIREX, Data Sheet GM-TDS-106, Airex Baltek Banova, Switzerland. Available at <https://www.3accorematerials.com/uploads/documents/TDS-AIREX-C70-E_1106.pdf> [Accessed 1 November 2017].
- Aktay, L., Johnson, A., Toksoy, A., Kröplin, B.H., and Güden, M. (2008) Modeling the progressive axial crushing of foam-filled aluminum tubes using smooth particle hydrodynamics and coupled finite element model/smooth particle hydrodynamics. *Materials & Design*, 29 (3): 569–575.
- Aktay, L., Toksoy, A. and Güden, M. (2006) Quasi-static axial crushing of extruded polystyrene foam-filled thin-walled aluminum tubes: experimental and numerical analysis. *Materials & Design*, 27 (7): 556–565.
- Andersson, M. and Larsson, E. (2016) *Benchmarking study of steel-composite structures in CAE crash applications*. Master Thesis, Chalmers University of Technology.

- Annett, M.S. (2010) LS-DYNA analysis of a full-scale helicopter crash test. *Proceedings of the 11th International LS-DYNA Users Conference*, Dearborn, MI.
- APP (2014) Polystyrene packaging. Available at <<http://www.advanced-pp.co.uk/products/polystyrene-packaging>> [Accessed 25 February 2014].
- ASTM (2003) ASTM Standards D 1596 – 97, Standard test method for dynamic shock cushioning characteristics of packaging material, ASTM International, US.
- Atas, C. and Sevim, C. (2010) On the impact response of sandwich composites with cores of balsa wood and PVC foam. *Composite Structures*, 93 (1): 40–48.
- ATMOS (2014) ATMOS™. Available at <http://www.giro.com/eu_en/products/men/helmets/atmos.html> [Accessed 25 February 2014].
- AWG (2013) Modeling guidelines document. *LS DYNA Aerospace Working Group*, Version 13-1.
- Bala, S. (2006) Best practices for modeling recoverable low density foams-by example. Available at <<http://www.d3view.com/best-practices-for-modeling-recoverable-low-density-foams-by-example/>> [Accessed 15 January 2013].
- Balendra, G., Turner, M., McCrory, P., Halley, W. (2007) Injuries in amateur horse racing (point to point racing) in Great Britain and Ireland during 1993-2006. *British Journal of Sports Medicine*, 41 (3): 162–166.
- Beheshti, H.K. and Lankarani, H. (2006) A simplified test methodology for crashworthiness evaluation of aircraft seat cushions. *International Journal of Crashworthiness*, 11 (1): 27–35.
- Bennett, L., Frank, A., McLoughlin, T., Moreton, R., Randell, S., and Wong, S. (2005) *Wing in ground Effect (WIG) aircraft Aerodynamics*. School of Mechanical Engineering, Adelaide, Mech Eng 3016.
- Bhonge, P.S. (2008) *A methodology for aircraft seat certification by dynamic finite element analysis*, PhD Dissertation, Wichita State University.
- Bhonge, P.S., Thorbole, C.K. and Lankarani, H.M. (2010) Computational modeling and performance evaluation of a DAX-foam aircraft seat cushion utilizing high loading rate dynamic characteristics, *ASME 2010 International Mechanical Engineering Congress and Exposition*, pp. 667–674.
- Bond, G.R., Christoph, R.A. and Rodgers, B.M. (1995) Pediatric equestrian injuries: assessing the impact of helmet use. *Pediatrics*, 95 (4): 487–489.

- Boshevski, B. and Mircheski, I. (2017) Bicycle helmet design and the virtual validation of the impact, aerodynamics and production process. *Facta Universitatis, Series: Mechanical Engineering*, 15 (3): 353–366.
- Brown, K.A. (2007) *Finite element modelling of the static and dynamic impact behaviour of thermoplastic composite sandwich structures*. PhD Thesis, University of Nottingham.
- Caliskan, U. and Apalak, M.K. (2017) Low velocity bending impact behavior of foam core sandwich beams: Experimental. *Composites Part B: Engineering*, 112:158–175.
- Cernicchi, A., Galvanetto, U. and Iannucci, L. (2008) Virtual modelling of safety helmets: practical problems. *International Journal of Crashworthiness*, 13 (4): 451–467.
- Cheng, M., Bueley, D., Chin, L. S., Dionne, J.P., Wright, N., and Makris, A. (2014) Evaluation of ATD models for simulating occupant responses under vertical impact. *13th International LS-DYNA Users Conference*, Session-Occupant Safety, 2014.
- Cipolla, V., Frediani, A., Oliviero, F., Rossi, R., Rizzo, E., and Pinucci, M. (2016) Ultralight amphibious PrandtlPlane: the final design. *Aerotecnica Missili & Spazio*, 95: 125–135.
- Coastal Automotive (n.d.). IMPAXX™: premier energy management foam solution for maximum efficiency. Available at <<https://coastal-automotive.com/products-energy-absorbing-materials/impaxx-energy-absorbing-extruded-polystyrene-foam/>> [Accessed 7 November 2018].
- Coltman, J.W., Van Ingen, C., Johnson, N.B, and Zimmermann, R.E. (1989) Aircraft crash survival design guide. *Volume II - Aircraft Design Crash Impact Conditions and Human Tolerance*. Final Report, USAAVSCOM TR 89-D-22B.
- Croop, B. and Lobo, H. (2009) Selecting material models for the simulation of foams in LS-DYNA. *7th European LS-DYNA Conference*, 2009.
- Cui, L., Kiernan, S. and Gilchrist, M.D. (2009) Designing the energy absorption capacity of functionally graded foam materials. *Materials Science and Engineering: A*, 507 (1): 215–225.
- Desjardins, S.P., Laananen, D.H. (1980) Aircraft crash survival design guide. volume IV: aircraft seats, restraints, litters and padding. *USARTL-TR-79-22D*, Applied Technology Laboratory, U.S. Army.
- De Vries, D. V. W. M. (2009) *Characterization of polymeric foams*. Master Thesis, Eindhoven University of Technology.

- Di Landro, L., Sala, G. and Olivieri, D. (2002) Deformation mechanisms and energy absorption of polystyrene foams for protective helmets. *Polymer Testing*, 21 (2): 217–228.
- Dow (2006) Tech data sheet IMPAXX™ 700 energy absorbing foam. Available at < <https://www.rollbarpadding.com/FS/CO/84/0/IMPAXX700.pdf>> [Accessed 17 June 2018].
- Dow (2009a) Finite element analysis with IMPAXX energy absorbing foams in headliner applications. Available at < <http://www.dowautomotive.com/>> [Accessed 1 July 2018].
- Dow (2009b) Product safety assessment IMPAXX™ energy absorbing foam. Available at <http://msdssearch.dow.com/PublishedLiteratureDOWCOM/dh_0932/0901b80380932357.pdf?filepath=productsafety/pdfs/noreg/233-00581.pdf&fromPage=GetDoc> [Accessed 7 November 2018].
- EASA (2012) Certification specifications for normal, utility, aerobatic, and commuter category aeroplanes. Amendment 3. ED Decision 2012/012/R. Available at <<https://www.easa.europa.eu/sites/default/files/dfu/CS-23%20Amdt%203.pdf>> [Accessed 7 November 2018].
- Eiband, A.M. (1959) *Human tolerance to rapidly applied accelerations: a summary of the literature*. National Aeronautics and Space Administration (NASA), Memo 5-19-59E.
- Equator (n.d.) Equator Aircraft Norway SA. Available at < <http://www.equatoraircraft.com/>> [Accessed 8 November 2018].
- FAA (1989) *Advisory circular: dynamic testing of part 23 airplane seat/restraint systems and occupant protection*. U.S. Department of Transportation, Federal Aviation Administration.
- FAA (2004a) *Airplane flying handbook*. U. S. Department of Transportation, Federal Aviation Administration.
- FAA (2004b) *Seaplane, skiplane, and float/ski equipped helicopter operations handbook*. FAA-H-8083–23. U.S. Department of Transportation, Federal Aviation Administration.
- FAA (2006) *Advisory circular: dynamic evaluation of seat restraint systems and occupant protection on transport airplanes*. 25.562-1B. U.S. Department of Transportation, Federal Aviation Administration.

- FAA (2009) *Advisory circular: 14 CFR part 23 type certification of an airplane originally certificated to European Aviation Safety Agency (EASA) (CS-VLA) standards or joint aviation requirements – very light airplane (JAR-VLA)*, U.S. Department of Transportation, Federal Aviation Administration.
- FAA (2015) *Advisory circular: dynamic evaluation of seat restraint systems and occupant protection on transport airplanes. 25.562-1B CHG 1*. U.S. Department of Transportation, Federal Aviation Administration.
- Franklyn, M. and Laing, S. (2016) Evaluation of military helmets and roof padding on head injury potential from vertical impacts. *Traffic Injury Prevention*, 17 (7): 750–757.
- FSF (2000) Flight safety foundation ALAR briefing note 8.2 -the final approach speed. Flight Safety Foundation ALAR Tool Kit. Available at <<https://skybrary.aero/bookshelf/books/866.pdf>> [Accessed 8 November 2018].
- Gibson, L.J. and Ashby., M.F. (1997) *Cellular solids- structure and properties*. 2nd ed. Cambridge University Press.
- Gionta, M., Karkow, J., Roncz, J., Kohler, D., Lednicer, D. (2018) *Spin resistant aircraft configuration*. Patent US9926071B2.
- Global, S. (2013) Seaplanes. Available at <www.globalsecurity.org/military/world/seaplanes.htm> [Accessed 10 February 2013].
- Gobbi, G., Smrcek, L., Galbraith, R., Mohr, B., and Schömann, J. (2011) Report on current strength and weaknesses of existing seaplane/amphibian transport system as well as future opportunities. FP7-AAT-20070RTD1. FUSETRA Version 1.0. Available at <http://www.fusetra.eu/documents/FUSETRA_D41_SWOT_v01_strtot2.pdf> [Accessed 1 November 2018].
- Gover, R. and Gudimetla, P. (2011) Testing and simulation of extruded polystyrene foam at low to moderate strain rates. *Proceedings of the First International Conference on Engineering, Designing and Developing the Built Environment for Sustainable Wellbeing*, 2011.
- Guida, M. and Marulo, F. (2014) Partial modeling of aircraft fuselage during an emergency crash landing. *Procedia Engineering*, 88: 26–33.
- Halldin, P., Gilchrist, A. and Mills, N. (2001) A new oblique impact test for motorcycle helmets. *International Journal of Crashworthiness*, 6 (1): 53–64.

- Hassan, M.Z. (2012) *The Low Velocity Impact Response of Sandwich Structures*. PhD Thesis, University of Liverpool.
- Hearon, B. and Brinkley, J. (1986) Effect of seat cushions on human response to +Gz impact. *Aviation, Space, and Environmental Medicine*, 57 (2): 113–121.
- Hejna, A., Kirpluks, M., Kosmela, P., Cabulis, P., Haponiuk, J., and Piszczyk, L. (2017) The influence of crude glycerol and castor oil-based polyol on the structure and performance of rigid polyurethane-polyisocyanurate foams. *Industrial Crops and Products*, 95: 113–125.
- Hilyard, N. (1982) *Mechanics of cellular plastics*. MacMillan, NY.
- HSV (2013) Production: EPS and EPP production process. Available at <<http://www.hsv.nl/hsv-production-process.php>> [Accessed 15 December 2013].
- Hu, D., Song, B., Wang, D., and Chen, Z. (2016) Experiment and numerical simulation of a full-scale helicopter composite cockpit structure subject to a bird strike. *Composite Structures*, 149: 385–397.
- Hunziker, K.J., Pang, J., Pereira, M., et al. (2018) NASA ACC high energy dynamic impact methodology and outcomes. *2018 AIAA/ASCE/AHS/ASC Structures, Structural Dynamics, and Materials Conference*.
- ICA (2013) The manufacturing process. Available at <<http://insulationcorp.com/manufacturing/>> [Accessed 12 December 2013].
- Jackson, K.E. (2018) Advances in rotorcraft crashworthiness: trends leading to improved survivability. 37th Alexander A. Nikolsky Honorary Lecture. *Journal of the American Helicopter Society*, 63 (2): 1–25.
- Kang, S. and Xiao, P. (2008) Comparison of hybrid III rigid body dummy models. *10th International LSDYNA Users Conference, 2008*.
- Kostopoulos, V., Markopoulos, Y., Giannopoulos, G., and Vlachos, D.E. (2002) Finite element analysis of impact damage response of composite motorcycle safety helmets. *Composites Part B: Engineering*, 33 (2): 99–107.
- Lee, S., Byun, J. and Cho, H. (2011) Progressive damage structural analysis of carbon/epoxy composite laminates. *The 18th International Conference of Composite Materials*, ICC Jeju, Korea. 2011, pp. 21–26.

- Leijten, J., Bersee, H.E., Bergsma, O.K., Beukers, A. (2009) Experimental study of the low-velocity impact behaviour of primary sandwich structures in aircraft. *Composites Part A: Applied Science and Manufacturing*, 40 (2): 164–175.
- Leslie-Pelecky, D. (2008) Why is there foam in the car doors? Available at <http://stockcarscience.com/scienceTopics/scsCarSafety_IMPAXX.php> [Accessed 20 January 2014].
- Lewis, A.F. and Kim, Y.K. (2018) *Add-on impact energy absorbing pad structure for outside of military and sport helmets*. Patent US App. 15/706,962.
- Li, J., Cao, L., Guo, B., and Zhang, X. (2018a) Prediction of productivity of high energy gas-fractured oil wells. *Journal of Petroleum Science and Engineering*, 160: 510–518.
- Li, Z., Chen, R. and Lu, F. (2018b) Comparative analysis of crashworthiness of empty and foam-filled thin-walled tubes. *Thin-Walled Structures*, 124: 343–349.
- Liem, R.P. (2018) Review of design aspects and challenges of efficient and quiet amphibious aircraft. *Journal of Physics: Conference Series*, 1005, p. 012027.
- Loftin, L.K. (1985) *Quest for performance: the evolution of modern aircraft*. Scientific and Technical Information Branch, National Aeronautics and Space Administration (NASA).
- LSTC (2007) *LS-DYNA® keyword user's manual volume 1 (version 971)*. Livermore, California.
- Lubguban, A.A., Ruda, R.J.G., Aquiatan, R.H., Paclijan, S., Magadan, K.O., Balangao, J.K.B., Bayron, R.R., Debalucos, B., Lubguban, A.A., Hsieh, F.H., and Suppes, G.J. (2017) Soy-based polyols and polyurethanes. *Kimika*, 28 (1): 1–19.
- Mahéo, L. and Viot, P. (2013) Impact on multi-layered polypropylene foams. *International Journal of Impact Engineering*, 53: 84–93.
- Majka, A. (2012) The problem of choice of light passenger seaplane used for short-haul flights. *Journal of KONES Powertrain and Transport*, 19 (4):419-428.
- Mark, J.E. (2009) *Polymer data handbook*. Oxford University Press, Inc.
- McIntosh, A.S. and McCrory, P. (2005) Preventing head and neck injury. *British Journal of Sports Medicine*, 39 (6): 314–318.

- Mills, N., Fitzgerald, C., Gilchrist, A., and Verdejo, R. (2003) Polymer foams for personal protection: cushions, shoes and helmets. *Composites Science and Technology*, 63 (16): 2389–2400.
- Mills, N.J. (2003) Materials in sports equipment. In Jenkins, M. (ed.) *Materials in Sport Equipment*. 1st ed. Woodhead Pubs.
- Mills, N.J. (2007) *Polymer foams handbook: engineering and biomechanics applications and design guide*. Butterworth-Heinemann.
- Miyazaki, Y., Ujihashi, S., Jin, T., Akiyama, S., and Woong, K.C. (2006) Effects of the mechanical properties of the shell and liner on the shock absorption of helmets. *The Engineering of Sport 6*. Springer, pp. 145–150.
- Mohan, P. (2009) Finite element modeling and mesh quality checks. Lecture -1, CE-264 Non-Linear Element Modeling and Simulation. Available at < <https://www.scribd.com/document/89168959/Lecture-1> > [Accessed 2 November 2018].
- Moren, C.R. (1999) Pilots, airplanes, and the tangent of three (3) degrees. Embry-Riddle Aeronautical University. Available at < https://pumas.jpl.nasa.gov/files/10_13_99_1.pdf > [Accessed 7 November 2018].
- Moritz, A. (2012) IMPAXX™ energy absorbers: automotive interiors. Available at < <https://www.yumpu.com/en/document/view/27494000/impaxx-energy-absorbers-by-cellutec-ukintpress-conferencescom/2> > [Accessed November 2017].
- Morris, R.D. (2014) *VTOL twin fuselage amphibious aircraft with tilt-center wing, engine and rotor*. US Patent 8,702,031.
- Mozafari, H., Khatami, S., Molatefi, H., Crupi, V., Epasto, G., and Guglielmino, E. (2016) Finite element analysis of foam-filled honeycomb structures under impact loading and crashworthiness design. *International Journal of Crashworthiness*, 21 (2): 148–160.
- Newcomb, B. A. and Chae, H. G. (2018), The properties of carbon fibres. In Bunsell, A.R.,(ed) *Handbook of Properties of textile and technical fibres*. The textile Institute Book Series 2018, pp. 841-871.
- Nguyen, T.D. (2010) *Finite element analysis of a nose gear during landing*. Master Thesis, University of North Florida.
- Olivares, G. (2010) Certification by analysis of aircraft seats. *6th Triennial International Aircraft Fire and Cabin Safety Research Conference, 2010*.

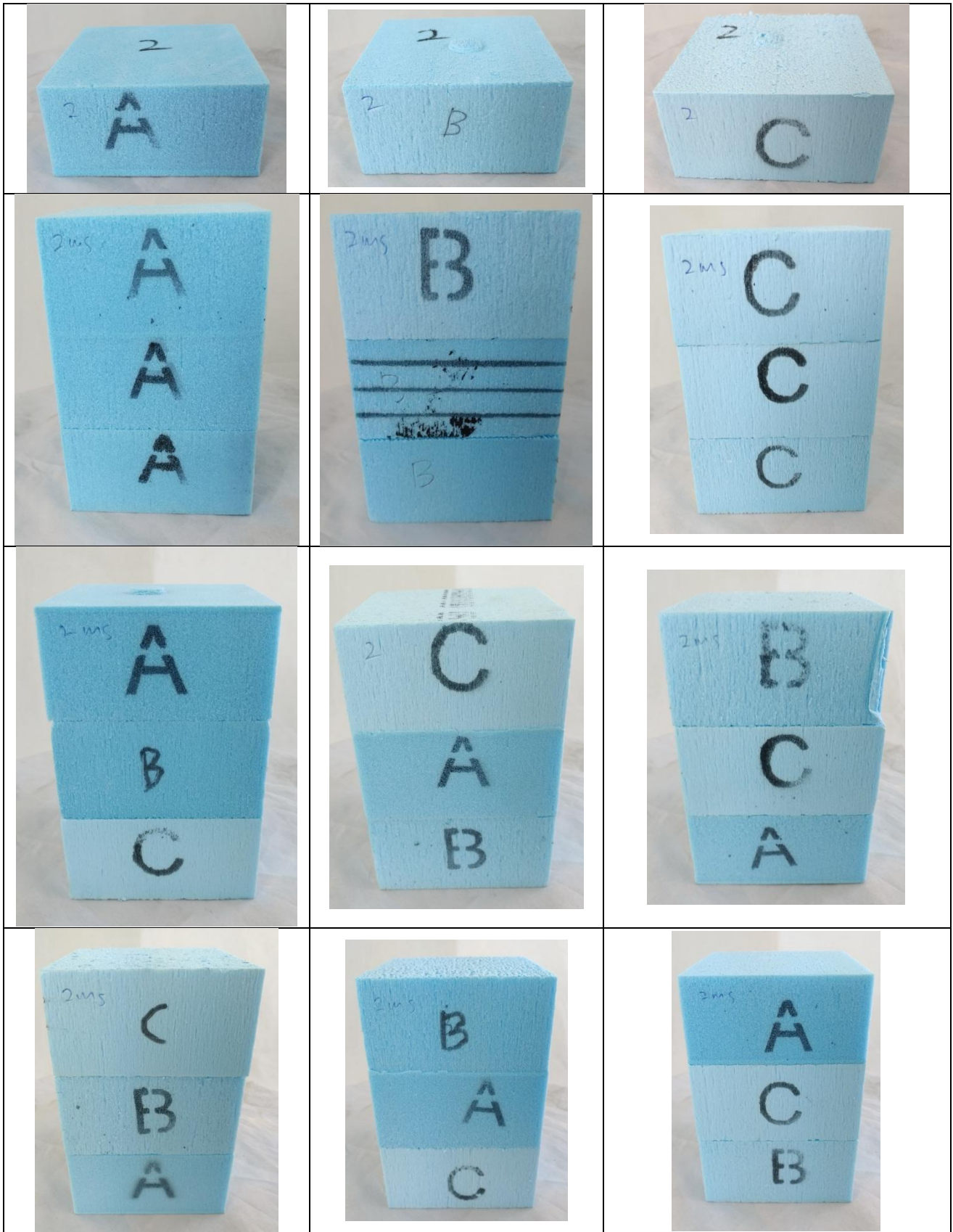
- Olivares, G., Acosta, J.F., and Yadav, V. (2010) Certification by analysis I and II. *FAA JAMS 2010 Technical Review Meeting*. Available at < https://depts.washington.edu/amtas/events/jams_10/pap16-Olivares.pdf> [Accessed 17 December 2017].
- Odedra, J., Hope, G., and Kennell, C. (2004) Use of seaplanes and integration within a sea base. *Technical Report NSWCCD-20-TR-2004/08, Naval Surface Warfare Center*. Available at < <https://apps.dtic.mil/dtic/tr/fulltext/u2/a476447.pdf>> [Accessed 12 December 2018].
- Ozturk, U.E. and Anlas, G. (2009) Energy absorption calculations in multiple compressive loading of polymeric foams. *Materials & Design*, 30 (1): 15–22.
- Paix, B.R. (1999) Rider injury rates and emergency medical services at equestrian events. *British Journal of Sports Medicine*, 33 (1): 46–48.
- Perry, C., Nguyen, T. and Pint, S. (2002) Evaluation of proposed seat cushions to vertical impact. *Safe Journal*, 30 (3): 197–207.
- Plastipedia (2013) Polystyrene (High Impact - HIPS). Available at < <http://www.bpf.co.uk/Plastipedia/Polymers/Default.aspx>> [Accessed November 2013].
- Potes, F., Silva, J. and Gamboa, P. (2016) Development and characterization of a natural lightweight composite solution for aircraft structural applications. *Composite Structures*, 136: 430–440.
- Qiu, L. and Song, W. (2015) Efficient multiobjective optimization of amphibious aircraft fuselage steps with decoupled hydrodynamic and aerodynamic analysis models. *Journal of Aerospace Engineering*, 29 (3): 0401507-1 - 0401507-14.
- Robinson, E.B. (2018) *Aircraft landing gear and method*. Patent WO2015035493A1.
- Rueda, F., Cui, L. and Gilchrist, M. (2009) Optimisation of energy absorbing liner for equestrian helmets. Part I: Layered foam liner. *Materials & Design*, 30 (9): 3405–3413.
- Segade, A., López-Campos, J.A., Fernández, J.R., Casarejos, R., and Vilán, J.A. (2016) Finite element simulation for analysing the design and testing of an energy absorption system. *Materials*, 9(660):1-13.
- Septevani, A.A., Evans, D.A., Chaleat, C., Martin, D.J., and Annamalai, P.K. (2015) A systematic study substituting polyether polyol with palm kernel oil based polyester polyol in rigid polyurethane foam. *Industrial Crops and Products*, 66: 16–26.

- Shanahan, D.F. (2004) Human tolerance and crash survivability. *RTO HFM Lecture Series on "Pathological Aspects and Associated Biodynamics in Aircraft Accident Investigation"*, 28-29 October 2004, Madrid, Spain.
- Slik, G., Vogel, G. and Chawda, V. (2006) Material model validation of a high efficient energy absorbing foam. *Proceedings of the 5th German LS-DYNA Forum, 2006*.
- Slik, G. and Vogel, G. (2007). Use of high efficient energy absorption foam in side impact padding. *Proceedings of the 20th Conf on the Enhanced Safety of Vehicles, 2007*.
- Stelzmann, U. and Hörmann, M. (2011) Ply-based composite modeling with the new *ELEMENT_SHELL_COMPOSITE keyword. *8th European Users Conference, 2011*.
- Styro (2013) Expanded polystyrene manufacturing process. Available at <<http://www.styrouae.com/environment/>> [Accessed 20 December 2013].
- Tabiei, A., Lawrence, C. and Fasanella, E.L. (2009) Validation of finite element crash test dummy models for predicting orion crew member injuries during a simulated vehicle landing. *10th International LS-DYNA® Users Conference. 2009*.
- Tay, Y.Y., Lim, C.S. and Lankarani, H.M. (2014) A finite element analysis of high-energy absorption cellular materials in enhancing passive safety of road vehicles in side-impact accidents. *International Journal of Crashworthiness*, 19 (3): 288–300.
- Teng, T.L., Liang, C.C., Shih, C.J., and Nguyen, V.H. (2013) Design and Analysis of Bicycle Helmet with Impaxx Foam Liner. *Advanced Materials Research*, 707-708:1778–1781.
- Toso, N.R.S. (2009) *Contribution to the modelling and simulation of aircraft structures impacting on water*. Dr-Ing, Thesis, the Universität Stuttgart.
- Trelleborg (n.d.) CONFOR® foams- cushioning and impact absorbing safety foam. Available at <<http://www.trelleborg.com/en/applied-technologies/products/protection/duplicate-of-advanced-energy-control-materials/confor-cushioning-and-impact-absorbing-safety-foam>>. [Accessed 2018].
- Troesch, A. and Kang, C. (1986) Hydrodynamic impact loads on three-dimensional bodies. *16th Symposium on Naval Hydrodynamics*, 1986.
- Troxel (2014) Troxel Sport. Available at <<http://www.troxelhelmets.com/products/sport>> [Accessed 25 February 2014].

- Turner, M., McCrory, P. and Halley, W. (2002) Injuries in professional horse racing in Great Britain and the Republic of Ireland during 1992-2000. *British Journal of Sports Medicine*, 36 (6): 403–409.
- Vagianos, N.J. and Thurston, D.B. (1970) *Hydrofoil seaplane design*. Report No.6912, May 1970, Thurston Aircraft Corporation.
- Valentini, S.C., Zou, H., Galbus, M.T., et al. (2016) *Polymeric foam composite for vehicle arresting system*. US Patent App. 14/972,991.
- Veronika, E. and Paul, D.B. (2012) Modelling of viscoelastic materials with LS-Dyna. DYNAMore GmbH (ed.). *11th German LS-Dyna Forum, 2012*.
- Veronika, E., Paul, D., Markus, F., et al. (2014). Nonlinear viscoelastic modeling for foams. *13th International LS-DYNA Users Conference, 2014*.
- Voloshchenko, V.Y. (2016) Seadrome: Increasing the safety of takeoff and landing operations in the seaplane basin. *Russian Aeronautics (Iz VUZ)*, 59 (2): 271–276.
- Wikipedia (n.d.) Grumman Goose G-21 (1937). Available at <http://en.wikipedia.org/wiki/File:JRF-5_NAS_Jax_1942.jpg> [Accessed 2013].
- Wu, J., Liu, X., Zhou, H., Li, L., and Lu, Z. (2018) Experimental and numerical study on soft-hard-soft (SHS) cement based composite system under multiple impact loads. *Materials & Design*, 139: 234–257.
- Xianfei, Z., Yunwen, F., Xiaofeng, X., and Qiang, Q. (2017) Evaluate the crashworthiness response of an aircraft fuselage section with luggage contained in the cargo hold. *International Journal of Crashworthiness*, 22 (4): 347–364.
- Yıldızhan, M., Efendioğlu, B., Kaya, N., Öztürk, I., Albak, E., and Öztürk, F. (2016) Design of improved energy absorbing pads to reduce occupant injuries in vehicle side impact. *International Journal of Vehicle Design*, 71 (1-4): 174–190.
- Zhang, J., Qin, Q., Chen, S., Yang, Y., Ye, Y., Xiang, C., and Wang, T.J. (2018) Low-velocity impact of multilayer sandwich beams with metal foam cores: analytical, experimental, and numerical investigations. *Journal of Sandwich Structures & Materials*, 0(0):1-32.
- Zhou, J., Guan, Z. and Cantwell, W. (2018) The energy-absorbing behaviour of composite tube-reinforced foams. *Composites Part B: Engineering*, 139: 227–237.

Appendix A

Example of IMPAXX EPS FOAM at 2 m/s



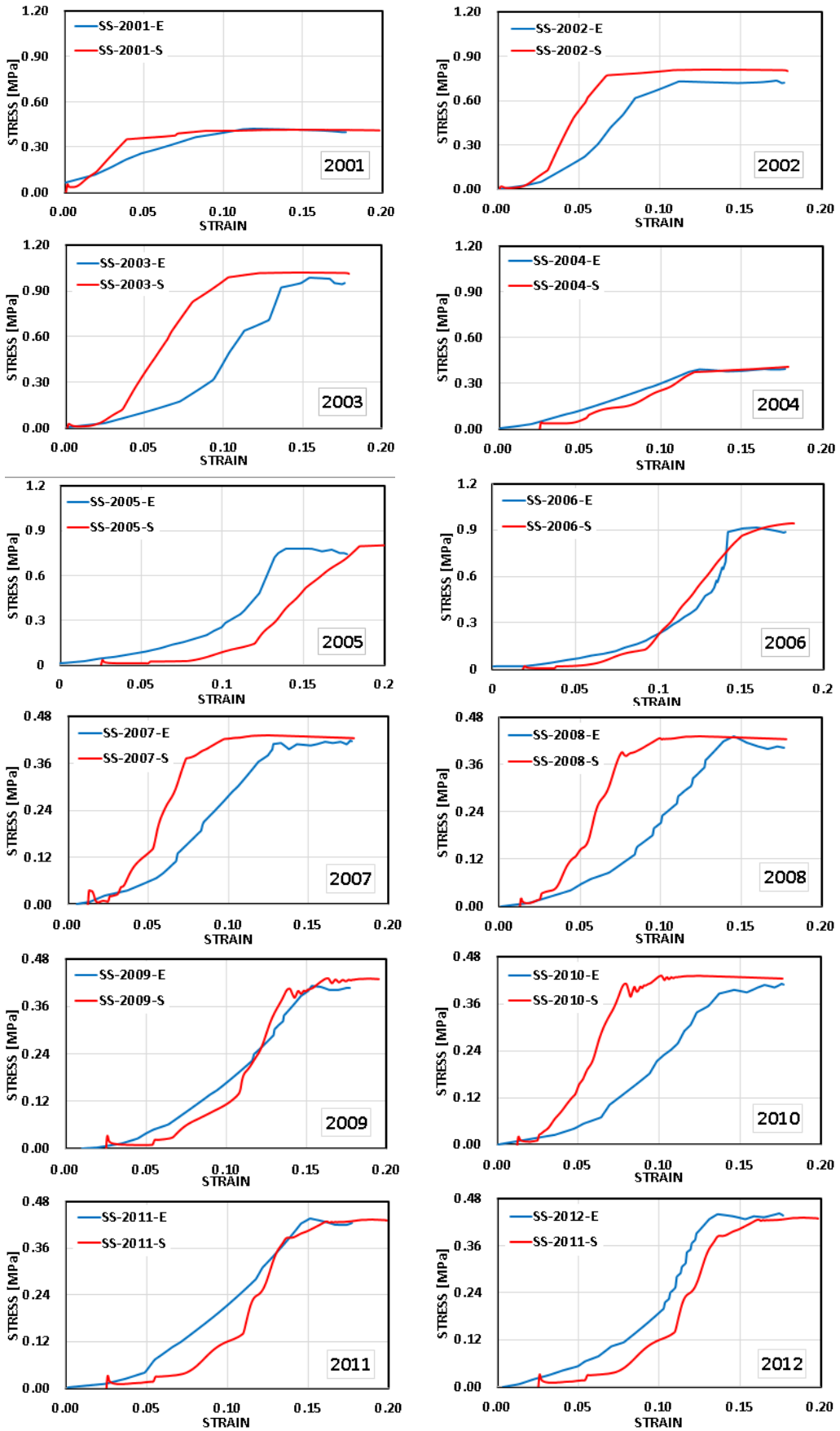
Arrangement of foam for experiment

Appendix B

Stress vs. Strain

Stress vs Strain

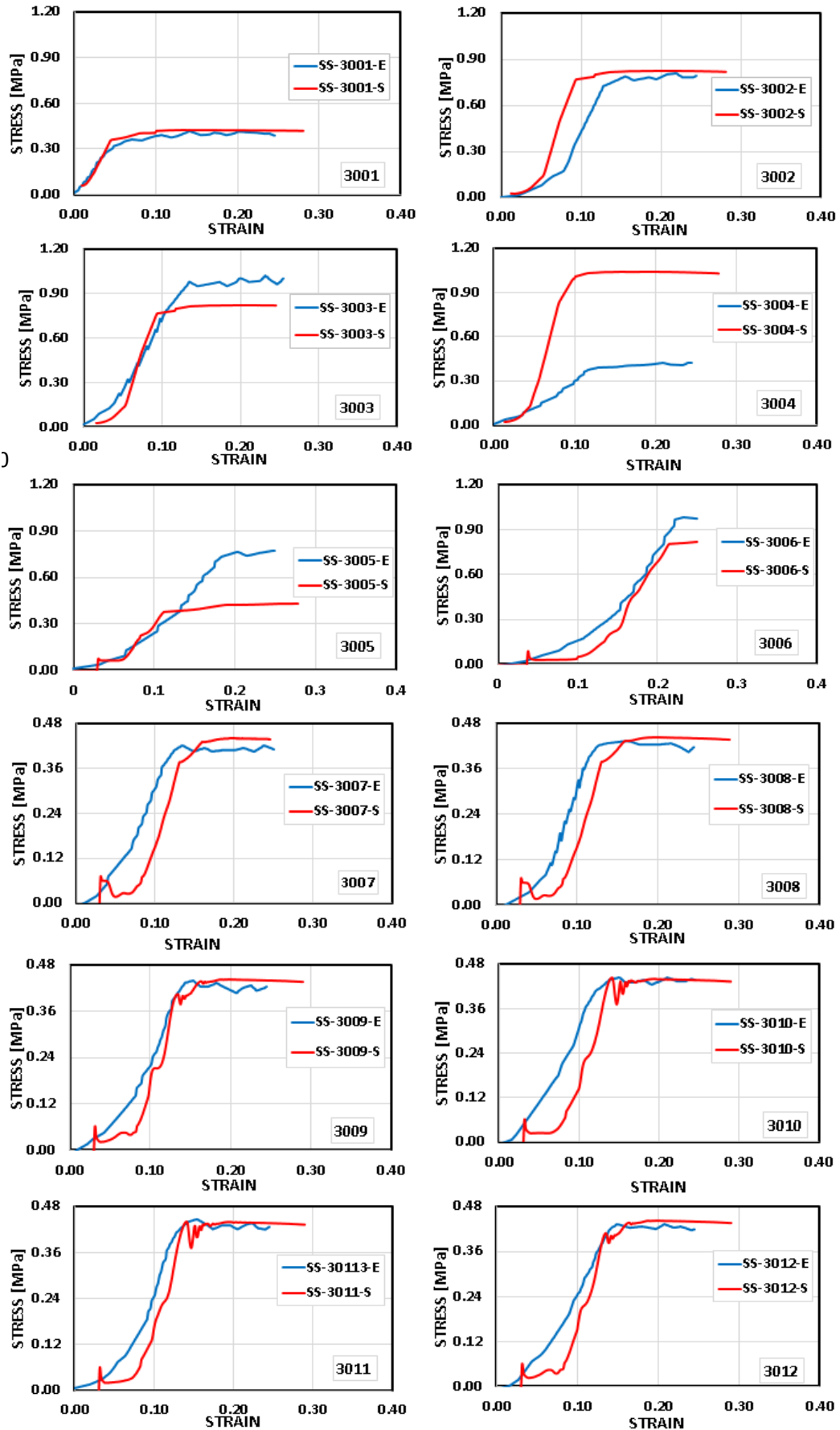
Impact Velocity 2 m/s



STRESS vs. STRAIN SIMULATION & EXPERIMENT 2 m/s

Stress vs Strain

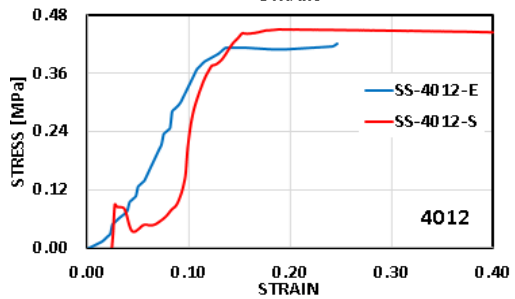
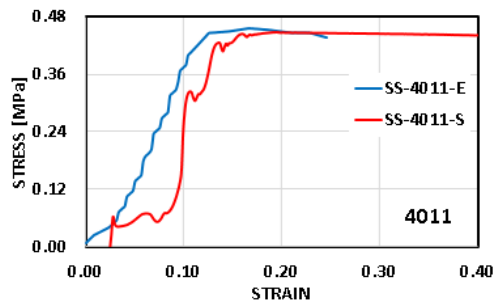
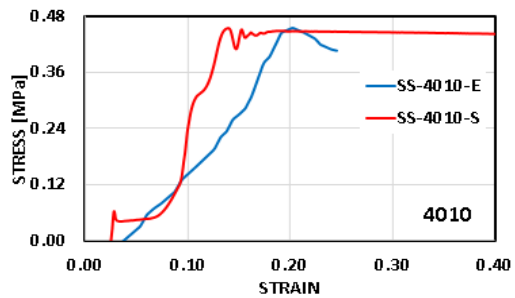
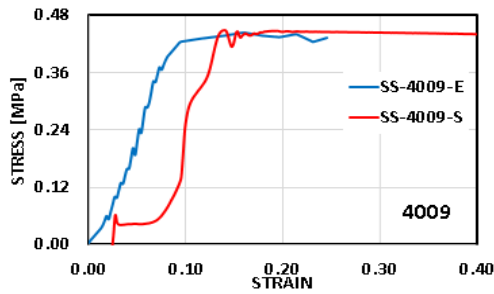
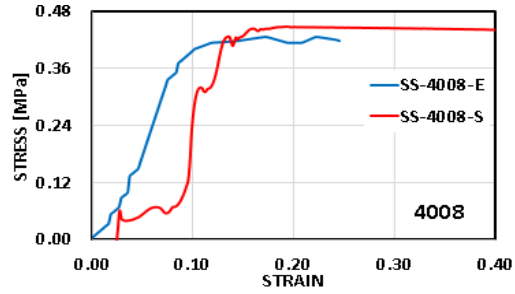
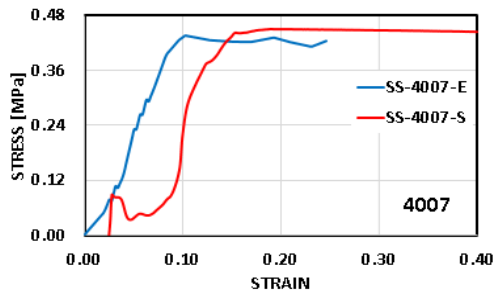
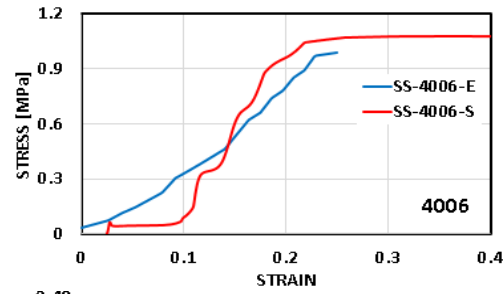
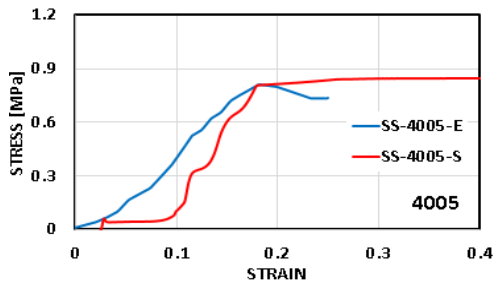
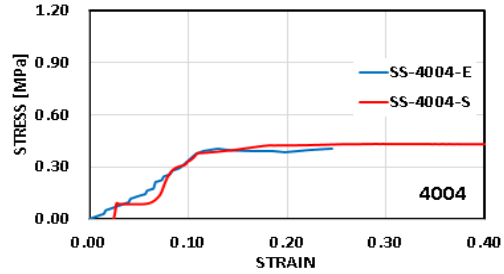
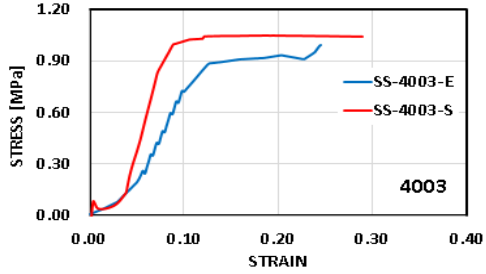
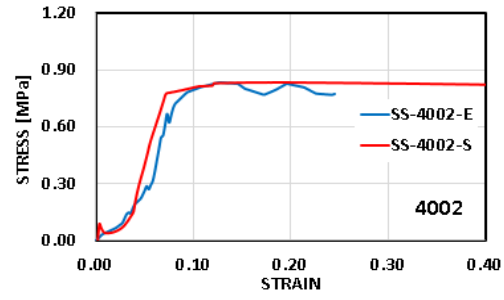
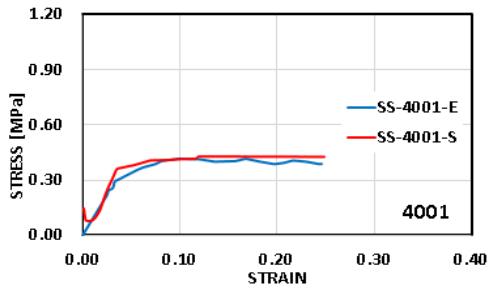
Impact Velocity 3 m/s



STRESS vs. STRAIN SIMULATION & EXPERIMENT 3 m/s

Stress vs Strain

Impact Velocity 4 m/s

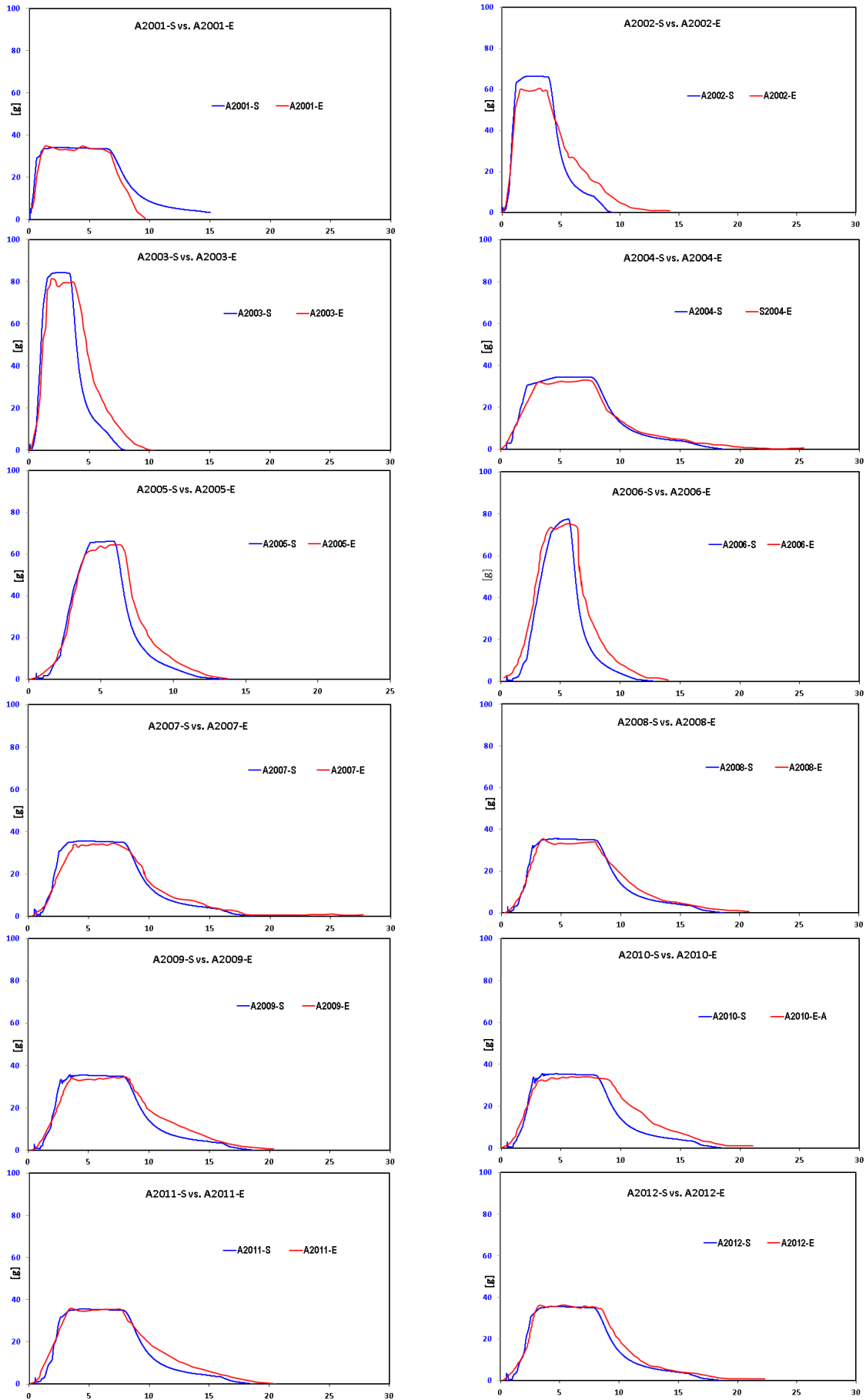


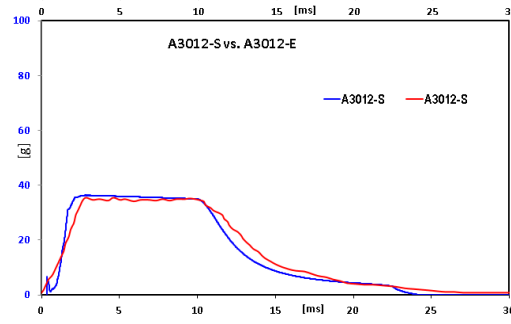
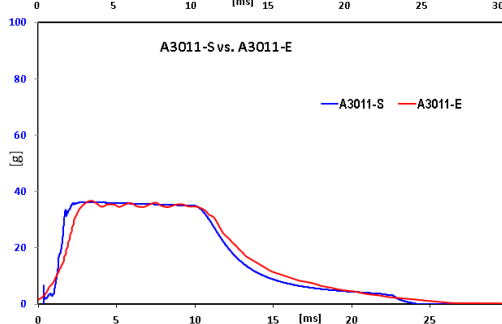
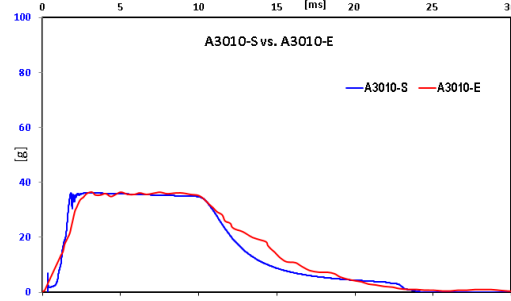
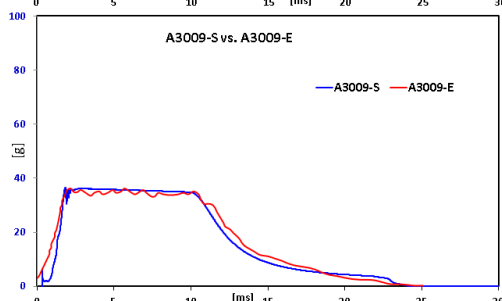
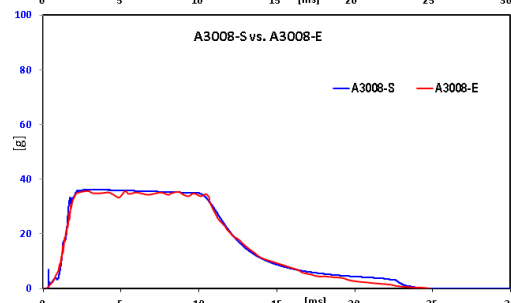
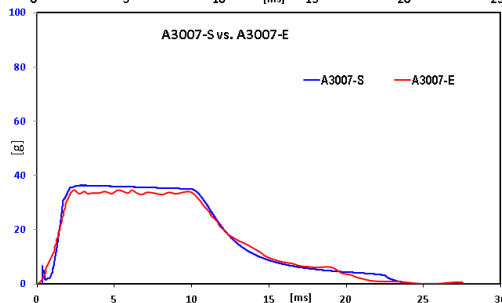
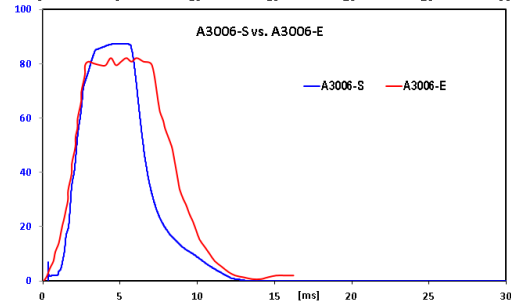
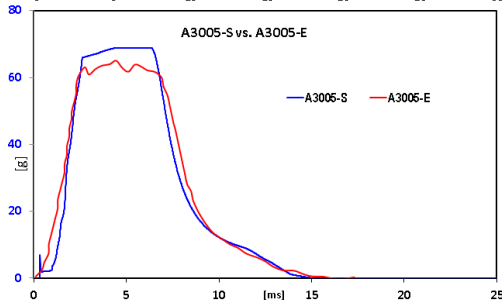
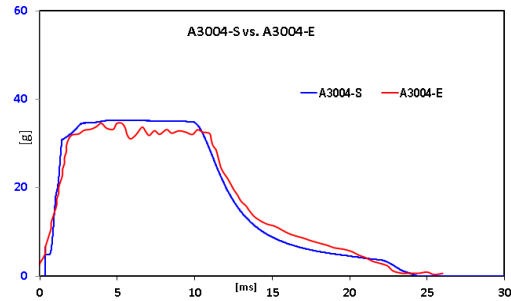
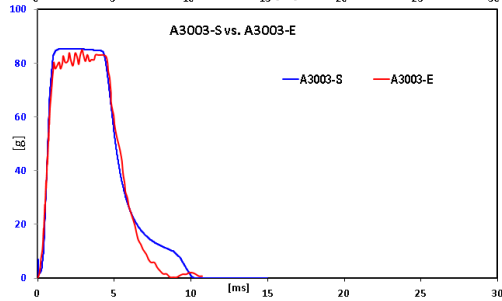
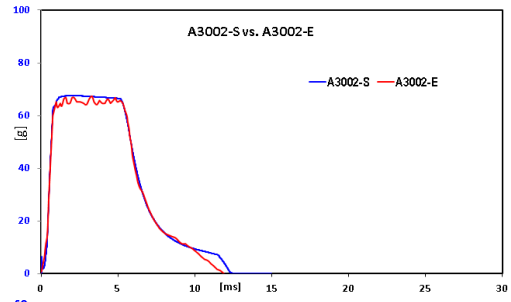
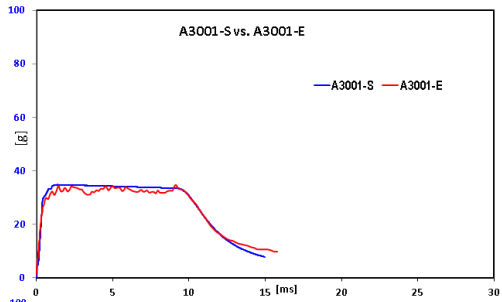
STRESS vs. STRAIN SIMULATION & EXPERIMENT 4 m/s

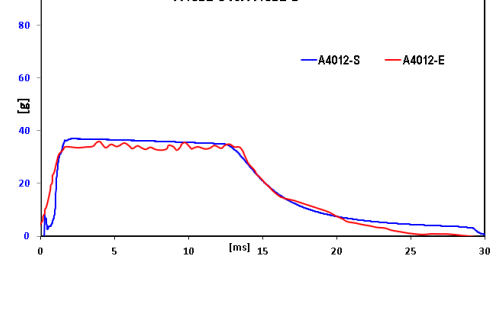
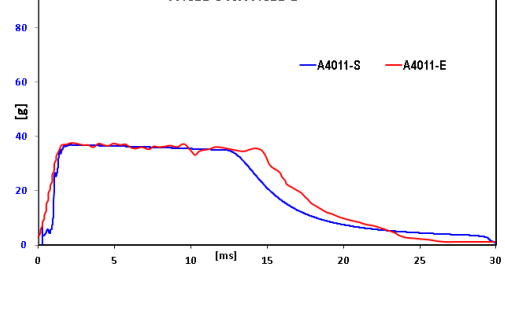
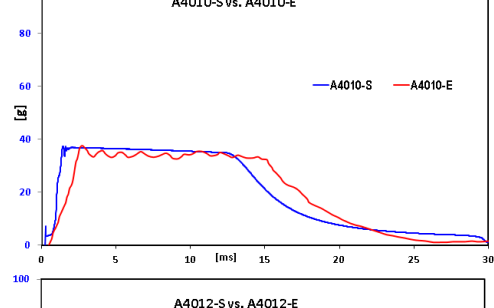
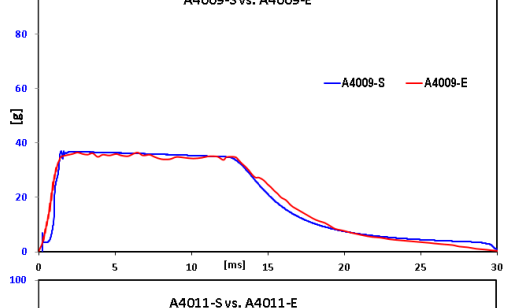
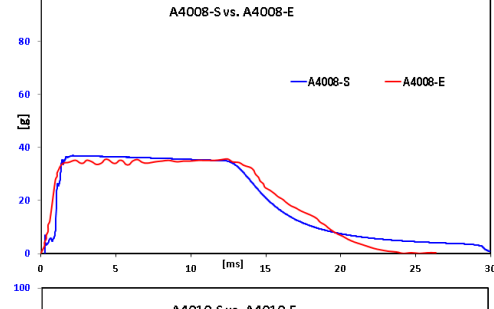
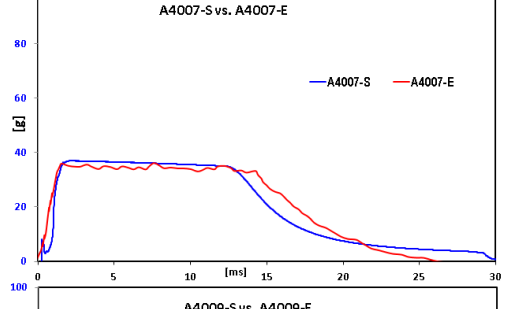
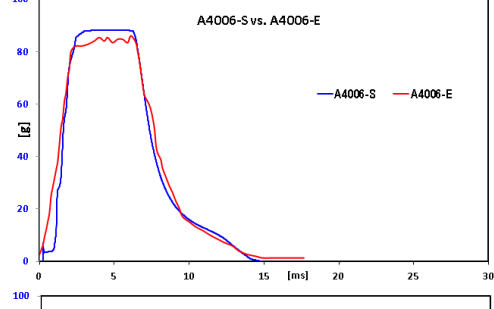
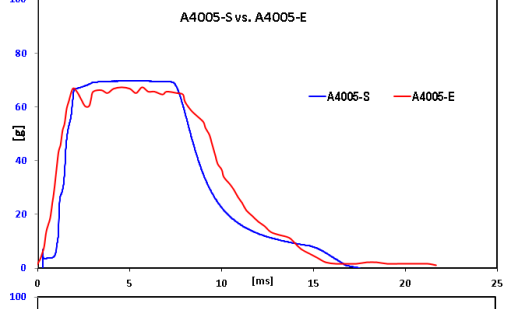
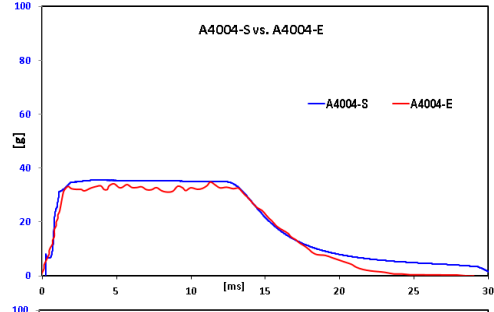
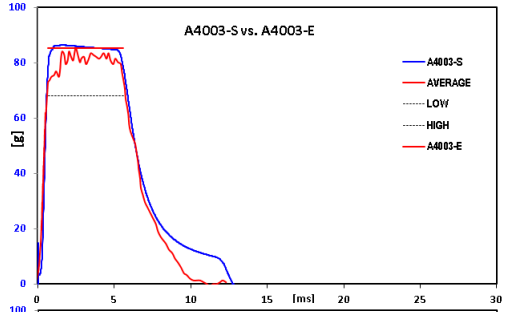
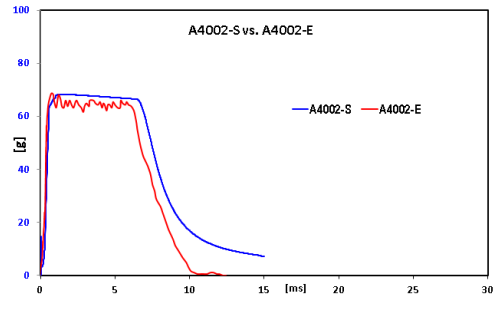
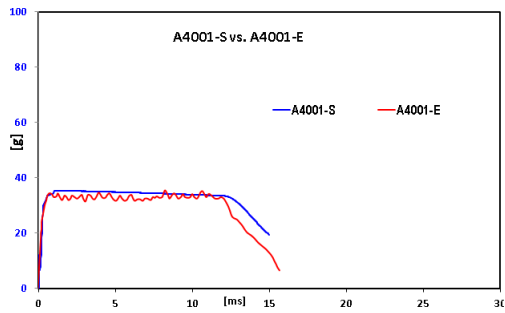
Appendix C

Acceleration

Simulation vs. Experiment



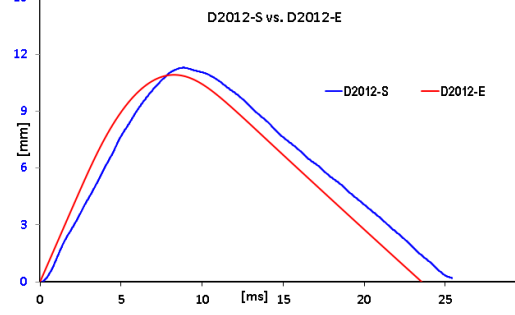
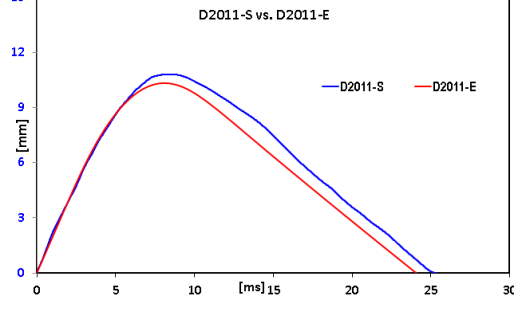
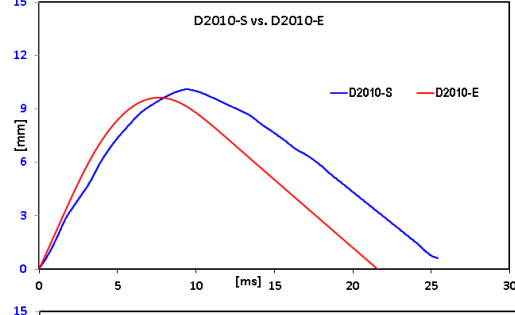
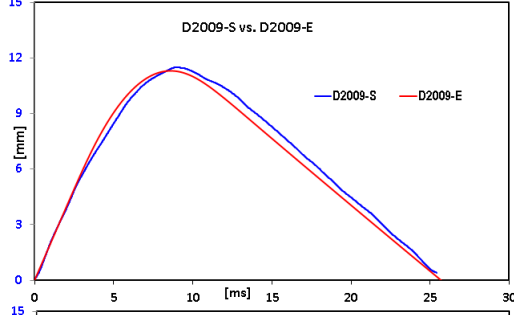
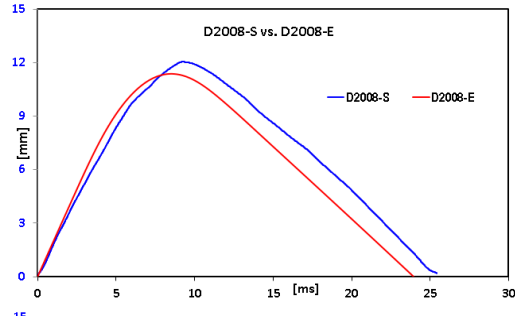
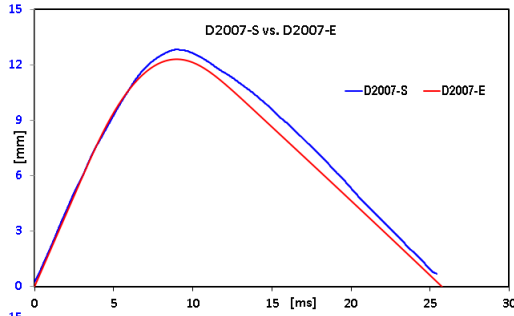
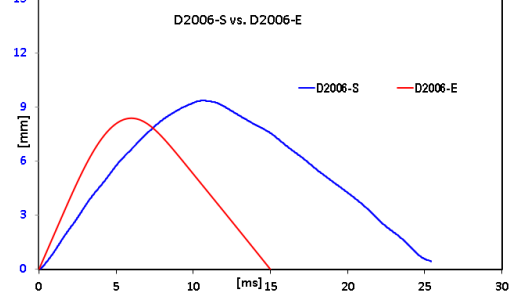
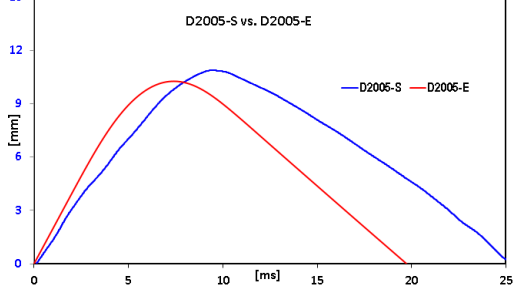
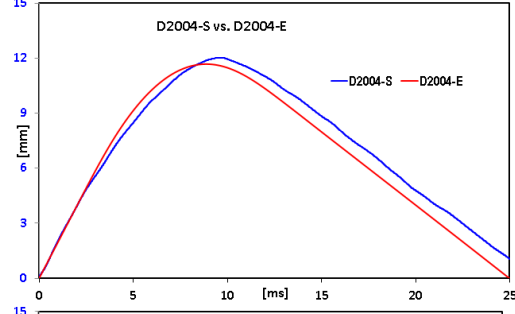
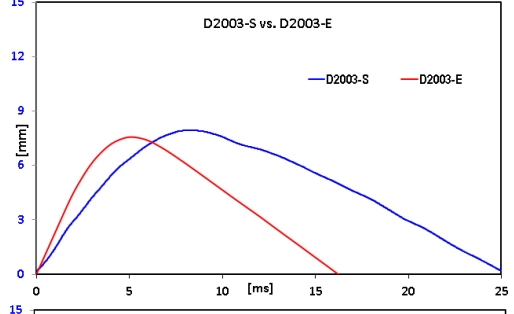
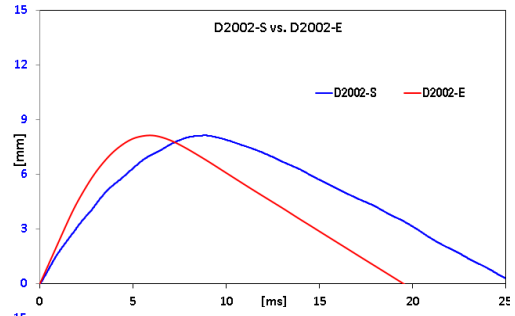
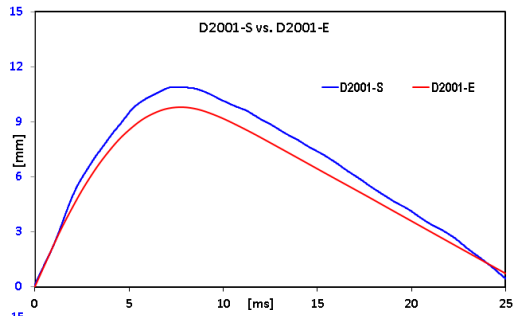


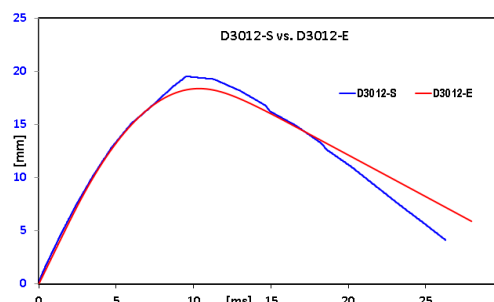
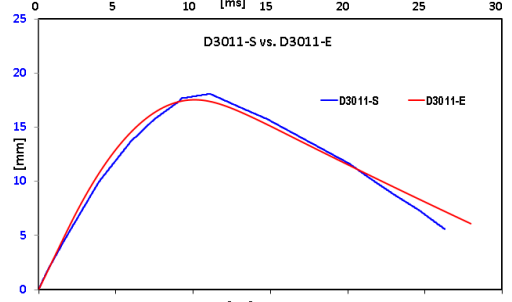
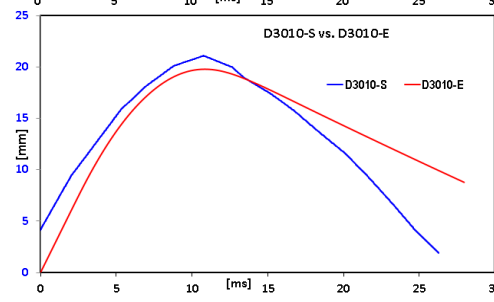
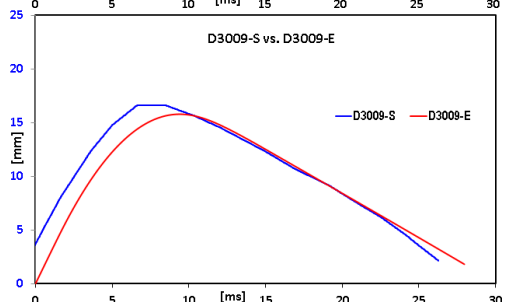
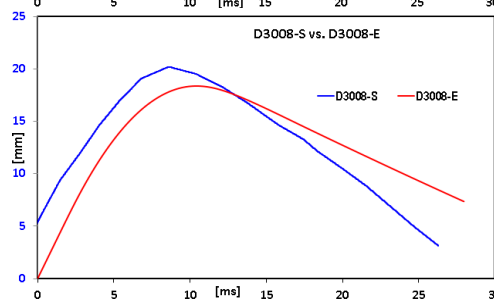
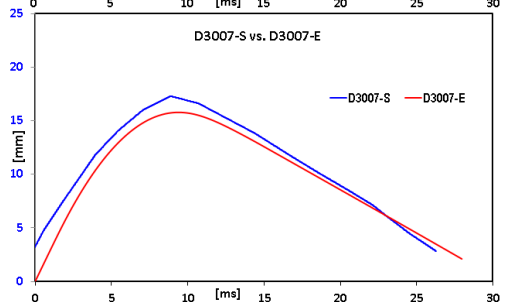
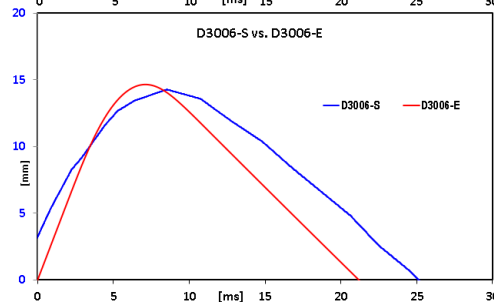
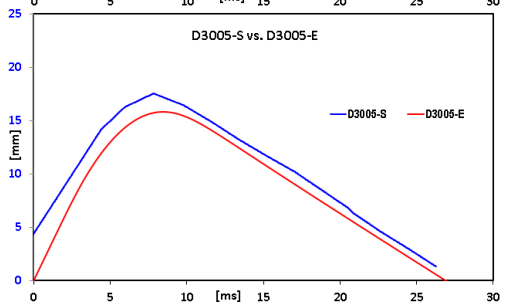
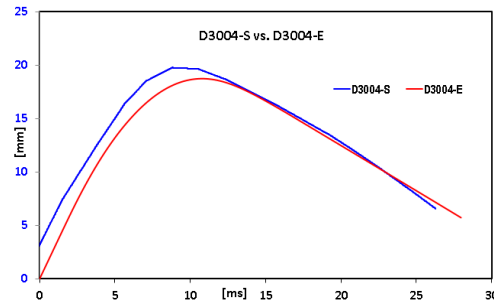
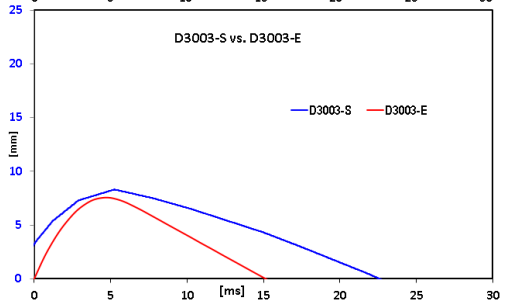
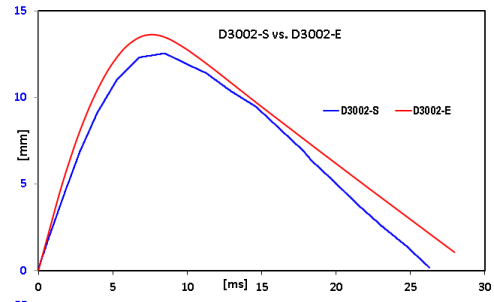
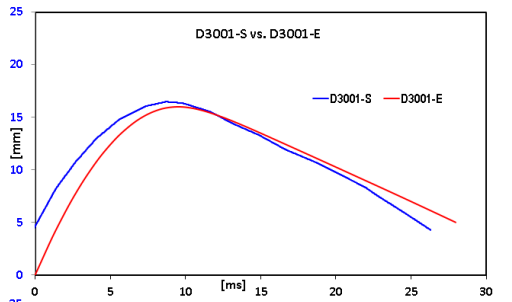


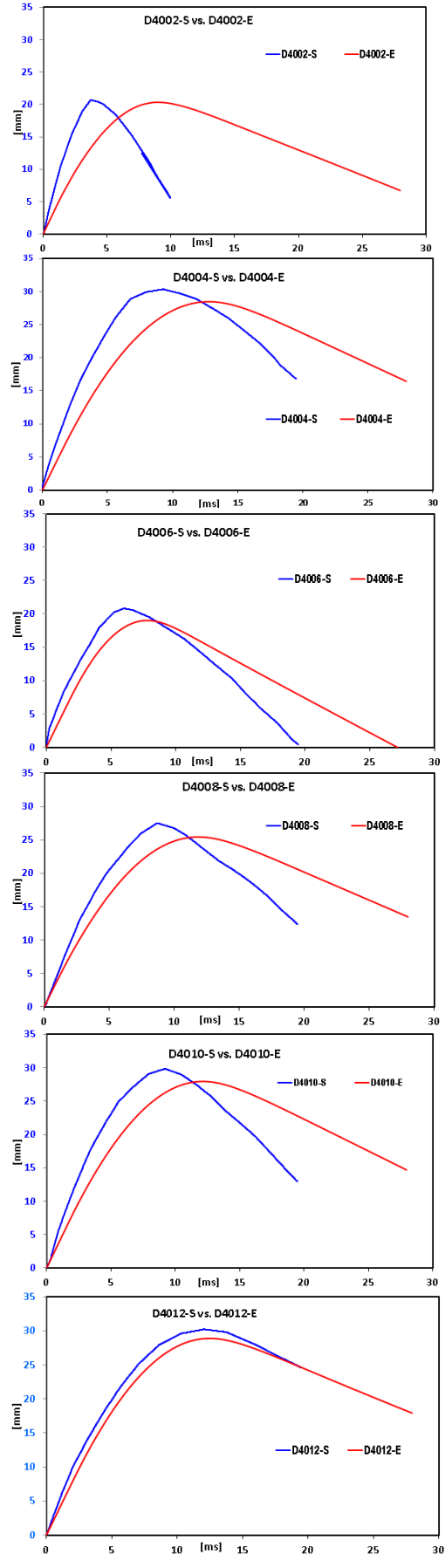
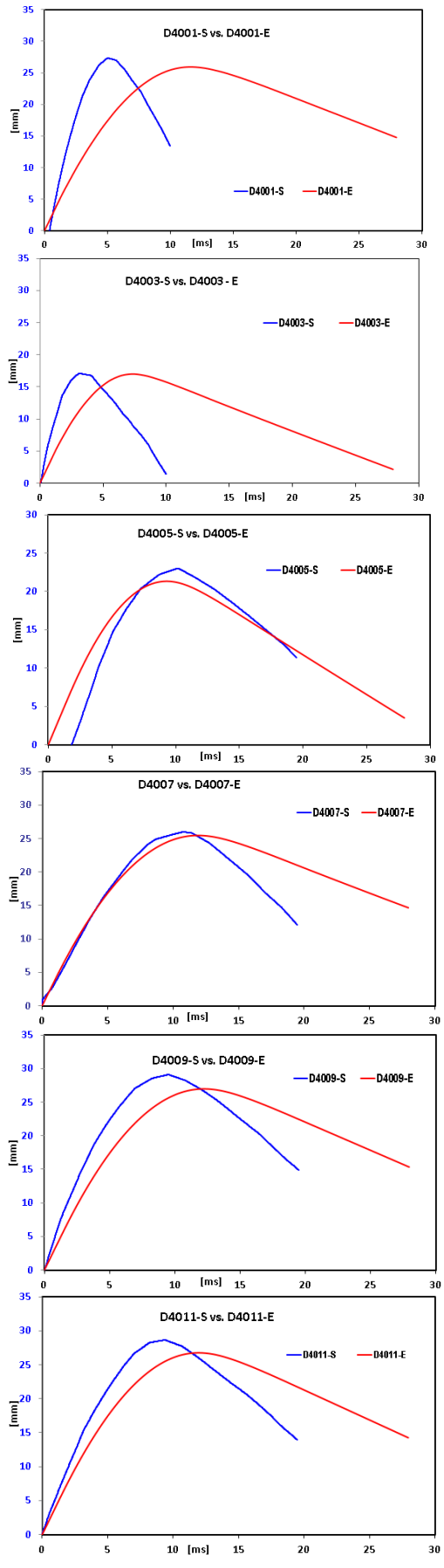
Appendix D

Displacement Data

Simulation Vs. Experiment







Appendix E

Finding the Tolerance

Correlation Between Simulation Vs. Experiment

This chapter starts with how to determine the accuracy of simulation towards experiment. A specific methodology is used to define the characteristics of each individual IMPAXX foam used and the results of the multiply layer with three same density foam arranged together to form an energy absorber. Later, the configuration is changed by using 3 multiply density foam to create a composition or hybrid component. This is to study the differences of the characteristics for all the possible configuration in impact absorption. All the foam design was tested and simulated to gather the reaction of foam arrangements towards impact velocity change. Interests were set to obtain the effects of foam arrangement towards acceleration (g) and displacement results.

The results of the acceleration (g) and displacement shows and opposing trend. Therefore, the research needs to determine the accuracy through the average and standard deviation process performed onto the data, based on tolerance trials.

For this purpose, tolerance was used to determine the accuracy or convergence between the simulation and experiment results which gathered from the acceleration (g) and displacement results. This values used to define the tolerances, this research will then apply specific tolerance values as a guidance towards the next process for determining the best materials used in this study based on impact velocity.

1.1 Analysis of Foam Design Based on Percentage Differences

This section discussed on the experimental and simulation findings of all foam layer configurations. Based from the findings previously, percentage difference need to identify the range between simulation and experimental values. The values that are look into are minimum, average and maximum values. This analysis is to predict tolerance percentage simulation toward experimental findings.

1.1.1 The Percentage Values Based on Average Values

Data collection in this section is to obtain deviation differences between the average point of simulation contrary to the average point of experiment called percentage differences. Based on this logic, this research calculates the percentage values between simulation compared to experiment (Table 1-1 and Table 1-2). Therefore, this section focus on finding the minimum, average and maximum percentage value of acceleration (g) and displacement using impact velocity of 2 m/s, 3 m/s and 4 m/s for all type of material arrangement (Table 1-3).

Table 1-1 shows the percentage value based on acceleration (g) parameter. There are three different table labelled as 2000, 3000 and 4000 symbolised as 2 m/s, 3 m/s and 4 m/s. The purpose of having this table is to observe the percentage deviation towards tolerance between simulation and experiment. This tolerance serves as range for the next chapter.

Table 1-1: The Percentage of Average Values towards the Acceleration (g) between Simulation versus Experiment

ACCELERATION (g) - AVERAGE - SIMULATION VS EXPERIMENT 2000													
MATERIAL	SINGLE LAYER			MULTIPLY LAYER			COMBINATION LAYER						AVE
DESIGN	A2001	A2002	A2003	A2004	A2005	A2006	A2007	A2008	A2009	A2010	A2011	A2012	
Deviation	0.06	0.47	0.63	0.14	0.14	0.14	0.03	0.09	0.05	0.14	0.14	0.03	
Percentage Deviation	0.28%	5.43%	7.35%	1.59%	1.59%	1.59%	0.30%	1.02%	0.61%	1.59%	1.59%	0.39%	1.94%
Percentage										MAX	7.35%	MIN	0.28%

ACCELERATION (g) - AVERAGE - SIMULATION VS EXPERIMENT 3000													
MATERIAL	SINGLE LAYER			MULTIPLY LAYER			COMBINATION LAYER						AVE
DESIGN	A3001	A3002	A3003	A3004	A3005	A3006	A3007	A3008	A3009	A3010	A3011	A3012	
Deviation	0.06	1.61	0.39	0.13	1.29	0.48	0.07	1.63	0.10	0.18	0.13	0.05	
Percentage Deviation	0.21%	5.36%	1.29%	1.01%	9.92%	3.69%	0.52%	12.6%	0.78%	1.36%	1.01%	0.40%	3.18%
Percentage										MAX	9.92%	MIN	0.21%

ACCELERATION (g) - AVERAGE - SIMULATION VS EXPERIMENT 4000													
MATERIAL	SINGLE LAYER			MULTIPLY LAYER			COMBINATION LAYER						AVE
DESIGN	A4001	A4002	A4003	A4004	A4005	A4006	A4007	A4008	A4009	A4010	A4011	A4012	
Deviation	0.20	0.67	1.85	0.13	0.13	0.13	3.26	0.13	0.13	0.56	0.13	0.69	
Percentage Deviation	0.60%	1.70%	4.62%	0.76%	0.76%	0.75%	19.0%	0.76%	0.76%	3.25%	0.76%	4.06%	3.15%
Percentage										MAX	19.0%	MIN	0.60%

Table 1-2: The Percentage of Average Values towards the Displacement between Simulation versus Experiment.

DISPLACEMENT (mm) - AVERAGE - SIMULATION VS EXPERIMENT 2000													
MATERIAL	SINGLE LAYER			MULTIPLY LAYER			COMBINATION LAYER						AVE
DESIGN	D2001	D2002	D2003	D2004	D2005	D2006	D2007	D2008	D2009	D2010	D2011	D2012	
Deviation	0.85	0.15	0.27	0.29	0.34	0.58	0.54	0.28	0.25	0.42	0.29	-0.06	
Percentage Deviation	13.15%	3.08%	5.94%	4.10%	5.43%	10.61%	7.13%	4.15%	3.74%	7.01%	4.70%	1.03%	5.84%
Percentage										MAX	13.15%	MIN	1.03%

DISPLACEMENT (mm) - AVERAGE - SIMULATION VS EXPERIMENT 3000													
MATERIAL	SINGLE LAYER			MULTIPLY LAYER			COMBINATION LAYER						AVE
DESIGN	D3001	D3002	D3003	D3004	D3005	D3006	D3007	D3008	D3009	D3010	D3011	D3012	
Deviation	0.26	-0.61	0.46	0.76	0.92	0.20	0.88	-0.12	0.70	-1.29	0.10	0.07	
Percentage Deviation	2.31%	8.27%	9.57%	5.69%	9.09%	2.39%	8.25%	0.97%	6.70%	9.90%	0.81%	0.54%	5.37%
Percentage										MAX	9.09%	MIN	0.54%

DISPLACEMENT (mm) - AVERAGE - SIMULATION VS EXPERIMENT 4000													
MATERIAL	SINGLE LAYER			MULTIPLY LAYER			COMBINATION LAYER						AVE
DESIGN	D4001	D4002	D4003	D4004	D4005	D4006	D4007	D4008	D4009	D4010	D4011	D4001	
Deviation	0.32	-0.05	0.55	1.70	3.19	0.21	-0.97	0.35	1.11	0.64	0.70	1.46	
Percentage Deviation	1.63%	0.39%	5.06%	7.43%	19.22%	1.95%	5.36%	1.86%	5.26%	3.02%	3.43%	6.30%	5.08%
Percentage										MAX	19.22%	MIN	0.39%

Table 1-2 shows the percentage value based on displacement parameter. There are three different table labelled as 2000, 3000 and 4000 symbolised as 2 m/s, 3 m/s and 4 m/s. The purpose of having this table is to observe the percentage deviation towards tolerance between

simulation and experiment.

Table 1-3 shows that, the maximum and minimum percentage values were 19.22% and 0.21% towards all values collected from the acceleration (g) and displacement between experiment and simulation conducted.

Table 1-3: The Percentage Values of Displacement and Acceleration (g) Based on Average Values.

TEST	ACCELERATION (g)			DISPLACEMENT (mm)		
VELOCITY	MIN	AVERAGE	MAX	MIN	AVERAGE	MAX
2000	0.28%	1.94%	7.35%	1.03%	5.84%	13.15%
3000	0.21%	3.18%	9.92%	0.54%	5.37%	9.09%
4000	0.60%	3.15%	19.0%	0.39%	5.08%	19.22%

1.1.2 The Percentage Values Based on the Maximum Values

Based on the data collected, the deviation differences between the maximum point of simulation contrary to the maximum point of experiment called percentage differences. Based on this logic, this research calculates the percentage values between simulation compared to experiment (Table 1-4 and Table 1-5). Therefore, this section focus on finding the minimum, average and maximum percentage value of acceleration (g) and displacement using impact velocity of 2 m/s, 3 m/s and 4 m/s for all type of material arrangement (Table 1-6).

Table 1-4 shows the percentage value based on acceleration (g) parameter. There are three different table labelled as 2000, 3000 and 4000 symbolised as 2 m/s, 3 m/s and 4 m/s. The purpose of having this table is to observe the percentage deviation towards tolerance between simulation and experiment. This tolerance serves as range for the next chapter.

Table 1-4: The Percentage Values of Acceleration (g) Maximum Values between Simulation versus Experiment

ACCELERATION (g) - MAXIMUM - SIMULATION VS EXPERIMENT 2000															
MATERIAL	SINGLE LAYER			MULTIPLY LAYER			COMBINATION LAYER						AVE		
DESIGN	A2001	A2002	A2003	A2004	A2005	A2006	A2007	A2008	A2009	A2010	A2011	A2012			
Deviation	-0.76	5.92	3.03	1.39	1.70	2.11	1.22	0.06	1.04	1.42	-0.38	-0.71			
Percentage Deviation	2.24%	8.90%	3.59%	4.05%	2.57%	2.73%	3.44%	0.17%	2.94%	3.99%	1.05%	1.99%	3.14%		
Percentage												MAX	8.90%	MIN	0.17%

ACCELERATION (g) - MAXIMUM - SIMULATION VS EXPERIMENT 3000															
MATERIAL	SINGLE LAYER			MULTIPLY LAYER			COMBINATION LAYER						AVE		
DESIGN	A3001	A3002	A3003	A3004	A3005	A3006	A3007	A3008	A3009	A3010	A3011	A3012			
Deviation	0.11	0.23	0.53	0.73	3.90	5.34	1.75	0.62	0.32	-0.16	-0.40	0.89			
Percentage Deviation	0.31%	0.35%	0.62%	2.06%	5.66%	6.10%	4.80%	1.72%	0.87%	0.43%	1.11%	2.45%	2.21%		
Percentage												MAX	6.10%	MIN	0.31%

ACCELERATION (g) - MAXIMUM - SIMULATION VS EXPERIMENT 4000															
MATERIAL	SINGLE LAYER			MULTIPLY LAYER			COMBINATION LAYER						AVE		
DESIGN	A4001	A4002	A4003	A4004	A4005	A4006	A4007	A4008	A4009	A4010	A4011	A4012			
Deviation	-0.04	-0.33	0.98	0.74	2.34	2.31	0.85	1.31	0.52	-0.17	-0.65	1.06			
Percentage Deviation	0.12%	0.48%	1.14%	2.08%	3.36%	2.62%	2.31%	3.55%	1.39%	0.45%	1.75%	2.86%	1.84%		
Percentage												MAX	3.55%	MIN	0.12%

Table 1-5: The Percentage Values of Displacement Maximum Values between Simulation versus Experiment

DISPLACEMENT (mm) - MAXIMUM - SIMULATION VS EXPERIMENT 2000															
MATERIAL	SINGLE LAYER			MULTIPLY LAYER			COMBINATION LAYER						AVE		
DESIGN	D2001	D2002	D2003	D2004	D2005	D2006	D2007	D2008	D2009	D2010	D2011	D2012			
Deviation	1.10	0.00	0.36	0.36	0.62	0.98	0.52	0.67	0.19	0.47	0.49	0.38			
Percentage Deviation	10.12%	0.01%	4.60%	2.99%	5.67%	10.45%	4.08%	5.60%	1.65%	4.61%	4.50%	3.38%	4.80%		
Percentage												MAX	10.45%	MIN	0.01%

DISPLACEMENT (mm) - MAXIMUM - SIMULATION VS EXPERIMENT 3000															
MATERIAL	SINGLE LAYER			MULTIPLY LAYER			COMBINATION LAYER						AVE		
DESIGN	D3001	D3002	D3003	D3004	D3005	D3006	D3007	D3008	D3009	D3010	D3011	D3012			
Deviation	0.49	-1.08	0.75	1.04	1.73	-0.37	1.51	1.84	0.83	1.31	0.55	1.15			
Percentage Deviation	2.95%	8.61%	9.05%	5.25%	9.84%	2.61%	8.75%	9.10%	5.03%	6.21%	3.06%	5.89%	6.36%		
Percentage												MAX	9.84%	MIN	2.61%

DISPLACEMENT (mm) - MAXIMUM - SIMULATION VS EXPERIMENT 4000															
MATERIAL	SINGLE LAYER			MULTIPLY LAYER			COMBINATION LAYER						AVE		
DESIGN	D4001	D4002	D4003	D4004	D4005	D4006	D4007	D4008	D4009	D4010	D4011	D4001			
Deviation	1.41	0.37	0.08	1.88	1.70	1.80	0.53	2.07	2.13	1.90	1.89	1.34			
Percentage Deviation	5.17%	1.77%	0.45%	6.20%	7.37%	8.67%	2.05%	7.51%	7.32%	6.36%	6.61%	4.44%	5.33%		
Percentage												MAX	8.67%	MIN	0.45%

Table 1-5 shows the percentage value based on displacement parameter. There are three different table labelled as 2000, 3000 and 4000 symbolised as 2 m/s, 3 m/s and 4 m/s. The purpose of having this table is to observe the percentage deviation towards tolerance between simulation and experiment. This tolerance serves as range for the next chapter.

Table 1-6 shows that, the maximum and minimum percentage values were 10.45% and 0.01% towards all values collected from the acceleration and displacement between experiment and simulation conducted.

Table 1-6: The Percentage of the Displacement and Acceleration Based on Maximum Values

TEST	ACCELERATION (g)			DISPLACEMENT (mm)		
VELOCITY	MIN	AVERAGE	MAX	MIN	AVERAGE	MAX
2000	0.17%	3.14%	8.90%	0.01%	4.80%	10.45%
3000	0.31%	2.21%	6.10%	2.61%	6.36%	9.84%
4000	0.12%	1.84%	3.55%	0.45%	5.33%	8.67%

1.1.3 Summary of Flat Foam Design Based on Percentage Differences

Table 1-3 shows that, the maximum percentage values were 10.45% collected from the acceleration (g) and displacement between experiment and simulation conducted. From Table 1-6 shows that, the maximum percentage value was 19.22% towards all values collected from the acceleration (g) and displacement between experiment and simulation conducted. Therefore, from percentage 10.45% and 19.22%, these numbers were round off to determine range for observing significant difference between simulation and experiment findings.

Using the tolerance defined (10% ~ 20%); this research verified gap between simulation against experiment conducted for acceleration (g) and displacement. This means that results is a reflection of data collected from experiment and simulation needed to be compared with the gap between each other. In this instance, appropriate percentage value needs to be determined so that all simulation and experiment values lies between the percentage bracket. This is crucial to evaluate the possible tolerance of final experiment. Hence, objective 1 was reflected in this portion of analysis.

1.2 Analysis of Tolerance Trials Based on Acceleration (g) and Displacement

This section discussed on the experimental and simulation findings of all foam layer configurations. Based from the findings previously, percentage difference need to identify the range between simulation and experimental values. The values that are look into are minimum, average and maximum values. This analysis is to predict tolerance percentage simulation toward experimental findings.

1.2.1 Tolerance Trials for Acceleration (g)

Based on the tolerance values found (stated in subpart 1.1.3); this research conducted trial using 20% tolerance for TR 1 (tolerance 1 towards the maximum point). All data between maximum point to 20% and below maximum point were collected for creation of average line based on maximum point. Moreover, the TR 2 (the tolerance 2 towards the average line) constructed for the upper and lower lines limit or boundary lines. All data from experiment were checked if fall within the specified boundary.

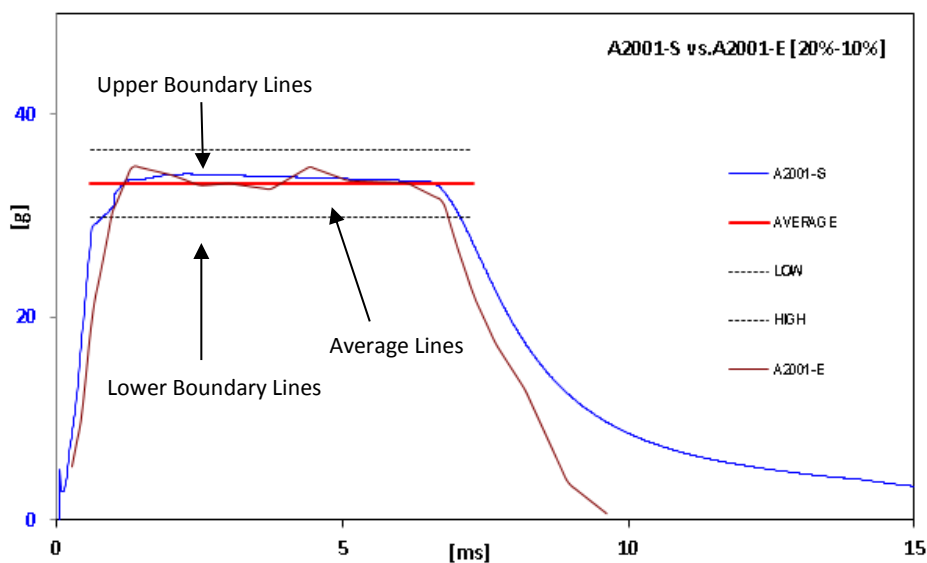


Figure 1-1: The Boundary and Average Lines Based on Tolerance Trials: 20% for TR 1 and 10% for TR 2.

Figure 1-1 shows an example using trial of 20% tolerance for TR 1 and 10% tolerance for TR 2. The research conducted towards all of 72 acceleration (g) and displacement data (experiment and simulation) respectively (*i.e.*, 2000, 3000, 4000 represents 2 m/s, 3 m/s, and 4 m/s)

These tolerances affect range of data taken from defined average lines based from maximum values that used to determine the upper and lower boundary line. The tolerance of TR 1 against the maximum values, while the tolerance of TR 2 towards the average line (see Figure 1-1).

Table 1-7: The Tolerance Trials: 20% for TR 1 and 10% for TR 2 for A-2001-S.

SIMULATION	A-2001-S
MAXIMUM POINT	34.15 g
[TR 1] UPPER FOR AVERAGE	40.98 g
[TR 1] LOWER FOR AVERAGE	27.32 g
AVERAGE LINE	33.21 g
[TR 2] UPPER BOUNDARY	36.53 g
[TR 2] LOWER BOUNDARY	29.89 g
STD DEVIATION	0.27

For example, data A-2001-S (Acceleration value of flat shape simulation with 2 m/s impact) constructed using blue line in graph (Figure 1-1), where the maximum point (S-Max) is 34.15 g. Using 20% tolerance (TR 1) as a trial for range data taken (that is between 27.32 g till 40.98 g), found that the average value was 33.21 g. This average value was then assumed and constructed as an average line in which the boundary for the upper and lower line (based on trials using 10% tolerance or TR 2) for the upper and the lower line were 29.89 g and 36.53 g (Table 1-7). On this boundary area, experiment data shown in brown lines (A-2001-E or Experiment of Acceleration (g) on the Flat shape with 2 m/s impact) must be within this limit as a representation of the tolerance capability (Figure 1-1). Based on defined tolerances (TR1 and TR 2 that were 20% and 10% respectively), research found that the standard deviation of

acceleration (g) from simulation data within range is 0.27 (Table 1-7).

1.2.1.1 Acceleration (g) – Simulation – [20% TR1 & 10% TR2]

Table 1-8 shows data simulation for 2 m/s, 3 m/s, and 4 m/s with 20% tolerance for TR 1 and 10% for TR 2. Based on this table, the research concluded that the standard deviation for design no. 2, 3, 5, and 6 were higher (>2) for all impactor velocity (*i.e.*, 2 m/s, 3 m/s, and 4 m/s respectively).

Table 1-8: The Acceleration (g) Data (Simulation) with 20% TR1 and 10% TR2

SIMULATION [2 m/s]	A2001-S	A2002-S	2003-S-A	2004-S-A	2005-S-A	2006-S-A	2007-S-A	2008-S-A	2009-S-A	2010-S-A	2011-S-A	2012-S-A
S-MAXIMUM POINT	34.15	66.51	84.31	34.36	66.07	77.42	35.64	35.56	35.54	35.50	35.56	35.64
S-AVERAGE LINE	33.21	65.01	81.85	33.18	63.49	73.18	34.60	34.55	34.49	34.50	34.52	34.61
S-STD DEVIATION	0.27	2.77	4.23	1.60	3.82	4.24	1.52	1.48	1.46	1.47	1.53	1.51
[TR 1] UPPER FOR AVERAGE	40.98	79.82	101.17	41.23	79.28	92.90	42.77	42.67	42.65	42.60	42.67	42.77
[TR 1] LOWER FOR AVERAGE	27.32	53.21	67.45	27.49	52.86	61.93	28.51	28.45	28.43	28.40	28.45	28.51
[TR 2] UPPER BOUNDARY	36.53	71.51	90.03	36.50	69.84	80.50	38.06	38.00	37.94	37.95	37.97	38.07
[TR 2] LOWER BOUNDARY	29.89	58.51	73.66	29.86	57.15	65.86	31.14	31.09	31.04	31.05	31.07	31.15

SIMULATION [3 m/s]	A3001-S	A3002-S	3003-S-A	3004-S-A	3005-S-A	3006-S-A	3007-S-A	3008-S-A	3009-S-A	3010-S-A	3011-S-A	3012-S-A
S-MAXIMUM	34.80	67.54	85.47	35.29	68.93	87.46	36.36	36.31	36.53	36.31	36.31	36.36
S-AVERAGE	33.69	66.19	83.74	34.37	67.09	84.00	35.25	35.18	35.18	35.16	35.19	35.25
S-STD DEVIATION	1.27	2.44	3.58	1.46	3.04	4.77	1.35	1.32	1.22	1.27	1.30	1.35
[TR 1] UPPER FOR AVERAGE	41.76	81.05	102.57	42.34	82.72	104.95	43.63	43.57	43.84	43.57	43.57	43.63
[TR 1] LOWER FOR AVERAGE	27.84	54.03	68.38	28.23	55.14	69.97	29.09	29.04	29.23	29.05	29.05	29.09
[TR 2] UPPER BOUNDARY	37.06	72.80	92.11	37.81	73.79	92.40	38.77	38.69	38.70	38.68	38.71	38.77
[TR 2] LOWER BOUNDARY	30.32	59.57	75.36	30.93	60.38	75.60	31.72	31.66	31.67	31.64	31.67	31.72

SIMULATION [4 m/s]	A4001-S	A4002-S	4003-S-A	4004-S-A	4005-S-A	4006-S-A	4007-S-A	4008-S-A	4009-S-A	4010-S-A	4011-S-A	4012-S-A
S-MAXIMUM	35.36	68.32	86.38	35.57	69.65	88.37	36.98	36.95	37.01	37.34	36.95	36.98
S-AVERAGE	34.09	66.69	84.46	34.74	68.31	86.18	35.68	35.66	35.60	35.63	35.66	35.67
S-STD DEVIATION	1.24	2.36	3.22	1.32	2.74	4.09	1.35	1.25	1.25	1.20	1.26	1.37
[TR 1] UPPER FOR AVERAGE	42.43	81.99	103.66	42.68	83.58	106.05	44.38	44.34	44.41	44.80	44.34	44.38
[TR 1] LOWER FOR AVERAGE	28.29	54.66	69.11	28.45	55.72	70.70	29.59	29.56	29.61	29.87	29.56	29.58
[TR 2] UPPER BOUNDARY	37.50	73.36	92.90	38.21	75.14	94.80	39.25	39.22	39.16	39.19	39.22	39.24
[TR 2] LOWER BOUNDARY	30.69	60.02	76.01	31.27	61.48	77.56	32.12	32.09	32.04	32.06	32.09	32.11

This means that individual data for each design within the range of upper and lower boundary is more dynamic compared to other designs. Since the multiply layer design represented by single layer (design no 4 is 3 layers of design no 1, design no 5 is 3 layers of design no 2, and design no 6 is 3 layers of design no 3), this research found higher standard deviation values on design no 2 and 3 reflected on design no 5 and 6. Unfortunately, based on

the graph between simulations versus the experiment (see the data), found that experiment graphs for design no. 4 and 5 (with impact velocity 4 m/s) lies outside of the boundary in simulation graph (Figure 1-2). This shows that the trials tolerance using 20% and 10% is not suitable to predict the experiment results.

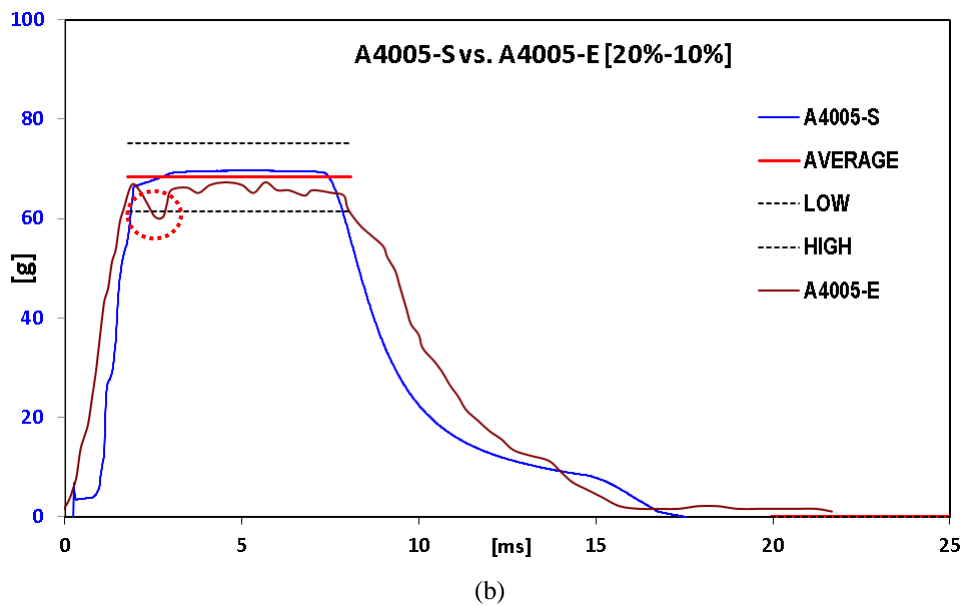
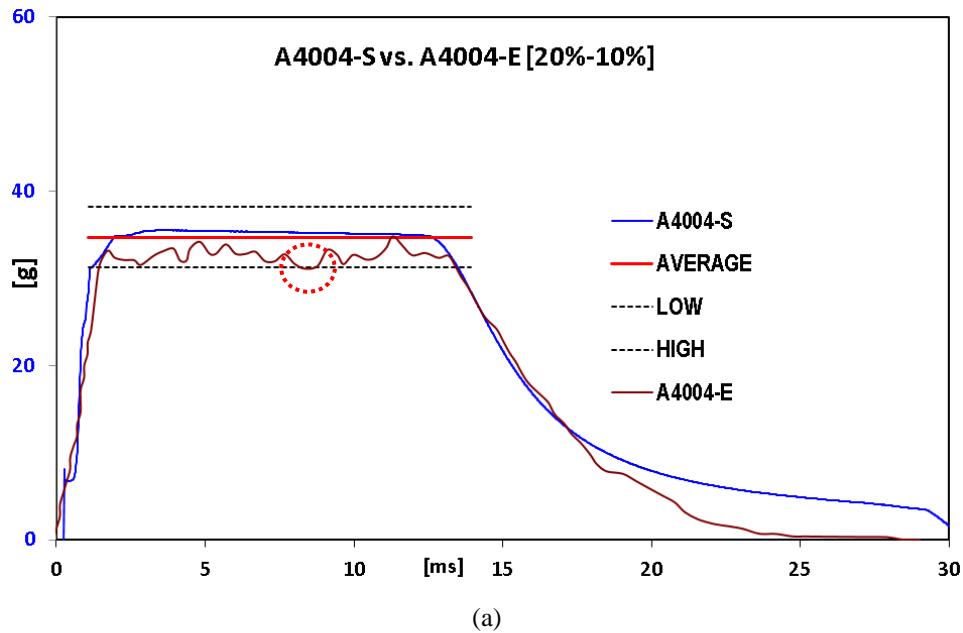


Figure 1-2 : Data Falls Outside Boundary Limit of the Acceleration (g) using Trials Tolerance 20% and 10%; (a) Acceleration (g) of Design 4 with 4 m/s Impact Velocity, (b) Acceleration (g) of Design 5 with 4 m/s Impact Velocity

1.2.1.2 Acceleration (g) – Experiment – [20% TR1 & 10% TR2]

Table 1-9 shows the impact test results of 2 m/s, 3 m/s, and 4 m/s impactor velocity with 20% tolerance for TR 1 and 10% for TR 2. Based on experimental data, the research found that higher standard deviation (>2) were captured on design no. 2,3, 5, and 6 with all velocities respectively. Since the multiply layer design is somehow an exact representation of single layer design, this research found that the higher standard deviation values occurred on design no 2 (B) and 3 (C) similar that the higher standard deviation values occurred on design no 2 (BBB) and 3 (CCC).

Table 1-9: The Acceleration (g) Data (Experiment) with 20% TR1 and 10% TR2.

EXPERIMENT [2 m/s]	A2001-E	A2002-E	A2003-E	A2004-E	A2005-E	A2006-E	A2007-E	A2008-E	A2009-E	A2010-E	A2011-E	A2012-E
E-MAXIMUM POINT	34.92	60.59	81.28	32.97	64.37	75.30	34.41	35.50	34.50	34.09	35.94	36.35
S-AVERAGE LINE	33.48	56.56	76.75	31.02	60.55	70.26	32.27	32.65	32.46	32.12	33.61	34.30
E-STD DEVIATION	0.52	3.76	4.00	1.89	3.95	4.90	2.17	1.84	2.07	1.99	2.40	2.05
[TR 1] UPPER FOR AVERAGE	38.41	72.71	97.54	39.56	77.24	90.37	41.30	42.59	41.39	40.90	43.12	43.62
[TR 1] LOWER FOR AVERAGE	31.43	48.47	65.03	26.37	51.50	60.24	27.53	28.40	27.60	27.27	28.75	29.08
[TR 2] UPPER BOUNDARY	40.17	62.22	84.42	34.12	66.60	77.28	35.49	35.92	35.71	35.34	36.97	37.73
[TR 2] LOWER BOUNDARY	26.78	50.90	69.07	27.92	54.49	63.23	29.04	29.39	29.22	28.91	30.25	30.87

EXPERIMENT [3 m/s]	A3001-E	A3002-E	A3003-E	A3004-E	A3005-E	A3006-E	A3007-E	A3008-E	A3009-E	A3010-E	A3011-E	A3012-E
E-MAXIMUM POINT	34.69	67.31	84.94	34.56	65.03	82.12	34.61	35.68	36.22	36.47	36.71	35.47
S-AVERAGE LINE	32.43	63.77	79.69	32.31	60.61	78.34	32.73	33.81	33.96	34.64	34.35	33.51
E-STD DEVIATION	1.32	3.44	4.03	1.56	3.59	4.58	1.84	1.77	1.61	2.18	1.73	2.01
[TR 1] UPPER FOR AVERAGE	41.63	80.77	101.93	41.47	78.03	98.54	41.54	42.82	43.46	43.76	44.05	42.56
[TR 1] LOWER FOR AVERAGE	27.75	53.85	67.96	27.65	52.02	65.70	27.69	28.55	28.97	29.17	29.37	28.37
[TR 2] UPPER BOUNDARY	35.68	70.15	87.66	35.54	66.67	86.17	36.00	37.19	37.36	38.10	37.78	36.87
[TR 2] LOWER BOUNDARY	29.19	57.39	71.72	29.08	54.55	70.51	29.46	30.43	30.56	31.17	30.91	30.16

EXPERIMENT [4 m/s]	A4001-E	A4002-E	A4003-E	A4004-E	A4005-E	A4006-E	A4007-E	A4008-E	A4009-E	A4010-E	A4011-E	A4012-E
E-MAXIMUM POINT	35.41	68.65	85.40	34.83	67.31	86.06	36.13	35.64	36.49	37.51	37.60	35.92
S-AVERAGE LINE	32.90	63.95	79.75	32.44	63.24	81.82	34.00	33.92	34.46	33.95	35.56	33.63
E-STD DEVIATION	1.12	2.62	3.92	1.05	3.89	4.28	1.35	1.71	1.72	1.30	1.56	1.22
[TR 1] UPPER FOR AVERAGE	42.49	82.38	102.48	41.80	80.77	103.27	43.35	42.77	43.79	45.01	45.12	43.11
[TR 1] LOWER FOR AVERAGE	28.32	54.92	68.32	27.86	53.85	68.85	28.90	28.51	29.19	30.00	30.08	28.74
[TR 2] UPPER BOUNDARY	36.19	70.34	87.73	35.68	69.56	90.01	37.40	37.31	37.90	37.35	39.11	36.99
[TR 2] LOWER BOUNDARY	29.61	57.55	71.78	29.20	56.92	73.64	30.60	30.53	31.01	30.56	32.00	30.26

In addition, higher standard deviation (>2) were detected on combined layer (hybrid) when using only 2 m/s and 3 m/s impactor velocity. This shows that combined layer for impact velocity 4 m/s will provide a more consistent acceleration (g) result.

1.2.1.3 Acceleration (g) – Simulation – [10% TR1 & 20% TR2]

Since this research found that the higher standard deviation (>2) of the experiment (Table 1-9) more than the standard deviation of simulation (Table 1-8) (especially for impact velocity 2 m/s and 3 m/s), then this research used the trials tolerance for TR 1 and TR 2 at 10% and 20% respectively as shown in Table 1-10.

This research found that higher standard deviation (>2) occurred on design no. 6 with the impactor velocity of 2 m/s and 3 m/s, which is 2.20 and 2.08 respectively. While using 4 m/s impactor velocity, all of the acceleration (g) standard deviation were less than 2.

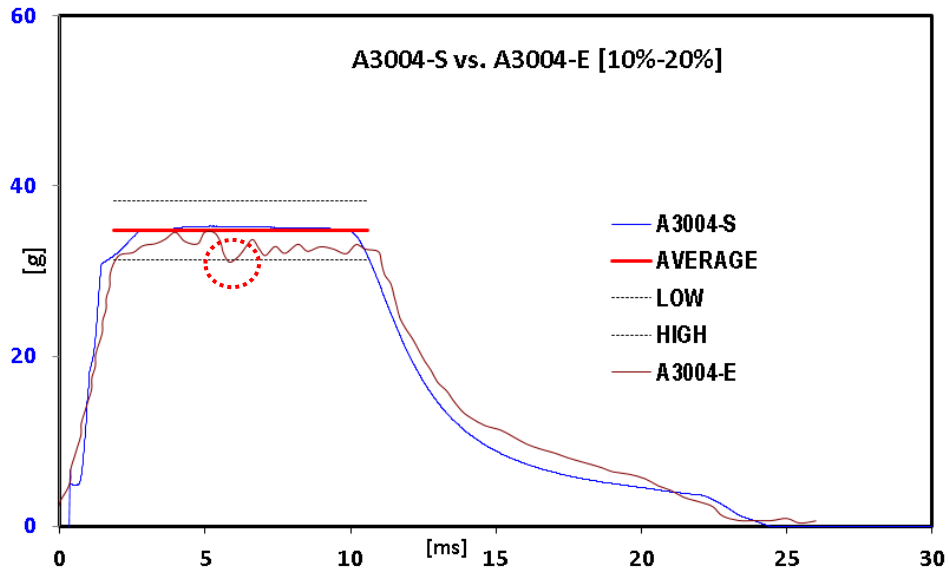
Table 1-10: The Acceleration (g) Data (Simulation) with 10% TR1 and 20% TR2.

SIMULATION [2 m/s]	A2001-S	A2002-S	A2003-S	A2004-S	A2005-S	A2006-S	A2007-S	A2008-S	A2009-S	A2010-S	A2011-S	A2012-S
S-MAXIMUM POINT	34.15	66.51	84.31	34.36	66.07	77.42	35.64	35.56	35.54	35.50	35.56	35.64
SVERAGE LINE	33.64	65.69	83.26	33.60	65.09	75.01	35.04	34.92	34.86	34.86	34.96	35.05
S-STD DEVIATION	0.27	1.29	1.86	1.06	1.64	2.20	0.73	0.82	0.78	0.77	0.74	0.73
[TR 1] UPPER FOR AVERAGE	37.57	73.17	92.74	37.80	72.68	85.16	39.20	39.11	39.09	39.05	39.12	39.20
[TR 1] LOWER FOR AVERAGE	30.74	59.86	75.88	30.92	59.46	69.68	32.07	32.00	31.99	31.95	32.00	32.07
[TR 2] UPPER BOUNDARY	40.36	78.83	99.91	40.31	78.11	90.01	42.05	41.90	41.83	41.83	41.96	42.05
[TR 2] LOWER BOUNDARY	26.91	52.55	66.61	26.88	52.07	60.00	28.04	27.93	27.89	27.89	27.97	28.04

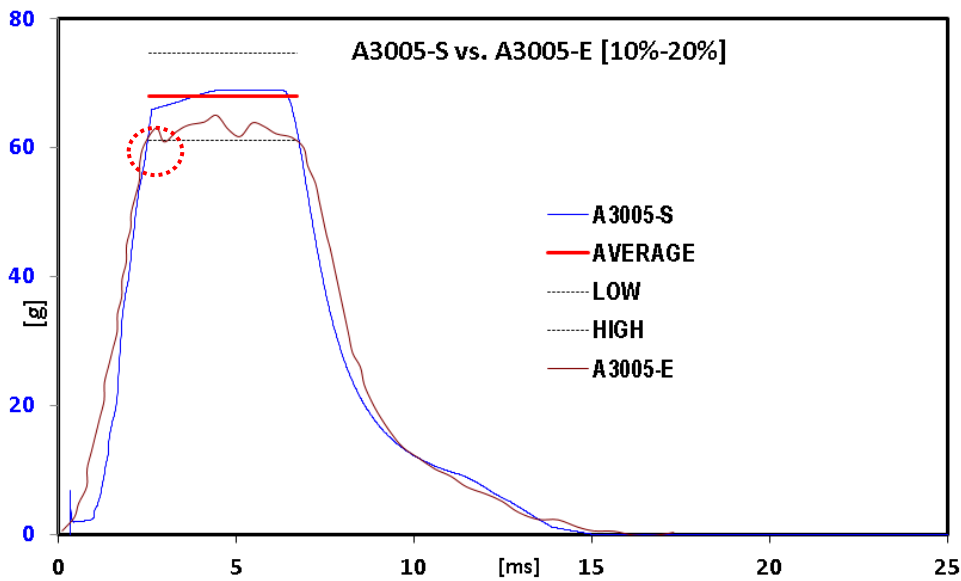
SIMULATION [3 m/s]	A3001-S	A3002-S	A3003-S	A3004-S	A3005-S	A3006-S	A3007-S	A3008-S	A3009-S	A3010-S	A3011-S	A3012-S
S-MAXIMUM POINT	34.80	67.54	85.47	35.29	68.93	87.46	36.36	36.31	36.53	36.31	36.31	36.36
SVERAGE LINE	34.00	66.70	84.68	34.77	67.92	85.93	35.59	35.48	35.46	35.44	35.48	35.58
S-STD DEVIATION	0.62	1.19	1.45	0.77	1.37	2.08	0.63	0.69	0.59	0.62	0.68	0.63
[TR 1] UPPER FOR AVERAGE	38.28	74.30	94.02	38.82	75.82	96.20	40.00	39.94	40.19	39.94	39.94	39.99
[TR 1] LOWER FOR AVERAGE	31.32	60.79	76.93	31.76	62.04	78.71	32.72	32.68	32.88	32.68	32.68	32.72
[TR 2] UPPER BOUNDARY	37.40	73.37	93.15	38.24	74.71	94.52	39.14	39.02	39.00	38.99	39.03	39.14
[TR 2] LOWER BOUNDARY	30.60	60.03	76.21	31.29	61.13	77.34	32.03	31.93	31.91	31.90	31.93	32.03

SIMULATION [4 m/s]	A4001-S	A4002-S	A4003-S	A4004-S	A4005-S	A4006-S	A4007-S	A4008-S	A4009-S	A4010-S	A4011-S	A4012-S
S-MAXIMUM POINT	35.36	68.32	86.38	35.57	69.65	88.37	36.98	36.95	37.01	37.34	36.95	36.98
SVERAGE LINE	34.36	67.18	85.21	35.05	68.94	87.44	35.99	35.90	35.86	35.88	35.91	35.99
S-STD DEVIATION	0.70	1.14	1.36	0.64	1.22	1.78	0.71	0.72	0.70	0.68	0.72	0.71
[TR 1] UPPER FOR AVERAGE	38.90	75.16	95.02	39.12	76.61	97.21	40.68	40.64	40.71	41.07	40.64	40.68
[TR 1] LOWER FOR AVERAGE	31.83	61.49	77.75	32.01	62.68	79.53	33.28	33.25	33.31	33.60	33.25	33.28
[TR 2] UPPER BOUNDARY	41.23	80.61	102.25	42.06	82.73	104.93	43.19	43.08	43.03	43.05	43.09	43.19
[TR 2] LOWER BOUNDARY	27.49	53.74	68.17	28.04	55.16	69.96	28.79	28.72	28.69	28.70	28.73	28.79

Based on the result between simulation versus the experiment (see data complete), few experiment graphs for design no. 4 and 5 (with the impactor velocity of 3 m/s) plotted below the boundary limits of the simulation graph (Figure 1-3). Hence, the trials tolerance using 10% and 20% is not suitable to predict the experimental result of acceleration (g).



(a)



(b)

Figure 1-3: Acceleration (g)- Experiment Data for Single Layer [10% TR1 & 20% TR2] a) Acceleration (g) of Design 4 with 3 m/s Impact Velocity, (b) Acceleration (g) of Design 5 with 3 m/s Impact Velocity

1.2.1.4 Acceleration (g) – Experiment – [10% TR1 & 20% TR2]

This research found that higher standard deviation (>2) occurred for design no. 3 when impact velocity 2 m/s and 3 m/s were applied during experiment. The standard deviation calculated were 2.08 and 2.018 respectively for design A-2003-E and A3003-E (Table 1-11).

Table 1-11: The Acceleration (g) Data (Experiment) with 10% TR1 and 20% TR2

EXPERIMENT [2 m/s]	A2001-E	A2002-E	A2003-E	A2004-E	A2005-E	A2006-E	A2007-E	A2008-E	A2009-E	A2010-E	A2011-E	A2012-E
E-MAXIMUM POINT	34.92	60.59	81.28	32.97	64.37	75.30	34.41	35.50	34.50	34.09	35.94	36.35
SVERAGE LINE	33.48	58.52	78.11	32.07	62.29	73.12	33.36	33.60	33.48	33.20	35.02	35.19
E-STD DEVIATION	0.52	1.88	2.08	0.62	1.90	1.81	1.00	0.75	0.79	0.77	0.60	0.84
[TR 1] UPPER FOR AVERAGE	38.41	66.65	89.41	36.26	70.81	82.84	37.85	39.05	37.95	37.50	39.53	39.98
[TR 1] LOWER FOR AVERAGE	31.43	54.53	73.15	29.67	57.93	67.77	30.97	31.95	31.05	30.68	32.34	32.71
[TR 2] UPPER BOUNDARY	40.17	70.23	93.73	38.49	74.74	87.74	40.03	40.32	40.18	39.84	42.03	42.23
[TR 2] LOWER BOUNDARY	26.78	46.82	62.49	25.66	49.83	58.50	26.69	26.88	26.78	26.56	28.02	28.15

EXPERIMENT [3 m/s]	A3001-E	A3002-E	A3003-E	A3004-E	A3005-E	A3006-E	A3007-E	A3008-E	A3009-E	A3010-E	A3011-E	A3012-E
E-MAXIMUM POINT	34.69	67.31	84.94	34.56	65.03	82.12	34.61	35.68	36.22	36.47	36.71	35.47
SVERAGE LINE	32.81	65.17	81.16	32.92	62.48	80.23	33.52	34.56	34.53	35.59	35.04	34.57
E-STD DEVIATION	0.78	1.20	2.01	0.82	1.46	1.56	0.68	0.68	0.88	0.74	0.82	0.66
[TR 1] UPPER FOR AVERAGE	38.16	74.04	93.44	38.02	71.53	90.33	38.07	39.25	39.84	40.11	40.38	39.01
[TR 1] LOWER FOR AVERAGE	31.22	60.58	76.45	31.10	58.52	73.91	31.15	32.11	32.59	32.82	33.04	31.92
[TR 2] UPPER BOUNDARY	39.37	78.20	97.40	39.50	74.97	96.27	40.23	41.47	41.44	42.71	42.05	41.48
[TR 2] LOWER BOUNDARY	26.25	52.13	64.93	26.33	49.98	64.18	26.82	27.65	27.62	28.47	28.03	27.65

EXPERIMENT [4 m/s]	A4001-E	A4002-E	A4003-E	A4004-E	A4005-E	A4006-E	A4007-E	A4008-E	A4009-E	A4010-E	A4011-E	A4012-E
E-MAXIMUM POINT	35.41	68.65	85.40	34.83	67.31	86.06	36.13	35.64	36.49	37.51	37.60	35.92
S-AVERAGE LINE	33.16	64.75	81.72	32.67	65.21	83.47	34.33	34.52	35.10	34.85	36.05	33.90
E-STD DEVIATION	0.81	1.45	1.67	0.77	1.63	1.78	0.82	0.75	0.79	0.87	0.96	0.82
[TR 1] UPPER FOR AVERAGE	38.95	75.51	93.94	38.31	74.04	94.66	39.74	39.20	40.14	41.26	41.36	39.51
[TR 1] LOWER FOR AVERAGE	31.86	61.78	76.86	31.35	60.58	77.45	32.52	32.07	32.84	33.75	33.84	32.33
[TR 2] UPPER BOUNDARY	39.79	77.70	98.07	39.20	78.25	100.17	41.19	41.42	42.12	41.82	43.26	40.68
[TR 2] LOWER BOUNDARY	26.53	51.80	65.38	26.13	52.17	66.78	27.46	27.62	28.08	27.88	28.84	27.12

1.2.1.5 Summary of Simulation vs. Experiment – [20% TR1 & 10% TR2]

Based on Acceleration (g)

Whilst using the impactor velocity of 4 m/s, this research found that all the acceleration (g) standard deviation were less than 2 (Table 1-11). Based on the finding stated as in part 1.2.1.1, 1.2.1.2, 1.2.1.3 and 1.2.1.4, this could conclude that the use of tolerance TR 1 (10%) and TR 2 (20%) were better than TR 1 (20%) and TR 2 (10%). The reason behind this argument is due to the acceleration (g) using trials tolerance at 10% and 20% for TR 1 and TR 2 is less than the higher standard deviation (>2) compared to the acceleration (g) using trials tolerance at 20% and 10% for TR 1 and TR 2.

Since the standard deviation values represented the dissimilarity of every single data to their average, it can be concluded that higher standard detected (>2), more data will be collected referring to the maximum points and wider trial tolerance used. In this sense, the gap between the upper and lower limit would represent the tolerance precision while making sure that all the data satisfy within the upper and lower boundary line.

It is important highlight that this research found that both trials tolerance failed to satisfy with the experiment values for design no. 4 and 5 when using the impact velocity 3 m/s (3004 and 3005 in Figure 1-2 and Figure 1-3). This is mainly due to the experiment data falls outside the lower limit of simulation graph.

1.2.2 Tolerance Trials for Displacement

Based on the tolerance values found (stated in subpart 1.1.3); this research conducted trial using 20% tolerance for TR 1 (tolerance 1 towards the maximum point). All data between maximum point to 20% and below maximum point were collected for creation of average line based on maximum point. Moreover, the TR 2 (the tolerance 2 towards the average line) constructed for the upper and lower lines limit or boundary lines. All data from experiment were checked if fall within the specified boundary.

Figure 1-4 shows an example using trial of 20% tolerance for TR 1 and 10% tolerance for TR 2. The research conducted towards all of 72 acceleration (g) and displacement data (experiment and simulation) respectively (*i.e.*, 2000, 3000, 4000 represents 2 m/s, 3 m/s, and 4 m/s)

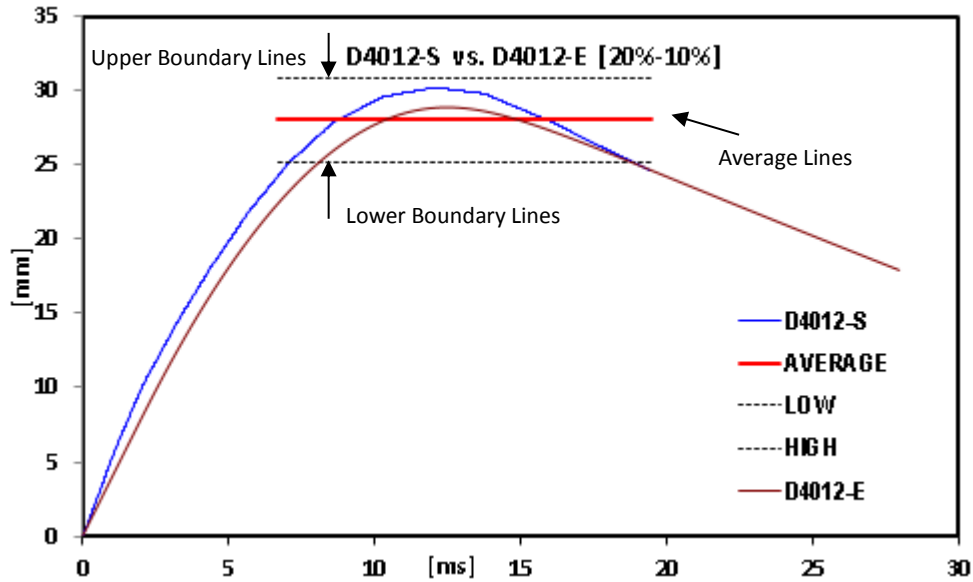


Figure 1-4: The Boundary and Average Lines Based on Tolerance Trials: 20% for TR 1 and 10% for TR 2.

These tolerances affect range of data taken from defined average lines that used to determine the upper and lower boundary line. The tolerance of TR 1 against the maximum point data, while the tolerance of TR 2 towards the average point line (see Figure 1-4).

For example, data D-4012-S (Displacement of flat shape simulation with 4 m/s impact) constructed using blue line in graph (Figure 1-4), where the maximum point (S-Max) is 30.22 mm. Using 20% tolerance (TR 1) as a trial for range data taken (that is between 24.17 mm till 36.26 mm), found that the average value was 28.02 mm. This average value was then assumed and constructed as an average line in which the boundary for the upper and lower line (based on trials using 10% tolerance or TR 2) for the upper and the lower line were 25.22 mm and 30.82 mm (Table 1-12). On this boundary area, experiment data shown in brown lines (D-4012-E or Experiment of Displacement on the Flat shape with 2 m/s impact) must be within this limit as a representation of the tolerance capability (see Figure 1-4). Based on defined tolerances (TR1 and TR 2 that were 20% and 10% respectively), research found that the standard deviation of displacement from data simulation within range is 1.76 (Table 1-12).

Table 1-12: The Tolerance Trials: 20% for TR 1 and 10% for TR 2 for D-2001-S.

SIMULATION	D-4012-S
MAXIMUM POINT	30.22
[TR 1] UPPER FOR AVERAGE	36.26
[TR 1] LOWER FOR AVERAGE	24.17
AVERAGE LINE	28.02
[TR 2] UPPER BOUNDARY	30.82
[TR 2] LOWER BOUNDARY	25.22
STD DEVIATION	1.76

1.2.2.1 Displacement – Simulation – [20% TR1 & 10% TR2]

This research found that there was no higher standard deviation (>2) occurred for simulation with impactor velocity 2 m/s, 3 m/s, and 4 m/s (Table 1-13). All displacement's standard deviation for impact velocity 2 m/s were calculated below 1 (<1).

Table 1-13: The Displacement Data (Simulation) with 20% TR1 and 10% TR2.

SIMULATION [2 m/s]	D2001-S	D2002-S	D2003-S	D2004-S	D2005-S	D2006-S	D2007-S	D2008-S	D2009-S	D2010-S	D2011-S	D2012-S
S-MAXIMUM POINT	10.90	8.13	7.93	12.04	10.88	9.35	12.83	12.05	11.49	10.10	10.82	11.31
S-AVERAGE LINE	10.08	7.49	7.30	11.07	10.01	8.58	11.83	11.05	10.62	9.30	10.01	10.45
S-STD DEVIATION	0.66	0.49	0.49	0.73	0.66	0.57	0.78	0.73	0.67	0.58	0.68	0.68
[TR 1] UPPER FOR AVERAGE	13.08	9.76	9.52	14.44	13.06	11.22	15.40	14.46	13.79	12.12	12.98	13.57
[TR 1] LOWER FOR AVERAGE	8.72	6.50	6.35	9.63	8.71	7.48	10.26	9.64	9.20	8.08	8.65	9.05
[TR 2] UPPER BOUNDARY	11.09	8.24	8.03	12.17	11.01	9.44	13.01	12.15	11.68	10.23	11.01	11.50
[TR 2] LOWER BOUNDARY	9.07	6.74	6.57	9.96	9.01	7.72	10.65	9.94	9.55	8.37	9.01	9.41

SIMULATION [3 m/s]	D3001-S	D3002-S	D3003-S	D3004-S	D3005-S	D3006-S	D3007-S	D3008-S	D3009-S	D3010-S	D3011-S	D3012-S
S-MAXIMUM	16.49	12.55	8.31	19.77	17.54	14.29	17.29	20.21	16.61	21.10	18.09	19.51
S-AVERAGE	15.20	11.58	7.57	18.26	16.03	13.19	15.80	18.59	15.39	19.30	16.58	17.94
S-STD DEVIATION	1.01	0.76	0.46	1.21	1.02	0.83	1.03	1.19	1.04	1.26	1.09	1.22
[TR 1] UPPER FOR AVERAGE	19.79	15.05	9.98	23.72	21.05	17.14	20.75	24.25	19.94	25.32	21.71	23.41
[TR 1] LOWER FOR AVERAGE	13.19	10.04	6.65	15.81	14.03	11.43	13.84	16.17	13.29	16.88	14.47	15.61
[TR 2] UPPER BOUNDARY	16.72	12.73	8.33	20.08	17.64	14.51	17.39	20.45	16.92	21.23	18.23	19.74
[TR 2] LOWER BOUNDARY	13.68	10.42	6.82	16.43	14.43	11.87	14.22	16.73	13.85	17.37	14.92	16.15

SIMULATION [4 m/s]	D4001-S	D4002-S	D4003-S	D4004-S	D4005-S	D4006-S	D4007-S	D4008-S	D4009-S	D4010-S	D4011-S	D4012-S
S-MAXIMUM	27.33	20.68	17.07	30.34	23.01	20.80	25.98	27.49	29.09	29.84	28.63	30.22
S-AVERAGE	25.17	19.07	15.81	28.19	21.11	19.13	24.06	25.20	26.86	27.52	26.42	28.02
S-STD DEVIATION	1.68	1.23	1.09	1.79	1.34	1.26	1.56	1.66	1.72	1.75	1.75	1.76
[TR 1] UPPER FOR AVERAGE	32.79	24.82	20.48	36.41	27.61	24.95	31.18	32.99	34.90	35.81	34.36	36.26
[TR 1] LOWER FOR AVERAGE	21.86	16.54	13.65	24.27	18.41	16.64	20.79	21.99	23.27	23.87	22.91	24.17
[TR 2] UPPER BOUNDARY	27.69	20.98	17.39	31.01	23.22	21.04	26.46	27.71	29.54	30.27	29.07	30.82
[TR 2] LOWER BOUNDARY	22.66	17.17	14.23	25.37	19.00	17.22	21.65	22.68	24.17	24.77	23.78	25.22

Based on the trials of tolerance defined for the displacement (see the data), shows that the

displacement for design no. 2 and 6 with TR 1 and TR 2 tolerances (20% and 10% respectively) for 3 m/s impact were outside of top boundary limit. In addition, simulation conducted at 3 m/s impact velocity showing design no. 2 and 6 plotted higher results than upper boundary limit (Figure 1-5).

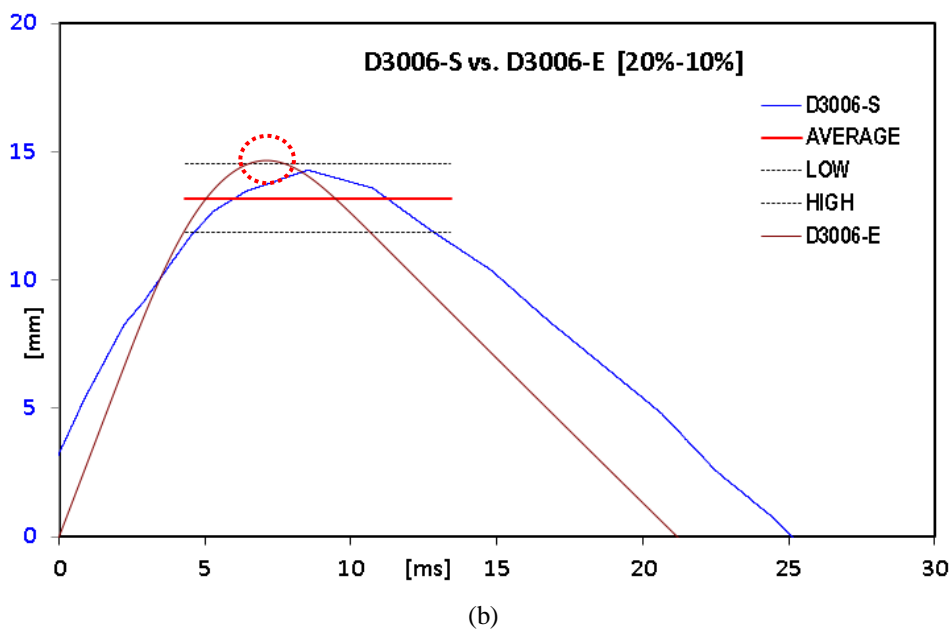
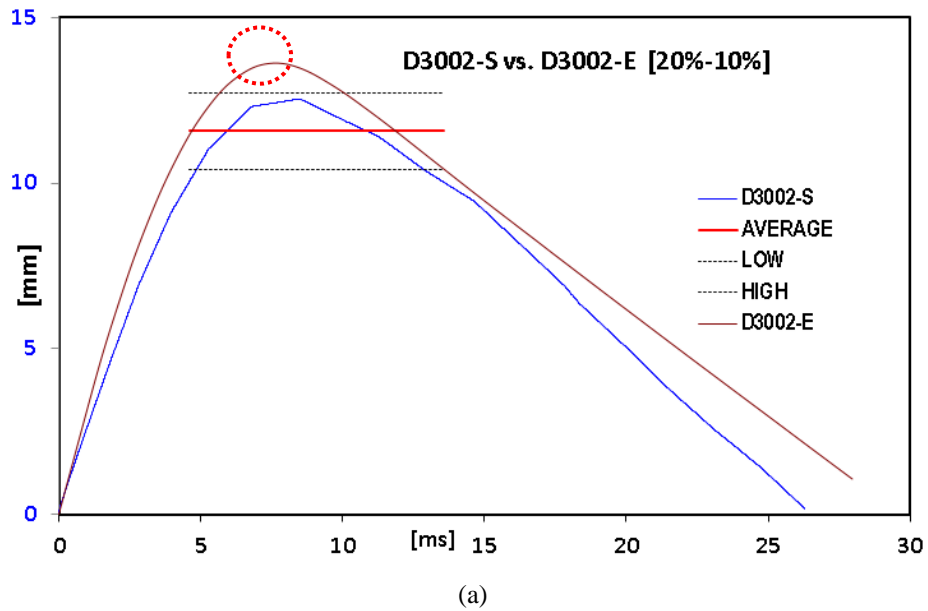


Figure 1-5: Displacement Result of Simulation conducted at 3 m/s which is Outside of the Boundary Limit. (a) Displacement of Design 6 with 3 m/s Impact Velocity, (b) Displacement of Design 6 with 3 m/s Impact Velocity

1.2.2.2 Displacement – Experiment – [20% TR1 & 10% TR2]

Table 1-14 shows that there were no higher standard deviation (>2) occurred for the displacement result when experiment was conducted with all impact velocity.

Table-14: The Displacement Data (Experiment) with 20% TR1 and 10% TR2

EXPERIMENT [2 m/s]	D2001-E	D2002-E	D2003-E	D2004-E	D2005-E	D2006-E	D2007-E	D2008-E	D2009-E	D2010-E	D2011-E	D2012-E
S-MAXIMUM POINT	9.80	8.13	7.57	11.68	10.27	8.37	12.31	11.37	11.31	9.64	10.33	10.92
S-AVERAGE LINE	9.07	7.53	7.01	10.85	9.54	7.78	11.42	10.56	10.49	8.96	9.59	10.15
S-STD DEVIATION	0.60	0.50	0.46	0.71	0.62	0.51	0.75	0.70	0.69	0.59	0.63	0.67
[TR 1] UPPER FOR AVERAGE	11.76	9.76	9.08	14.01	12.32	10.04	14.77	13.65	13.57	11.56	12.40	13.11
[TR 1] LOWER FOR AVERAGE	7.84	6.50	6.05	9.34	8.21	6.70	9.84	9.10	9.04	7.71	8.26	8.74
[TR 2] UPPER BOUNDARY	9.98	8.28	7.71	11.93	10.50	8.56	12.56	11.62	11.54	9.85	10.55	11.16
[TR 2] LOWER BOUNDARY	8.17	6.78	6.31	9.76	8.59	7.00	10.28	9.51	9.44	8.06	8.63	9.13

EXPERIMENT [3 m/s]	D3001-E	D3002-E	D3003-E	D3004-E	D3005-E	D3006-E	D3007-E	D3008-E	D3009-E	D3010-E	D3011-E	D3012-E
S-MAXIMUM	16.00	13.63	7.56	18.73	15.81	14.66	15.78	18.37	15.78	19.79	17.54	18.36
S-AVERAGE	14.80	12.59	7.01	17.36	14.66	13.60	14.62	16.99	14.63	18.28	16.22	17.00
S-STD DEVIATION	0.98	0.84	0.46	1.15	0.97	0.90	0.97	1.13	0.97	1.22	1.08	1.13
[TR 1] UPPER FOR AVERAGE	19.21	16.35	9.07	22.48	18.98	17.59	18.94	22.05	18.93	23.74	21.05	22.03
[TR 1] LOWER FOR AVERAGE	12.80	10.90	6.05	14.98	12.65	11.73	12.62	14.70	12.62	15.83	14.03	14.69
[TR 2] UPPER BOUNDARY	16.28	13.85	7.71	19.10	16.13	14.96	16.09	18.69	16.09	20.11	17.85	18.70
[TR 2] LOWER BOUNDARY	13.32	11.33	6.31	15.63	13.20	12.24	13.16	15.29	13.16	16.46	14.60	15.30

EXPERIMENT [4 m/s]	D4001-E	D4002-E	D4003-E	D4004-E	D4005-E	D4006-E	D4007-E	D4008-E	D4009-E	D4010-E	D4011-E	D4012-E
S-MAXIMUM	25.92	20.31	16.99	28.46	21.31	18.99	25.45	25.43	26.96	27.94	26.74	28.88
S-AVERAGE	23.94	18.77	15.68	26.33	19.74	17.58	23.50	23.51	24.91	25.84	24.72	26.65
S-STD DEVIATION	1.60	1.25	1.04	1.75	1.31	1.17	1.57	1.57	1.66	1.72	1.65	1.79
[TR 1] UPPER FOR AVERAGE	31.10	24.38	20.39	34.15	25.57	22.79	30.54	30.51	32.35	33.53	32.09	34.65
[TR 1] LOWER FOR AVERAGE	20.73	16.25	13.59	22.77	17.05	15.19	20.36	20.34	21.57	22.35	21.39	23.10
[TR 2] UPPER BOUNDARY	26.33	20.65	17.24	28.96	21.71	19.34	25.85	25.86	27.41	28.43	27.19	29.31
[TR 2] LOWER BOUNDARY	21.54	16.90	14.11	23.70	17.77	15.82	21.15	21.16	22.42	23.26	22.25	23.98

1.2.2.3 Displacement – Simulation – [10% TR1 & 20% TR2]

This section acknowledges that less standard deviation (<1) occurred for all design range when 2 m/s and 3 m/s impact velocity was applied. However, for higher impact velocity 4 m/s, the deviation shows a slight increase but still maintained a standard deviation value below than 2 (<2) (Table 1-15).

Based on the trials of tolerance defined for the displacement (Appendix D), found also that all design for displacement mode with TR 1 and TR 2 tolerances (20% and 20% respectively) plotted within the boundary limit.

Table 1-15: The Displacement Data (Simulation) with 10% TR1 and 20% TR2.

SIMULATION [2 m/s]	D2001-S	D2002-S	D2003-S	D2004-S	D2005-S	D2006-S	D2007-S	D2008-S	D2009-S	D2010-S	D2011-S	D2012-S
S-MAXIMUM POINT	10.90	8.13	7.93	12.04	10.88	9.35	12.83	12.05	11.49	10.10	10.82	11.31
S-AVERAGE LINE	10.49	7.82	7.65	11.55	10.45	8.99	12.34	11.57	11.02	9.68	10.44	10.89
S-STD DEVIATION	0.35	0.25	0.25	0.36	0.34	0.29	0.40	0.36	0.35	0.31	0.34	0.33
[TR 1] UPPER FOR AVERAGE	11.99	8.94	8.73	13.24	11.97	10.28	14.11	13.25	12.64	11.11	11.90	12.44
[TR 1] LOWER FOR AVERAGE	9.81	7.32	7.14	10.83	9.79	8.41	11.55	10.84	10.35	9.09	9.74	10.18
[TR 2] UPPER BOUNDARY	12.59	9.38	9.18	13.87	12.54	10.78	14.81	13.89	13.22	11.62	12.53	13.07
[TR 2] LOWER BOUNDARY	8.40	6.25	6.12	9.24	8.36	7.19	9.87	9.26	8.82	7.75	8.36	8.71

SIMULATION [3 m/s]	D3001-S	D3002-S	D3003-S	D3004-S	D3005-S	D3006-S	D3007-S	D3008-S	D3009-S	D3010-S	D3011-S	D3012-S
S-MAXIMUM	16.49	12.55	8.31	19.77	17.54	14.29	17.29	20.21	16.61	21.10	18.09	19.51
S-AVERAGE	15.87	12.05	7.90	19.05	16.75	13.70	16.55	19.38	16.04	20.24	17.35	18.77
S-STD DEVIATION	0.49	0.38	0.24	0.59	0.48	0.39	0.49	0.57	0.54	0.58	0.55	0.59
[TR 1] UPPER FOR AVERAGE	18.14	13.80	9.14	21.74	19.29	15.71	19.02	22.23	18.27	23.21	19.90	21.46
[TR 1] LOWER FOR AVERAGE	14.84	11.29	7.48	17.79	15.79	12.86	15.56	18.19	14.95	18.99	16.28	17.56
[TR 2] UPPER BOUNDARY	19.04	14.46	9.48	22.87	20.10	16.44	19.86	23.25	19.25	24.29	20.82	22.53
[TR 2] LOWER BOUNDARY	12.69	9.64	6.32	15.24	13.40	10.96	13.24	15.50	12.83	16.19	13.88	15.02

SIMULATION [4 m/s]	D4001-S	D4002-S	D4003-S	D4004-S	D4005-S	D4006-S	D4007-S	D4008-S	D4009-S	D4010-S	D4011-S	D4012-S
S-MAXIMUM	27.33	20.68	17.07	30.34	23.01	20.80	25.98	27.49	29.09	29.84	28.63	30.22
S-AVERAGE	25.17	19.07	15.81	28.19	21.11	19.13	24.06	25.20	26.86	27.52	26.42	28.02
S-STD DEVIATION	1.68	1.23	1.09	1.79	1.34	1.26	1.56	1.66	1.72	1.75	1.75	1.76
[TR 1] UPPER FOR AVERAGE	32.79	24.82	20.48	36.41	27.61	24.95	31.18	32.99	34.90	35.81	34.36	36.26
[TR 1] LOWER FOR AVERAGE	21.86	16.54	13.65	24.27	18.41	16.64	20.79	21.99	23.27	23.87	22.91	24.17
[TR 2] UPPER BOUNDARY	27.69	20.98	17.39	31.01	23.22	21.04	26.46	27.71	29.54	30.27	29.07	30.82
[TR 2] LOWER BOUNDARY	22.66	17.17	14.23	25.37	19.00	17.22	21.65	22.68	24.17	24.77	23.78	25.22

1.2.2.4 Displacement – Experiment – [10% TR1 & 20% TR2]

This research found that there were no higher standard deviation (>2) occurred for the simulation with the impact velocity 2 m/s, 3 m/s, and 4 m/s (Table 1-16). Lower standard deviation (<1) occurred on all design based on the displacement when the impact velocity was 2 m/s and 3 m/s.

Based on the findings, stated as in 0, 0 and 0, we can conclude that the used tolerance of TR 1 (10%) and TR 2 (20%) were better than TR 1 (20%) and TR 2 (10%). The reason behind this argument was due to acceleration (g) using trials tolerance 10% and 20% for TR 1 and TR 2. TR1 and TR2 are less high than standard deviation (>2) compared to the acceleration (g) using trials tolerance 20% and 10% for TR 1 and TR 2.

Table 1-16: The Displacement Data (Experiment) with 10% TR1 and 20% TR2

EXPERIMENT [2 m/s]	D2001-E	D2002-E	D2003-E	D2004-E	D2005-E	D2006-E	D2007-E	D2008-E	D2009-E	D2010-E	D2011-E	D2012-E
S-MAXIMUM POINT	9.80	8.13	7.57	11.68	10.27	8.37	12.31	11.37	11.31	9.64	10.33	10.92
S-AVERAGE LINE	9.45	7.84	7.30	11.28	9.91	8.08	11.88	10.98	10.91	9.31	9.97	10.55
S-STD DEVIATION	0.30	0.25	0.23	0.35	0.31	0.25	0.37	0.34	0.34	0.29	0.31	0.33
[TR 1] UPPER FOR AVERAGE	10.78	8.94	8.32	12.84	11.29	9.21	13.54	12.51	12.44	10.60	11.36	12.02
[TR 1] LOWER FOR AVERAGE	8.82	7.32	6.81	10.51	9.24	7.53	11.08	10.24	10.17	8.67	9.30	9.83
[TR 2] UPPER BOUNDARY	11.34	9.41	8.76	13.53	11.90	9.70	14.26	13.18	13.10	11.17	11.97	12.66
[TR 2] LOWER BOUNDARY	7.56	6.27	5.84	9.02	7.93	6.47	9.51	8.79	8.73	7.45	7.98	8.44

EXPERIMENT [3 m/s]	D3001-E	D3002-E	D3003-E	D3004-E	D3005-E	D3006-E	D3007-E	D3008-E	D3009-E	D3010-E	D3011-E	D3012-E
S-MAXIMUM	16.00	13.63	7.56	18.73	15.81	14.66	15.78	18.37	15.78	19.79	17.54	18.36
S-AVERAGE	15.43	13.13	7.30	18.08	15.26	14.15	15.23	17.71	15.23	19.08	16.91	17.71
S-STD DEVIATION	0.49	0.42	0.23	0.57	0.48	0.44	0.48	0.56	0.48	0.60	0.53	0.56
[TR 1] UPPER FOR AVERAGE	17.61	14.99	8.32	20.60	17.40	16.12	17.36	20.21	17.36	21.76	19.29	20.20
[TR 1] LOWER FOR AVERAGE	14.40	12.26	6.80	16.86	14.23	13.19	14.20	16.53	14.20	17.81	15.78	16.53
[TR 2] UPPER BOUNDARY	18.52	15.76	8.76	21.69	18.32	16.98	18.27	21.26	18.27	22.89	20.30	21.25
[TR 2] LOWER BOUNDARY	12.34	10.51	5.84	14.46	12.21	11.32	12.18	14.17	12.18	15.26	13.53	14.17

EXPERIMENT [3 m/s]	D3001-E	3002-E	3003-E	3004-E	3005-E	3006-E	3007-E	3008-E	3009-E	3010-E	3011-E	3012-E
S-MAXIMUM	25.92	20.31	16.99	28.46	21.31	18.99	25.45	25.43	26.96	27.94	26.74	28.88
S-AVERAGE	24.97	19.58	16.36	27.44	20.56	18.32	24.53	24.52	25.99	26.94	25.78	27.82
S-STD DEVIATION	0.79	0.62	0.52	0.87	0.65	0.58	0.78	0.78	0.82	0.85	0.82	0.88
[TR 1] UPPER FOR AVERAGE	28.51	22.35	18.69	31.30	23.44	20.89	27.99	27.97	29.65	30.74	29.41	31.76
[TR 1] LOWER FOR AVERAGE	23.32	18.28	15.29	25.61	19.18	17.09	22.90	22.89	24.26	25.15	24.07	25.99
[TR 2] UPPER BOUNDARY	29.97	23.49	19.64	32.93	24.67	21.99	29.43	29.42	31.18	32.33	30.93	33.39
[TR 2] LOWER BOUNDARY	19.98	15.66	13.09	21.96	16.45	14.66	19.62	19.61	20.79	21.55	20.62	22.26

1.2.2.1 Summary of Simulation vs. Experiment – [10% TR1 & 20% TR2]

Based on Displacement

Since the standard deviation values represents the dissimilarities of every single data to their average, can be concluded when wider range of data are collected, standard deviation will be higher (>2). In this sense, the gap between upper and lower limit are representation of how precise the tolerances to cope with the data represented through the graph within the boundary line.

However, occurs that used trial tolerance fail to satisfy the experiment result. At impact velocity of 3 m/s, design no. 2 and 6 (3002 and 3006 in Figure 1-5) were outside the lower limit. Therefore, this tolerance is not suitable for displacement.

1.2.3 The Tolerances that Satisfy Simulation and Experiment

Since acceleration (g) uses the tolerance of TR 1 (10%) and TR 2 (20%), TR 1(20%) and TR 2(10%) have few setbacks. Same goes to displacement tolerances. Therefore, tolerance trials of TR 1 and TR 2 used were 15% to fulfil the simulation tolerance versus experimental for both acceleration (g) and displacement.

1.2.3.1 Acceleration (g) – Simulation – [15% TR1 & 15% TR2]

Since this research focused on the simulation against the experiment results (as for the final experiment prediction purpose), this research continues to adjust the tolerance values in next trials. In this research, the tolerance trials of TR 1 and TR 2 used were 15% each as a trade-off between tolerances towards the maximum values and the upper-lower boundary lines. In this context, the research found that all experiment values were within simulation boundary of the acceleration (g) values.

Table 1-17: The Acceleration (g) Data (Simulation) with 15% TR1 and 15% TR2.

SIMULATION [2 m/s]	A2001-S	A2002-S	A2003-S	A2004-S	A2005-S	A2006-S	A2007-S	A2008-S	A2009-S	A2010-S	A2011-S	A2012-S
S-MAXIMUM POINT	34.15	66.51	84.31	34.36	66.07	77.42	35.64	35.56	35.54	35.50	35.56	35.64
SVERAGE LINE	33.36	65.43	82.62	33.36	64.38	74.14	34.77	34.71	34.68	34.69	34.72	34.78
S-STD DEVIATION	1.12	1.88	3.00	1.33	2.69	3.15	1.22	1.16	1.10	1.09	1.16	1.20
[TR 1] UPPER FOR AVERAGE	39.28	76.49	96.96	39.51	75.98	89.03	40.98	40.89	40.87	40.83	40.89	40.98
[TR 1] LOWER FOR AVERAGE	29.03	56.54	71.66	29.21	56.16	65.80	30.29	30.22	30.21	30.18	30.23	30.29
[TR 2] UPPER BOUNDARY	38.36	75.25	95.01	38.37	74.03	85.26	39.98	39.92	39.89	39.89	39.93	39.99
[TR 2] LOWER BOUNDARY	28.35	55.62	70.22	28.36	54.72	63.02	29.55	29.51	29.48	29.49	29.51	29.56

SIMULATION [3 m/s]	A3001-S	A3002-S	A3003-S	A3004-S	A3005-S	A3006-S	A3007-S	A3008-S	A3009-S	A3010-S	A3011-S	A3012-S
S-MAXIMUM	34.80	67.54	85.47	35.29	68.93	87.46	36.36	36.31	36.53	36.31	36.31	36.36
SVERAGE	33.83	66.46	84.26	34.51	67.60	84.96	35.39	35.32	35.33	35.31	35.33	35.39
S-STD DEVIATION	0.97	1.77	2.45	1.19	2.05	3.52	1.05	1.01	0.89	0.93	0.98	1.05
[TR 1] UPPER FOR AVERAGE	40.02	77.67	98.29	40.58	79.27	100.57	41.81	41.75	42.01	41.76	41.75	41.81
[TR 1] LOWER FOR AVERAGE	29.58	57.41	72.65	29.99	58.59	74.34	30.91	30.86	31.05	30.86	30.86	30.90
[TR 2] UPPER BOUNDARY	38.90	76.43	96.90	39.69	77.73	97.71	40.70	40.62	40.63	40.60	40.64	40.70
[TR 2] LOWER BOUNDARY	28.75	56.49	71.62	29.34	57.46	72.22	30.08	30.02	30.03	30.01	30.03	30.08

SIMULATION [4 m/s]	A4001-S	A4002-S	A4003-S	A4004-S	A4005-S	A4006-S	A4007-S	A4008-S	A4009-S	A4010-S	A4011-S	A4012-S
S-MAXIMUM	35.36	68.32	86.38	35.57	69.65	88.37	36.98	36.95	37.01	37.34	36.95	36.98
S-AVERAGE	34.22	66.96	84.87	34.88	68.68	86.74	35.85	35.79	35.75	35.77	35.80	35.85
S-STD DEVIATION	0.96	1.68	2.23	1.00	1.87	3.12	0.99	0.94	0.92	0.88	0.94	0.99
[TR 1] UPPER FOR AVERAGE	40.67	78.57	99.34	40.90	80.10	101.63	42.53	42.49	42.56	42.94	42.49	42.53
[TR 1] LOWER FOR AVERAGE	30.06	58.07	73.43	30.23	59.20	75.12	31.43	31.41	31.46	31.73	31.41	31.43
[TR 2] UPPER BOUNDARY	39.36	77.01	97.60	40.11	78.99	99.75	41.23	41.16	41.11	41.13	41.16	41.23
[TR 2] LOWER BOUNDARY	29.09	56.92	72.14	29.65	58.38	73.73	30.48	30.43	30.38	30.40	30.43	30.48

Table 1-17 showed that higher standard deviation (>2) occurred on design no.3, 5, and 6 with the impactor velocity 2 m/s and 3 m/s. While, for the impactor velocity 4 m/s it only occurs on the design 3 and 6. Hence, Figure 1-6 shows A2003 – S versus A2003 – E whereby average line and maximum values fall within TR1 (15%) and TR2 (15%). Even though the standard deviation is more than 2, yet theory from simulation supported through experiment.

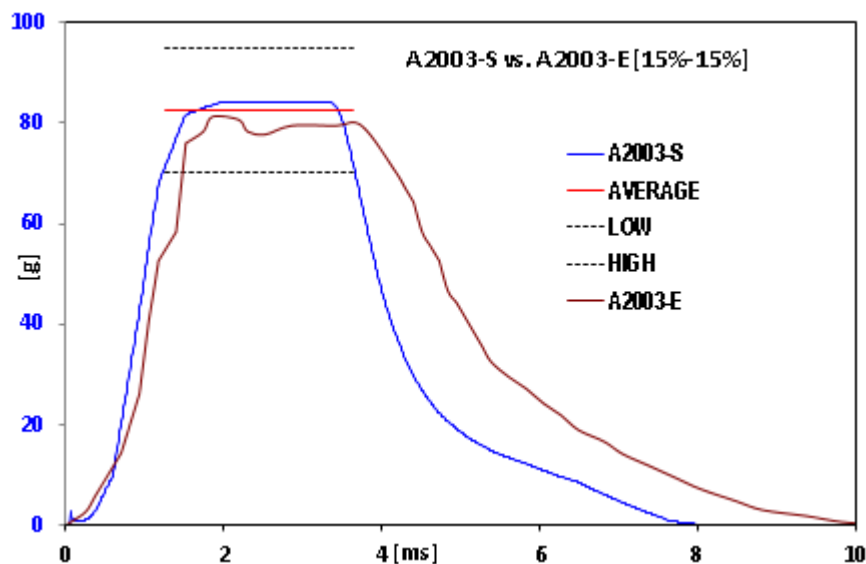


Figure 1-6: Acceleration (g): A2003-S vs A2003-E for 15% TR1 and 15% TR2 for 2 m/s impact velocity

1.2.3.2 Acceleration (g) – Experiment – [15% TR1 & 15% TR2]

Table 1-18 shows the higher standard deviation (>2) occurred on design no.2, 3, 5, and 6 based on the experiment for acceleration (g) with the impact velocity 2 m/s and 3 m/s. While, for the impact velocity 4 m/s only occurred on design 3, 5, and 6.

Figure 1-7 shows A2006–S versus A2006–E whereby average line and maximum values fall within TR1 (15%) and TR2 (15%). Even though the standard deviation was 3.38 bigger than 2, yet theory from simulation supported through experiment.

Table 1-18: The Acceleration (g) Data (Experiment) with 15% TR1 and 15% TR2

EXPERIMENT [2 m/s]	A2001-E	A2002-E	A2003-E	A2004-E	A2005-E	A2006-E	A2007-E	A2008-E	A2009-E	A2010-E	A2011-E	A2012-E
E-MAXIMUM POINT	34.92	60.59	81.28	32.97	64.37	75.30	34.41	35.50	34.50	34.09	35.94	36.35
SVERAGE LINE	33.37	58.03	77.49	31.49	61.81	71.81	32.96	33.29	33.06	32.53	34.52	34.87
E-STD DEVIATION	0.88	2.47	2.99	1.40	2.45	3.38	1.47	1.11	1.32	1.56	1.42	1.34
[TR 1] UPPER FOR AVERAGE	40.15	69.68	93.48	37.91	74.03	86.60	39.58	40.82	39.67	39.20	41.33	41.80
[TR 1] LOWER FOR AVERAGE	29.68	51.50	69.09	28.02	54.71	64.01	29.25	30.17	29.32	28.97	30.55	30.89
[TR 2] UPPER BOUNDARY	38.38	66.74	89.11	36.21	71.08	82.58	37.90	38.29	38.02	37.41	39.70	40.10
[TR 2] LOWER BOUNDARY	28.37	49.33	65.87	26.76	52.54	61.03	28.01	28.30	28.10	27.65	29.34	29.64

EXPERIMENT [3 m/s]	A3001-E	3002-E	3003-E	3004-E	3005-E	3006-E	3007-E	3008-E	3009-E	3010-E	3011-E	3012-E
E-MAXIMUM POINT	34.69	67.31	84.94	34.56	65.03	82.12	34.61	35.68	36.22	36.47	36.71	35.47
SVERAGE LINE	32.59	64.53	80.79	32.52	61.85	79.74	33.18	34.12	34.36	35.42	34.80	34.02
E-STD DEVIATION	1.02	2.25	2.47	1.23	2.18	2.42	1.22	1.34	1.11	1.07	1.14	1.44
[TR 1] UPPER FOR AVERAGE	39.89	77.40	97.69	39.74	74.78	94.44	39.80	41.04	41.65	41.94	42.22	40.79
[TR 1] LOWER FOR AVERAGE	29.49	57.21	72.20	29.38	55.27	69.80	29.42	30.33	30.78	31.00	31.20	30.15
[TR 2] UPPER BOUNDARY	37.48	74.21	92.91	37.40	71.13	91.70	38.16	39.23	39.52	40.74	40.02	39.12
[TR 2] LOWER BOUNDARY	27.70	54.85	68.67	27.64	52.58	67.77	28.20	29.00	29.21	30.11	29.58	28.91

EXPERIMENT [4 m/s]	A4001-E	4002-E	4003-E	4004-E	4005-E	4006-E	4007-E	4008-E	4009-E	4010-E	4011-E	4012-E
E-MAXIMUM POINT	35.41	68.65	85.40	34.83	67.31	86.06	36.13	35.64	36.49	37.51	37.60	35.92
S-AVERAGE LINE	33.02	64.41	80.27	32.52	64.28	82.50	34.21	34.27	34.83	34.12	35.76	33.79
E-STD DEVIATION	0.92	1.83	3.27	0.91	2.60	3.26	0.94	1.16	1.18	1.10	1.28	0.97
[TR 1] UPPER FOR AVERAGE	40.72	78.95	98.21	40.05	77.40	98.97	41.55	40.98	41.96	43.13	43.24	41.31
[TR 1] LOWER FOR AVERAGE	30.09	58.35	72.59	29.61	57.21	73.15	30.71	30.29	31.02	31.88	31.96	30.53
[TR 2] UPPER BOUNDARY	37.97	74.07	92.31	37.40	73.92	94.88	39.35	39.41	40.05	39.24	41.12	38.86
[TR 2] LOWER BOUNDARY	28.07	54.75	68.23	27.64	54.64	70.13	29.08	29.13	29.60	29.00	30.40	28.72

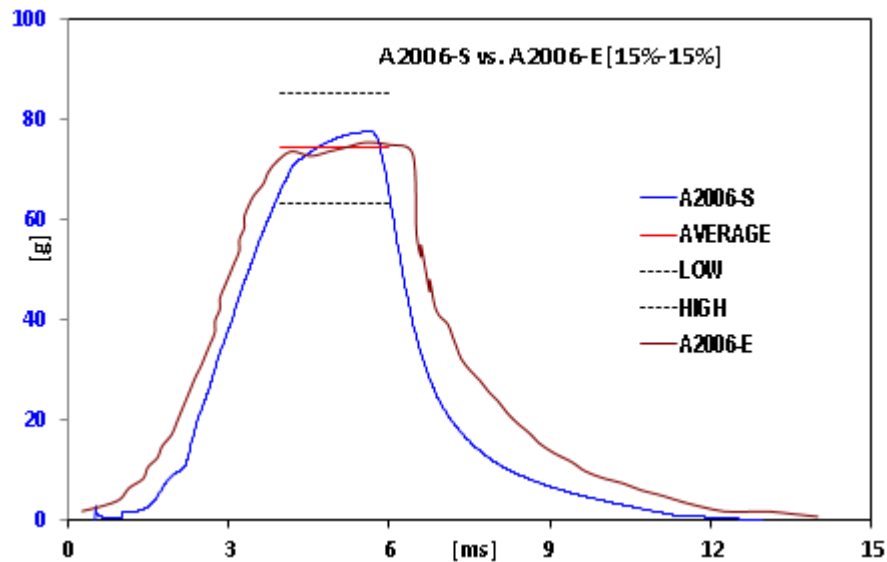


Figure 1-7 Acceleration (g): A2006-S vs A2006-E for 15% TR1 and 15% TR2 for 2 m/s impact velocity

1.2.3.3 Displacement – Simulation – [15% TR1 & 15% TR2]

The research found that all displacement graphs (related to the simulation against the experiment) were within the boundary. Table 1-19 shows that all plotted values provide a standard deviation value below than 2 (<2). In general, experiment values were within simulation boundary of the acceleration (g) values. Need to note that, 15% tolerance for TR 1 and 15 % tolerances for TR 2 can be used to predict the final experiment through simulation.

Table 1-19: The Displacement Data (Simulation) with 15% TR1 and 15% TR2

SIMULATION [2 m/s]	D2001-S	D2002-S	D2003-S	D2004-S	D2005-S	D2006-S	D2007-S	D2008-S	D2009-S	D2010-S	D2011-S	D2012-S
S-MAXIMUM POINT	10.90	8.13	7.93	12.04	10.88	9.35	12.83	12.05	11.49	10.10	10.82	11.31
S-AVERAGE LINE	10.30	7.65	7.46	11.33	10.23	8.78	12.09	11.30	10.81	9.47	10.23	10.67
S-STD DEVIATION	0.49	0.38	0.38	0.53	0.50	0.44	0.59	0.56	0.50	0.45	0.51	0.51
[TR 1] UPPER FOR AVERAGE	12.54	9.35	9.12	13.84	12.52	10.75	14.75	13.86	13.22	11.62	12.44	13.00
[TR 1] LOWER FOR AVERAGE	9.27	6.91	6.74	10.23	9.25	7.95	10.91	10.24	9.77	8.59	9.20	9.61
[TR 2] UPPER BOUNDARY	11.84	8.79	8.58	13.03	11.76	10.10	13.90	13.00	12.44	10.89	11.77	12.27
[TR 2] LOWER BOUNDARY	8.75	6.50	6.34	9.63	8.69	7.47	10.27	9.61	9.19	8.05	8.70	9.07

SIMULATION [3 m/s]	D3001-S	D3002-S	D3003-S	D3004-S	D3005-S	D3006-S	D3007-S	D3008-S	D3009-S	D3010-S	D3011-S	D3012-S
S-MAXIMUM	16.49	12.55	8.31	19.77	17.54	14.29	17.29	20.21	16.61	21.10	18.09	19.51
S-AVERAGE	15.55	11.83	7.74	18.65	16.40	13.46	16.19	18.99	15.72	19.76	16.95	18.38
S-STD DEVIATION	0.75	0.55	0.34	0.91	0.75	0.60	0.76	0.88	0.79	0.94	0.82	0.89
[TR 1] UPPER FOR AVERAGE	18.96	14.43	9.56	22.73	20.17	16.43	19.89	23.24	19.10	24.26	20.81	22.44
[TR 1] LOWER FOR AVERAGE	14.02	10.66	7.07	16.80	14.91	12.14	14.70	17.18	14.12	17.93	15.38	16.58
[TR 2] UPPER BOUNDARY	17.89	13.60	8.90	21.45	18.86	15.48	18.62	21.84	18.08	22.72	19.50	21.14
[TR 2] LOWER BOUNDARY	13.22	10.05	6.57	15.86	13.94	11.44	13.76	16.14	13.36	16.79	14.41	15.62

SIMULATION [4 m/s]	D4001-S	D4002-S	D4003-S	D4004-S	D4005-S	D4006-S	D4007-S	D4008-S	D4009-S	D4010-S	D4011-S	D4012-S
S-MAXIMUM	27.33	20.68	17.07	30.34	23.01	20.80	25.98	27.49	29.09	29.84	28.63	30.22
S-AVERAGE	25.75	19.48	16.18	28.71	21.56	19.55	24.55	25.80	27.41	28.04	27.02	28.52
S-STD DEVIATION	1.25	0.91	0.80	1.34	0.99	0.94	1.16	1.22	1.28	1.34	1.29	1.37
[TR 1] UPPER FOR AVERAGE	31.43	23.78	19.63	34.89	26.46	23.91	29.88	31.62	33.45	34.31	32.93	34.75
[TR 1] LOWER FOR AVERAGE	23.23	17.58	14.51	25.79	19.56	17.68	22.08	23.37	24.72	25.36	24.34	25.68
[TR 2] UPPER BOUNDARY	29.61	22.40	18.61	33.02	24.80	22.48	28.23	29.66	31.52	32.25	31.07	32.80
[TR 2] LOWER BOUNDARY	21.89	16.56	13.75	24.41	18.33	16.62	20.87	21.93	23.30	23.84	22.96	24.25

Figure 1-8 shows D4012 – S versus D4012 – E whereby average line and maximum values fall within TR1 (15%) and TR2 (15%). Even though the standard deviation was 1.37 highest among other design, yet theory from simulation supported through experiment.

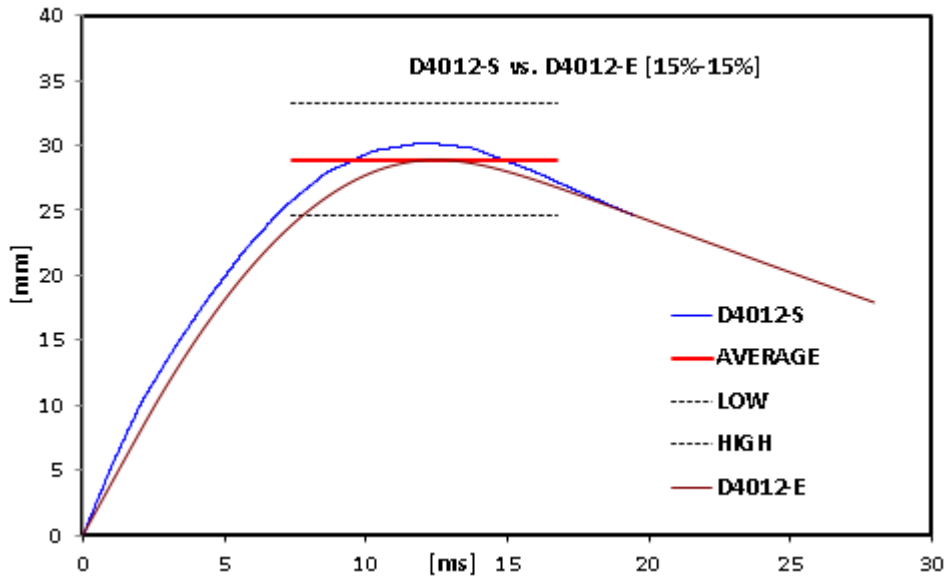


Figure 1-8: Displacement: D4012-S vs D4012-E for 15% TR1 and 15% TR2 for 4 m/s impact velocity

1.2.3.4 Displacement – Experiment – [15% TR1 & 15% TR2]

The research found that all standard deviation values were below than 2 (Table 1-20). In this context, the research found that, all experiment values within simulation boundary of the acceleration (g) values (see the data). Hence, the 15% tolerance for TR 1 and 15 % tolerances for TR 2 could be used for simulation to predict the experiment.

Figure 1-9 shows D4005 – S versus D4005 – E whereby average line and maximum values fall within TR1 (15%) and TR2 (15%). This proves that theory from simulation supported through experiment.

Table 1-20: The Displacement Data (Experiment) with 15% TR1 and 15% TR2.

EXPERIMENT [2 m/s]	D2001-E	D2002-E	D2003-E	D2004-E	D2005-E	D2006-E	D2007-E	D2008-E	D2009-E	D2010-E	D2011-E	D2012-E
S-MAXIMUM POINT	9.80	8.13	7.57	11.68	10.27	8.37	12.31	11.37	11.31	9.64	10.33	10.92
S-AVERAGE LINE	9.27	7.69	7.16	11.07	9.73	7.94	11.66	10.78	10.71	9.13	9.79	10.35
S-STD DEVIATION	0.30	0.25	0.23	0.35	0.31	0.25	0.37	0.34	0.34	0.29	0.31	0.33
[TR 1] UPPER FOR AVERAGE	11.27	9.35	8.70	13.43	11.81	9.63	14.15	13.08	13.00	11.08	11.88	12.56
[TR 1] LOWER FOR AVERAGE	8.33	6.91	6.43	9.93	8.73	7.12	10.46	9.67	9.61	8.19	8.78	9.29
[TR 2] UPPER BOUNDARY	10.65	8.84	8.23	12.73	11.19	9.13	13.41	12.39	12.31	10.50	11.25	11.90
[TR 2] LOWER BOUNDARY	7.88	6.54	6.08	9.41	8.27	6.75	9.91	9.16	9.10	7.76	8.32	8.80

EXPERIMENT [3 m/s]	D3001-E	D3002-E	D3003-E	D3004-E	D3005-E	D3006-E	D3007-E	D3008-E	D3009-E	D3010-E	D3011-E	D3012-E
S-MAXIMUM	16.00	13.63	7.56	18.73	15.81	14.66	15.78	18.37	15.78	19.79	17.54	18.36
S-AVERAGE	15.12	12.87	7.15	17.73	14.97	13.88	14.93	17.36	14.93	18.69	16.58	17.36
S-STD DEVIATION	0.49	0.42	0.23	0.57	0.48	0.44	0.48	0.56	0.48	0.60	0.53	0.56
[TR 1] UPPER FOR AVERAGE	18.41	15.67	8.70	21.54	18.19	16.86	18.15	21.13	18.14	22.75	20.17	21.12
[TR 1] LOWER FOR AVERAGE	13.60	11.58	6.43	15.92	13.44	12.46	13.41	15.62	13.41	16.82	14.91	15.61
[TR 2] UPPER BOUNDARY	17.39	14.80	8.23	20.39	17.22	15.96	17.17	19.96	17.17	21.49	19.06	19.96
[TR 2] LOWER BOUNDARY	12.85	10.94	6.08	15.07	12.72	11.80	12.69	14.75	12.69	15.89	14.09	14.76

EXPERIMENT [4 m/s]	D4001-E	D4002-E	D4003-E	D4004-E	D4005-E	D4006-E	D4007-E	D4008-E	D4009-E	D4010-E	D4011-E	D4012-E
S-MAXIMUM	25.92	20.31	16.99	28.46	21.31	18.99	25.45	25.43	26.96	27.94	26.74	28.88
S-AVERAGE	24.46	19.18	16.02	26.90	20.16	17.96	24.03	24.02	25.46	26.40	25.26	27.25
S-STD DEVIATION	0.79	0.62	0.52	0.87	0.65	0.58	0.78	0.78	0.82	0.85	0.82	0.88
[TR 1] UPPER FOR AVERAGE	29.80	23.36	19.54	32.72	24.51	21.84	29.27	29.24	31.00	32.13	30.75	33.21
[TR 1] LOWER FOR AVERAGE	22.03	17.27	14.44	24.19	18.12	16.14	21.63	21.61	22.91	23.75	22.73	24.55
[TR 2] UPPER BOUNDARY	28.13	22.06	18.43	30.93	23.18	20.65	27.63	27.62	29.28	30.36	29.05	31.34
[TR 2] LOWER BOUNDARY	20.79	16.31	13.62	22.86	17.13	15.27	20.42	20.42	21.64	22.44	21.47	23.16

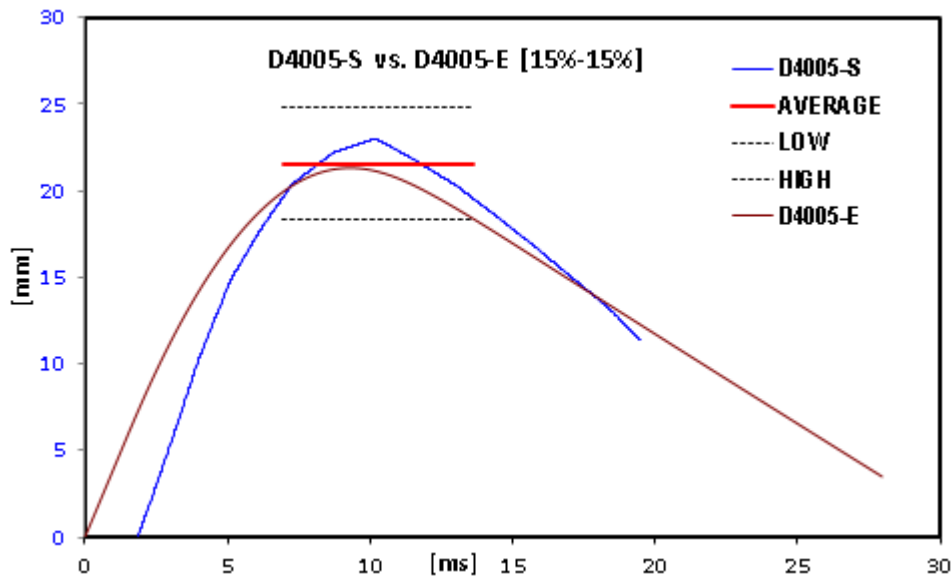


Figure 1-9: Displacement: D4005-S vs D4005-E for 15% TR1 and 15% TR2 for 4 m/s impact velocity

1.2.3.5 Summary of Simulation vs. Experiment – [15% TR1 & 15% TR2]

Based on the findings stated in subpart 1.2.3.1, 1.2.3.2, 1.2.3.3, and 1.2.3.4, this research concluded the use of tolerance TR 1 (15%) and TR 2 (15%) provides better result on the case of simulation against experiment data where all maximum points fall within the upper and lower limit. However, a higher standard deviation was detected in the results associated to acceleration (g). The higher standard deviation (>2) detected for simulation of acceleration (g) on design 3, 5, and 6. Whilst on the experiment, the higher standard deviation (>2) occurred on design 2, 3, 5, and 6 for impactor velocity 2 m/s and 3 m/s. In addition, for the impactor velocity 4 m/s, the higher standard deviation (>2) occurred on design no. 3, 5, and 6.

Based on the graph between simulation against experiment using tolerances TR1 15% and TR2 15% this research found that all experiment and simulation data, within 15% tolerance. Thus, standard deviation needs to be considered throughout the average and standard deviation values approach to determine the best material and configuration. In this context, the standard deviation is also a representation of average values. This statistical approach used to predict the final experiment result since this research will not be conducting an actual aircraft drop test experiment.

1.3 Summary

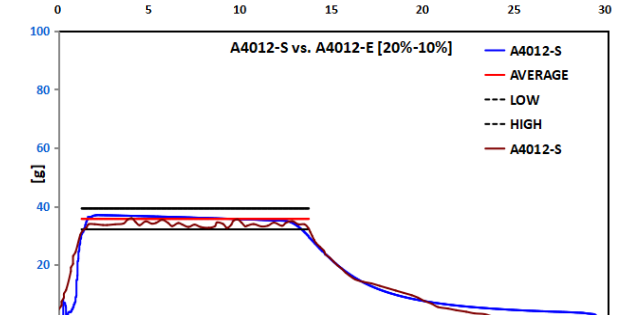
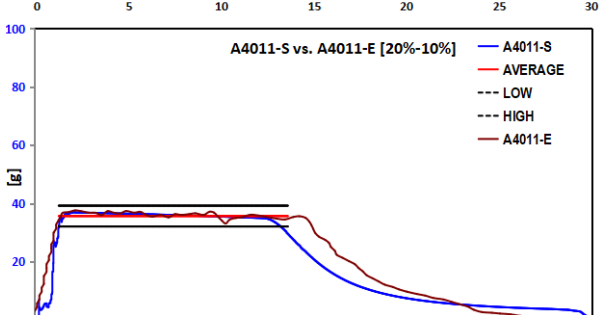
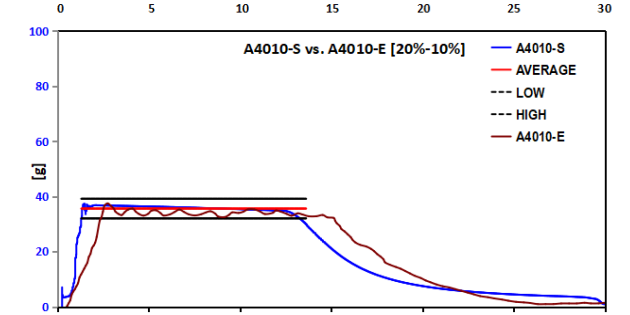
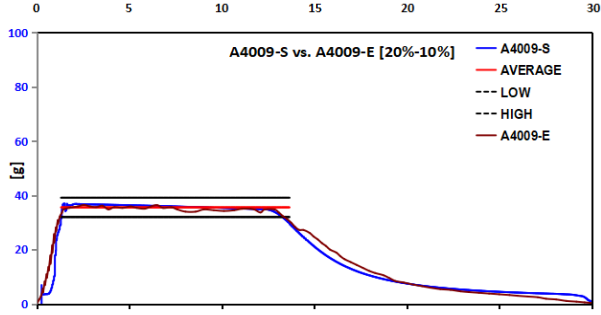
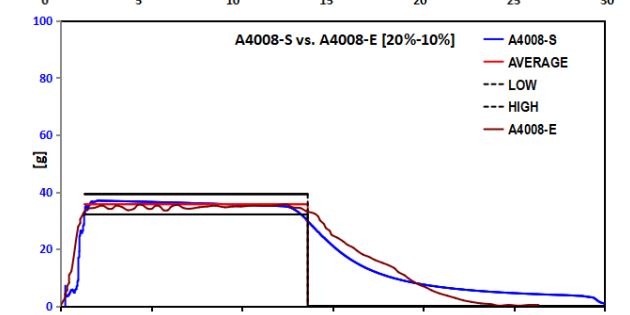
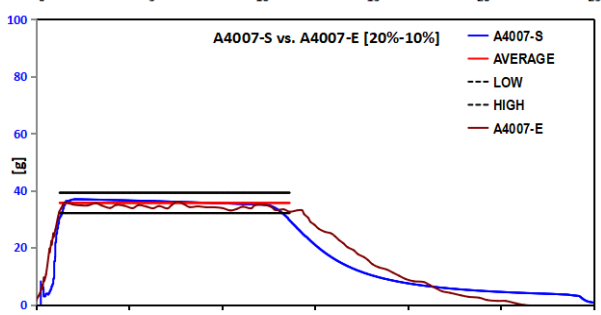
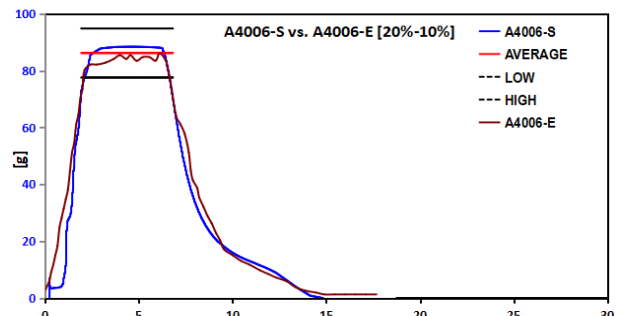
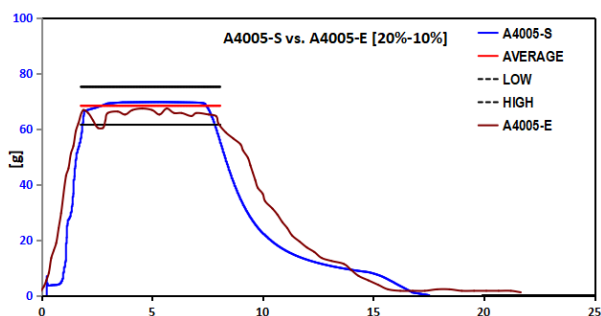
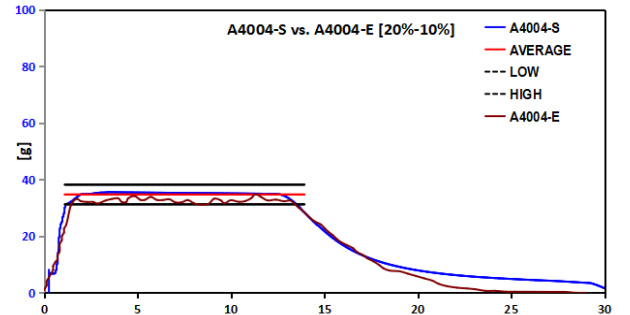
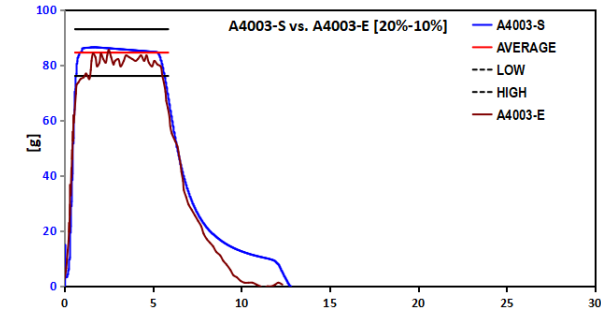
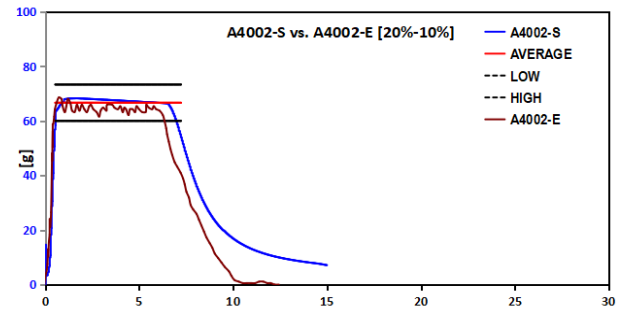
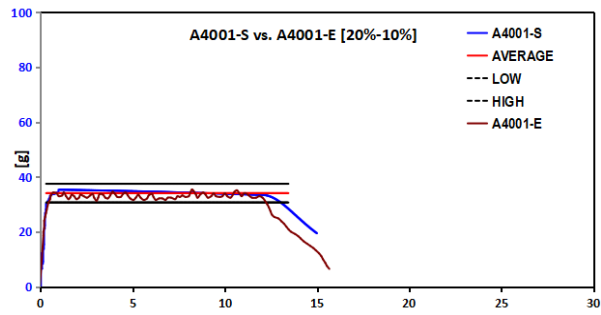
In this chapter, comparison between simulation and experiments finding were carried out. By using maximum, average and standard deviation values, maximum percentage values were 10.45% collected from the acceleration (g) and displacement between experiment and simulation conducted. Another maximum percentage value was 19.22% towards all values collected from the acceleration (g) and displacement between experiment and simulation conducted.

However, after identified the upper and lower limit 10.45% and 19.22% respectively, these percentages were rounded up. The tolerances were between 10% and 20 %. After conducting computation to observe the simulation and experiment difference, there are some values plotted outside of the tolerances range.

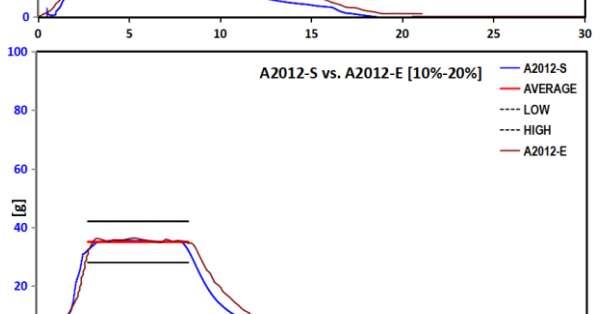
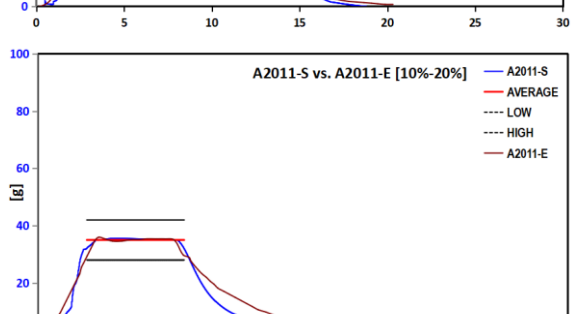
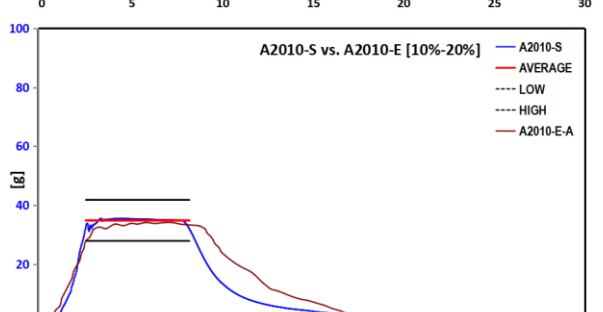
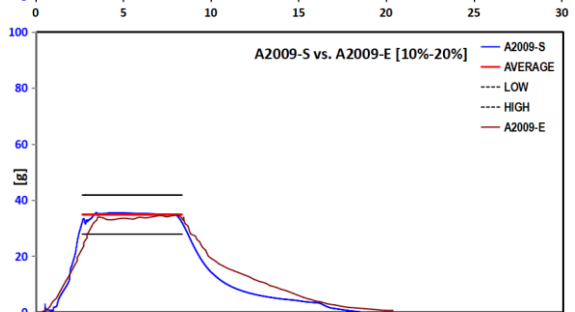
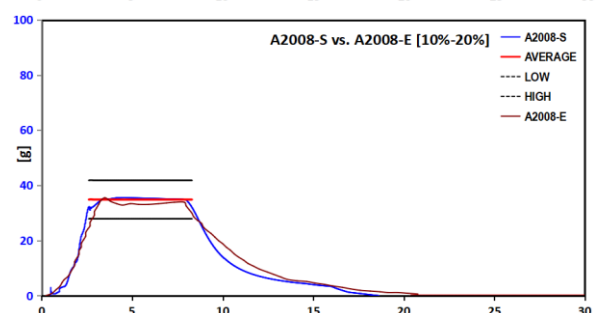
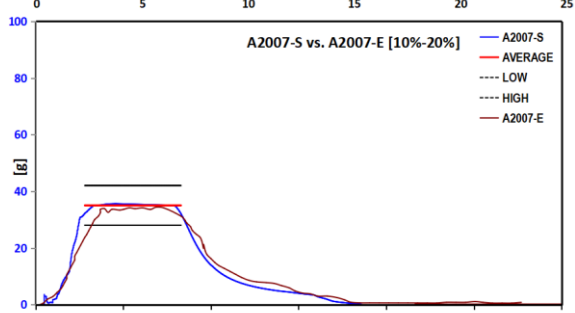
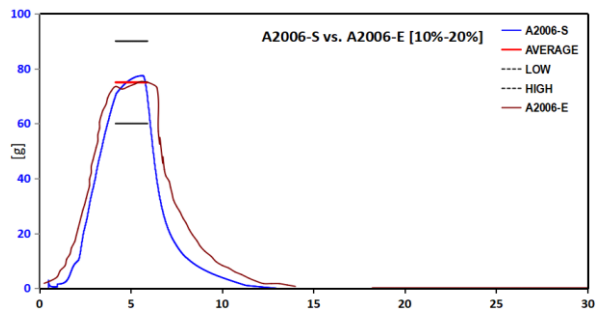
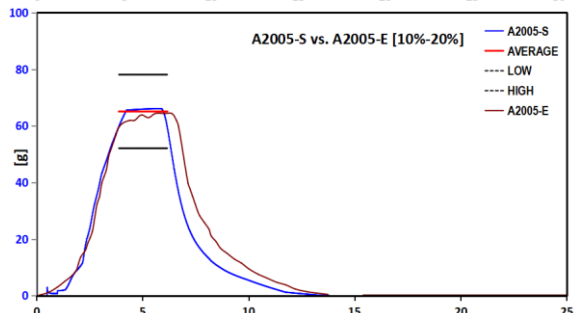
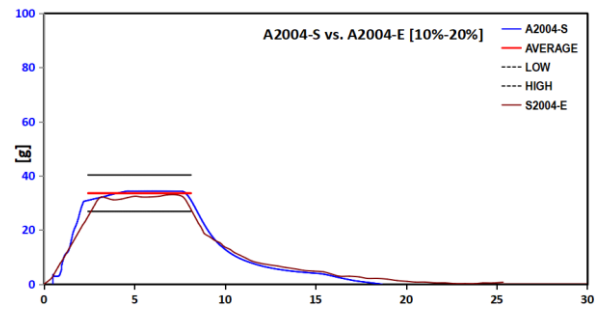
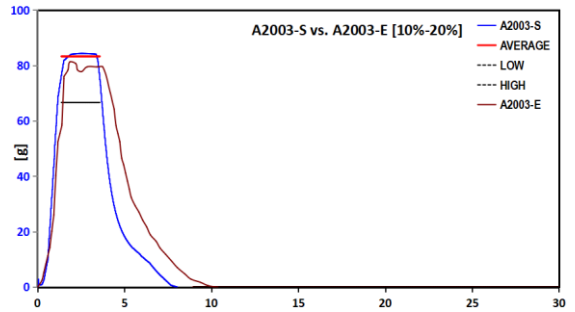
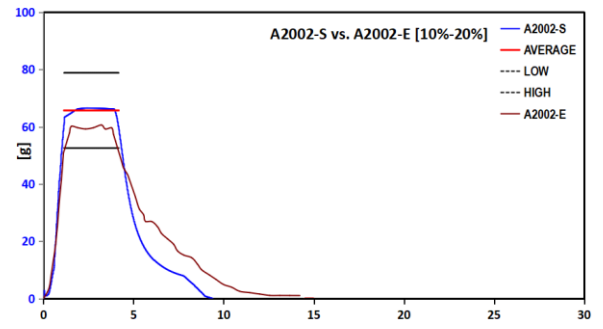
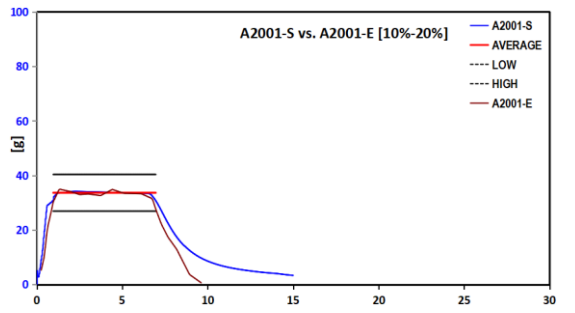
This chapter was further carried out to determine the best tolerance. Based on the graph between simulation against experiment using tolerances TR1 15% and TR2 15% this research found that all experiment and simulation data, within 15% tolerance. In this context, the standard deviation is also a representation of average values. This statistical approach used to predict the final experiment result since this research will not be conducting an actual aircraft drop test experiment.

Appendix F

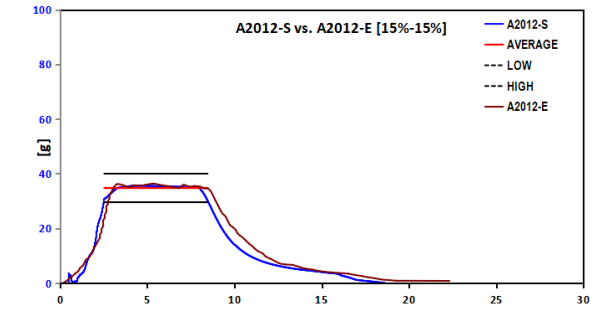
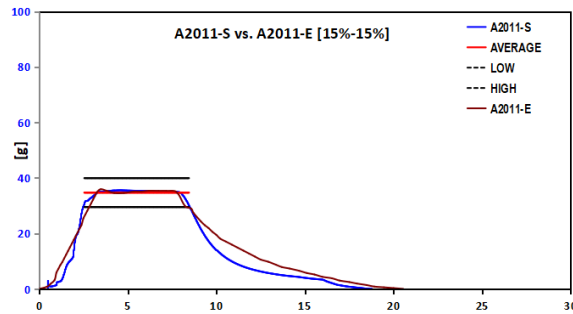
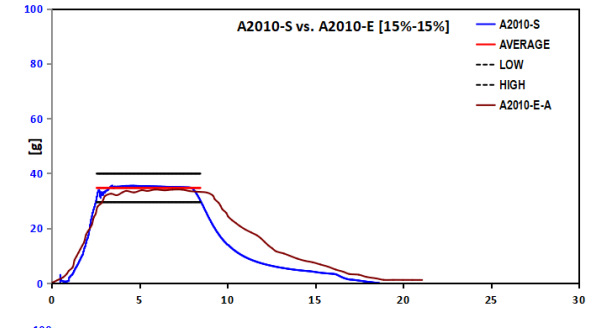
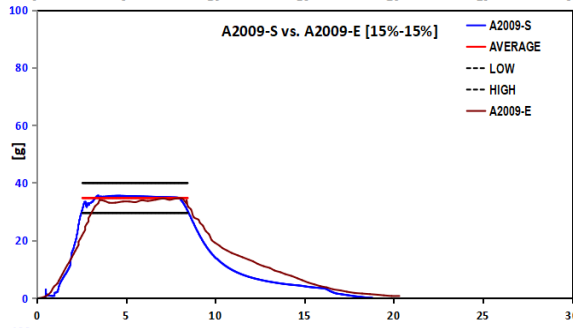
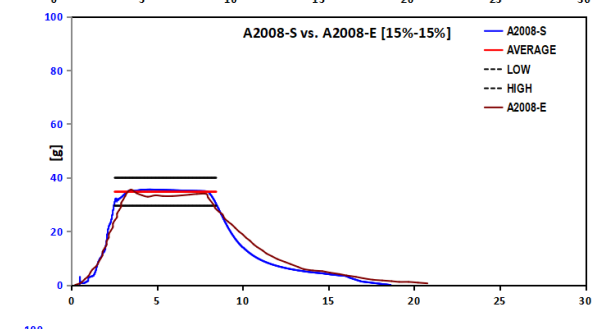
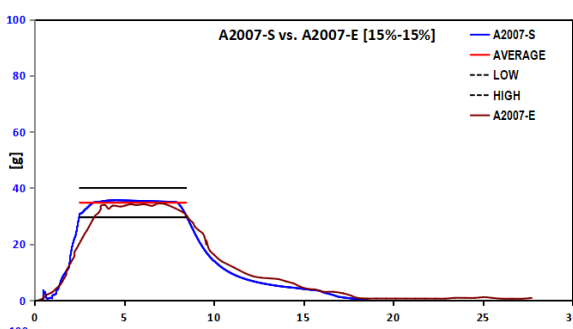
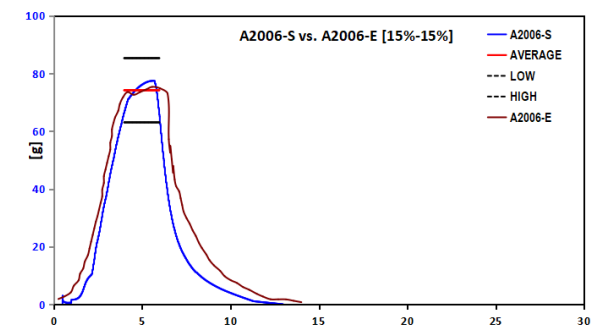
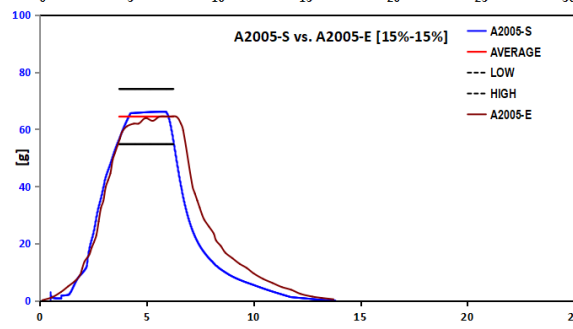
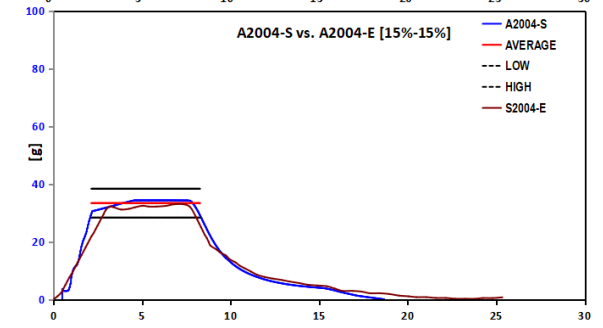
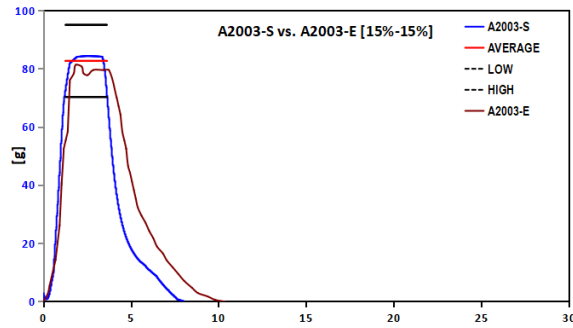
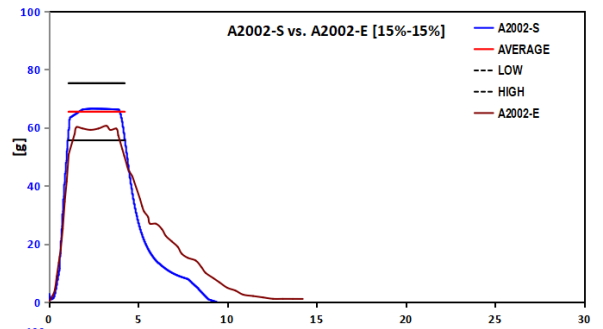
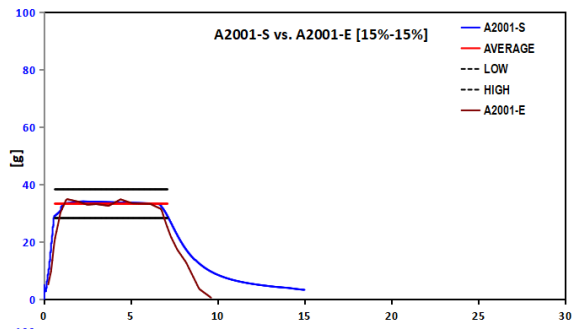
Acceleration [20 % & 10%]

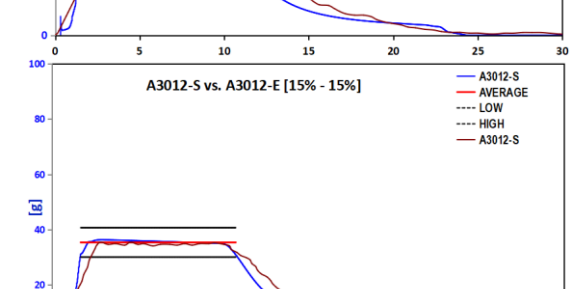
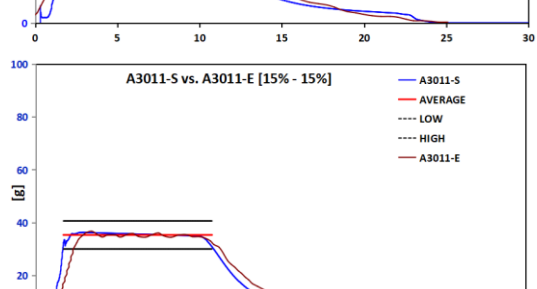
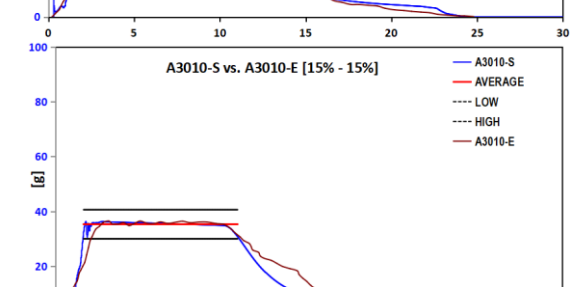
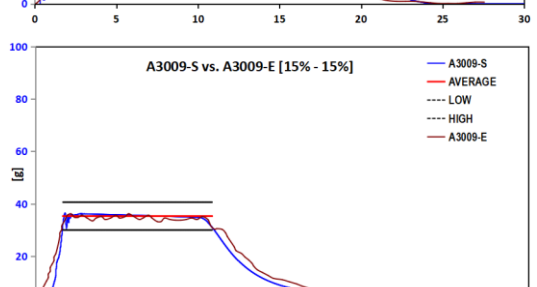
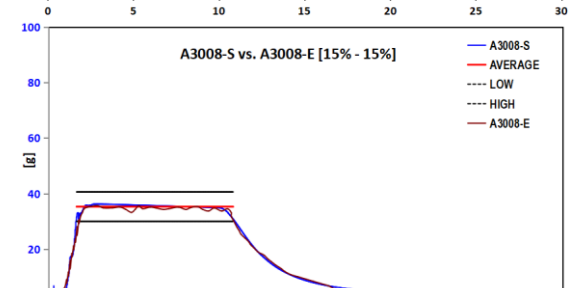
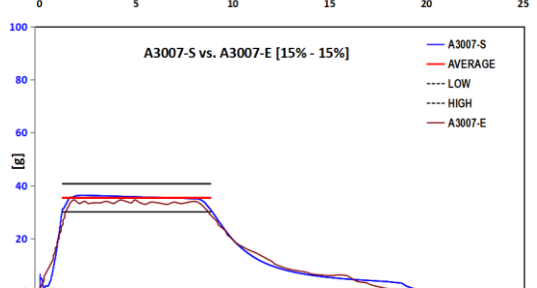
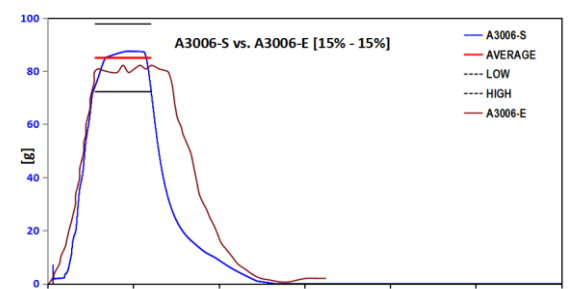
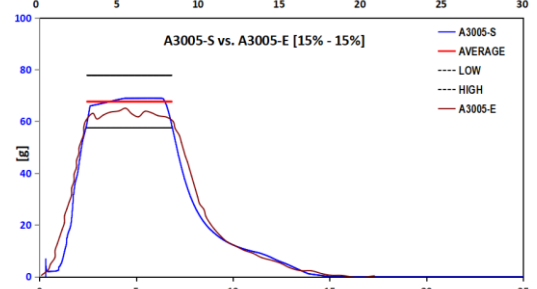
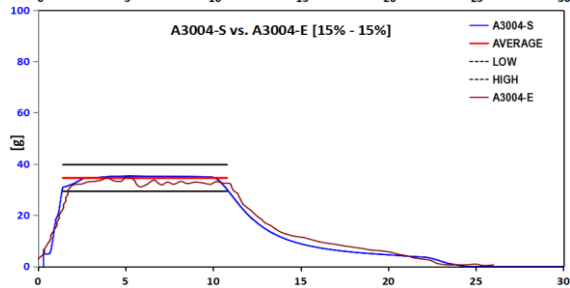
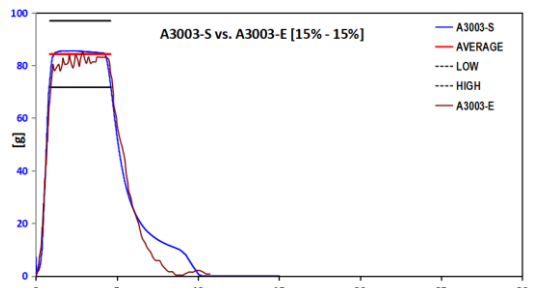
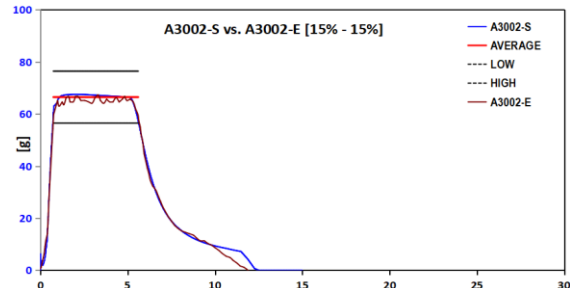
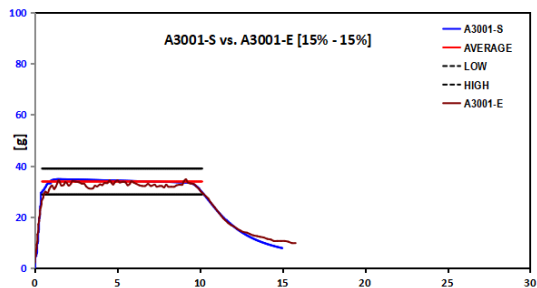


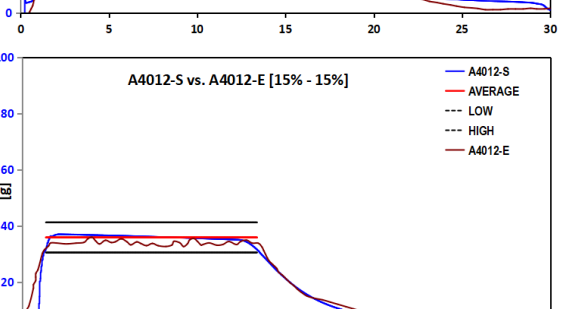
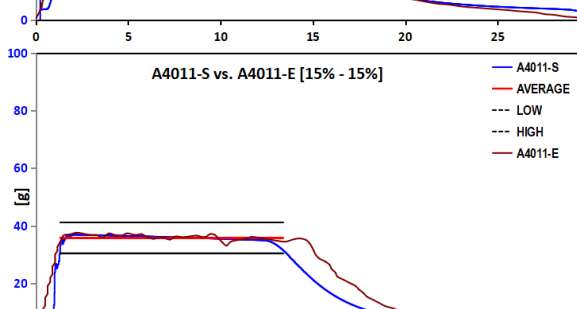
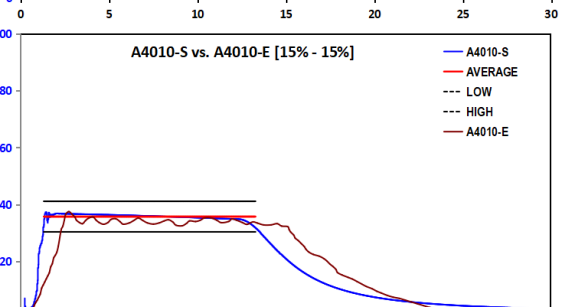
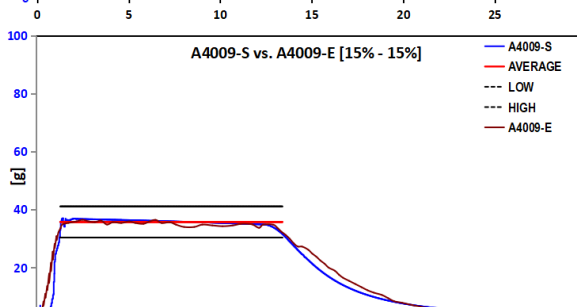
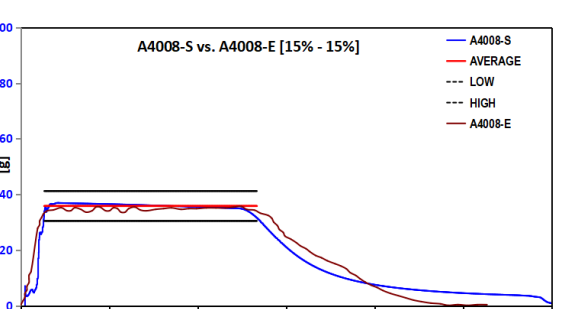
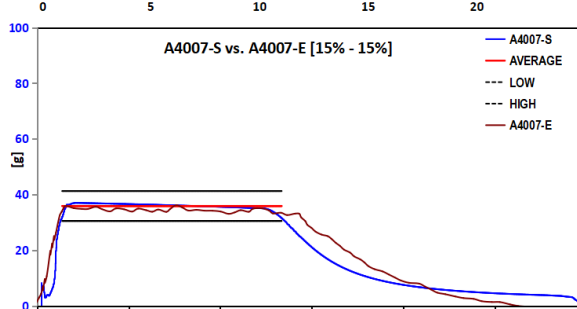
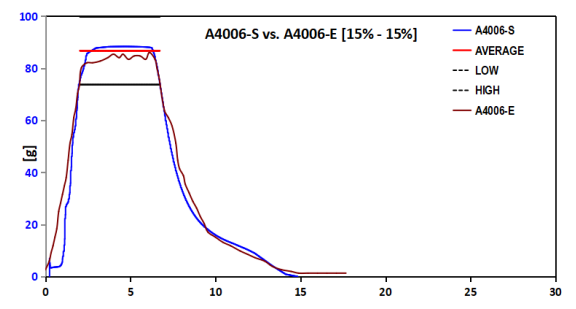
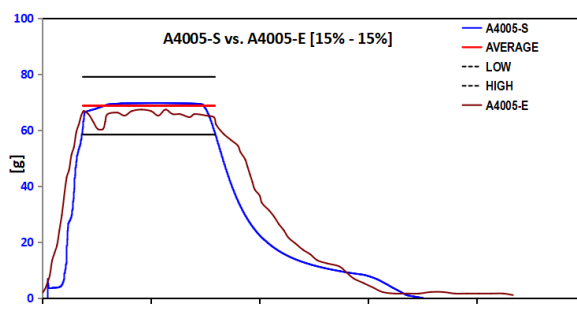
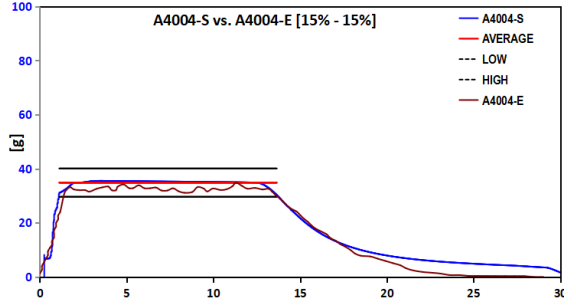
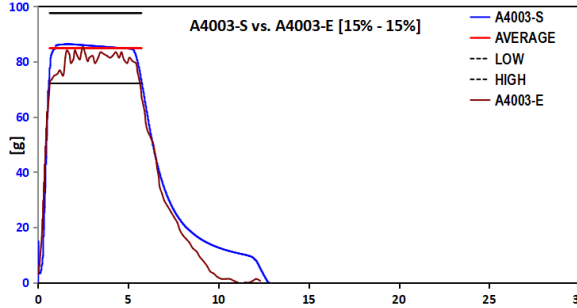
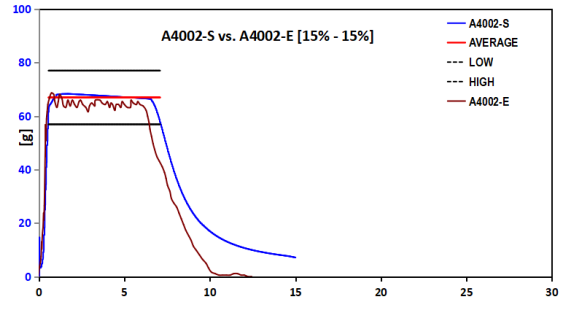
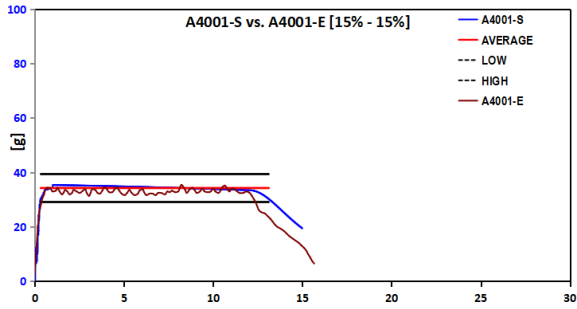
ACCELERATION [10 % & 20%]



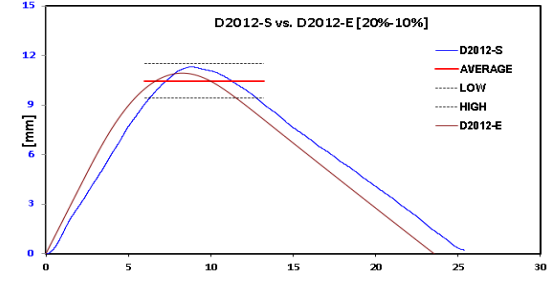
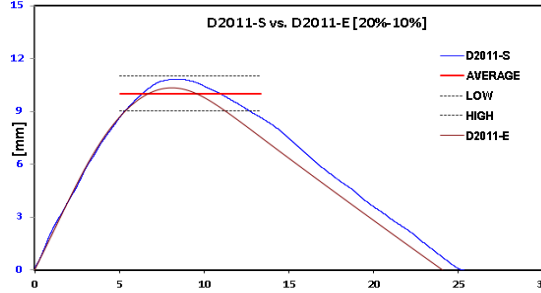
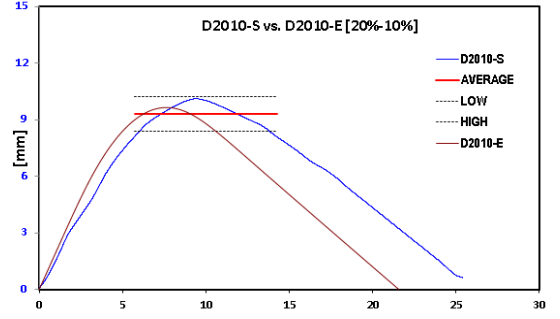
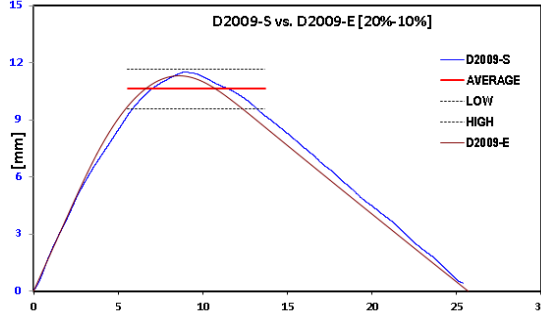
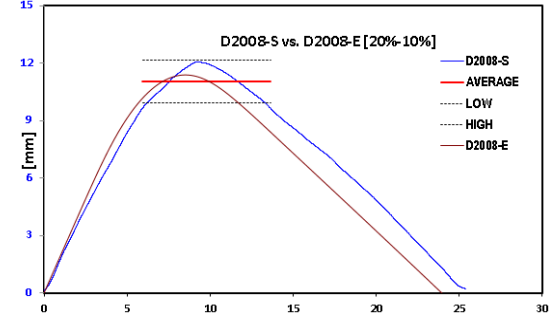
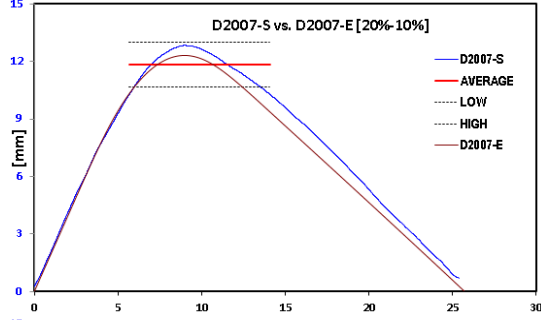
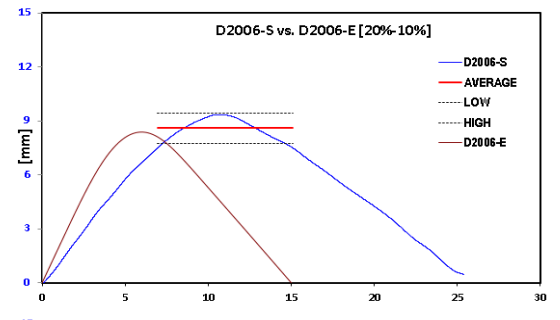
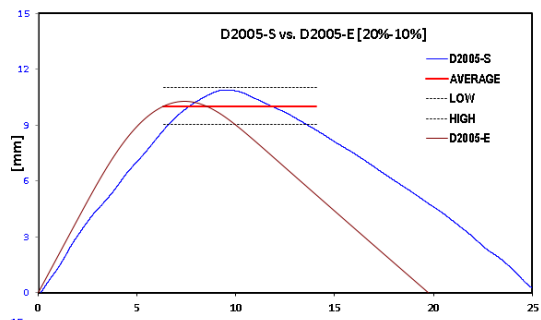
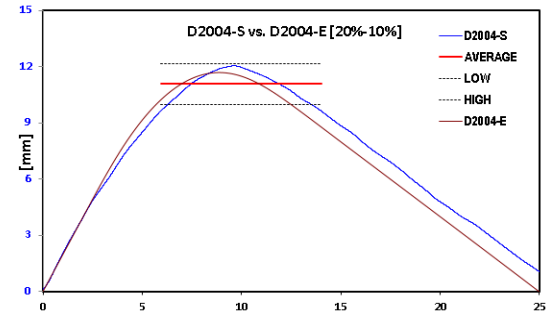
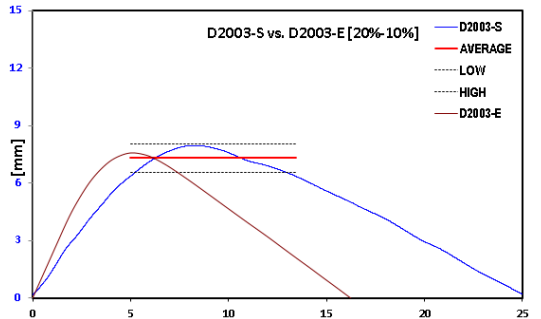
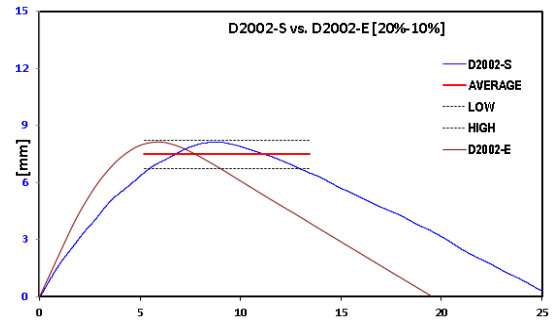
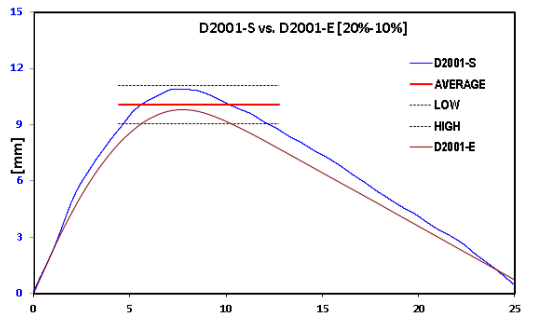
ACCELERATION [15 % & 15%]

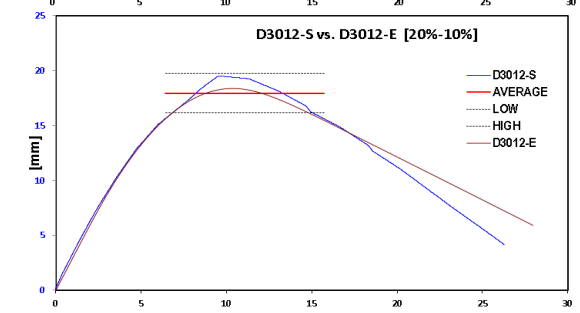
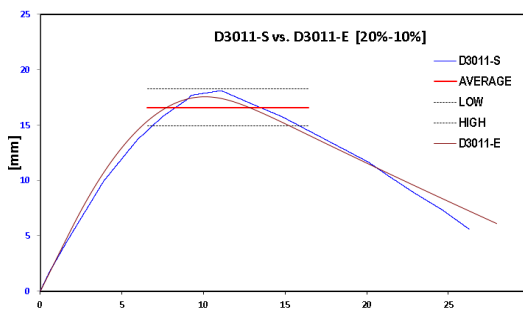
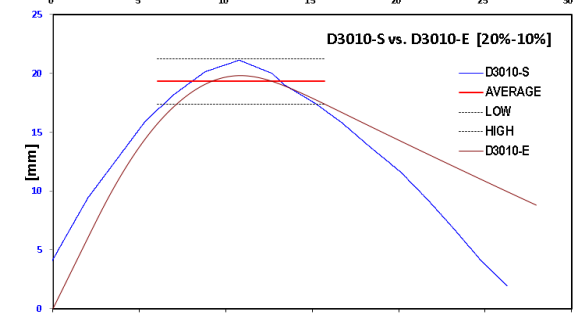
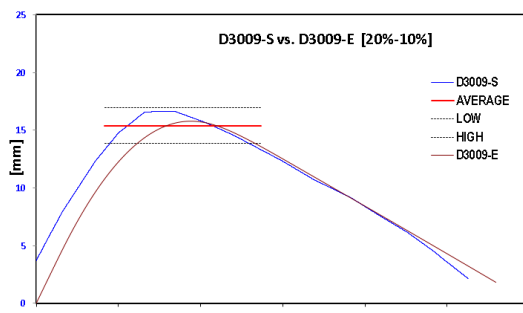
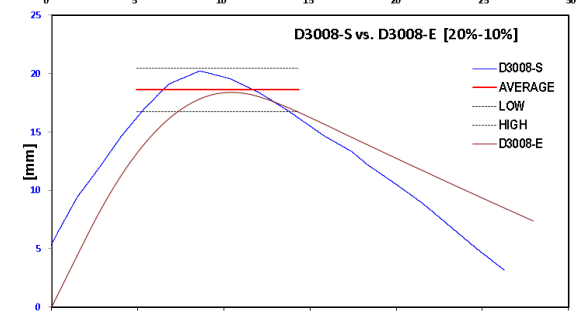
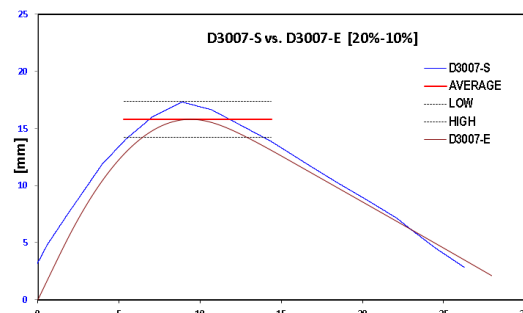
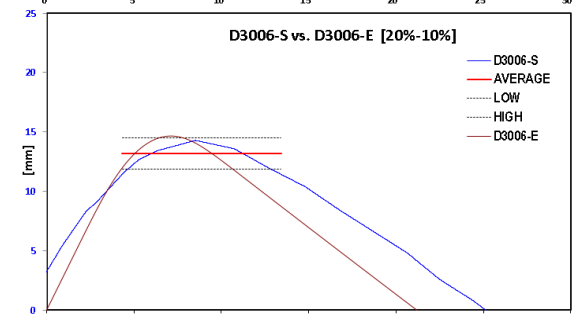
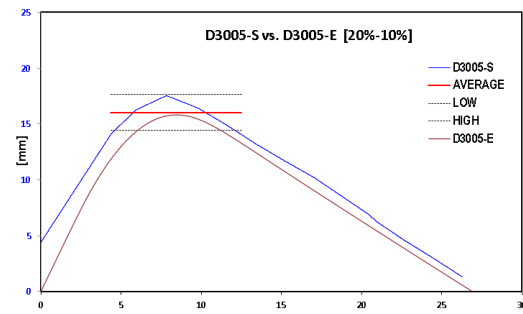
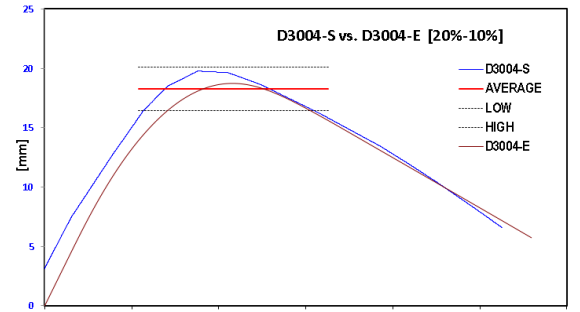
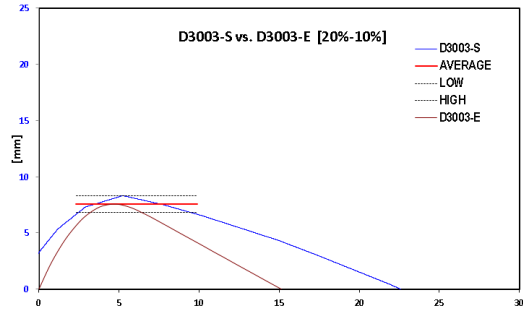
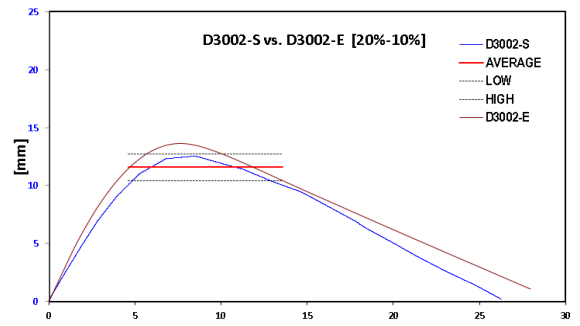
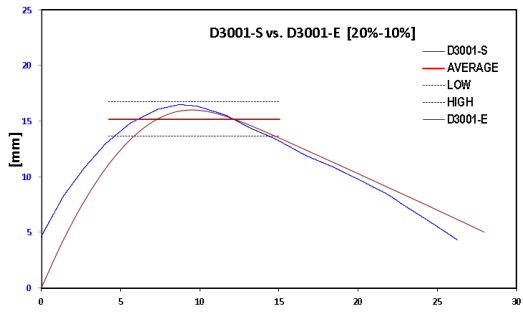




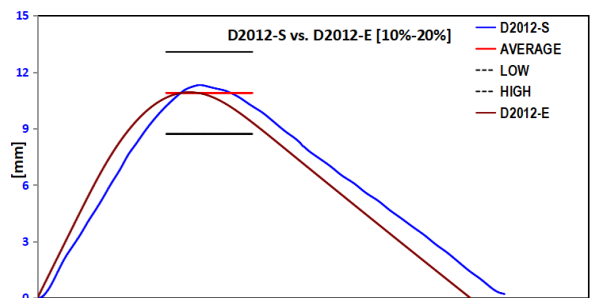
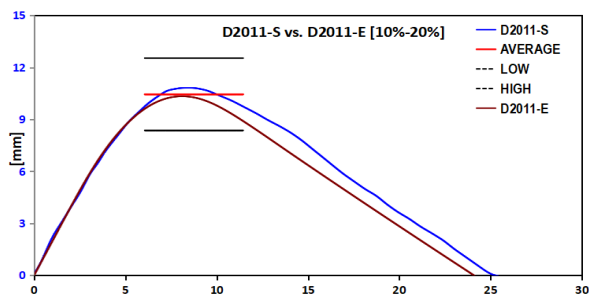
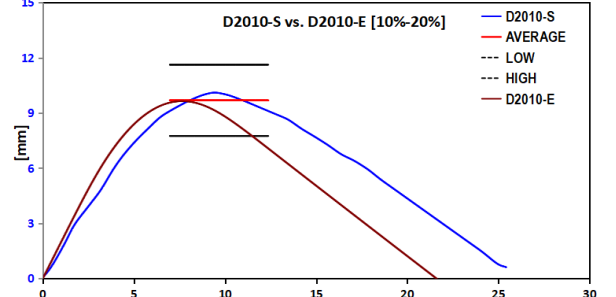
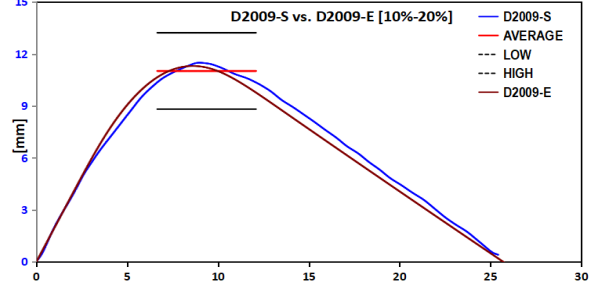
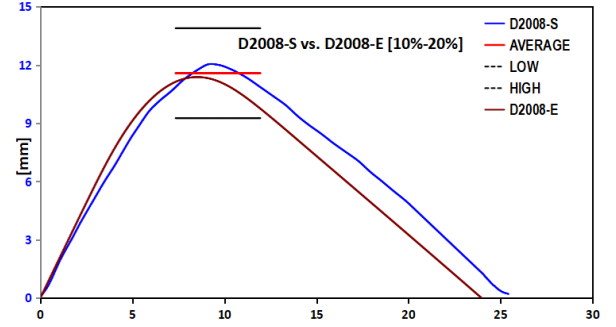
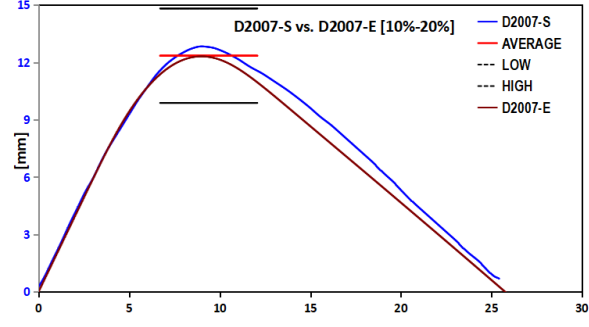
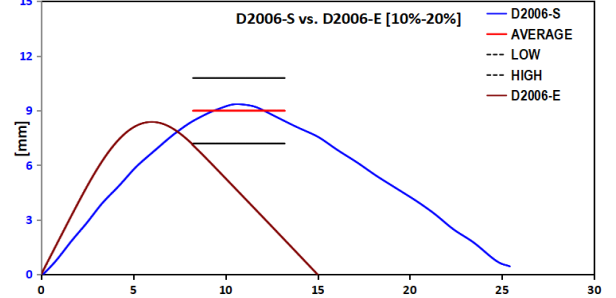
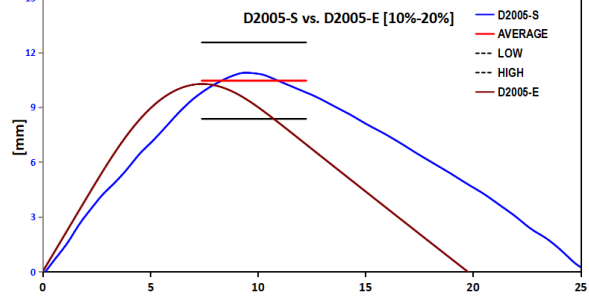
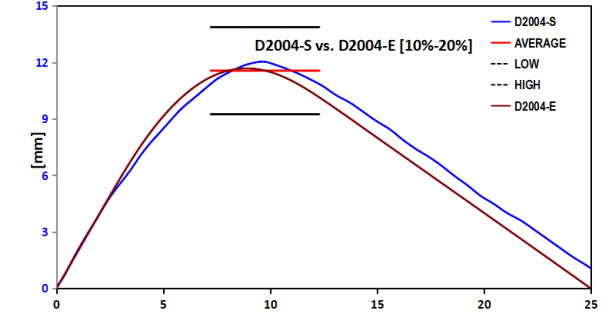
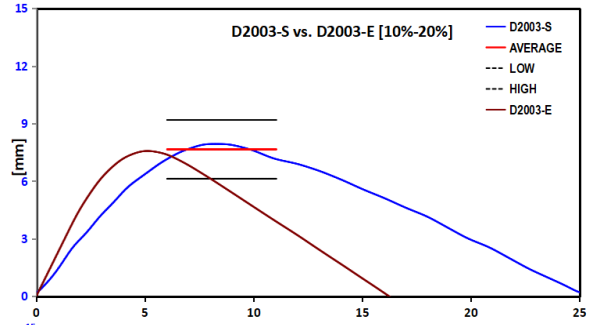
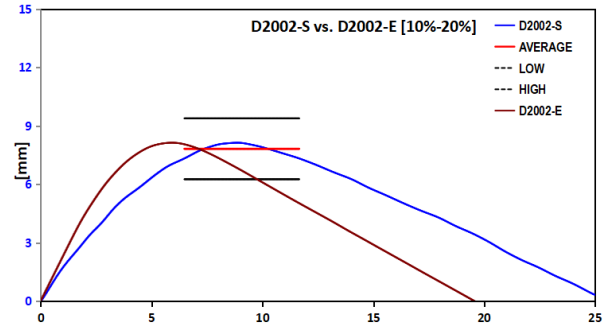
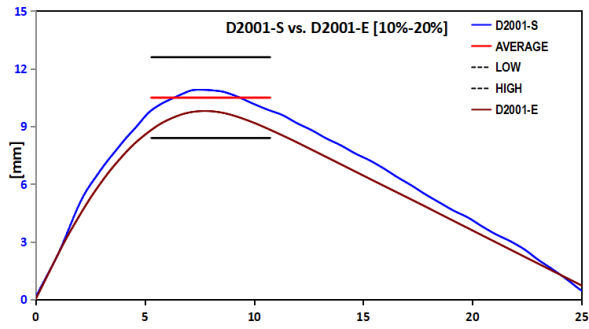


DISPLACEMENT [20 % & 10%]

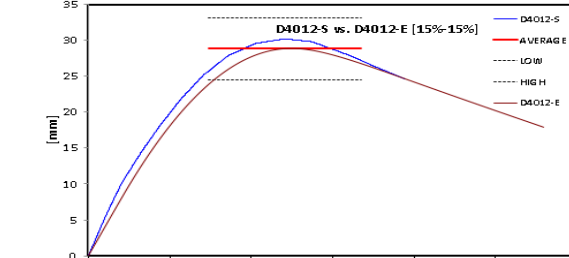
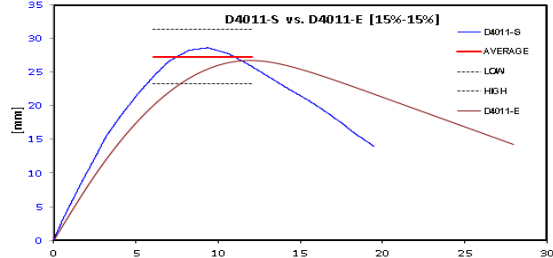
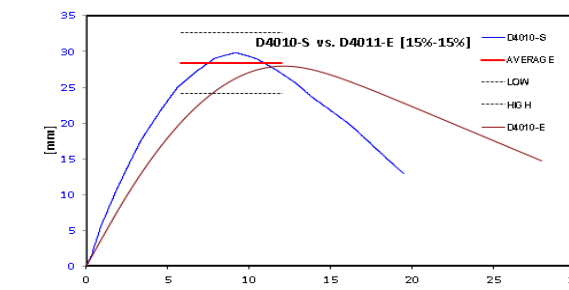
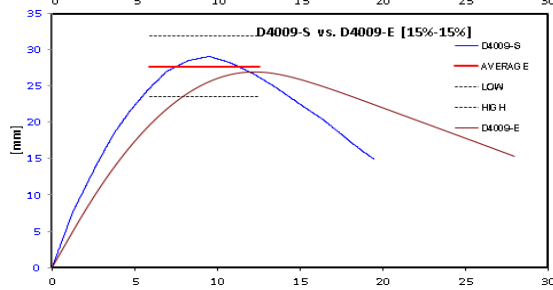
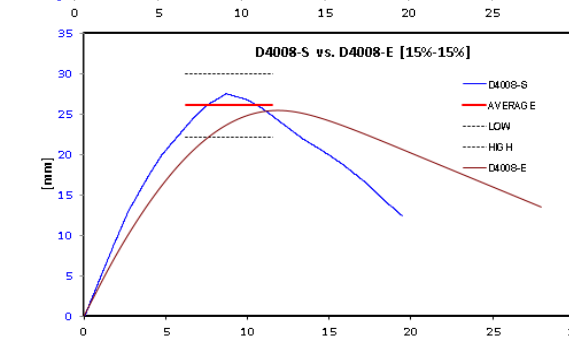
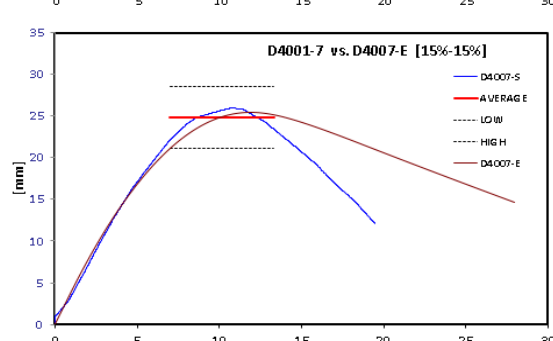
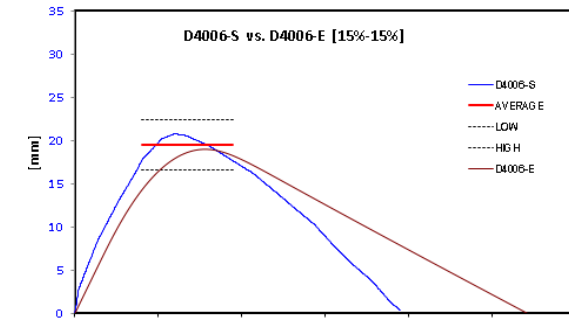
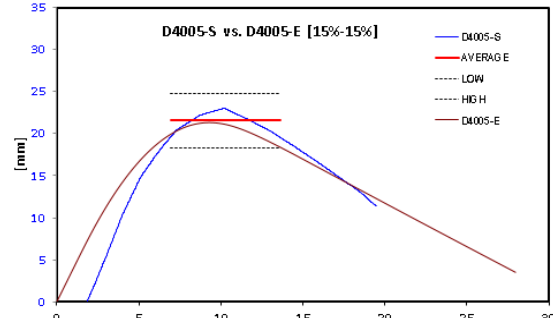
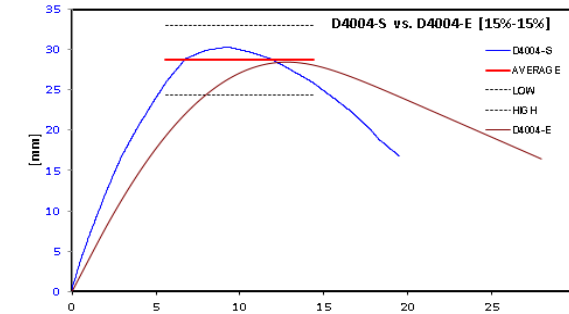
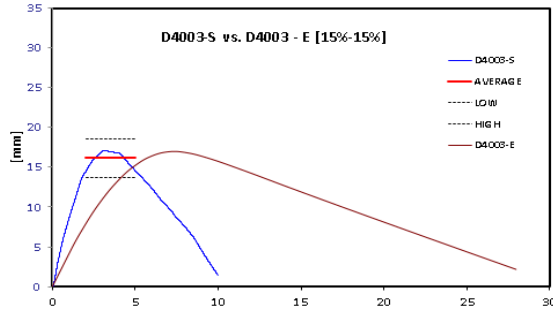
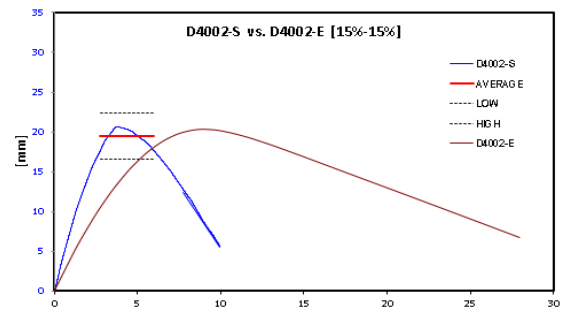
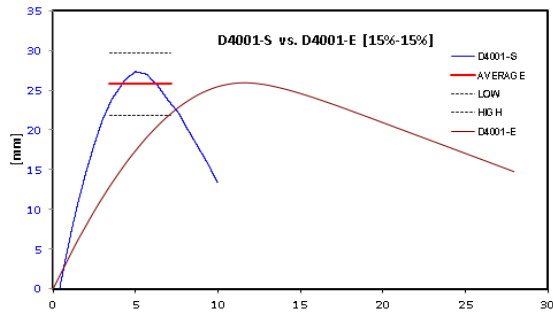




DISPLACEMENT [10 % & 20%]



DISPLACEMENT [15 % & 15%]

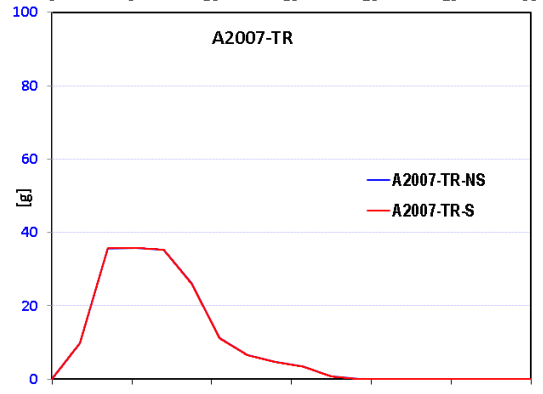
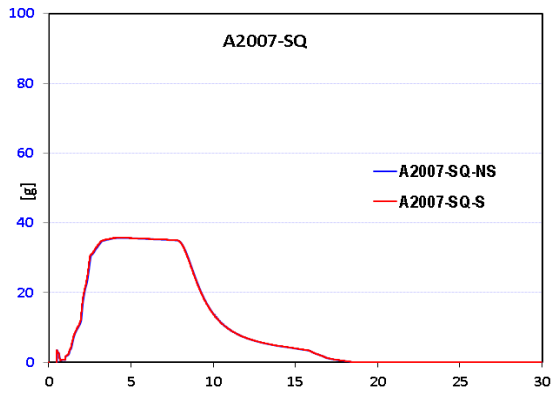
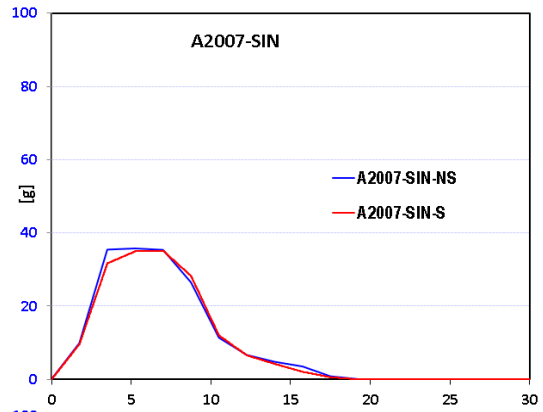
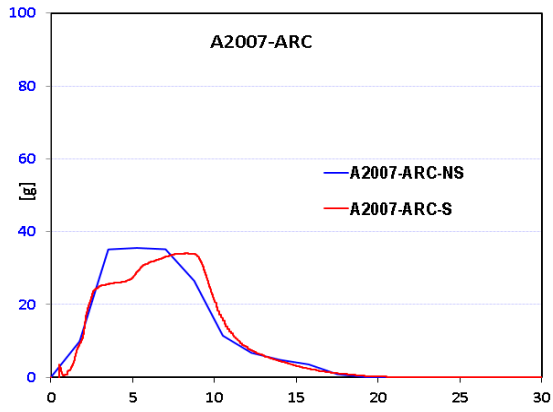


Appendix G

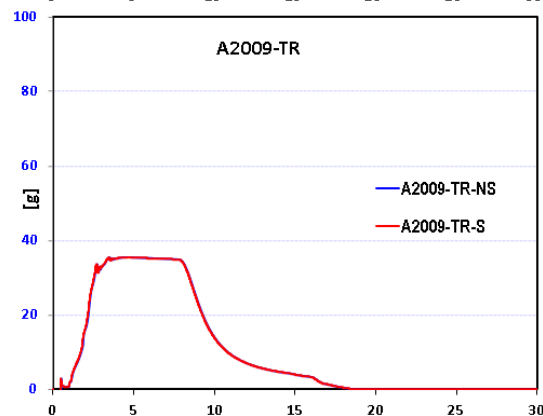
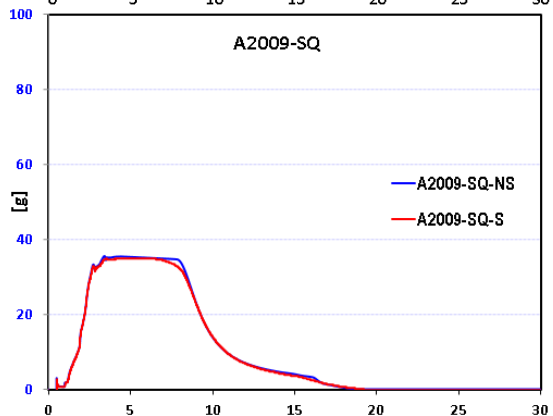
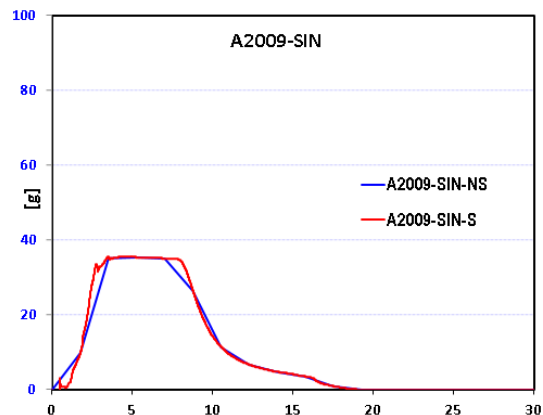
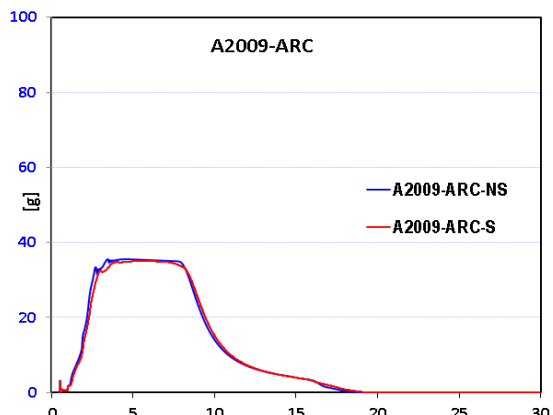
Acceleration (g) Value for Shape Design

Acceleration 2 m/s Shape

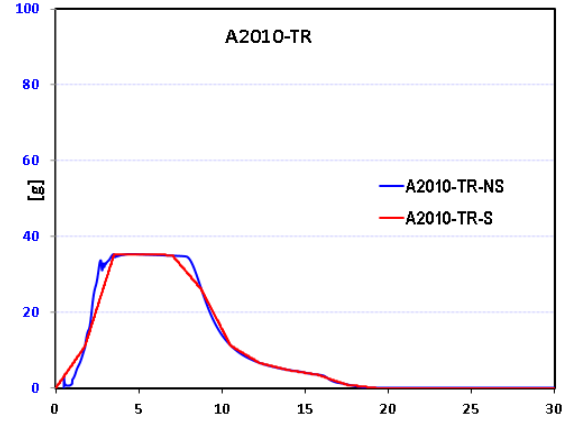
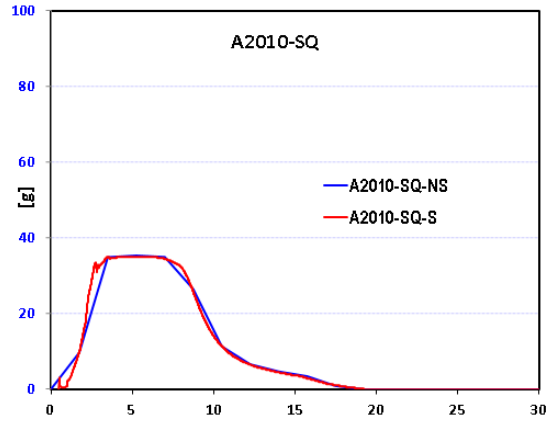
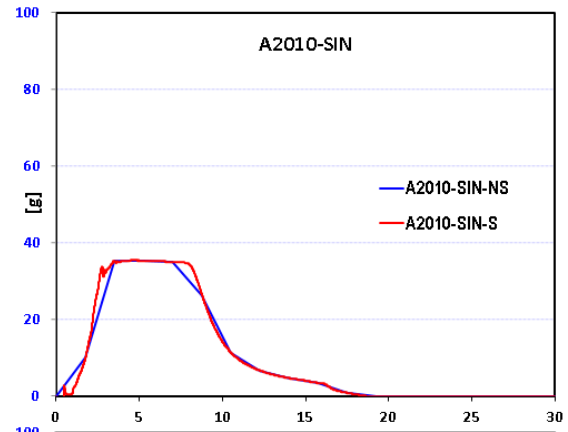
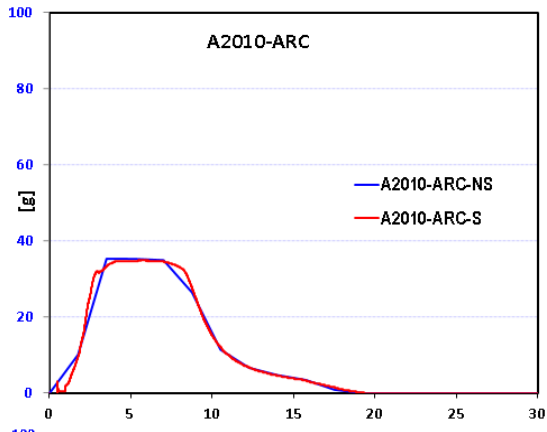
(No-Space Vs. Space)



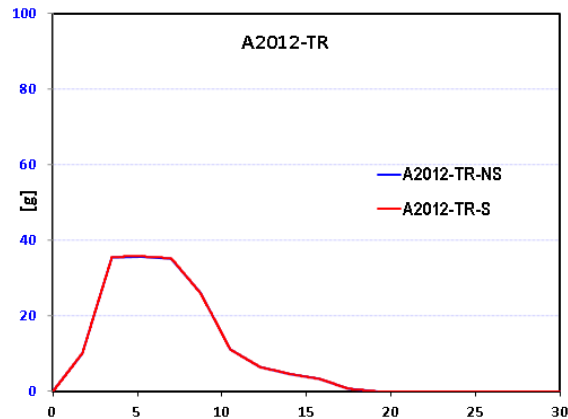
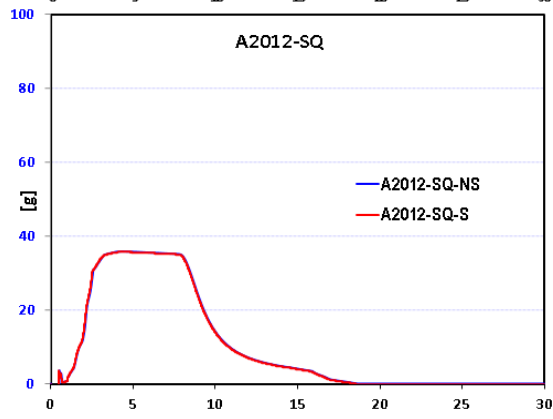
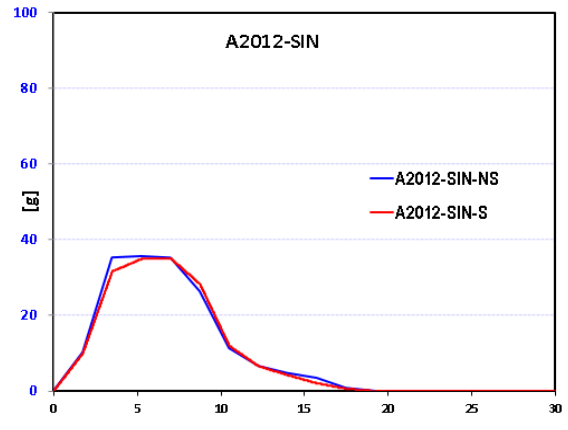
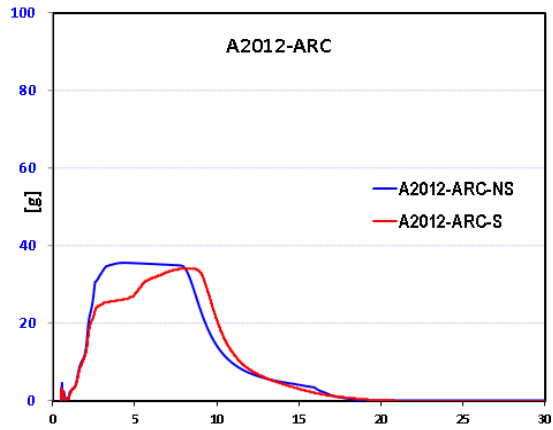
ACCELERATION SHAPE 2007 NO-SPACE vs. SPACE



ACCELERATION SHAPE 2009 NO-SPACE vs. SPACE

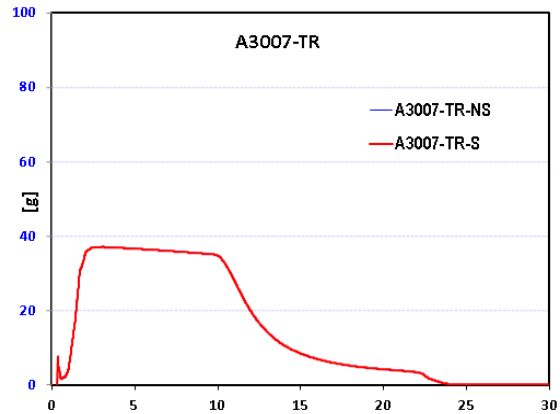
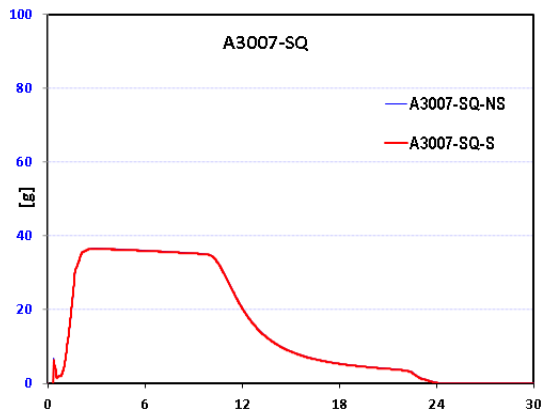
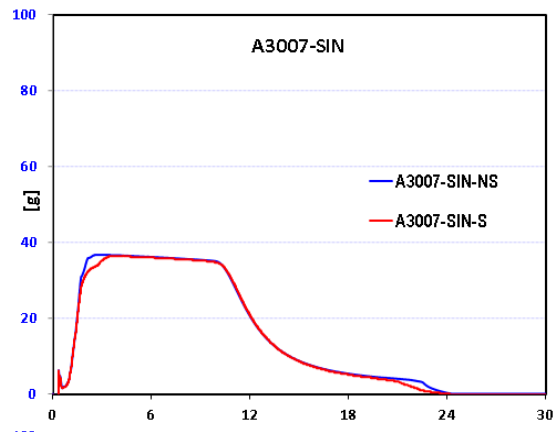
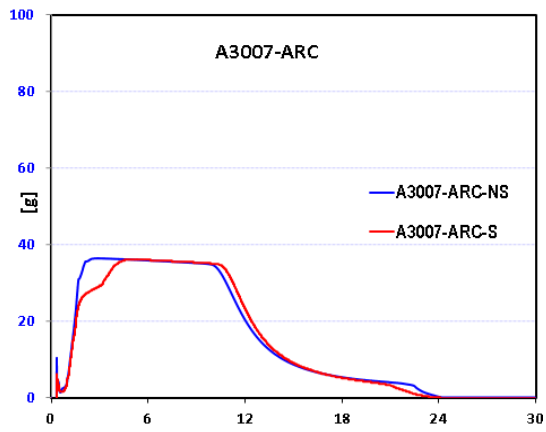


ACCELERATION SHAPE 2010 NO-SPACE vs. SPACE

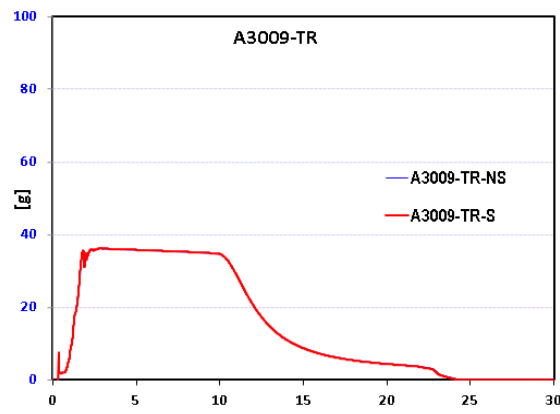
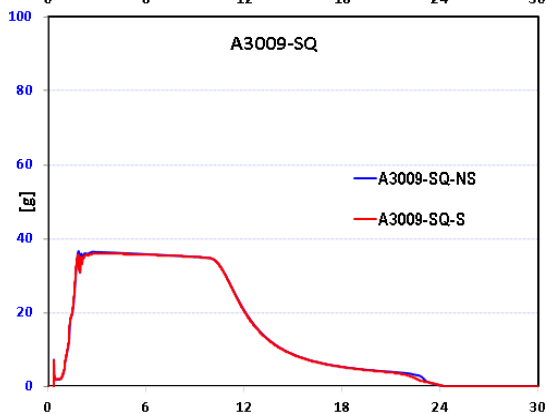
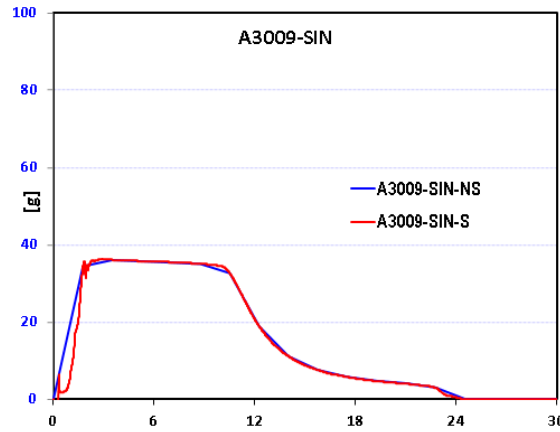
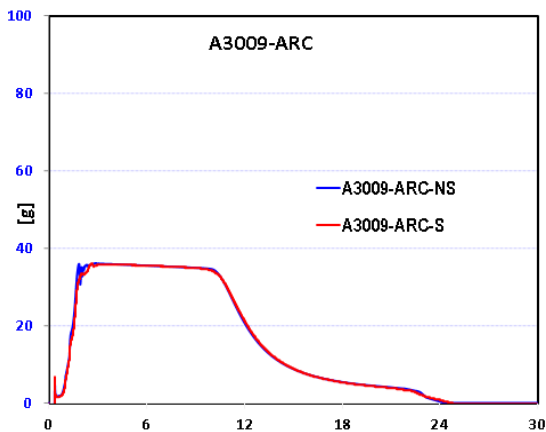


ACCELERATION SHAPE 2012 NO-SPACE vs. SPACE

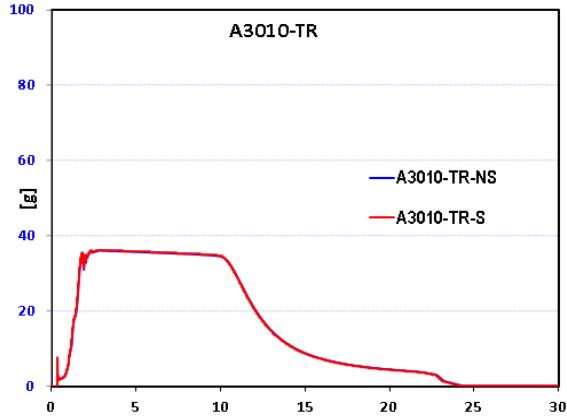
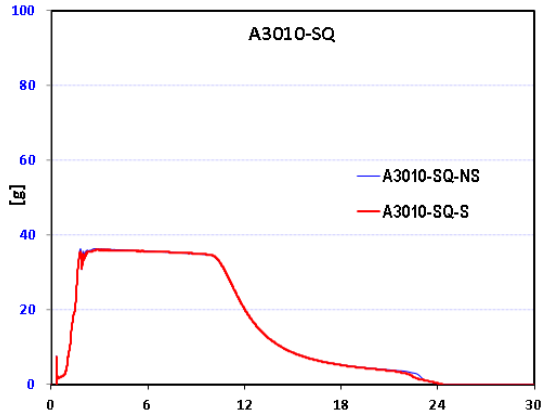
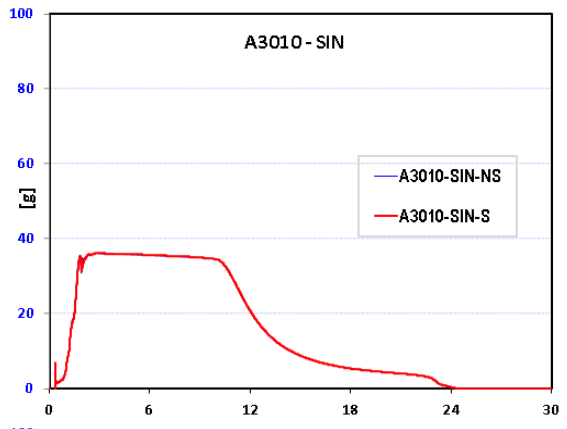
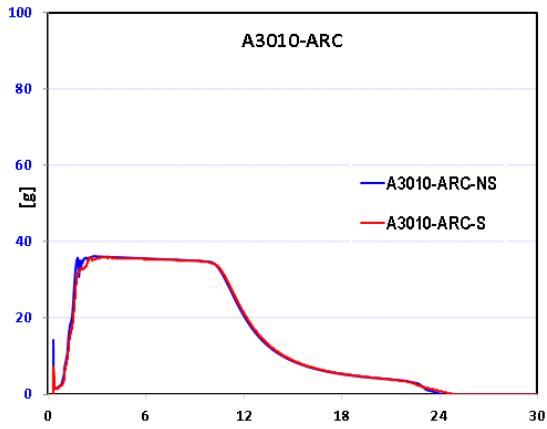
Acceleration 2 m/s Shape
(No-Space Vs. Space)



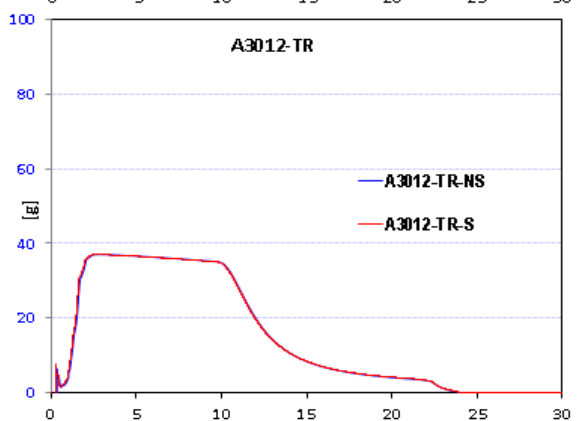
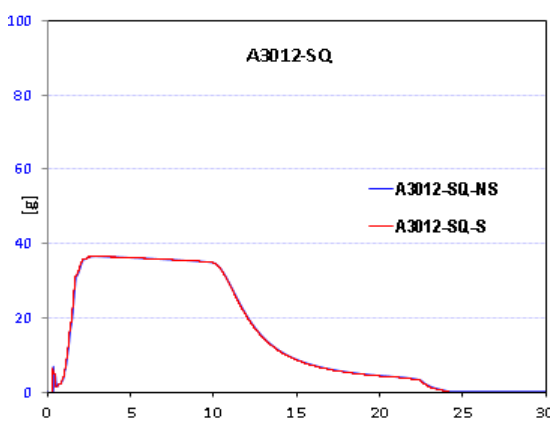
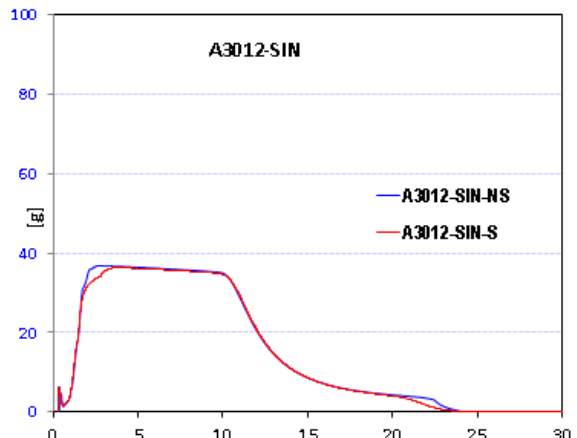
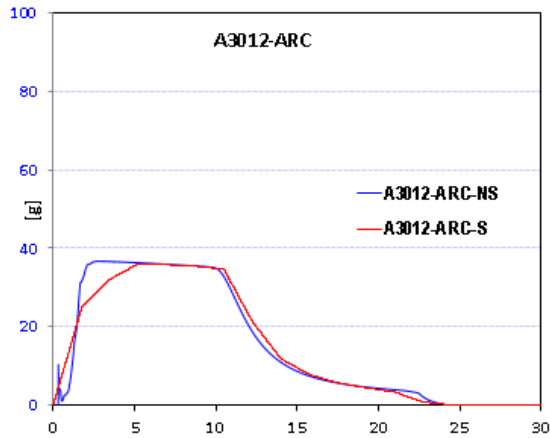
ACCELERATION SHAPE 3007 NO-SPACE vs. SPACE



ACCELERATION SHAPE 3009 NO-SPACE vs. SPACE

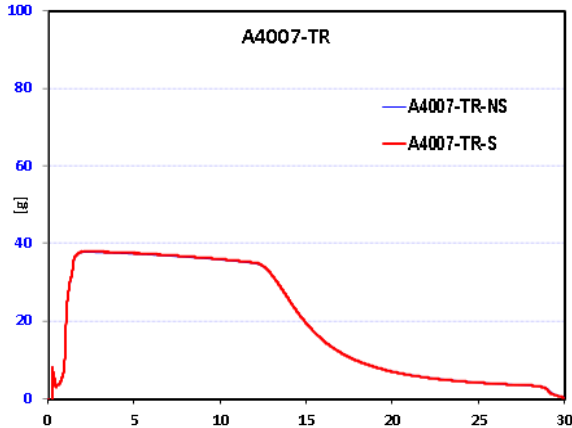
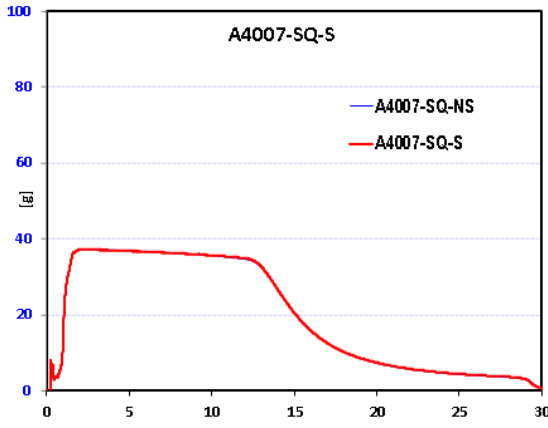
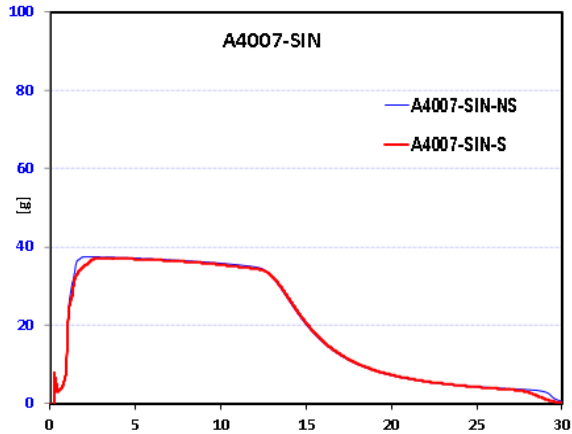
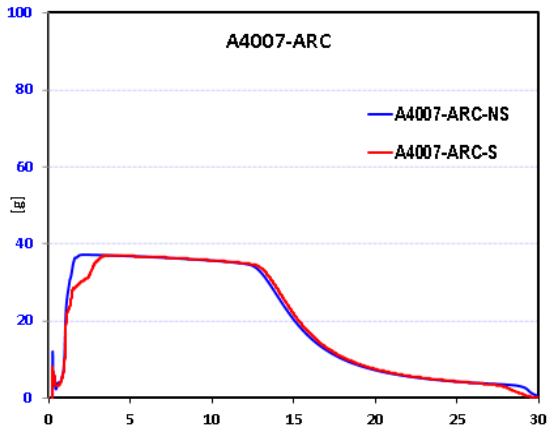


ACCELERATION SHAPE 3010 NO-SPACE vs. SPACE

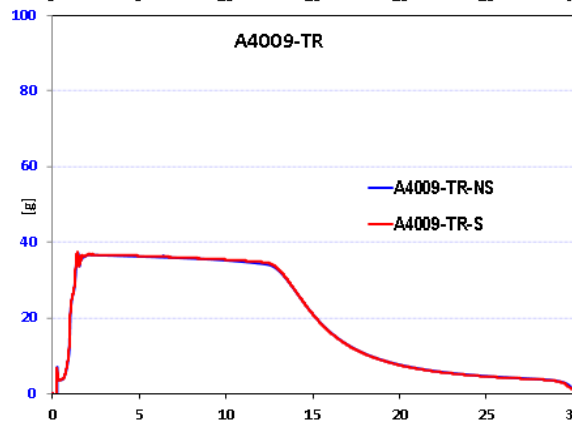
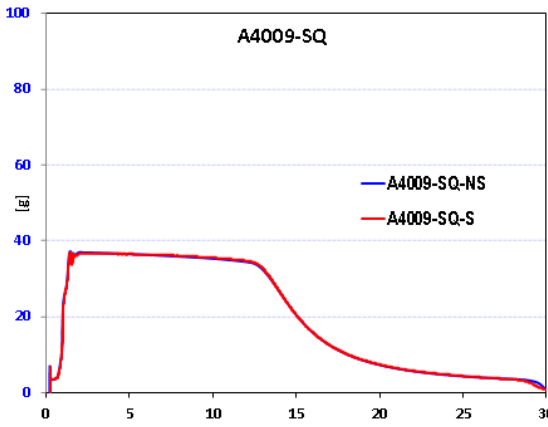
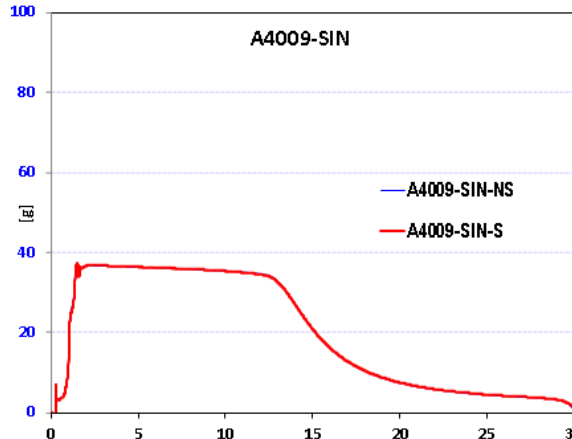
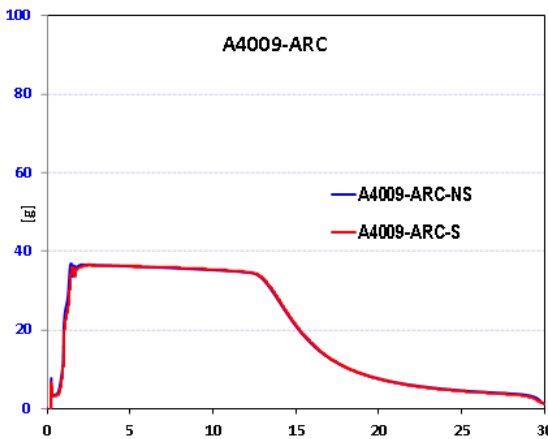


ACCELERATION SHAPE 3012 NO-SPACE vs. SPACE

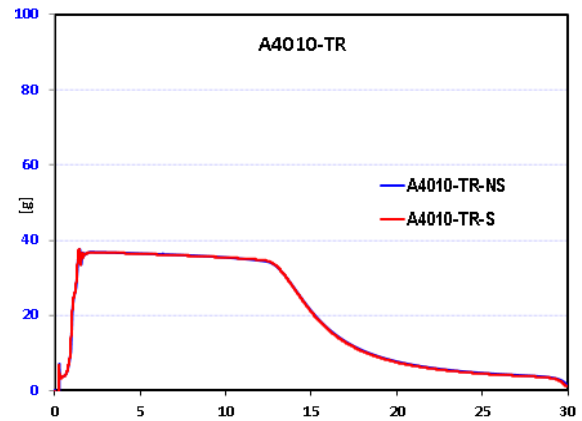
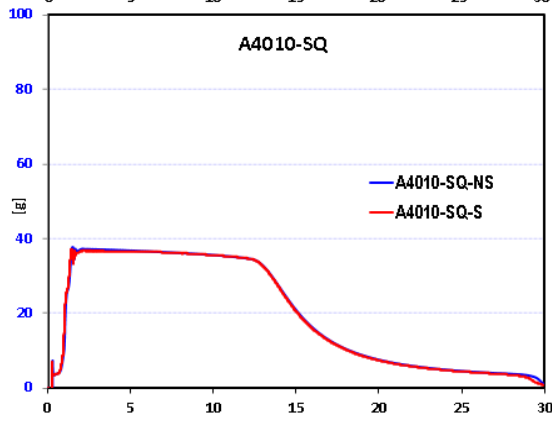
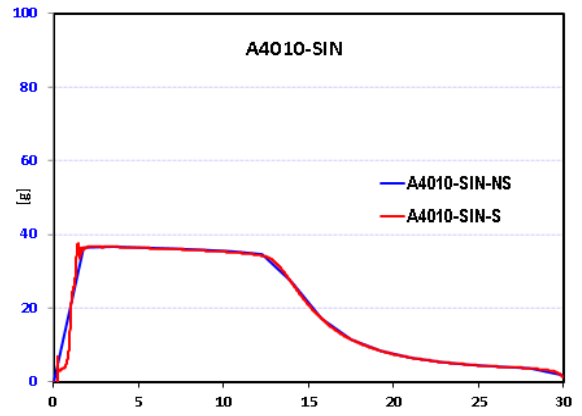
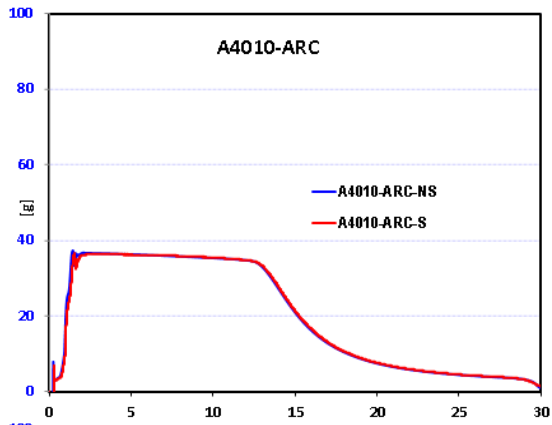
Acceleration 2 m/s Shape
(No-Space Vs. Space)



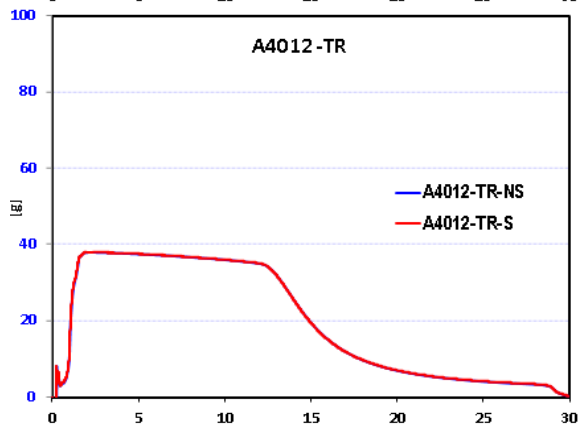
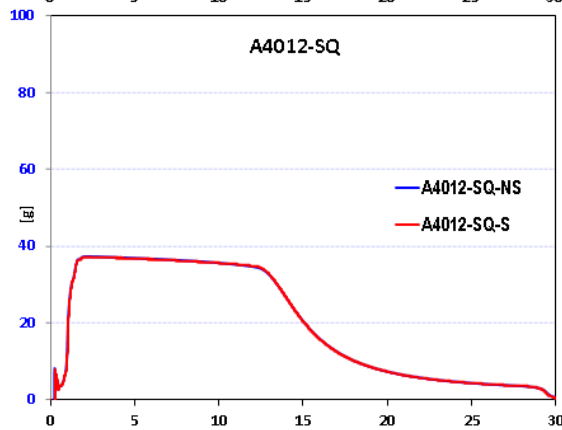
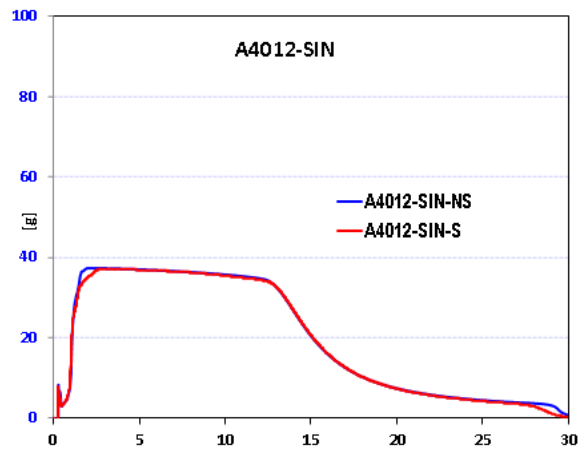
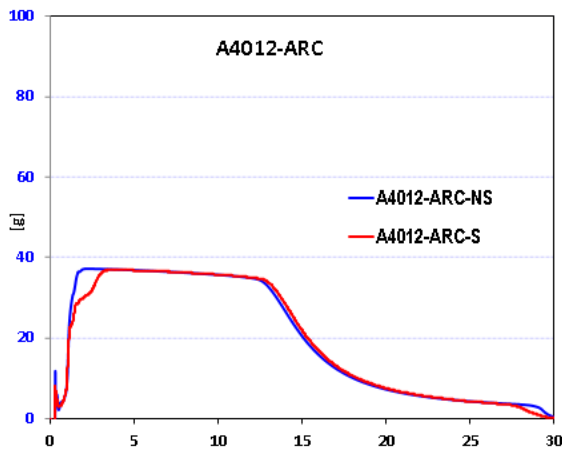
ACCELERATION SHAPE 4007 NO-SPACE vs. SPACE



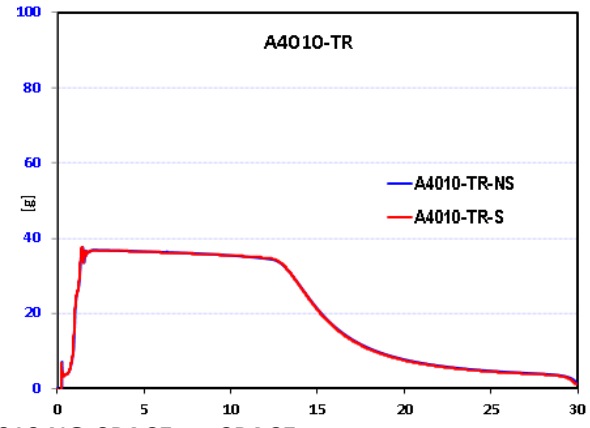
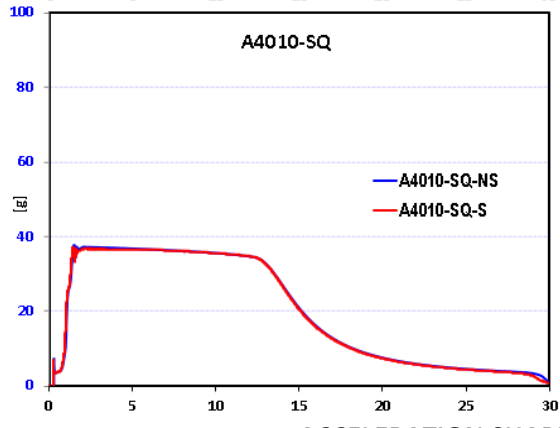
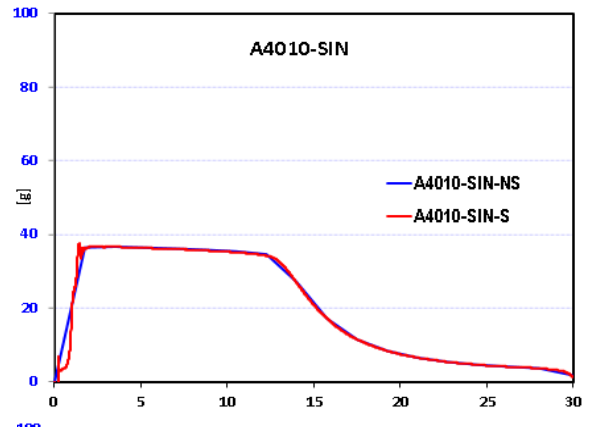
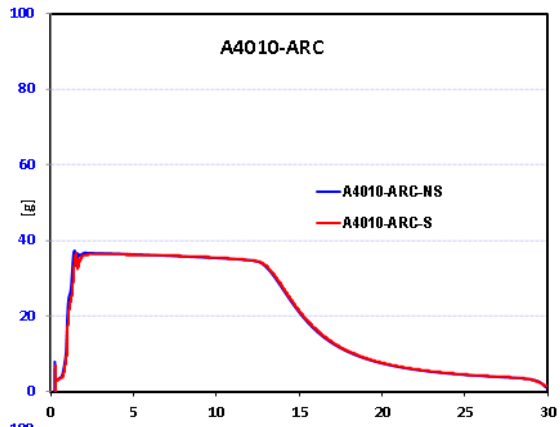
ACCELERATION SHAPE 4009 NO-SPACE vs. SPACE



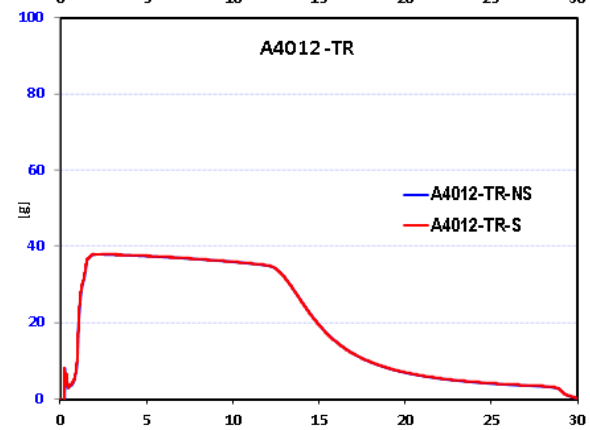
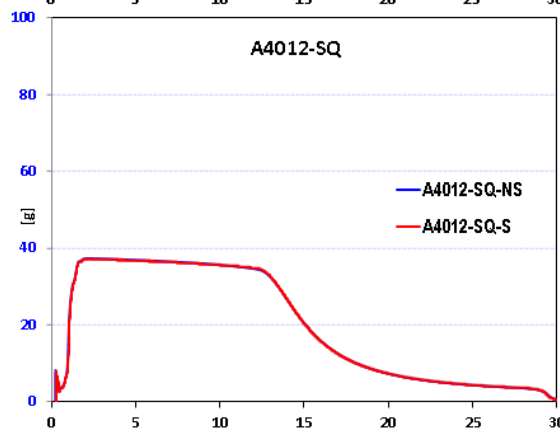
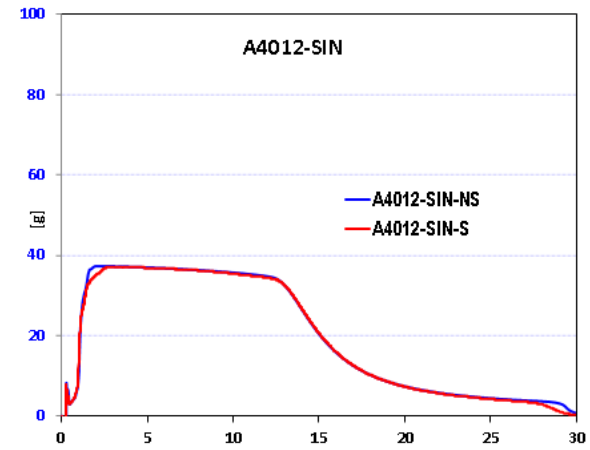
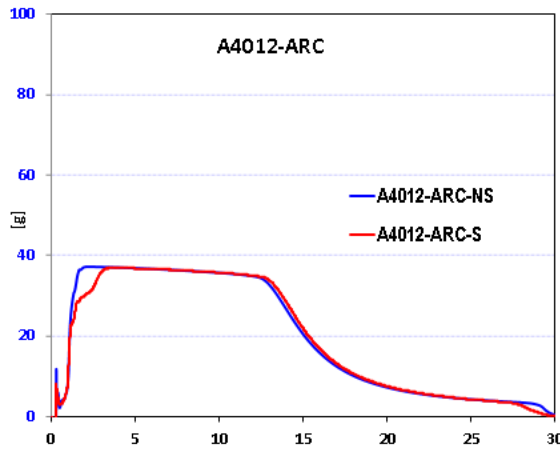
ACCELERATION SHAPE 4010 NO-SPACE vs. SPACE



ACCELERATION SHAPE 4012 NO-SPACE vs. SPACE



ACCELERATION SHAPE 4010 NO-SPACE vs. SPACE



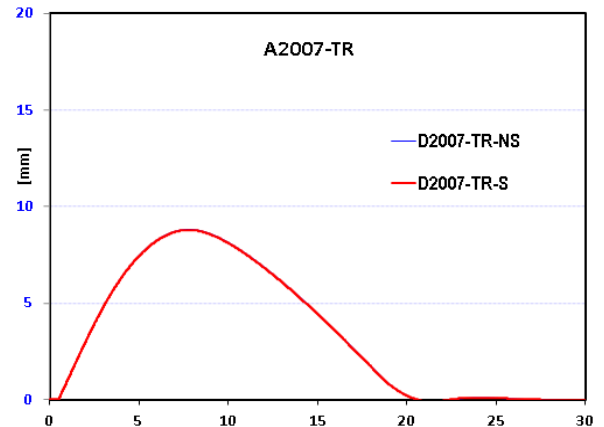
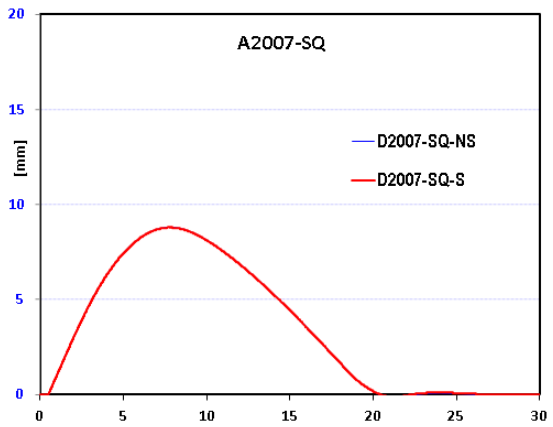
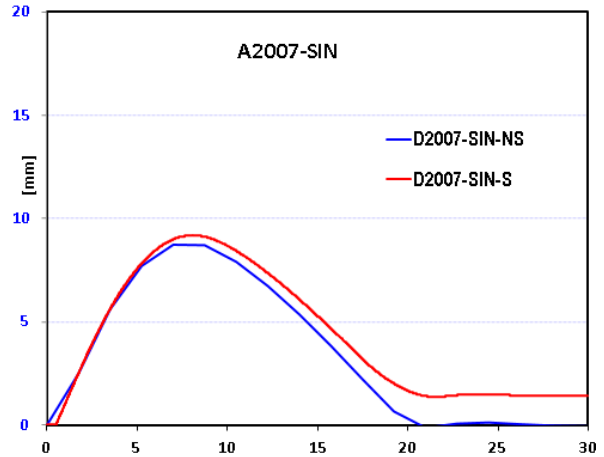
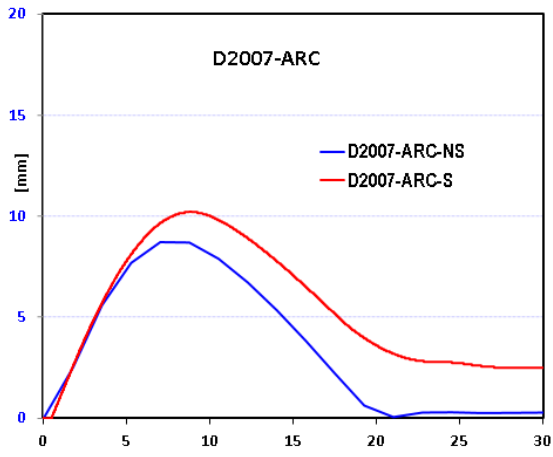
ACCELERATION SHAPE 4012 NO-SPACE vs. SPACE

Appendix H

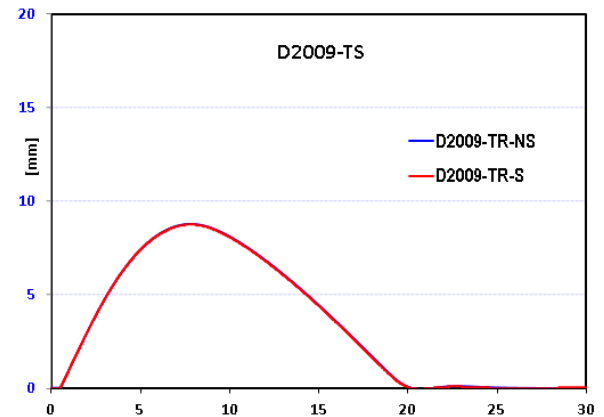
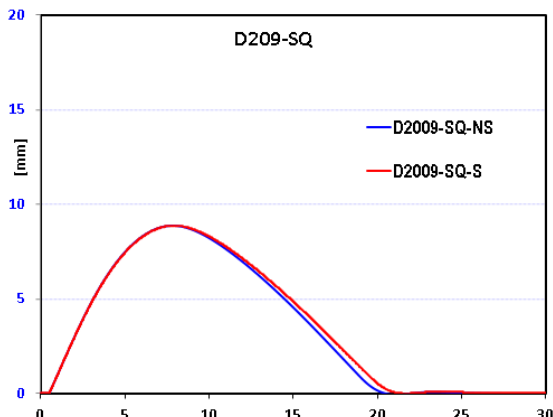
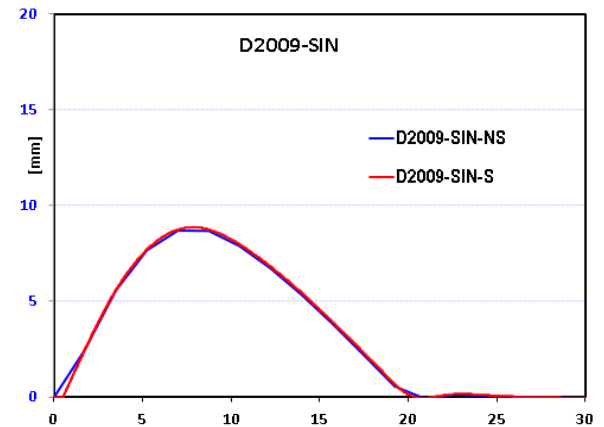
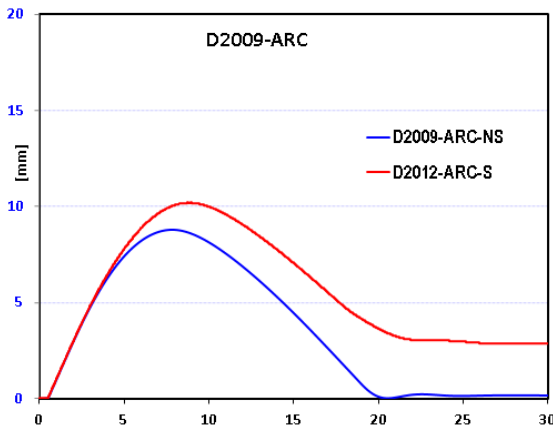
Displacement value for Shape Design

Displacement 2 m/s Shape

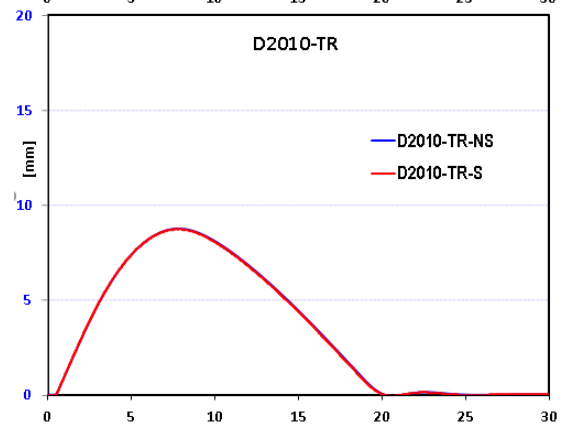
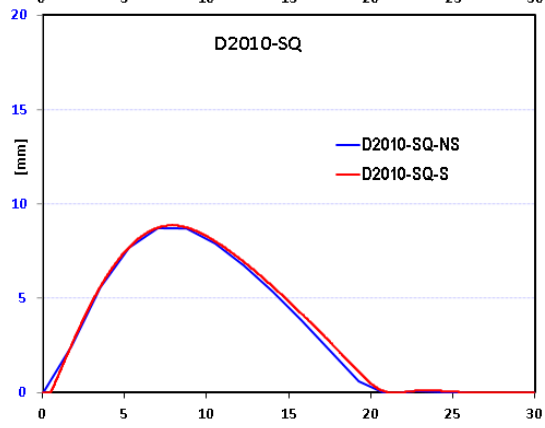
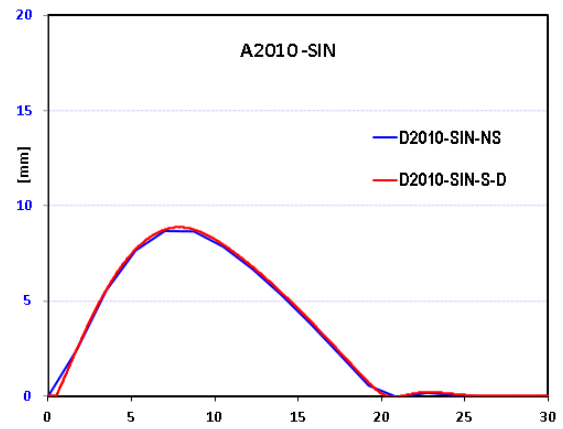
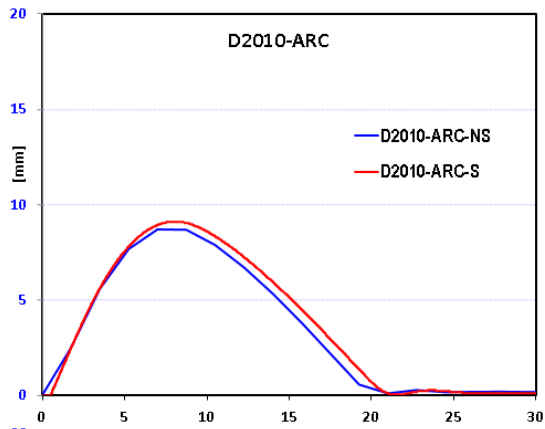
(No-Space Vs. Space)



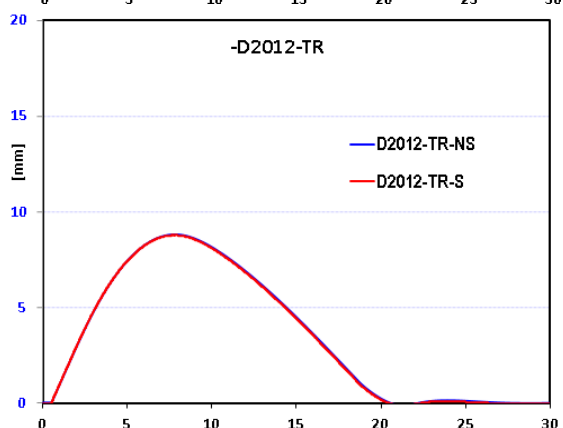
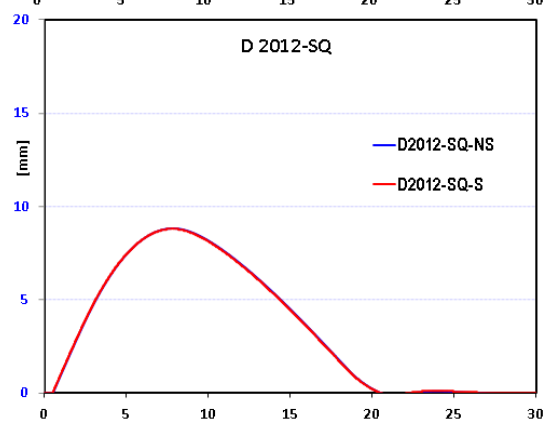
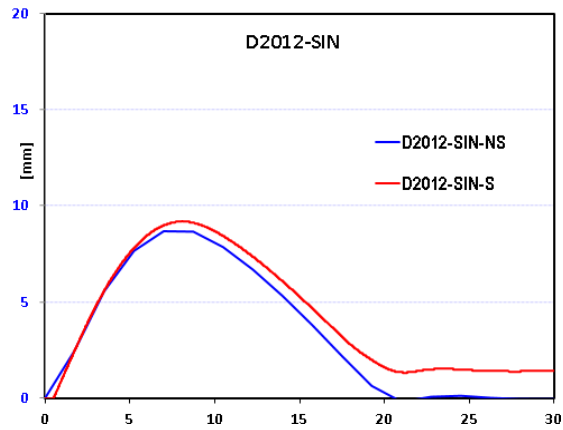
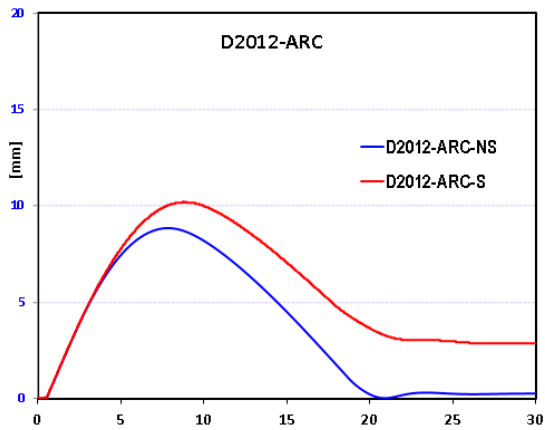
DISPLACEMENT 2007 NO-SPACE vs. SPACE



DISPLACEMENT 2009 NO-SPACE vs. SPACE



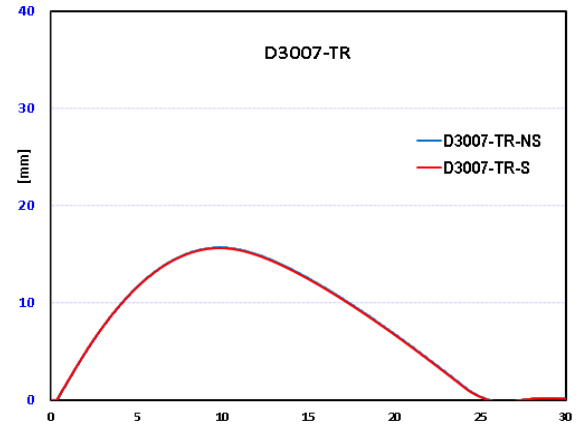
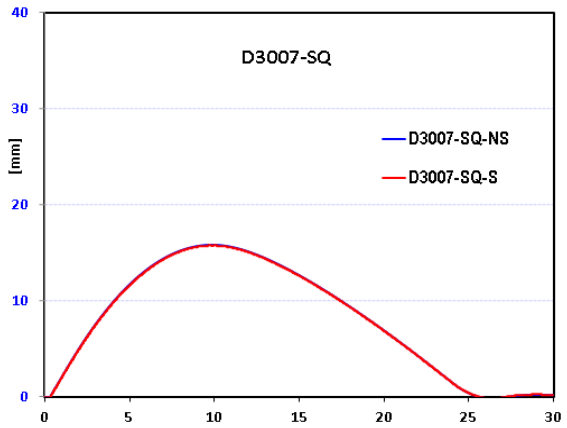
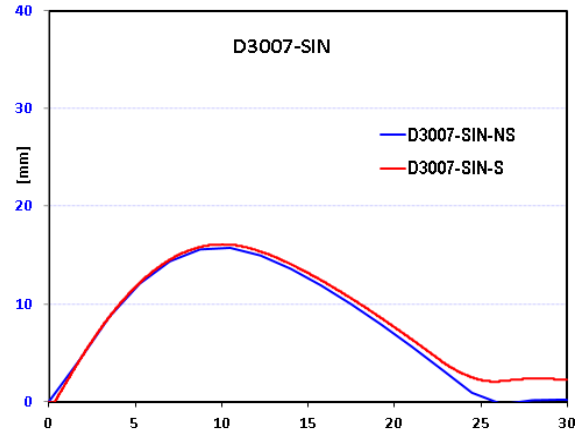
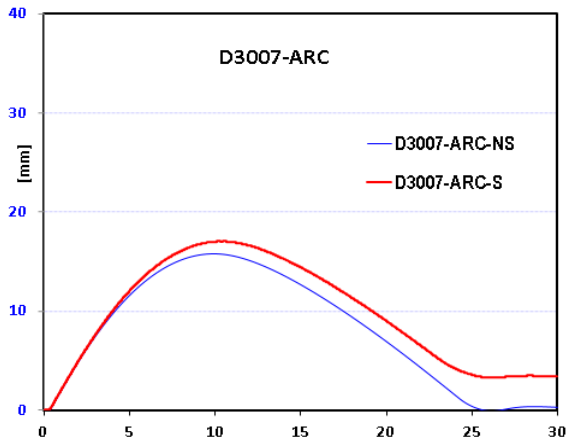
DISPLACEMENT 2010 NO-SPACE vs. SPACE



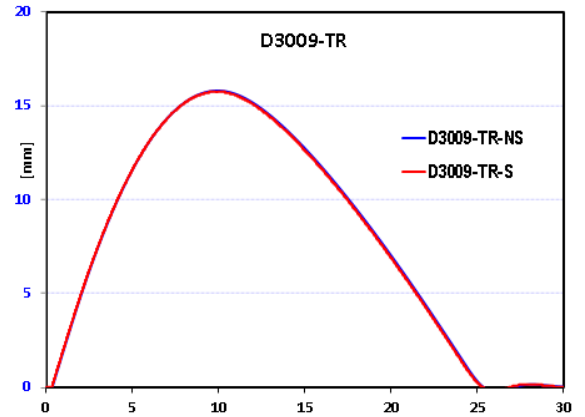
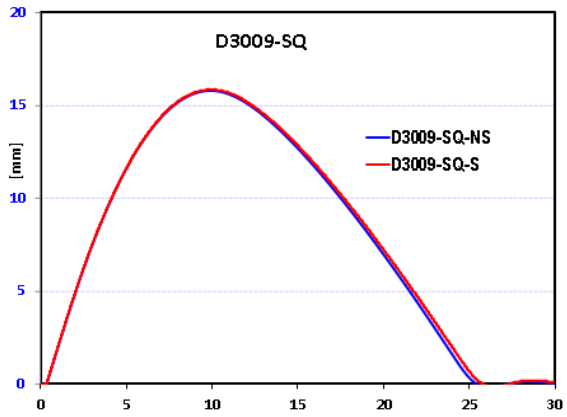
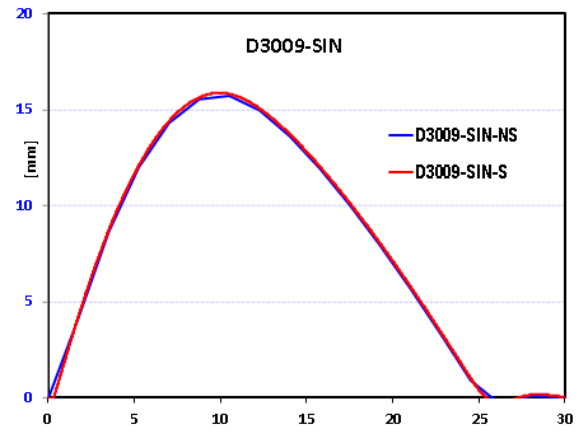
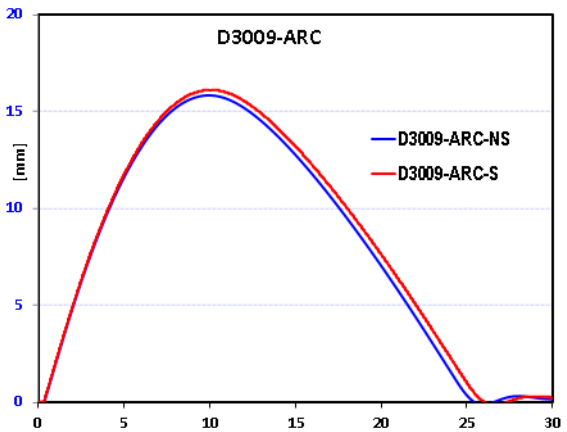
DISPLACEMENT 2012 NO-SPACE vs. SPACE

Displacement 3 m/s Shape

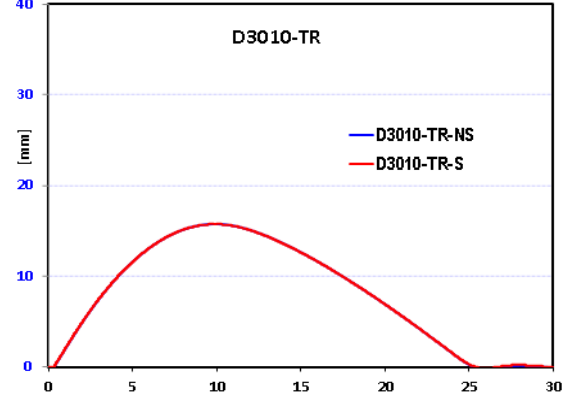
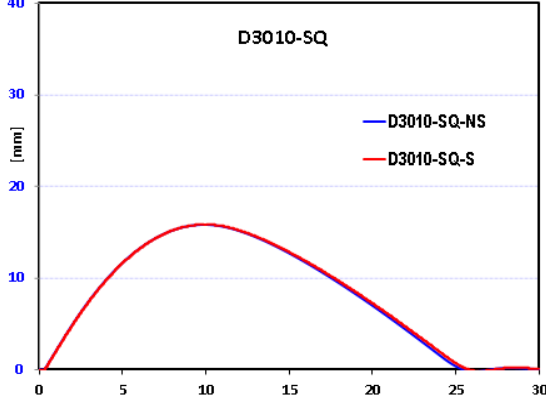
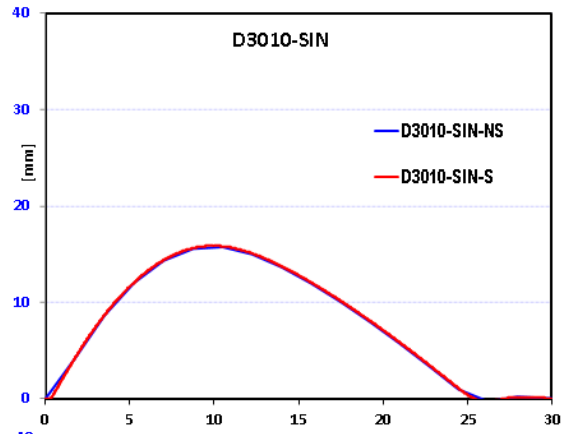
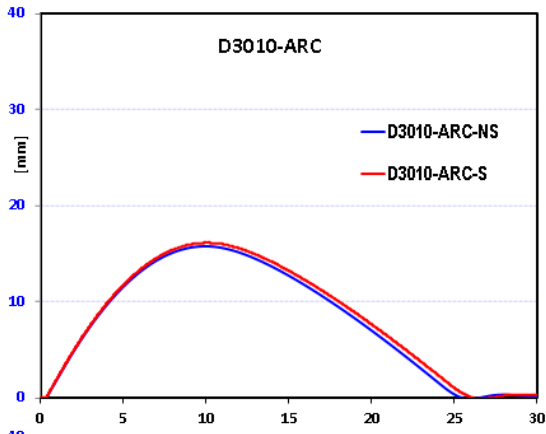
(No-Space Vs. Space)



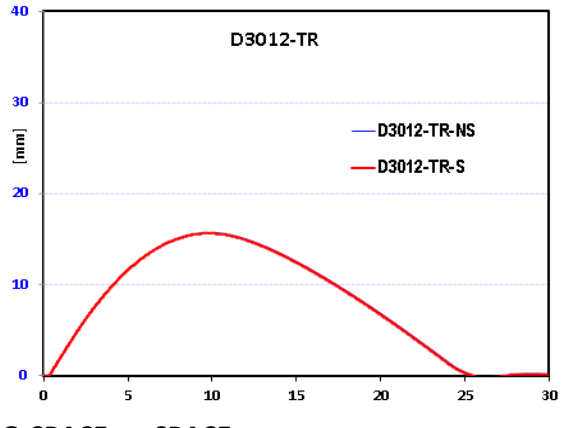
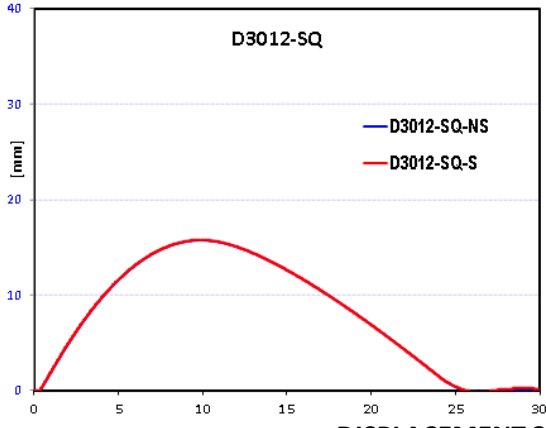
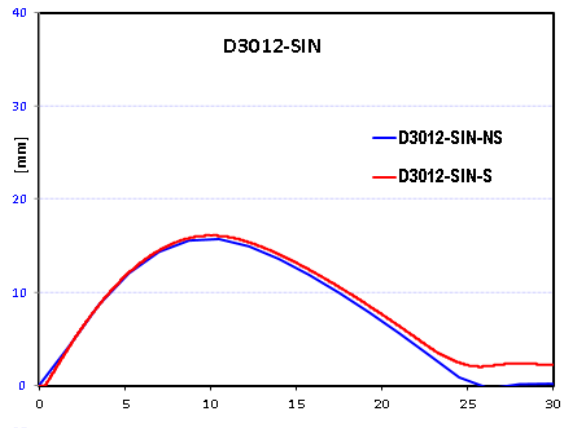
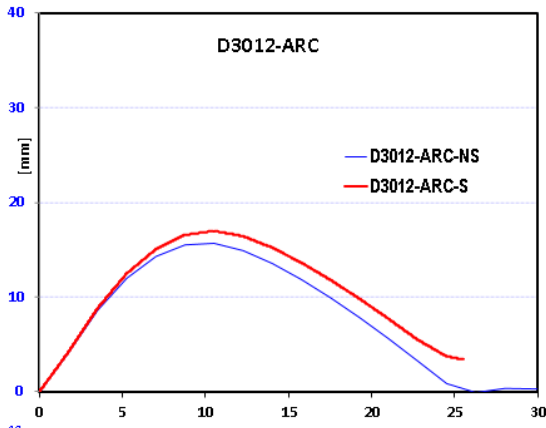
DISPLACEMENT 3007 NO-SPACE vs. SPACE



DISPLACEMENT 3009 NO-SPACE vs. SPACE



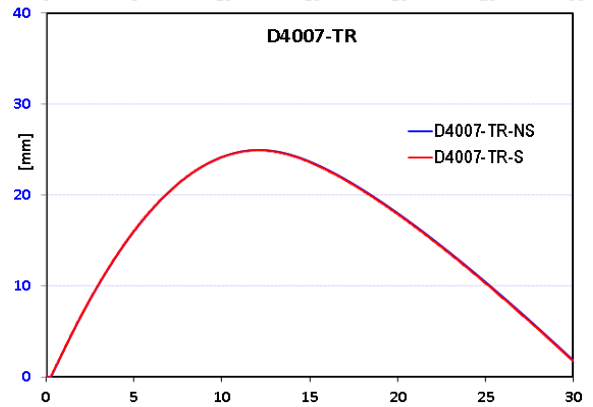
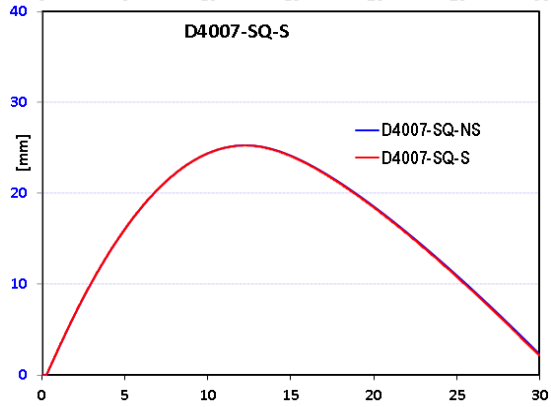
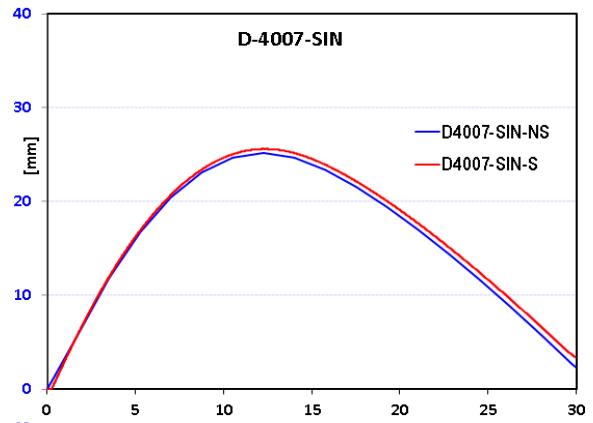
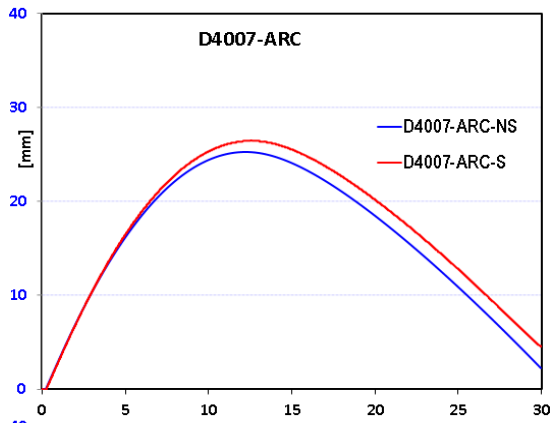
DISPLACEMENT 3010 NO-SPACE vs. SPACE



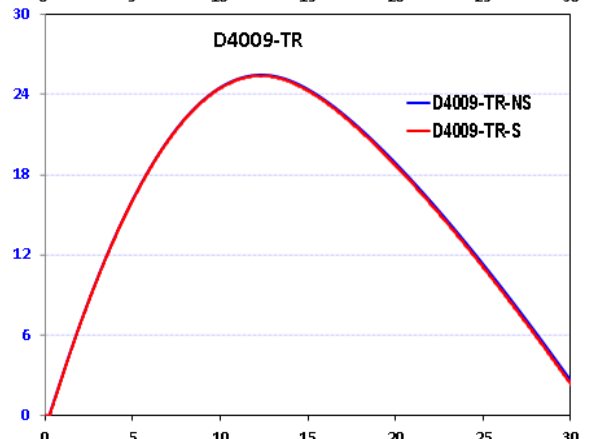
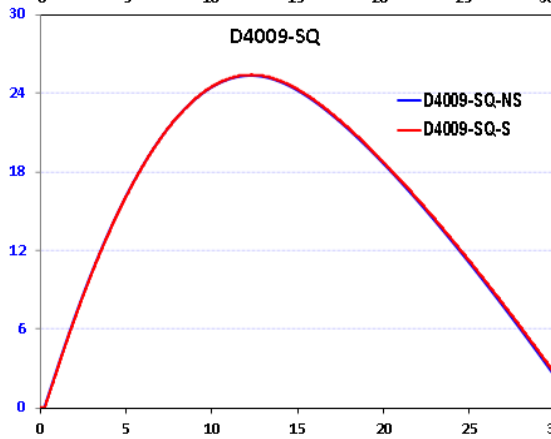
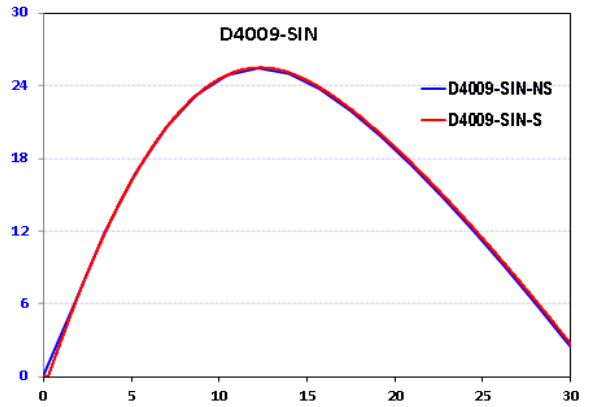
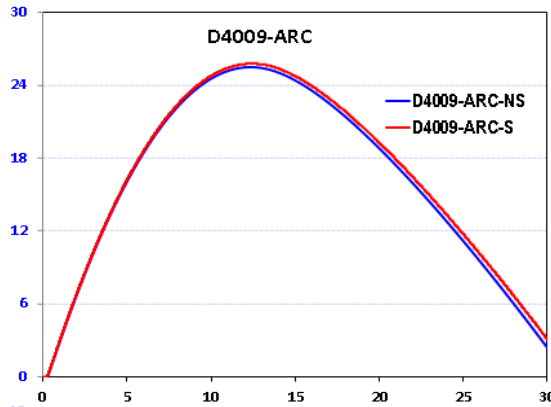
DISPLACEMENT 3012 NO-SPACE vs. SPACE

Displacement 4 m/s Shape

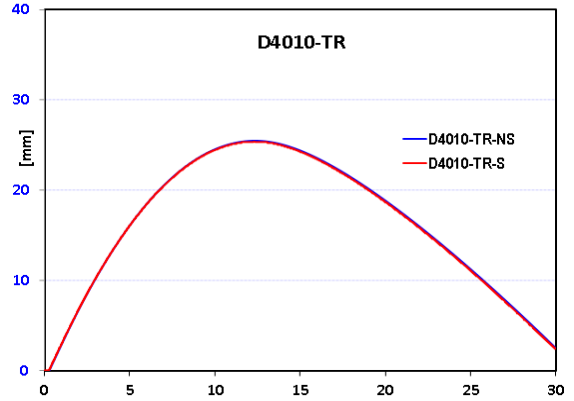
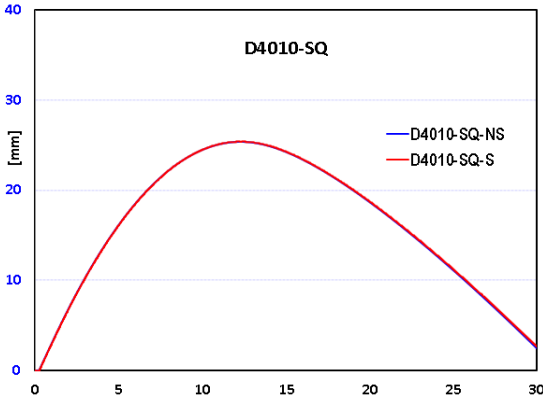
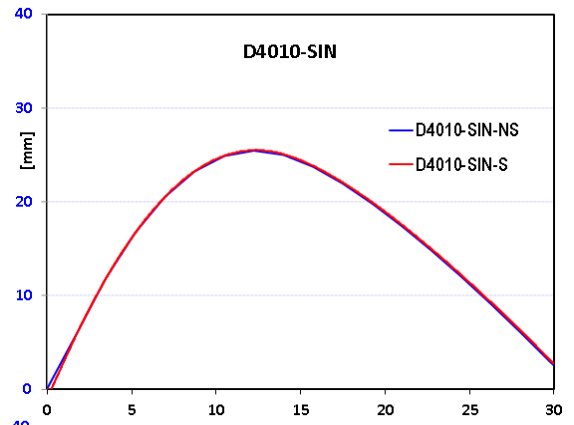
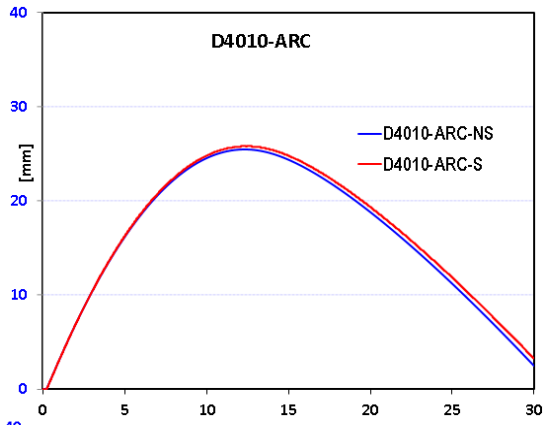
(No-Space Vs. Space)



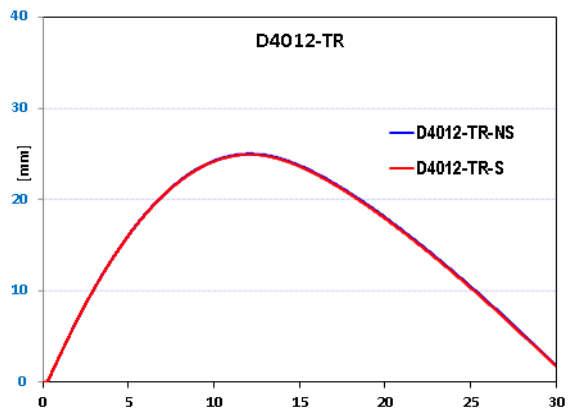
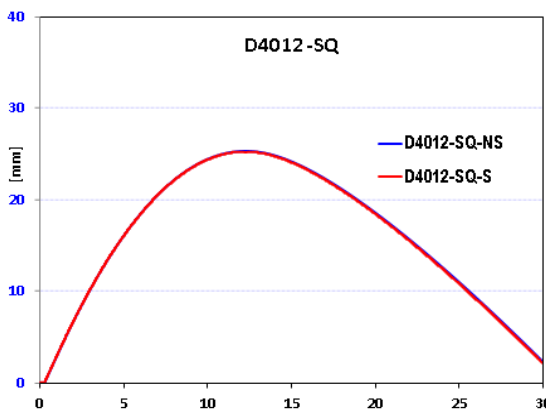
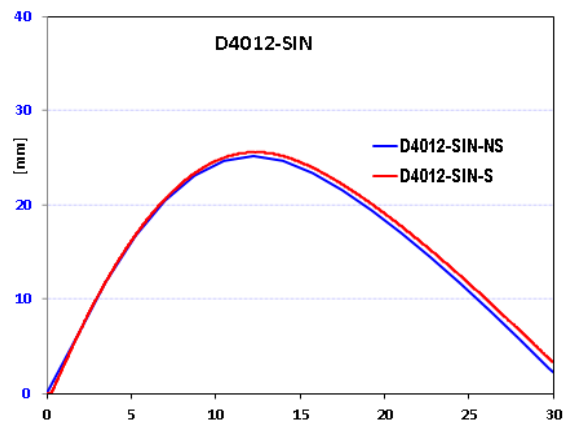
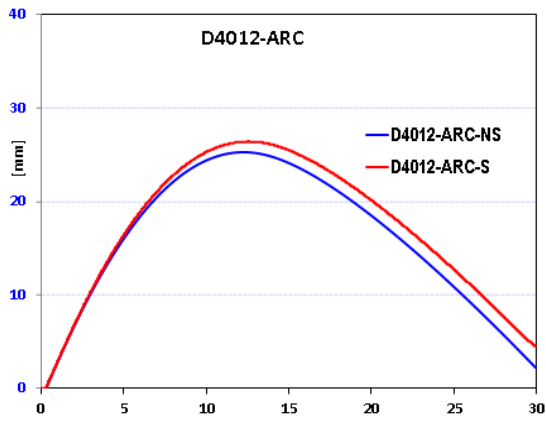
DISPLACEMENT 4007 NO-SPACE vs. SPACE



DISPLACEMENT 4009 NO-SPACE vs. SPACE



DISPLACEMENT 4010 NO-SPACE vs. SPACE



DISPLACEMENT 4012 NO-SPACE vs. SPACE